NASA-CR-174697-Vol-2

Configuration Study for a 30 GHz Monolithic Receive Array

Volume II: Appendixes

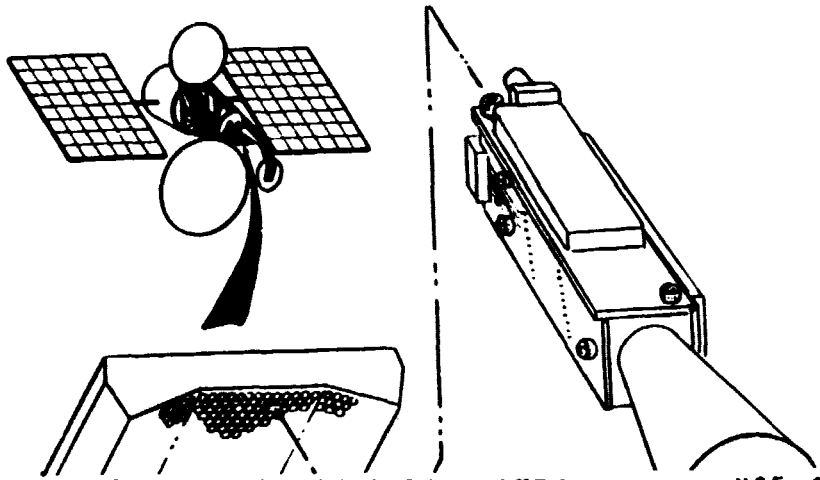

Prepared for
NASA LEWIS RESEARCH CENTER
Cleveland, Ohio

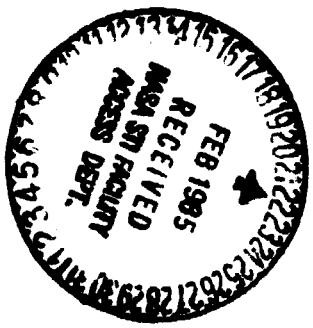

Contract NAS3-23780

ELECTRONICS LABORATORY
Syracuse, New York 13221

GENERAL ELECTRIC

1. Report No.	2. Government Accession No.	3. Recipient's Catalog No.
NASA CR-174-697		

4. Title and Subtitle	5. Report Date
Configuration Study for a 30 GHz Monolithic Receive Array	1 November 1984
	6. Performing Organization Code

7. Author(s)	8. Performing Organization Report No.
W.H. Nester, Bryan Cleaveland, Brian Edward, Steve Gotkis, Gary Hesserbacker, Jack Loh, Bruce Mitchell	
	10. Work Unit No.

9. Performing Organization Name and Address	11. Contract or Grant No.
General Electric Company Electronics Laboratory Electronics Park Syracuse, New York 13221	NAS3-23780
	13. Type of Report and Period Covered

12. Sponsoring Agency Name and Address	14. Sponsoring Agency Code
National Aeronautics & Space Administration Lewis Research Center 21000 Brookpark Road Cleveland, OH 44135	

15. Supplementary Notes

Technical Monitor, Richard Lee, Space Communication Division
NASA Lewis Research Center

16. Abstract

This report summarizes the results of configuration and design studies for 30 GHz receive antennas on a communications satellite. The antennas use reflector focusing systems with phased array feeds for beampointing, aberration correction, and interference suppression. The phased array feed designs are based on MMIC module technology. The antennas form simultaneous multiple beams in both scanning beam and fixed beam designs. Polarization diversity is used for beam isolation.

The initial configuration study and parametric design analyses encompassed Gregorian, Cassegrain, and single reflector systems. Parametric design and performance curves were generated. A preliminary design of each reflector/feed system was derived including radiating elements, beamformer network, beamsteering system, and MMIC module architecture. Performance estimates and component requirements were developed for each design. A recommended design was selected for both the scanning beam and the fixed beam case.

Detailed design and performance analysis results are presented for the selected Cassegrain configurations. The final design point is characterized in detail and performance measures evaluated in terms of gain, sidelobe level, noise figure, carrier-to-interference ratio, prime power, and beamsteering. The effects of mutual coupling and excitation errors (including phase and amplitude quantization errors) are evaluated. Mechanical assembly drawings are given for the final design point. Thermal design requirments are addressed in the mechanical design.

17. Key Words (Suggested by Author(s))	18. Distribution Statement
Cassegrain, Gregorian, Reflector, Phased Array Feed, MMIC Multiple Beam Antenna	For General Release

19. Security Classif. (of this report)	20. Security Classif. (of this page)	21. No. of Pages	22. Price*
Unclassified	Unclassified	549	

* For sale by the National Technical Information Service, Springfield Virginia 22161

APPENDIX A

THE FORMALISM OF THE SIDELOBE SUPPRESSION ALGORITHM

A. Given $\hat{e}_k(\theta_j)$ for k = 1, K elements j = O, J pattern points, choose a main-beam direction "θ_o", a sidelobe suppression region "θ_j", and an initial set of sidelobe suppression weights "β_j". (A caret designates a complex quantity)

B. Select the main-lobe gain vector

$$\hat{G}] = \hat{e}_k(\theta_o)] \quad ; \quad k = 1, \text{----}, K \qquad \text{A-(1)}$$

C. Compute a Sidelobe Covariance Matrix

$$[\hat{M}] = \left[\sum_{i=1}^{I} \beta_i \hat{e}_k^*(\theta_i)\hat{e}_\ell(\theta_i)\right] \; ; \; \begin{matrix} k = 1, \text{----}, K \\ \ell = 1, \text{----}, K \end{matrix} \qquad \text{A-(2)}$$

(An asterisk designates a complex conjugate)

D. Solve for the Excitation Vector

$$\hat{W}] = \hat{W}_k] \qquad k = 1, \text{----}, k \qquad \text{A-(3)}$$

Using the matrix equation

$$\hat{W}] = [I + \hat{M}]^{-1} \quad \hat{G}^*] \qquad \text{A-(4)}$$

where

$[I]$ = Identity Matrix

$[\;]_T^{-1}$ = Inverse of the Transposed Matrix

Normalize the weight vector $\hat{W}_{NEW}] = \dfrac{\hat{W}_{OLD}]}{\underbrace{\hat{W}_{OLD}^*}\cdot \hat{W}_{OLD}]}$

E. Compute the Resulting Gain

$$G_o = |\underbrace{\hat{G}}\quad \hat{W}]\;|^2 \qquad \text{A-(5)}$$

F. Compute the Resulting Sidelobe Performance

$$(SL)_j = \left|\sum_{k=1}^{K} \hat{W}_k \hat{e}_k(\theta_j)\right|^2 \qquad \text{A-(6)}$$

$$\overline{SL} = \frac{\sum_{j=1}^{J} (SL)_j}{J} \qquad \text{A-(7)}$$

G. If lower sidelobe performance at the expense of reduced gain is desired, based upon a comparison of the results from steps "D" and "E" to corresponding peformance requirements, iterate the optimization by proceeding to step "H", otherwise stop.

H. Increase "β_j" in high sidelobe regions and return to step "C";

i.e., If $(SL)_j > \gamma * SL$ A-(8)

Then $(\beta j)_{NEW} = (\beta j)_{OLD} + \Delta\beta$ A-(9)

APPENDIX B. SYSTEM NOISE FIGURE CALCULATION

The overall noise figure for a general system is defined as the quotient of a reference signal-to-noise ratio and the signal-to-noise ratio at the output of the system,

$$NF = \frac{(S/N)_{REF}}{(S/N)_{OUT}} \quad . \tag{B1}$$

For a two port system as shown in Figure B-1, the reference is usually taken at the system input making

$(S/N)_{IN}$ G, NF $(S/N)_{OUT}$

Figure B-1. Two Port System

$$NF = \frac{(S/N)_{IN}}{(S/N)_{OUT}} \quad . \tag{B2}$$

For a system with gain G and internally added noise N_{ADD}, (B2) may be written as

$$NF = \frac{S_{IN}/N_{IN}}{S_{OUT}/N_{OUT}} \tag{B3}$$

$$= \frac{S_{IN}/N_{IN}}{GS_{IN}/(GN_{IN} + N_{ADD})} \tag{B4}$$

$$= \frac{GN_{IN} + N_{ADD}}{GN_{IN}} \quad . \tag{B5}$$

This is an equivalent definition which states that noise figure is the net noise present at the output of a system which imparts additive noise referenced to the noise present at the output of an equivalent ideal system which contributes no additive noise.

In a multi-port beamforming network such as shown in Figure B-2, the signals at the element ports may not be identical. Additionally, if elemental receiver modules are employed, each having different gains and noise figures, then the signal-to-noise ratios at the combiner inputs will not be equal. In this situation, to determine the overall system noise figure, the reference signal-to-noise ratio is defined as the ratio that would be present at the output of a system which has noiseless receiver modules and a lossless combiner. It is assumed the combiner has matched inputs (features an isolated port). Such a system is shown in Figure B-3. This reference signal-to-noise ratio is in accordance with the definition given earlier.

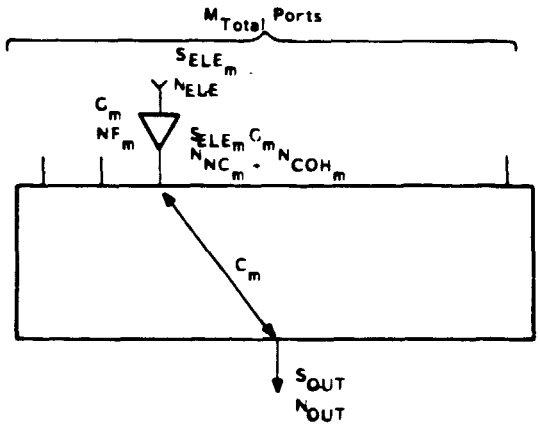

Figure B-2. General Multi-Port Beamforming Network

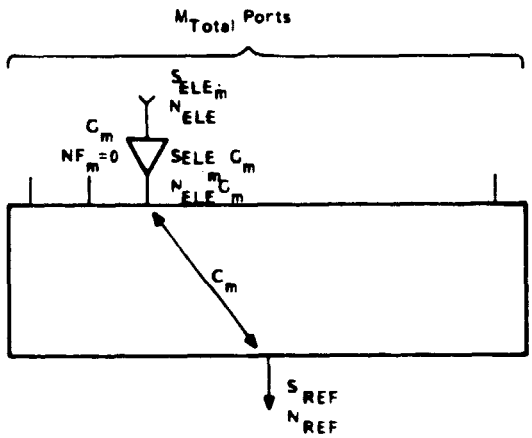

Figure B-3. Reference Multi-Port Beamforming Network

S_{ELE_m} and N_{ELE} are the signal and noise powers at the m^{th} element input while S_{REF} and N_{REF} are the signal and noise powers at the reference beamformer output. Notice that it has been assumed that the noise powers at each of the element inputs are equal which is a reasonable assumption when all elements are pointed in the same direction. G_m and NF_m are the power gain and noise figure respectively of the m^{th} elemental receiver module with the noise figures identically zero in the reference system. For non-active or "OFF" modules, G_m equals zero. C_m are the voltage coupling coefficients which may be complex.

The signals at the combiner output add coherently, therefore

$$S_{REF} = \left| \sum_{m=1}^{M_{Total}} \sqrt{S_{ELE_m}} \sqrt{G_m} \quad C_m \right|^2. \tag{B6}$$

The noise at the combiner output adds non-coherently so that

$$N_{REF} = \sum_{m=1}^{M_{Total}} \left| \sqrt{N_{ELE}} \sqrt{G_m} \quad C_m \right|^2. \tag{B7}$$

The reference signal-to-noise ratio is therefore from equations (B6) and (B7),

$$(S/N)_{REF} = \frac{\left| \sum_{m=1}^{M_{Total}} \sqrt{S_{ELE_m}} \sqrt{G_m} \quad C_m \right|^2}{N_{ELE} \sum_{m=1}^{M_{Total}} G_m \left| C_m \right|^2} . \tag{B8}$$

To derive the noise figure expression for the general multi-port beamforming network, the signal-to-noise ratio at the output must be determined for the case where the elemental receiver module noise figures are non-zero. Referring to Figure B-2, the signal power at the combiner is given by

$$S_{OUT} = \left| \sum_{m=1}^{M_{Total}} \sqrt{S_{ELE_m}} \sqrt{G_m} \quad C_m \right|^2. \tag{B9}$$

The noise power at the output can consist of two components. A non-coherent part which is amplified element noise and non-coherent additive noise, and a coherent part which may be due to noise from a common local oscillator if frequency translation takes place in each of the receiver modules. If N_{NC_m} and N_{COH_m} represent these non-coherent and coherent noises at the m^{th} amplifier module output, then the noise power at the beamforming network output is

$$N_{OUT} = \sum_{m=1}^{M_{Total}} |\sqrt{N_{NC_m}}\, C_m|^2 + |\sum_{m=1}^{M_{Total}} \sqrt{N_{COH_m}}\, C_m|^2. \qquad \text{(B10)}$$

From equations (B9) and (B10), the output signal-to-noise ratio is

$$(S/N)_{OUT} = \frac{|\sum_{m=1}^{M_{Total}} \sqrt{S_{ELE_m}}\, \sqrt{G_m}\, C_m|^2}{\sum_{m=1}^{M_{Total}} |\sqrt{N_{NC_m}}\, C_m|^2 + |\sum_{m=1}^{M_{Total}} \sqrt{N_{COH_m}}\, C_m|^2}. \qquad \text{(B11)}$$

A non-active or "OFF" module contributes no coherent noise. Further, the coherent noise contributions from active modules may be assumed to be equal. Therefore, the output signal-to-noise ratio may be expressed as

$$(S/N)_{OUT} = \frac{|\sum_{m=1}^{M_{Total}} \sqrt{S_{ELE_m}}\, \sqrt{G_m}\, C_m|^2}{\sum_{m=1}^{M_{Total}} N_{NC_m} |C_m|^2 + N_{COH} |\sum_{m=1}^{M_{Active}} C_m|^2}. \qquad \text{(B12)}$$

where M_{active} is the number of "ON" receiver modules.

Substituting the signal-to-noise ratio expressions (B8) and (B12) into the noise figure expression, equation (B1), gives for the beamforming network

$$NF = \frac{\sum_{m=1}^{M_{Total}} N_{NC_m} |C_m|^2 + N_{COH} |\sum_{m=1}^{M_{Active}} C_m|^2}{N_{ELE} \sum_{m=1}^{M_{Total}} G_m |C_m|^2}. \qquad \text{(B13)}$$

Using the noise figure definition of equation (B5), the noise figure for the m^{th} receiver module may be written as

$$NF_m = \frac{N_{NC_m} + N_{COH_m}}{G_m \, N_{ELE}} \qquad \text{(B14)}$$

where as before, N_{NC_m} contains the contribution of both additive non-coherent noise and amplified non-coherent element noise $G_m \, N_{ELE}$. Solving equation (B14) for N_{NC_m} gives

$$N_{NC_m} = NF_m \, G_m \, N_{ELE} - N_{COH_m} \qquad \text{(B15)}$$

which when substituted into equation (B13) yields

$$NF = \frac{N_{ELE} \sum_{m=1}^{M_{Total}} NF_m \, G_m |C_m|^2 - \sum_{m=1}^{M_{Total}} N_{COH_m} |C_m|^2 + N_{COH} \left| \sum_{m=1}^{M_{Active}} C_m \right|^2}{N_{ELE} \sum_{m=1}^{M_{Total}} G_m |C_m|^2} \qquad \text{(B16)}$$

As before, the coherent noise contributions are equal for active amplifier modules and zero for non-active modules. Thus, the noise figure expression becomes

$$NF = \frac{\sum_{m=1}^{M_{Total}} NF_m \, G_m |C_m|^2 + \frac{N_{COH}}{N_{ELE}} \left(\left| \sum_{m=1}^{M_{Active}} C_m \right|^2 - \sum_{m=1}^{M_{Active}} |C_m|^2 \right)}{\sum_{m=1}^{M_{Total}} G_m \, |C_m|^2} \, . \qquad \text{(B17)}$$

For the "OFF" or non-active receiver modules G_m equals zero. For these modules

$$\left[NF_m \, G_m = \frac{N_{NC_m} + N_{COH}}{N_{ELE}} \right]_{G_m \to 0} = \frac{N_{OFF}}{N_{ELE}} \qquad \text{(B18)}$$

where N_{OFF} is the non-coherent additive noise from an "OFF" receiver module. Using this expression in equation (B17) results in

$$NF = \frac{\sum_{m=1}^{M_{active}} NF_m G_m |C_m|^2 + \frac{N_{OFF}}{N_{ELE}} \sum_{m=M_{Active}+1}^{M_{Total}} |C_m|^2 + \frac{N_{COH}}{N_{ELE}} \left(\left| \sum_{m=1}^{M_{Active}} C_m \right|^2 - \sum_{m=1}^{M_{Active}} |C_m|^2 \right)}{\sum_{m=1}^{M_{Active}} G_m |C_m|^2} \tag{B19}$$

If the combiner under consideration is uniformly weighted, then the voltage coupling coefficients C_m are given by

$$|C_m| = \frac{1}{\sqrt{M_{Total}}} \quad . \tag{B20}$$

Therefore, the noise figure expression (B19) for this special case becomes

$$NF = \frac{\sum_{m=1}^{M_{active}} NF_m G_m + \frac{N_{OFF}}{N_{ELE}} (M_{Total} - M_{Active}) + \frac{N_{COH}}{N_{ELE}} (M_{Active}^2 - M_{Active})}{\sum_{m=1}^{M_{Active}} G_m} \quad . \tag{B21}$$

Equations (B19) and (B21) represent the noise figure of a beamforming network having non-equal signal inputs, non-equal elemental receiver module characteristics, and a lossless combiner. The mean gain for this system is simply

$$G = \frac{\sum_{m=1}^{M_{Active}} G_m}{M_{Total}} \tag{B22}$$

The overall noise figure which includes the effects of combiner loss may be determined by considering two cascaded networks as shown in Figure B-4. The first network has a noise figure and gain as calculated by equataions (19) or (21) and (22). The second network accounts for the combiner loss L_{COMB} and has a noise figure numerically equal to this loss. Therefore, the overall noise figure is given by

$$NF_{OVERALL} = NF + \frac{L_{COMB} - 1}{G} \qquad (B23)$$

and the overall gain is

$$G_{OVERALL} = G/L_{COMB}. \qquad (B24)$$

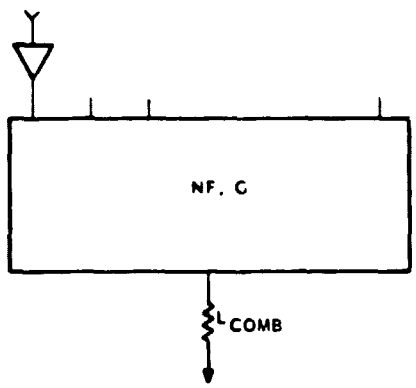

Figure B-4. Beamforming network with combiner losses

Appendix C

TABLE OF CONTENTS

Appendix C

TABLE OF CONTENTS (CONTINUED)

SECTION 1

INTRODUCTION AND SUMMARY

1.1 INTRODUCTION

The primary effort of G.E. SSD during Phase I of this program was aimed at analyzing a confocal parabolic, electronically scanned, Gregorian type antenna system. This effort was broken up into two main tasks , namely the analysis of the optical system and the analysis of the MMIC beam combining network. The early part of phase I was devoted to determining a baseline optical system capable of imaging a desired far field pattern to a phased array system such that proper element weights could be determined. The primary parameters which were investigated included the F/D, the magnification (M),the subreflector size , and the reflector offset. Once the optical system was defined, several array configurations were considered to verify the spherical mode approach as well as to define the initial design point for the Gregorian system. The verification was accomplished by comparing the secondary patterns produced using spherical mode techniques with those produced using a near field physical optics approach. This verification was required since the spherical mode approach had not previously been used in the analysis of apertures of this size. A description of the spherical mode technique appears in section 1.3.2. Several reflector program modifications including a non-linear offset grid were made to significantly reduce the computation time by optimally selecting the number of modes required to accurately descibe the pattern. The reflector program is discussed in section 1.3.1.

It was originally intended that the weights for the individual array elements would be optimized using a secondary pattern synthesis approach. This approach entails computing the secondary pattern of each element in the array. The elemental information furnishes a data base utilized in the optimization of the system secondary pattern. Due to the number of elements (600-1200) that are used in the Gregorian system, the computation time for determining these individual element far field patterns (approximately 4 Hrs/element on a HP 1000) was prohibitive. The optimization program is extremely powerful to fine tune the element weights once an optical system is properly selected. However, this program provides no direct information regarding the optical system parameter selection. An approach which determines the amplitude and phase on each element in the array prior to computing the secondary pattern was developed based on an inverse ray tracing technique. This approach can be used to provide optical system information such as the selection of the magnification factor, and the size and location of the subreflector and the array aperture. This method is descibed in detail in section 1.3.3.

Once the weight of each element was determined, the system performance, as well as the parameters which characterize the beam forming network was investigated. These parameters included phase quantization, phase shifter error, phase shifter failure, amplitude taper, amplitude error, and amplifier failure. These parameters were varied, primarily, to determine their effect on peak gain and maximum sidelobe level. The information obtained from this parametric study is contained in sections 3 and 4.

1.2 THE GREGORIAN SYSTEM

The system configuration being studied consisted of two confocal paraboloids arranged in a Gregorian fashion, and an offset phased array located parallel to the focal plane. The offset plane cross sectional view of the system is depicted in figure 1.2-1 and a conceptual sketch is shown in figure 1.2-2.

1.3 SUMMARY OF COMPUTER PROGRAMS

1.3.1 MAIN REFLECTOR PROGRAM

The reflector program used to analyze the Gregorian system under consideration is based on physical optics theory. The reflector surface is projected onto a polar grid as shown in figure 1.3-1. This polar form requires approximately 1/3 the number of samples that would be required for a cartesian system. The number of angular and radial cuts are determined from sampling theory. Once the grid has been defined, the current in each element bounded by the grid is determined. This current is assumed to be constant throughout each incremental area. The grid definition is extremely important in large aperture systems, such as the one under consideration, since, improper sampling may introduce ficticious power (grating lobes). If the grid increments are large in areas where the current distribution is changing rapidly, the elemental current may not accurately describe the actual current distributions. In the present large diameter offset reflector system, the distance between grid points could be several wavelengths near the peak current point. Thus a much finer grid system must be defined. A finer grid system is a rather inefficient way to solve the sampling problem. Therefore several techniques were implemented to reduce the number of grid points while maintaining accurate current representation. First an offset grid system was developed. This allows the grid center to be shifted to the peak current point where the surface current will tend to change most rapidly and where the current magnitude is most concentrated. In addition , a non-linear angular and radial step size can be specified. This allows more samples to be taken near the peak of the current thereby providing a more accurate surface current description. The offset non-linear polar grid configuration is shown in figure 1.3-2 Comparisions of subreflector far field patterns using a standard polar grid and an offset non-linear polar grid are given in figures 1.3-3 and 1.3-4. As can be seen from this data the offset non-linear grid is required to accurately represent the current on the reflector surface.

1.3.2 DESCRIPTION OF THE SPHERICAL MODE APPROACH

General Electric S.S.D. has been working with a unique method of simulating feeds and analyzing reflector configurations using spherical mode techniques since 1978. One merit of the spherical mode approach is that, in general, the far field of a reflector or feed element can be accurately described in a relatively small number of complex coefficients which makes the programs very efficient. For 10λ apertures the spherical mode approach is approximately 5 times faster than a true near field physical optics approach. For 50λ apertures the spherical mode approach is twice as fast as the physical optics technique.

The spherical mode technique is based on the solution of the vector wave equation in spherical coordinates. For EM fields of a radiating structure expressed by E and H conventionally, the coefficients of the vector wave equation of the form Amn

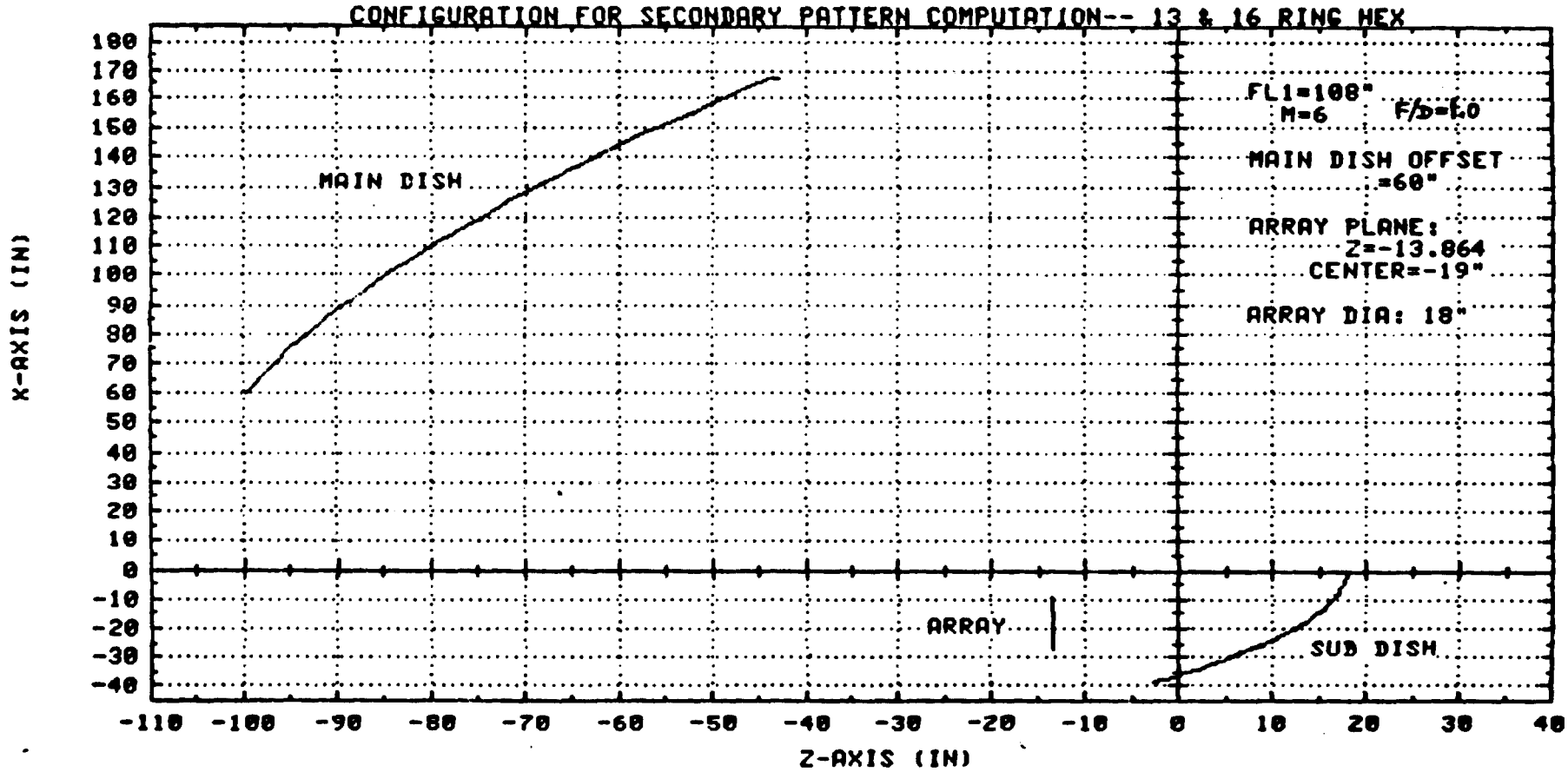

FIG. 1.2-1 GREGORIAN SYSTEM CONFIGURATION

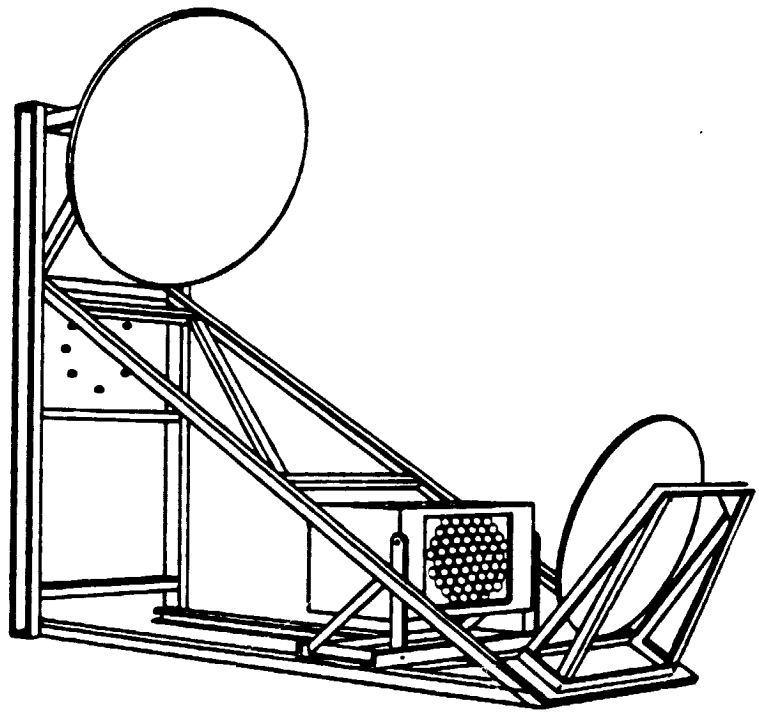

FIG. 1.2-2 **Confocal Paraboloids in Gregorian Arrangement**

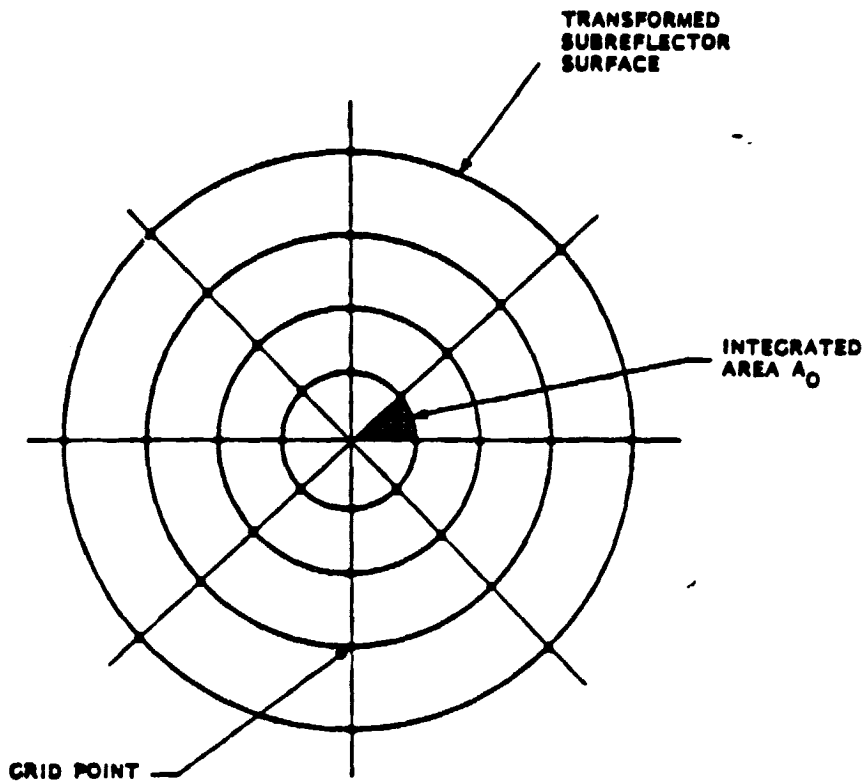

Figure 1.3-1 Polar Grid Configuration for Main Reflector Program

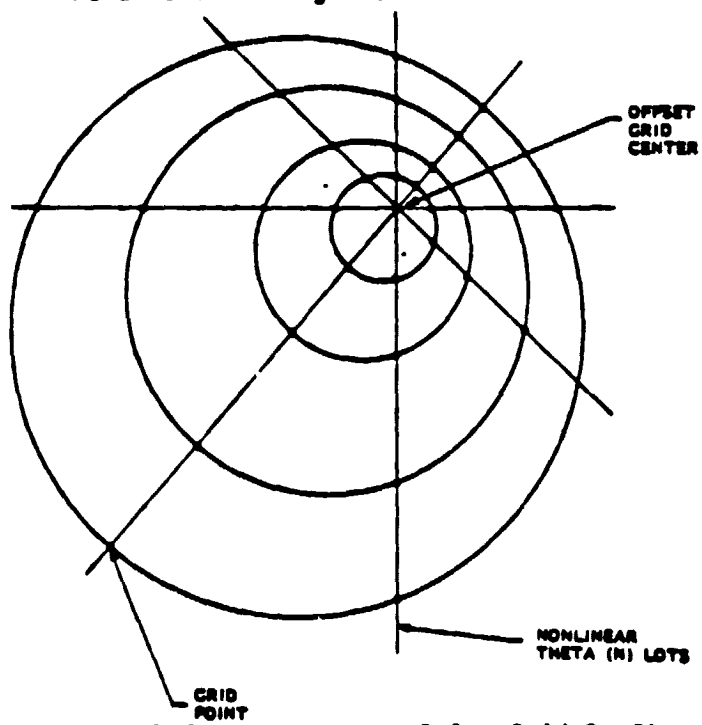

Figure 1.3-2 Offset Non-Linear Polar Grid Configuration for Main Reflector Program

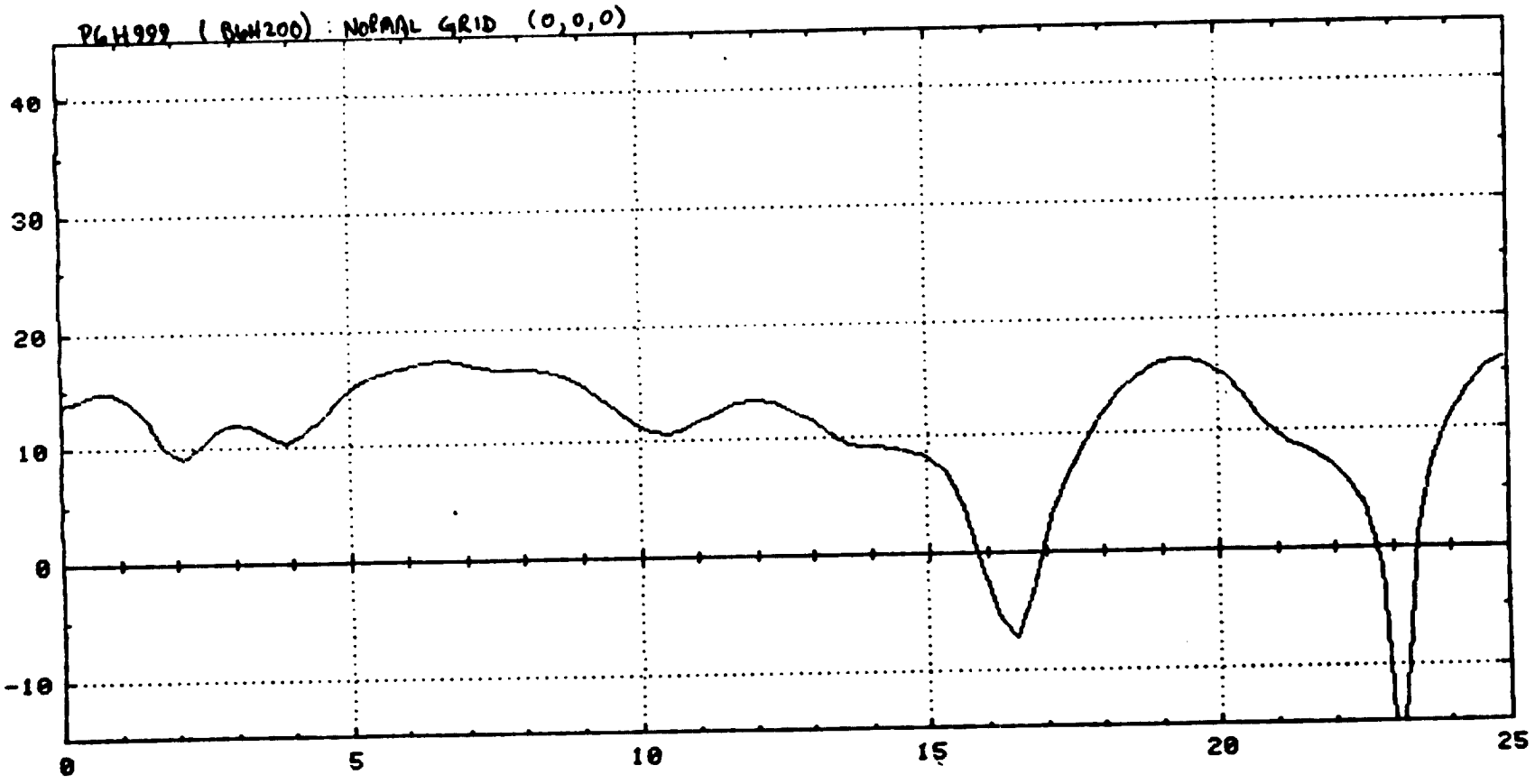

FIG 1.3-3 20 RING C.S. HEX SCAN (AZ/EL = 0°/0°)

NO GRID OFFSET, (0,0)

EXPONENTIAL MAPPING FACTOR : 0.0

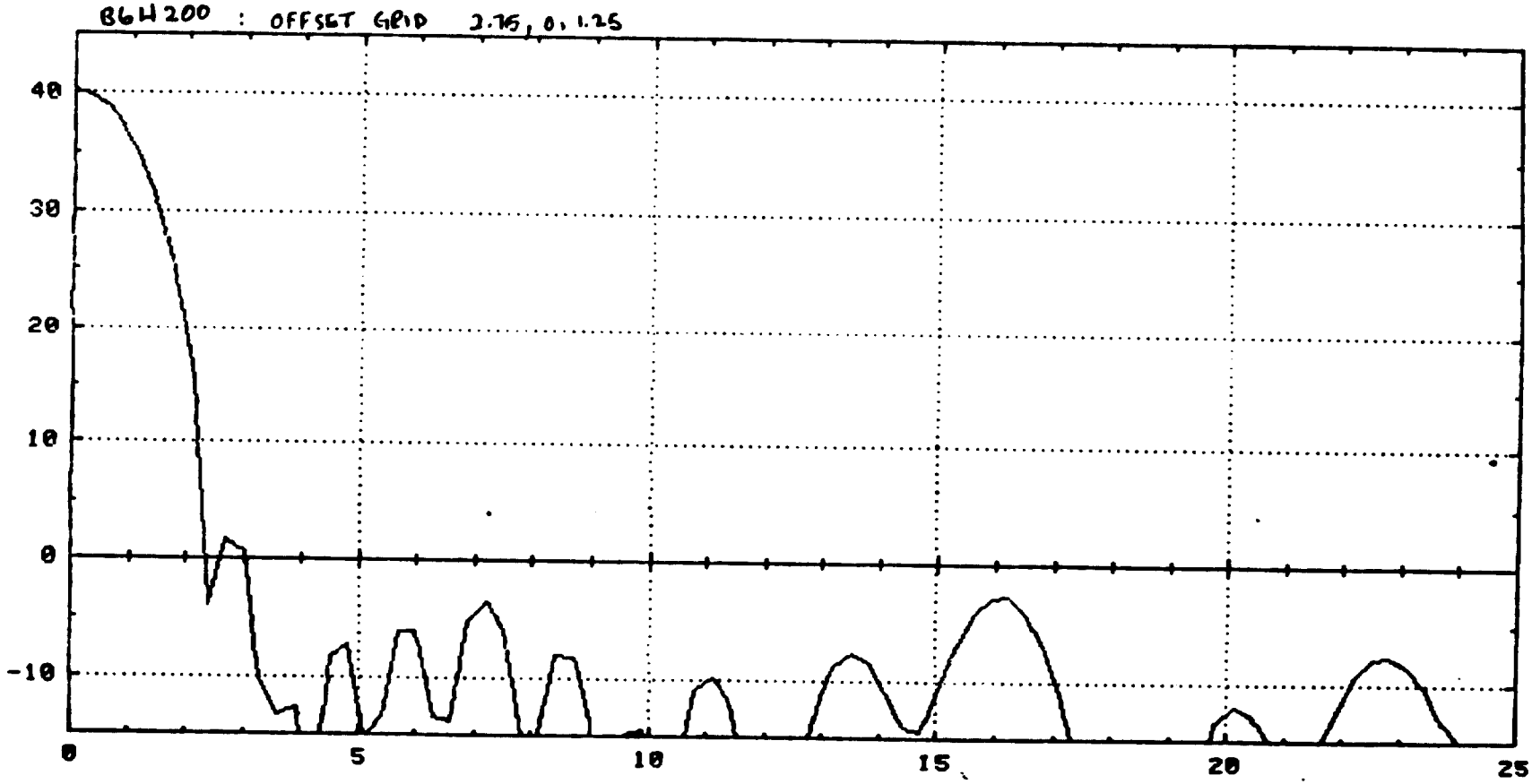

FIG 1.3-4 20 RING C.S. HEX SCAN (AZ/EL = 0°/0°)

OFFSET GRID · (2.75, 0)

EXPONENTIAL MAPPING FACTOR : 1.25

and Bmn in spherical coordinates can be determined. This process is referred to as spherical mode expansion (SME). For a given set of spherical mode coefficients, the EM fields (E,H) can be determined from a knowledge of the vector orthogonal functions. This process of determining E and H from spherical mode coefficients is referred to as spherical mode reconstruction (SMR). Since, in the far field, the radial function can be factored out of the wave equation, a set of spherical mode coefficients can easily be determined. By reinserting the radial function into the vector orthogonal functions, the near field can be computed. This far to near transformation is extemely important for the system under consideration in that the subreflector is within the near field of the array aperture and the main reflector is within the near field of the subreflector.

1.3.3 DESCRIPTION OF ARRAY SYNTHESIS APPROACH

The array systhesis is designed to produce the following array parameters complying with the system performance requirements.

1) Array location
2) Array size
3) Element size & spacing
4) Element weight, phase & amplitude
5) Phase quantization, number of bits
6) Sensitivity to random errors

The first synthesis method evaluated was the secondary pattern optimization approach. The advantages of this method are:

1) It provides an overal view of the system performance.
2) It optimizes performance parameters simultaneously on a global basis.
3) It provides the insight to performance tradeoffs.

The disadvantages are:

1) It provides no physical insight regarding the initial system design.
2) It requires the individual secondary pattern of each of the array elements; and the patterns have to be re-computed once the array or any other system parameter is adjusted.

The computational efforts become prohibitive, if the number of array element is large, or the initial choice of the array and/or system parameters is not close to optimum.

The second synthesis method was developed based on inverse ray tracing technique(IRTT). This method has effectively decoupled the array synthesis from the optical system design. It also provides the designer with the near-optimum optical system design efficiently and economically. However, IRTT is not a replacement for the synthesis by the secondary pattern optimization. Instead, it supplements the first array synthesis approach.

The following describes the IRTT development.

In the early stages of the study, secondary patterns were computed (re: Table 7.1-1). In almost all of the unscanned cases, reasonable secondary patterns were obtained. But none of the scanned cases showed satisfactory results.

To better understand the results that were obtained, an investigation was conducted in three major areas. The first was aimed at verifying the imaging concept where an array with 6 times the feed array diameter and element spacing (i.e. 3.18"=6x0.53) and with the same number of elements (1039) was assumed to replace the main reflector aperture. The unscanned far field patterns of the "magnified" array show excellent agreement with the actual unscanned system secondary pattern as can be seen in figures 1.3-5 and 1.3-6. The aperture image concept was thus established for the unscanned case.

The second area of investigation was aimed at explaining the unsatisfactory results for the scanned case. A ray tracing technique was implemented to aid in this investigation. It was found that rays leaving the array plane in the same direction corresponding to a specific scan angle arrived at the scan plane with different path lengths leading to phase error problems. This concept is shown in figure 1.3-7. Figures 1.3-8 - 1.3-11 show these path length errors as a function of element position and array scan angle for two different geometries. In addition, these rays will arrive in different directions as can be seen in figure 1.3-12. The far field scanning angle as a function of element position and array scan pointing angle for two different geometries is depicted in figures 1.3-13 - 1.3-16. Both of these effects become more pronounced at larger scan angles. The scan plane is a plane passing through the focus, perpendicular to the system scan direction . If the system scan becomes zero, all the secondary rays are parallel to each other and all the ray path lengths are equal. Based upon these results, the reasons for the unsatisfactory scanned results are well understood.

The third area of investigation dealt with finding a method to handle the scanned cases, leading to the development of the inverse ray tracing technique (IRTT). The word "inverse" was used to imply that the rays were traced from the secondary back to the primary, i.e., from the main dish through the subreflector to the array. See figure 1.3-17. A necessary condition to obtain peak radiation in the scanned direction is that the rays in the scanned direction must be in phase. To have the secondary rays parallel to each other in the scanned direction, they must leave the array plane at specific angles. The ray emmiting angle at the array element to produce an in phase secondary ray in the scanned direction is a function of the element location and the parameters of the optical system. Once the ray emitting angle is determined, the path length from the array element to the scan plane can be calculated. The phase of each of the array elements can thus be equalized by using the phase shifters to provide equal phase across the scan plane. This procedure provides a basis for array element phase settings. Figure 1.3-18 shows the path length from a point on the reflector to a point on the array for a given scan direction as the point moves in both the X and Y directions across the reflector surface. The amplitude settings of the array elements can also be determined using the inverse ray tracing technique, since the amplitude taper across the scan plane dictated by the performance requirements can be mapped back to the array plane to obtain the desired array amplitude taper.

1.3.4 VERIFICATION OF COMPUTER PROGRAMS

The use of spherical modes for apertures exceeding 100 wavelengths had not been completely verified prior to the start of this contract. Therefore, before the spherical mode approach could be confidently utilized, a justification of the method had to be made. This justification involved computing the secondary pattern of the system using both spherical mode techniques and a near field

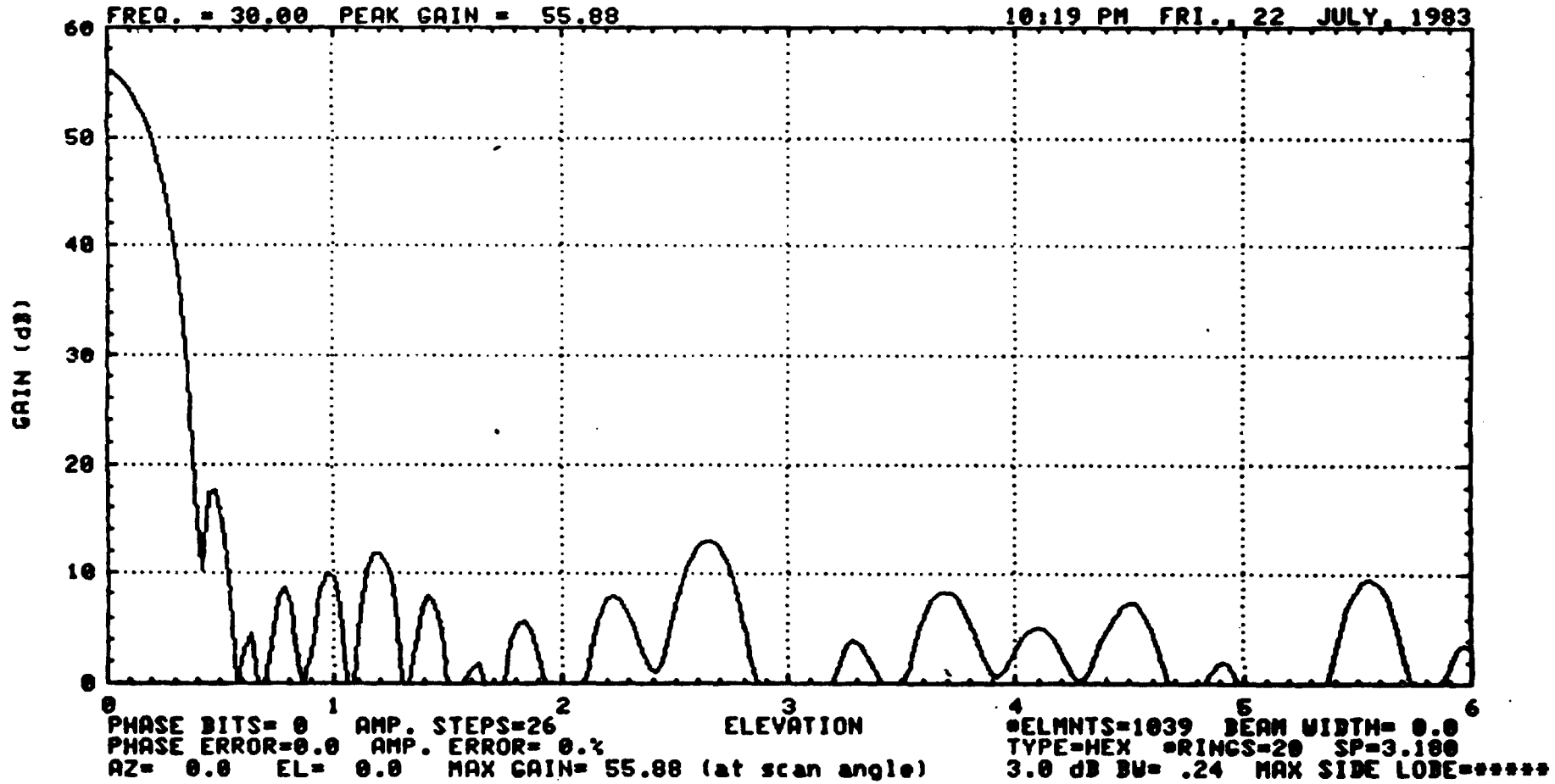
FREQ. = 30.00 PEAK GAIN = 55.88
10:19 PM FRI., 22 JULY, 1983
GAIN (dB)
60
50
40
30
20
10
0
0
1
2
3
4
5
6
ELEVATION
PHASE BITS= 0 AMP. STEPS=26
PHASE ERROR=0.0 AMP. ERROR= 0.%
AZ= 0.0 EL= 0.0 MAX GAIN= 55.88 (at scan angle)
*ELMNTS=1039 BEAM WIDTH= 0.0
TYPE=HEX *RINGS=20 SP=3.180
3.0 dB BW= .24 MAX SIDE LOBE=*****

FIGURE 1.3-5

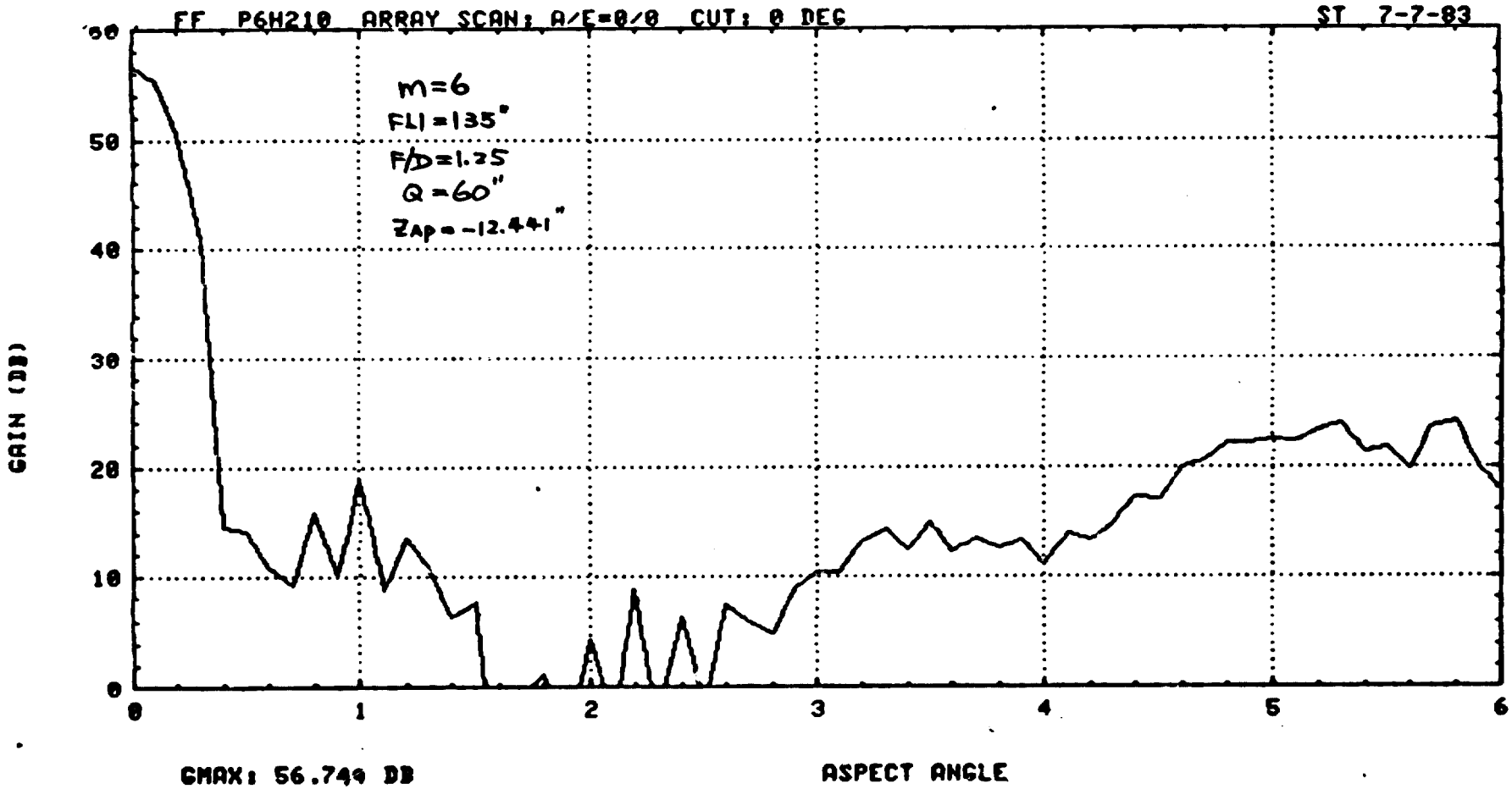
FF P6H210 ARRAY SCAN; A/E=0/0 CUT: 0 DEG
ST 7-7-83
m=6
FLI=135°
F/D=1.25
Q=60"
Zap=-12.441"
GAIN (DB)
60
50
40
30
20
10
0
0
1
2
3
4
5
6
GMAX: 56.749 DB
ASPECT ANGLE

FIGURE 1.3-6

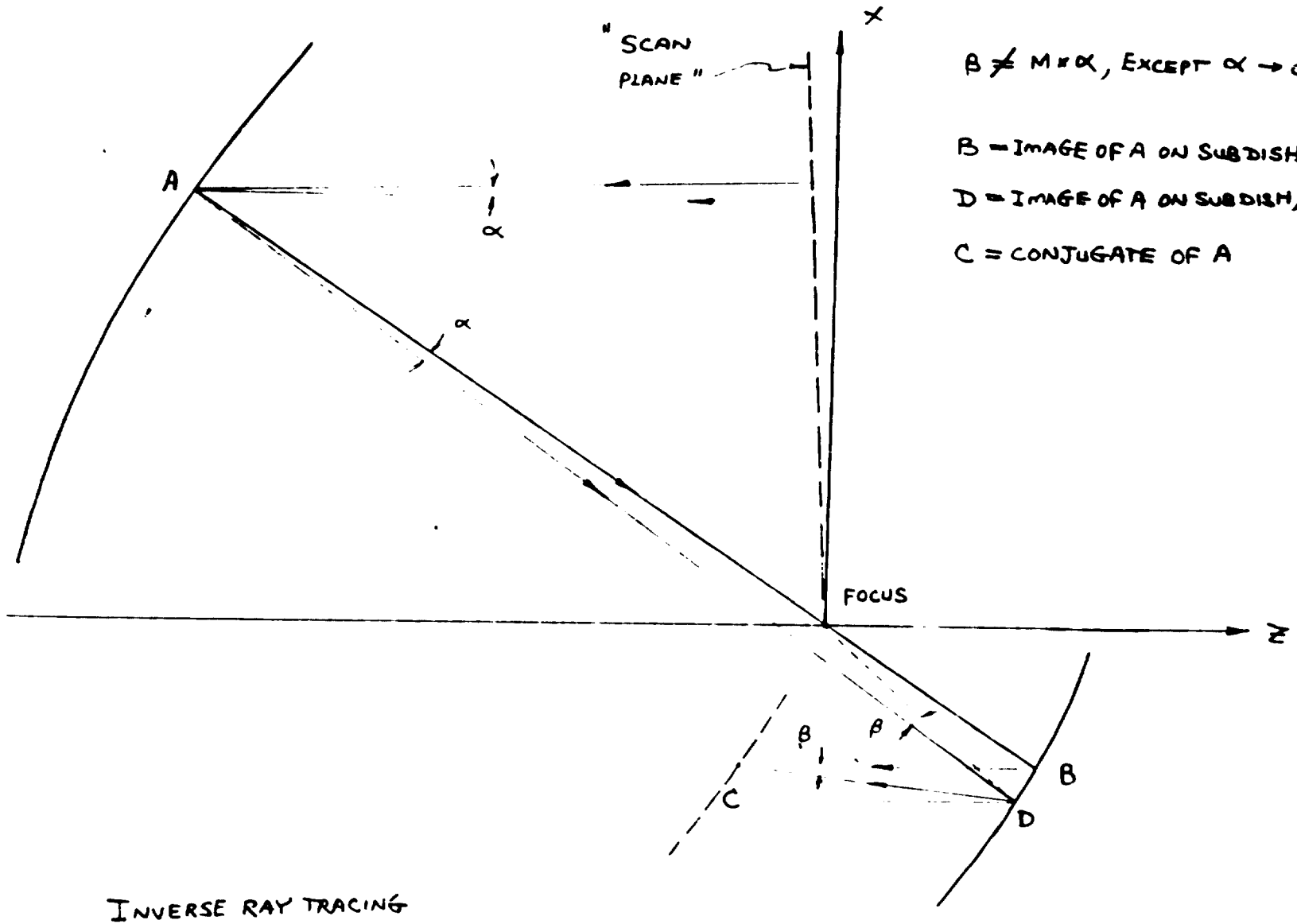

INVERSE RAY TRACING
& CONJUGATE POINT

FIGURE 1.3-7

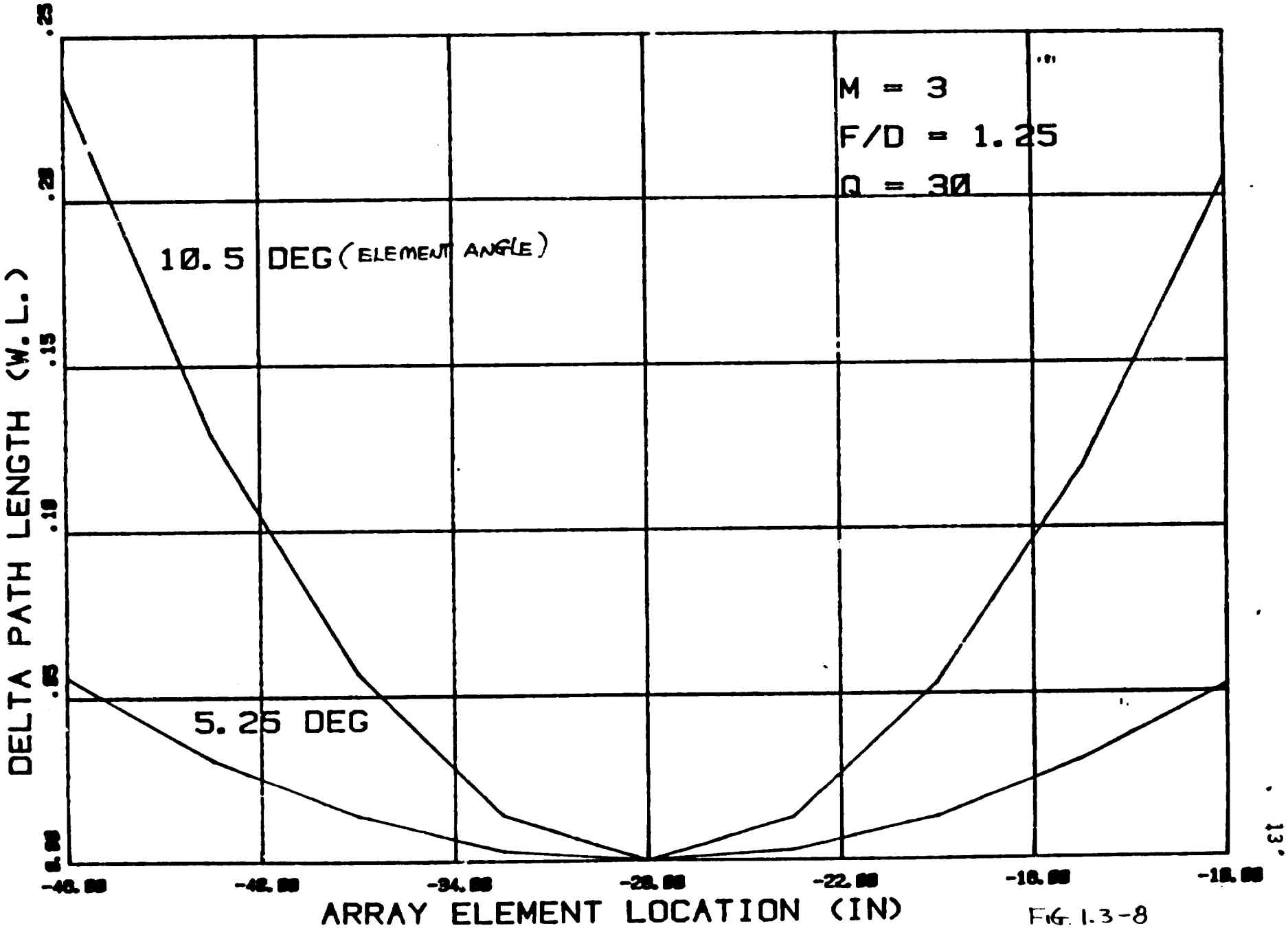
M = 3
F/D = 1.25
Q = 30
10.5 DEG (ELEMENT ANGLE)
5.25 DEG
DELTA PATH LENGTH (W.L.)
ARRAY ELEMENT LOCATION (IN)

FIG. 1.3-8

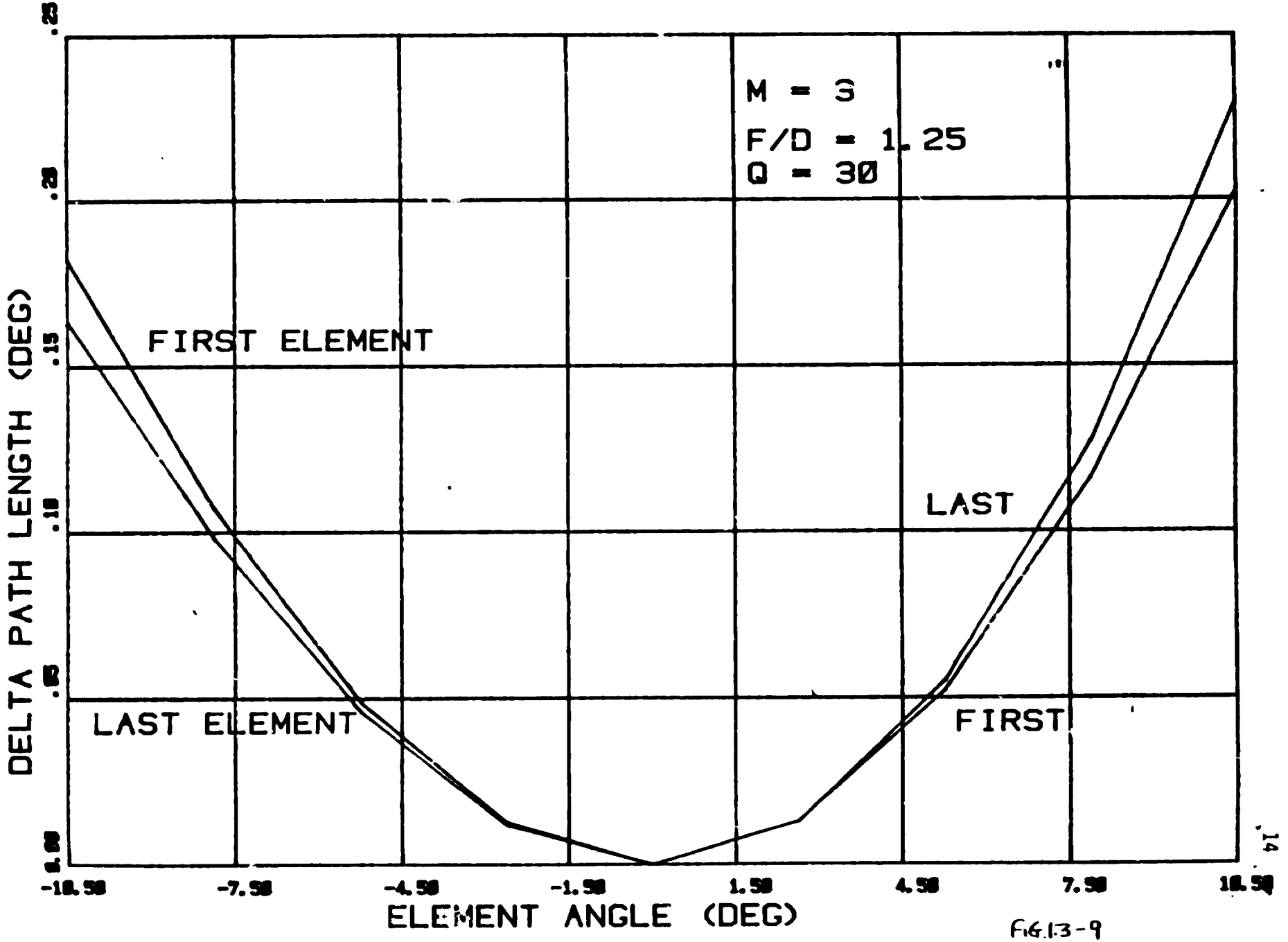
M = 3
F/D = 1.25
Q = 30
FIRST ELEMENT
LAST
LAST ELEMENT
FIRST
DELTA PATH LENGTH (DEG)
.23
.20
.15
.10
.05
0.00
-10.50
-7.50
-4.50
-1.50
1.50
4.50
7.50
10.50
ELEMENT ANGLE (DEG)

FIG 13-9

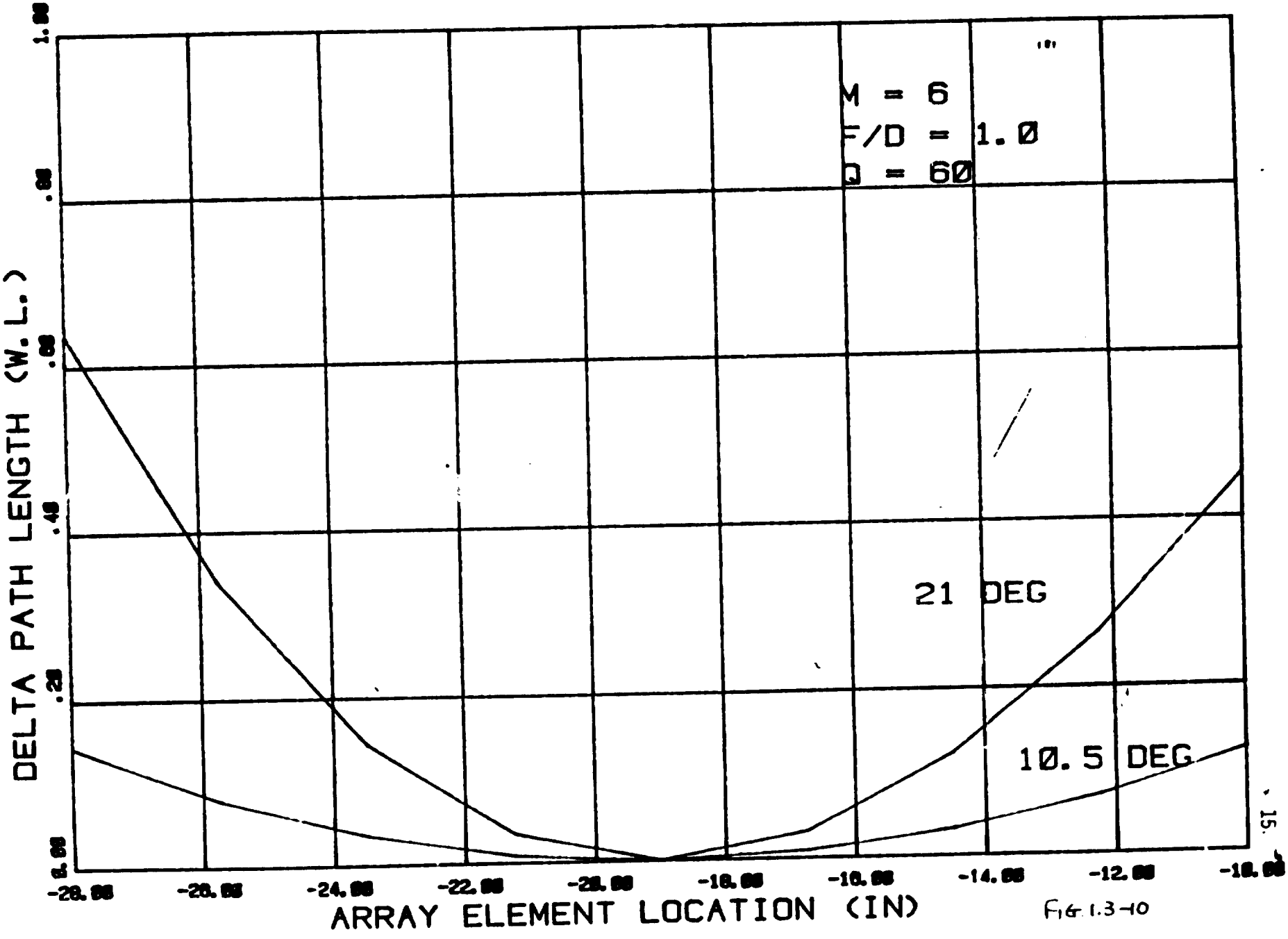
M = 6
F/D = 1.0
Q = 60
21 DEG
10.5 DEG
DELTA PATH LENGTH (W.L.)
ARRAY ELEMENT LOCATION (IN)

FIG 1.3-10

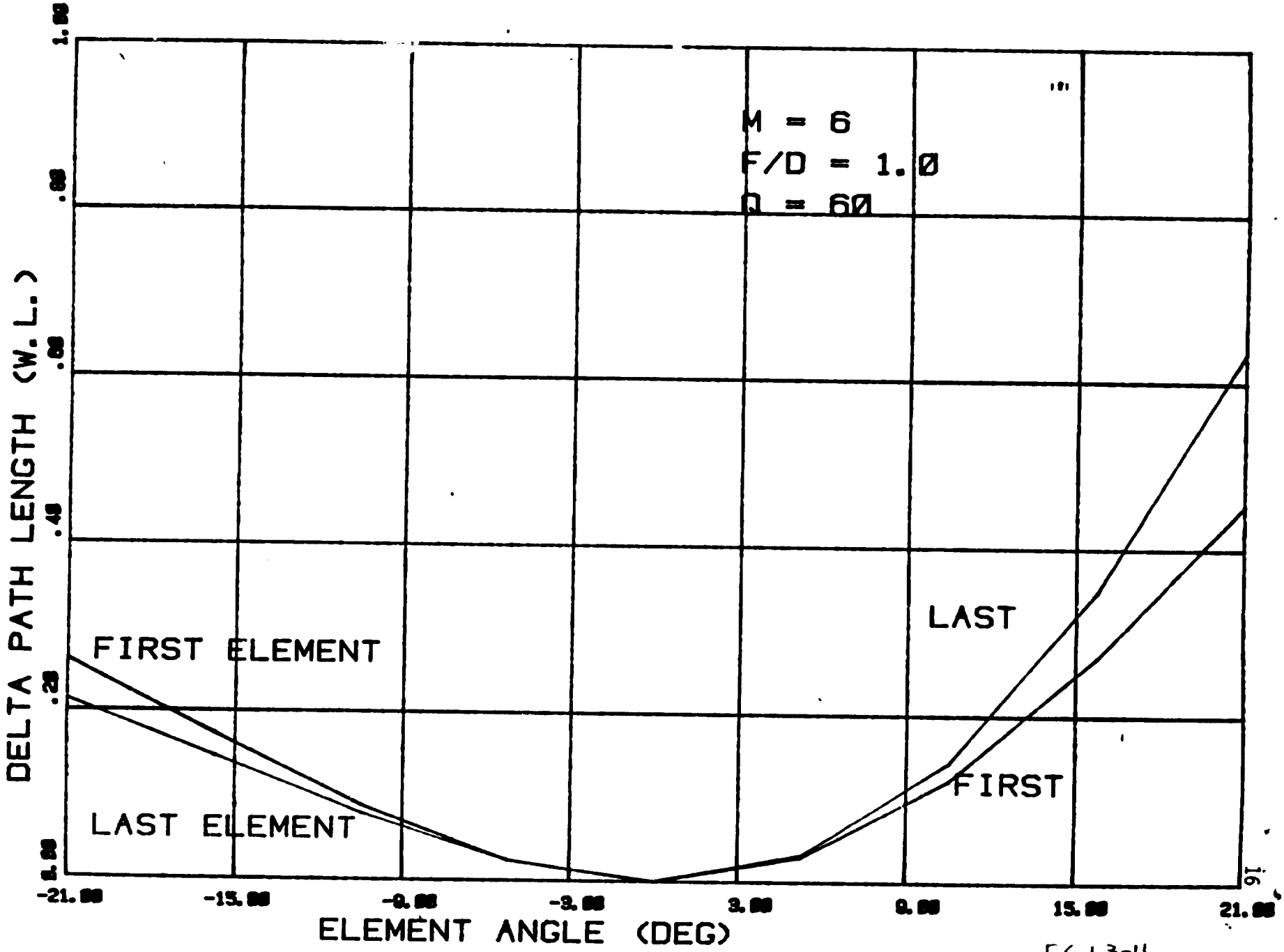
M = 6
F/D = 1.0
Θ = 60
FIRST ELEMENT
LAST ELEMENT
LAST
FIRST
DELTA PATH LENGTH (W.L.)
ELEMENT ANGLE (DEG)
-21.
-15.
-9.
-3.
3.
9.
15.
21.

FIG. 1.3-11

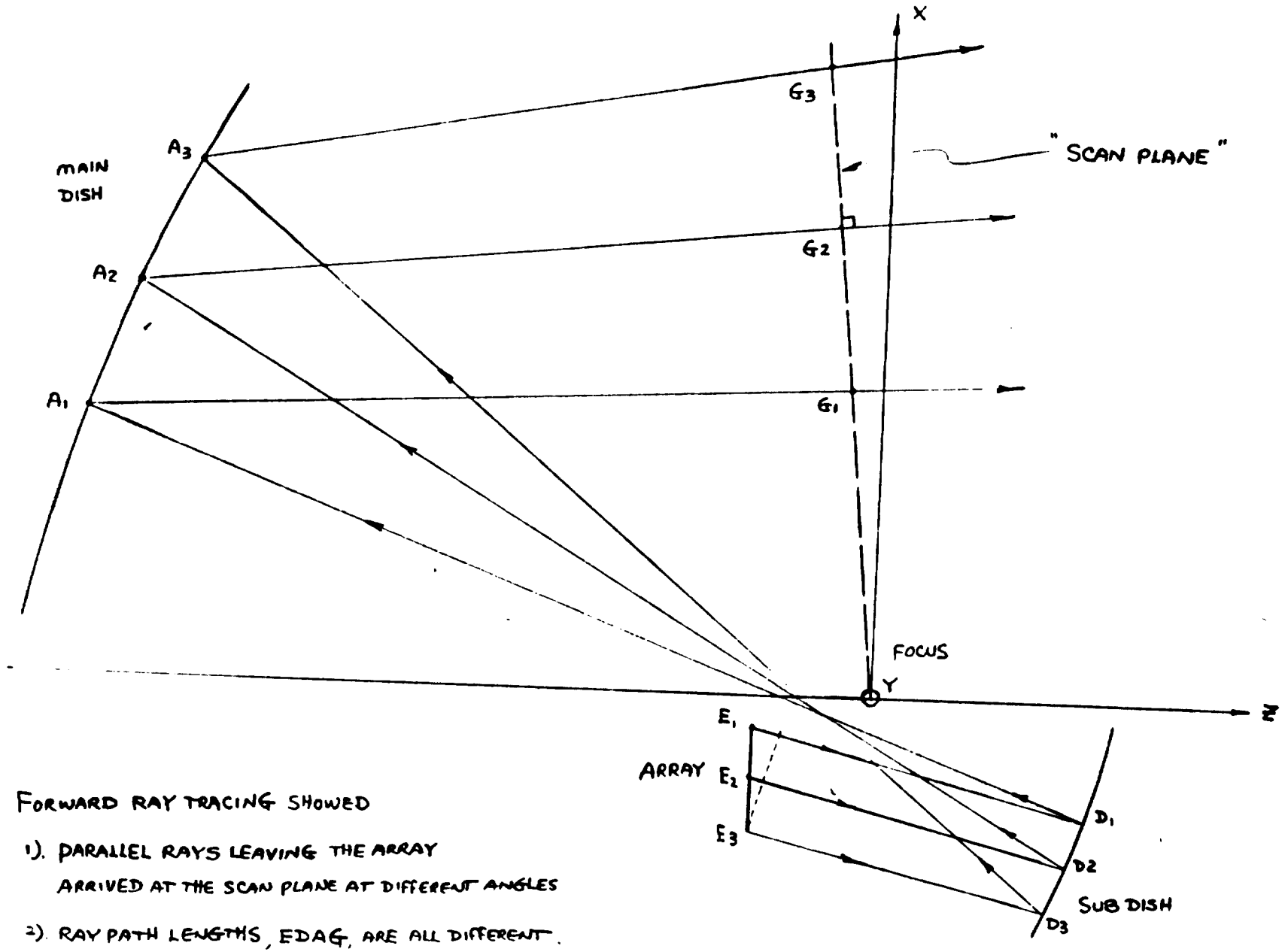

FORWARD RAY TRACING SHOWED

1). PARALLEL RAYS LEAVING THE ARRAY ARRIVED AT THE SCAN PLANE AT DIFFERENT ANGLES

2). RAY PATH LENGTHS, EDAG, ARE ALL DIFFERENT.

FIGURE 1.3-12

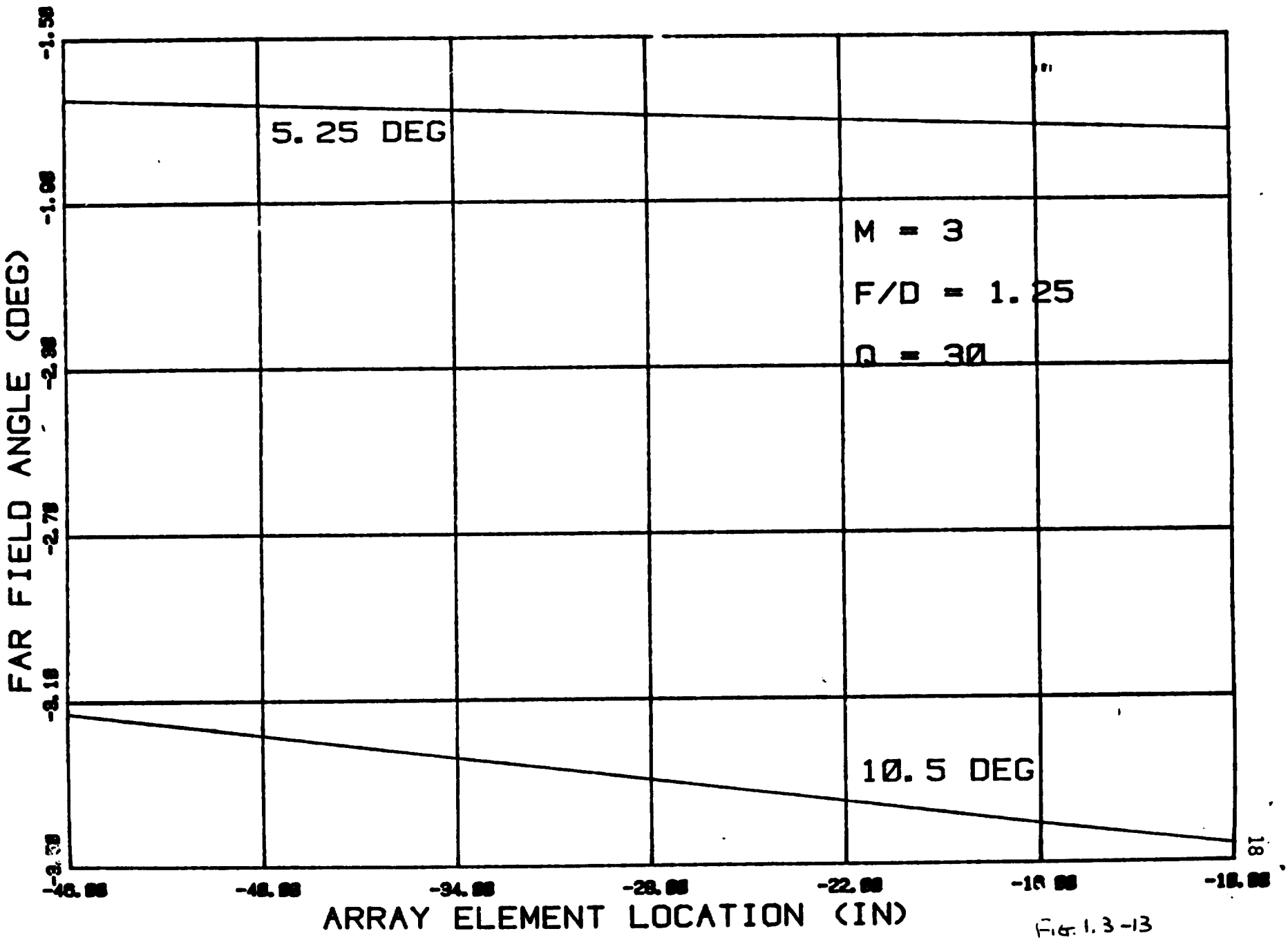
5.25 DEG
M = 3
F/D = 1.25
Q = 30
10.5 DEG
FAR FIELD ANGLE (DEG)
ARRAY ELEMENT LOCATION (IN)

Fig. 1.3-13

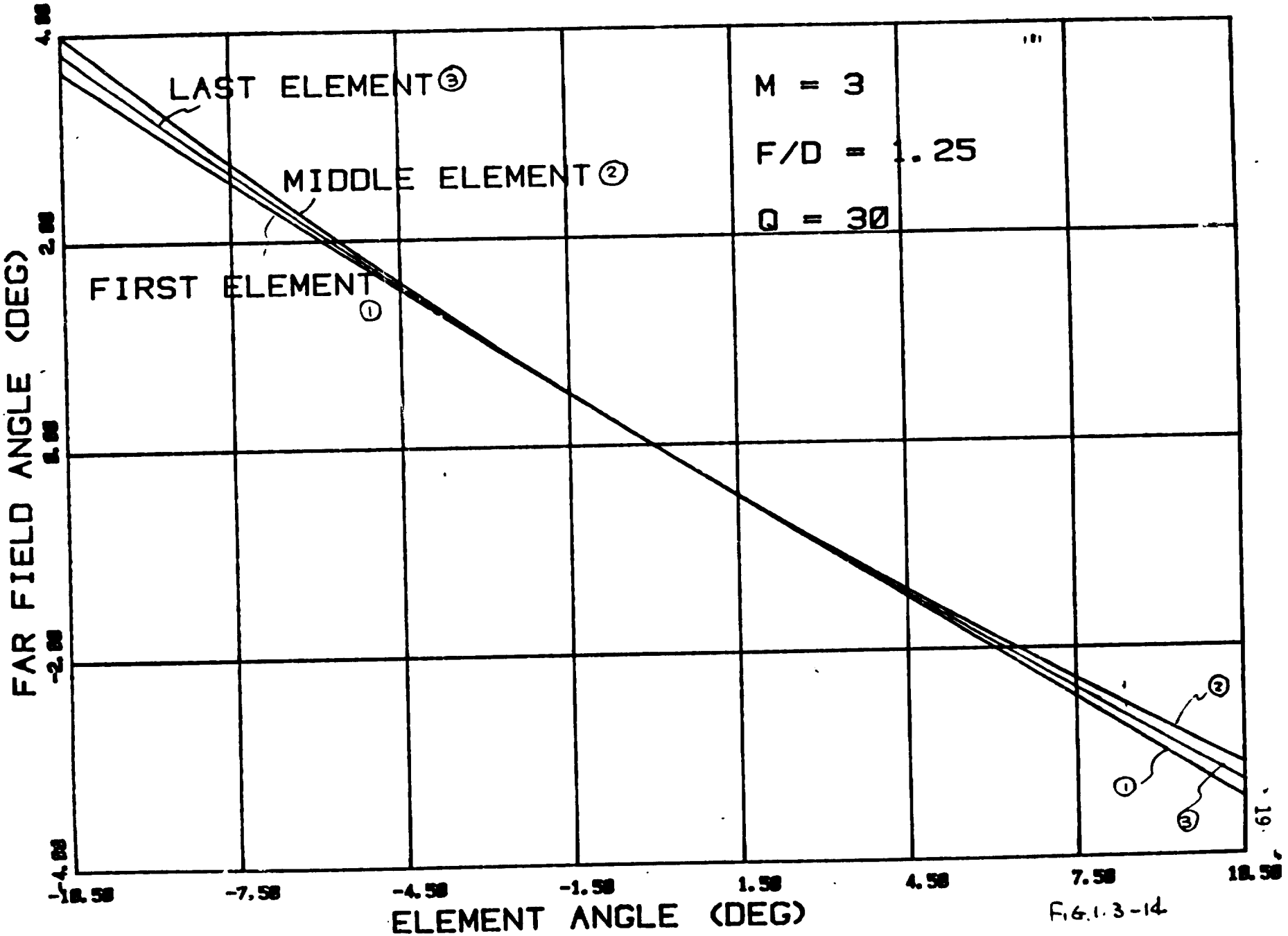
LAST ELEMENT ③
MIDDLE ELEMENT ②
FIRST ELEMENT ①
M = 3
F/D = 1.25
Q = 30
FAR FIELD ANGLE (DEG)
ELEMENT ANGLE (DEG)
-10.5B
-7.5B
-4.5B
-1.5B
1.5B
4.5B
7.5B
10.5B

Fig. 1.3-14

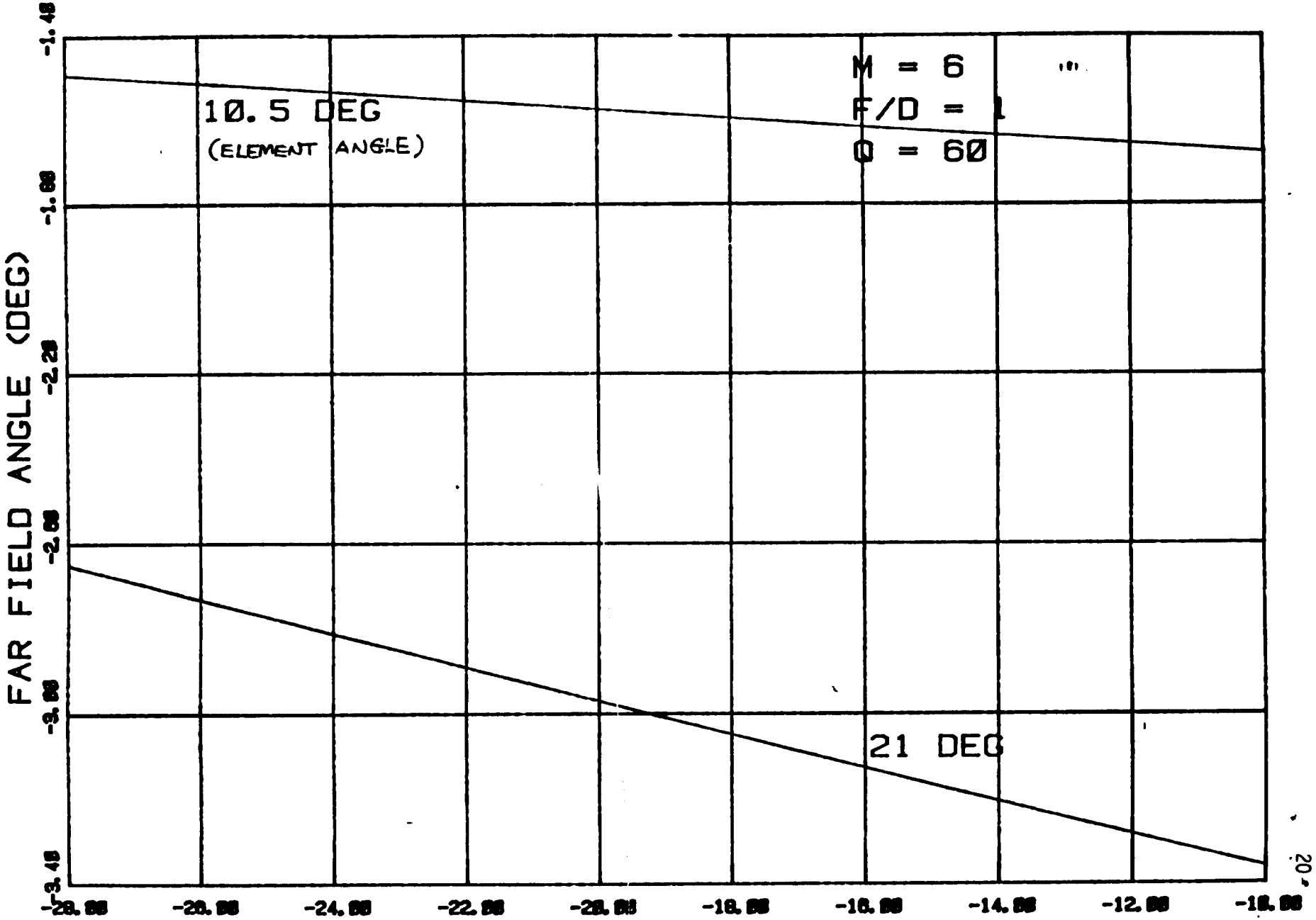
M = 6
F/D = 1
Θ = 60
10.5 DEG
(ELEMENT ANGLE)
21 DEG
FAR FIELD ANGLE (DEG)
-1.40
-1.80
-2.20
-2.60
-3.00
-3.40
-26.00
-20.00
-24.00
-22.00
-20.00
-18.00
-16.00
-14.00
-12.00
-10.00
ARRAY ELEMENT LOCATION (IN)

FIG. 1.3-15

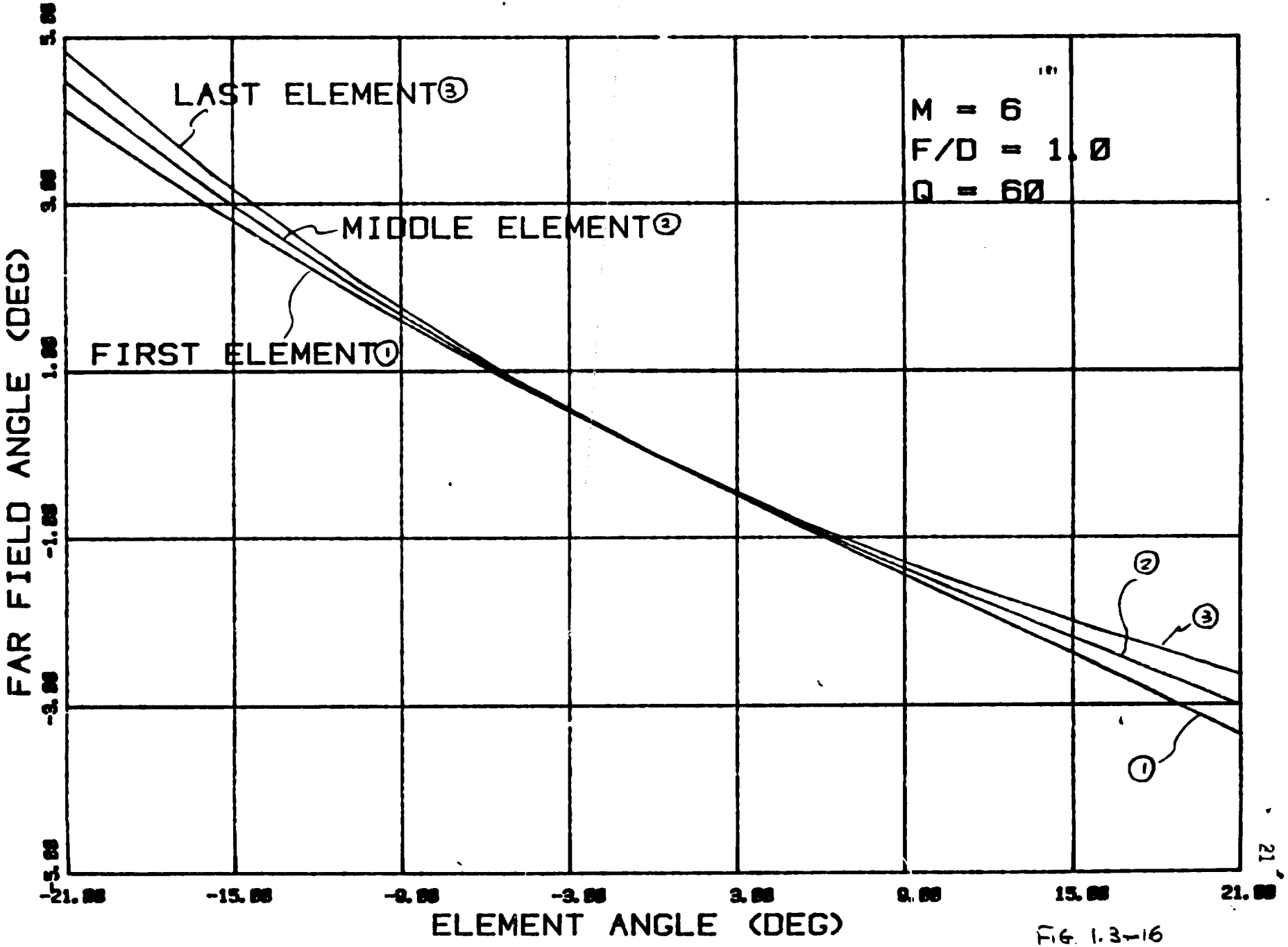
LAST ELEMENT③
MIDDLE ELEMENT②
FIRST ELEMENT①
M = 6
F/D = 1.0
Θ = 60
FAR FIELD ANGLE (DEG)
ELEMENT ANGLE (DEG)
-21.00
-15.00
-9.00
-3.00
3.00
9.00
15.00
21.00
3.00
1.00
-1.00
-3.00
-5.00
①
②
③

Fig. 1.3-16

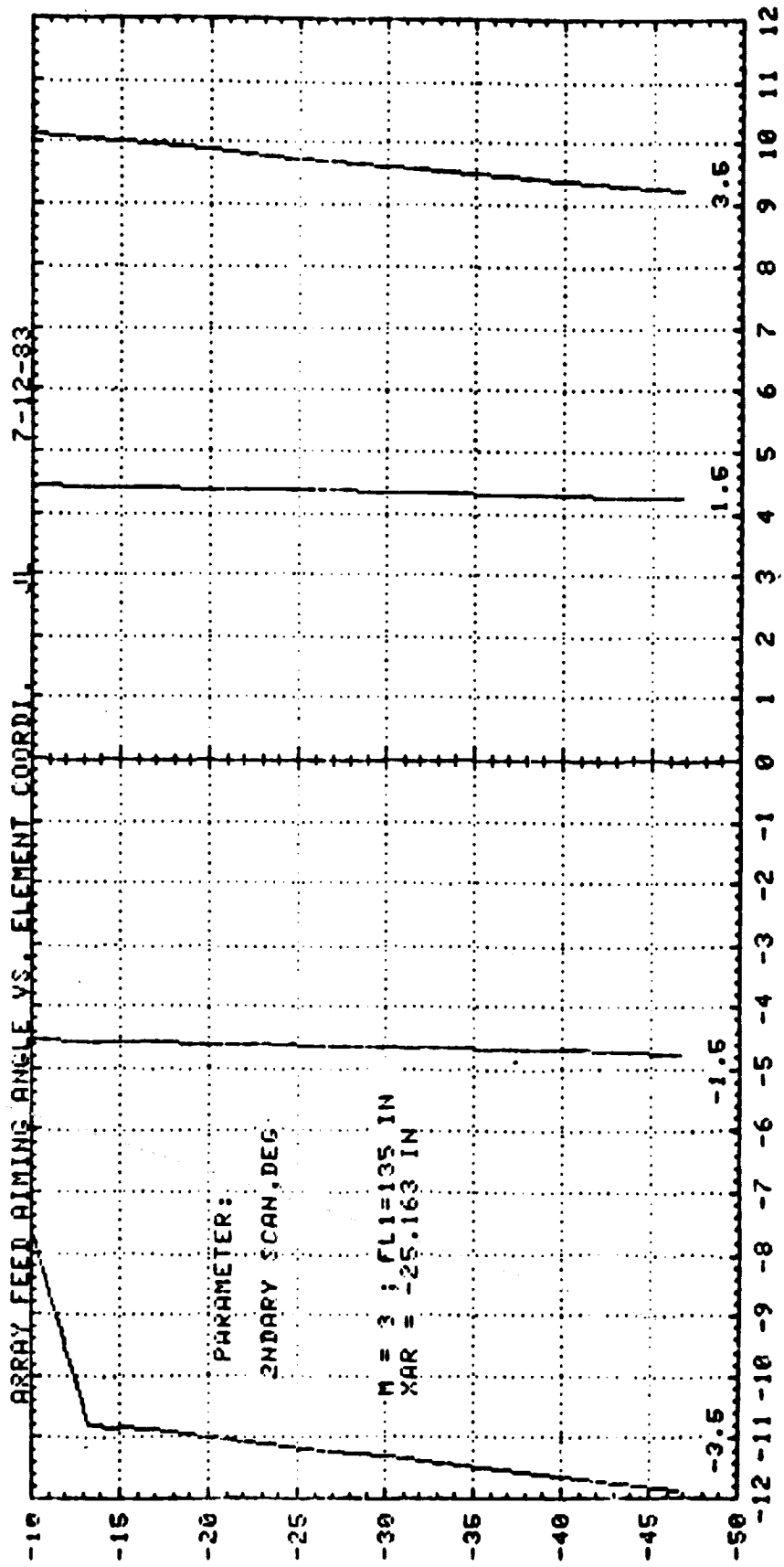

FIG. 1.3-17 RAY ANGLE AT ARRAY ELEMENT, SCAN ANGLE AS PARAMETER

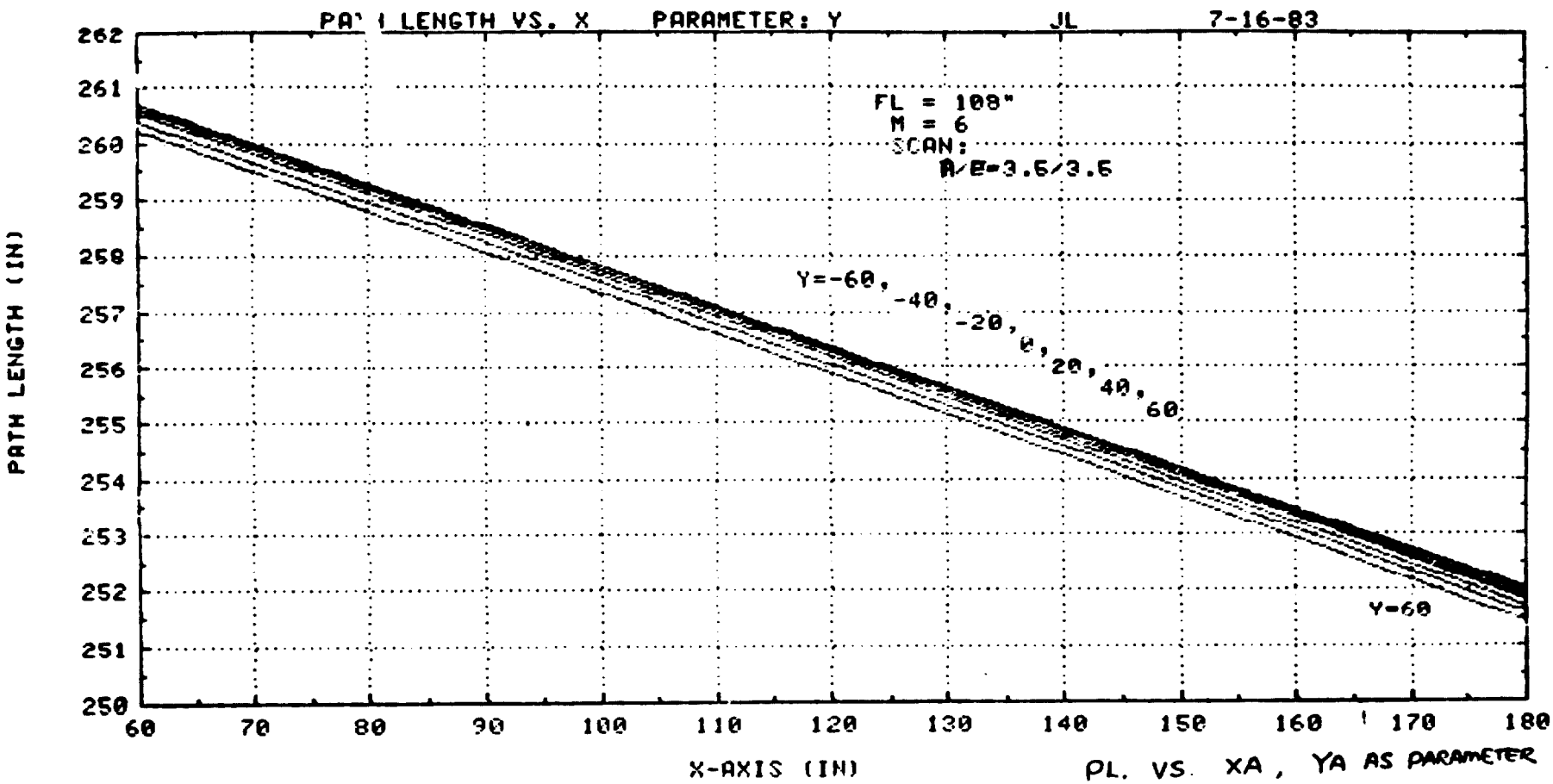
PA' I LENGTH VS. X PARAMETER: Y JL 7-16-83
FL = 108"
M = 6
SCAN:
A/E=3.6/3.6
Y=-60, -40, -20, 0, 20, 40, 60
Y=60
PATH LENGTH (IN)
262
261
260
259
258
257
256
255
254
253
252
251
250
60
70
80
90
100
110
120
130
140
150
160
170
180
X-AXIS (IN)
PL. VS. XA, YA AS PARAMETER

FIG 1.3-18

physical optics aproach. Since the nearfield physical optics method is an accepted approach, good correlation between the two techniques would justify the method. Several cases were analyzed in verifying the spherical mode approach for the Gregorian system under consideration. These cases are summarized in Table 1.3-1. The first involved computing the current induced on the main reflector for a single feed element using the two techniques described above. The results of this comparision are shown in figures 1.3-19 - 1.3-24. As can be seen, there is a good correlation between the two approaches. The second comparision involved the investigation of a seven element hex array. In this case, the secondary pattern of the array was treated as a single feed element. The results of the comparision using spherical mode techniques (SMT) and near field pysical optics (NFPO) are presented in figures 1.3-25 - 1.3-30. Again excellent correlation between the two approaches is evident. The final benchmark of the SMT approach involved the analysis of a 397 element (12 ring) hex array. The results of this analysis are given in figures 1.3-31 - 1.3-36. A comparision of SMT with the NFPO approach provided results which are considered to be well within acceptable limits. As a result of the SMT verification effort it was concluded that the SMT approach provides results which can accurately represent the secondary far field pattern of systems with aperture diameters in excess of 100 wavelengths. The upper limit of SMT capability on the size of aperture diameters is determined by the number of modes dimensioned in the program which is a function of the computer on which the SMT programs are implemented.

TABLE 1-3.1: Summary of Cases For SMT Verification

CASE NO.	ARRAY	OPTICAL SYSTEM D	F/D	M	Q	Z	PARAMETERS COMPARED		FIGURE #
1	Single Element 0.59" Diameter 1.5 @ 30 GHz TE_{11}, YP	108"	1	6	36"	0"	Induced Main Dish Current	SMT	1.3-19 - 1.3 21
								NFPO	1.3-22 - 1.3-24
2	7-Element Hex 0.59" Diameter 1.5 @ 30 GHz TE_{11}, YP	108"	1	6	36"	-9.711"	FF Patterns	SMT	1.3-25 - 1.3-27
								NFPO	1.3-28 - 1.3-30
3	12 Ring (397-Element) Hex 0.59" Diameter 1.5 @ 30 GHz TE_{11}, YP	108"	1	6	36"	-13.864	FF Patterns	SMT	1.3-21 - 1.3-33
								NFPO	1.3-34 - 1.3.36

D = Main Dish Diameter
M = System Magnification
Q = Main Dish Offset
Z = Array Plane Location

TRUE NF PO — CUT #1 MAGNITUDE

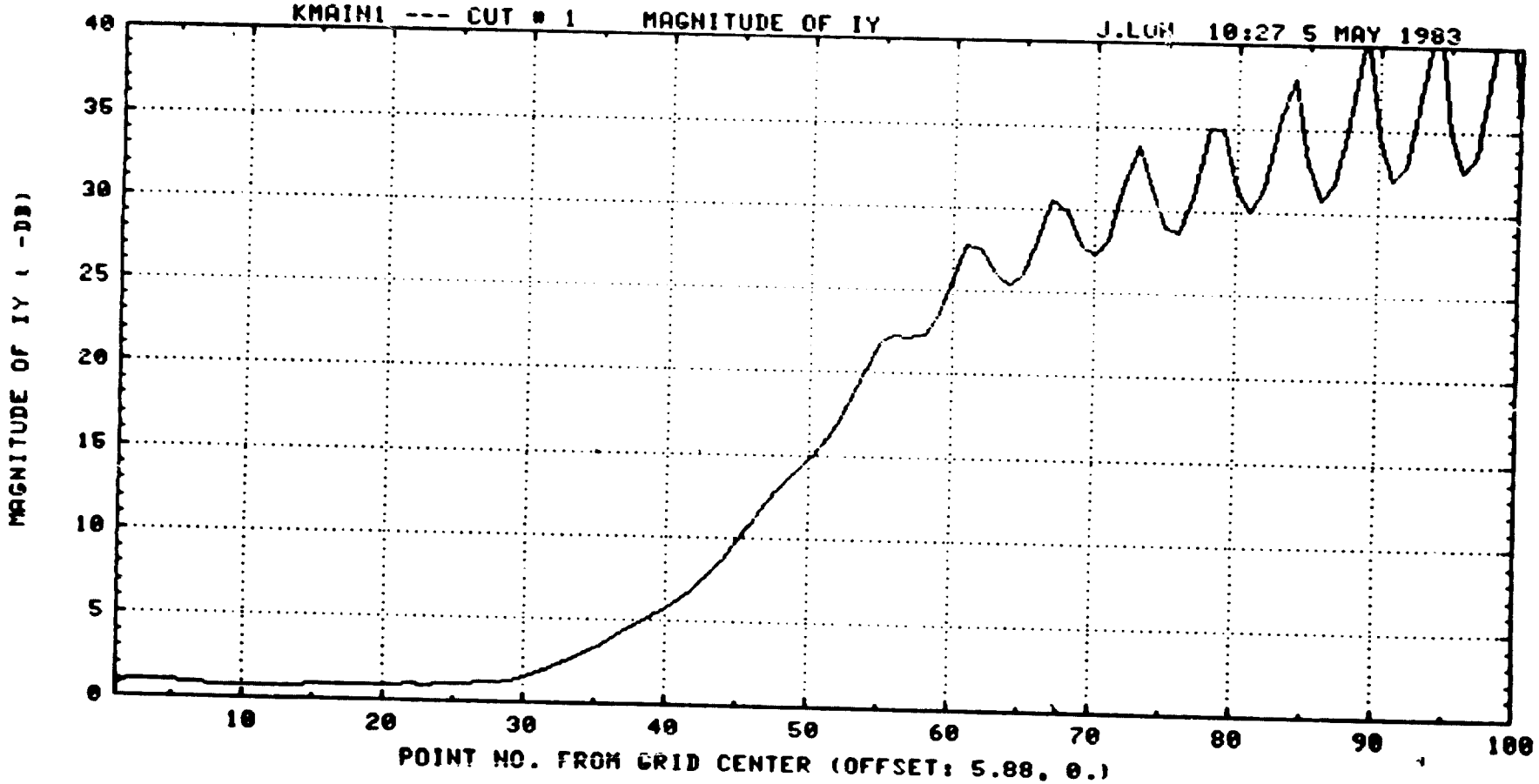

FIG. 1.3-19 SINGLE ELEMENT

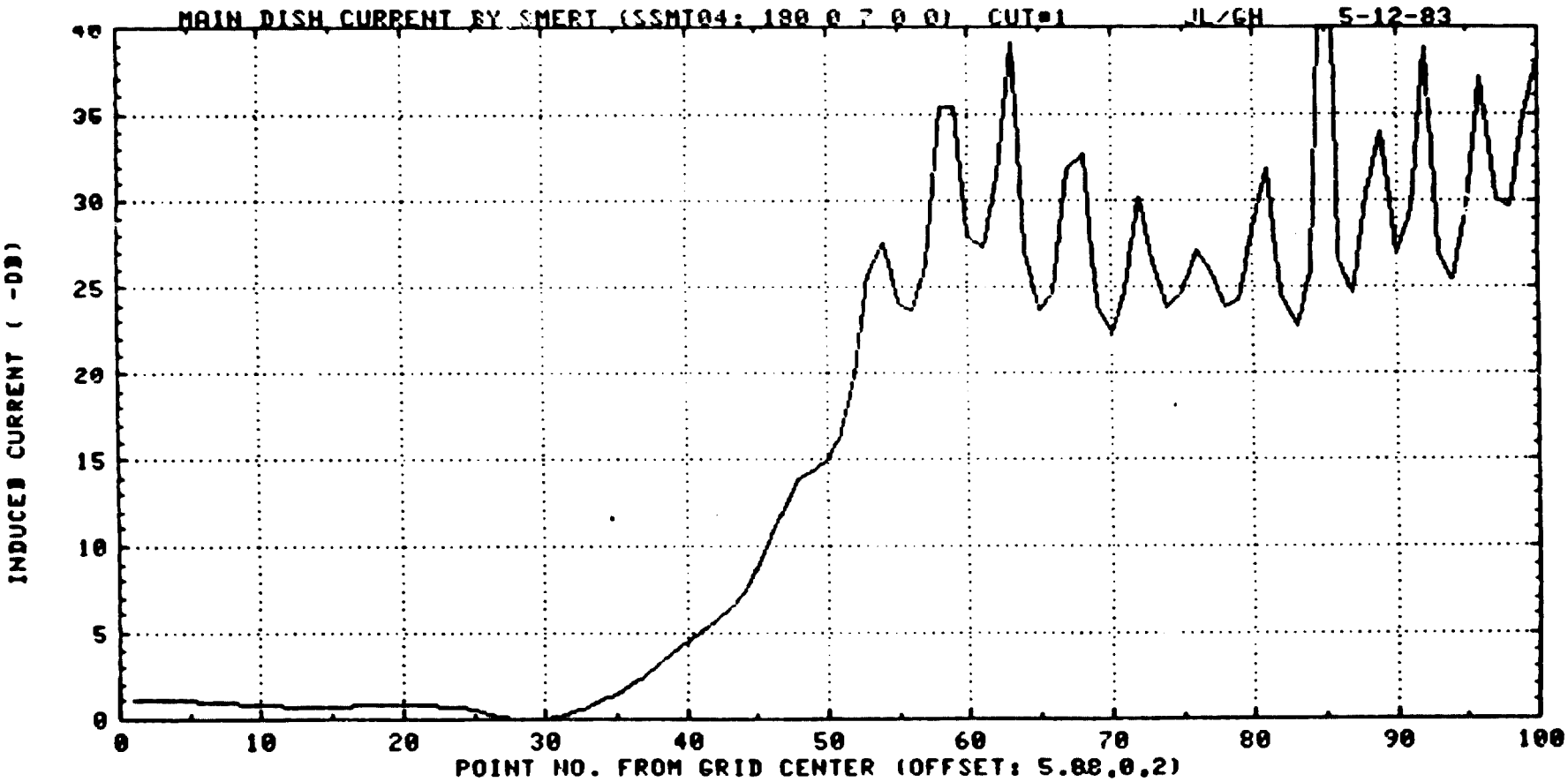

FIG. 1.3-20 SINGLE ELEMENT

TRUE NF PO — CUT #2 MAGNITUDE

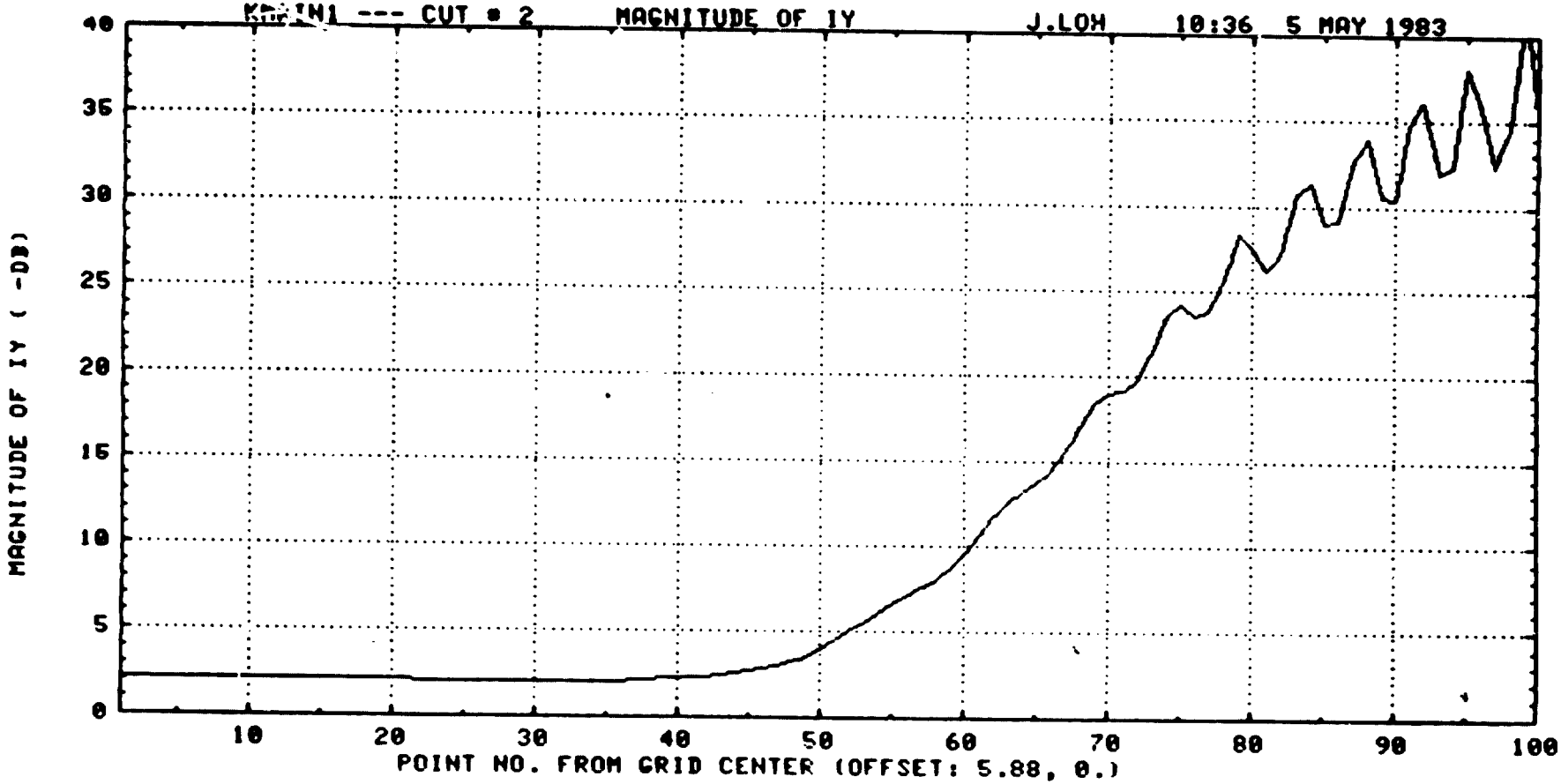

FIG 1.3-21 SINGLE ELEMENT

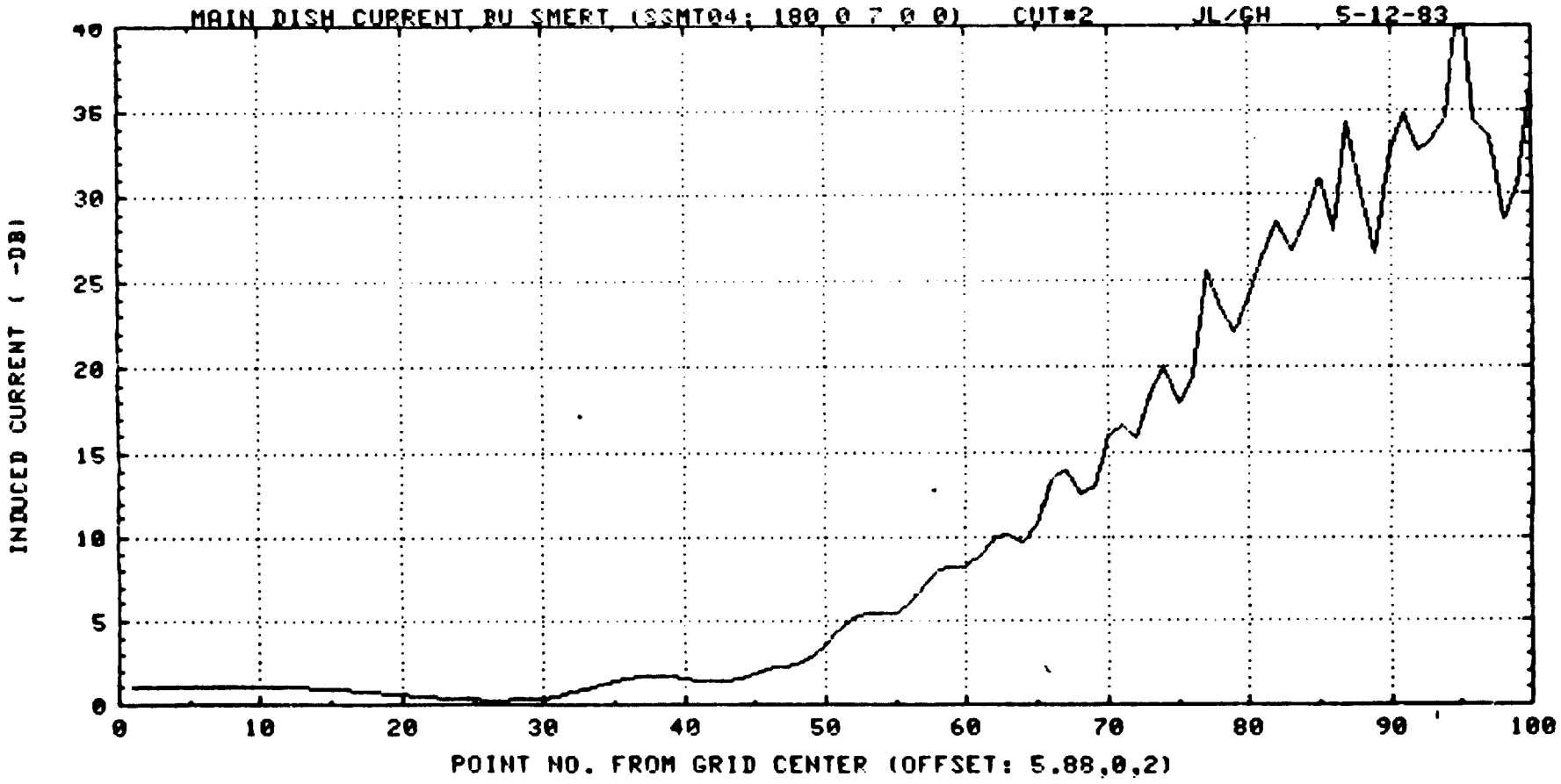

FIG 1.3-22 SINGLE ELEMENT

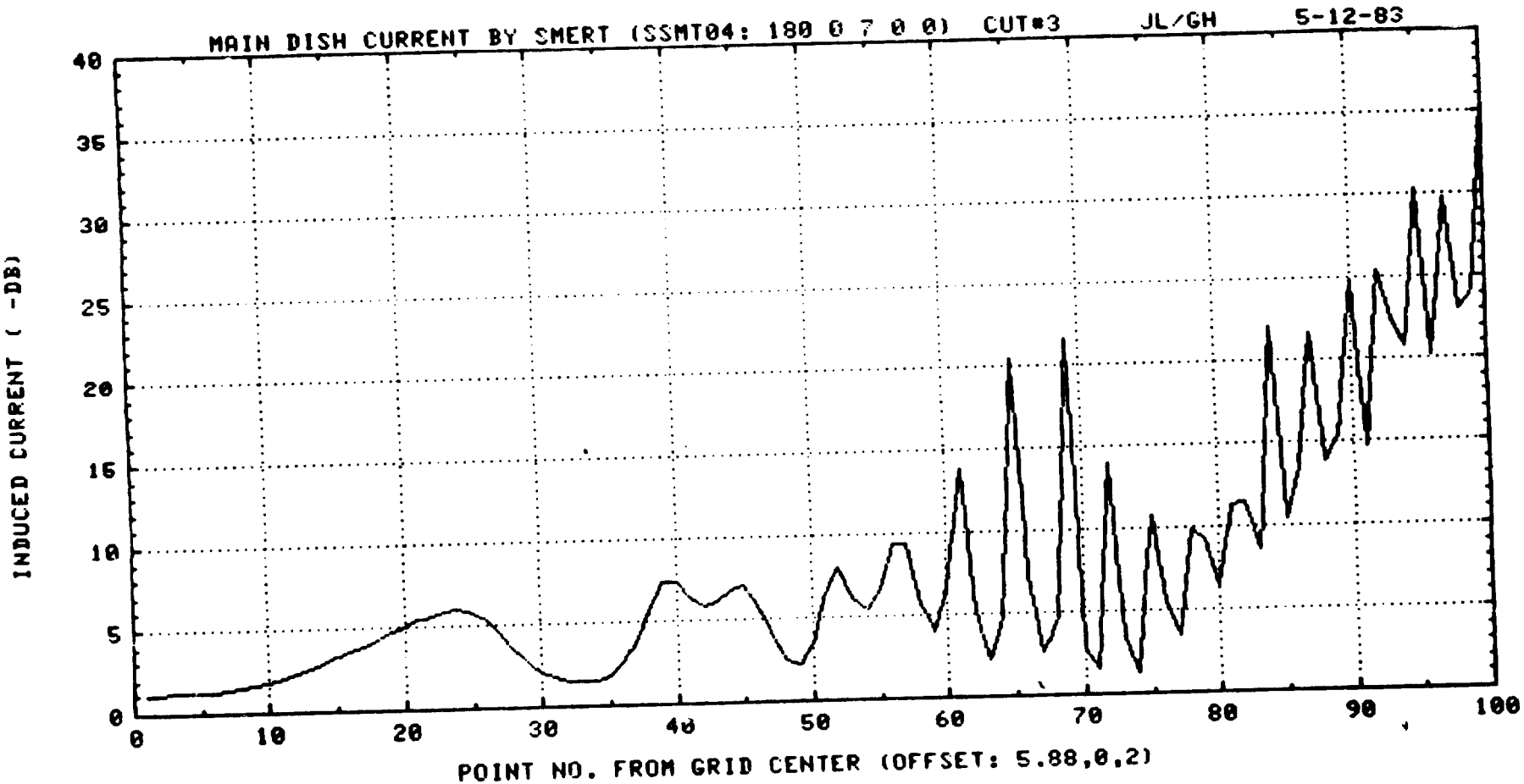

FIG. 1.3-23 SINGLE ELEMENT

TRUE NF PO – CUT #3 MAGNITUDE

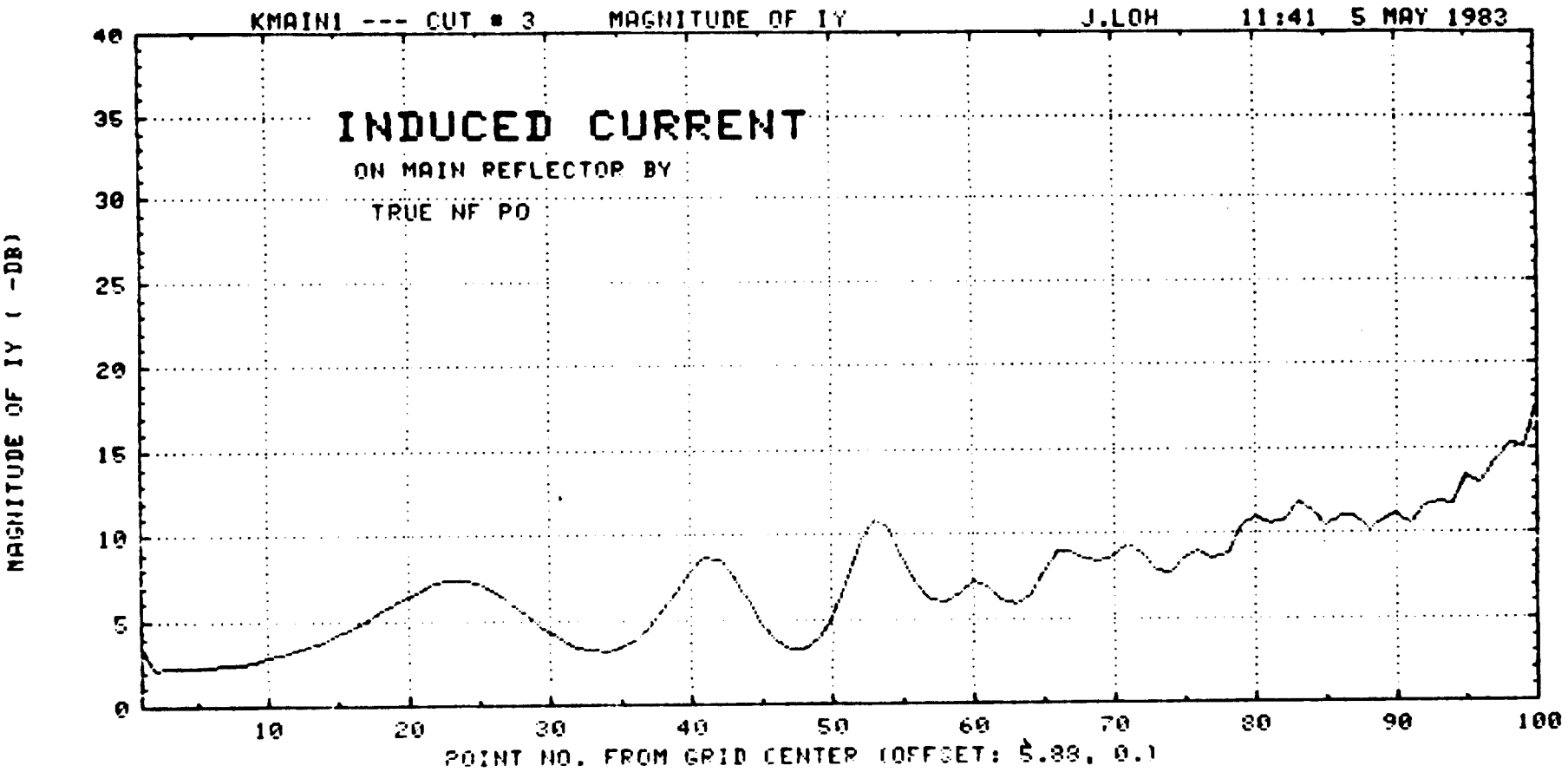

FIG 1.3-24 SINGLE ELEMENT

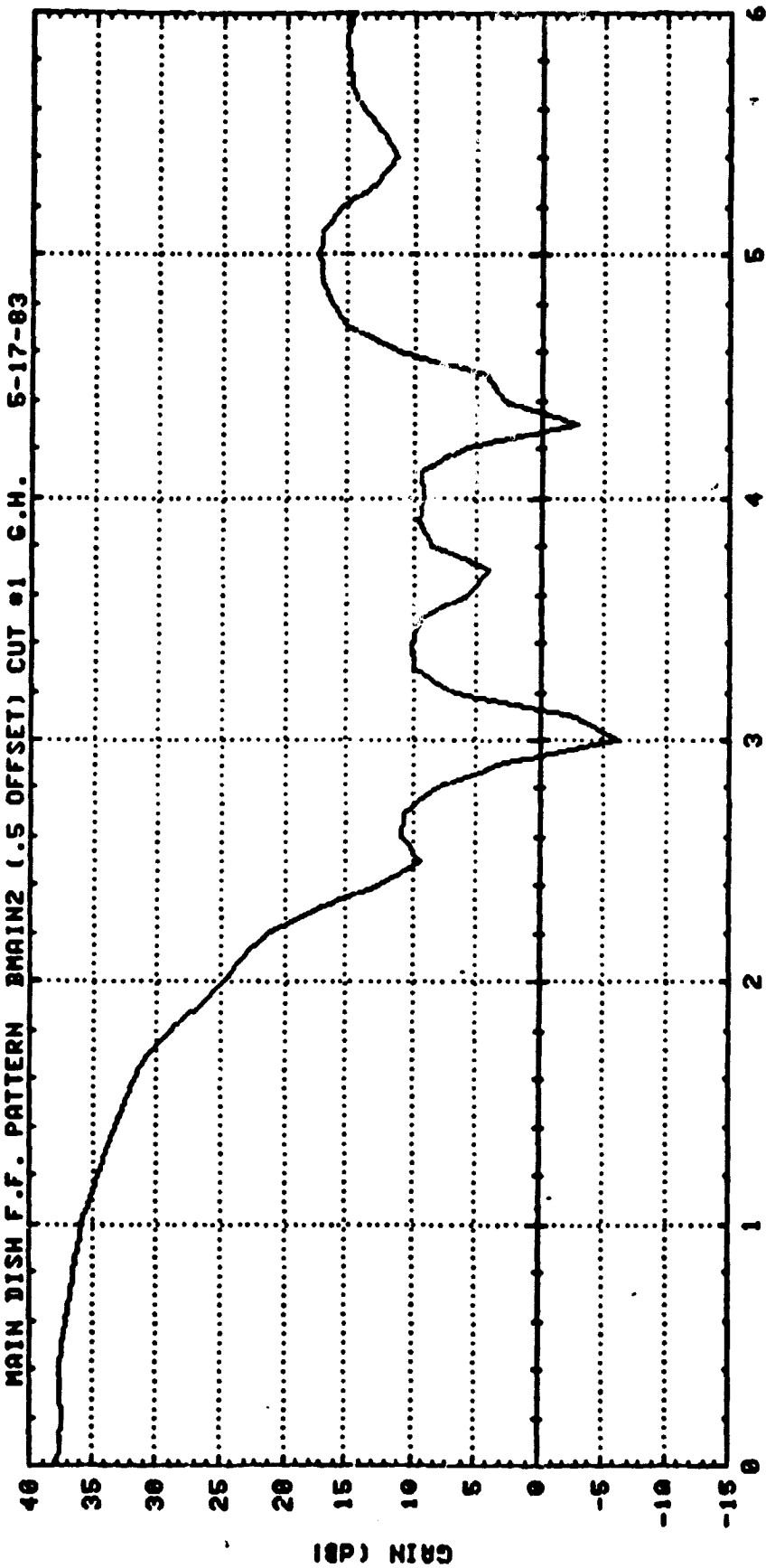

FIG. 1.3-25 7-ELEMENT ARRAY

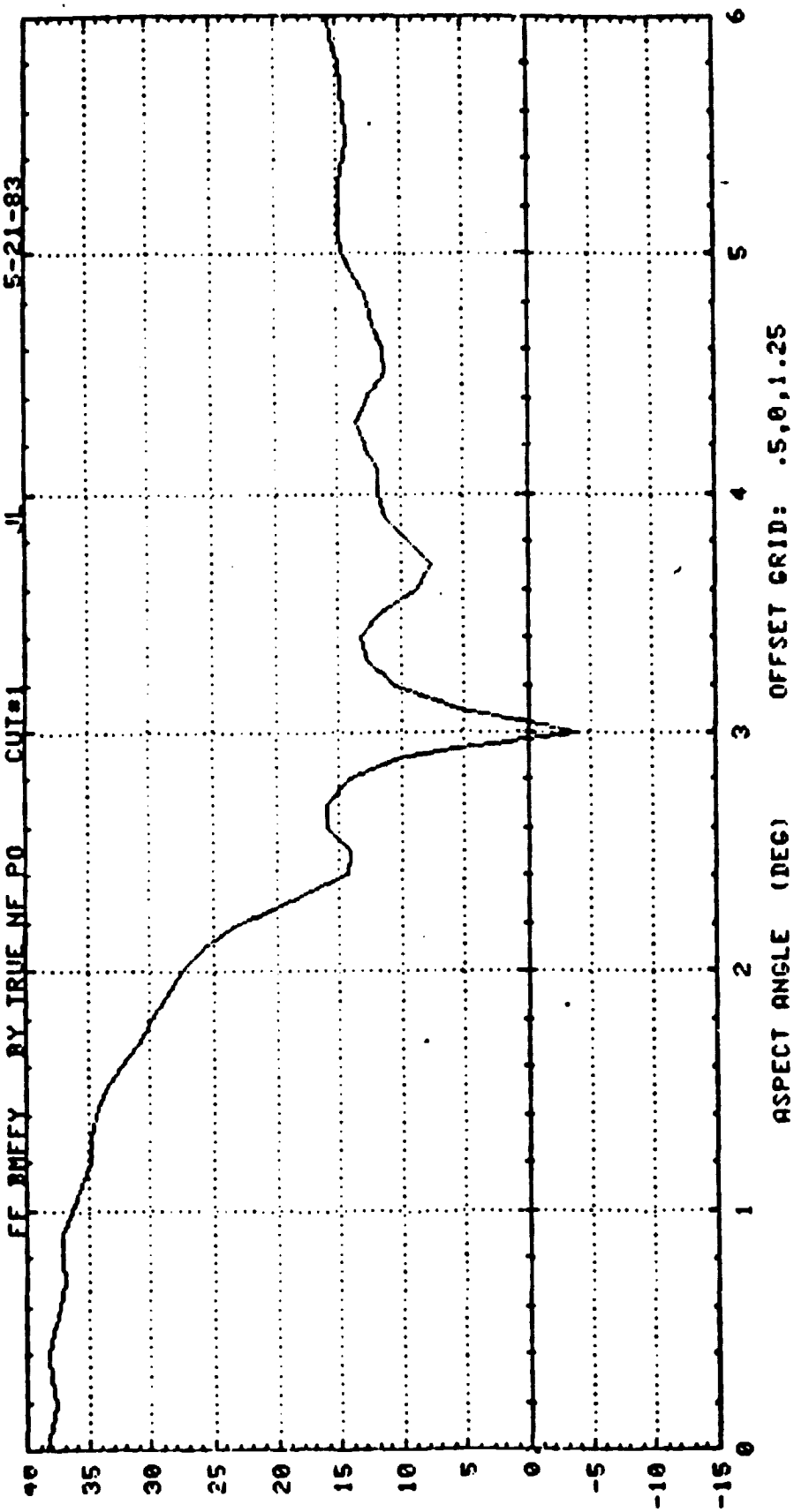

Fig. 1.3-26 7-Element Array

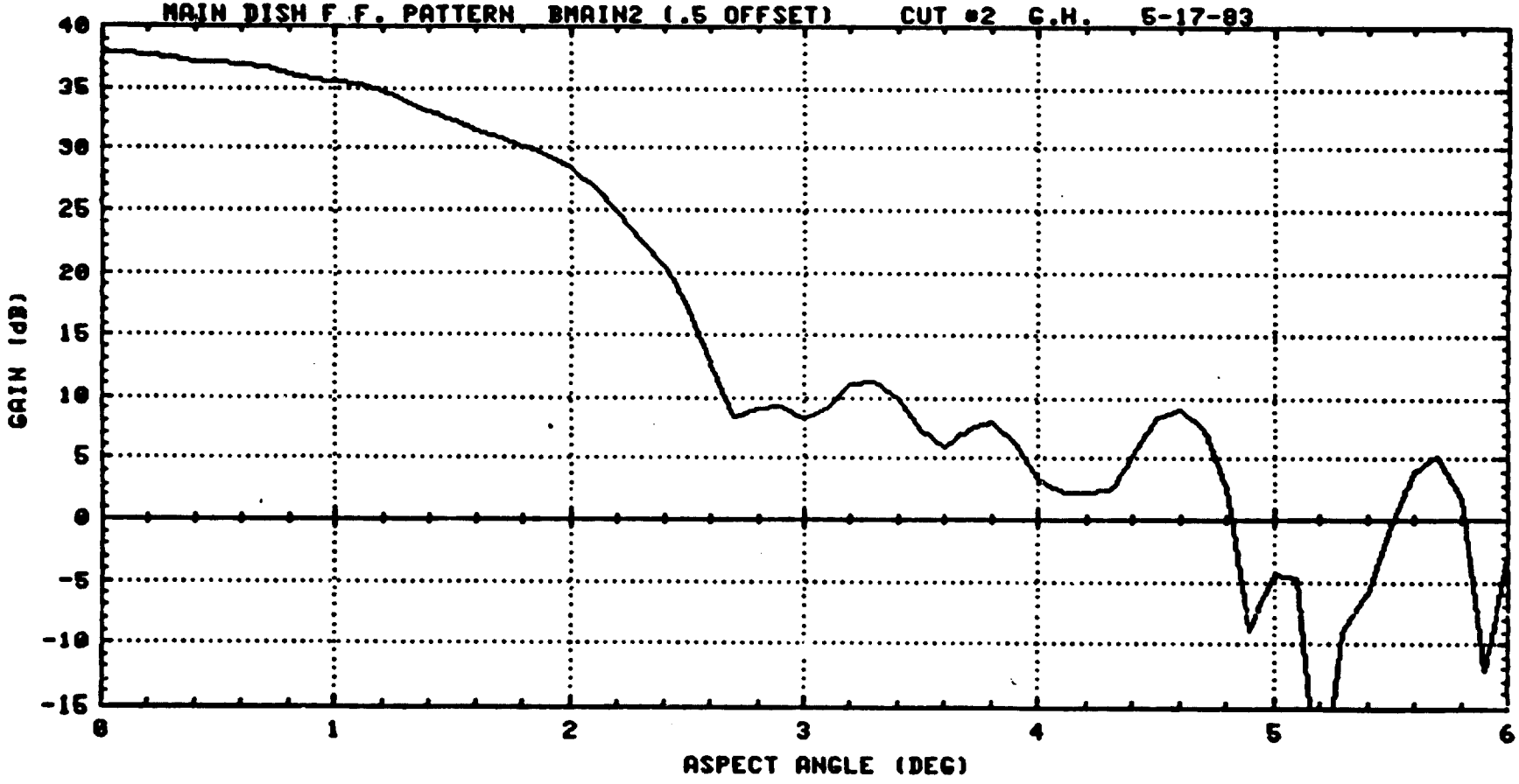

FIG. 1.3-27 7-ELEMENT ARRAY

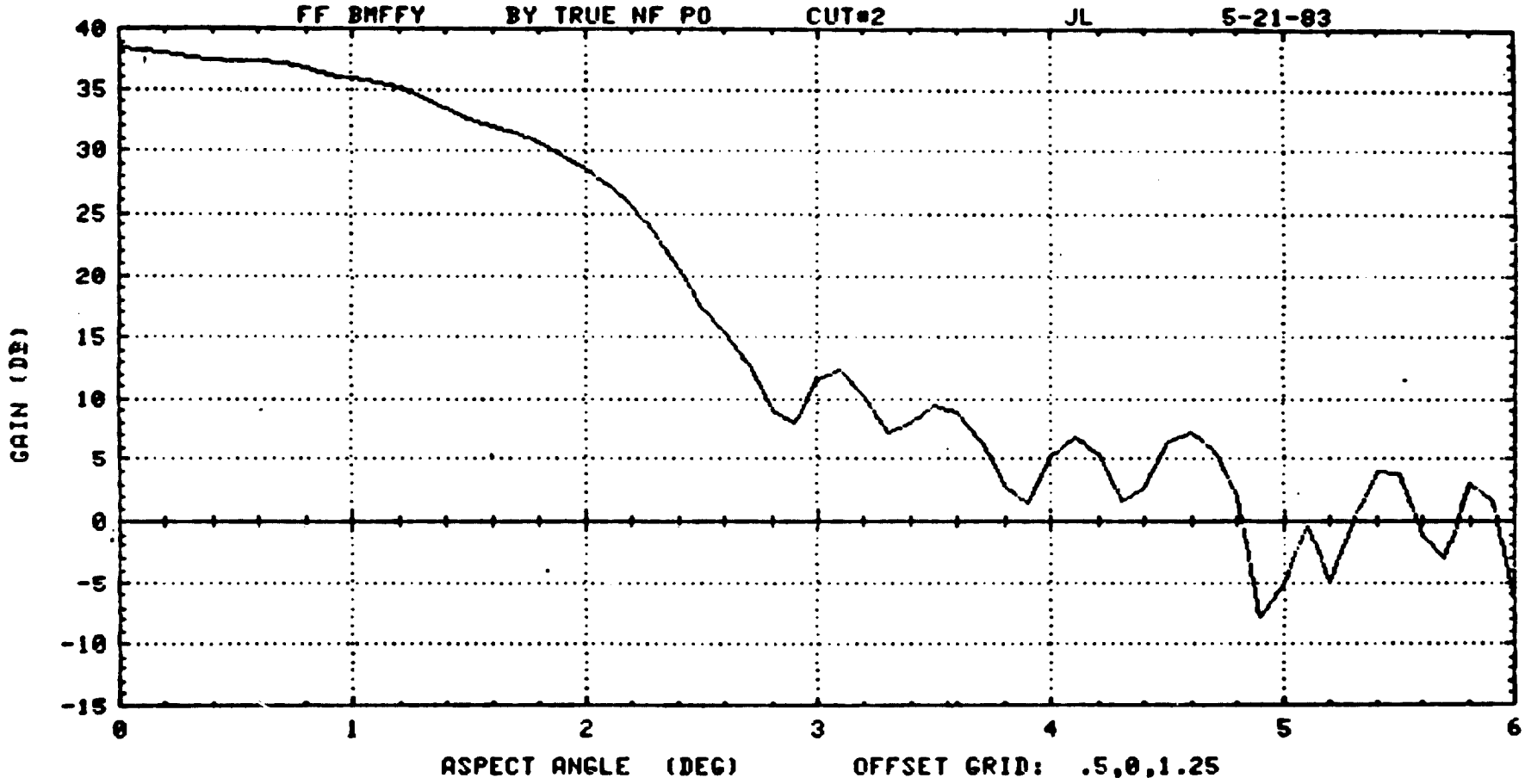

FIG. 1.3-28 7-ELEMENT ARRAY

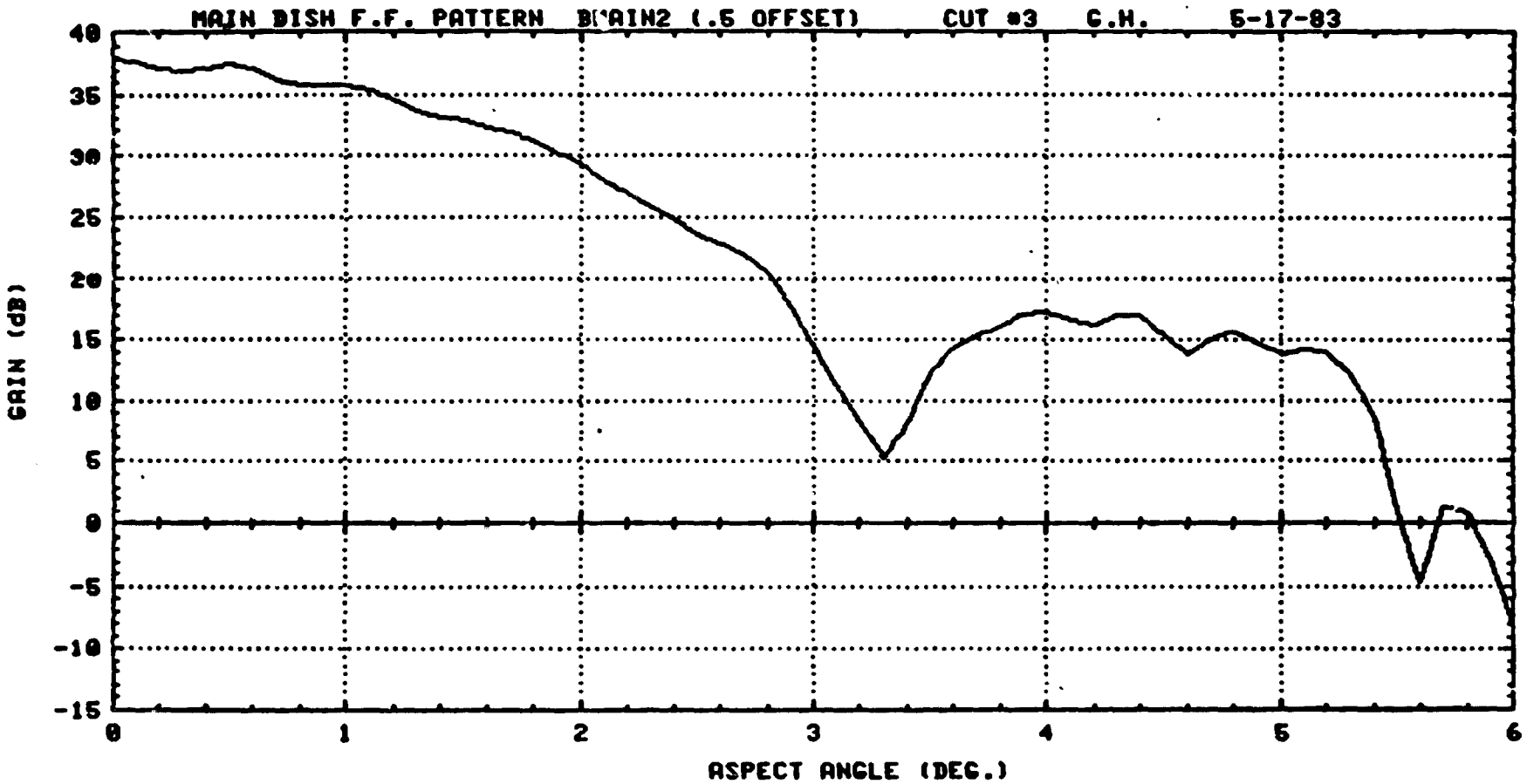

FIG. 1.3-29 7-ELEMENT ARRAY

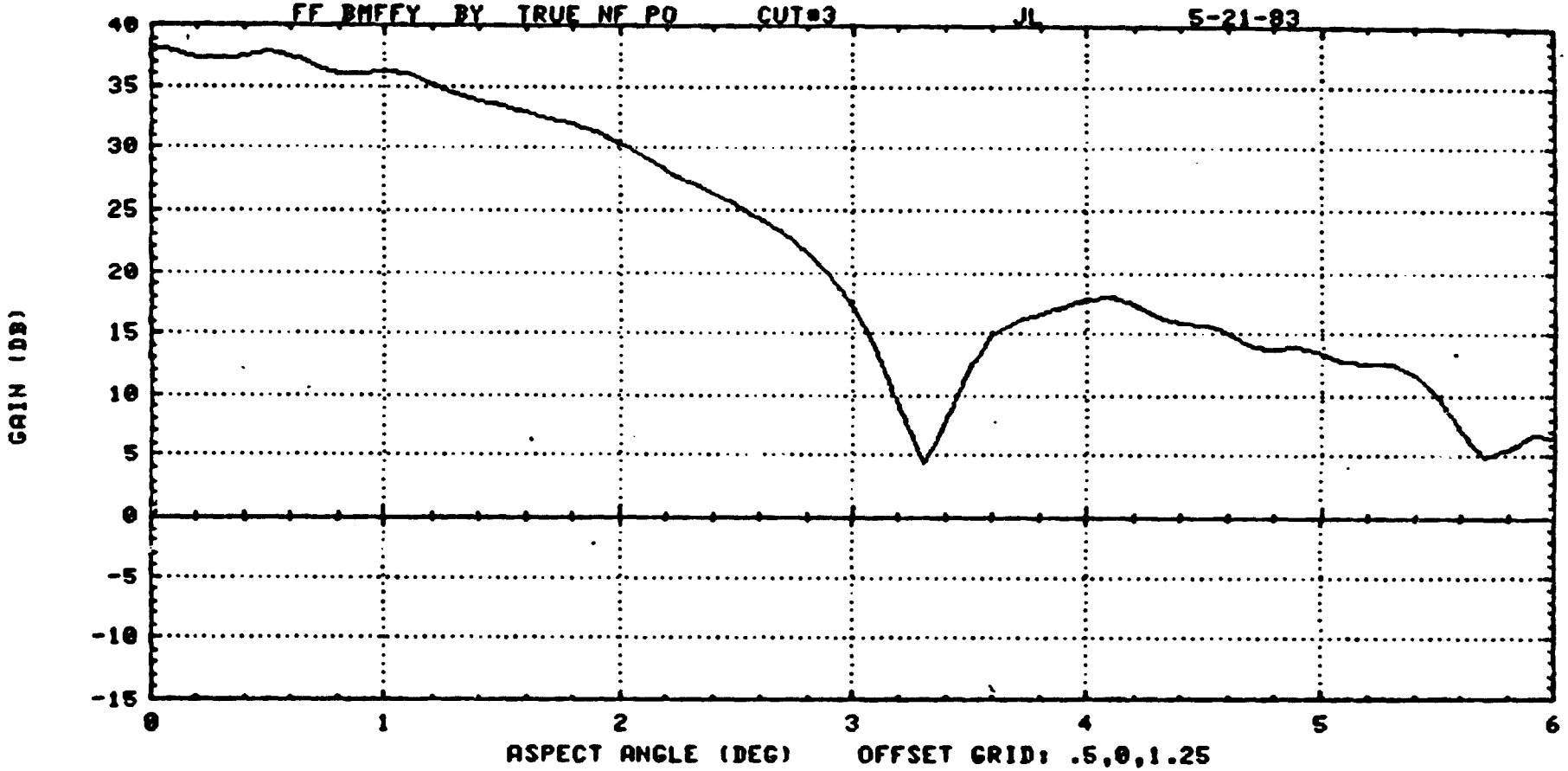

FIG. 1.3-30 7-ELEMENT ARRAY

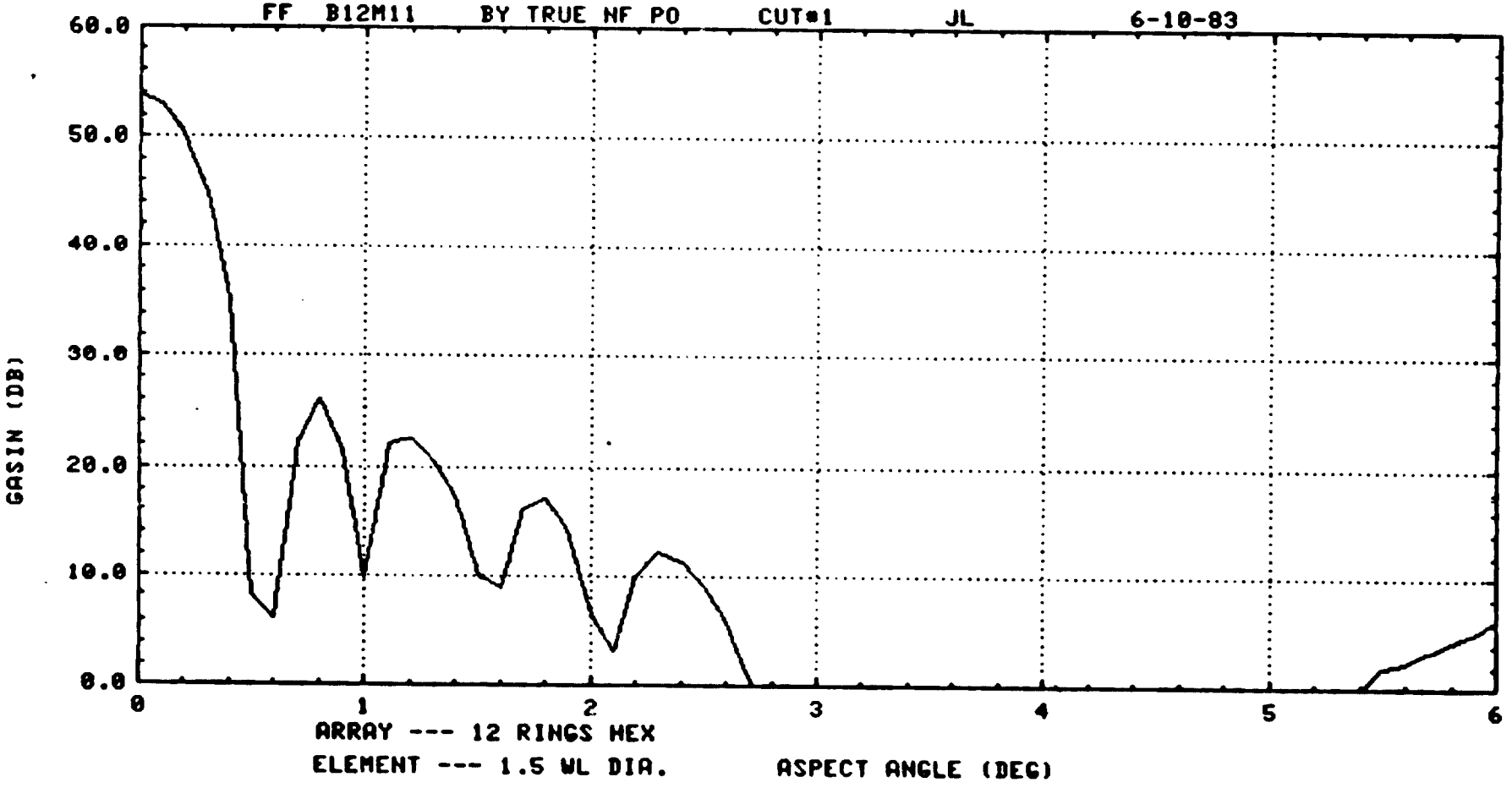

FIG 13-31 12-RING HEX ARRAY—SYSTEM FF

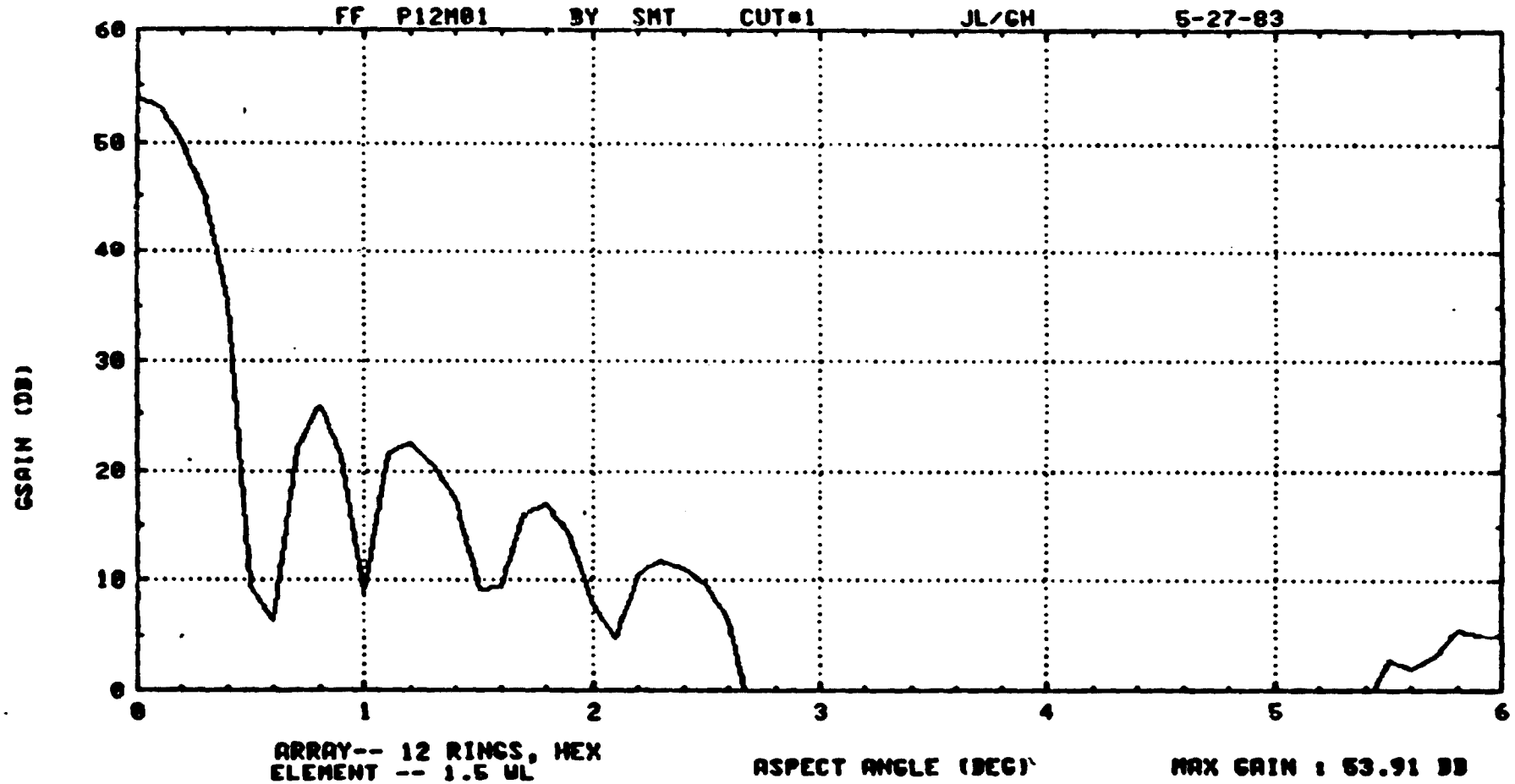

FIG. 1.3-32 12-RING HEX ARRAY — SYSTEM FF

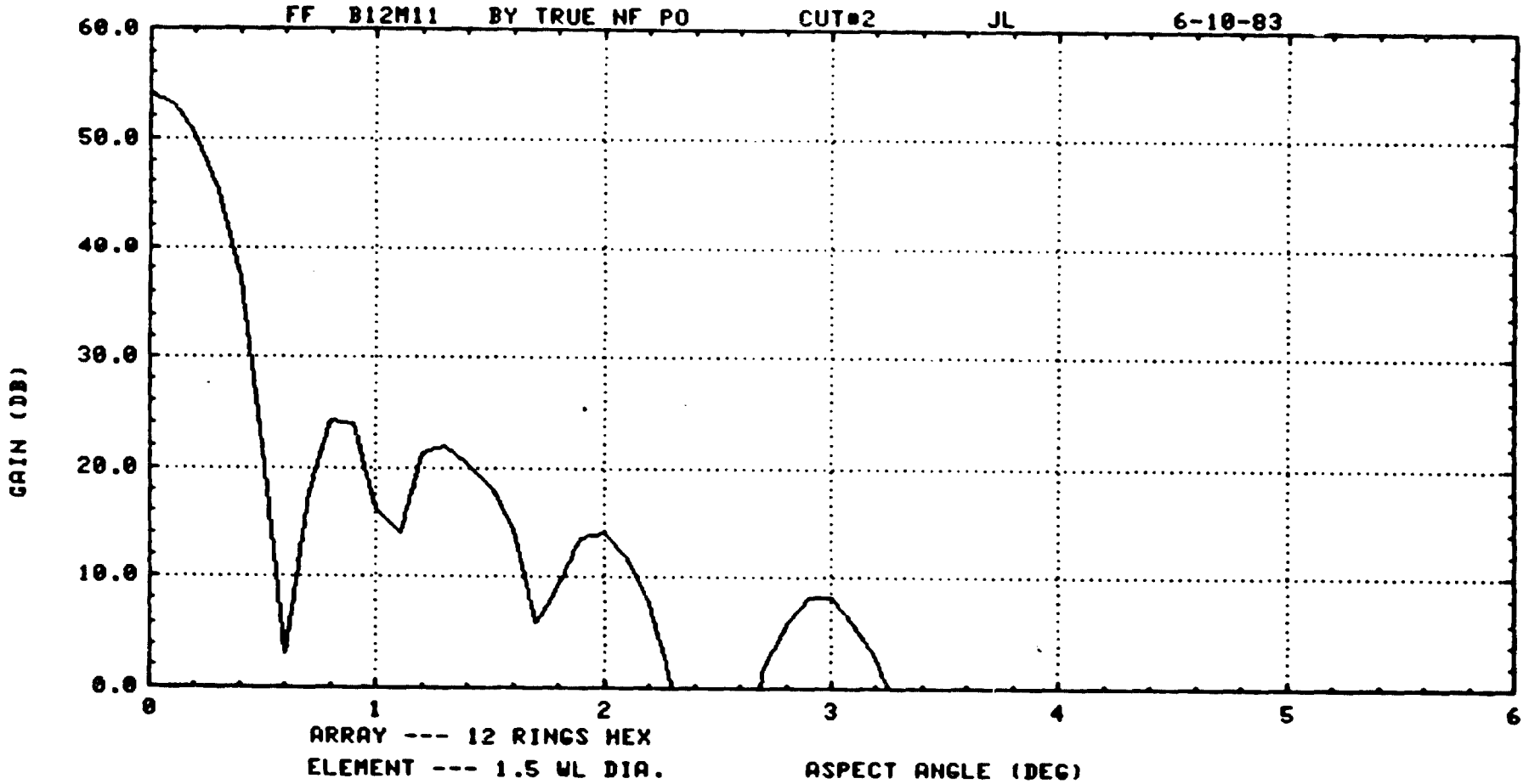

FIG 1.3-33 12-RING HEX ARRAY — SYSTEM FF

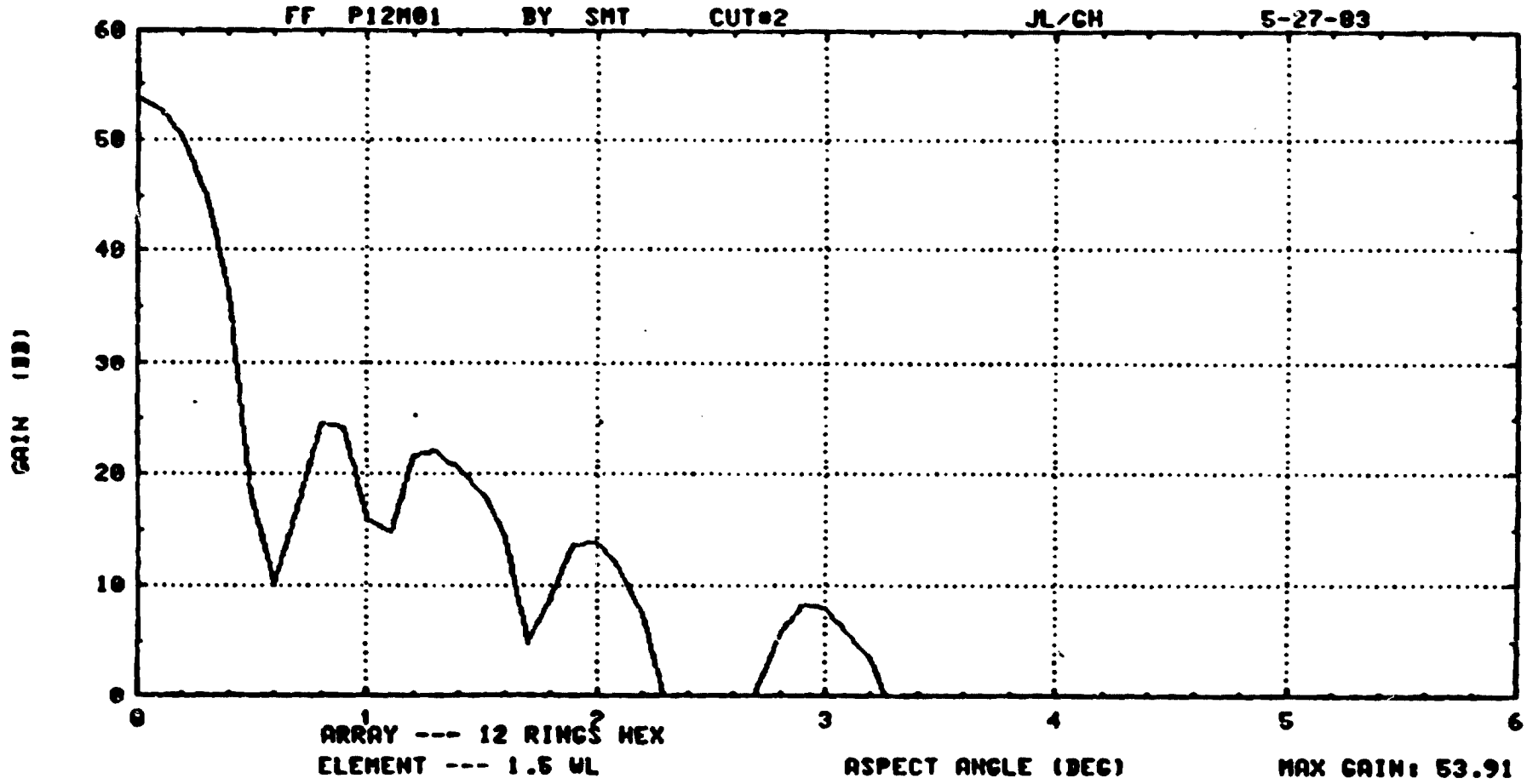

FIG 1.3-34 12-RING HEX ARRAY—SYSTEM FF

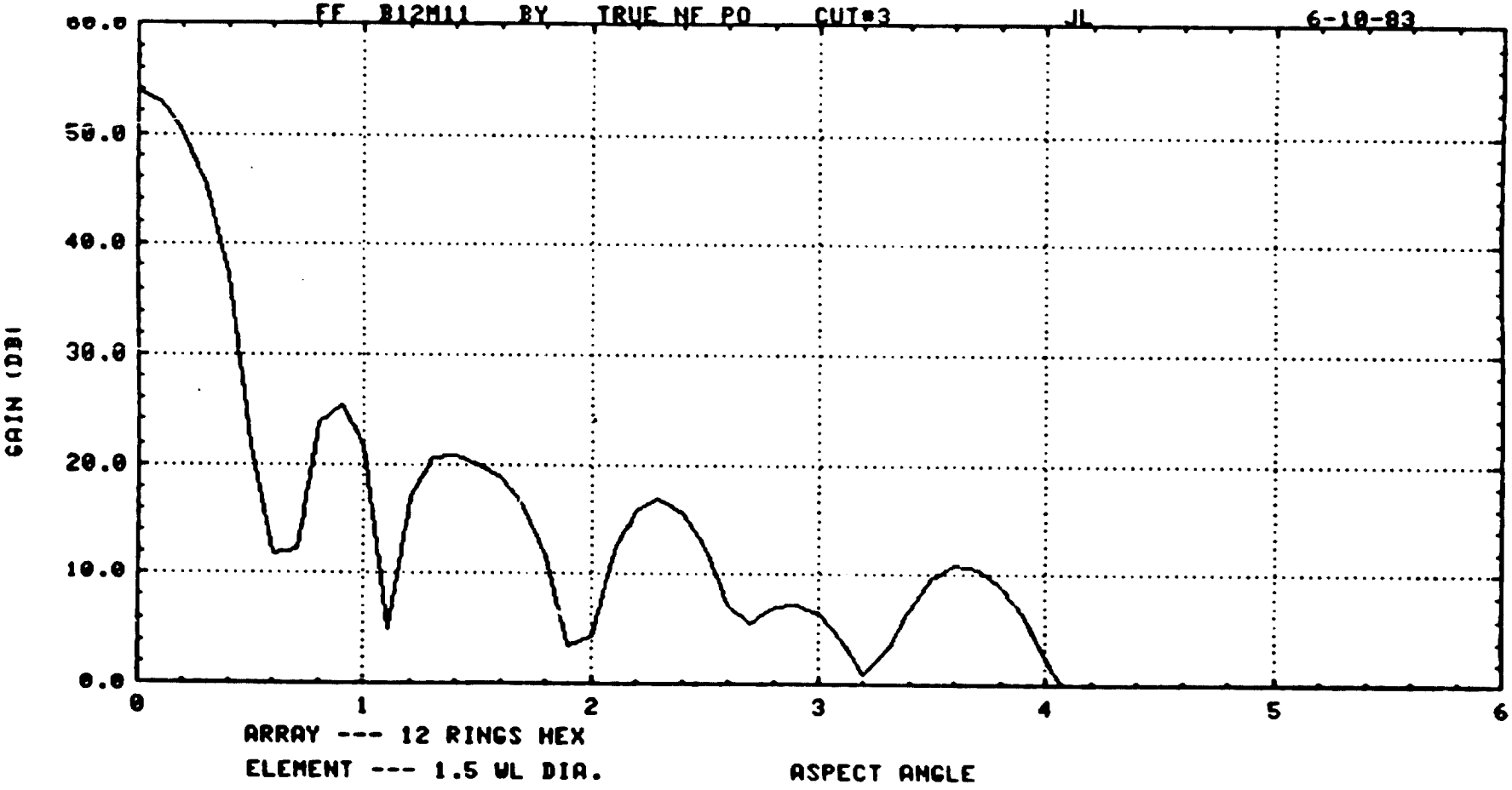

FIG 1.3-35 12-RING HEX ARRAY — SYSTEM FF

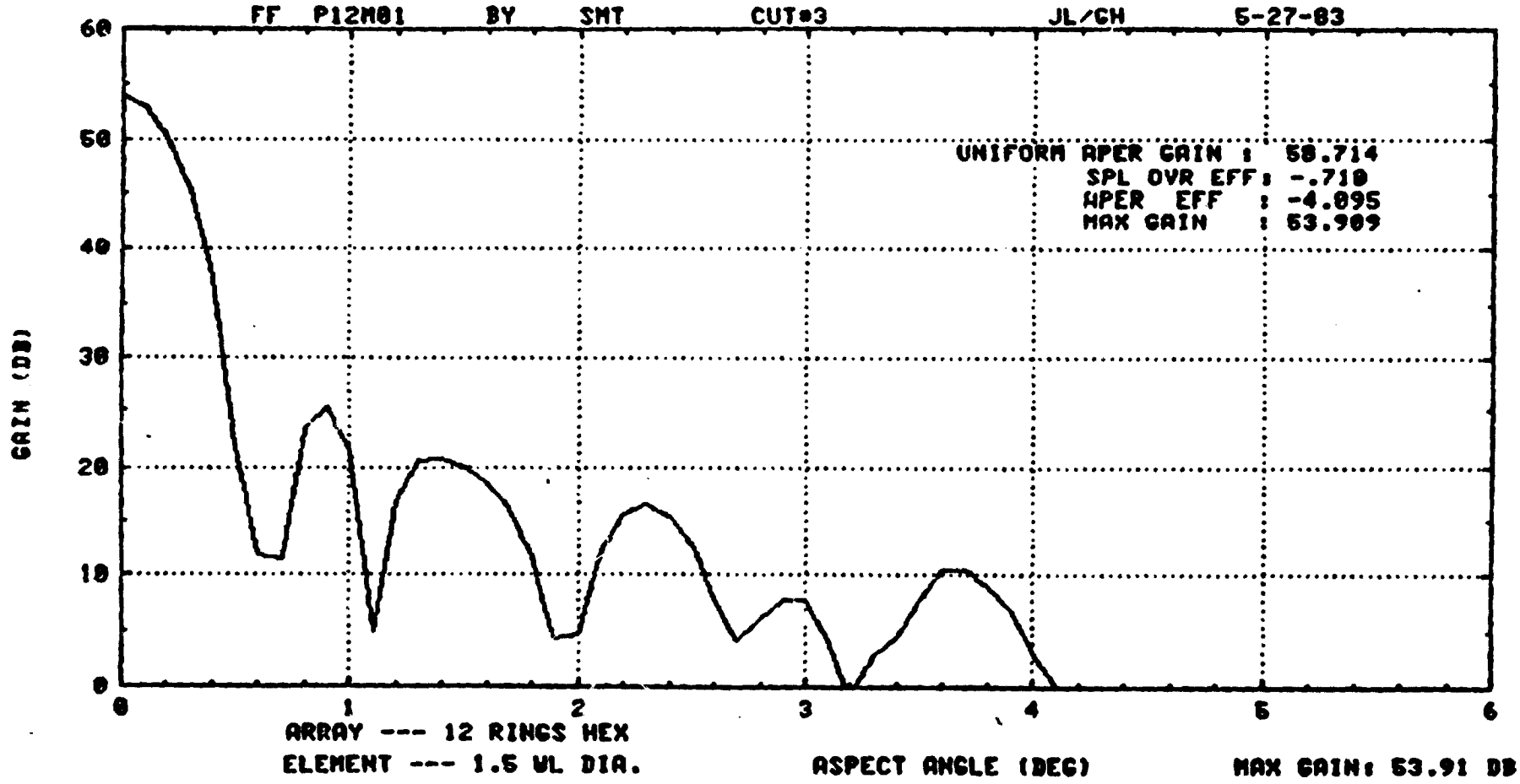

FIG. 1.3-36 12-RING HEX ARRAY — SYSTEM FF

SECTION 2

OPTICAL SYSTEM DESIGN

2.1 BASELINE CONFIGURATIONS

In determining the optical system set-up, there are several important parameters to be considered. These parameters include the F/D, the magnification (M), the subreflector size, and the reflector offset. The primary objective of the optical system trade off was aimed at determining a system which would provide the required gain for a given array aperture size. In order to achieve the minimum gain requirement, a 108 inch main reflector was chosen. The maximum theoretical gain that can be achieved with such a reflector is 58 db at 27.5 GHz. This leaves a 5 dB margin for a scanning beam system, which is satisfactory for an initial baseline design. Three optical systems were investigated using the above main dish. For the first, an F/D fo 1.25 was chosen with a magnification factor of 3. For the required array scan angles (which are approximatrly M times the far field scan angles), a subreflector size of 55.8inches would be required. To avoid blockage a reflector offset (Q) of 30" is necessary. This optical system is sketched in figure 2.1-1. For the second and third systems a magnification of 6 was chosen with F/D of 1.0 and 1.25, respectively. To include the array scan angles to cover CONUS, a subreflector size of 37 inches is required for an F/D of 1.0 and a 39.5 inch subreflector is required for an F/D of 1.25. A reflector offset of 60" was specified to avoid blockage. These configurations are shown in figures 2.1-2 and 2.1-3. Since the magnification factor directly influences the number of array elements required, the second and third systems described above were chosen as baselines.

2.2 DESIGN CONSIDERATIONS

2.2.1 DESIGN BY IRTT

The inverse ray tracing technique provides a simple and straight forward means to determine the main dish images on the sub-dish, the array plane and the scan plane, while the rays at the scan plane are forced to be in the same (scan) direction. It can also be used to determine the images of the array on the sub-dish, main dish and the scan plane, while the rays at the scan plane are all in the scan direction.

IRTT can also be used to plot the "conjugate" surface of the main dish, which is formed by the loci of the conjugates of the points on the main dish (Ref.1). A two dimensional plot of the conjugate surfaces was shown in Fig.2.2-1 and 2.2-2.

By examining the main dish images on the sub-dish for various scan angles, the size and location of the sub-dish can easily be determined, see Figs. 2.2-3--2.2-7. The effects of the array plane location on the array size and location were depicted in Fig.2.2-8--2.2-10.

Figures 2.2-11 - 2.2-17 show the mapping of the main reflector surface onto the array plane and the subreflector for magnifications of 3, 4, and 5. In these plots the ideal array plane location was estimated. As can be seen, a lower magnification factor will tend to maximize the common mapped region. Figures 2.2-18 and 2.2-19 show the effects of changing the reflector offset. It can be determined that as the offset distance is reduced, the mapped area tends to

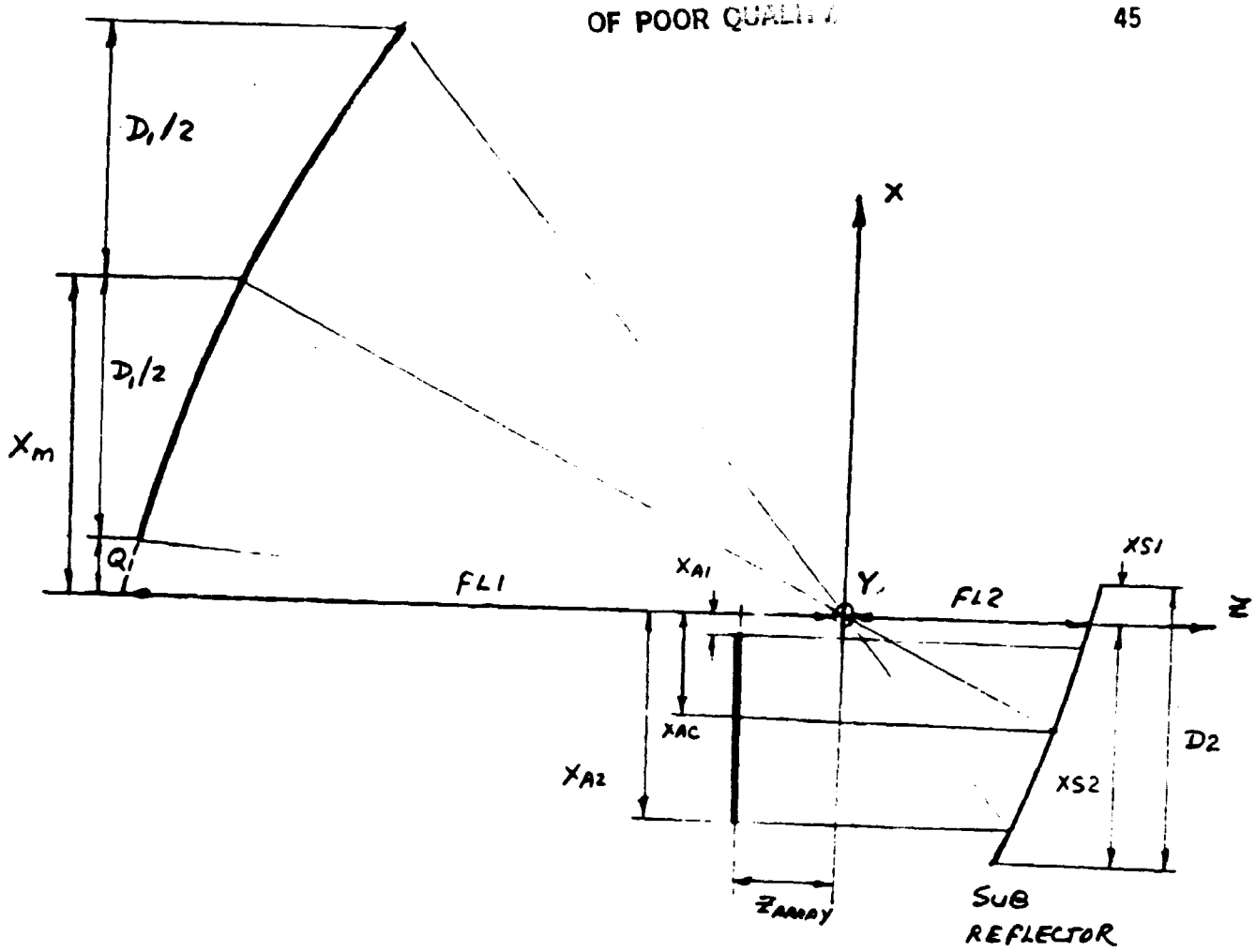

MAIN DISH:

$m = FL1/FL2 = 3$

$FL1 = 135"$

$D1 = 108"$

$F/D = FL1/D1 = 1.25$

$Q = 30"$

$X_m = 84"$

SUB DISH:

$XS1 = 2.995"$

$XS2 = 55.798"$

$D2 = 58.793"$

FIG. 2.1-1

ARRAY:

$Z_{ARRAY} = -25.163"$

$XA1 = -10"$

$XA2 = -46"$

$XAc = -28"$

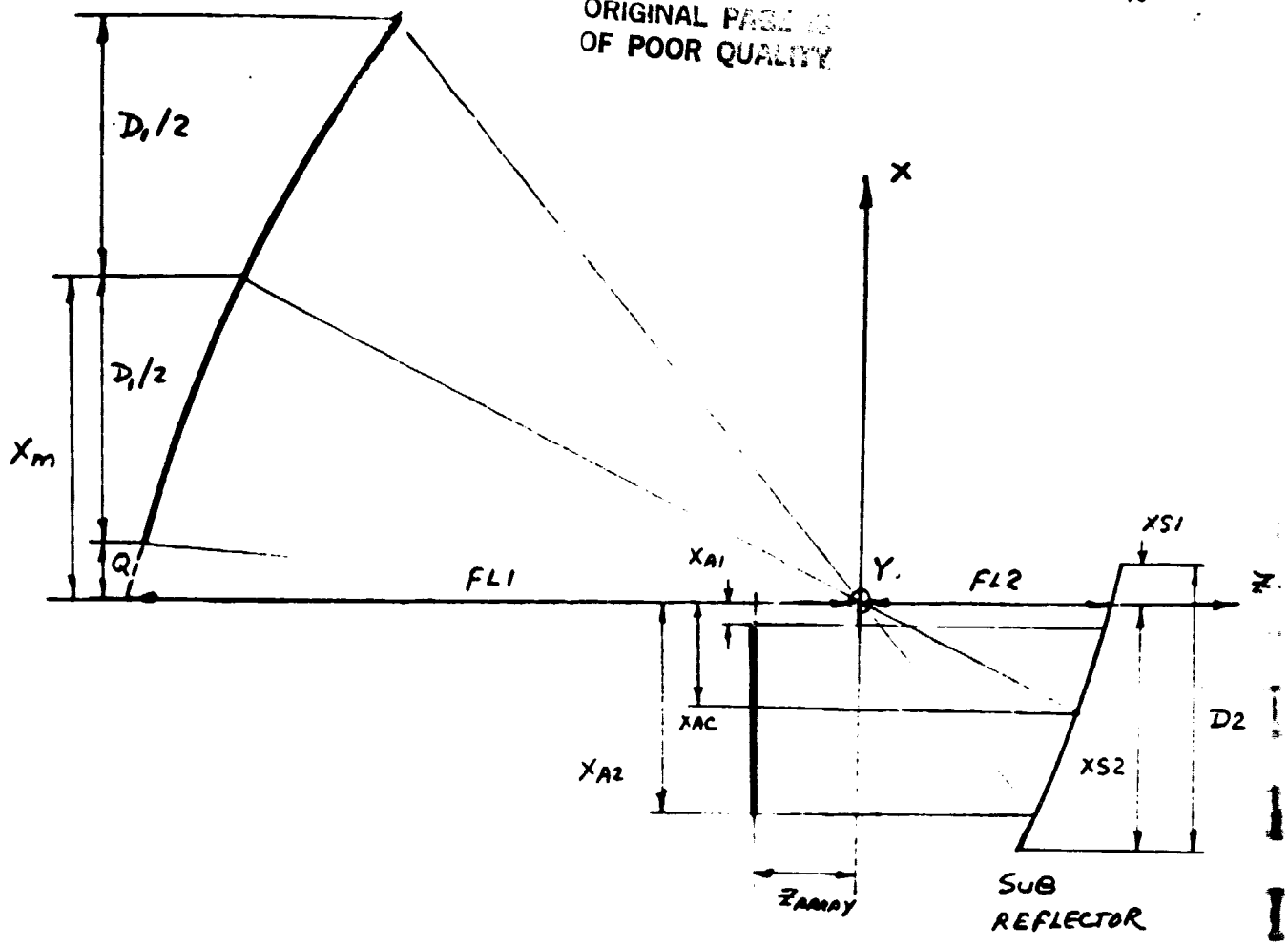

MAIN DISH:

$m = FL1/FL2 = 6$

$FL1 = 108"$

$D1 = 108"$

$F/D = FL1/D1 = 1.0$

$Q = 60"$

$Xm = 114"$

SUB DISH:

$XS1 = 3"$

$XS2 = 34"$

$D2 = 37"$

FIG. 2.1-2

ARRAY: $Z_{ARRAY} = -13.864"$

$XA1 = -10"$

$XA2 = -28"$

$XAc = -19"$

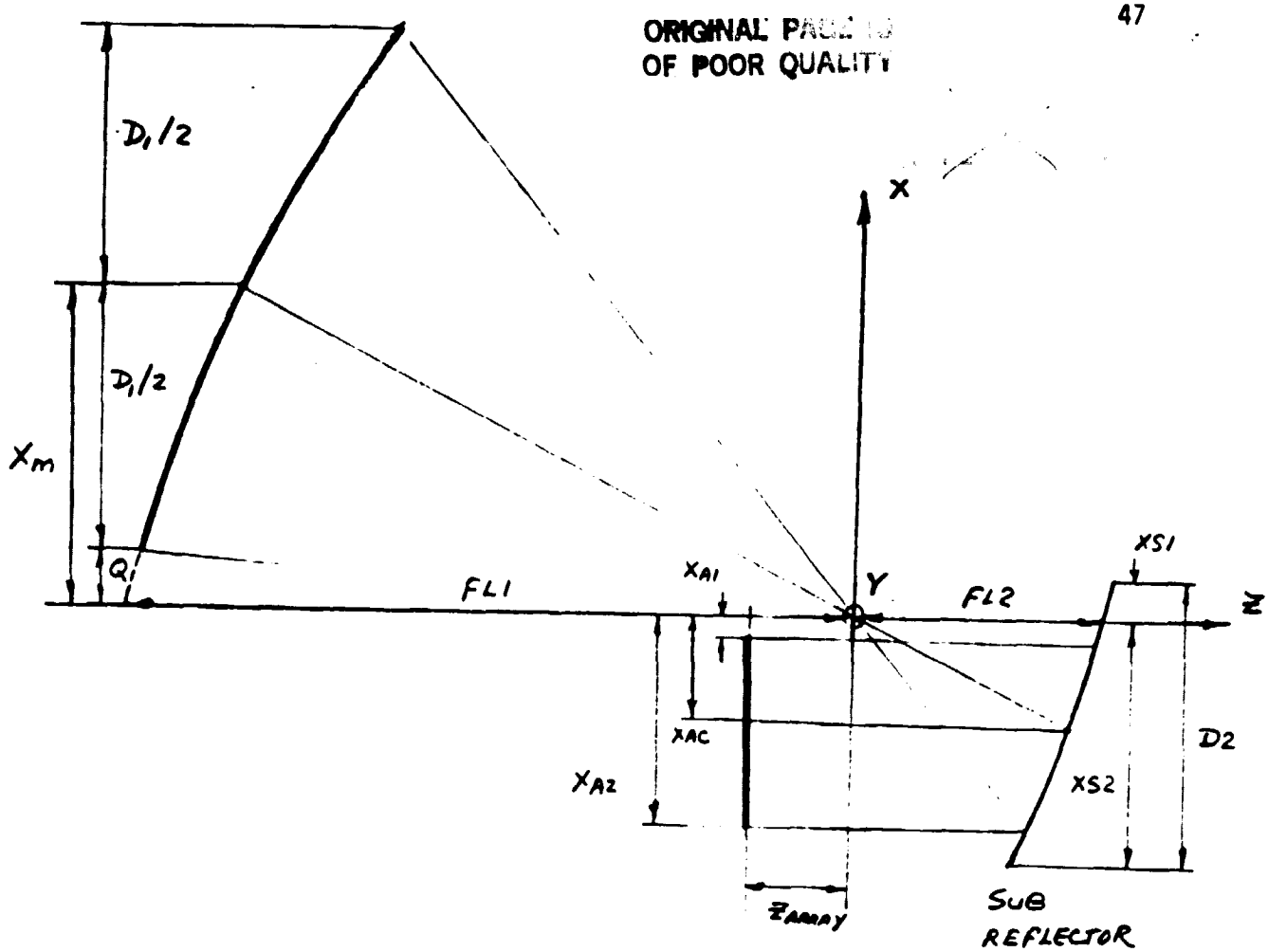

MAIN DISH:

$m = FL1/FL2 = 6$

$FL1 = 135"$

$D1 = 108"$

$F/D = FL1/D1 = 1.25$

$Q = 60"$

$X_m = 114"$

SUB DISH:

$XS1 = +3.364"$

$XS2 = -35.912"$

$D2 = 39.276"$

FIG. 2.1-3

ARRAY: $Z_{ARRAY} = -12.441"$

$XA1 = -10"$

$XA2 = -28"$

$XAc = -19"$

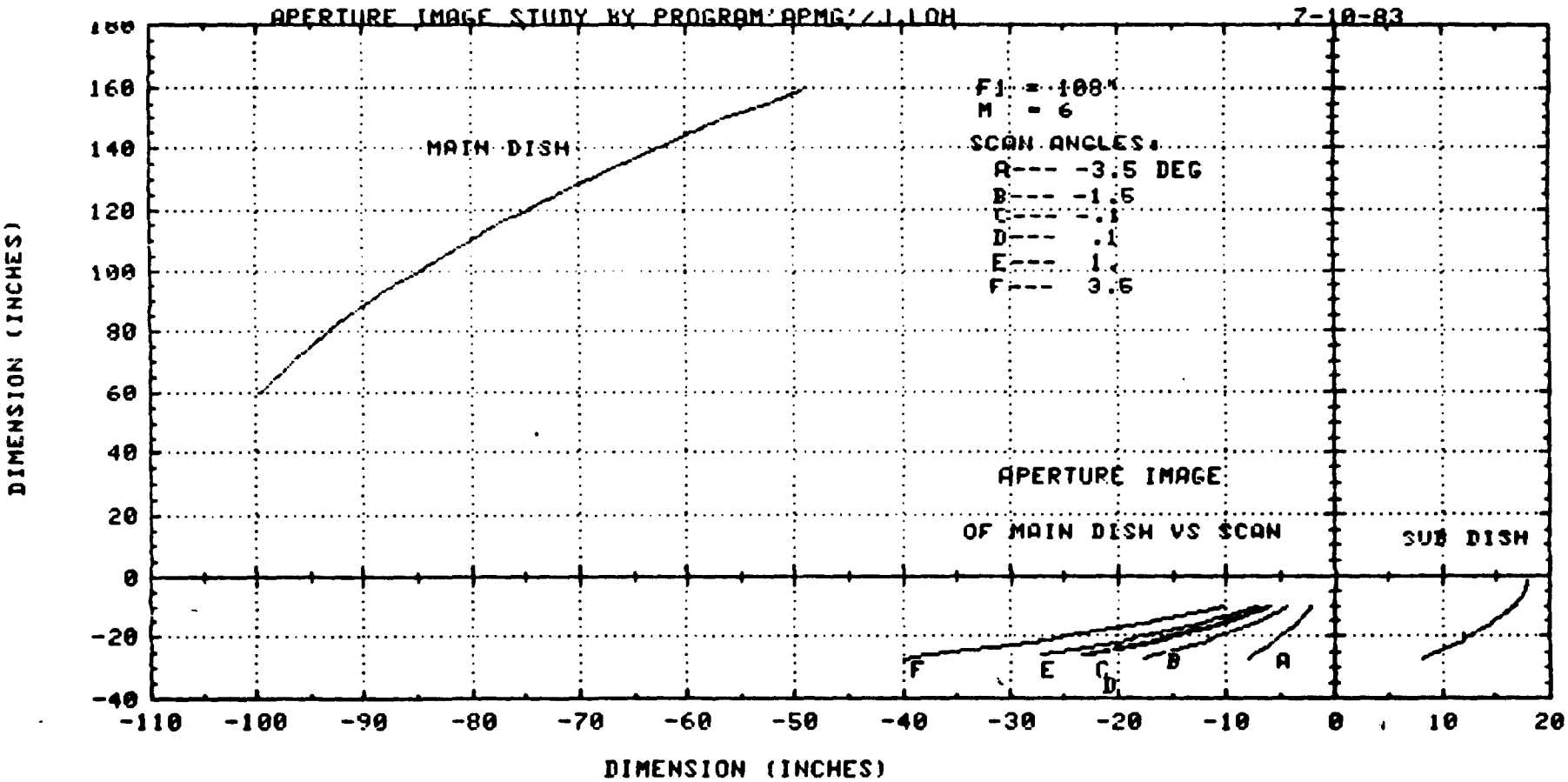

OFFSET PLANE (XZ-PLANE) CROSS-SECTION OF MAIN DISH, SUB-DISH, & MAIN DISH IMAGES, M=6

FIG. 2.2-1

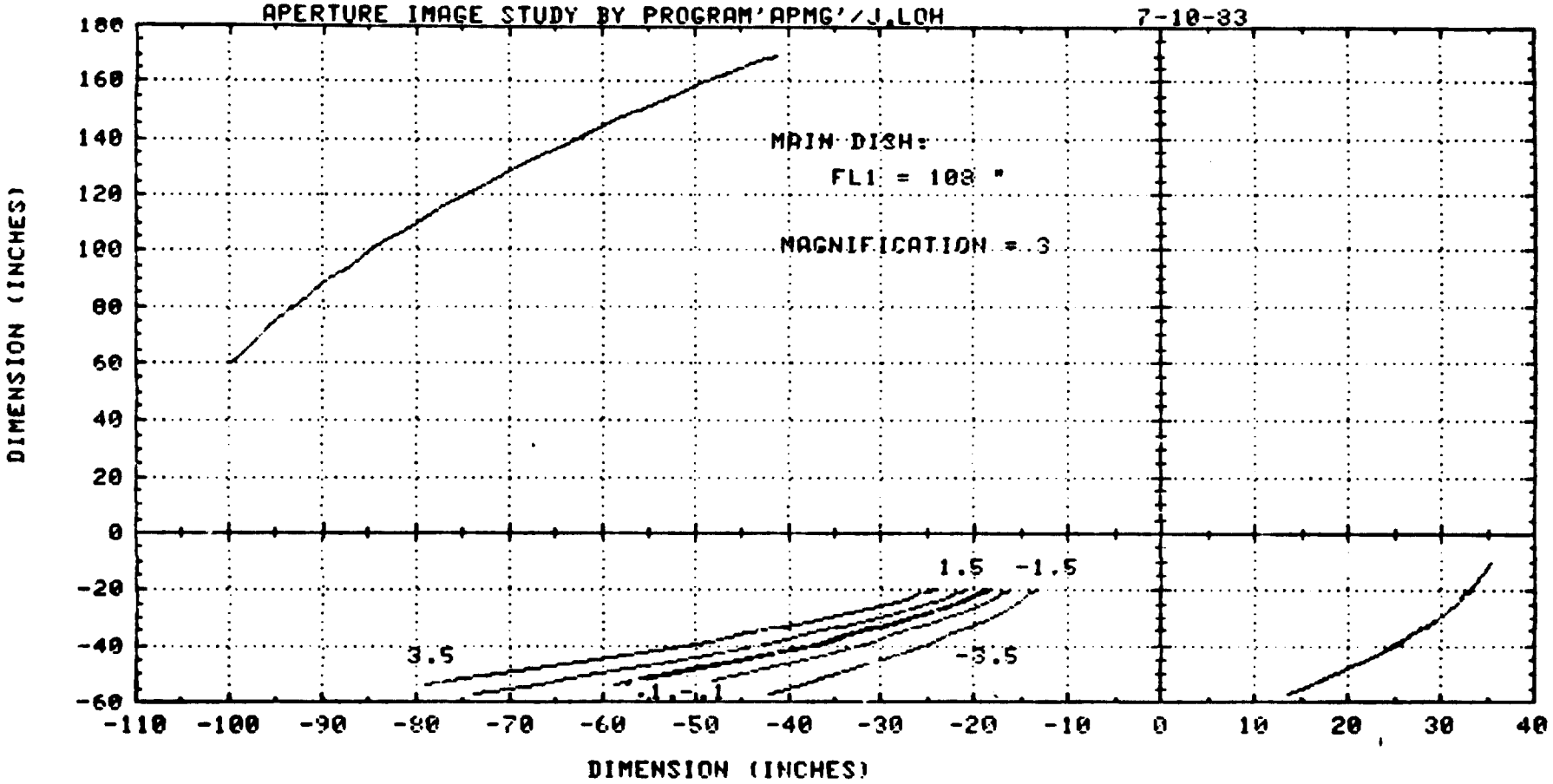

OFFSET PLANE (X Z-PLANE) CROSS SECTIONS OF MAIN DISH, SUB-DISH & MAIN DISH IMAGES, m=3

FIG. 2.2-2

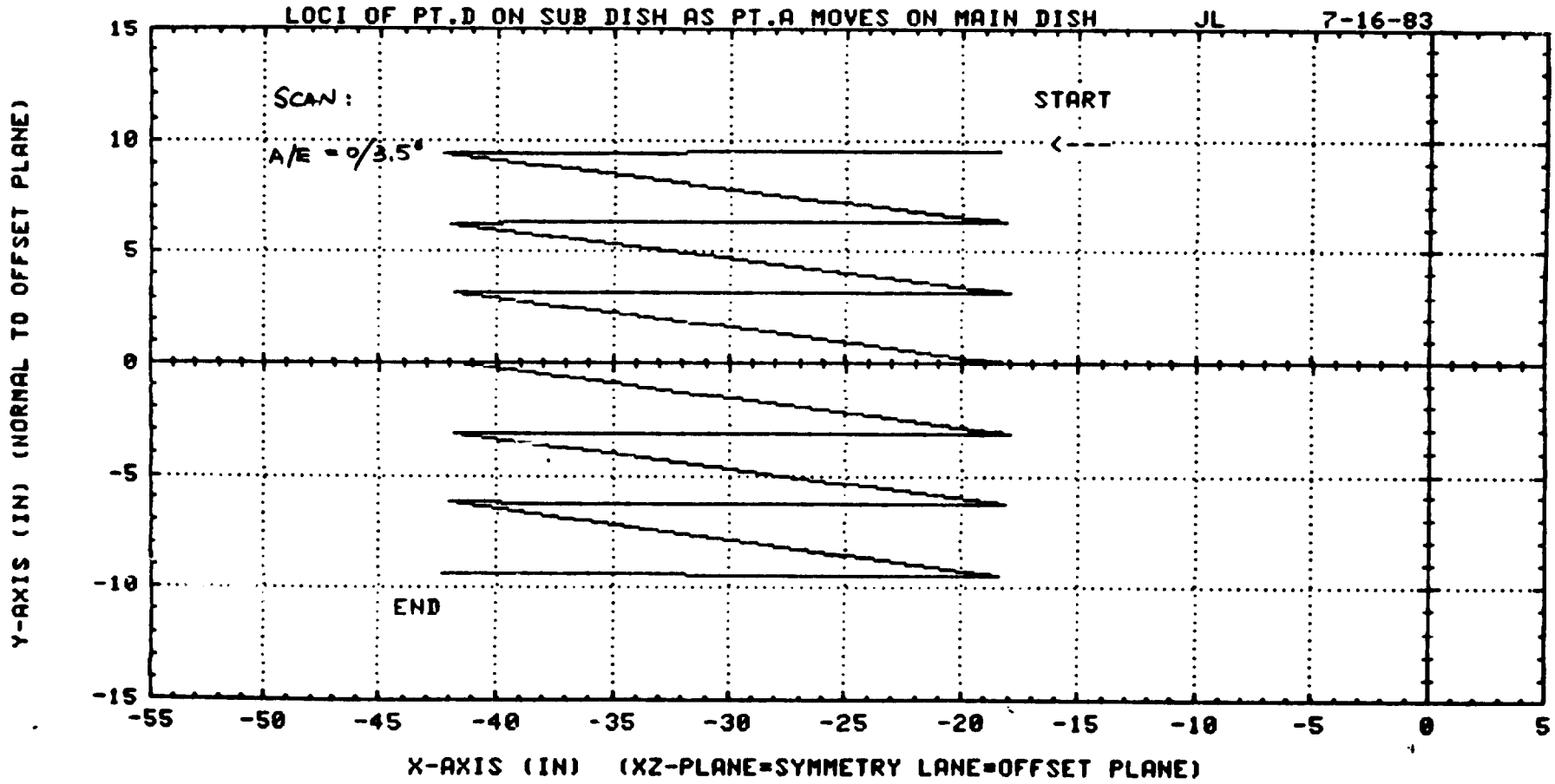

Y_D V.S. XD, AS PT. A SCANS ON MAIN DISH

FIG 2 2-3 SCANNING POINT ON SUB DISH

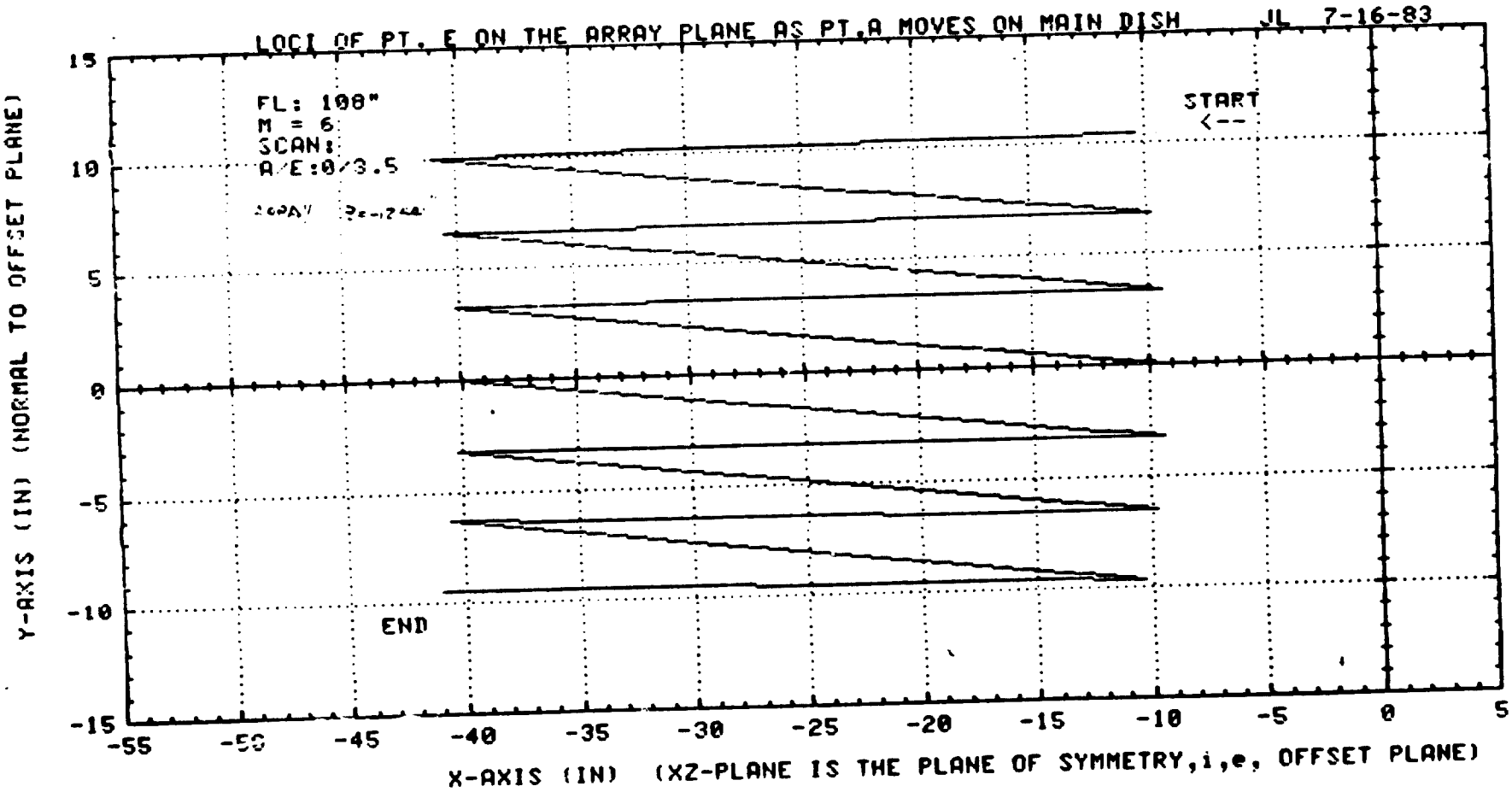

YE VS. XE

FIG 2.2-4 SCANNING POINT ON ARRAY PLANE

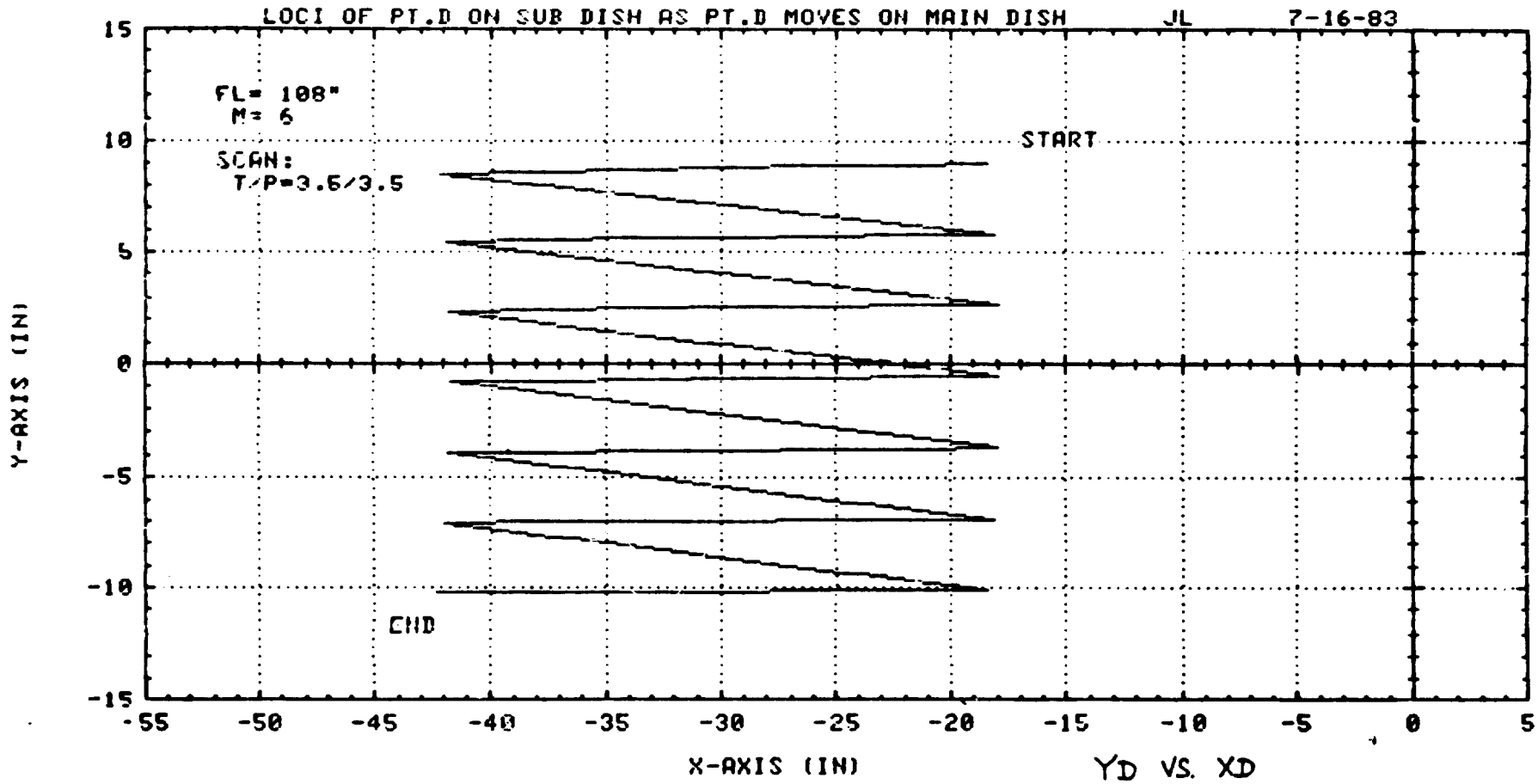

FIG 2 2-5 SCANNING POINT ON SUB DISH

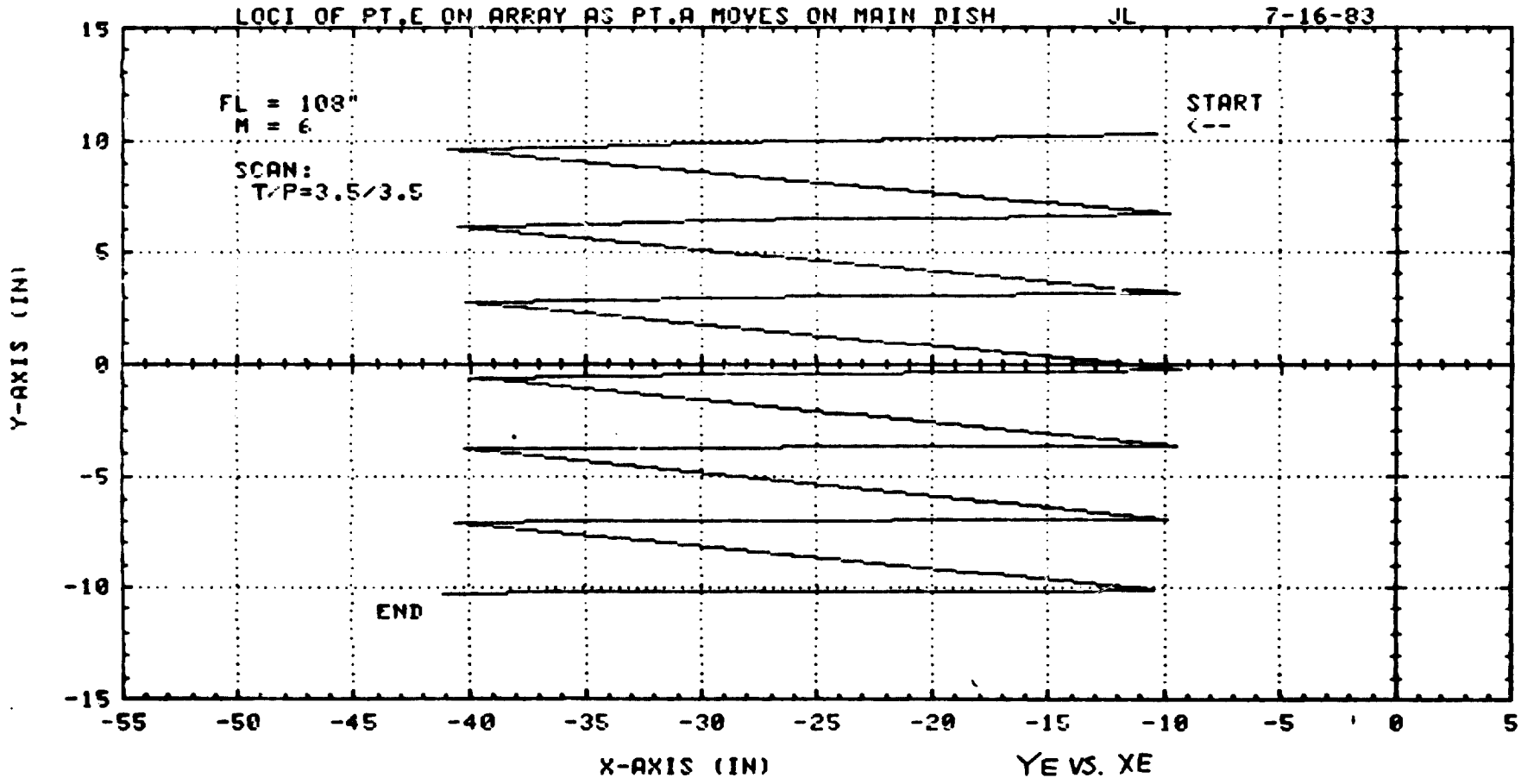

SCANNING IMAGE ON THE ARRAY PLANE, Z= -12.1.1.1

FIG. 2.2-6 SCANNING POINT ON ARRAY PLANE

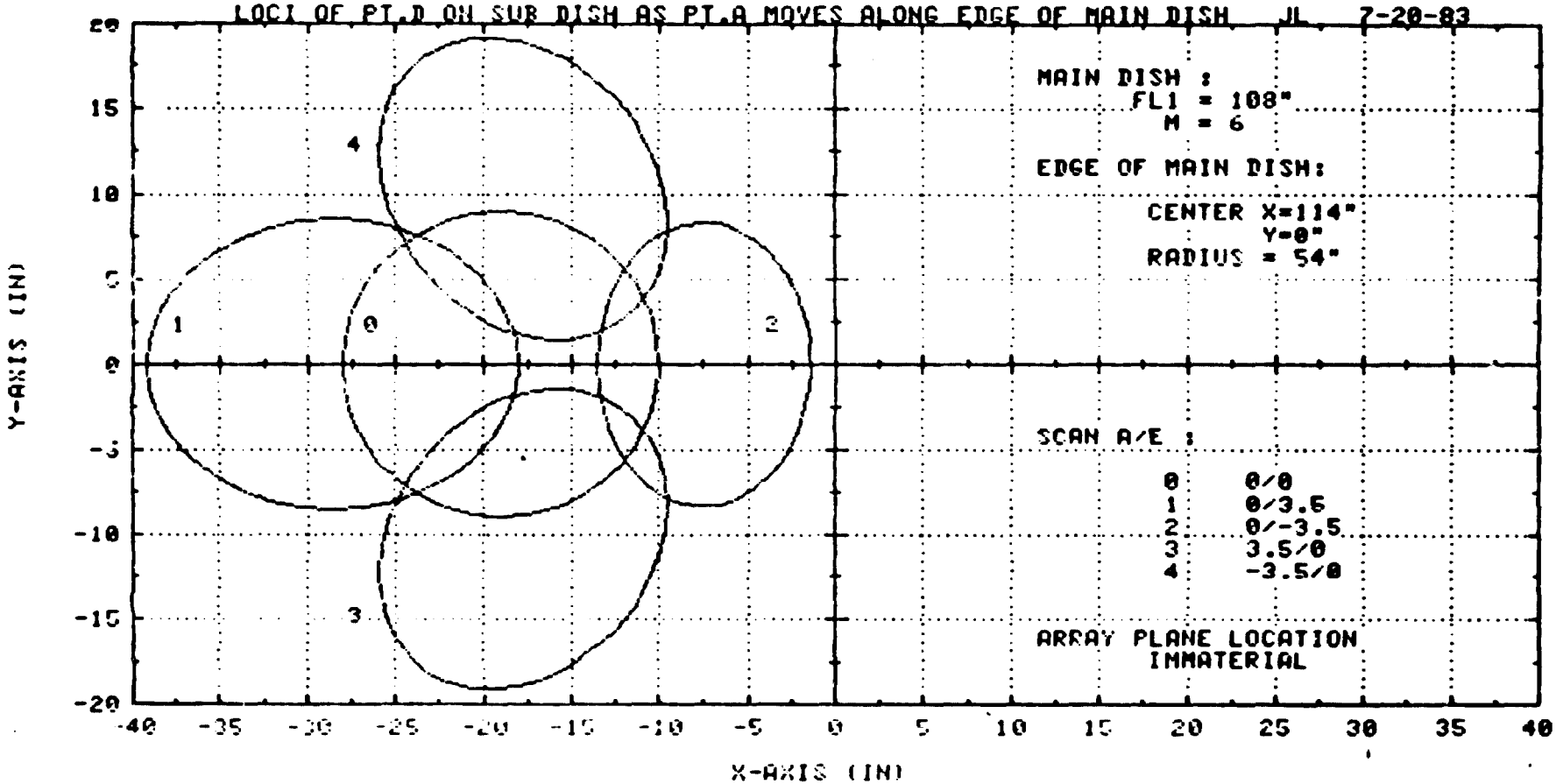

FIG. 2.2-1 IMAGE OF MAIN DISH ON SUB-DISH, 3.5° SCAN IN PRINCIPAL DIRECTIONS

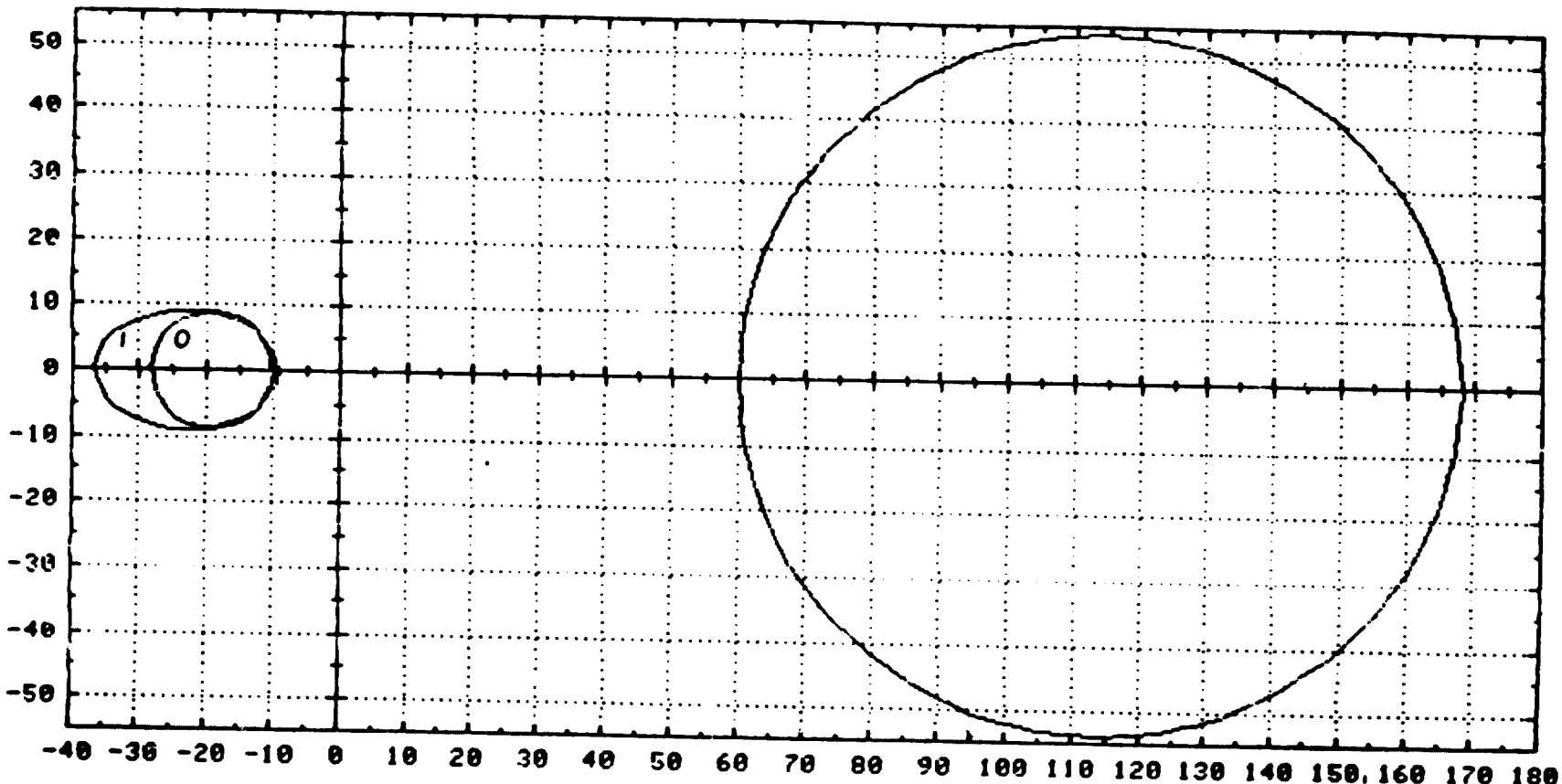

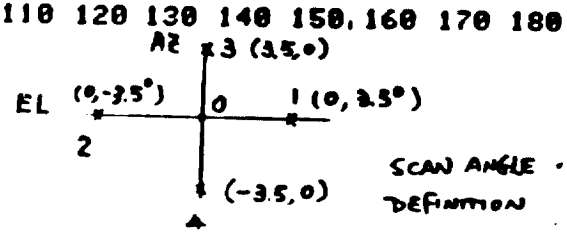

FIG. 2 2-8 MAIN DISH IMAGE ON ARRAY PLANE

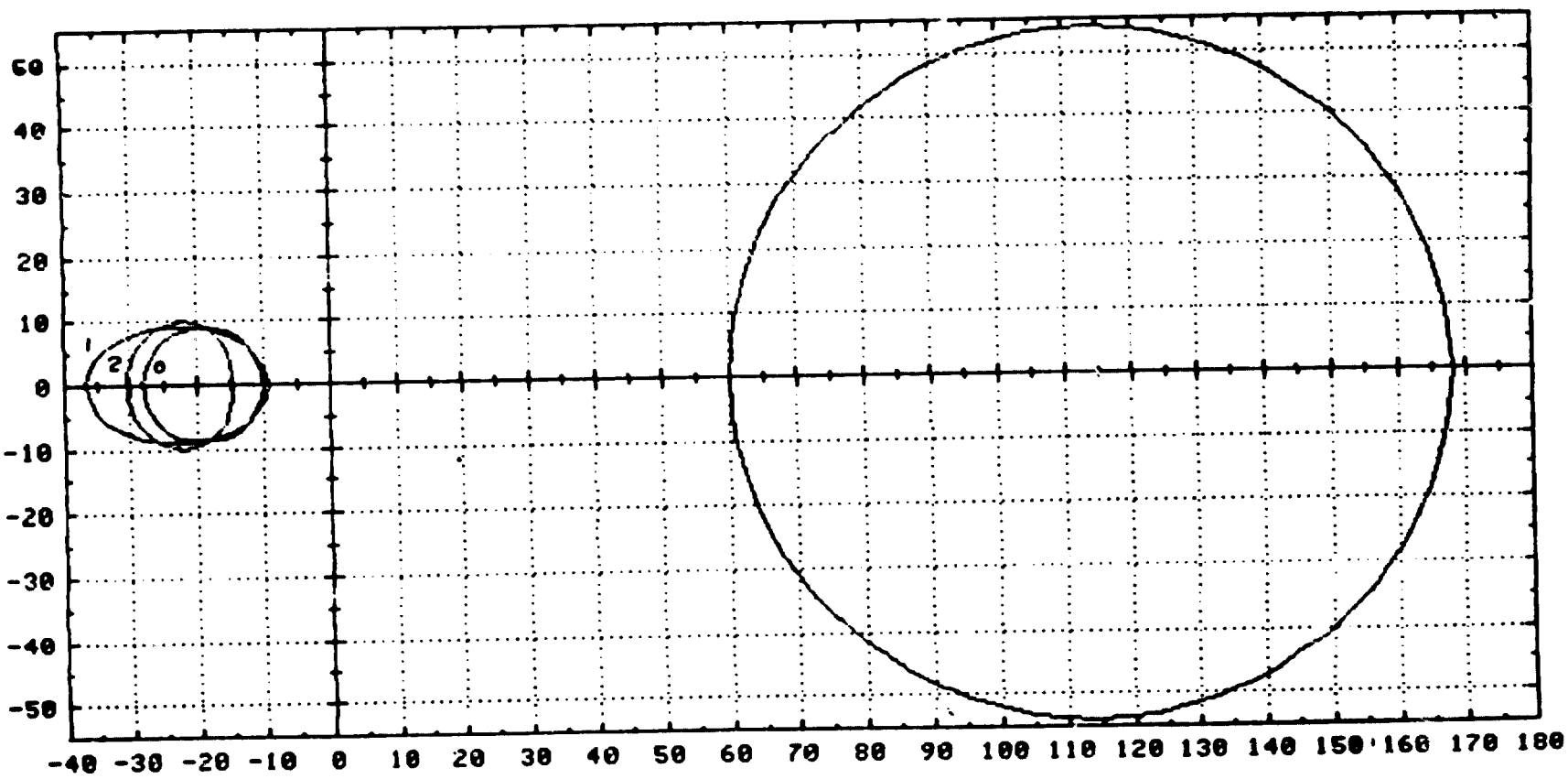

FIG 2 2-9 MAIN DISH IMAGE ON ARRAY PLANE

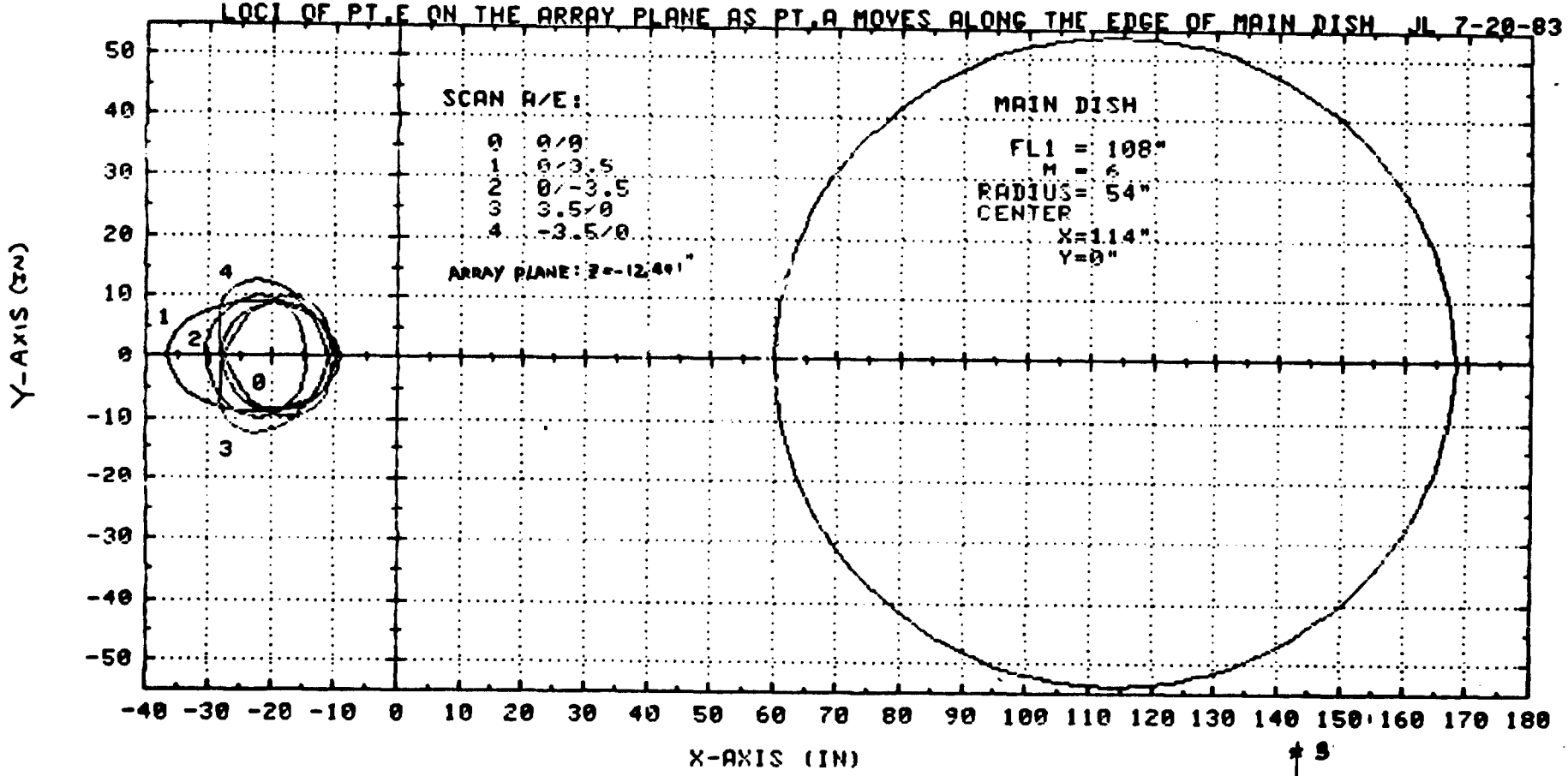

IMAGE OF MAIN DISH ONTO THE ARRAY PLANE.

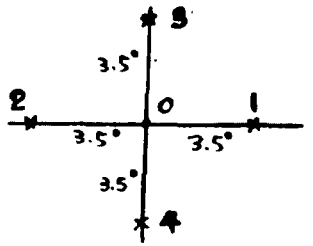

FIG. 2.2-10 MAIN DISH IMAGE ON ARRAY PLANE

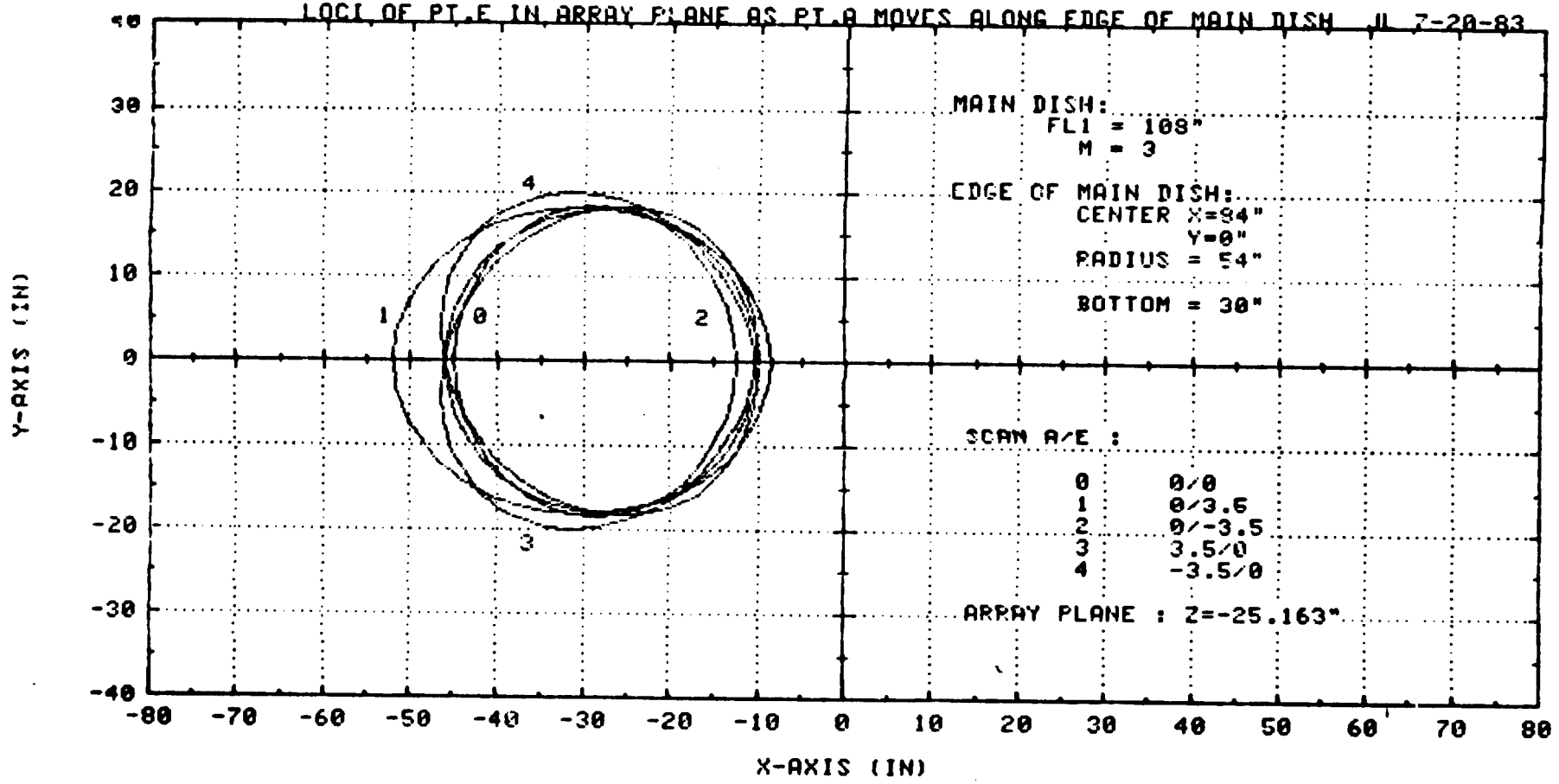

FIG. 2.2-11 MAIN DISH IMAGE ON ARRAY PLANE, m = 3

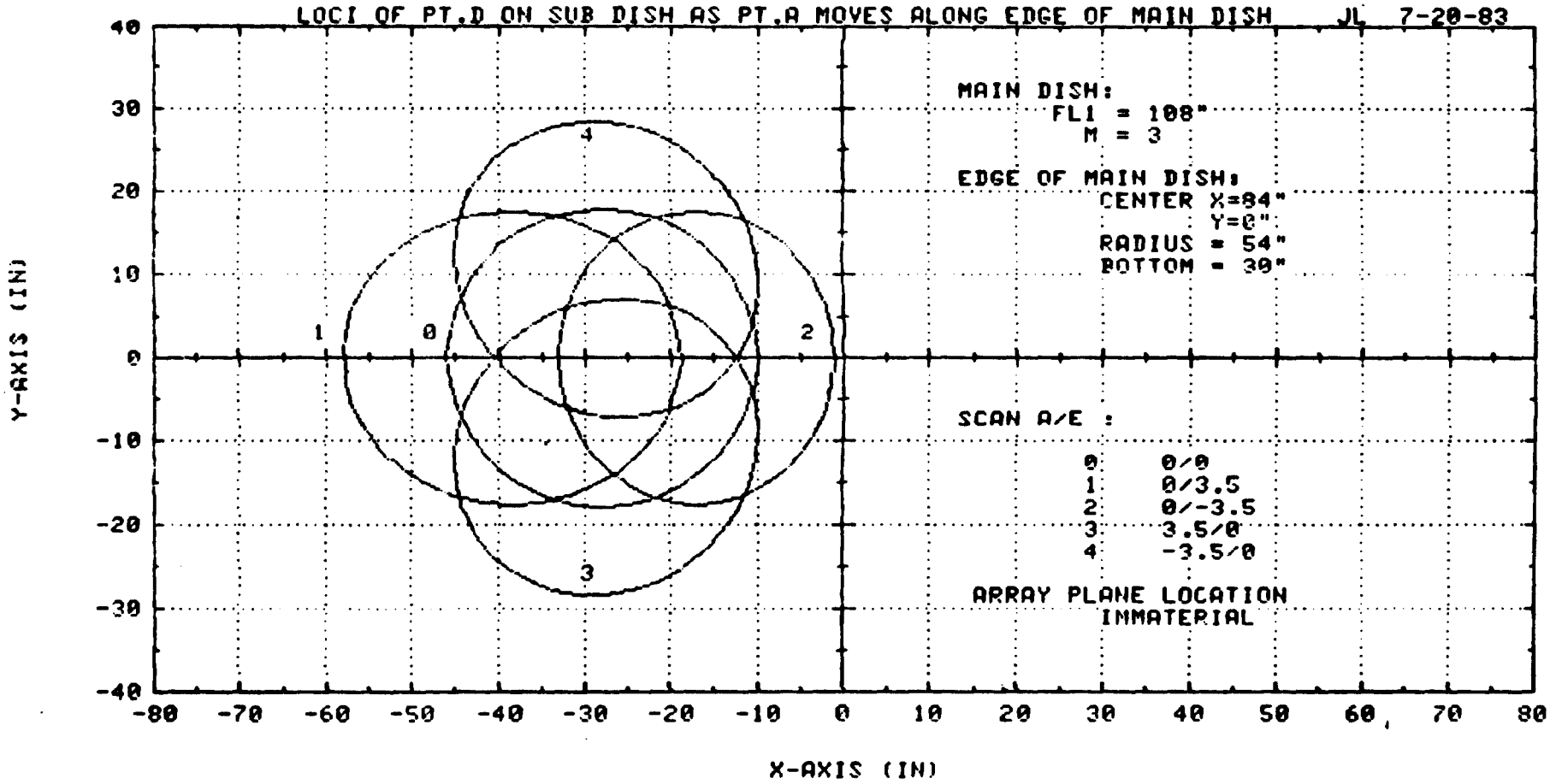

FIG. 2.2-12 MAIN DISH IMAGE ON SUB DISH, m=3

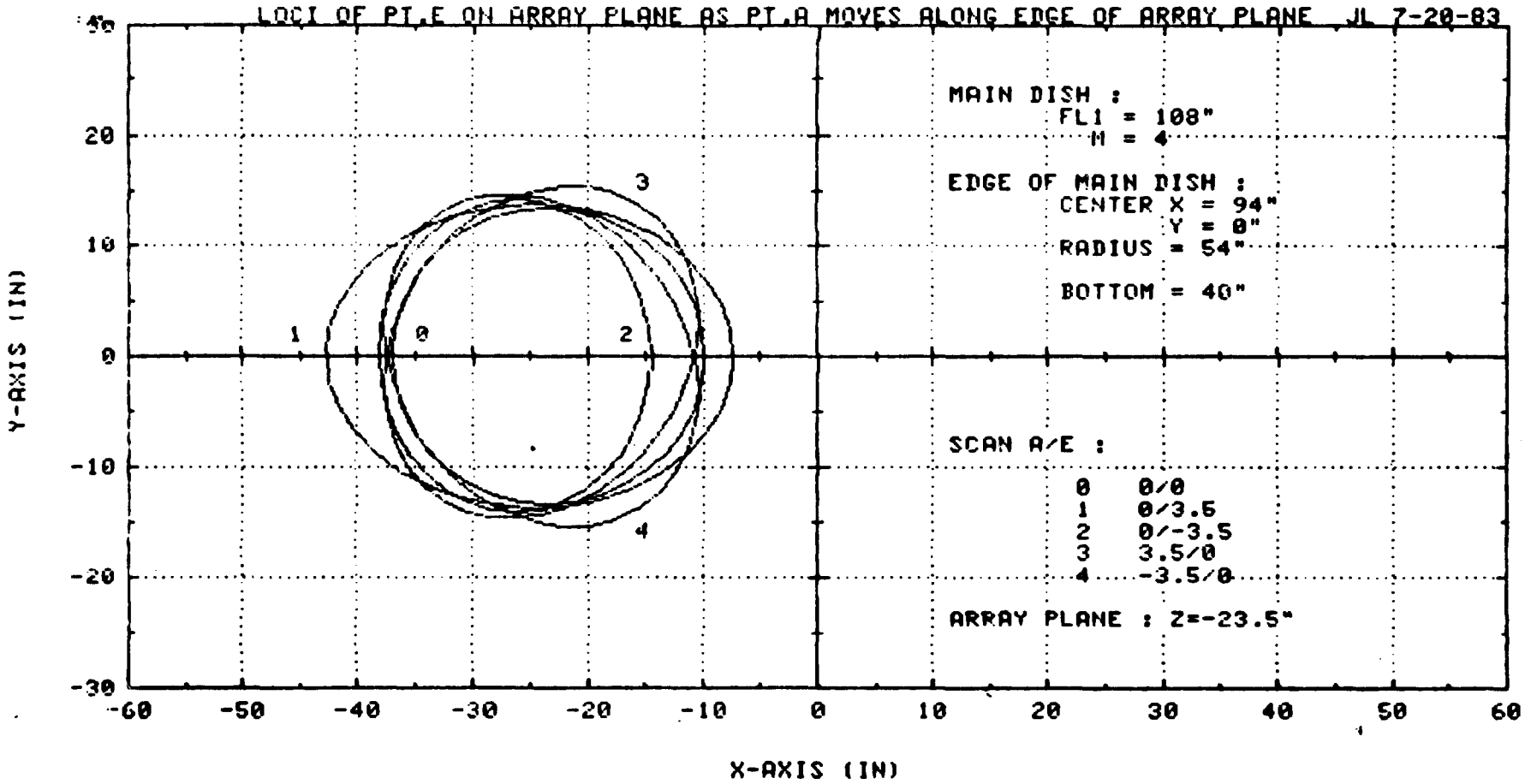

FIG. 2.2-13 MAIN DISH IMAGE ON ARRAY PLANE, M=4

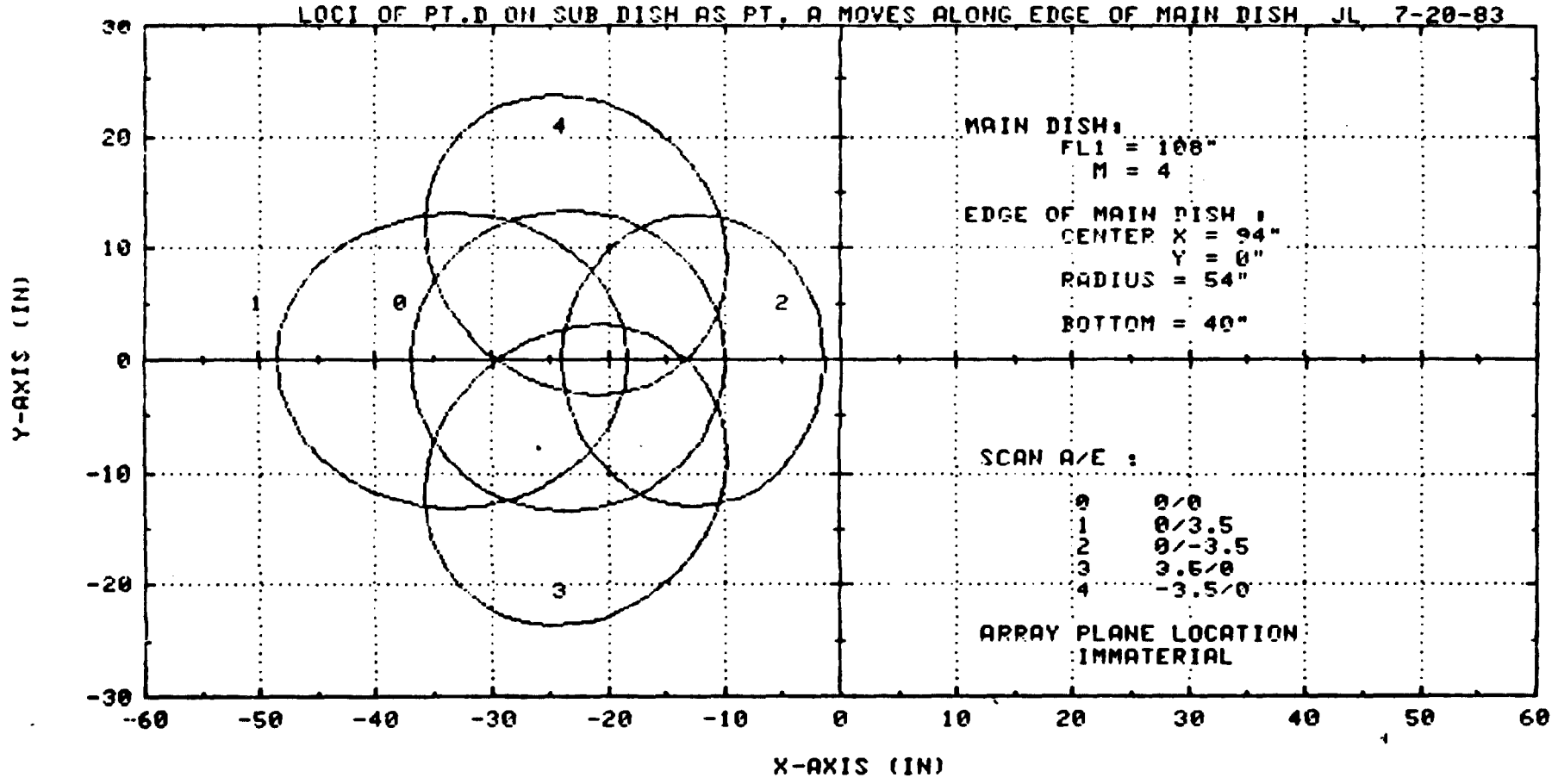

FIG 2-14 MAIN DISH IMAGE ON SUBDISH, m=4

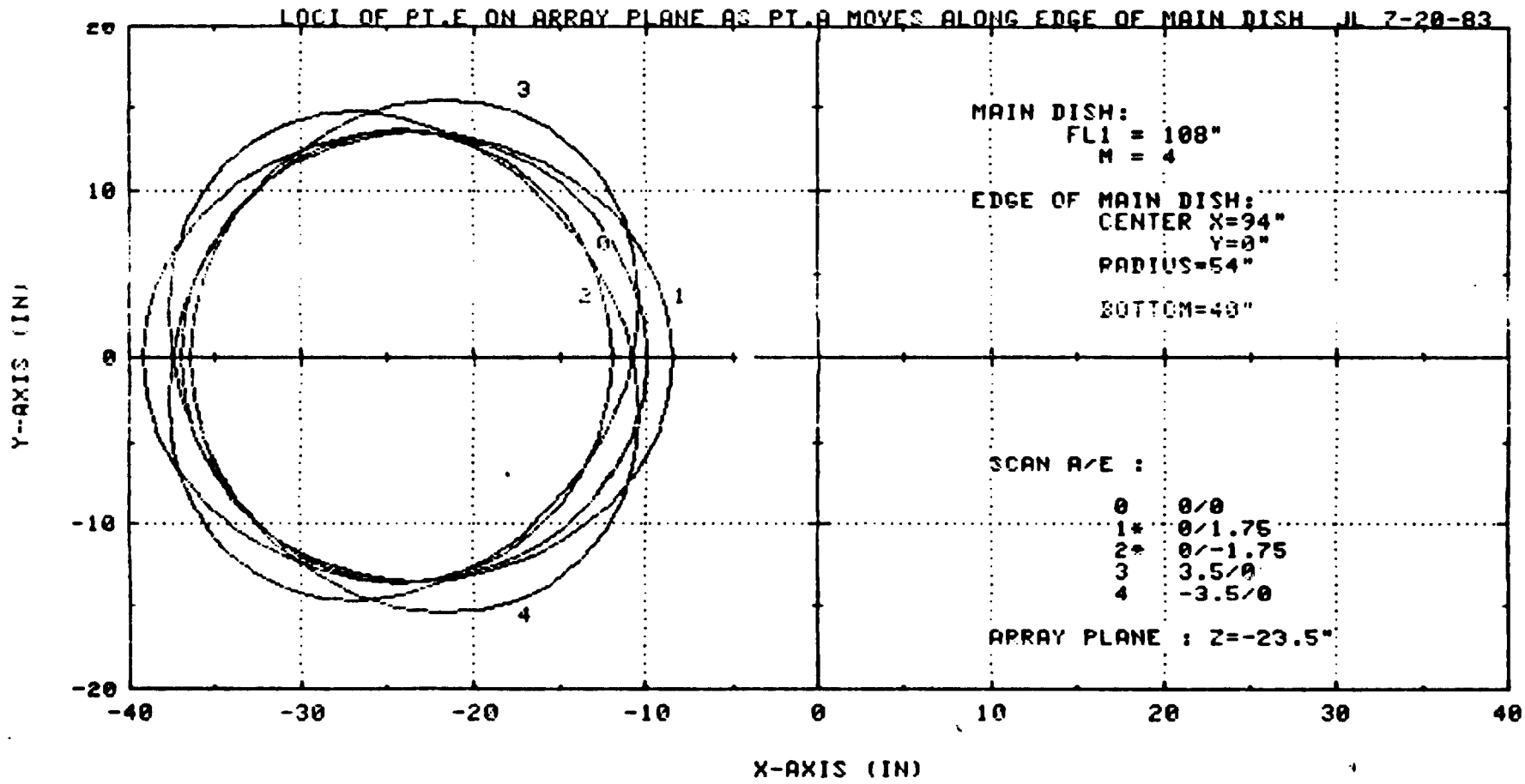

FIG. 2 2-15 MAIN DISH IMAGE ON ARRAY PLANE, $m=4$

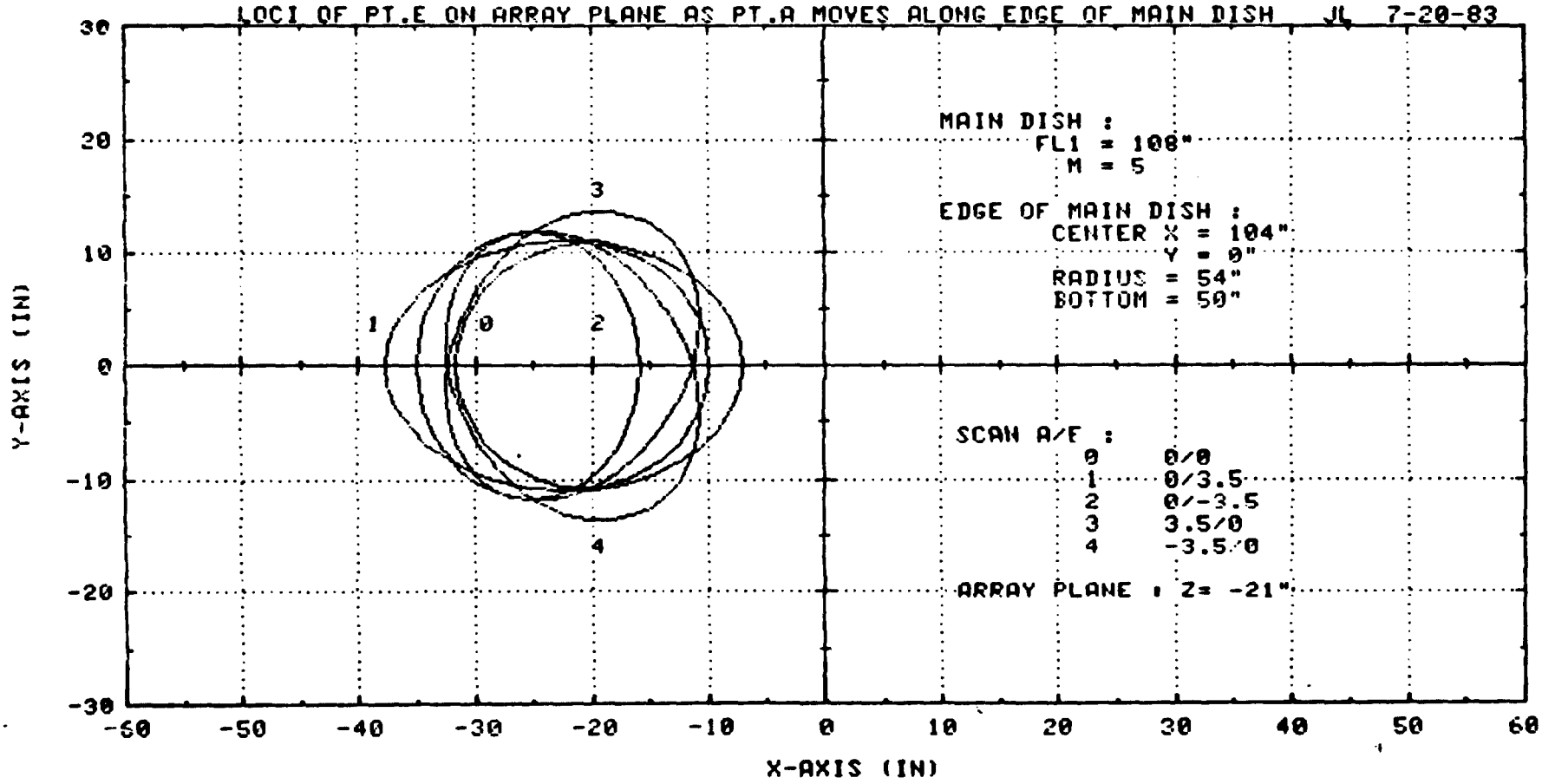

FIG 2.2-16 MAIN DISH IMAGE ON ARRAY PLANE, m=5

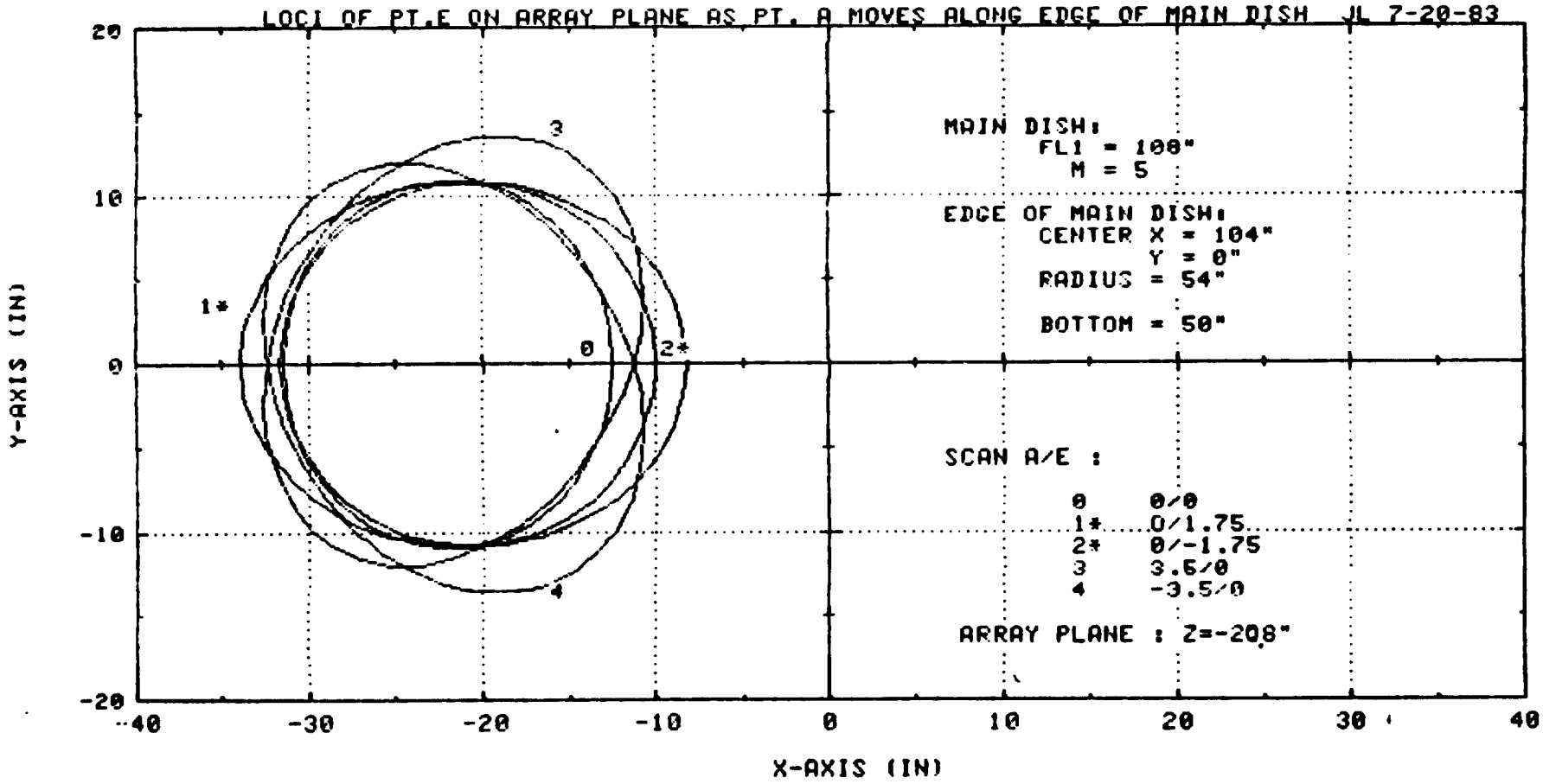

FIG. 2.2-17 MAIN DISH IMAGE ON ARRAY PLANE, m = 5

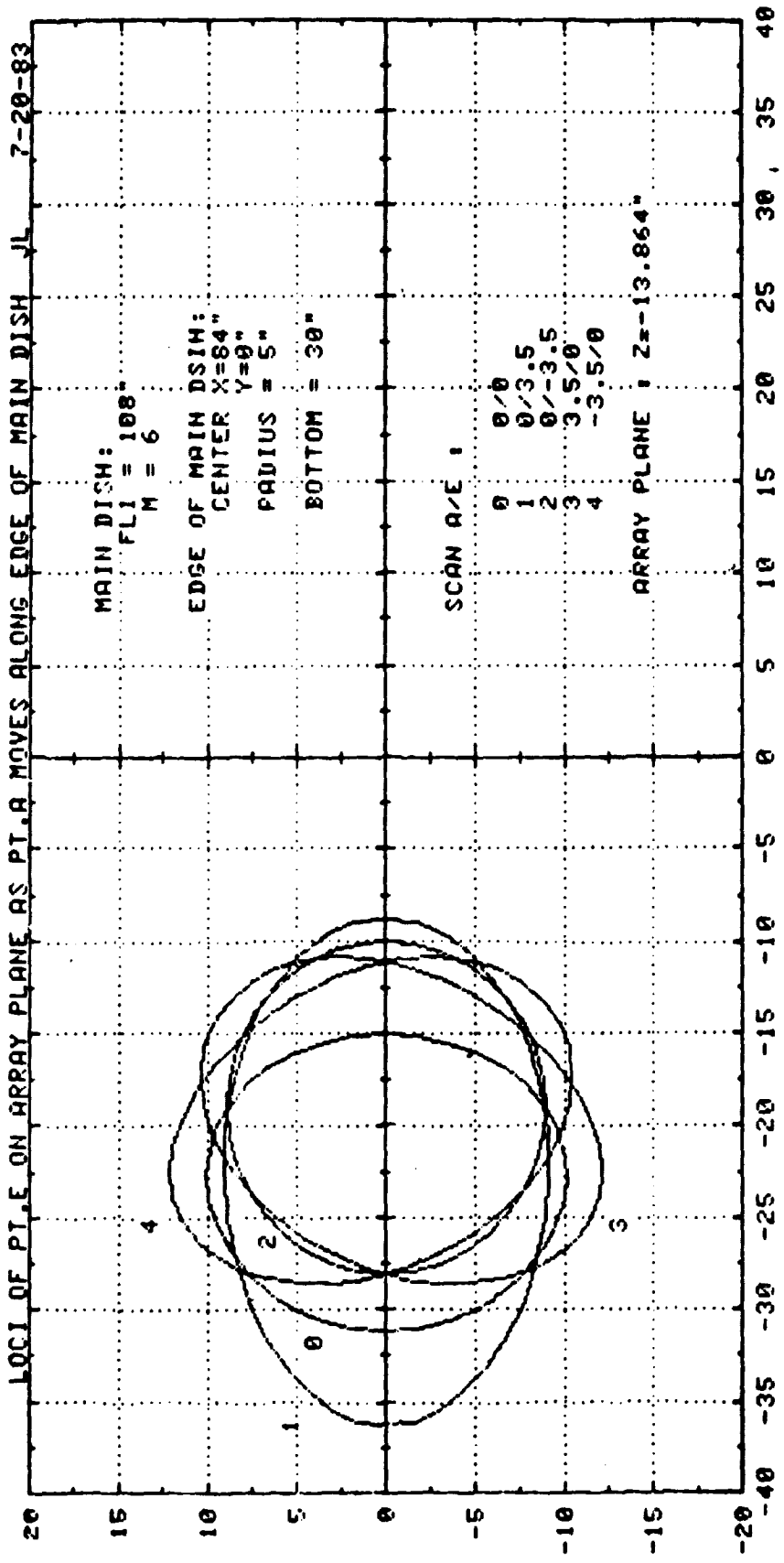

FIG.2.2-18 MAIN DISH OFFSET = 30", EFFECTS ON ARRAY PLANE

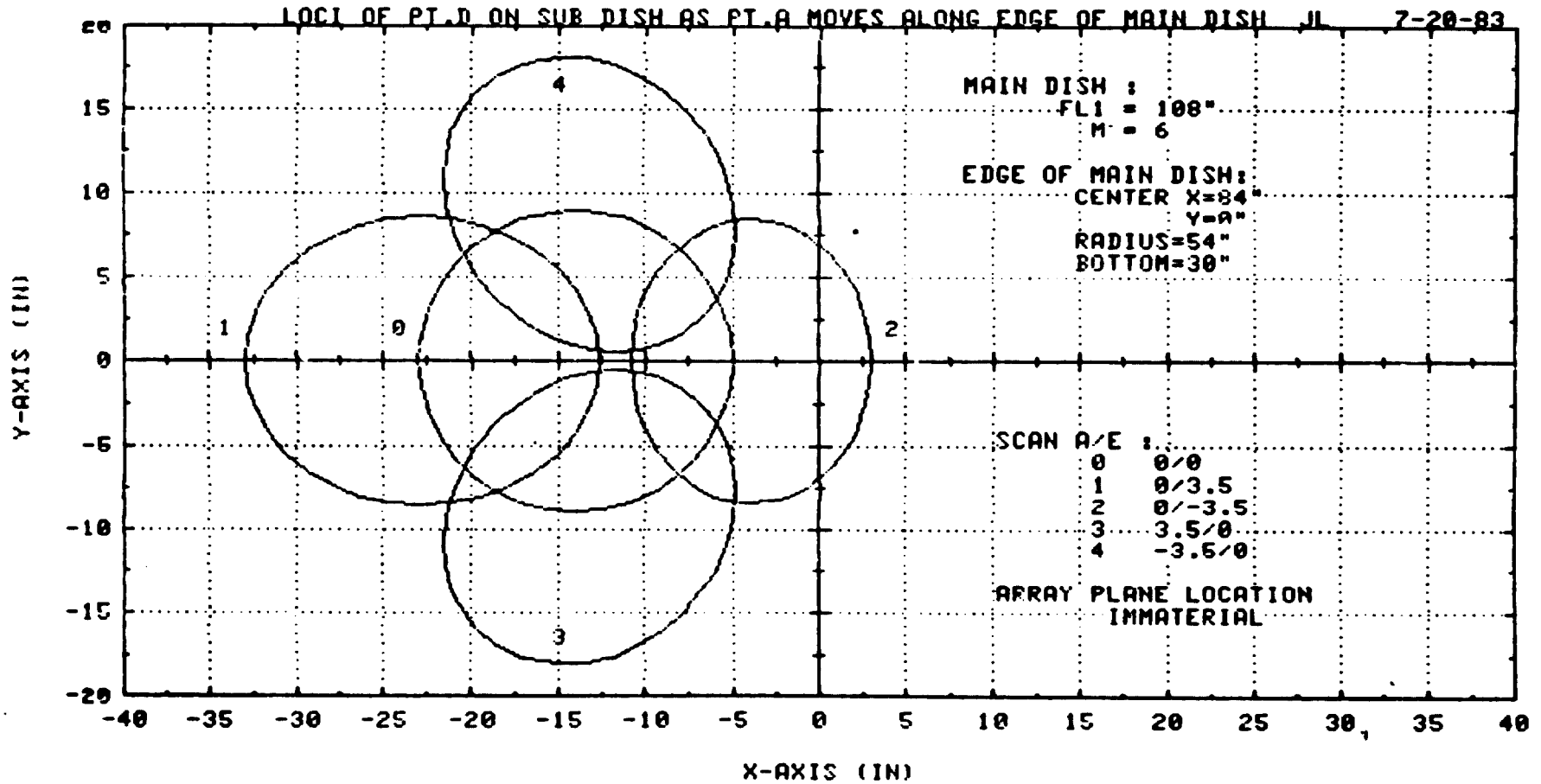

FIG. 2.2-19 MAIN DISH OFFSET 30", EFFECTS ON SUB DISH.

converge, thereby maximizing the common area. This point will be elaborated in Section 2.2.2.

2.2.2 MAIN REFLECTOR OFFSET

The bottom edge of the main dish is to be as close to the optical axis as possible. The blockage considerations place a limitation on how close it can be. However, there exists another type of restriction, which is not at all obvious but sometimes more stringent than the blockage. This new restriction surfaces when one uses IRTT to determine the conjugate surface of the main reflector. There exists a distinct conjugate surface for a specific system scan angle. It looks as if all the conjugate surfaces are moving toward the focus as the points on the main dish are moving toward the optical axis. But, this is true only initially. As the points on the main dish move further toward the axis, the conjugate surfaces bend over and move away from the focus, then oscillations start in a fashion similar to the tangent fuction about 90 degrees. This image fold-back phenomenon is physically explainable and imposes a restriction on the minimum main dish offset. The fold-back phenomenon was depicted in figures 2.2-20 and 2.2-21, which often occured with negative scan angles (scan toward the optical axis).

2.2.3 ARRAY LOCATION & SIZE

The system performance is very sensitive to the array plane location. The array plane should be located such that the main dish images corresponding to all possible scan angles have a maximum overlap. If the extent of system scan is symmetrical with respect to both the offset plane and the asymmetry plane, then the array center should coincide with the conjugate of the main dish center point in the unscanned case. Otherwise, the array location has to be derived from the knowledge of the main dish images on the intended array plane, where maximum overlap of the images is obtained. The overlapped images as a function of array plane location are shown in figures 2.2-22 - 2.2-25.

Once the array location is determined, the size of the array aperture should be chosen to be equal to or slightly smaller than the overlap area. The reason for selecting the 'overlap' area instead of the 'image coverage' area is to be chosen for the array aperture is explained below.

If an array element is in the 'image coverage' area but not in the 'overlap' area, then it does not contribute to system main beam in all of the scan directions. If it does not contribute to the main beam, its contribution then goes to the sidelobes and hence must be avoided to prevent performance degradation.

2.2.4 SYSTEM ORIENTATION ASSIGNMENT

To cover the entire CONUS, the required E-W scan is +- 3.5 degrees and the required N-S scan is +- 1.75 degrees. The effects of system orientation assignments were studied and shown in Figures 2.2-26 - 2.2-29. It was evident that the system offset plane should be assigned North-South to minimize the sub-dish as well as the array size needed.

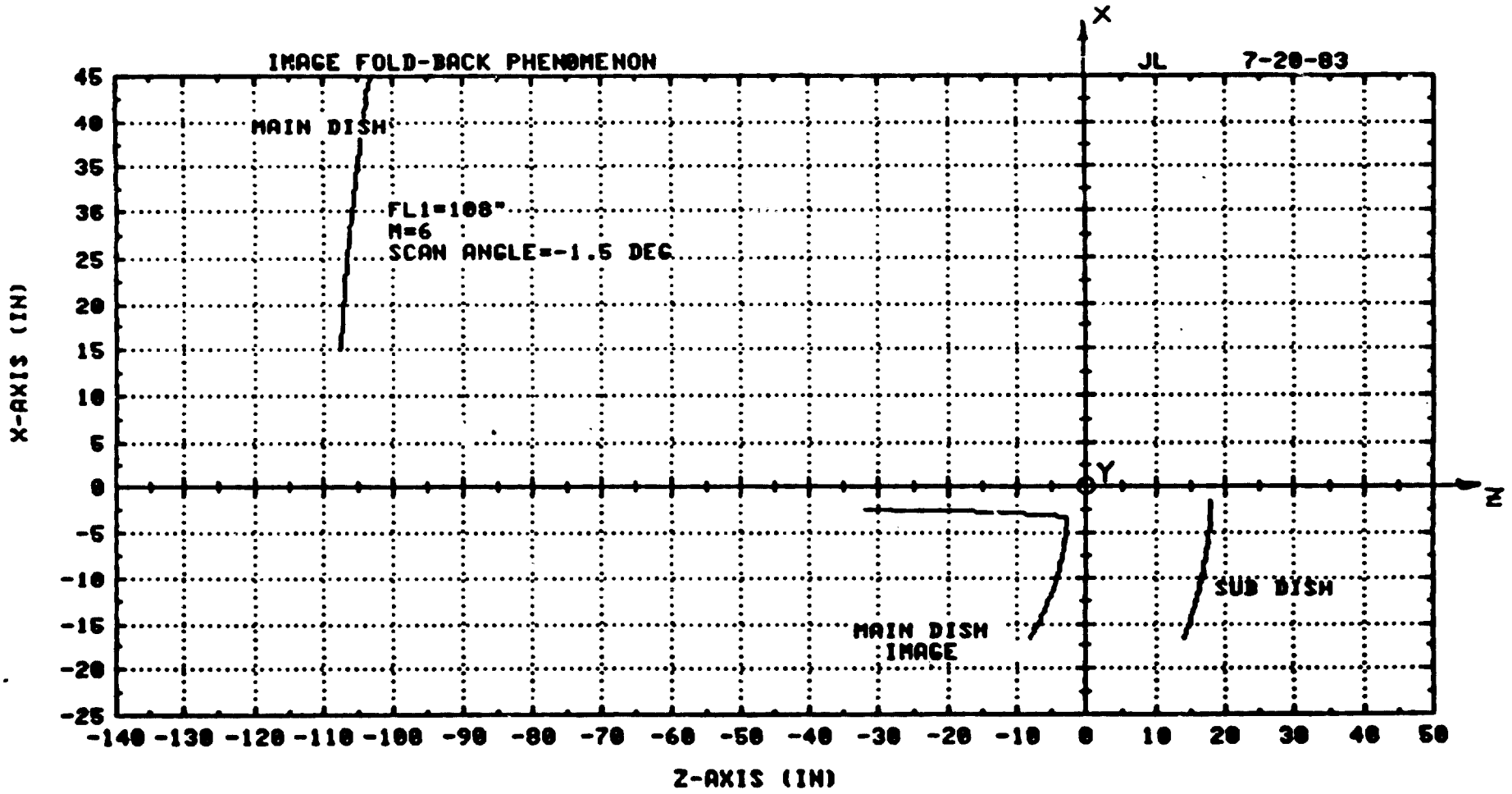

FIG. 2.1-20 IMAGE FOLD-BACK IMPOSES MIN. OFFSET REQUIREMENT OF MAIN DISH

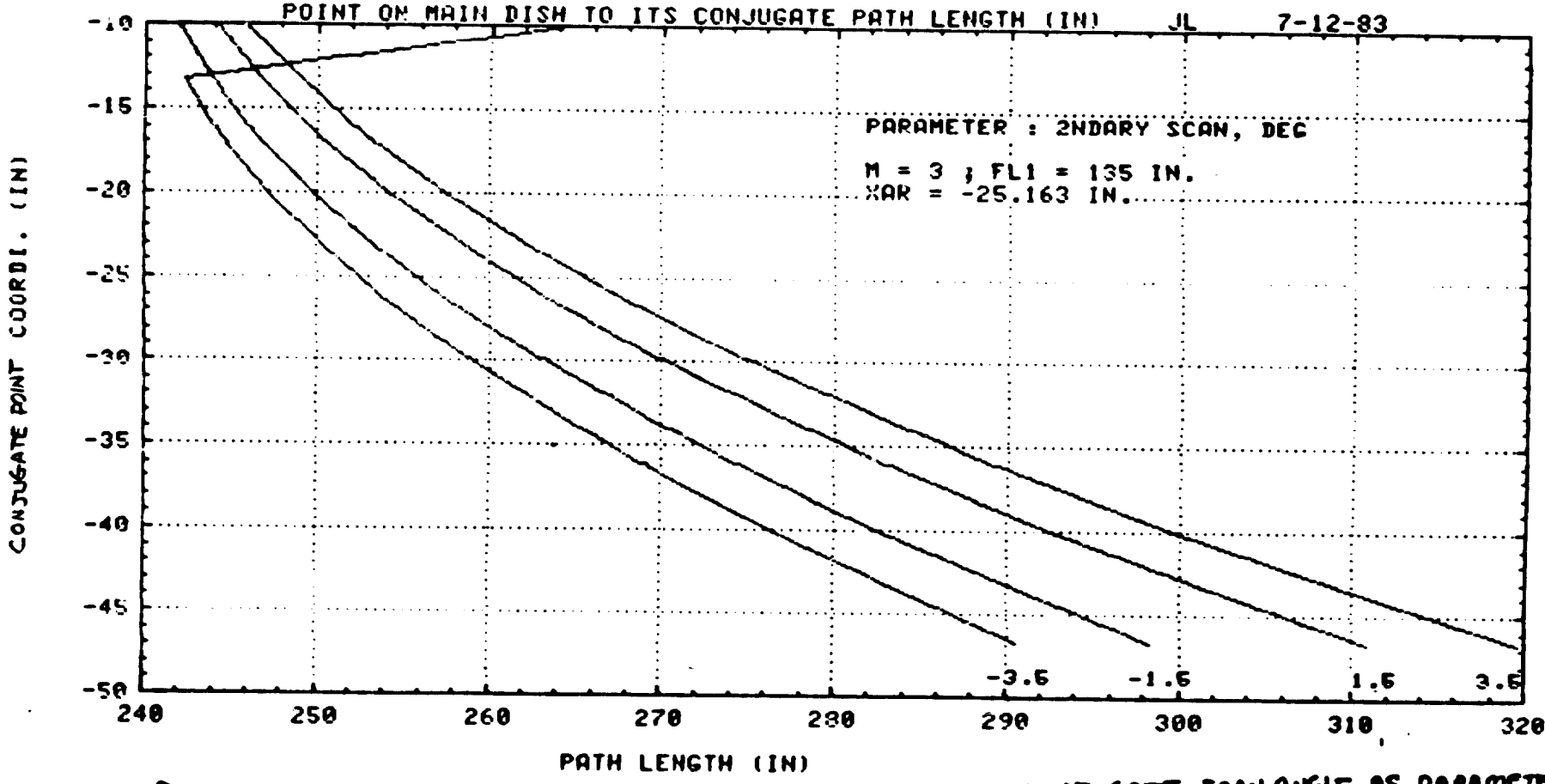

FIG. 22-21 PATH LENGTH FROM PT. A ON MAIN DISH TO ITS CONJUGATE, SCAN ANGLE AS PARAMETER

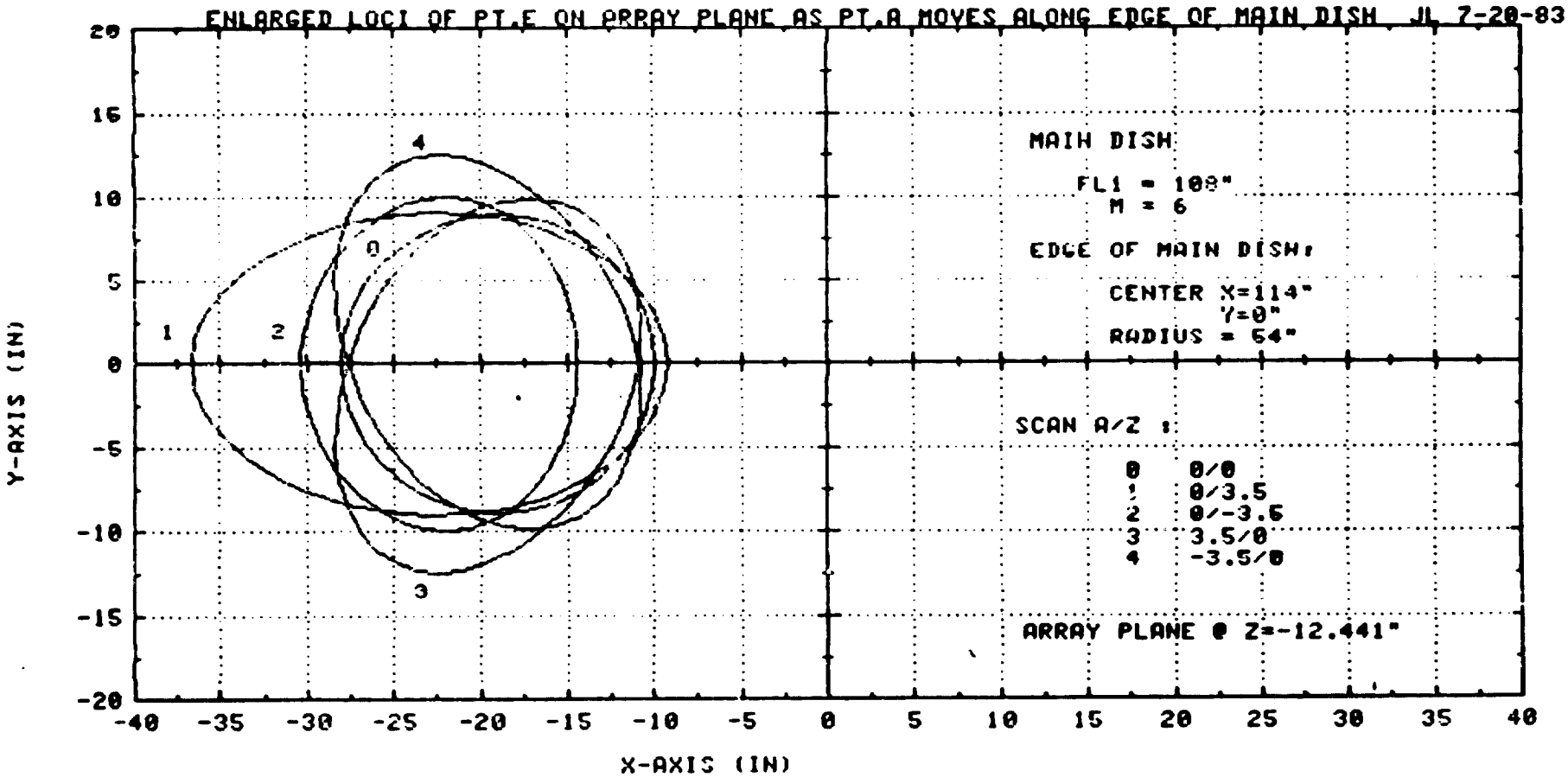

FIG. 2.2-22 ENLARGED VIEW OF THE MAIN DISH IMAGE ON THE ARRAY PLANE, Z=-12.441

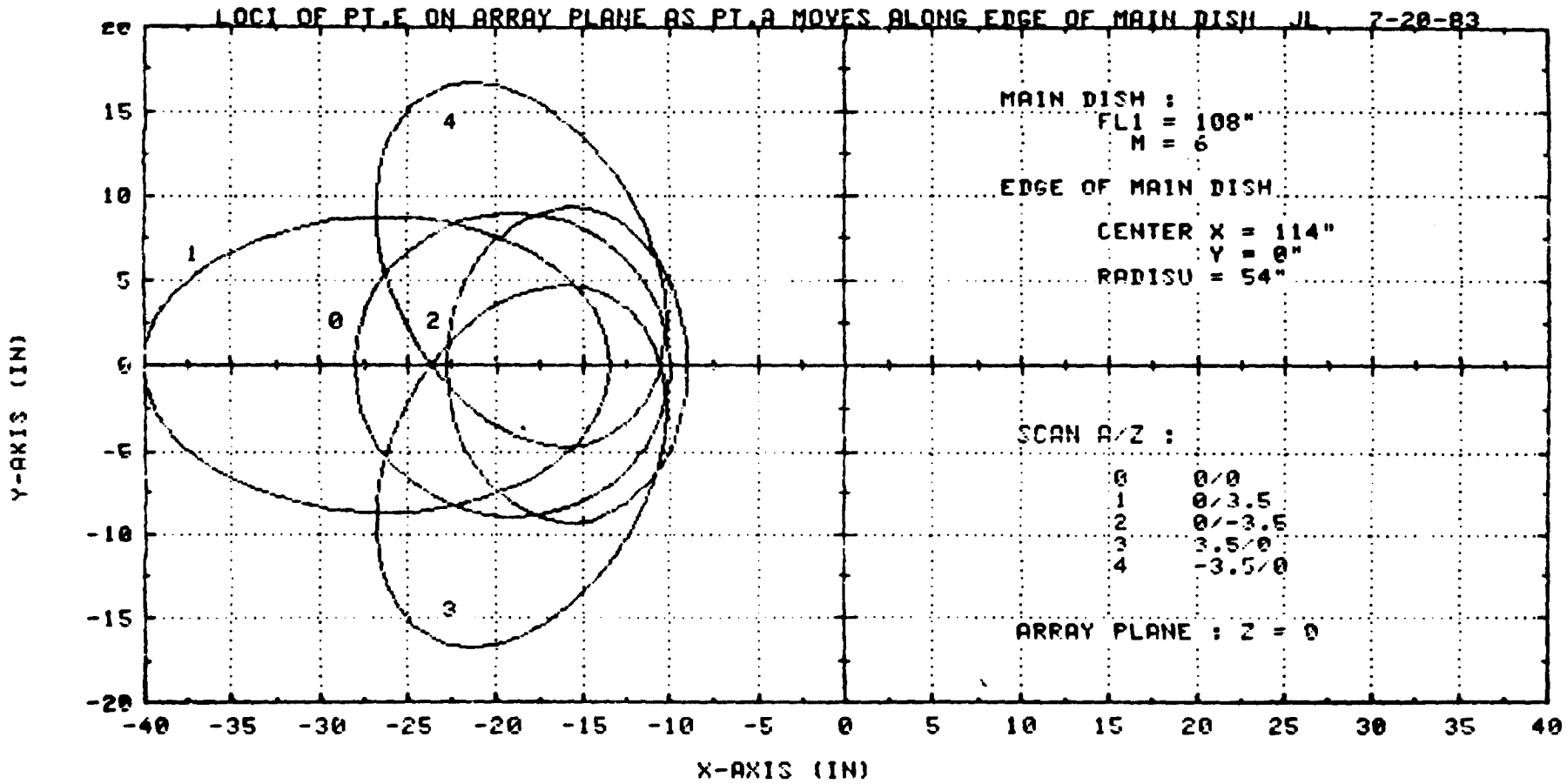

FIG 2.2-23 MAIN DISH IMAGE ON THE ARRAY PLANE, Z = 0

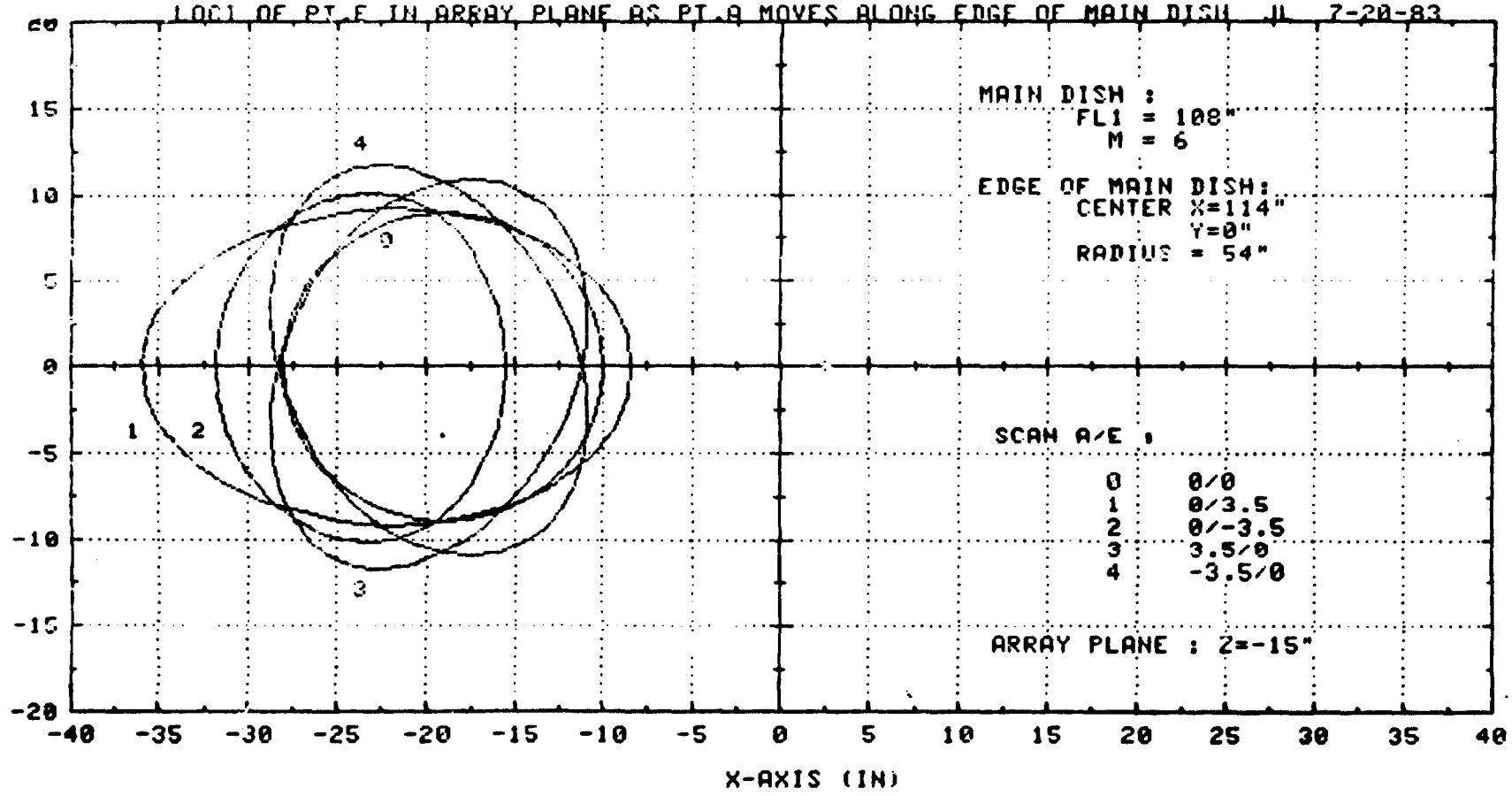

FIG 2.2-24 MAIN DISH IMAGE ON THE ARRAY PLANE, Z=-15"

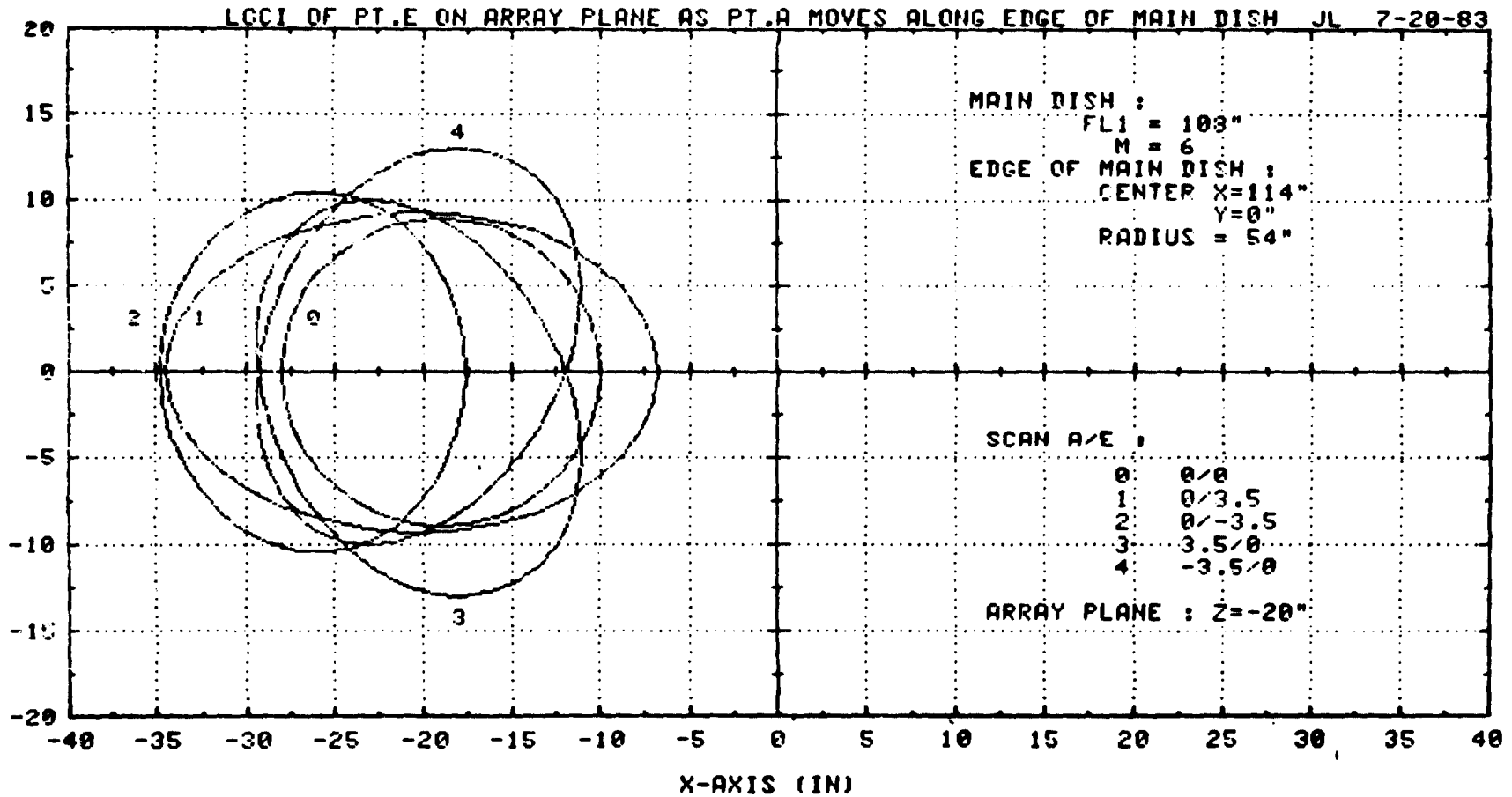

FIG.2.2-25 MAIN DISH IMAGE ON THE ARRAY PLANE, $Z = -20"$

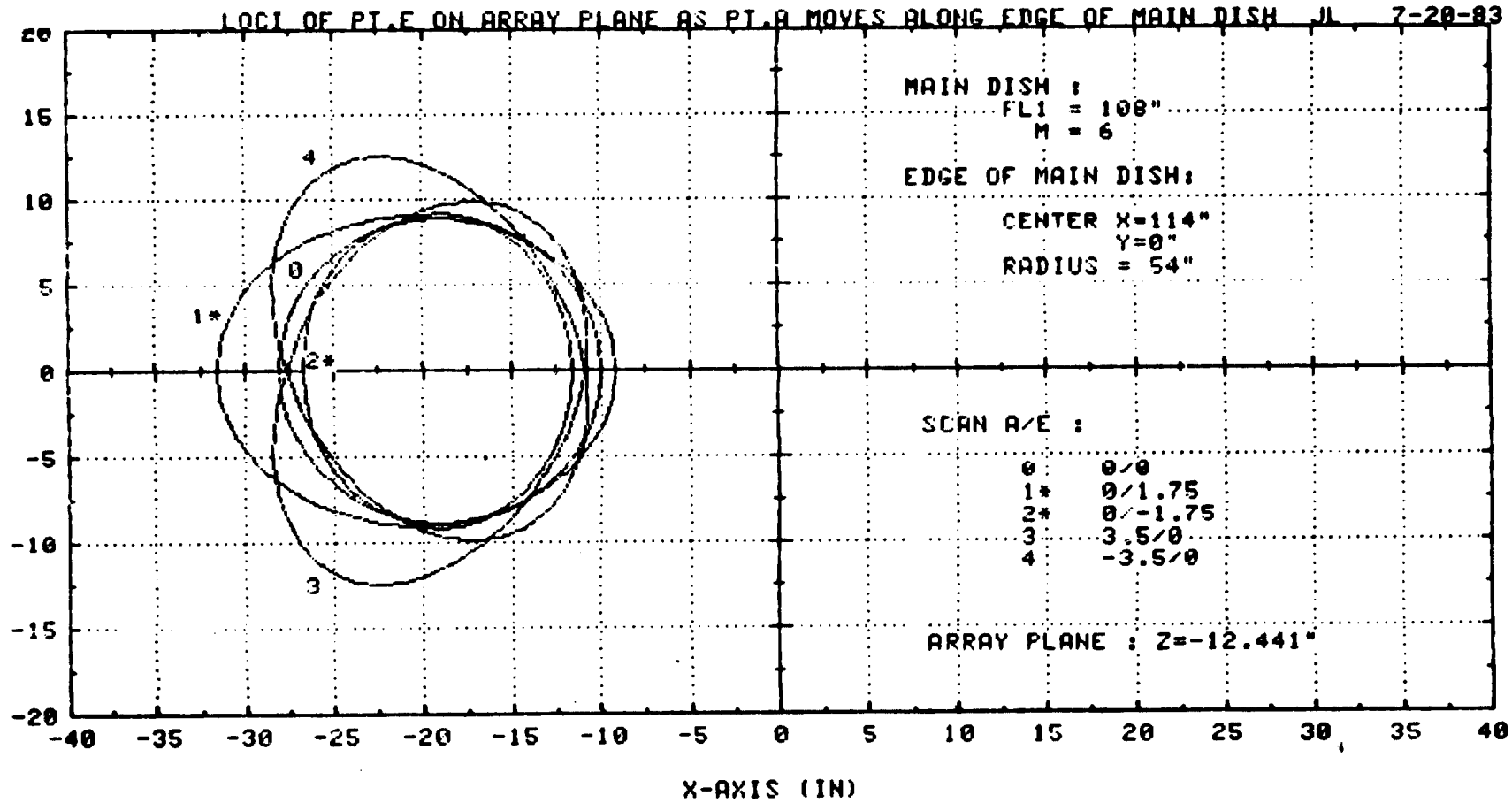

FIG. 2.2-26 SYSTEM ORIENTATION SELECTION : OFFSET PLANE — NS (ARRAY PLANE IMAGE)

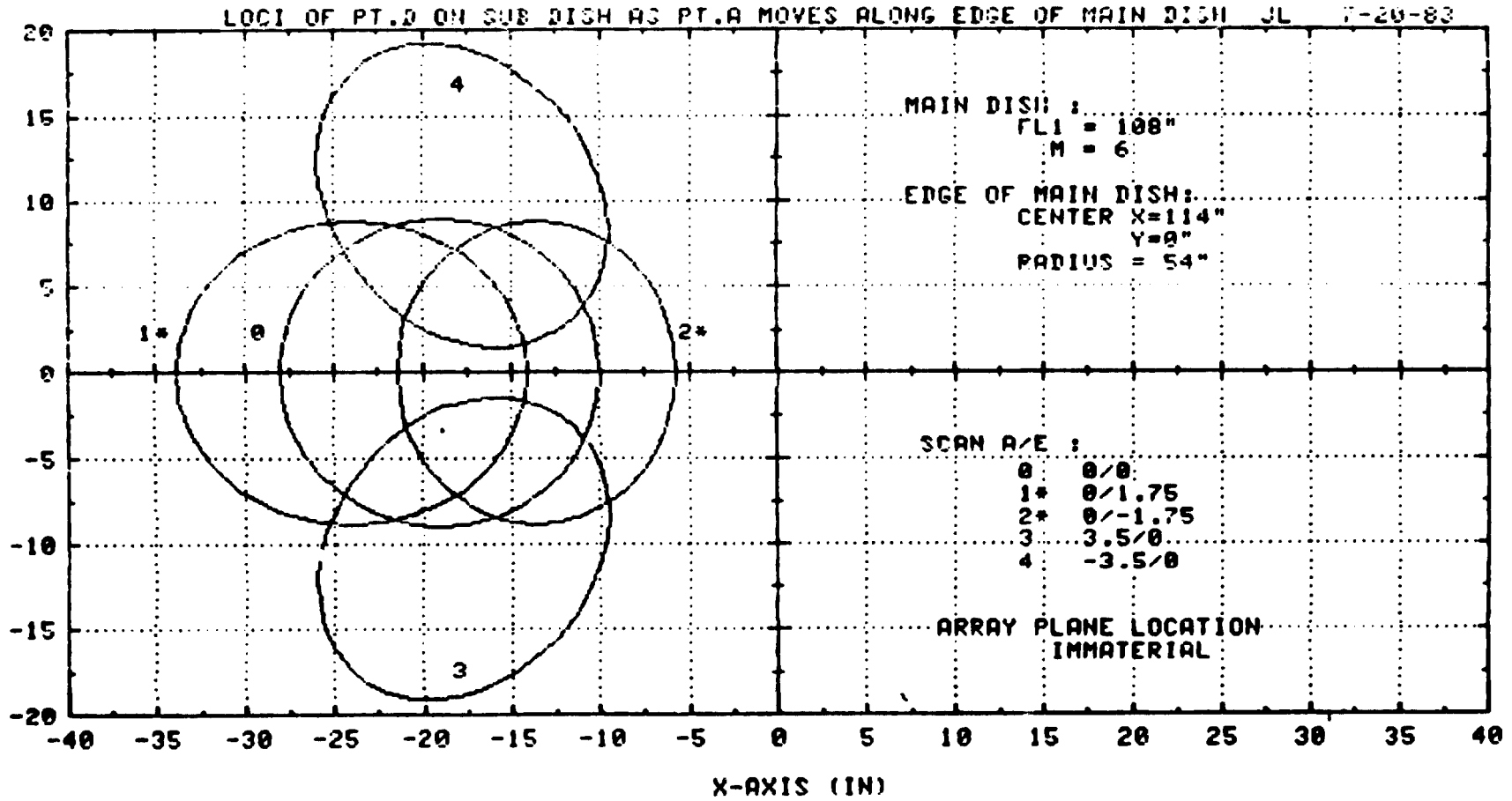

FIG 2.2-11 SYSTEM ORIENTATION SELECTION : OFFSET PLANE — NS (IMAGE ON SUB DISH)

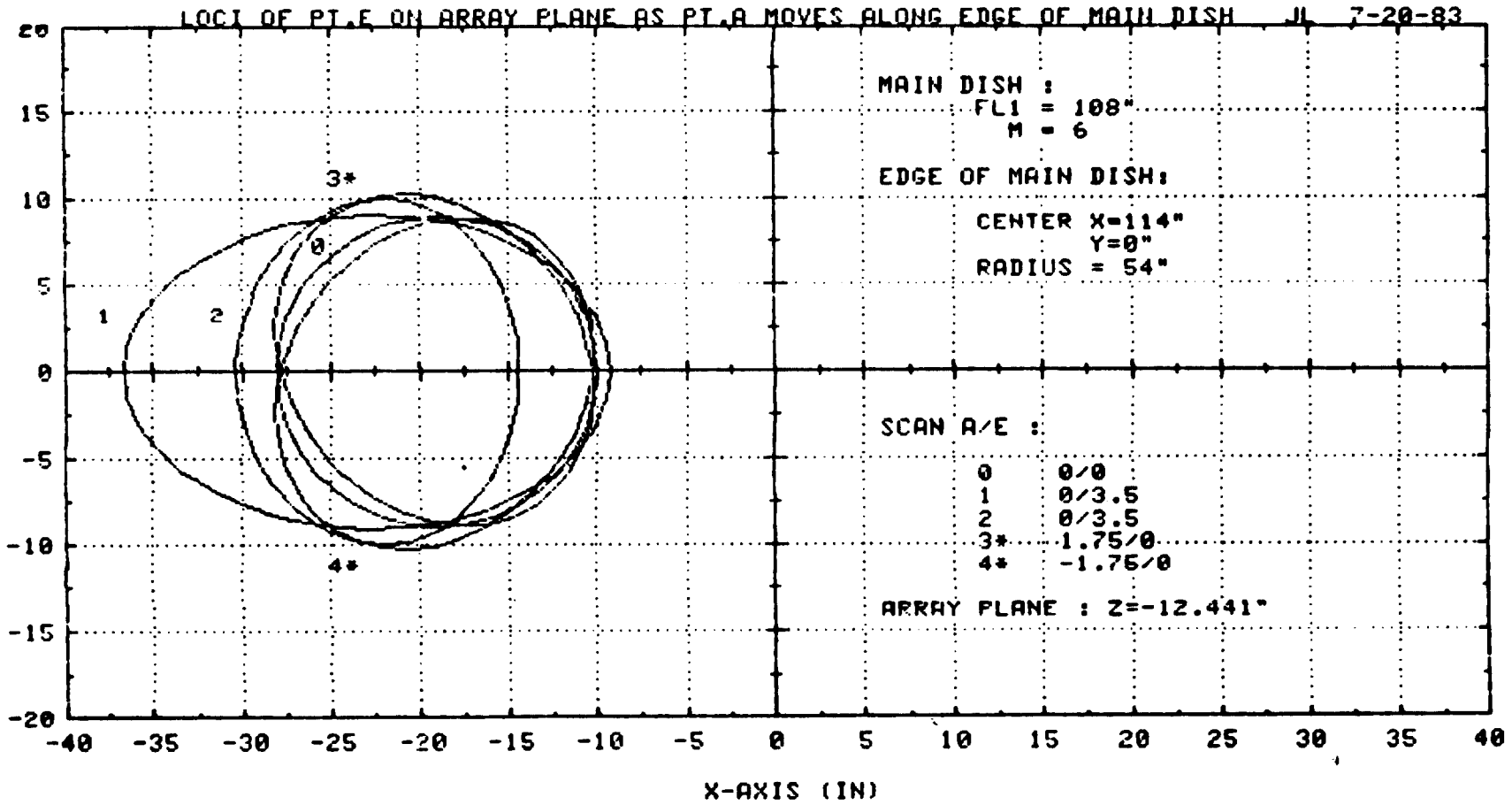

FIG.2.2-28 SYSTEM ORIENTATION SELECTION: OFFSET PLANE — EW (ARRAY PLANE IMAGE)

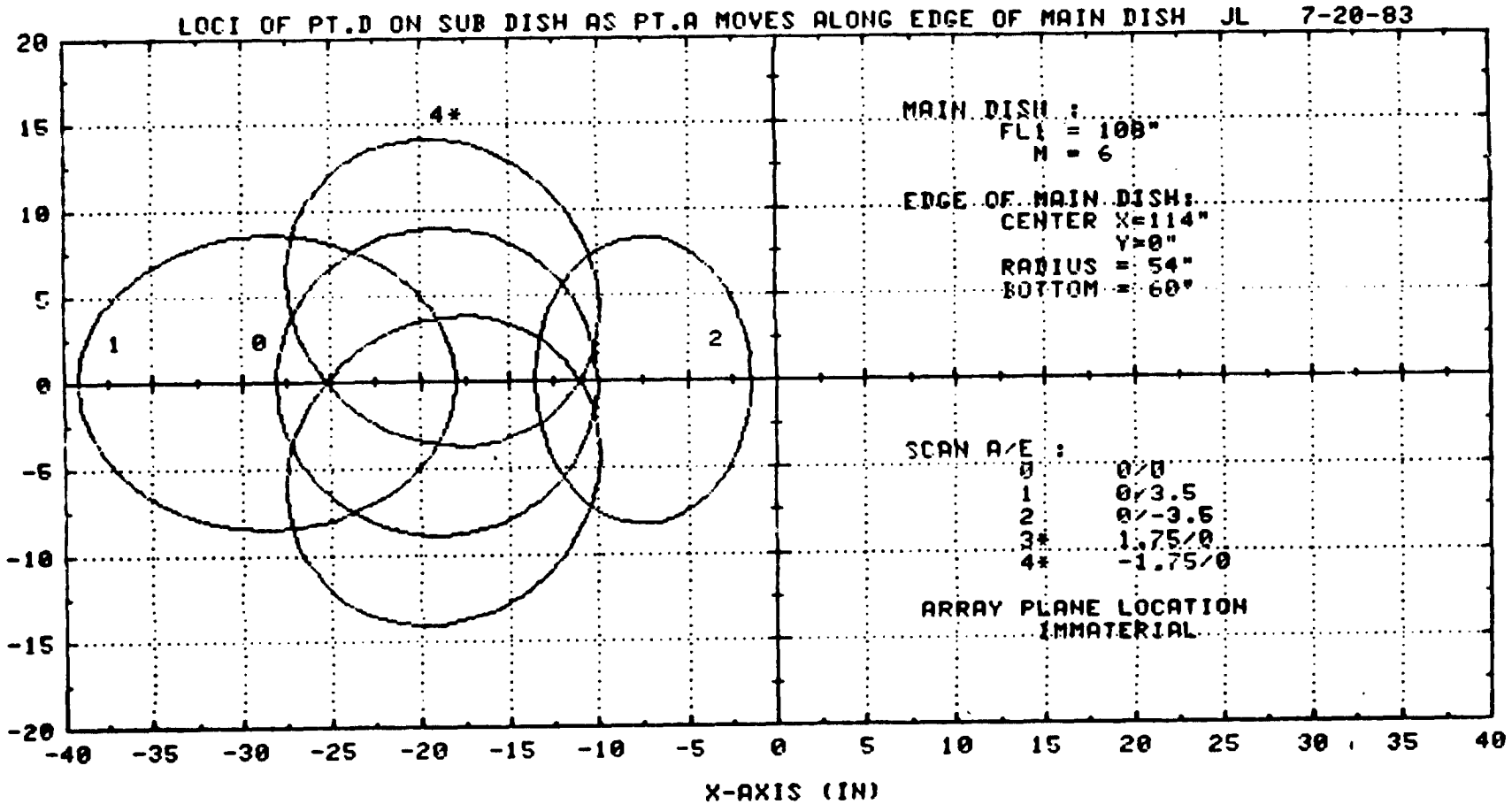

FIG. 2.2-29 SYSTEM ORIENTATION SELECTION: OFFSET PLANE — EW (IMAGE ON SUB DISH)

SECTION 3

DETERMINATION OF PHASED ARRAY SYSTEM

3.1 ARRAY CONFIGURATION STUDY

3.1.1 DEFINITION OF ARRAY TYPE

Before a tradeoff of the MMIC parameters can be made the phased array system must be determined. The primary concern with setting up the array system is the location of the grating lobes. Basically the grating lobe location is a function of the element spacing as well as the array packaging. From the expression relating the element spacing and the grating lobe location, it can be determined that as the element spacing decreases, the angle at which the grating lobe will occur becomes larger. As the array is scanned this grating lobe moves toward the main lobe. The extent to which the grating lobe will converge is dependent upon the scan angle and the element packaging. Since it is desirable to minimize the number of elements, the element spacing should be chosen such that the grating lobes do not impinge on the subreflector for the array scan angles required for CONUS coverage. There are three basic array configurations which can be specified namely a rectangular array, a circular array or a hexagonal array. In this study a rectangular array was not considered due to the regularity of the lattice structure as well as the loose packing of the elements, both of which tend to cause the grating lobes to move in towards the main lobe.

Several circular configurations were investigated. Although the circular configuration tends to have loosely packed elements, a randomness can be added to the structure by specifying the starting location of each ring as well as the spacing between the rings. This random nature will tend to suppress the grating lobes thus making a circular configuration a viable candidate. Two configurations were investigated. The first was a 13 ring setup utilizing a .72 inch (1.825 wavelength) element spacing. This configuration is shown in Figure 3.1-1. (This pattern as well as other array far field patterns are located in Appendix A). The far field pattern for an unscanned beam is plotted in Figure 3.1-2. For an array scan of 21 degrees which corresponds to an approximate secondary scan of 3.5 degrees, the array far field pattern is shown in Figure 3.1-3. A 16 ring circular configuration was also investigated. A .59 inch (1.5 wavelength) element spacing was implemented in this set-up. This configuration is shown in Figure 3.1-4. The array far field pattern is plotted for the unscanned case in Figure 3.1-5. For a 21 degree array scan the far field pattern is shown in Figure 3.1-6.

Two hexagonal and one modified hexagonal array configurations were also analyzed. Due to the dense packing of elements afforded by this set-up, the hexagonal array becomes the prime candidate, in that the grating lobes of a tightly packed array will tend to move away from the main lobe. The first configuration which was investigated was a 13 ring hex array with .72 inch (1.825 wavelength spacing). This set-up is depicted in Figure 3.1-7. The unscanned array pattern corresponding to this configuration is plotted in Figure 3.1-8. For an array scan angle of 21 degrees the far field pattern is found in Figure 3.1-9.

A 16 ring hexagonal array was also considered. The element spacing for the array was .59 inches (1.5 wavelengths). This set-up is shown in Figure 3.1-10. The unscanned array pattern and a 21 degree scanned array pattern are plotted in

Figures 3.1-11 and 3.1-12., respectively.

A 20 ring hexagonal array modified to fit into a circular aperture was also analyzed. This configuration is shown in Figure 3.1-13. It was felt that the contribution of the corner elements in the hex array was minimal and they could therefore be eliminated without introducing adverse effects. The unscanned array pattern for this modified configuration is plotted in Figure 3.1-14. The array far field pattern for a beam scanned to 21 degrees is shown in Figure 3.1-15.

A composite plot of grating lobe location versus element spacing for the five configurations which were analyzed is shown in Figure 3.1-16 for an unscanned array beam and in Figure 3.1-17 for a beam scanned to 21 degrees. The peak gain within the angles subtended by the subreflector are plotted for a 0 degree scan and a 21 degree scan in Figures 1.3-18 and 1.3-19, respectively. The overall conclusion that can be made as a result of this investigation is that the 20 ring modified hexagonal array produces the best overall results. On the basis of this conclusion, this configuration was adopted as the baseline array type.

3.2 STUDY OF ARRAY TAPER

To achieve the required sidelobe levels an amplitude taper across the array will be required. Several functions for determining the proper array taper were investigated including a binomial function, a cosine to the n function and a Chebyshev function. A trade off of the above functions showed that all three produced similar results, thus the binomial function was chosen for determining taper levels.

Since the 20 ring hexagonal array modified to fit into a circular aperture was initially chosen as a baseline prior to this investigation, the major emphasis on the taper analysis was aimed at this configuration. Data on the 13 ring hex array and 16 ring hex array was also taken for trade off purposes. The far field array patterns for these two configurations are shown in Figures 3.2-1 through 3.2-6 for three different taper levels. The first case considered for the 20 ring modified hex array utilized 5 taper levels corresponding to the levels of MMIC amplification which are available. The array far field pattern for this case is found in Figure 3.2-7. The maximum sidelobe was found to be 30 dB down from peak for an unscanned pattern. It was decided that sidelobe levels of 40 dB down (minimum) would be required for an unscanned array to assure that the secondary pattern sidelobe levels remain below 30 dB down under all situations. Sidelobe degradation due to the optical system as well as phase shifter and amplifier variations and random component failures were considered in mandating this extra 10 dB margin. To generate data for the parametric study 16 taper levels and 26 taper levels were also analyzed. The unscanned far field array patterns for these two cases are plotted in Figures 3.2-8 and 3.2-9.

Curves of peak gain versus taper level and maximum sidelobe level versus taper level for all the cases considered are found in Figures 3.2-10 and 3.2-11, respectively. For the 20 ring modified hex, a 26 level taper was chosen, although a 16 level taper would probably prove to be adequate. A 26 level taper allows a beter fit to the binomial curve. The amplitude levels used (referenced to zero dB) as well as the diameter (in centimeters) at which the level assumes a new value is given in Table 3.2.1. Since only 5 amplification levels are available, additional tapering would have to be incorporated into the beam combining network.

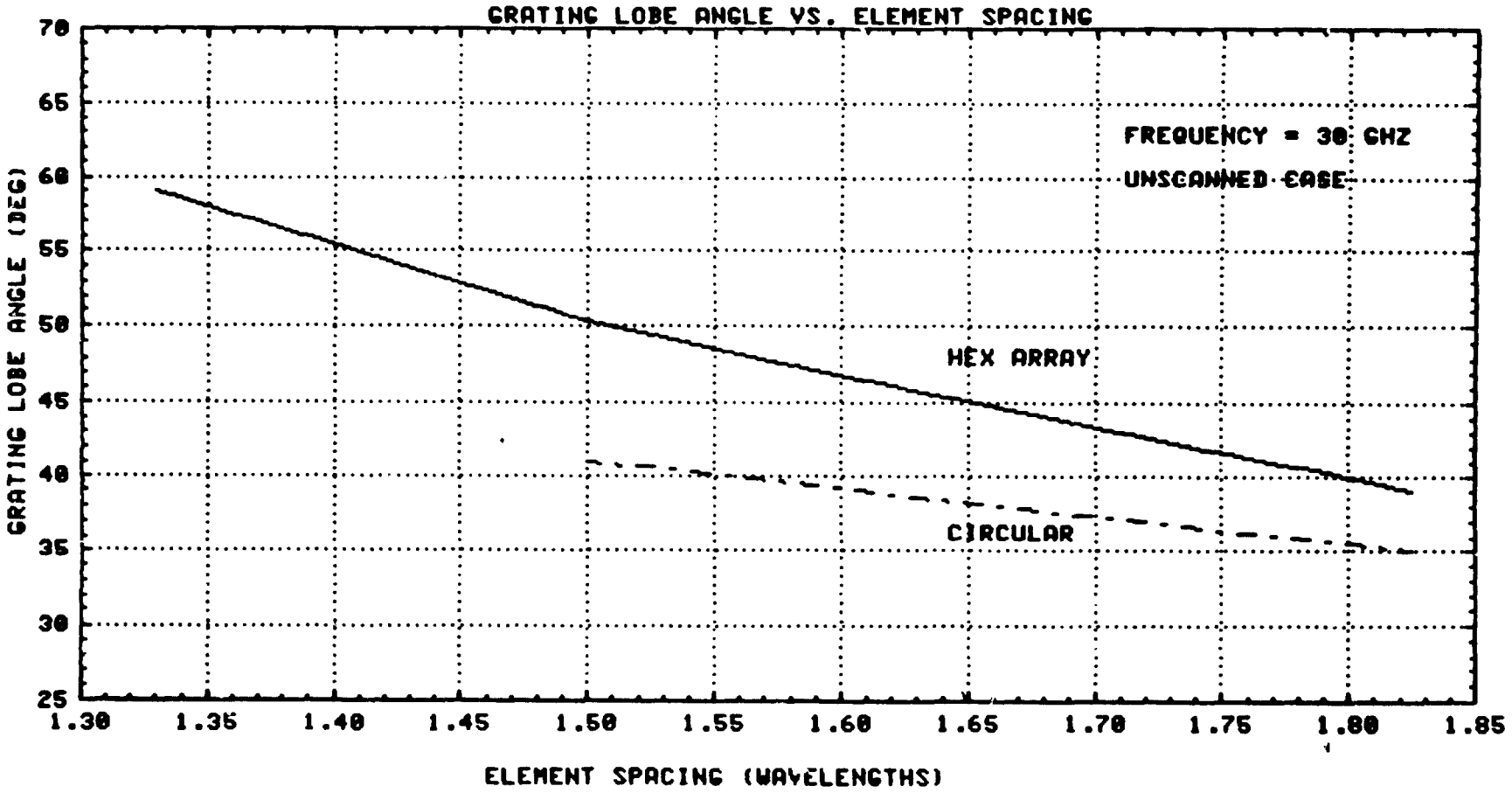

FIG. 3.1-16 UNSCANNED, GRATING LOBE LOCATION VS. SPACING

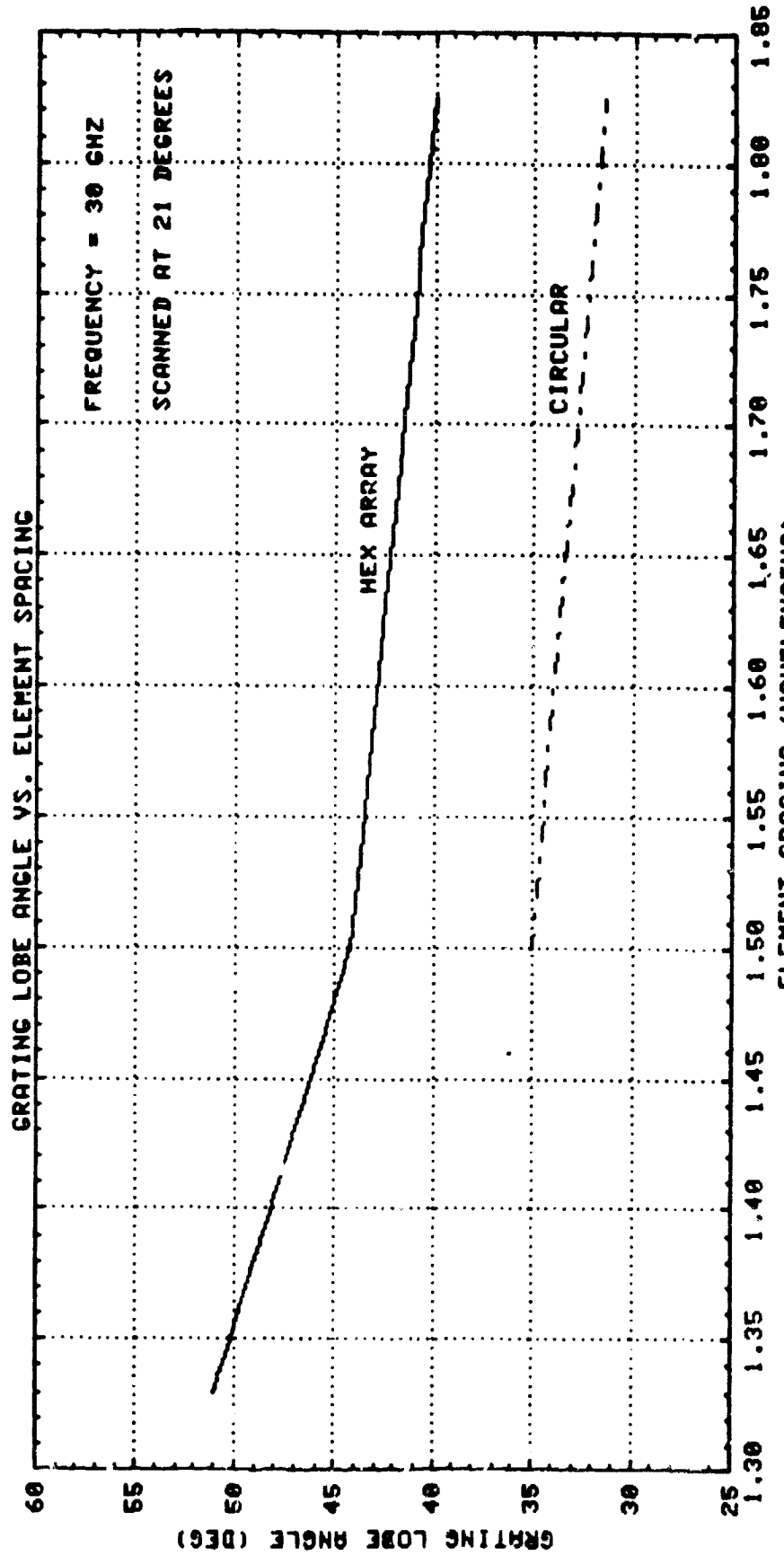
GRATING LOBE ANGLE VS. ELEMENT SPACING
FREQUENCY = 30 GHZ
SCANNED AT 21 DEGREES
HEX ARRAY
CIRCULAR
GRATING LOBE ANGLE (DEG)
60
55
50
45
40
35
30
25
1.30
1.35
1.40
1.45
1.50
1.55
1.60
1.65
1.70
1.75
1.80
1.85
ELEMENT SPACING (WAVELENGTHS)

FIG 3.1-17

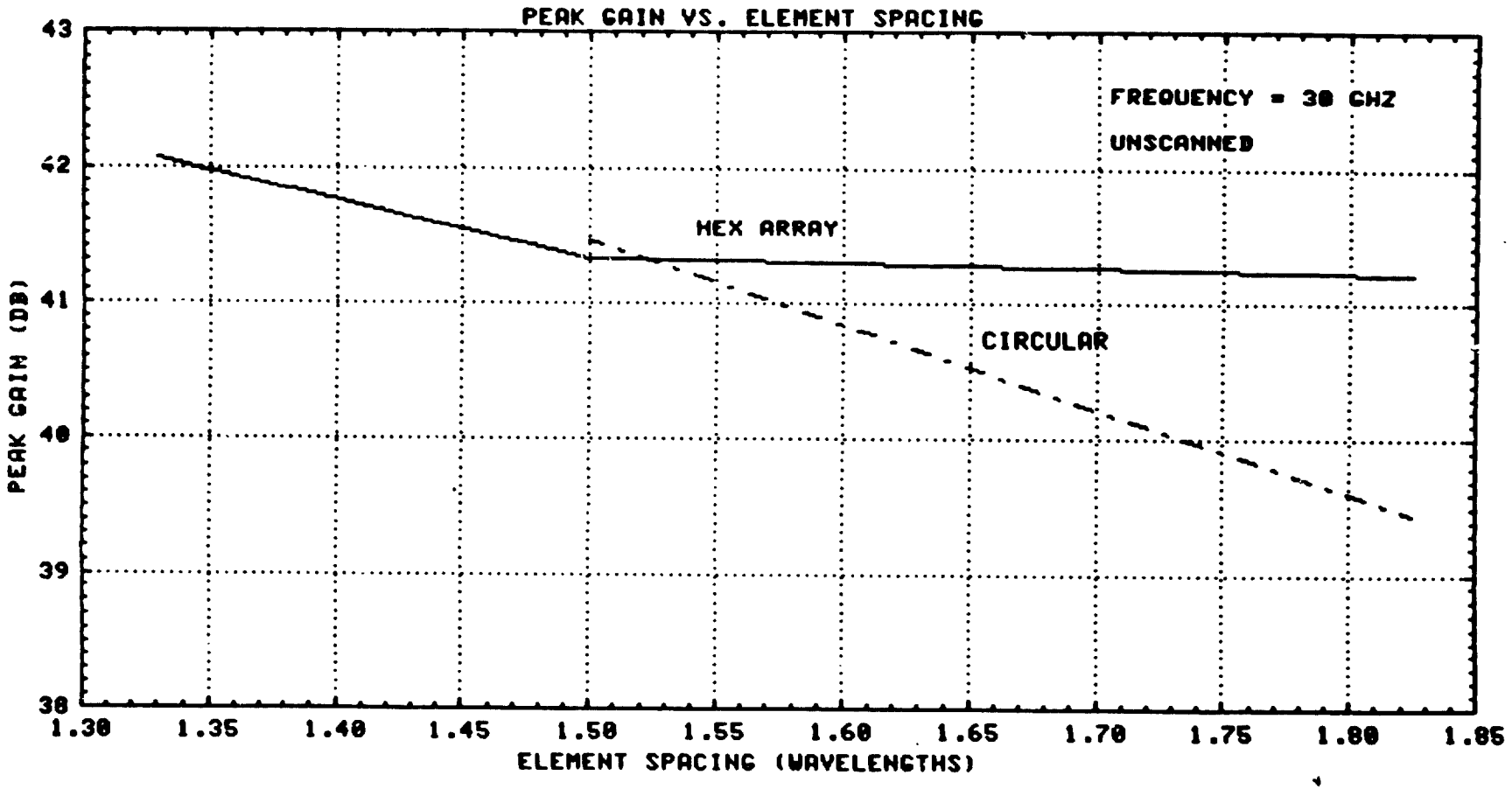
PEAK GAIN VS. ELEMENT SPACING
FREQUENCY = 30 GHZ
UNSCANNED
HEX ARRAY
CIRCULAR
PEAK GAIN (DB)
43
42
41
40
39
38
1.30
1.35
1.40
1.45
1.50
1.55
1.60
1.65
1.70
1.75
1.80
1.85
ELEMENT SPACING (WAVELENGTHS)

FIG. 3.1-18

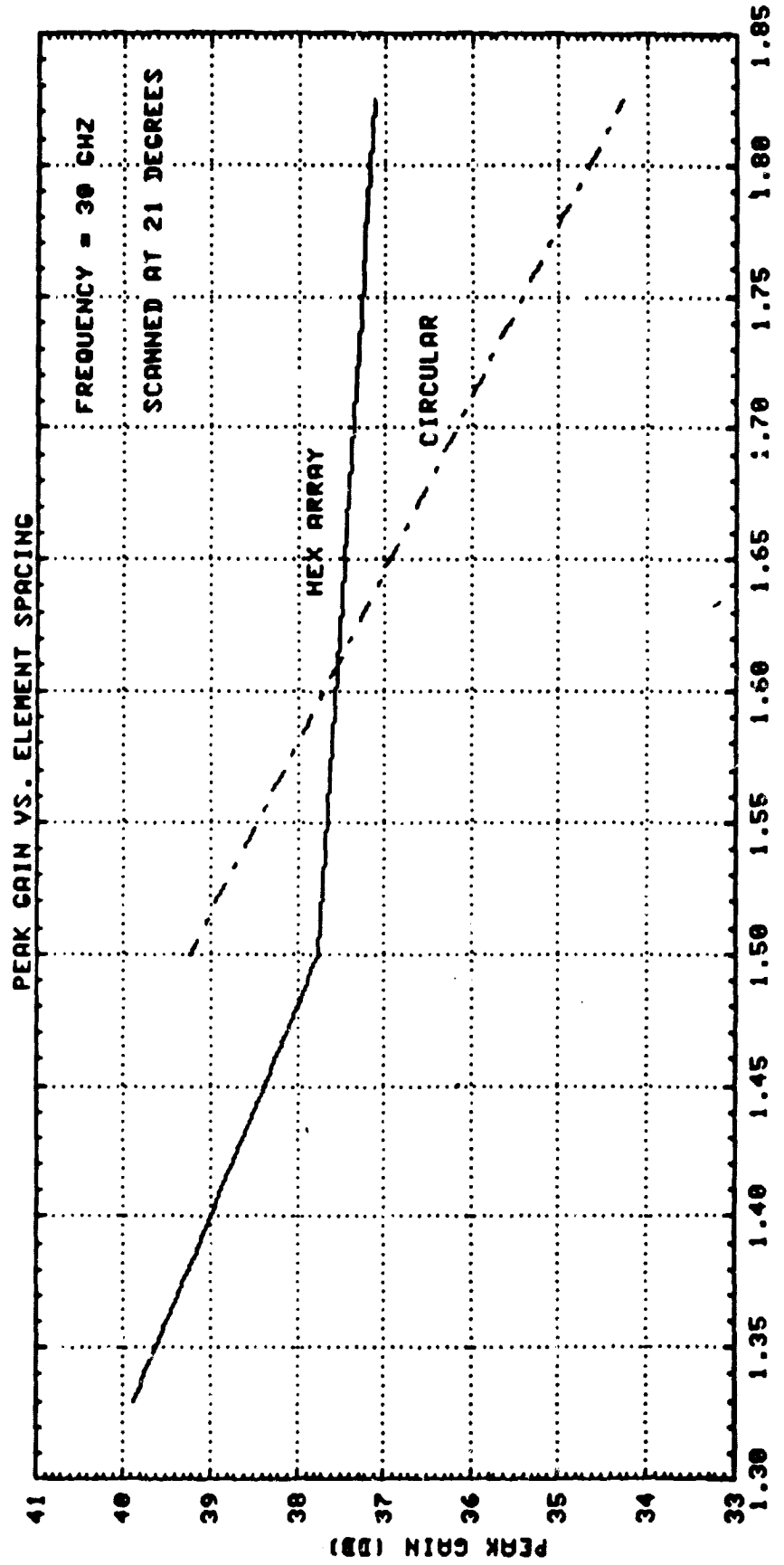
PEAK GAIN VS. ELEMENT SPACING
FREQUENCY = 30 GHZ
SCANNED AT 21 DEGREES
HEX ARRAY
CIRCULAR
PEAK GAIN (DB)
ELEMENT SPACING (WAVELENGTHS)
41
40
39
38
37
36
35
34
33
1.30
1.35
1.40
1.45
1.50
1.55
1.60
1.65
1.70
1.75
1.80
1.85

FIG. 3.1-19

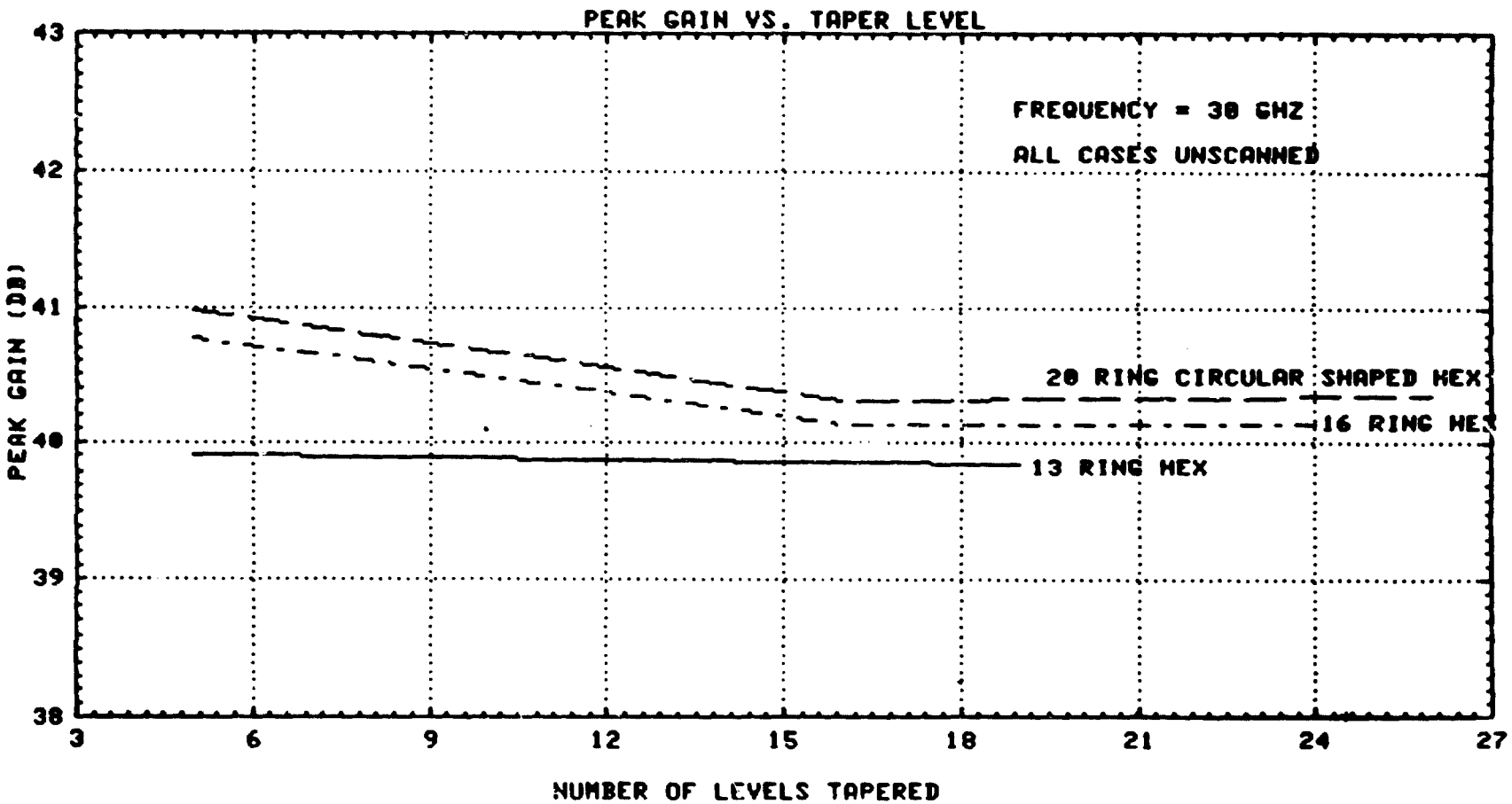
PEAK GAIN VS. TAPER LEVEL
FREQUENCY = 30 GHZ
ALL CASES UNSCANNED
20 RING CIRCULAR SHAPED HEX
16 RING HEX
13 RING HEX
PEAK GAIN (DB)
NUMBER OF LEVELS TAPERED
43
42
41
40
39
38
3
6
9
12
15
18
21
24
27

Fig 3.2-10

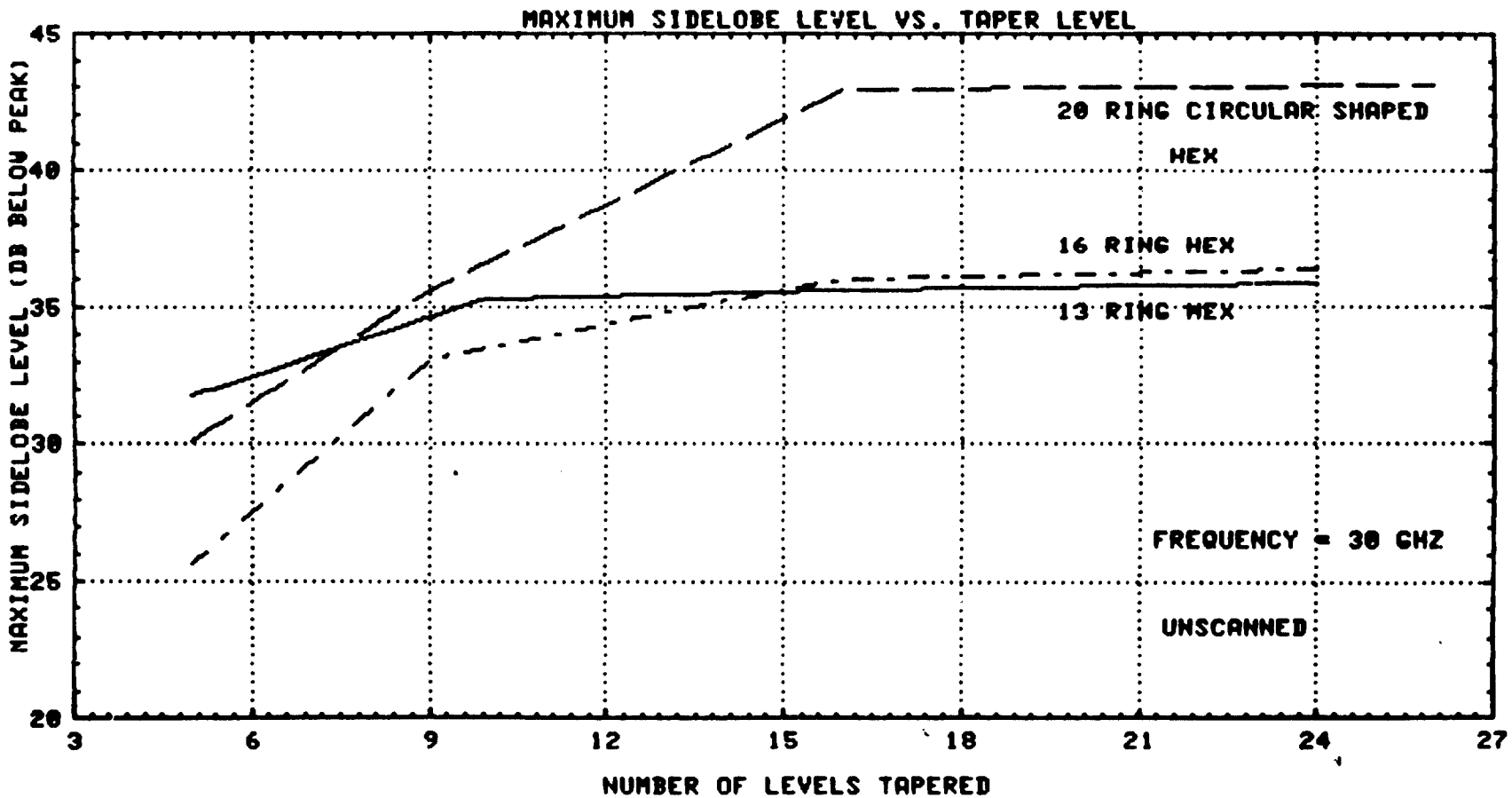
MAXIMUM SIDELOBE LEVEL VS. TAPER LEVEL
MAXIMUM SIDELOBE LEVEL (DB BELOW PEAK)
45
40
35
30
25
20
3
6
9
12
15
18
21
24
27
NUMBER OF LEVELS TAPERED
20 RING CIRCULAR SHAPED
HEX
16 RING HEX
13 RING HEX
FREQUENCY = 30 GHZ
UNSCANNED

FIG. 3.2-11

TABLE 3.2-1 TAPER LEVELS FOR CIRCULAR SHAPED 20 RING MODIFIED HEX ARRAY

Level #	dB Level	Diameter of Taper Level (cm)
1	-.054	2.7
2	-.163	4.7
3	-.218	5.4
4	-.493	8.1
5	-.660	9.3
6	-.885	10.8
7	-1.401	13.5
8	-1.518	14.0
9	-2.050	16.2
10	-2.783	18.7
11	-2.845	18.9
12	-3.802	21.5
13	-4.532	23.3
14	-4.941	24.2
15	-6.287	27.0
16	-6.877	28.0
17	-7.870	29.6
18	-9.721	32.3
19	-9.970	32.6
20	-11.863	35.0
21	-13.918	37.3
22	-14.280	37.7
23	-16.824	40.4
24	-18.215	42.0
25	-19.036	43.0
26	-20.000	46.0

SECTION 4

CONSIDERATION OF MMIC COMPONENTS

4.1 MMIC ANALYSIS OVERVIEW

The performance of solid state components in electronically scanned systems plays a crucial role in analyzing the overall system behavior. The major factors to be considered in the investigation of electronic components include phase quantization, phase shifter errors, phase shifter failures, amplifier fluctuations, and random amplifier failures. The next five sections are devoted to summarizing information that was collected while analyzing the above topics. In these sections a 13 ring hexagonal array with a 19 level taper, a 16 ring hexagonal array with 24 taper levels and a 20 ring hexagonal array (modified to fit into a circular aperture) with 26 taper levels are used for trade off purposes.

4.2 PHASE SHIFTER ANALYSIS

4.2.1 PHASE QUANTIZATION

Phase quantization plays a major role in determining array scan angle resolution. As more phase bits are used, descrete phase settings will more closely match a continuous phase taper across an aperture thereby giving higher resolution. A good correlation between the ideal phase distribution and the quantized phases will also tend to produce higher peak gains and lower sidelobes at scanned angles. For tradeoff purposes a 3 bit, 5 bit and a 6 bit phase shifter were analyzed. A 10 degree and a 21 degree array scan angle were investigated. The information obtained from this analysis is plotted in Figures 4.2.1-4.2.4. The corresponding array far field plots are given in Figures 4.2.5-4.2.23.

4.2.2 PHASE SHIFTER ERROR

Variations among phase shifter units will tend to have a degrading effect on peak gain and sidelobe performance. It is therefore important to determine the amount of error that can be tolerated while still maintaining the required system performance. Plots of peak gain and maximum sidelobe level versus random phase error are plotted in Figures 4.2.23 and 4.2.24. The corresponding array far field patterns are shown in Figures 4.2.25-4.2.33. As can be seen, the array gain is relatively unaffected by these perturbations were as the sidelobe levels are quite sensitive.

4.2.3 PHASE SHIFTER FAILURE

One of the attributes of an electronically scanned system is graceful degradation. From a system reliability viewpoint, the analysis of random phase shifter failures becomes quite important. In analyzing these random failures it is important to determine how many failures can be tolerated while still maintaining the required peak gain and sidelobe levels.

In this investigation 3, 5 and 8 random phase shifter failures were considered for an unscanned case as well as a 10 degree and a 21 degree array scan. Plots of peak gain and maximum sidelobe level versus number of random failures are located in

Figures 4.2.34-4.2.39 for the 0, 10, and 21 degree array scan angles respectively. The array far field patterns used in deriving this information are shown in Figures 4.2.40-4.2.67. Again the peak gain does not degrade notably for the cases considered, where as the sidelobe level is directly related to the number of failures.

4.2.4 RANDOM AMPLITUDE ERROR

In addition to the random phase errors discussed earlier, random amplitude errors can also play a major role in system performance. Variations in manufacturnig as well as in materials will cause fluctuations in amplifier performance. These perturbations will in general, affect the peak gain and sidelobe performance. To analyze the effects of there variations, a 0%, 5% and 10% uniformly distributed zero mean error function was used. In addition to the configurations mentioned above, a 13 ring hex array with 16 taper levels, a 16 ring hex array with 16 taper levels, and a modified 20 ring hex array with 16 taper levels were considered. Plots of peak gain and maximum sidelobe level as a function of amplitude error for all configurations are given in Figures 4.2.68 and 4.2.69, respectively. Both gain and sidelobe level appear to be insensitve to these random perturations for the unscanned case. The array far field patterns used in obtaining this information are found in Figures 4.2-70 through 4.2-87.

4.2.5 RANDOM AMPLIFIER FAILURES

In analyzing graceful degradation, random amplifier failures must also be considered. As in all cases previously discussed, the primary concerns when investigating these random failures are peak gain and sidelobe levels. The objective here is to determine the number of random amplifier failures that can occur while maintaining reasonable gain with relatively low side lobes. In this analysis 3, 7, 10 and 50 random failures were considered for a 0, 10 and 21 degree array scan. A summary of this analysis is contained in Figures 4.2-88 through 4.2-93. The array patterns from which this information was obtained can be found in Figures 4.2-94 through 4.2-129. As can be seen from the summary plots, both the gain and the sidelobe level are dependent on the number of amplifier failures. It is worth noting that 50 failures represent approximately 10% of the elements in the 13 ring case and about 5% of the elements in the 20 ring case.

4.3 FREQUENCY EFFECTS

The behavior of the array as a function of frequency must be considered in analyzing the system performance. Once again peak gain and sidelobe levels are the primary factors to be considered. For this investigation a Y-polarized circular aperture served as the feed element. The feed was modelled at 30 GHz. An analysis of the array performance was done for a 0 degree, 10 degree, and 21 degree array scan angle. A 27.5 to 30 GHz frequency band was considered. The peak gain and maximum sidelobe information derived from this analysis is summarized in Figures 4.3.1 through 4.3.6. As can be seen both the gain and the side lobes become more frequency sensitive as the array scan angle is increased. The array patterns used to obtain this information are shown in Figures 4.3.7 through 4.3.33.

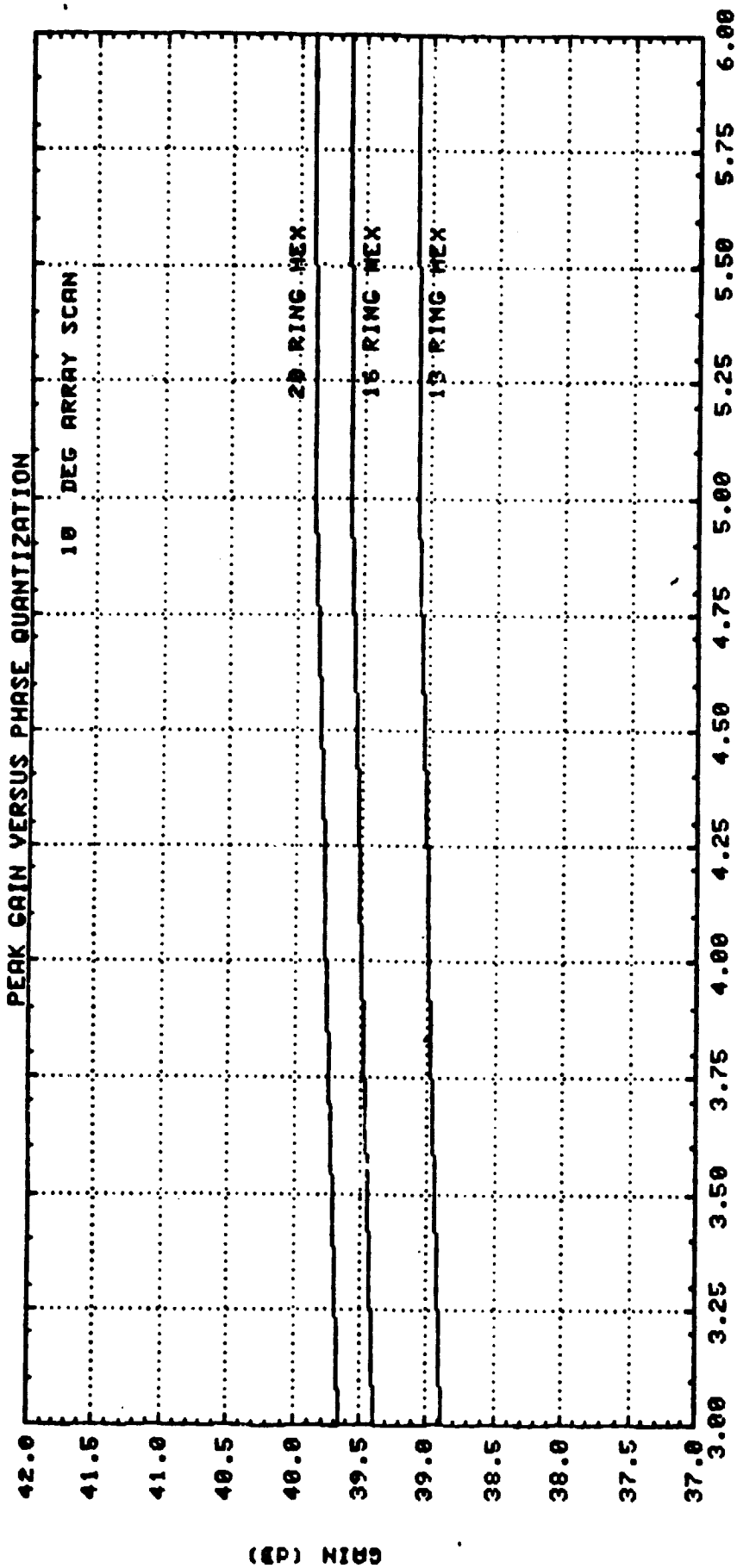
PEAK GAIN VERSUS PHASE QUANTIZATION
10 DEG ARRAY SCAN
20 RING HEX
15 RING HEX
13 RING HEX
GAIN (dB)
42.0
41.5
41.0
40.5
40.0
39.5
39.0
38.5
38.0
37.5
37.0
3.00
3.25
3.50
3.75
4.00
4.25
4.50
4.75
5.00
5.25
5.50
5.75
6.00
PHASE QUANTIZATION (BITS)

FIGURE 4.2-1

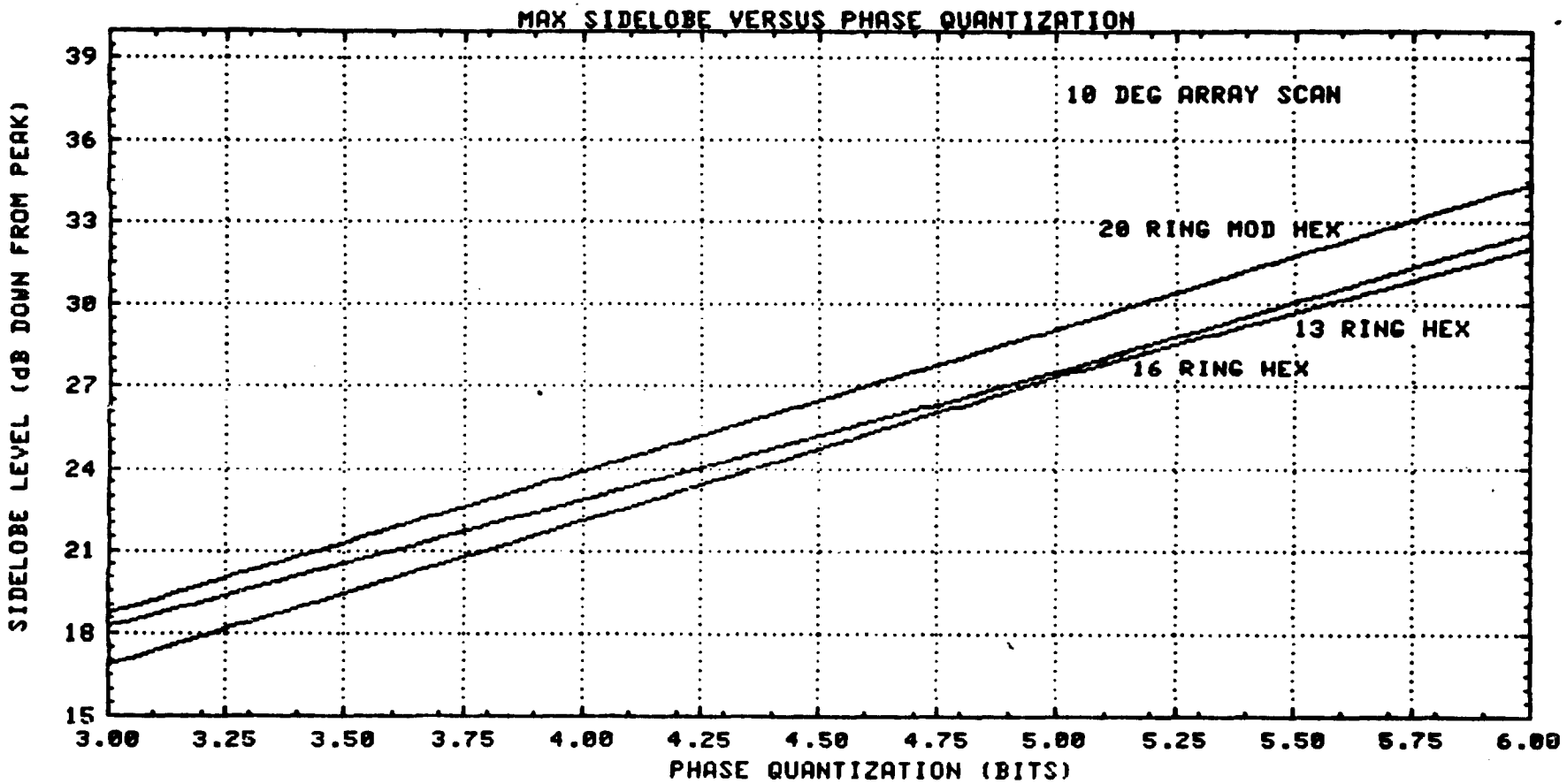
MAX SIDELOBE VERSUS PHASE QUANTIZATION
10 DEG ARRAY SCAN
20 RING MOD HEX
13 RING HEX
16 RING HEX
SIDELOBE LEVEL (dB DOWN FROM PEAK)
39
36
33
30
27
24
21
18
15
3.00
3.25
3.50
3.75
4.00
4.25
4.50
4.75
5.00
5.25
5.50
5.75
6.00
PHASE QUANTIZATION (BITS)

FIGURE 4.2-2

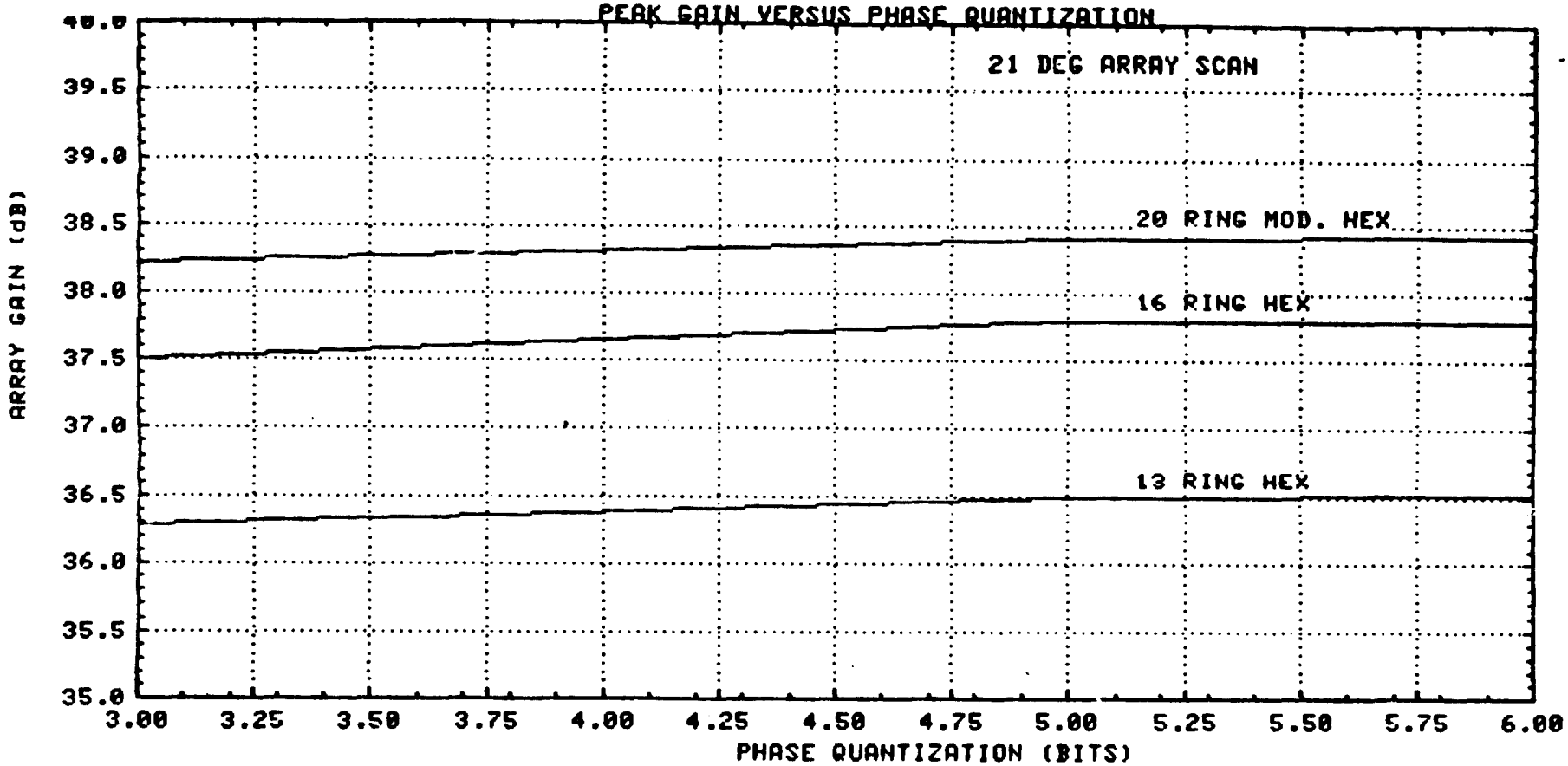
PEAK GAIN VERSUS PHASE QUANTIZATION
21 DEG ARRAY SCAN
20 RING MOD. HEX
16 RING HEX
13 RING HEX
ARRAY GAIN (dB)
40.0
39.5
39.0
38.5
38.0
37.5
37.0
36.5
36.0
35.5
35.0
3.00
3.25
3.50
3.75
4.00
4.25
4.50
4.75
5.00
5.25
5.50
5.75
6.00
PHASE QUANTIZATION (BITS)

FIGURE 4.2-3

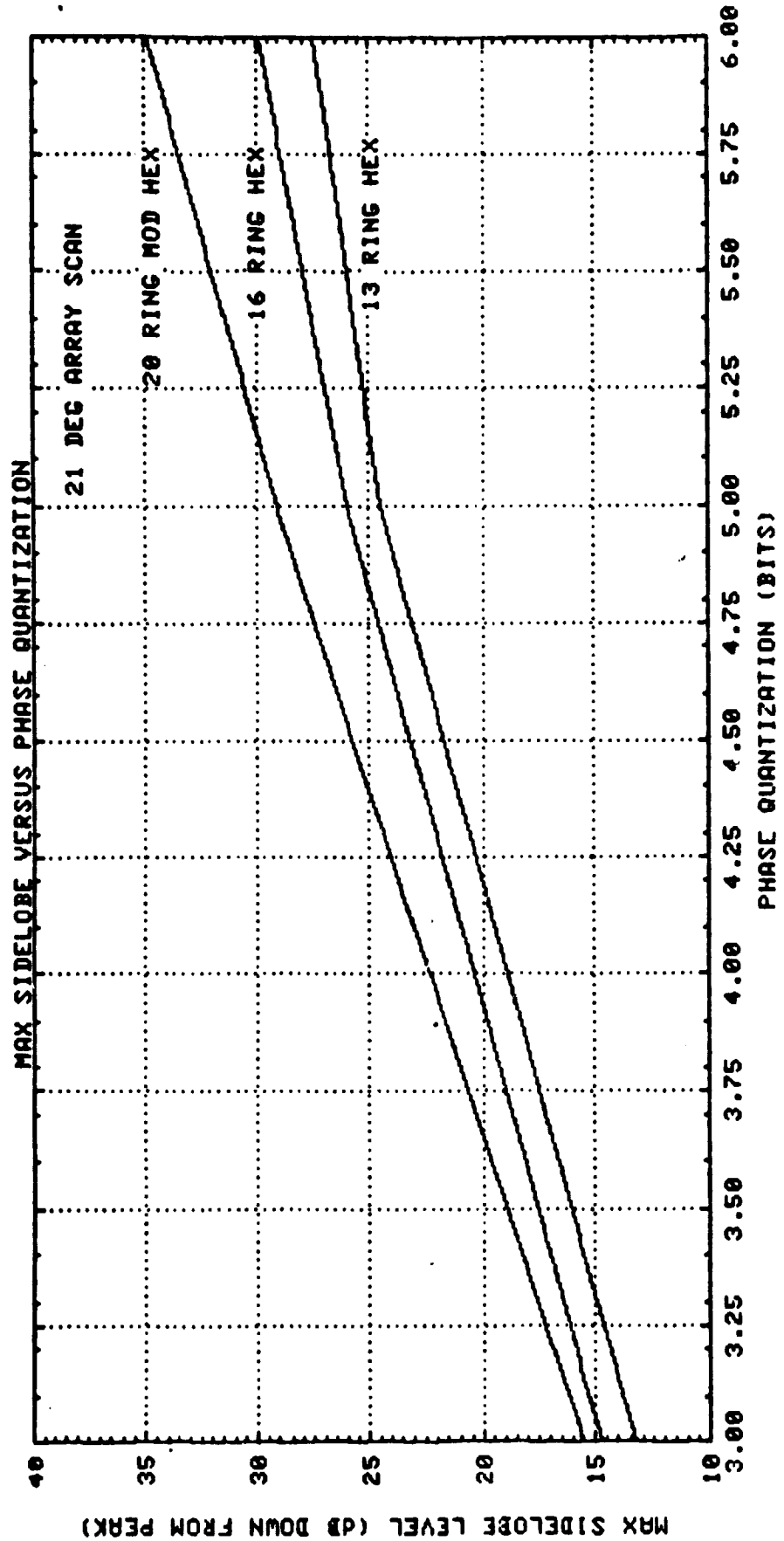
MAX SIDELOBE VERSUS PHASE QUANTIZATION
21 DEG ARRAY SCAN
20 RING MOD HEX
16 RING HEX
13 RING HEX
MAX SIDELOBE LEVEL (dB DOWN FROM PEAK)
PHASE QUANTIZATION (BITS)
40
35
30
25
20
15
10
3.00
3.25
3.50
3.75
4.00
4.25
4.50
4.75
5.00
5.25
5.50
5.75
6.00

FIGURE 4.2-4

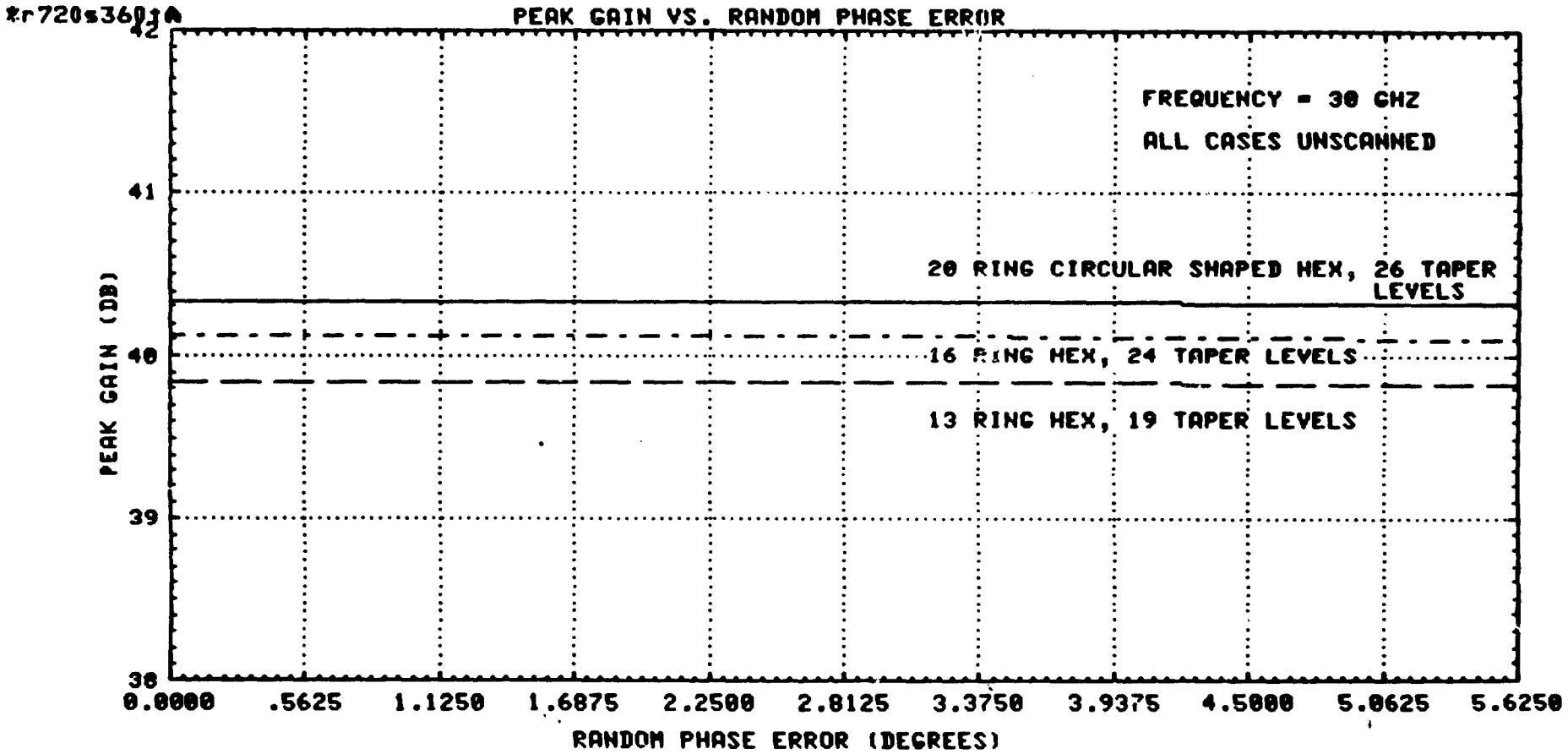
*r720s360j0
PEAK GAIN VS. RANDOM PHASE ERROR
FREQUENCY = 30 GHZ
ALL CASES UNSCANNED
20 RING CIRCULAR SHAPED HEX, 26 TAPER LEVELS
16 RING HEX, 24 TAPER LEVELS
13 RING HEX, 19 TAPER LEVELS
PEAK GAIN (DB)
42
41
40
39
38
0.0000
.5625
1.1250
1.6875
2.2500
2.8125
3.3750
3.9375
4.5000
5.0625
5.6250
RANDOM PHASE ERROR (DEGREES)

FIG. 4.2-23

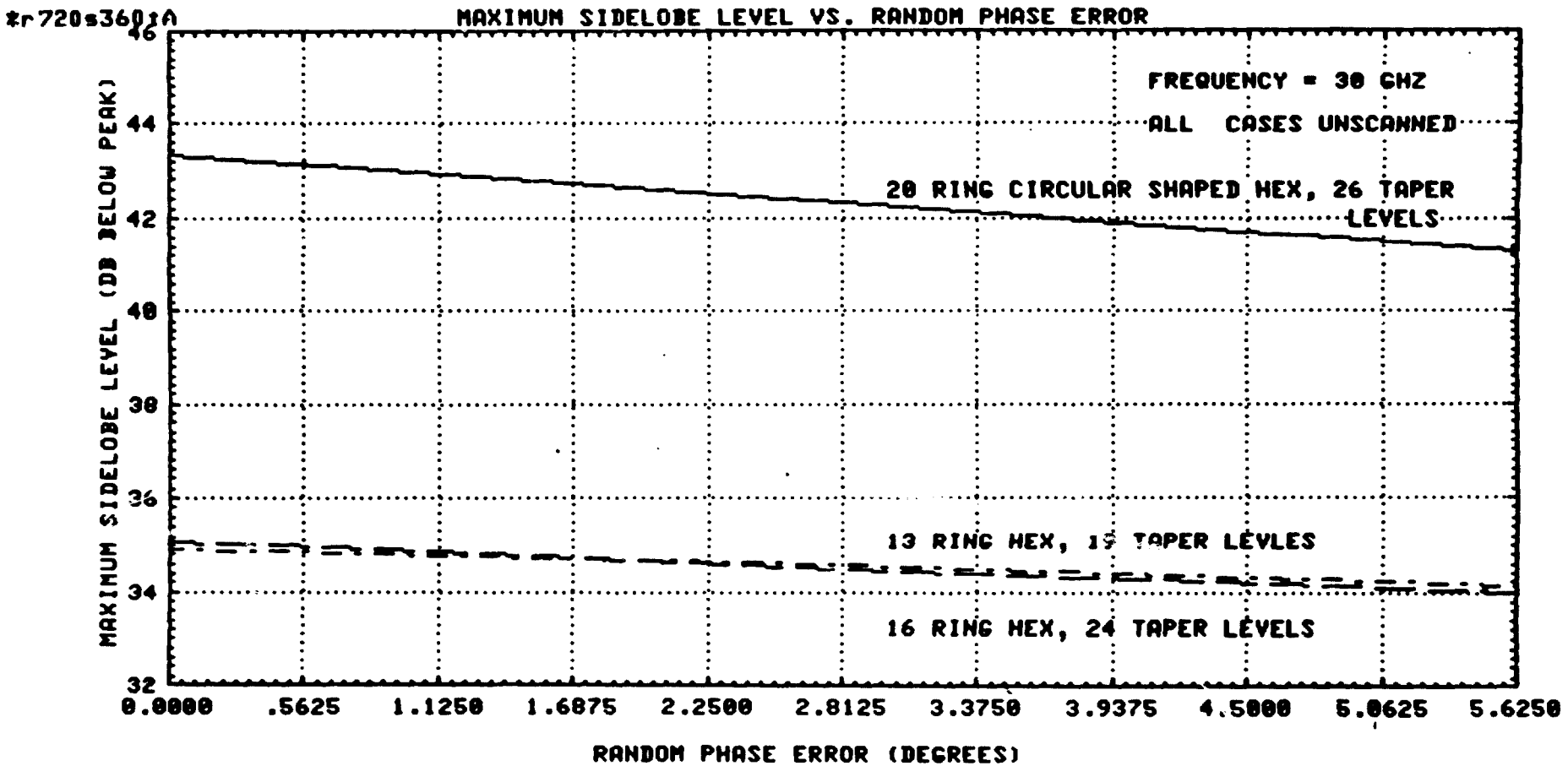
*r720s360iA
MAXIMUM SIDELOBE LEVEL VS. RANDOM PHASE ERROR
FREQUENCY = 30 GHZ
ALL CASES UNSCANNED
20 RING CIRCULAR SHAPED HEX, 26 TAPER LEVELS
13 RING HEX, 15 TAPER LEVLES
16 RING HEX, 24 TAPER LEVELS
MAXIMUM SIDELOBE LEVEL (DB BELOW PEAK)
46
44
42
40
38
36
34
32
0.0000
.5625
1.1250
1.6875
2.2500
2.8125
3.3750
3.9375
4.5000
5.0625
5.6250
RANDOM PHASE ERROR (DEGREES)

FIG 4.2-24

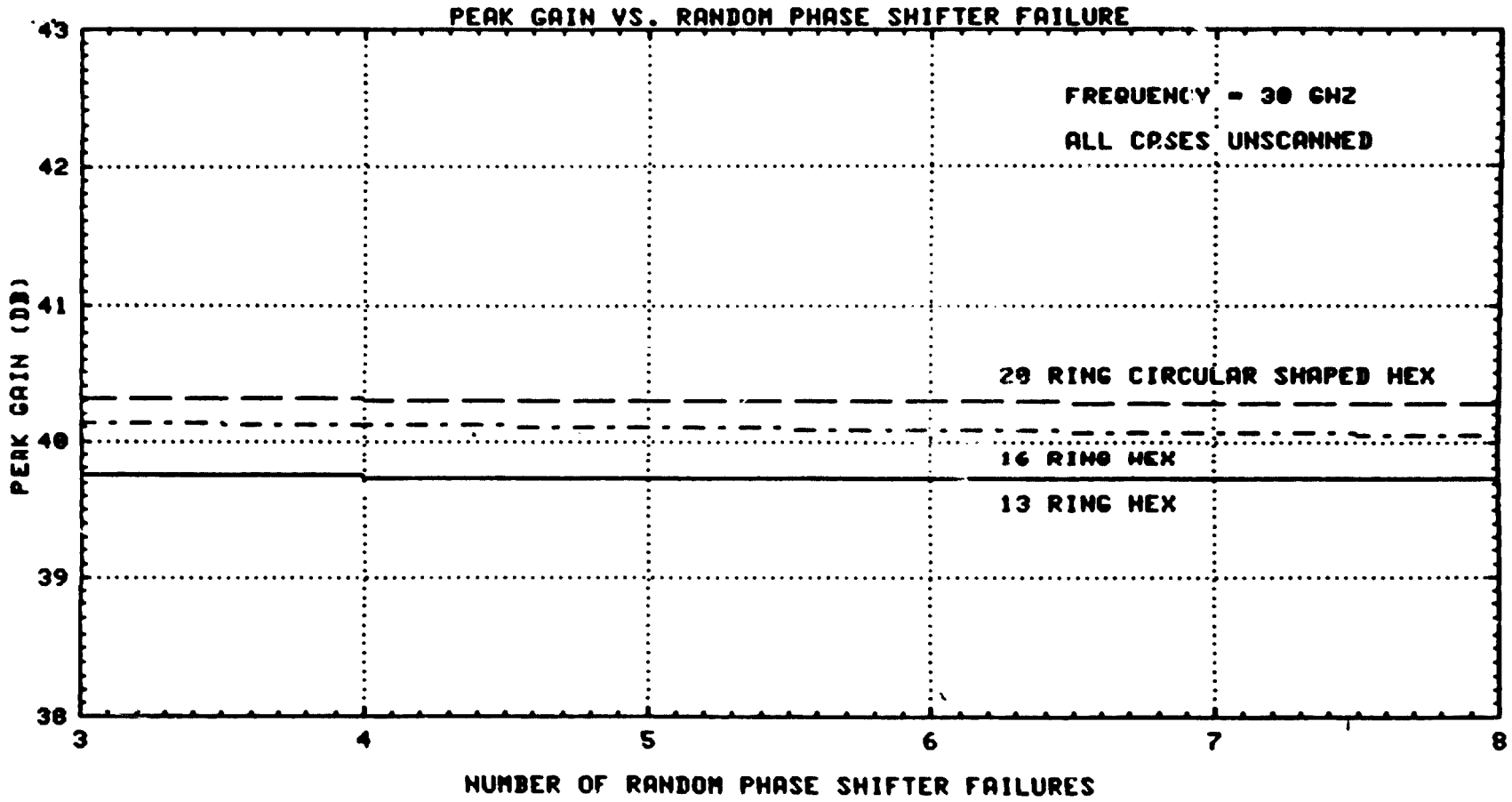

FIG 4.2-34

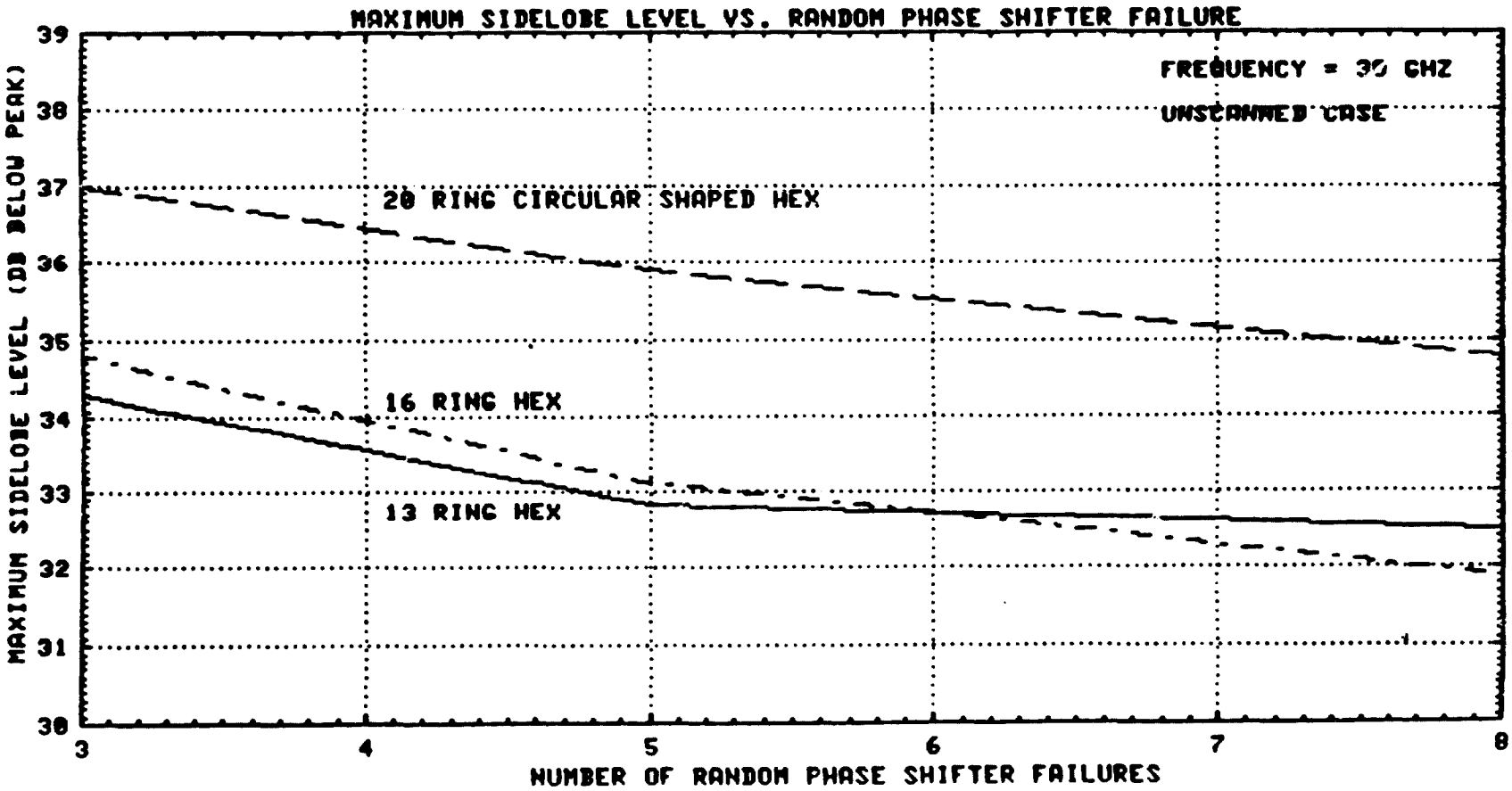
MAXIMUM SIDELOBE LEVEL VS. RANDOM PHASE SHIFTER FAILURE
FREQUENCY = 30 GHZ
UNSCANNED CASE
20 RING CIRCULAR SHAPED HEX
16 RING HEX
13 RING HEX
MAXIMUM SIDELOBE LEVEL (DB BELOW PEAK)
39
38
37
36
35
34
33
32
31
30
3
4
5
6
7
8
NUMBER OF RANDOM PHASE SHIFTER FAILURES

FIG. 4.2-35

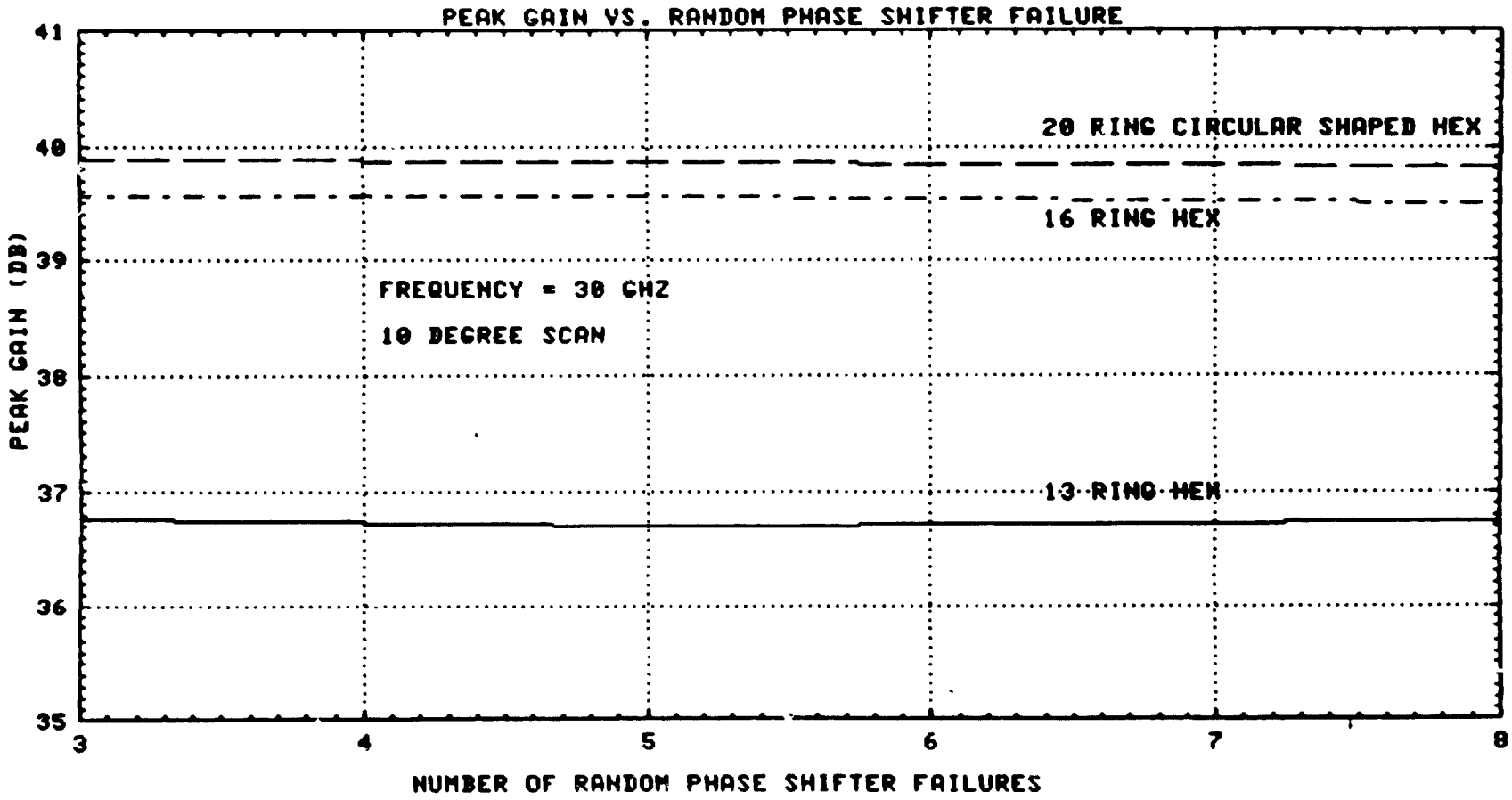
PEAK GAIN VS. RANDOM PHASE SHIFTER FAILURE
20 RING CIRCULAR SHAPED HEX
16 RING HEX
13 RING HEX
FREQUENCY = 30 GHZ
10 DEGREE SCAN
PEAK GAIN (DB)
41
40
39
38
37
36
35
3
4
5
6
7
8
NUMBER OF RANDOM PHASE SHIFTER FAILURES

FIG. 4.2-36

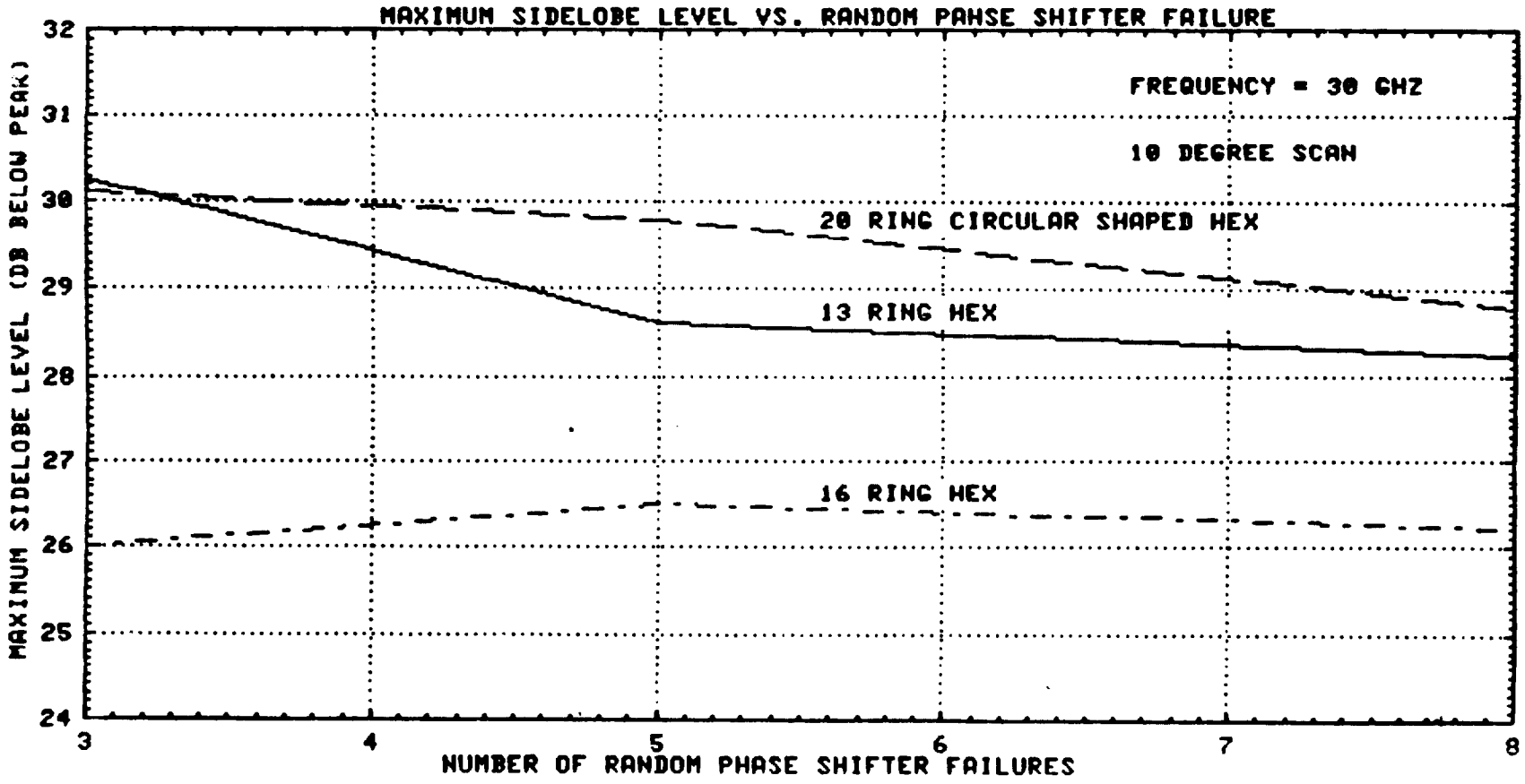
MAXIMUM SIDELOBE LEVEL VS. RANDOM PAHSE SHIFTER FAILURE
FREQUENCY = 30 GHZ
10 DEGREE SCAN
20 RING CIRCULAR SHAPED HEX
13 RING HEX
16 RING HEX
MAXIMUM SIDELOBE LEVEL (DB BELOW PEAK)
NUMBER OF RANDOM PHASE SHIFTER FAILURES
32
31
30
29
28
27
26
25
24
3
4
5
6
7
8

FIG. 4.2-37

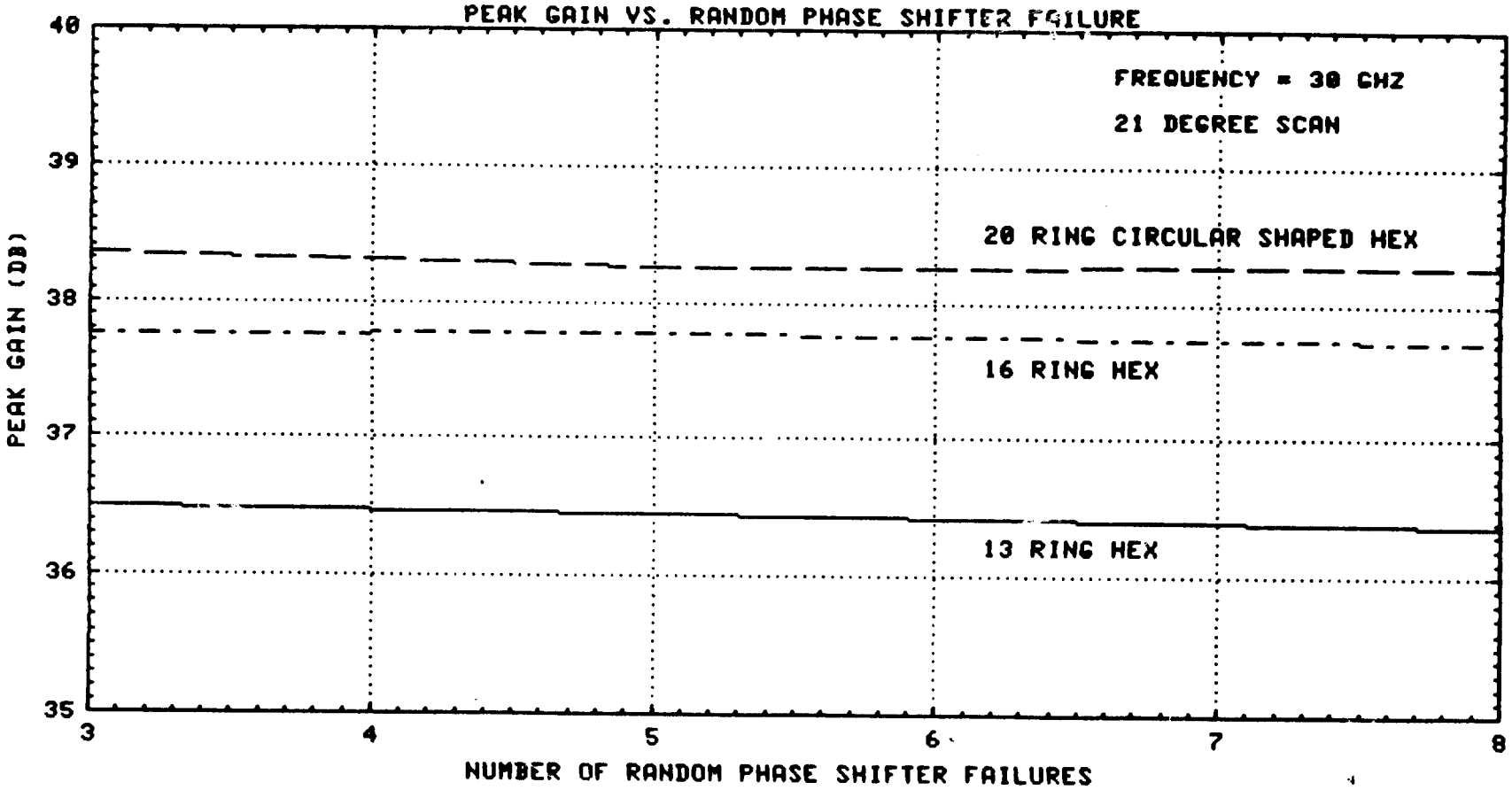
PEAK GAIN VS. RANDOM PHASE SHIFTER FAILURE
FREQUENCY = 30 GHZ
21 DEGREE SCAN
20 RING CIRCULAR SHAPED HEX
16 RING HEX
13 RING HEX
PEAK GAIN (DB)
40
39
38
37
36
35
3
4
5
6
7
8
NUMBER OF RANDOM PHASE SHIFTER FAILURES

FIG. 4.2-38

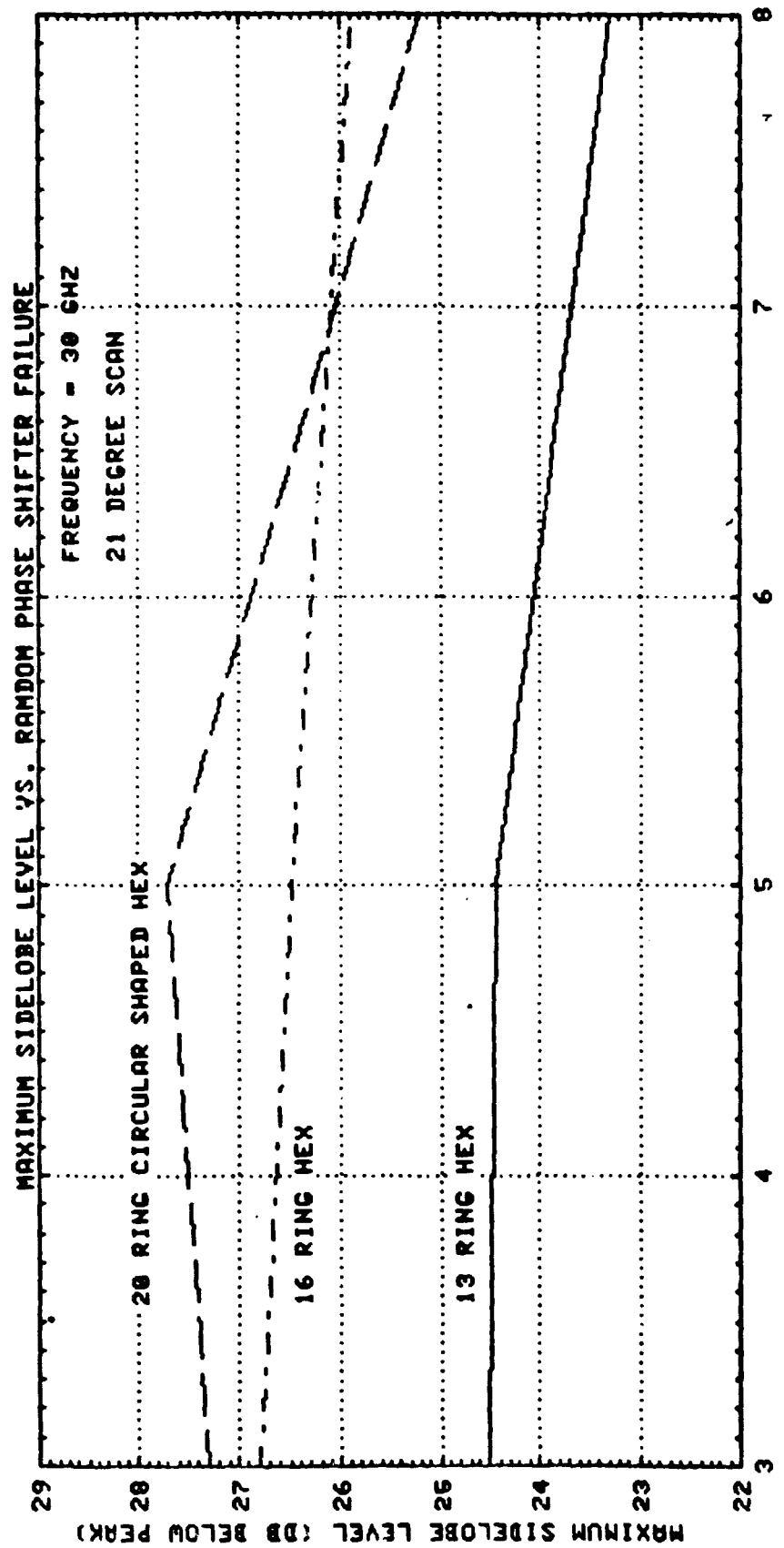
MAXIMUM SIDELOBE LEVEL VS. RANDOM PHASE SHIFTER FAILURE
FREQUENCY = 30 GHZ
21 DEGREE SCAN
20 RING CIRCULAR SHAPED HEX
16 RING HEX
13 RING HEX
MAXIMUM SIDELOBE LEVEL (DB BELOW PEAK)
NUMBER OF RANDOM PHASE SHIFTER FAILURES
29
28
27
26
25
24
23
22
3
4
5
6
7
8

F16.4.2-39

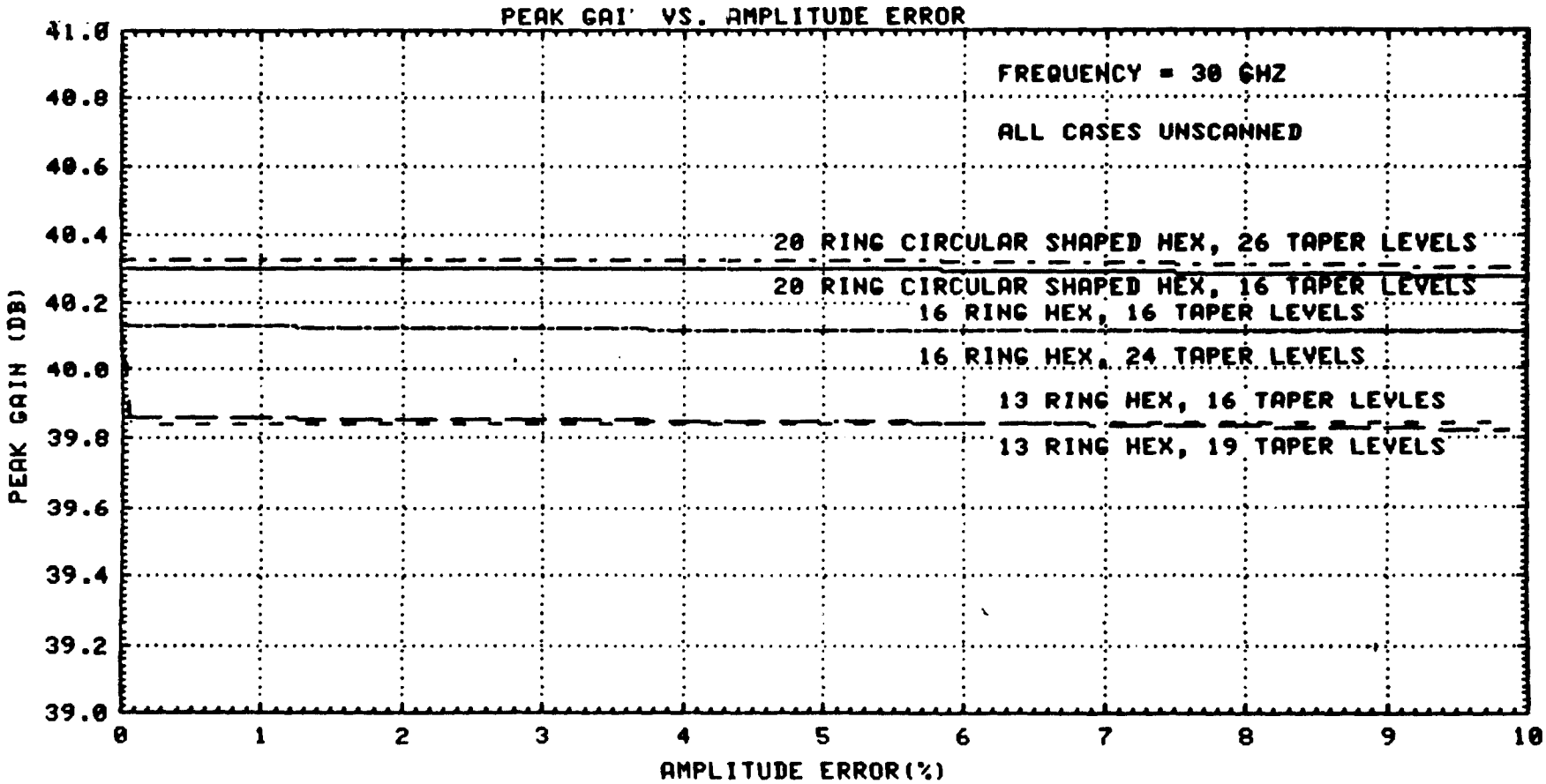
PEAK GAI' VS. AMPLITUDE ERROR
FREQUENCY = 30 GHZ
ALL CASES UNSCANNED
20 RING CIRCULAR SHAPED HEX, 26 TAPER LEVELS
20 RING CIRCULAR SHAPED HEX, 16 TAPER LEVELS
16 RING HEX, 16 TAPER LEVELS
16 RING HEX, 24 TAPER LEVELS
13 RING HEX, 16 TAPER LEVLES
13 RING HEX, 19 TAPER LEVELS
PEAK GAIN (DB)
41.0
40.8
40.6
40.4
40.2
40.0
39.8
39.6
39.4
39.2
39.0
0
1
2
3
4
5
6
7
8
9
10
AMPLITUDE ERROR(%)

FIG. 4.2-68

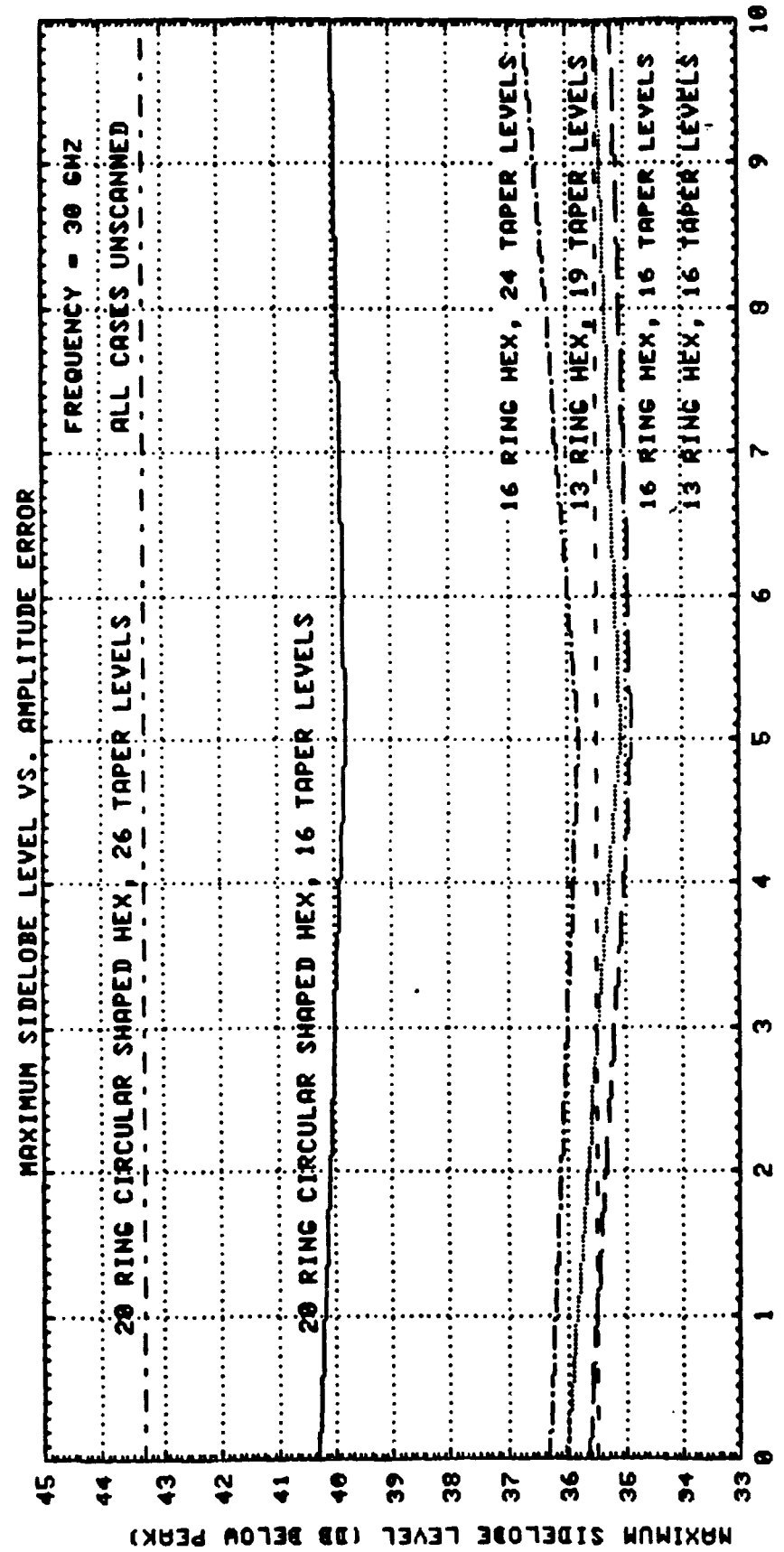
MAXIMUM SIDELOBE LEVEL VS. AMPLITUDE ERROR
FREQUENCY = 30 GHZ
ALL CASES UNSCANNED
20 RING CIRCULAR SHAPED HEX, 26 TAPER LEVELS
20 RING CIRCULAR SHAPED HEX, 16 TAPER LEVELS
16 RING HEX, 24 TAPER LEVELS
13 RING HEX, 19 TAPER LEVELS
16 RING HEX, 16 TAPER LEVELS
13 RING HEX, 16 TAPER LEVELS
MAXIMUM SIDELOBE LEVEL (DB BELOW PEAK)
AMPLITUDE ERROR (%)
45
44
43
42
41
40
39
38
37
36
35
34
33
0
1
2
3
4
5
6
7
8
9
10

FIG 4.2-69

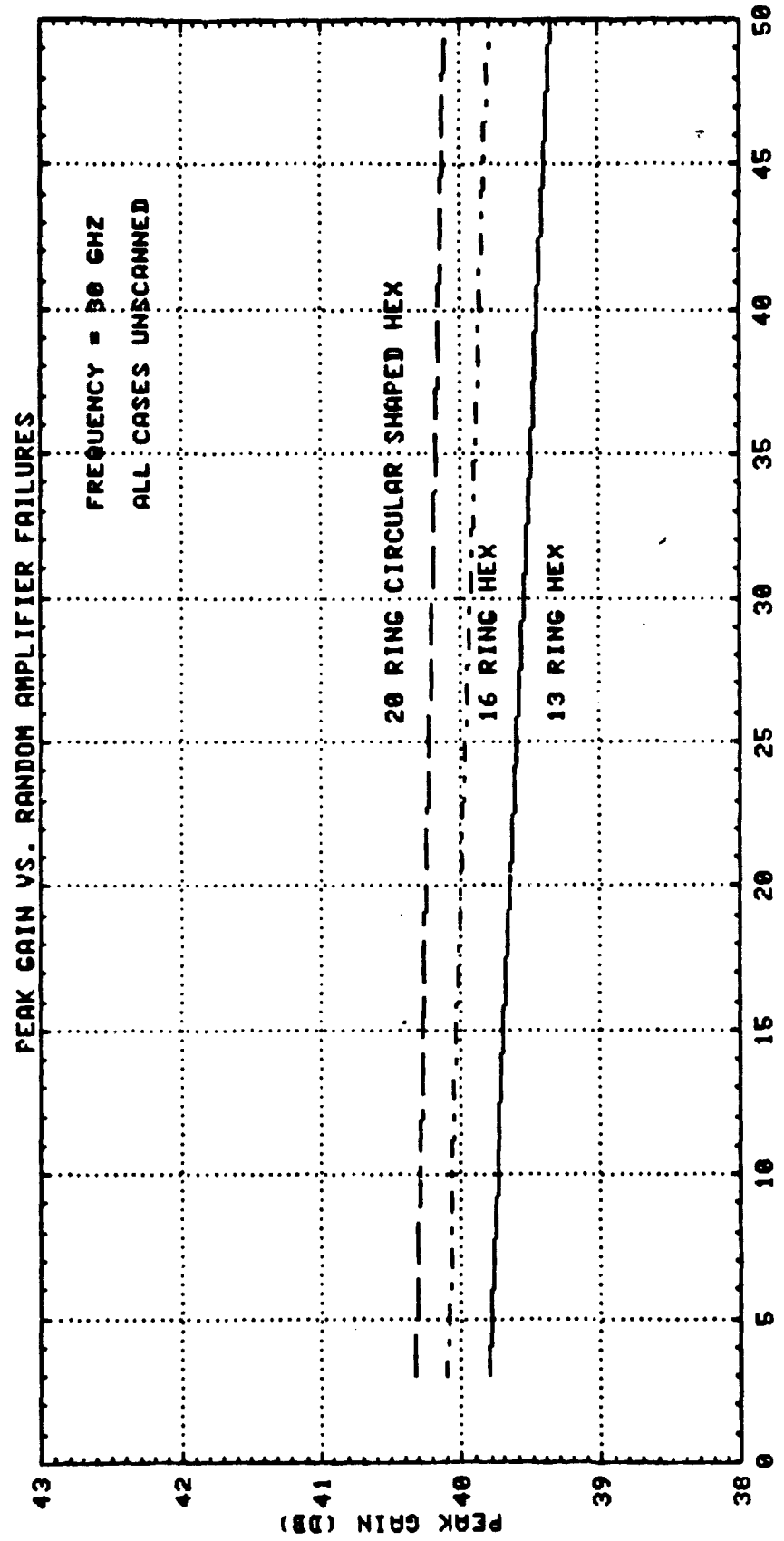
PEAK GAIN VS. RANDOM AMPLIFIER FAILURES
FREQUENCY = 30 GHZ
ALL CASES UNSCANNED
20 RING CIRCULAR SHAPED HEX
16 RING HEX
13 RING HEX
PEAK GAIN (DB)
NUMBER OF RANDOM AMPLIFIER FAILURES
43
42
41
40
39
38
0
5
10
15
20
25
30
35
40
45
50

FIG. 4.2-88

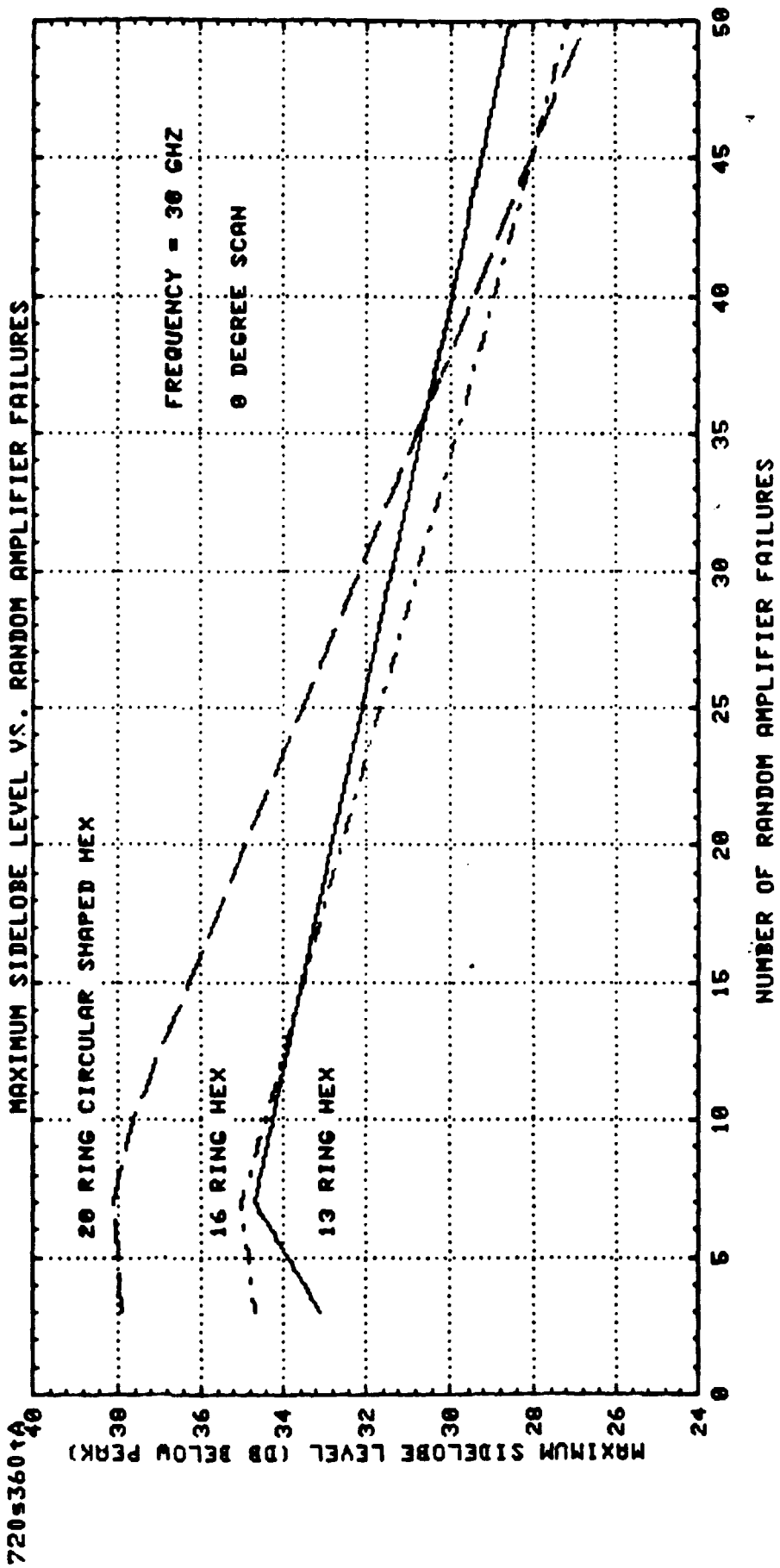
MAXIMUM SIDELOBE LEVEL VS. RANDOM AMPLIFIER FAILURES
FREQUENCY = 30 GHZ
0 DEGREE SCAN
20 RING CIRCULAR SHAPED HEX
16 RING HEX
13 RING HEX
MAXIMUM SIDELOBE LEVEL (DB BELOW PEAK)
NUMBER OF RANDOM AMPLIFIER FAILURES
720=360+0
40
30
36
34
32
30
28
26
24
0
5
10
15
20
25
30
35
40
45
50

Fig. 4.2-89

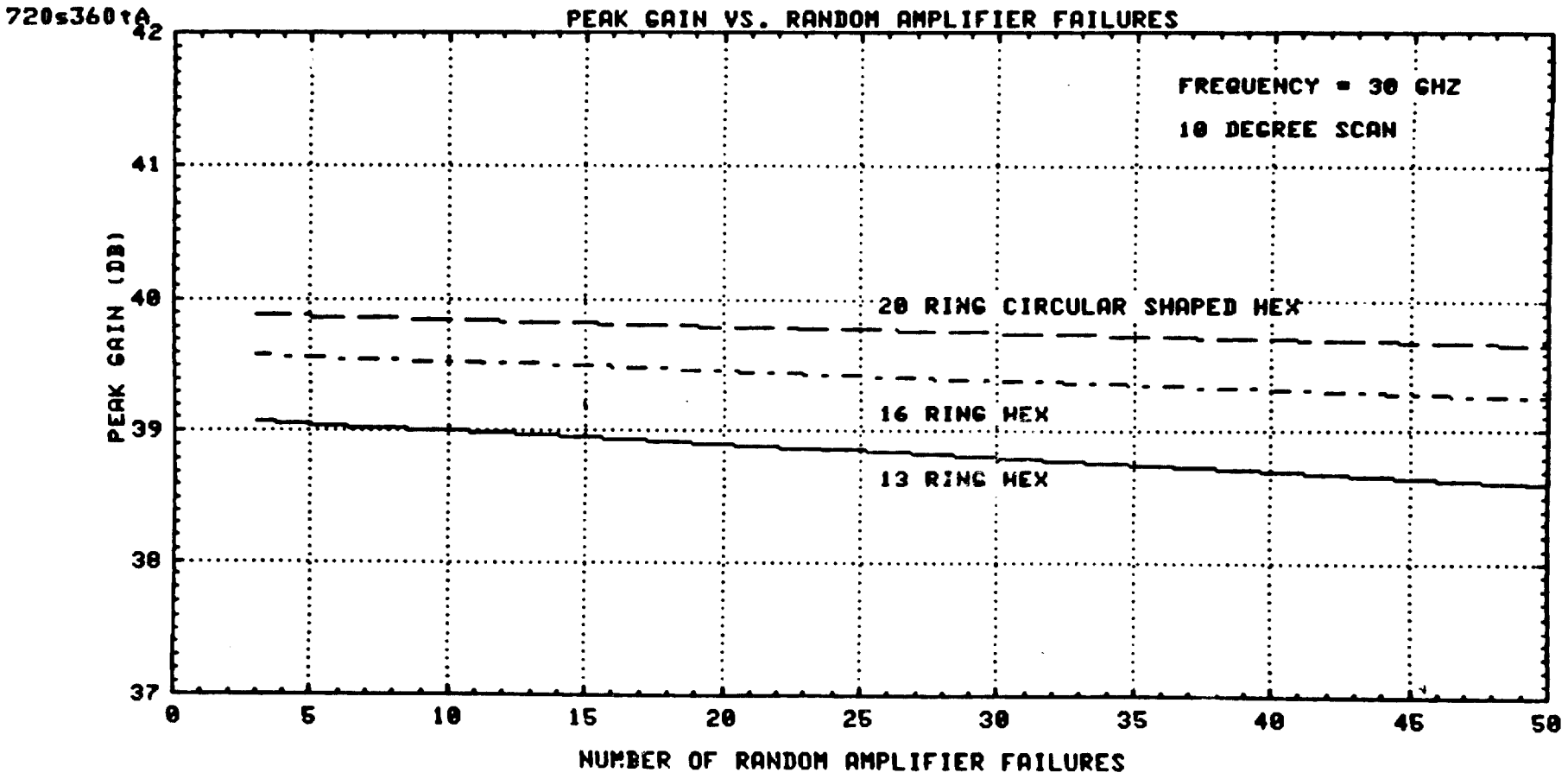
720s360tA
PEAK GAIN VS. RANDOM AMPLIFIER FAILURES
FREQUENCY = 30 GHZ
10 DEGREE SCAN
20 RING CIRCULAR SHAPED HEX
16 RING HEX
13 RING HEX
PEAK GAIN (DB)
42
41
40
39
38
37
0
5
10
15
20
25
30
35
40
45
50
NUMBER OF RANDOM AMPLIFIER FAILURES

FIG. 4.2-90

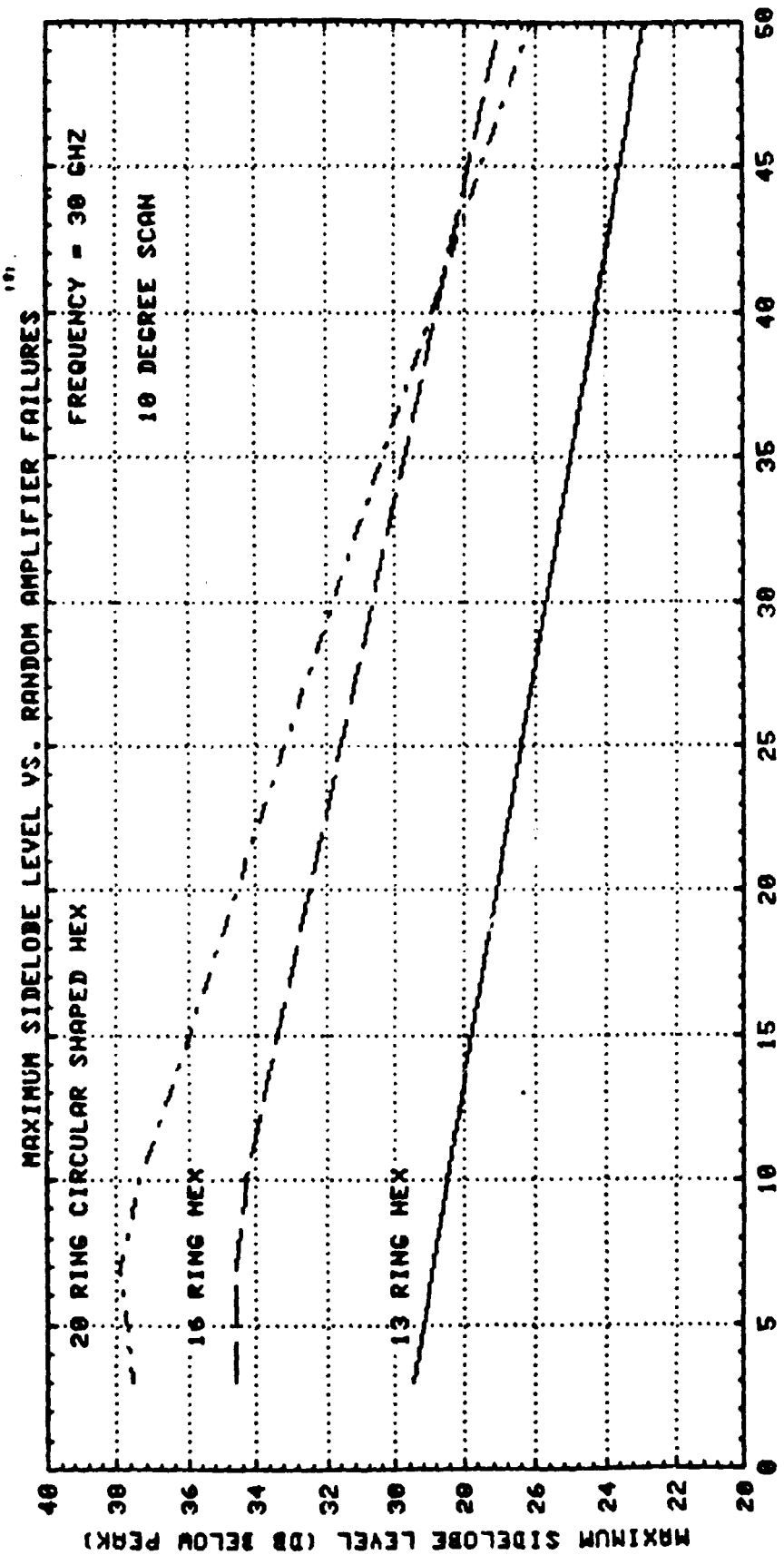
MAXIMUM SIDELOBE LEVEL VS. RANDOM AMPLIFIER FAILURES
FREQUENCY = 30 GHZ
10 DEGREE SCAN
20 RING CIRCULAR SHAPED HEX
16 RING HEX
13 RING HEX
MAXIMUM SIDELOBE LEVEL (DB BELOW PEAK)
NUMBER OF RANDOM AMPLIFIER FAILURES
40
38
36
34
32
30
28
26
24
22
20
0
5
10
15
20
25
30
35
40
45
50

Fig. 4.2-91

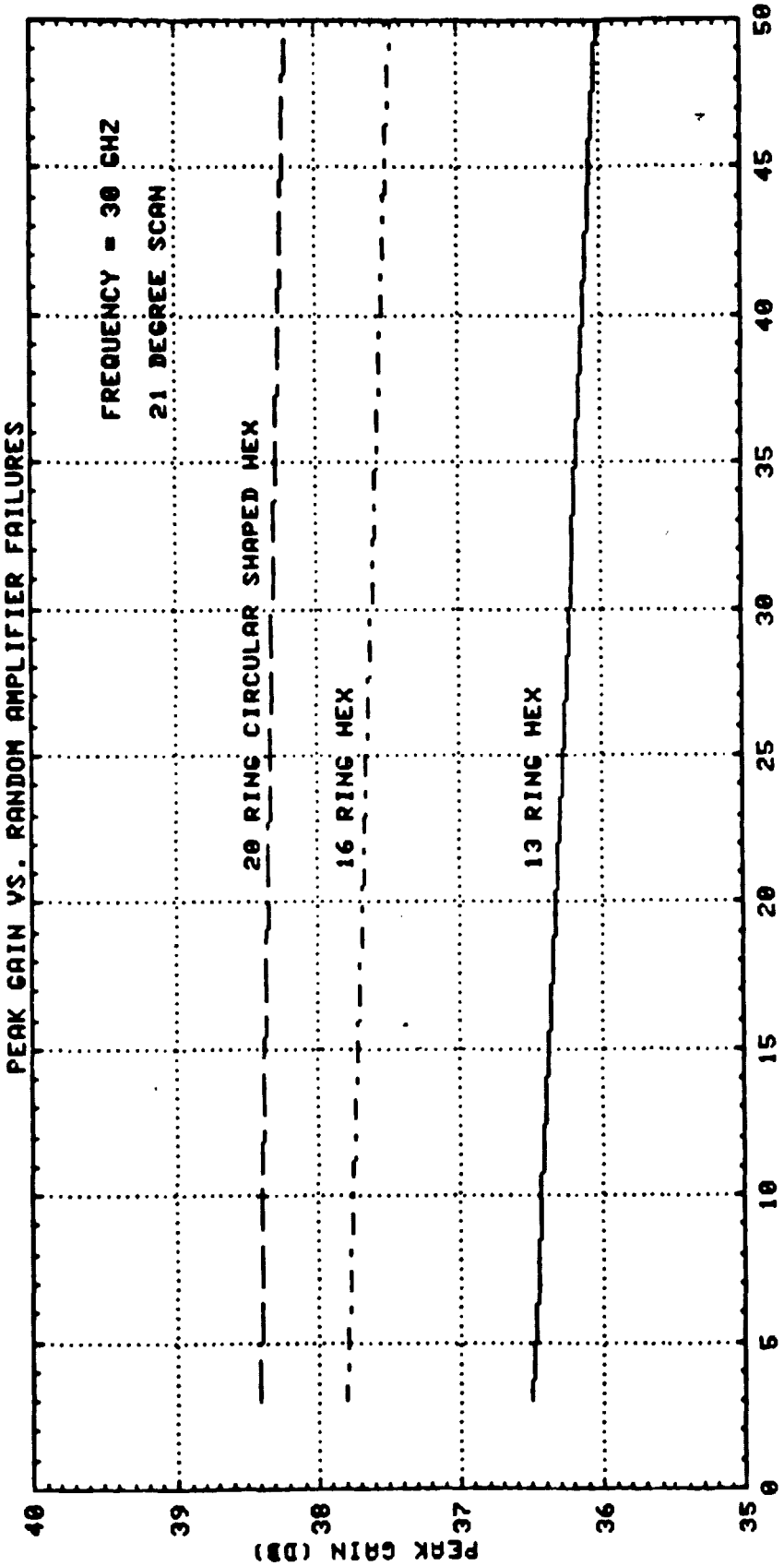
PEAK GAIN VS. RANDOM AMPLIFIER FAILURES
FREQUENCY = 30 GHZ
21 DEGREE SCAN
20 RING CIRCULAR SHAPED HEX
16 RING HEX
13 RING HEX
PEAK GAIN (DB)
NUMBER OF RANDOM AMPLIFIER FAILURES
40
39
38
37
36
35
0
5
10
15
20
25
30
35
40
45
50

FIG. 4.2-92

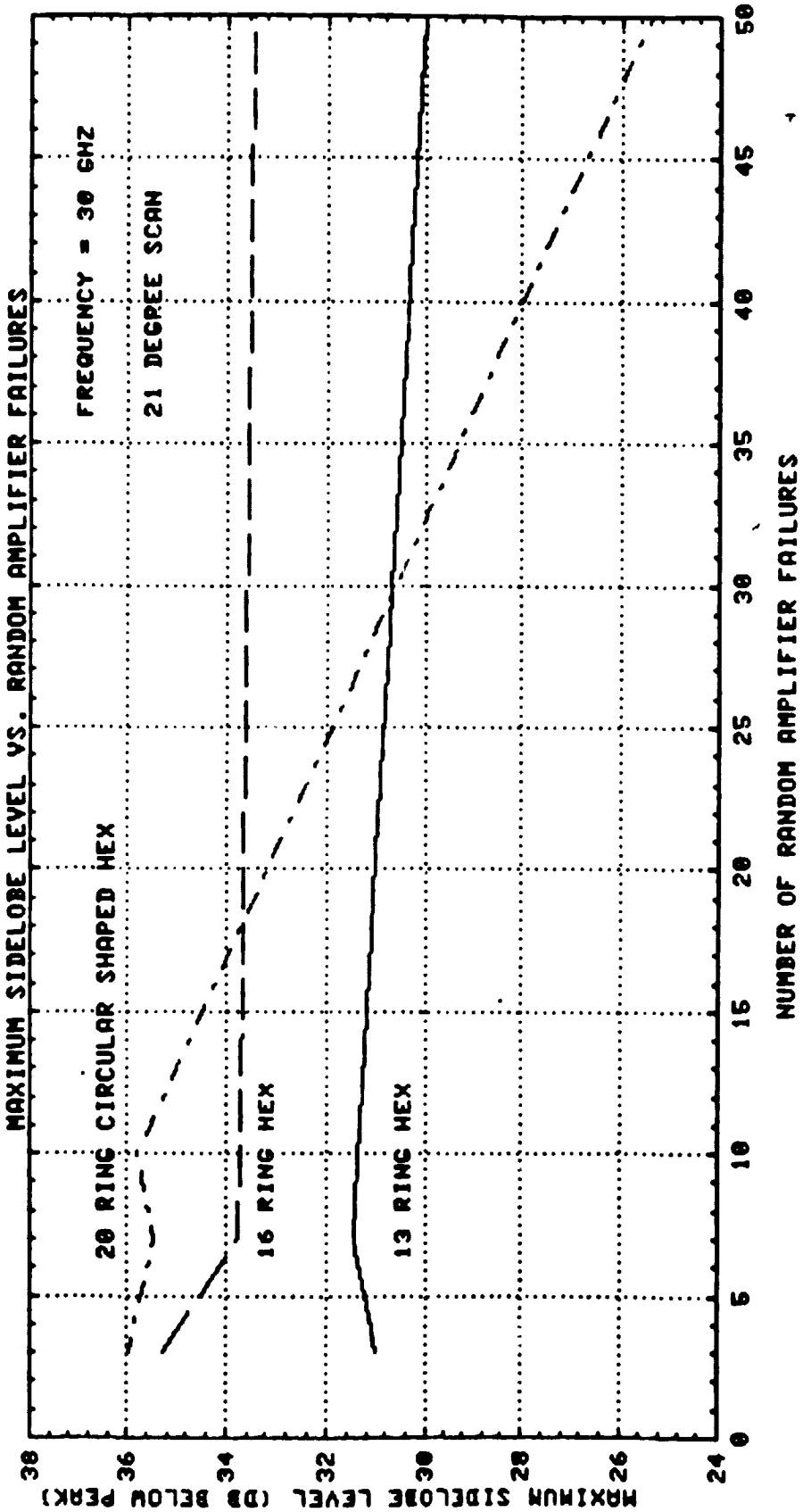
MAXIMUM SIDELOBE LEVEL VS. RANDOM AMPLIFIER FAILURES
FREQUENCY = 30 GHZ
21 DEGREE SCAN
20 RING CIRCULAR SHAPED HEX
16 RING HEX
13 RING HEX
MAXIMUM SIDELOBE LEVEL (DB BELOW PEAK)
NUMBER OF RANDOM AMPLIFIER FAILURES
30
36
34
32
30
28
26
24
0
5
10
15
20
25
30
35
40
45
50

FIG. 4.2-93

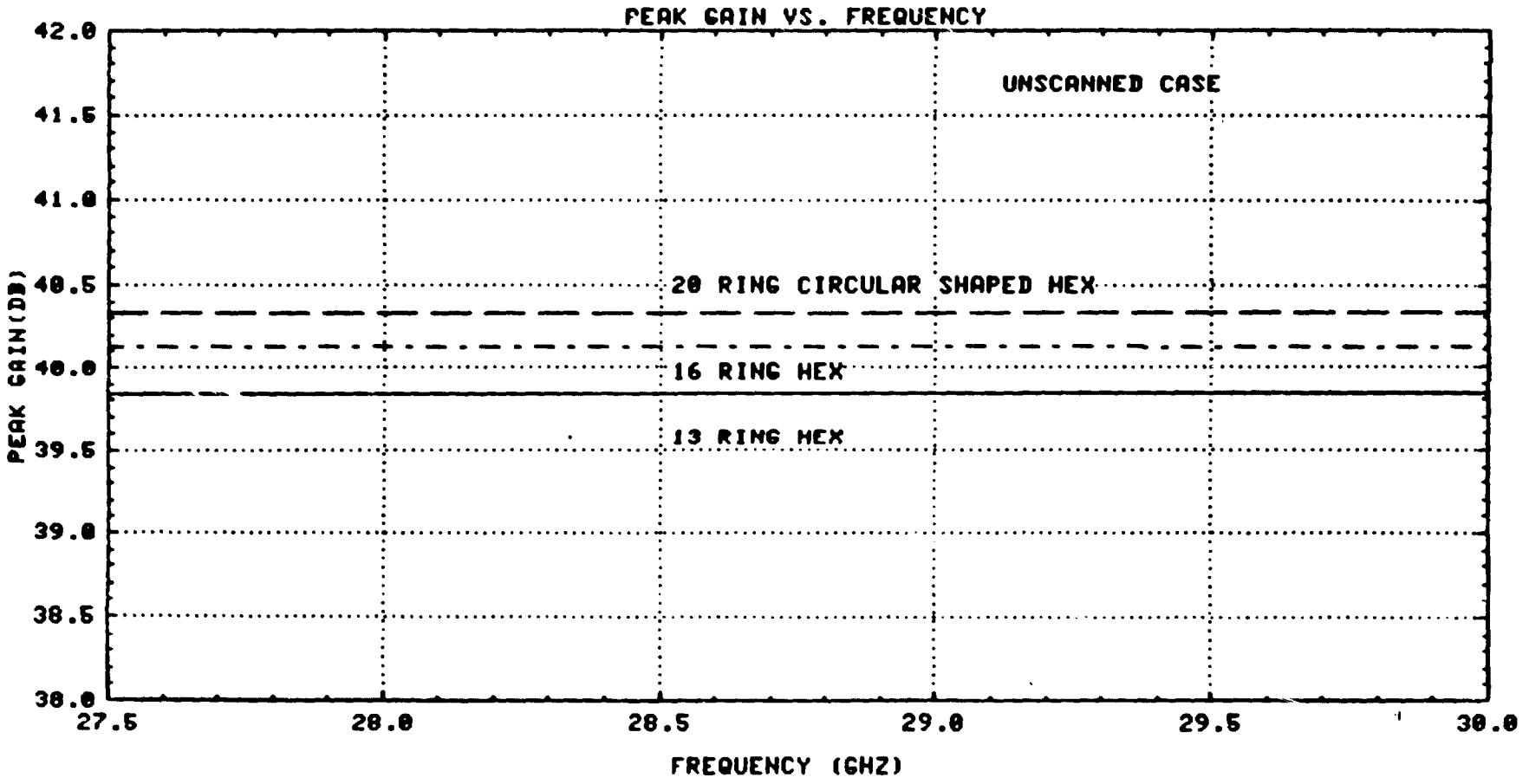
PEAK GAIN VS. FREQUENCY
UNSCANNED CASE
20 RING CIRCULAR SHAPED HEX
16 RING HEX
13 RING HEX
PEAK GAIN(DB)
42.0
41.5
41.0
40.5
40.0
39.5
39.0
38.5
38.0
27.5
28.0
28.5
29.0
29.5
30.0
FREQUENCY (GHZ)

FIG. 4.3-1

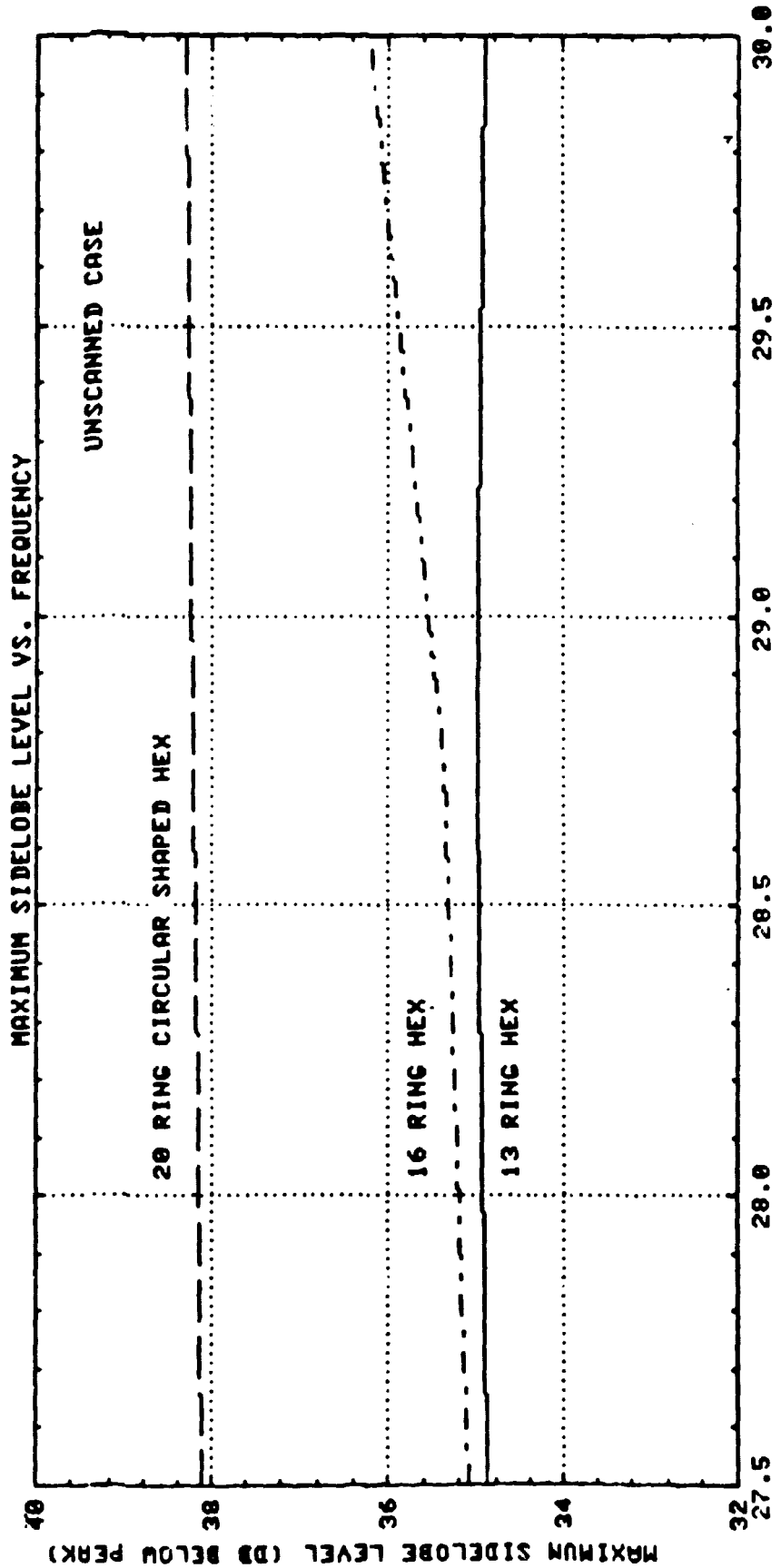
MAXIMUM SIDELOBE LEVEL VS. FREQUENCY
UNSCANNED CASE
20 RING CIRCULAR SHAPED HEX
16 RING HEX
13 RING HEX
MAXIMUM SIDELOBE LEVEL (DB BELOW PEAK)
40
38
36
34
32
27.5
28.0
28.5
29.0
29.5
30.0
FREQUENCY (GHZ)

FIG. 4.3-2

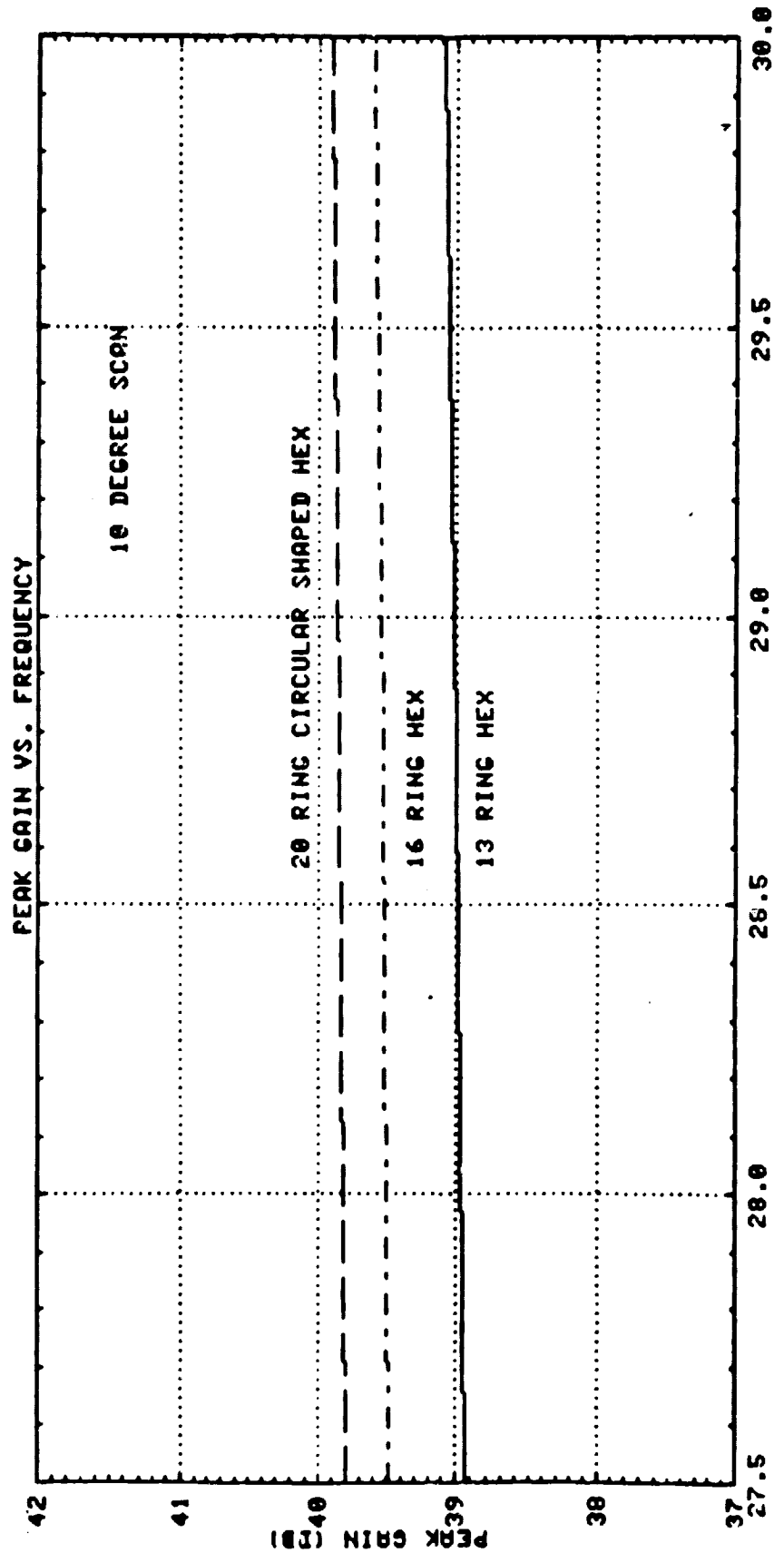
PEAK GAIN VS. FREQUENCY
10 DEGREE SCAN
20 RING CIRCULAR SHAPED HEX
16 RING HEX
13 RING HEX
PEAK GAIN (DB)
FREQUENCY (GHZ)
42
41
40
39
38
37
27.5
28.0
28.5
29.0
29.5
30.0

FIG. 4.3-3

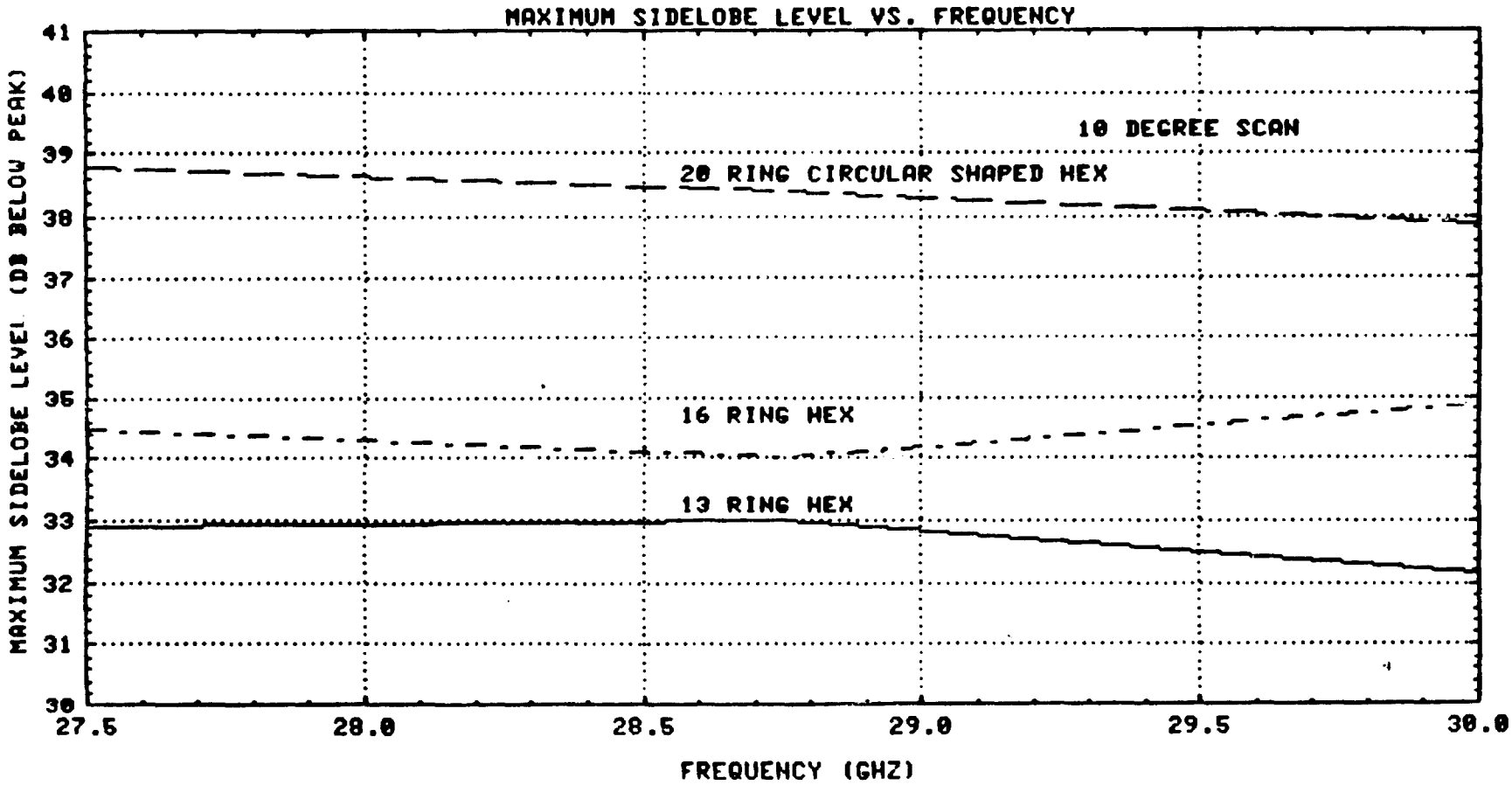
MAXIMUM SIDELOBE LEVEL VS. FREQUENCY
MAXIMUM SIDELOBE LEVEL (DB BELOW PEAK)
41
40
39
38
37
36
35
34
33
32
31
30
27.5
28.0
28.5
29.0
29.5
30.0
FREQUENCY (GHZ)
10 DEGREE SCAN
20 RING CIRCULAR SHAPED HEX
16 RING HEX
13 RING HEX

FIG 4.3-4

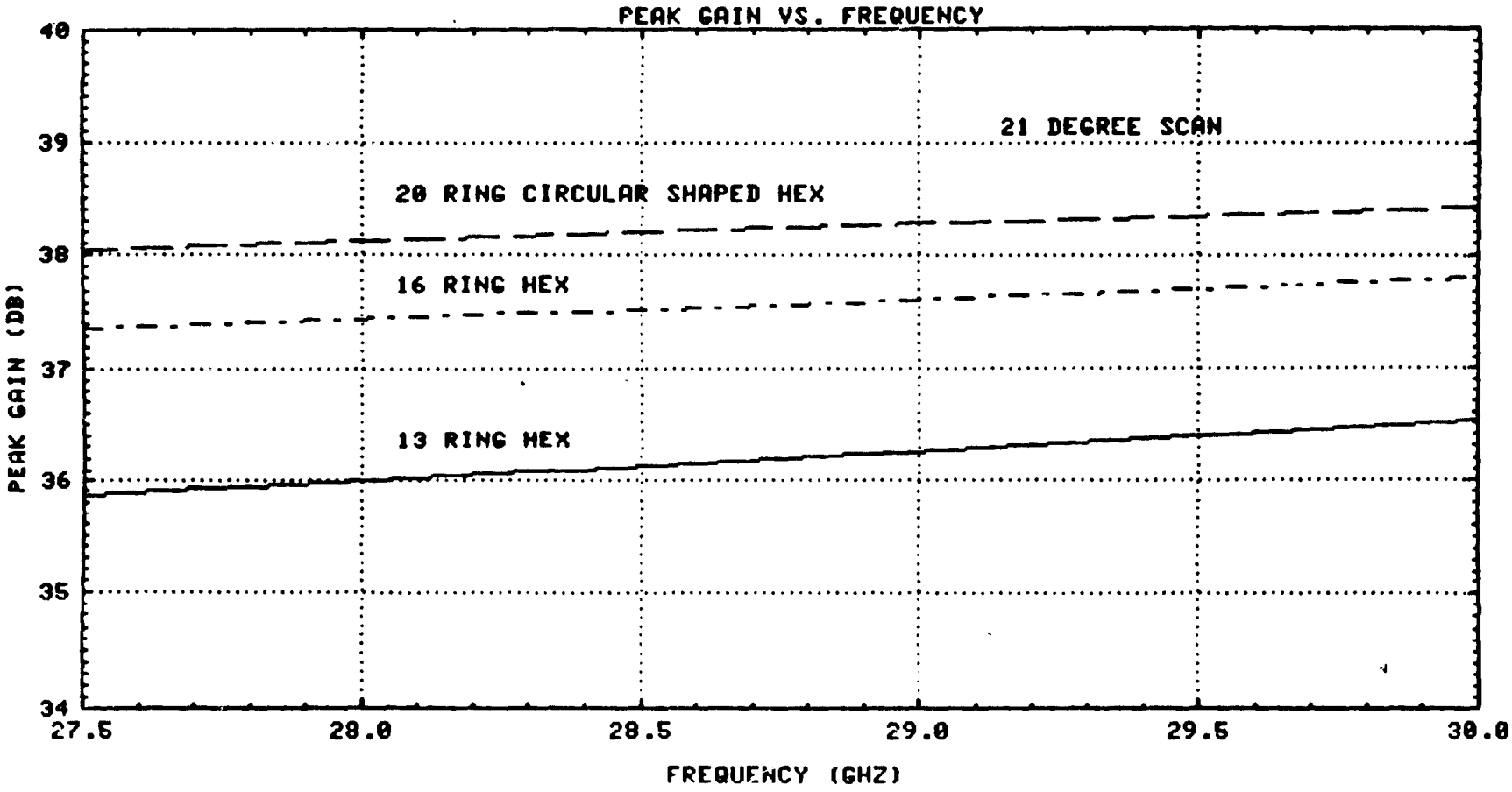
PEAK GAIN VS. FREQUENCY
21 DEGREE SCAN
20 RING CIRCULAR SHAPED HEX
16 RING HEX
13 RING HEX
PEAK GAIN (DB)
40
39
38
37
36
35
34
27.5
28.0
28.5
29.0
29.5
30.0
FREQUENCY (GHZ)

F.6 4.3-5

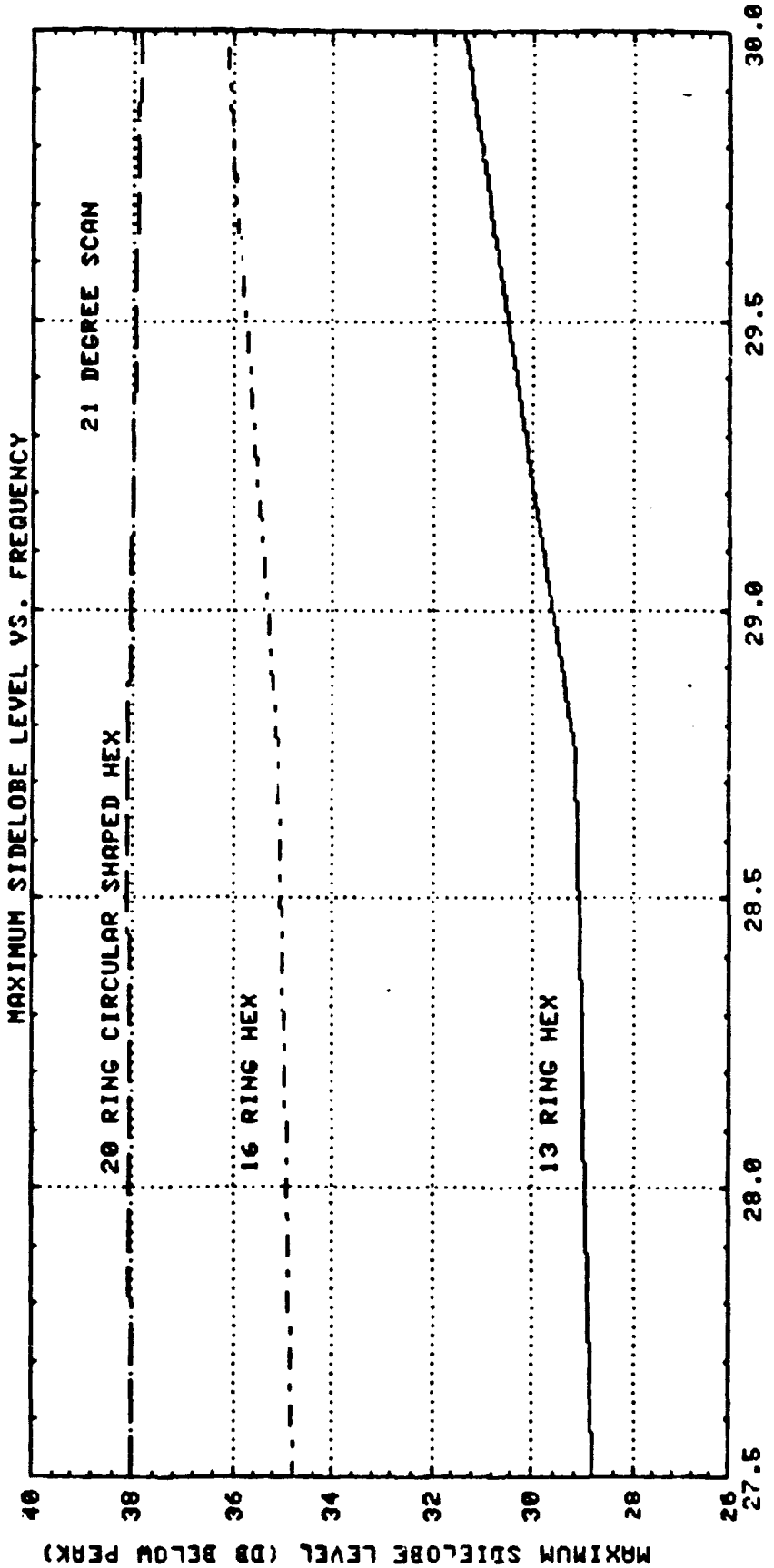
MAXIMUM SIDELOBE LEVEL VS. FREQUENCY
21 DEGREE SCAN
20 RING CIRCULAR SHAPED HEX
16 RING HEX
13 RING HEX
MAXIMUM SIDELOBE LEVEL (DB BELOW PEAK)
FREQUENCY (GHZ)
40
38
36
34
32
30
28
26
27.5
28.0
28.5
29.0
29.5
30.0

FIG. 4.3-6

SECTION 5

SECONDARY PATTERNS AND DISCUSSIONS

5.1 SECONDARY PATTERNS COMPUTATIONS

The procedure of computing the system secondary patterns are summarized below:

Step 1. Compute Far-Fields of the Array.

The array weight determination is described in detail in Section 5.2.

Step 2. Obtain the spherical mode coefficient representation of the array far fields obtained in Step 1.

Step 3. Reconstruct the array far fields for verification and perform far field to near field transformation to obtain the array near fields at the subrelfector surface.

Step 4. Determine the induced current on the subreflector.

Step 5. Compute the far fields contributed by the sub-dish current; represent the far fields in spherical mode coefficients (generally 180 complex numbers would be sufficient); reconstruct the far fields for verifications and perform far field to near field transformation; and compute near fields at the main dish surface.

An alternative is to use NFPO to compute the fields at the main dish surface directly at the expense of approximately twice the computation time.

Step 6. Comput the induced main dish current and calculate the far fields.

The method outlined above has been verified for three separate cases, for details see Section 1.3.

5.2 ELEMENT WEIGHT DETERMINATION

5.2.1 ELEMENT PHASE

Two methods were used in this study to compute thee weights of the array elements. The first method was based on the array far field scan, and the second based on the scan of the system far field.

In the first method, the phases are computed such that the rays emitted from the array elements are exactly in phase in the array scan direction. The computation is pertinent only to the array, and no knowledge of the optical system is assumed or needed. The resultant system main beam position depends upon the array scan angle and the characteristics of the optical system. The system beam deviation factor (system beam angle per degree of array scan) is a function of scan direction. Generally, the beam deviation factor is larger in directions away from the system optical axis and smaller in directions towards it. For instance, the system scan is 4.3 degrees for 3.5 degree array scan in the direction away from the optical axis, and is only 3.7 degrees for a 3.5 degrees array scan towards the

optical axis. This presents a difficulty in deteriming the exact location of the system scan. In addition to this difficulty the first method provides no assurance that the parallel rays emitted from the array will be either in phase or in the same direction when they reach the scan plane (a plane normal to the system scan direction and passing through the focus, as defined in Section 1). In fact, the forward ray tracing (from the array to the main reflector) showed how the rays were neither in phase nor in the same direction (see Figures 1.3-8 through 1.3-11 and 1.3-13 through 1.3-16). Due to these drawbacks, the second method was developed.

The second method is based on IRTT. The rays that reach the scan plane in the scan direction are forced to be in-phase. The rays must leave the elements at various angles in order to arrive at the scan plane in the same direction. Once the specific ray emitting angle from an element is known, the optical path length from the array element to the output scan plane can be determined. The path length is used to determine the phase setting of the array element.

5.2.2 ELEMENT AMPLITUDE

Since there exists a one-to-one mapping correspondence between an array element and its image on the scan plane, a prescribed amplitude ditribution required for a specific sidelobe level can be translated to the array plane. For the static taper case, the amplitude taper of the array elements follows a binomial distribution. The circular contours in the array plane image to "elliptical like" contours in the scan plane. Both the above cases were investigated in this study. The above discussion has assumed a "transmit" viewpoint, but the result applies equally well to the "receive" case due to reciprocity.

5.3 SECONDARY PATTERNS

Table 5.3-1 summarizes the secondary pattern data which was obtained using an array static amplitude taper. The cases for which the taper is determined in the scan plane and translated back to the array aperture are summarized in Table 5.3-2.

The secondary patterns used to generate Table 5.3-i can be seen in Figures 5.3-1 through 5.3-64 while the patterns used to generate Table 5.3.2 are plotted in Figures 5.3-65 thourgh 5.3-71 (located in Appendix A).

5.4 IMAGING CONCEPT

As implied in the last section, the array element weights computed by the inverse ray tracing technique (IRTT) should lead to a system scan angle exactly equal to the scan angle used in determining the element weights. This was indeed the case as shown in Figure 5.3-65, were the angles A/E=0/1.75 were used as the desired scan. The resultant system far field does point at exactly A/E=0/1.75. The verification can be considered as a first benchmark on the computer programs employed.

For the same unscanned case, the phase settings of array elements are all the same and the array amplitude taper is mapped onto the scan plane as concentric circles, see Figure 5.3-4. The implication of these two observations is that the system far field patterns should match that computed for an equivalent array, which is the primary array enlarged by the system magnification factor M, placed in the scan

TABLE 5.3-1 SUMMARY OF COMPUTED SYSTEM PERFORMANCE --- Phase setting by array FF scan

ARRAY				OPTICAL SYSTEM					PERFORMANCE @ 30 GHZ					FIGURE #
SHAPE	#ELM /#ring	SPACING "/λ@30GHz	MAIN POL	M	Q "	FL1 "	F/D	Zarray "	SCAN Ar'y	SCAN FF	GMAX Main	GMAX Xpol	SIDELOBE dBI/dB down	
HEX	397/12	.59/1.5	Y	6	60	108	1.0	-13.864	0/0	*0/0	53.9	31	25/28.9	1.3-31-36
HEX	469/13	.72/1.825	Y	6	60	108	1.0	-13.864	0/0	*0/0	54.1	32	28/26.1	5.3-1 - 8
HEX	469/13	.72/1.825	Y	6	60	108	1.0	-13.864	*18/0	*3.7/0	53.1	7.1	31.8/21.3	5.3-9 - 11
HEX	469/13	.72/1.825	Y	6	60	108	1.0	-13.864	*18/180	*2.5 /180	53.2	6.1	40.1/13.1	5.3-12 - 14
HEX	721/16	.59/1.5	Y	6	60	108	1.0	-13.864	0/0	*0/0	55.7	36	32/23.7	5.3-15 - 21
C.S.HEX	1039/20	.53/1.333	Y	6	60	135	1.25	-12.441	0/0	*0/0	56.7	34	27/29.7	5.3-23 - 27
(ENLARGED 6TIMES)				(NONE)					0/0	0/0	55.8	—	18/37.8	5.3-28 - 29
C.S.HEX	1039/20	.53/1.333	Y	6	60	135	1.25	-12.441	*21/0	*4.3/0	53.7	1	32/21.7	5.3-30 - 37
C.S.HEX	1039/20	.53/1.333	Y	6	60	135	1.25	-12.441	*21/180	*3/180	55.0	6.2	32/23	5.3-38 - 45
C.S.HEX	1039/20	.53/1.333	Y	6	60	135	1.25	-12.441	*21/90	-3.6/.6	54.4	39.4	27/27.4	5.3-46 - 47
C.S.HEX	1039/20	.53/1.333	Y	6	60	135	1.25	-12.441	*21/0	*3.1/0	53.8	2	29/24.8	5.3-48 - 55
C.S.HEX	1039/20	.53/1.333	X	6	60	135	1.25	-12.441	21/0	-3.5/.6	46.5#	36.3	24/22.5	5.3-56 - 57
C.S.HEX	1039/20	.53/1.333	X	6	60	135	1.25	-12.441	10/0	4.3/0#	53.7	-8	27/26.7	5.3-58 61
C.S.HEX	1039/20	.53/1.333	Y	6	60	135	1.25	-12.441	*10/180	3.1/0#	55.1	1	28/27.1	5.3-62 - 64

* indicates the angles are Theta/Phi; otherwise ,they are Az/El.
\# indicates that the validity of the values are in doubt.

TABLE 5. -2 SUMMARY OF COMPUTED SYSTEM PERFORMANCE --- PHASE SETTING BY SYSTEM FF SCAN

ARRAY				OPTICAL SYSTEM					PERFORMANCE @ 30GHZ					
									SCAN		GMAX		SIDELOBE	FIGURE #
SHAPE	#ELM /#ring	SPACING "λ@30GHZ	MAIN -POL	M	Q "	FL1 "	F/D	Zarray "	Ar'y	FF	Main	Xpol	dBI/dB down	
C.S.HEX	1039/20$	.53/1.333	Y	6	60	135	1.25	-12.441	0/0	0/0	56.7	34	27/29.7	5.3-23 - 27
(Enlarged Array,6 times)				(None)					0/0	0/0	55.8	-	18/37.8	5.3-28 - 29
C.S.HEX	1039/20	.53/1.333	Y	6	60	108	1.0	-13.864	0/9.41	0/ 1.75	55.4	5	27/28.4	5.3-65 - 68
(Enlarged Array,6 times)				(None)					0/1.75		55.45	-	18/37.45	5.3-69
C.S.HEX	1039/20	.53/1.333	Y	6	60	108	1.0	-13.864	0/-11.7	0/-1.75	55.7	1	27/28.7	5.3-70 71

* indicates that the angles are Theta/Phi; otherwise, they are Az/El.

$ indicates 102 Elements are deleted from the 20-ring HEX.

plane. Again, this deduction was verified by computer programs employed.

Although there was good agreement in the above verification, several problems were encounted.

1. The enlarged array did not produce cross-polarization patterns, while the computed system far fields in the unscanned case had a cross-pol peak gain about 23 dB below the man peak gain and occurred at one half beam width (3 dB) array from the main lobe. The de-polarization amounted ot 0.5% of the main beam power. Its presence was due to the nature of the offset reflector system.

2. In the unscanned case, the discrepancies between the secondary patterns of the system and the enlarged array occurred at 35 dB or more down from the main lobe peak region and are believed to be due to the offset nature of the system.

3. In the scanned case, the main lobe agreement between system far field and the enlarged array was limited to within one beam width about the main lobe, even though the sidelobe behavior was somewhat the same. This limited agreement was believed to be due to the effects of the element amplitude taper and the magnification factor (see figures 5.3-65 and 5.3-70) where M=6 was used in the cases which were considered. For smaller M's (e.g. M=3), the agreement is expected to improve greately (see figure 2.2-19).

SECTION 6

FEED ARRAY PACKAGING

The modified hexgonal feed array can be packaged in a housing similar to the arrangements shown in Figures 6.1 and 6.2. The MMIC modules are attached to transverse heat pipes that terminate in radiator panels placed in some distance form the antenna where the heat can be dissipated.

The corporate-feed waveguide network is attached directly behind the MMIC modules and the entire assembly is placed in a square housing. This approach provides the smallest size antenna feed array. The physical arrangement which permits the MMIC module assemblies to be individually inserted into or removed from the antenna is shown in Figure 6-3. The parallel rows of transverse heat pipes are spaced to provide adequate clearance for the modules to pass between them. Thru rods, which have stepped bosses for each amplifier, are placed on either side of the transverse heat pipe channel shown in Figure 6-3. The bosses on the through rods are at a spacing slightly less than that provided for the transverse heat pipes. When the thru rods are installed in the antenna, they pass through holes in the mounting flange of each output MMIC module. There are up to 33 rows of amplifiers and each thru rod has up to 33 bosses. The holes in the mounting flange of each MMIC module contain a steel bushing with a slotted hole, which is slightly larger than the thru rod bosses. The module assembly is inserted into the antenna and connected to the bulkhead containing the corporate feed output. Captive screws are provided in the module flange to make this connection. When all the the module assemblies are in place, the thru rods are put into the antenna and pass through the slotted holes in each module mounting flange. Rotating the rods 90 degrees causes the large area of the rod boss to contact the MMIC module flange and draw it down against the transverse heat pipe. When all the thru rods are in place, nuts are placed on the threaded end of the rod, which are then tightened to develop a pre-determined tension in the rod. This tensile force pulls each amplifier tightly against its transverse heat pipe permitting the amplifier heat to flow readily into the heat pipe.

If it becomes necessary to remove a module from the antenna this can be accomplished by removing the four thru rods which hold the module to its heat pipe and untightening the four captive screws in the module flange. The free module can now be removed from the antenna without disturbing any other modules.

The housing is the principal structure for the antenna feed array. The individual support members from each component section attach to and derive their support from it. The base of the housing contains the mounting surfaces (pads) for attaching the antenna to the spacecraft. The aperture across the feed horn cluster can be covered with an astroquartz fabric which provides an RF transparent window and also diffuses the sunlight to minimize temperature gradients across the antenna aperture. The housing is square measuring 18.0 inches on the side. Access to the antenna components is through removable access plates on the sides and base of the housing.

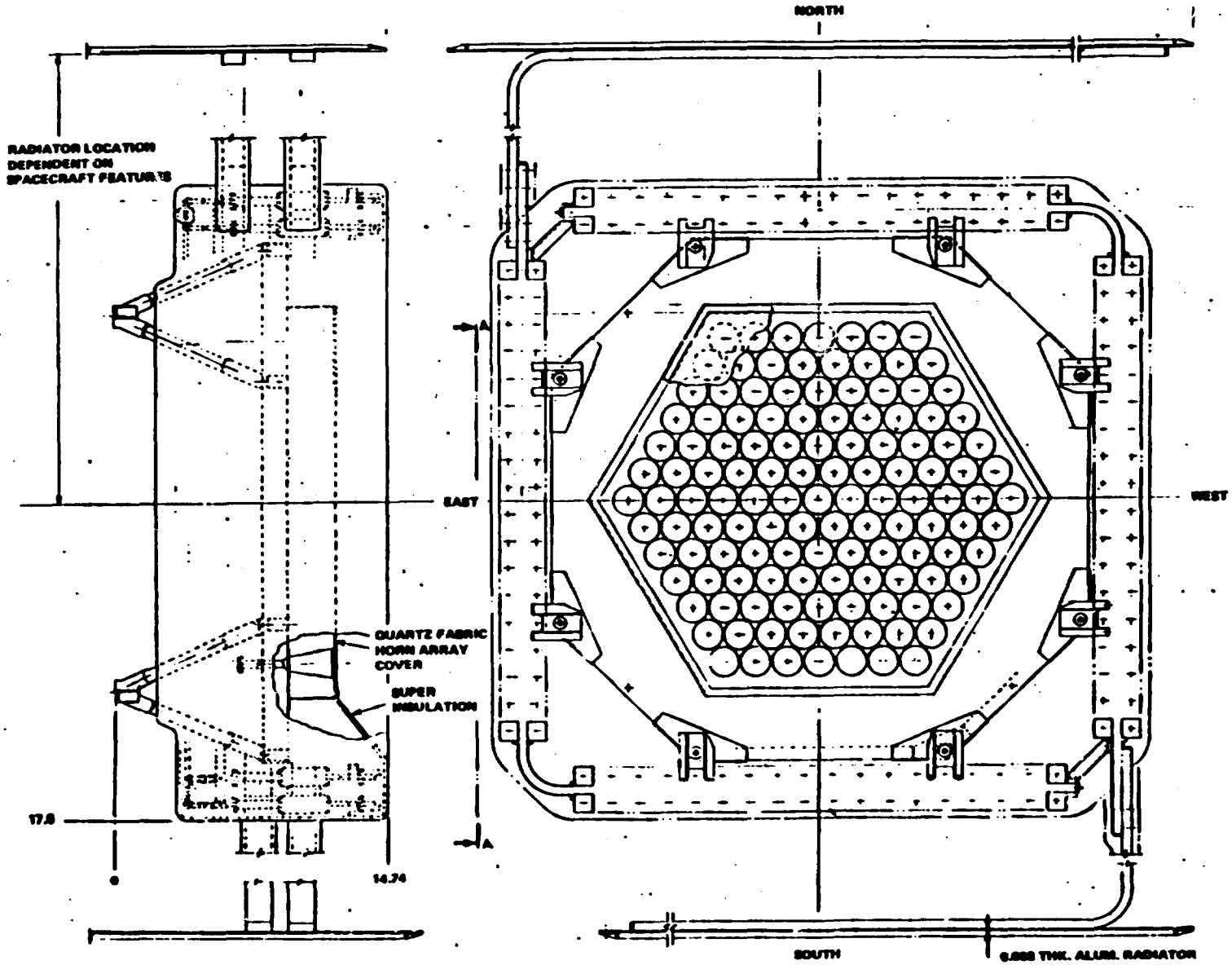

Figure 6.1 Peripherally Mounted Array

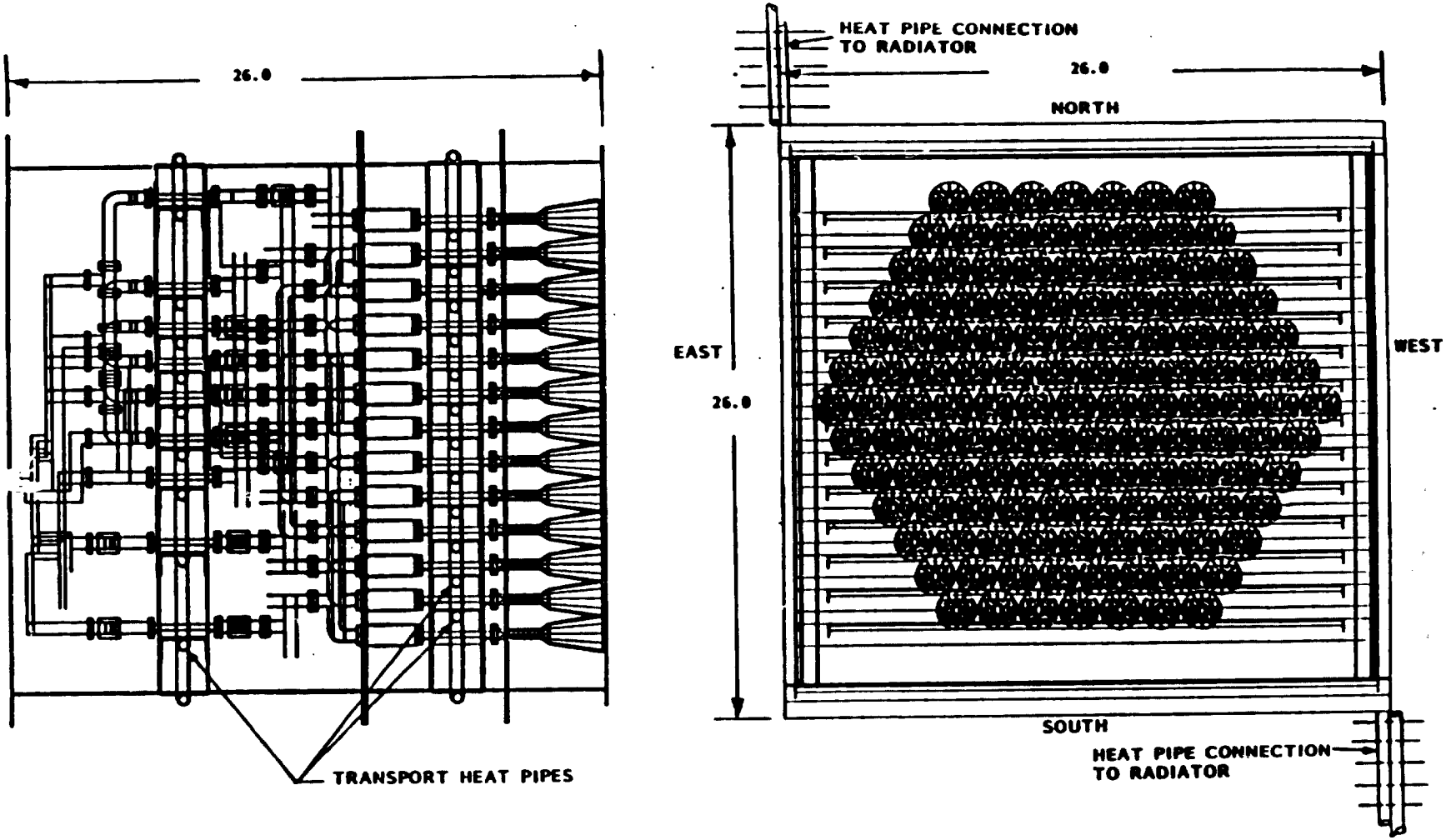

20GHZ SOLID STATE APERTURE ANTENNA
WITH OUTER STRUCTURE

Figure 6.2 Outer Structure

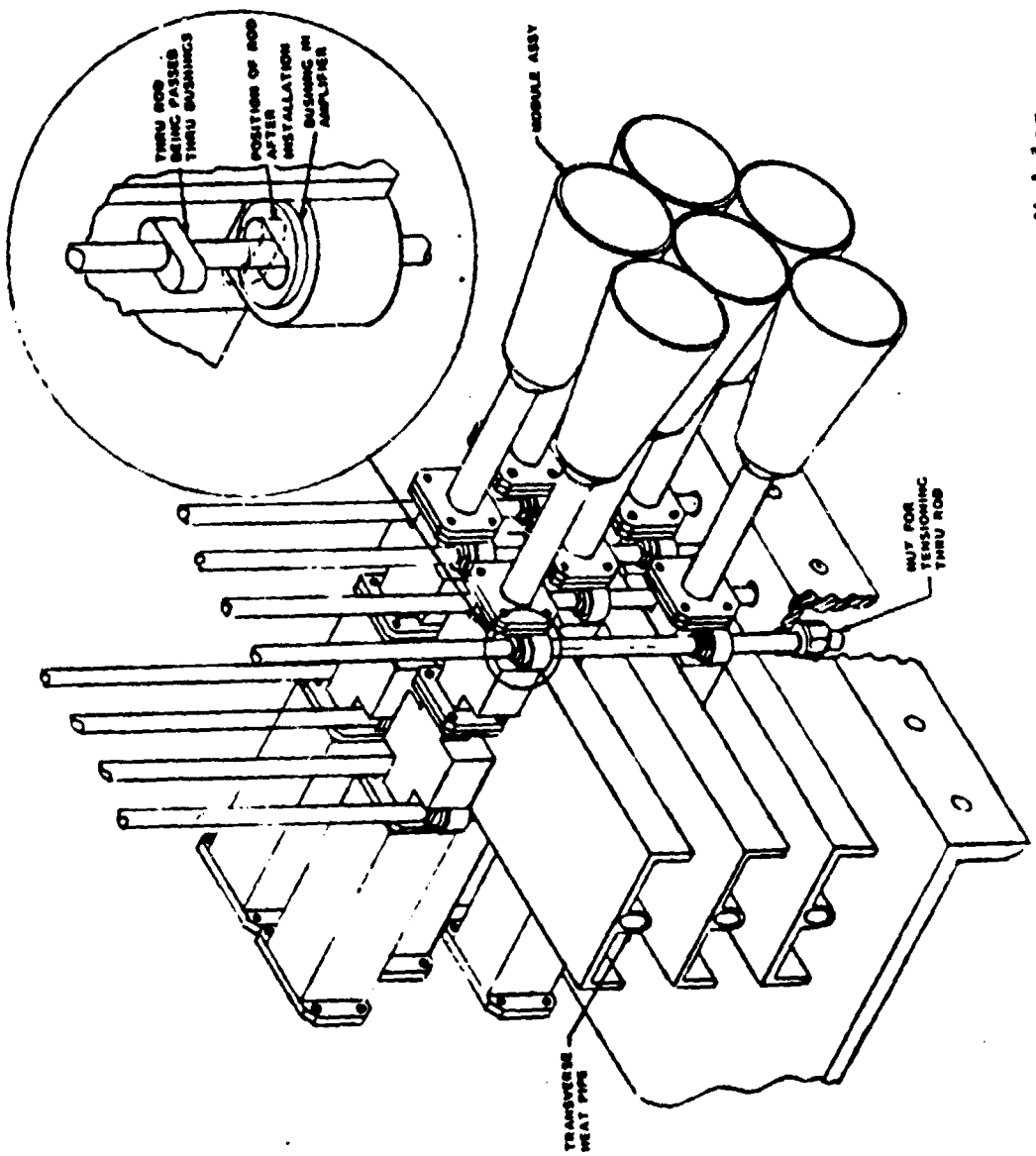

Figure 6.3 Physical Arrangement of Antenna Modules

SECTION 7

CONCLUSIONS

The confocal Gregorian offset parabolic antenna system, fed by a hexgonal phased array, was evaluated for CONUS scanning beam application. Several significant conclusions resulted from the study.

The inverse ray tracing technique (IRTT), a powerful analytic tool for designand optimization of complex multiple reflector antenna systems was developed and used extensively in this study. The word "inverse" refers to ray tracing from the scan plane (a plane normal to the system main beam and passing through the focal point) toward the source array plane. The tracing is performed on parallel rays in the direction of beam scan.

Using IRTT, the optical system can be designed optimally for a given M (magnification) and then array element weights (phase and amplitude) can be determined for any scan angle. The decoupling of the weight determination from the optical system design permits the designer to gain physical insight and obtain a near optimum design by an efficient and economical procedure. Elaborate optimization programs can later be used on the obtained design for further improvement such as sidelobe reduction and cross-polarization suppression.

Specifically, the following features were obtained using IRTT for a preselected magnification and main dish size:

(1) Location and size of the subdish
(2) Location and size of the array
(3) Main dish offset --- to clear the blockage and to avoid main dish image fold-back
(4) Path lengths from the array elements elements to their respective images on the scan plane
(5) Amplitude taper at the array plane which was mapped from the desired taper at the scan plane
(6) System orientation East-West, North-South assignment

Extensive parametric studies were performed on the array. Included in the obtained graphs were array performance parameters (peak gain, sidelobe level, and grating lobes) versus parameters such as array shape (circular, hex, and circular shaped hex), element spacing, number of elements, amplitude taper levels, phase quantization (3-6 bits), and number of element failures.

Elimination of potential grating lobes, due to size and position of the sub dish imposed the most stringent requirement on element spacing. Hence, determining the minimum number of array elements. For M=6 and a main dish diameter of 108", the required feed array was 18" in diameter and the grating lobe was required to be at least 50 degrees away from the scanned main lobe. The resultant array needed to meet these requirements was a 20-ring (1039 element) circular shaped hex array (102 elements deleted from a 20 ring hex array of 1141 elements), with an element

spacing of .53" (1.333 at 30 GHz). The hex array has the most dense element packaging and, hence, the largest angular discrimination between the grating lobe and the main lobe. Also, the corner elements of a hex array can be deleted without significant effect, due to the level of tapering. Therefore, the circular shaped hex was selected for this study. As a result of the parametric analysis, it can be concluded that a 5-bit phase shifter will provide adequate phase resolution. A 1/2 bit random phase error can be tolerated in the MMIC modules without introducing serious performance degradation. A 26 level taper with a 20 ring modified hex array provided ample margin on the sidelobe requirement. A sixteen level taper could also be utilized with satisfactory performance. Due to the number of elements used in the Gregorian set-up, a 10% random amplitude error has a very small effect on the system. A failure analysis showed that the system will maintain the sidelobe and peak gain requirements with up to 50 random amplifier failures or up to 8 random phase shifter failures. A more in depth failure analysis is required before any element failure conclusions can be made.

One of the main objectives of this study was to investigate the feasibility of an array static taper. The array amplitude taper was initially chosen to be 5 levels (0, -3, -6, -10, -13 dB), and was later expanded to 26 levels (from 0 to -20 dB according to a binamial distribution), since a 5 level taper could not provide a secondary pattern with sidelobe levels better than -26 dB.

As a comparision to the results of the static taper, the amplitude taper across the scan plane was assumed to have a binomial distribution of the form : A+B(1-(/a)**2))**2 with A=0.1, B=0.9; and this taper was mapped to the array plane to determine the array element amplitude setting (referred to as the imaged taper).

Secondary patterns scanned to an AZ/EL angle of 0/1.75 degrees were obtained for both the static and the imaged taper, (with M=6, main dish diameter= 108") and the array element phase settings were derived using IRTT. The static taper gave a better pattern than did the image taper. This result seemed improper at first but is actually quite realistic and explained in the following. The images of the constant level contours of a static taper appear in the scan plane as concentric ellipses. The outermost ellipse corresponds to the edge of the circular array and defines the boundary of the effective scan plane aperture. The constant level elliptical contours provide a better scan plane aperture utilization efficiency than do the circular contours of the imaged taper case. The aperture is not used efficiently in the imaged taper case, because there are disjointed "leftover" areas between the ellipse and the largest inscribing circle. The difference in utilizing the scan plane aperture leads to a higher tapering efficiency of the static taper than that of the imaged taper.

The imaged taper would have the highest efficiency if the effective scan plane aperture were made circular. Such an aperture implies an elliptical array for a non-zero scan (circular array for an unscanned case). If the array elements are stacked in a "hexagonal" manner, an elliptical array requires that all the array elements are to be of an elliptical shape in order to maximize the array aperture usage. Unfortunately, the elliptical shape changes as a function of scan angle. This implies that an imaged taper can be implemented only for a specific scan angle to obtain a maximum taper efficiency. The static taper would provide a global near optimum performance. A set of secondary patterns were obtained. They were divided into two groups. The first group was summarized in table 5.3-1, where the element phase was deteremined by the array far field scan and the optical system was neither needed or used. The second group is summarized in table 5.3-2,

where the element phase was determined from the path lengths calculated using IRTT. In this case the optical system information is required. The steps used in group 2 should be followed in future design work and are summarized below:

STEP 1 Select the optical system parameters
- M Magnification
- FL1 Main dish focal length
- F/D FL1 divided by main dish diameter
- Q Main dish offset
- Za Array plane distance to the focal plane

STEP 2 Verify the parameters by IRTT (Inverse Ray Tracing technique) for various system scans. Determine the main dish images on the subreflector and on the array plane. Specify the size and location of the sub dish and array aperture. Check for blockage as well as the occurance of "fold back".

STEP 3 Freeze the parameters and compute the weights of the array elements using IRTT for desired system scans.

STEP 4 Predict system performance for each scan direction.
- a) Gmax peak gain (main pol. and cross pol.)
- b) Gain versus Beam Angle (main pol. and cross pol.)
- c) Beamwidth vs. scan position
- d) Sidelobes, PPeak value and location

STEP 5 Optimize the system performance for a given scanning direction. Optimization programs may be employed to fine tune the weights of the array elements at a particular scanning direction. To utilize the optimization programs, the far field patterns of each of the array elements (or cluster of elements) are first computed based upon the optical system parameters obtained above. Target values are then selected at various points and the element weights (phase and magnitude) are optimized to match these specified values.

The aperture imaging concept has been justified in this study for both unscanned and scanned cases. It was fully justified for the unscanned case where excellent agreement was obtained between the system secondary pattern and the pattern obtained from an enlarged array placed in the scan plane.

The imaging concept was also justified for the scanned case where the system peak gain and location were in excellent agreement with the imaged array. A discrepency in the shape of the main lobe below ** dB is well understood as explained in conclusion #3. The discrepency could be eliminated for any specific scan angle provided that the array and horn element were both designed for the desired angle . Different array and horn shapes would be required for each scan angle in order to eliminate the afore mentioned discrepency.

It is desirable to minimize the main reflector offset . The constraints are the blockage clearance and the "image fold-back". The image fold-back phenomenon was discussed in section 2.2.2. In the fold-back region, the path length variation per element spacing changes sign and increases in magnitude almost exponentially, thus the fold-back region must be avoided. The limitation on the minimum main dish offset imposed by fold-back suppression may be more critical than the blockage restriction.

Mechanical considerations of the feed array packaging were included. (See section 6)

PLOTS

FOR

SECTION 3

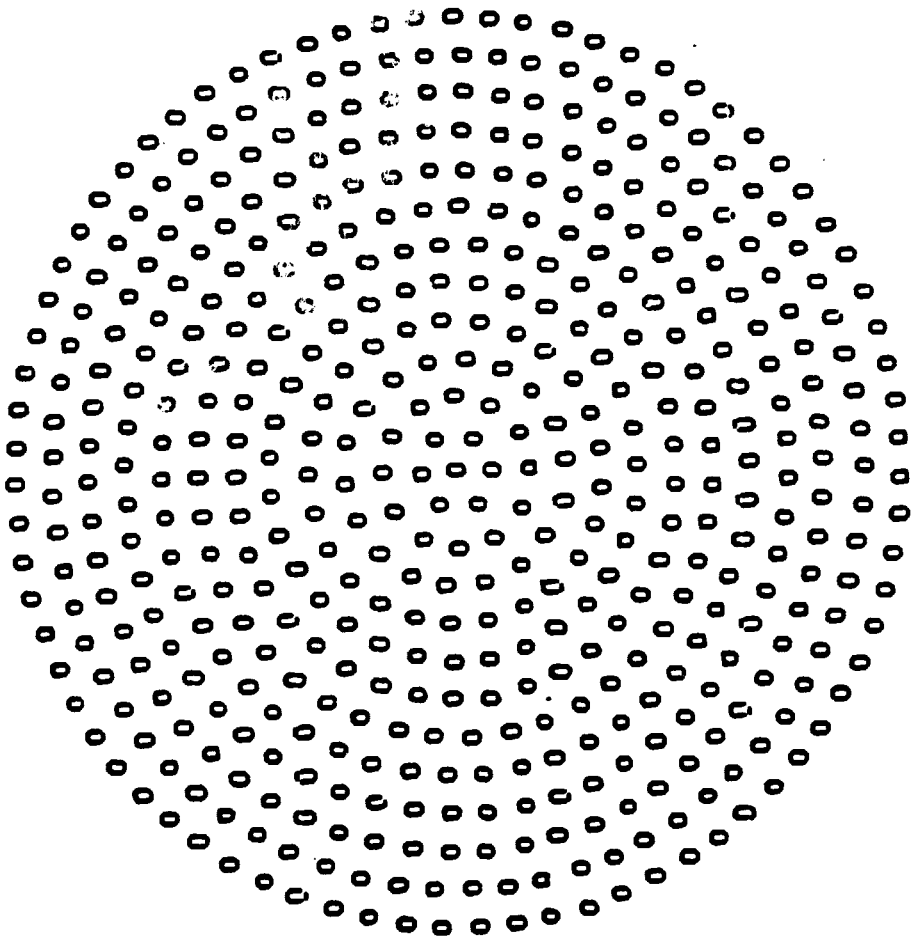

FIG. 3.1.1 485 ELEMENT CIRCULAR ARRAY (13 RINGS)

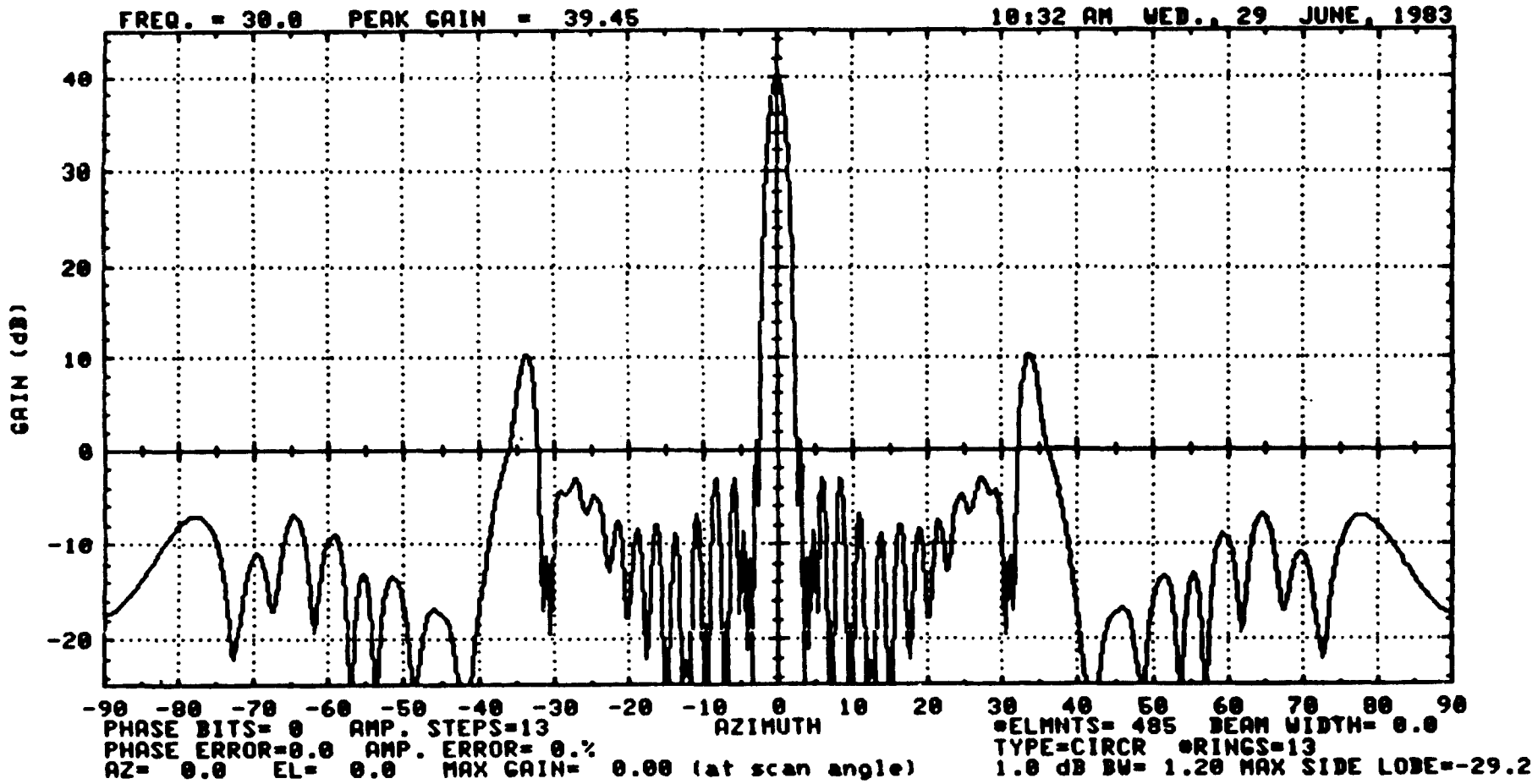

FIG. 3.1.2 UNSCANNED

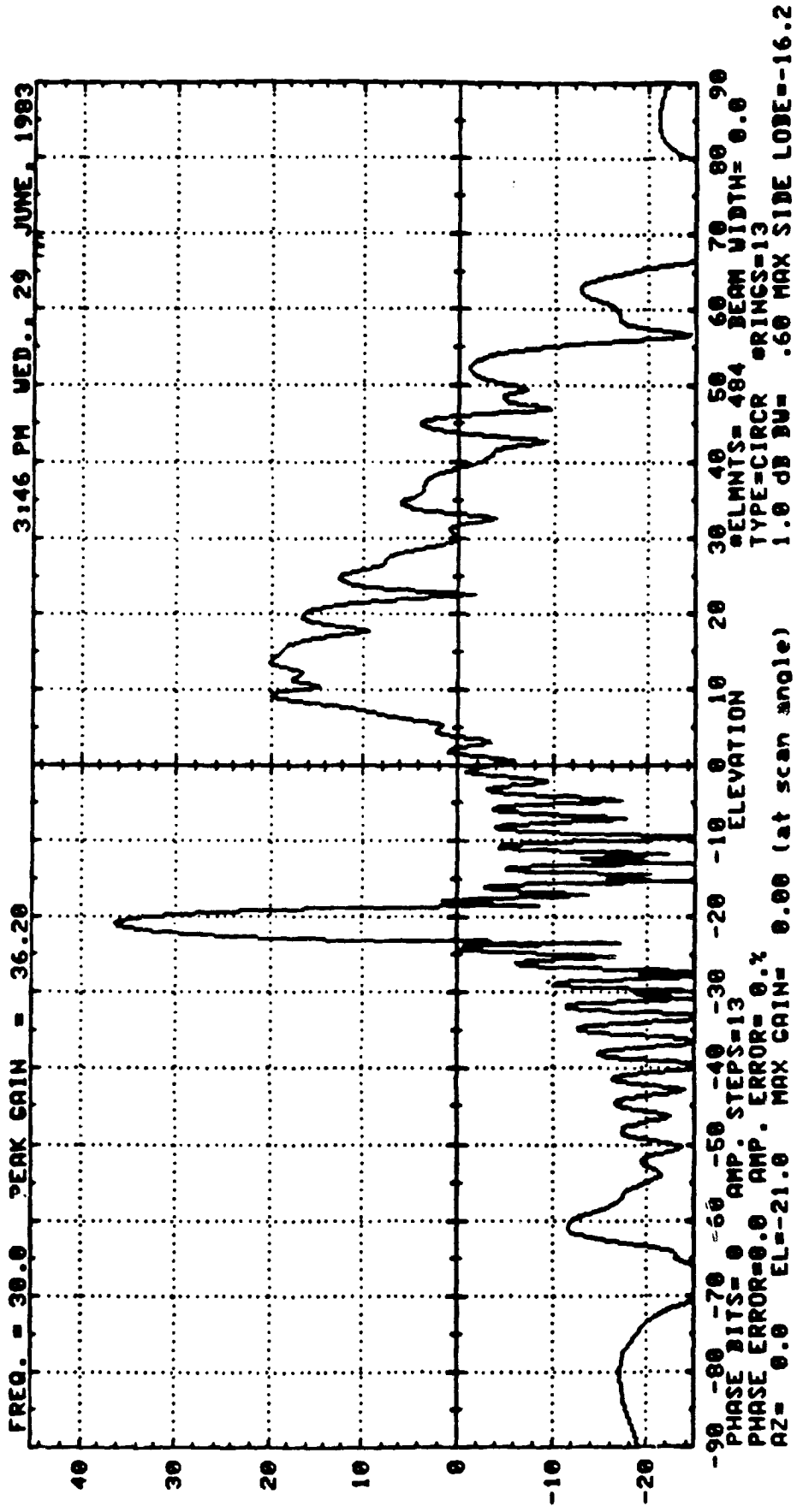

FIG. 3.1-3 SCAN: $A/E = 0°/21°$

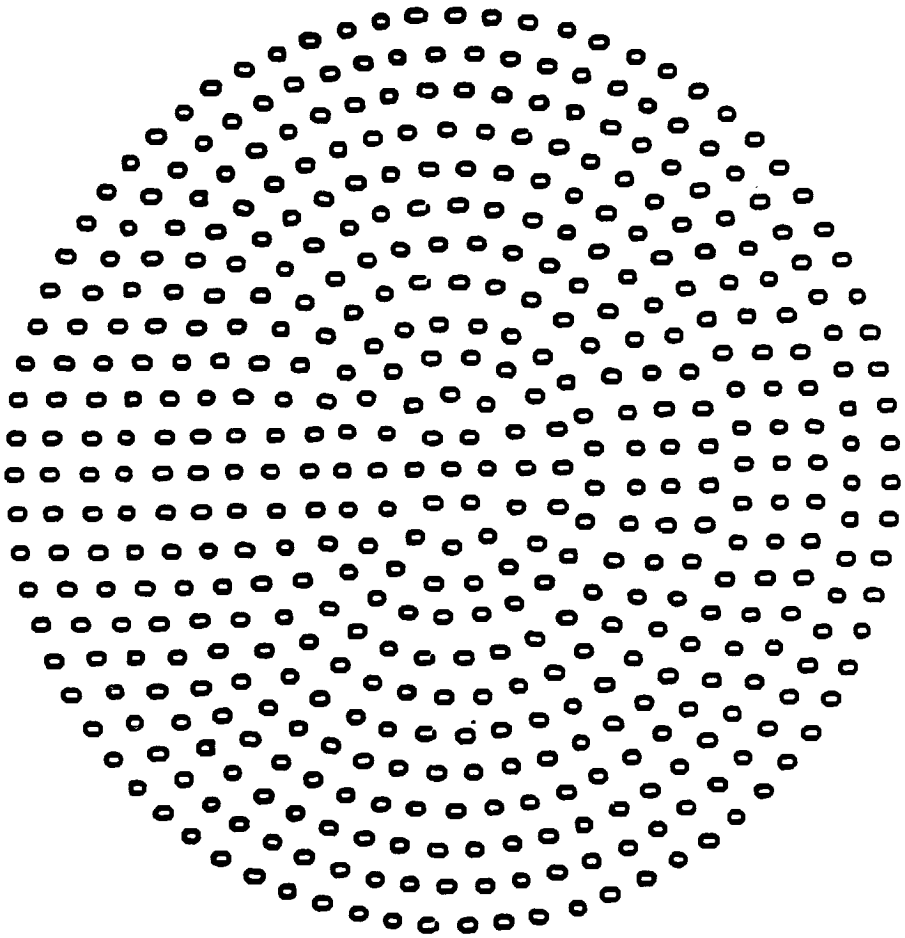

FIG. 3.1-4 747-ELEMENT CIRCULAR (16 RINGS)

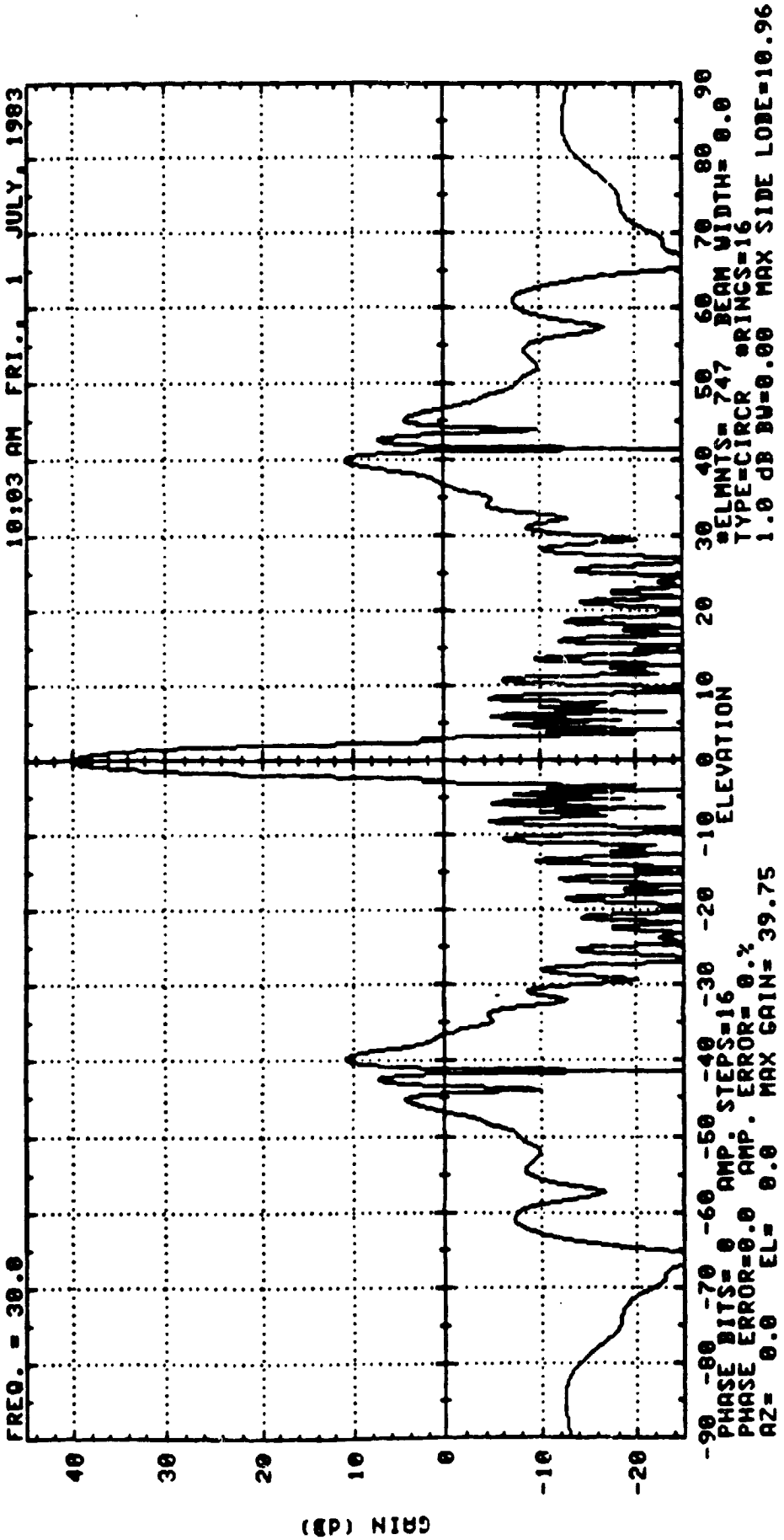

FIG. 3.1-5 UNSCANNED

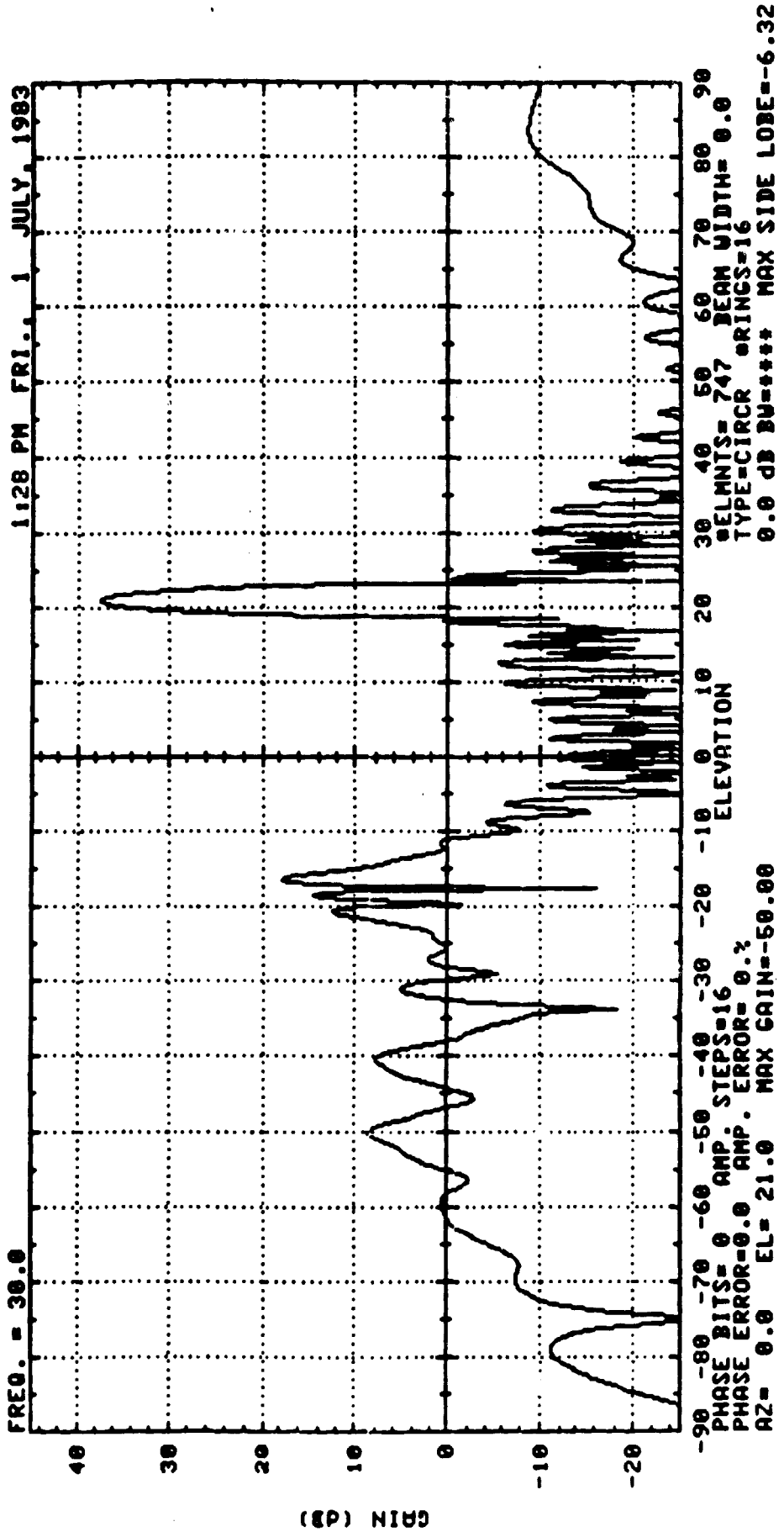

FIG 3.1-6 SCAN: $A/E = 0^\circ/21^\circ$

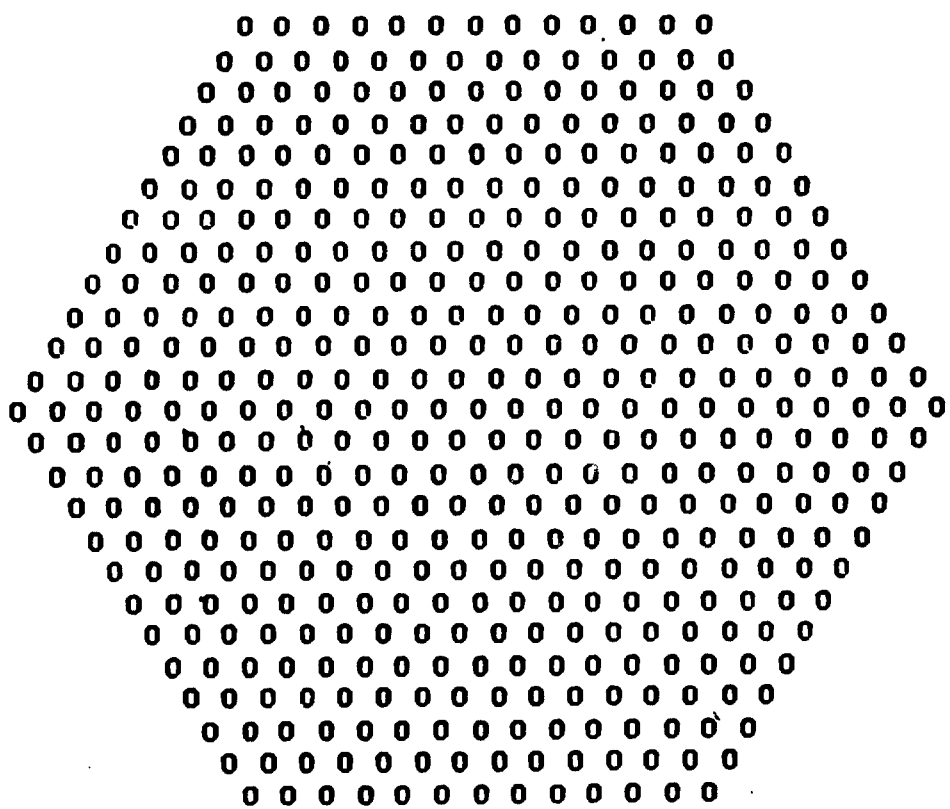

FIG. 3.1-7 13-RING HEX, 469 ELEMENTS

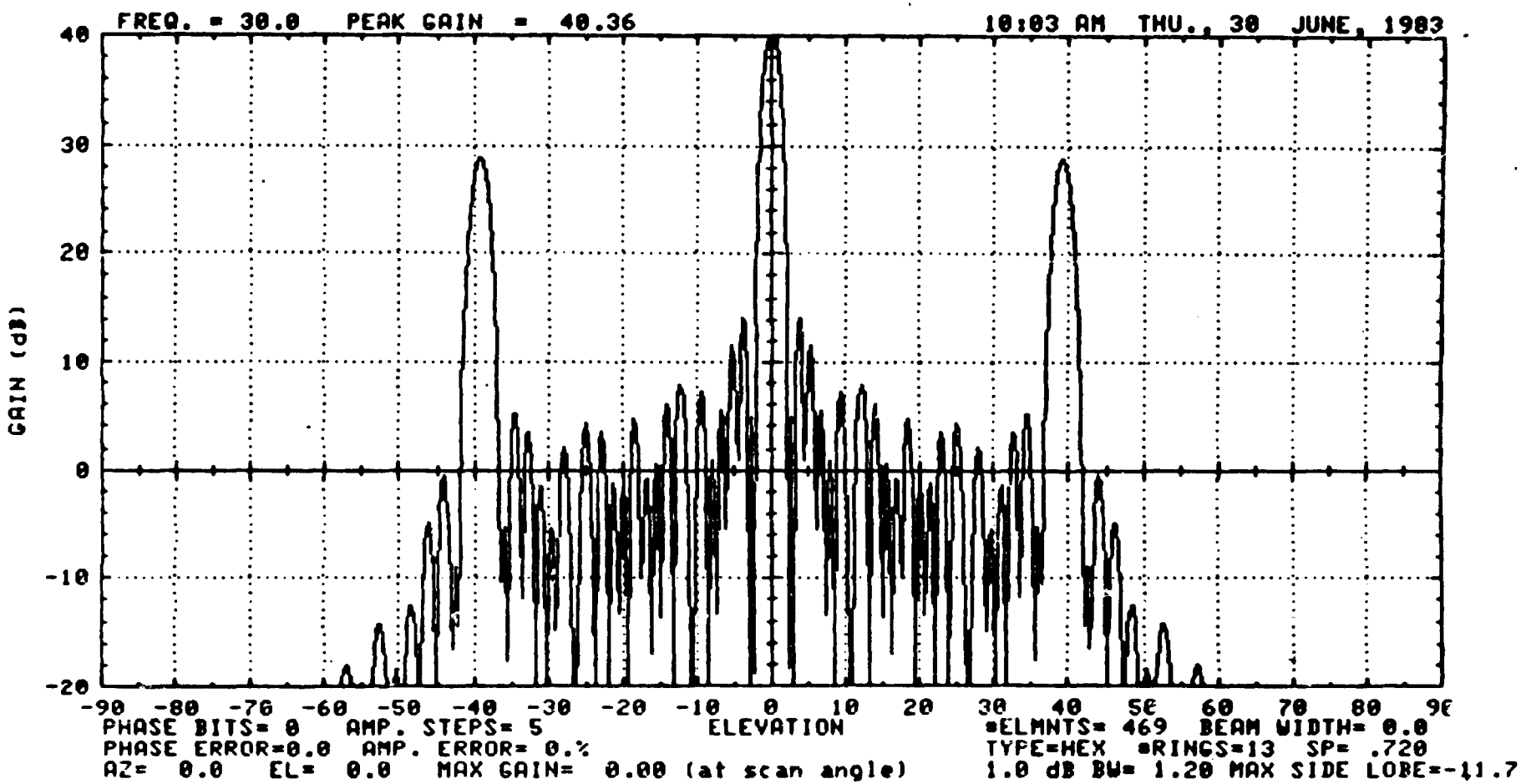

FIG 3.1-8 13 RING HEX, 5 LEVEL TAPER, UNSCANNED EL CUT

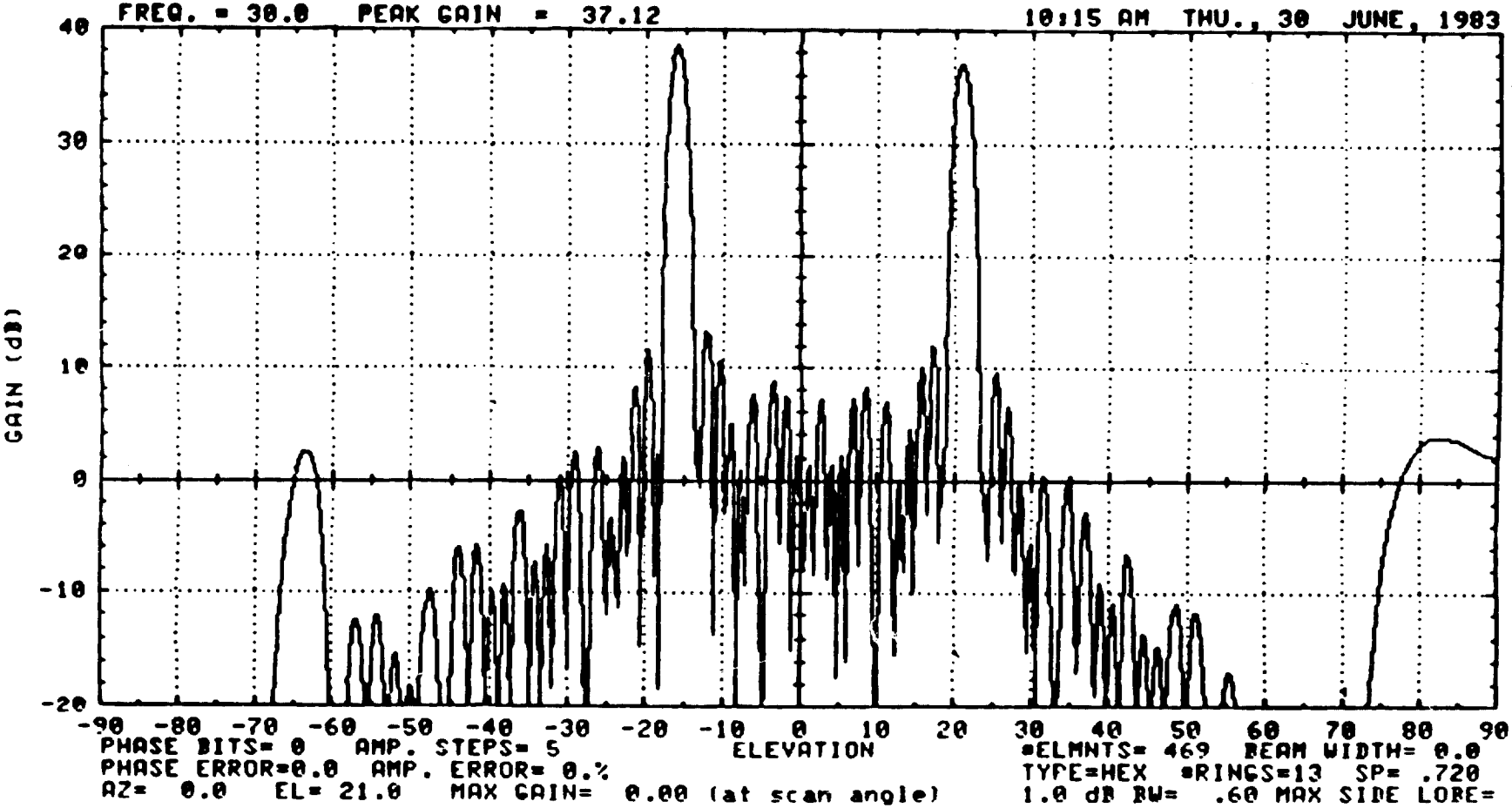

FIG 3.1-9 13 RING HEX, 5 LEVELS, SCAN: (0,21°), EL CUT

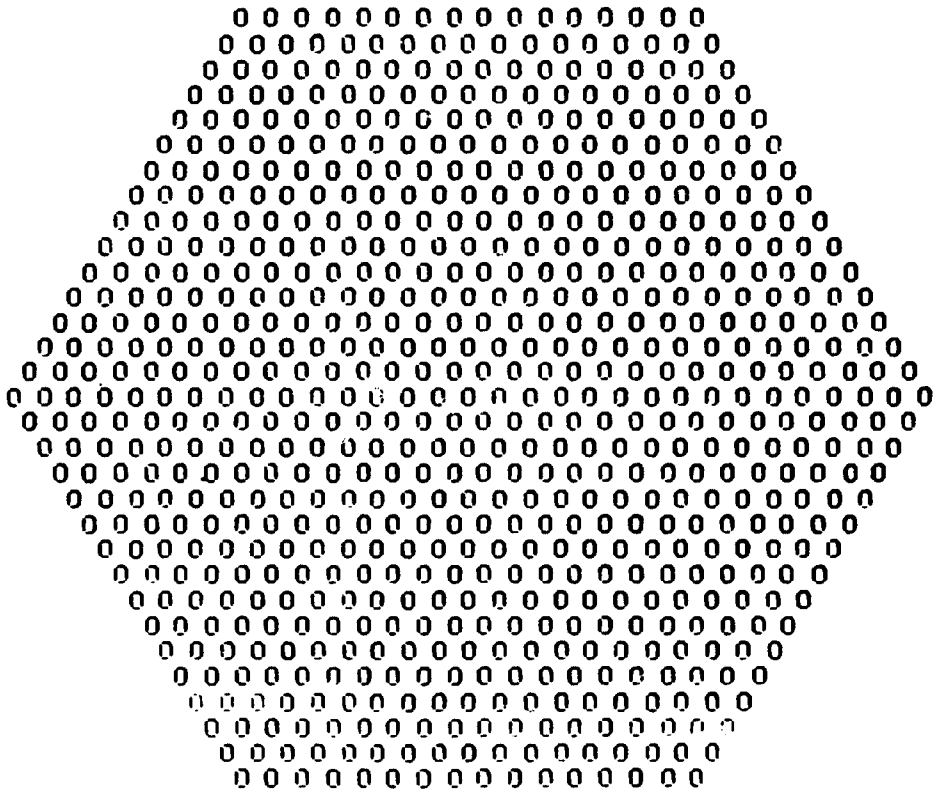

FIG. 3.1-10 16-RING HEX, 721 ELEMENTS

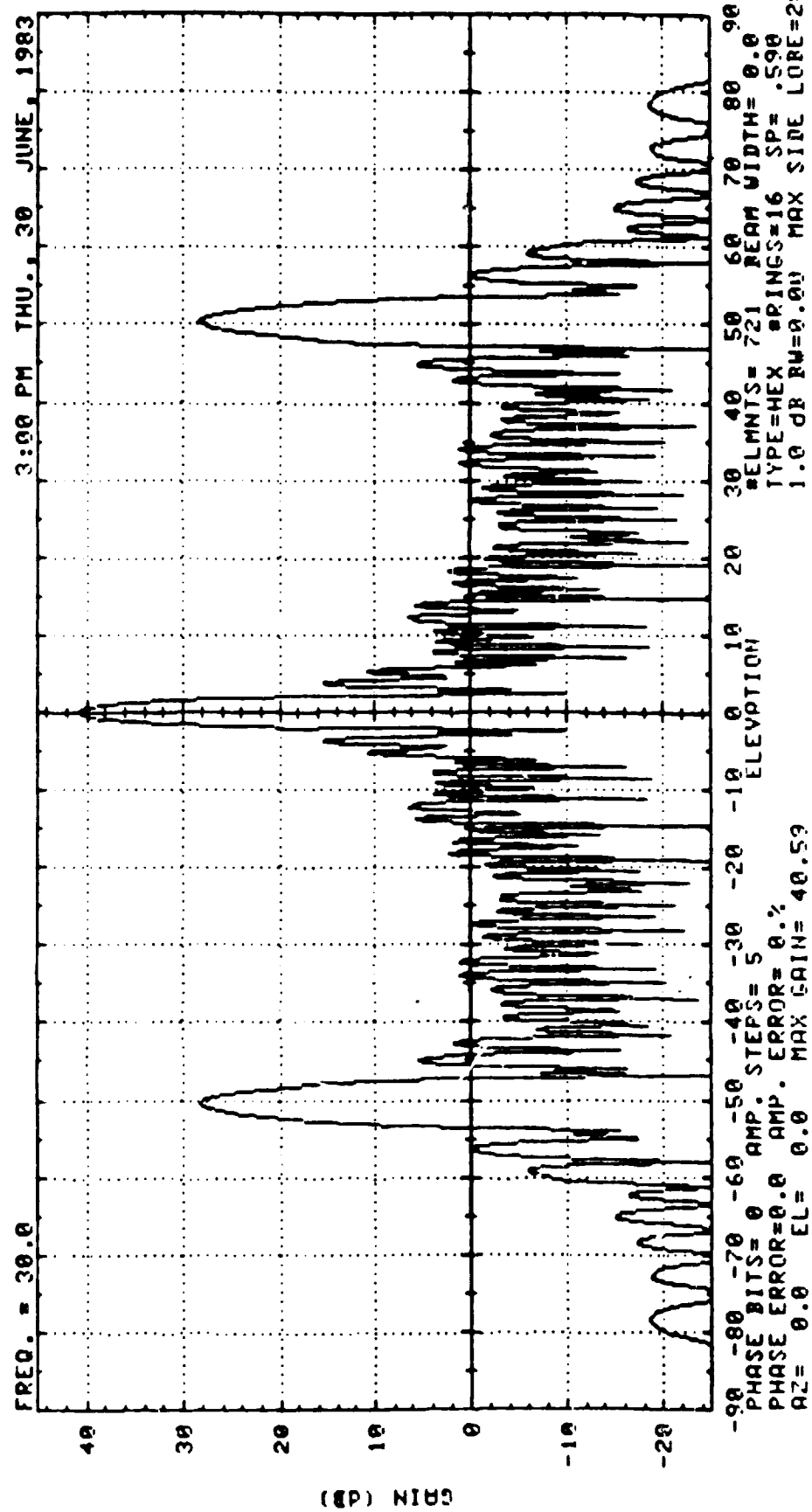

FIG 31-11 UNSCANNED

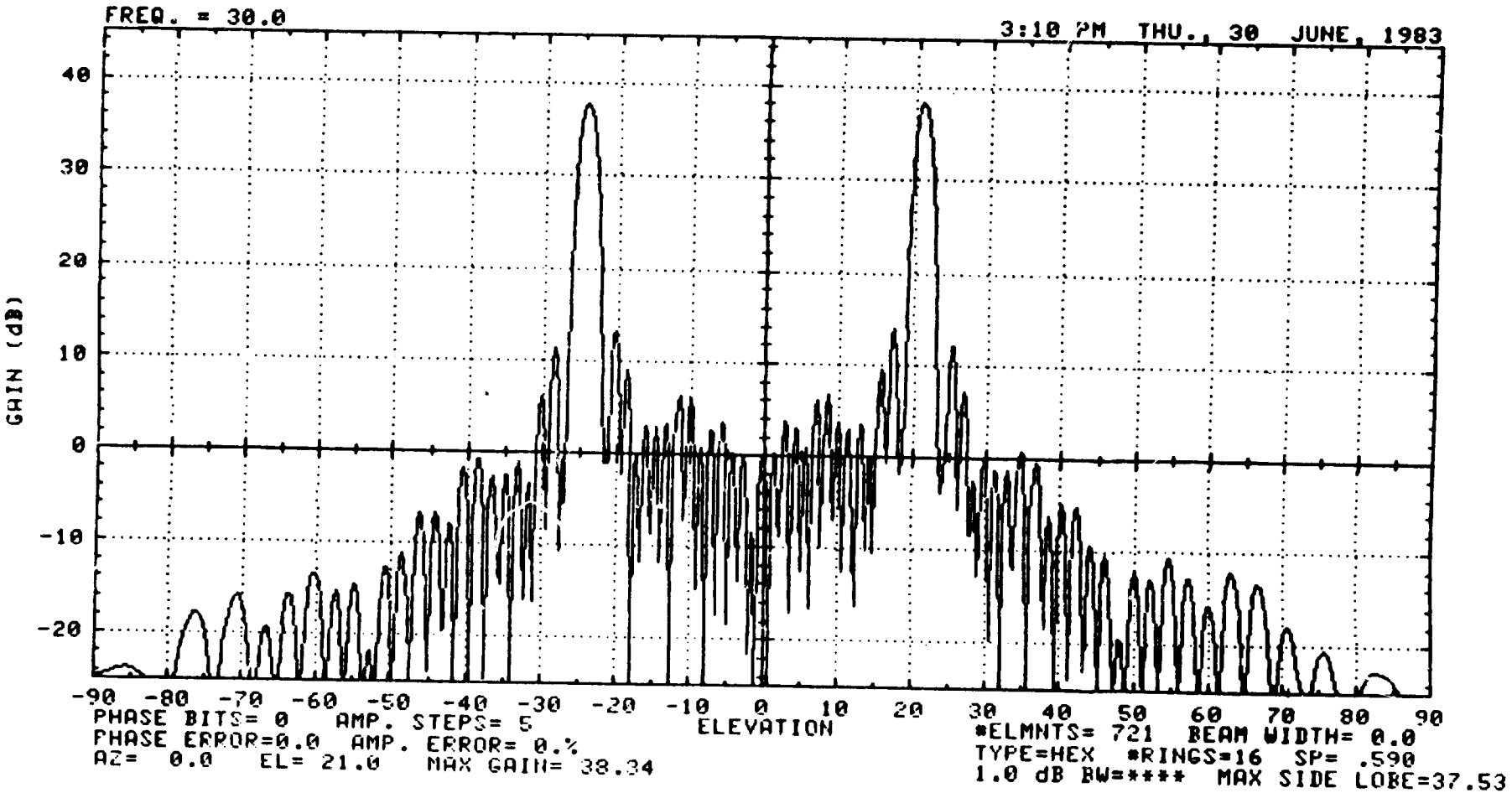

FIG. 3.1-12 SCAN: A/E = 0°/21°

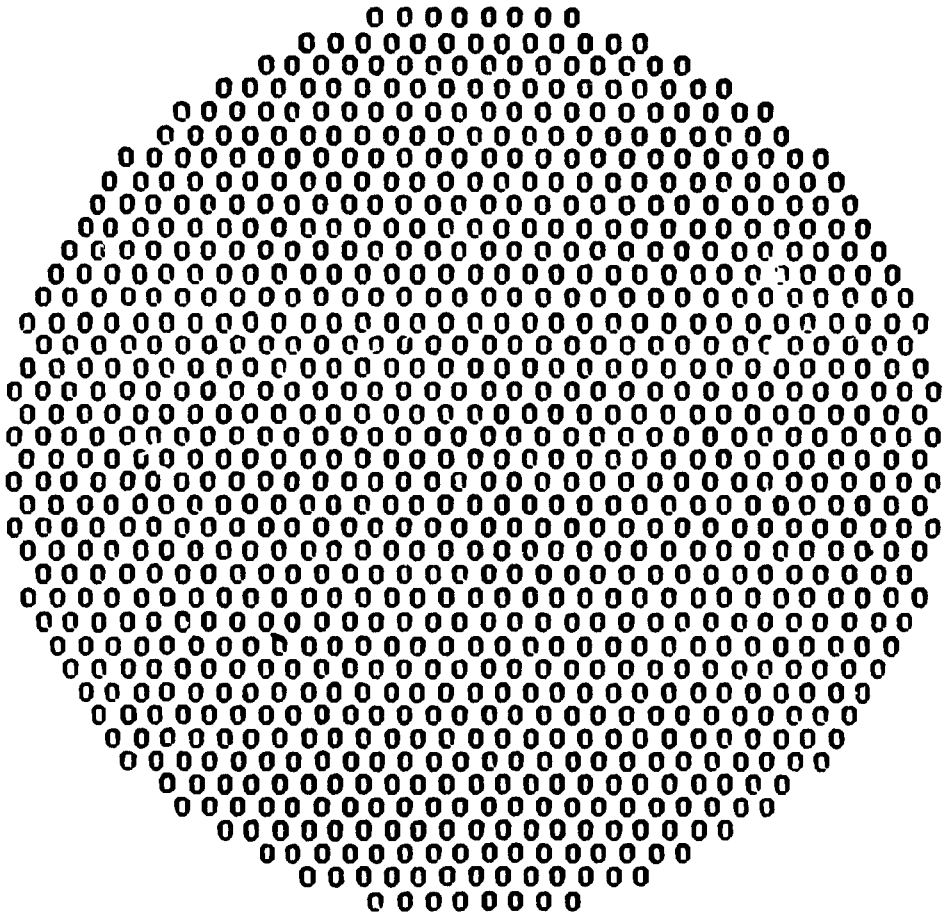

FIG. 3.1-13 20 RING CIRCULAR-SHAPED HEX, 1039 ELEMENTS

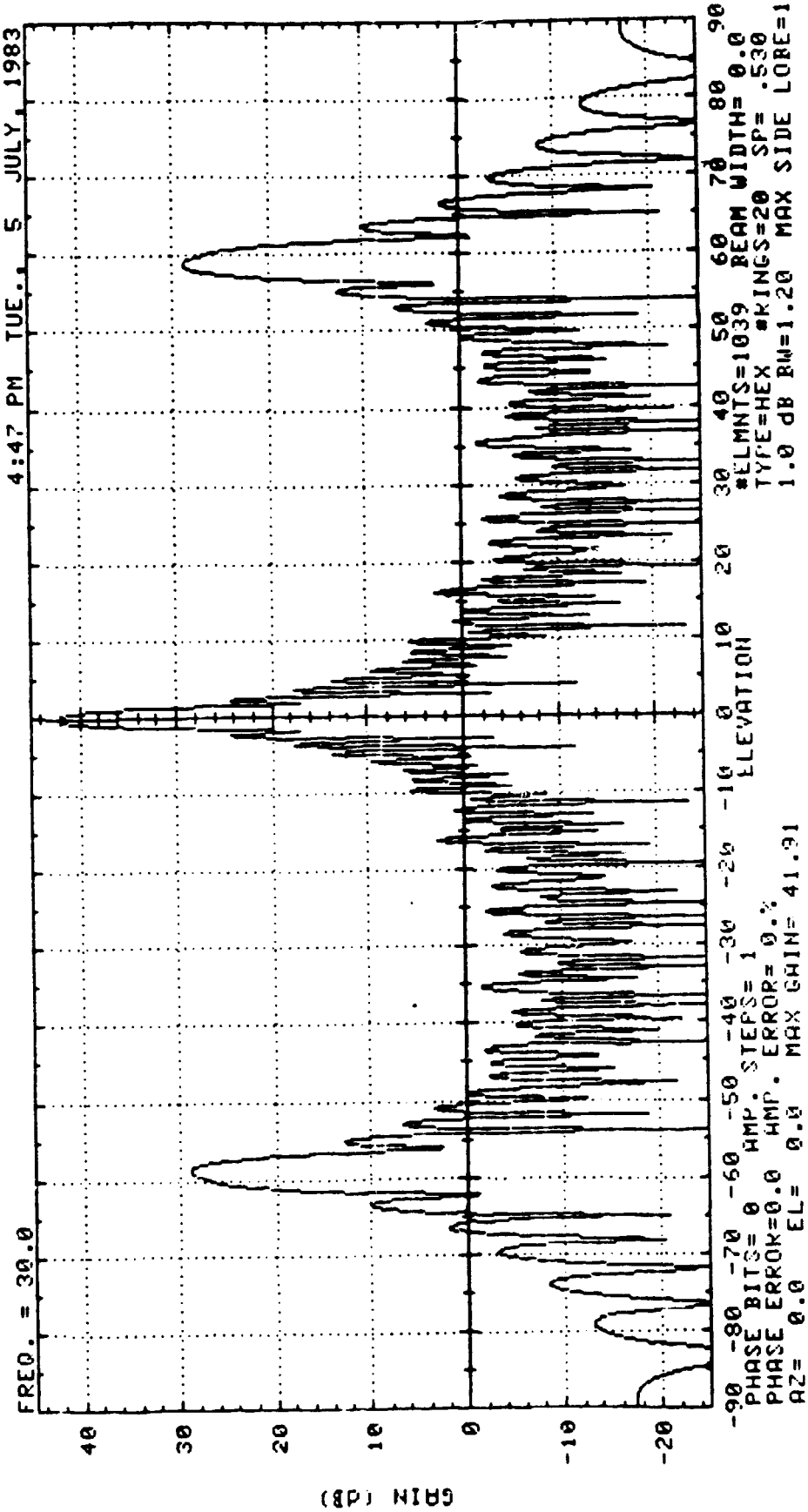

FIG. 3.1-14 UNSCANNED, UNIFORM TAPER

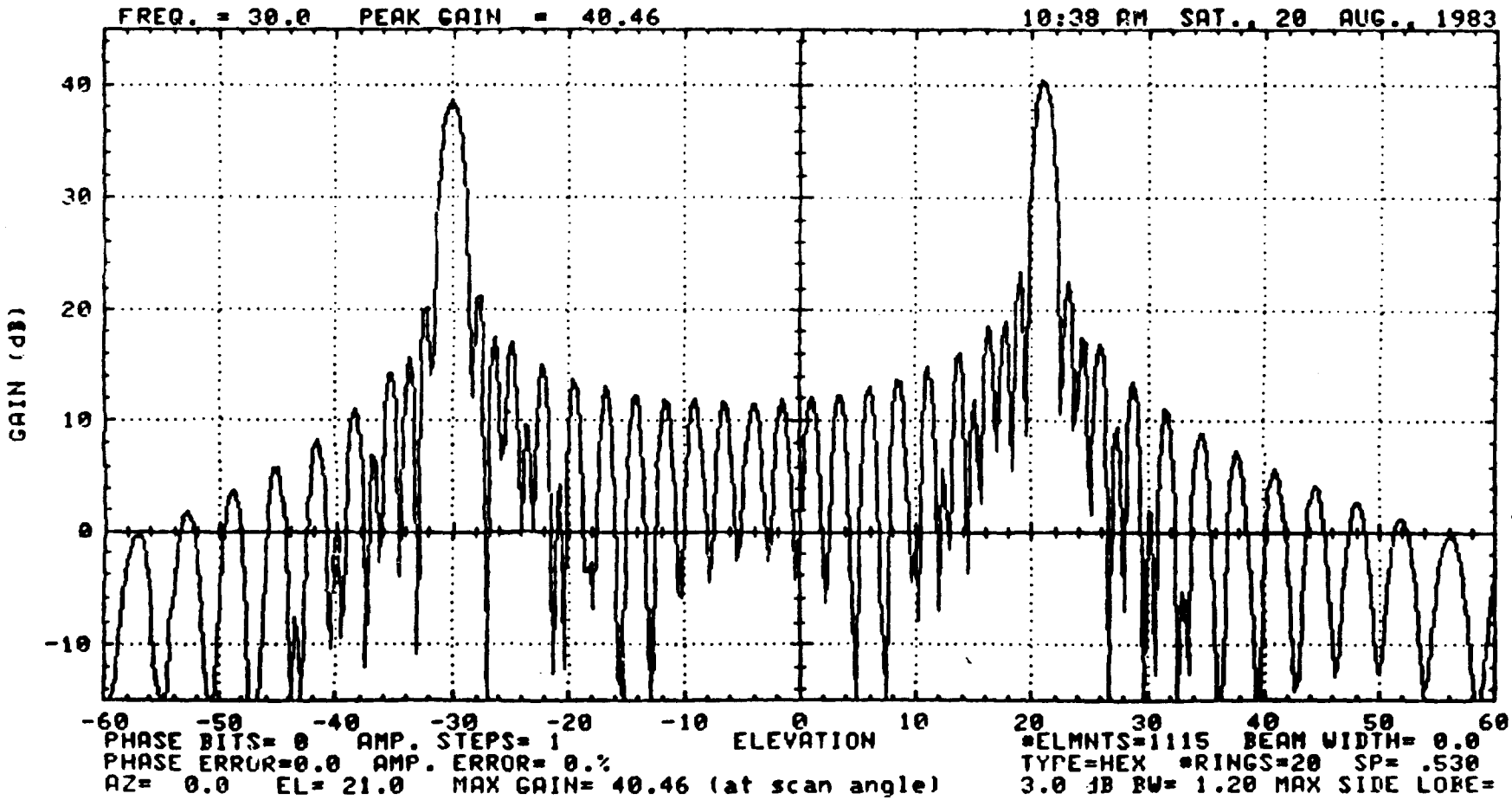

FIGURE 3.1-15

20 RING CC HEX SCAN CASE - 0°/0°) EL-CUT

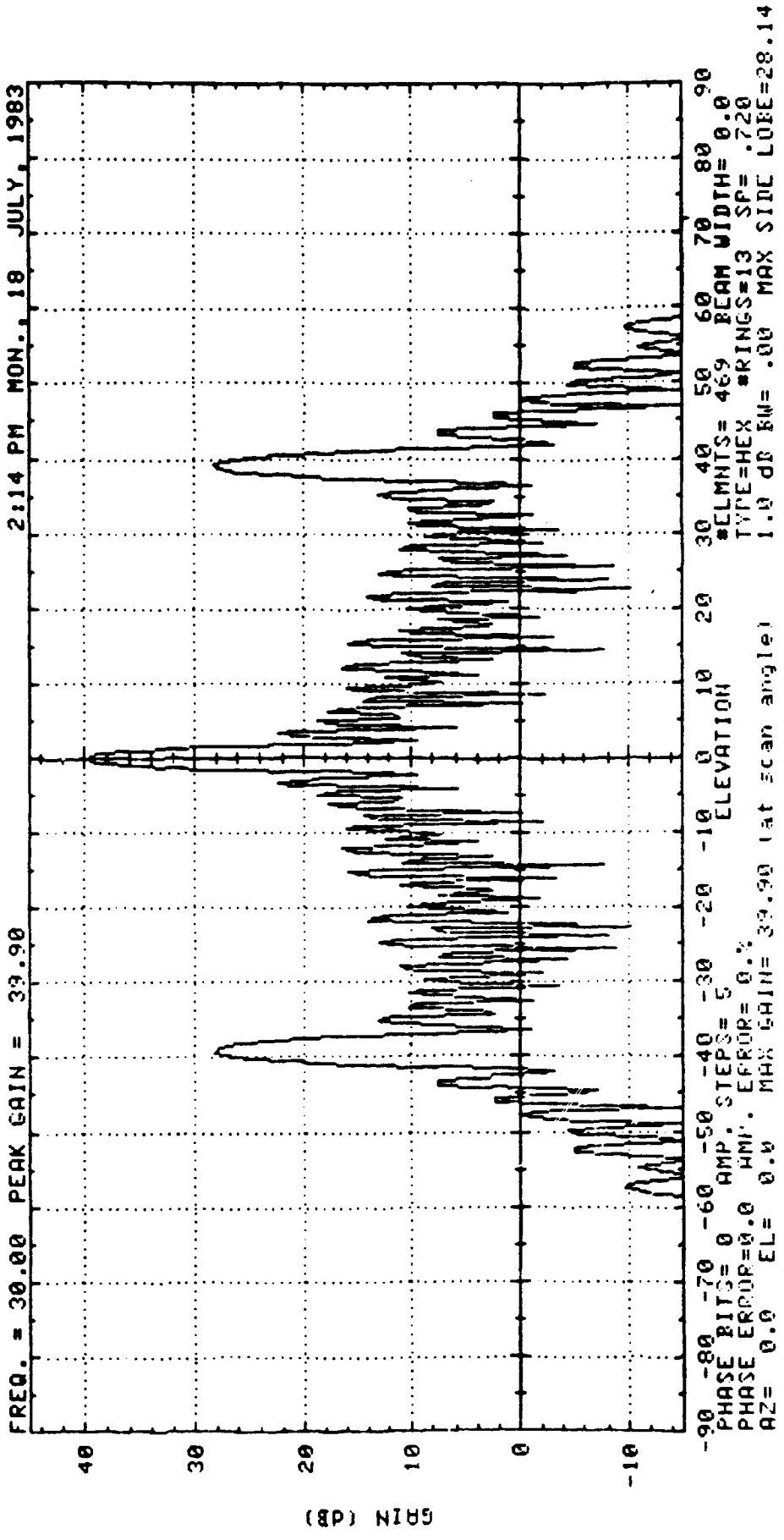
FREQ. = 30.00 PEAK GAIN = 39.90
2:14 PM MON., 18 JULY, 1983
GAIN (dB)
40
30
20
10
0
-10
-90 -80 -70 -60 -50 -40 -30 -20 -10 0 10 20 30 40 50 60 70 80 90
ELEVATION
PHASE BITS= 0 AMP. STEPS= 5 #ELMNTS= 469 BEAM WIDTH= 0.0
PHASE ERROR=0.0 AMP. ERROR= 0.% TYPE=HEX #RINGS=13 SP= .720
AZ= 0.0 EL= 0.0 MAX GAIN= 39.90 (at scan angle) 1.0 dB BW= .00 MAX SIDE LOBE=28.14

Fig 3.2-1

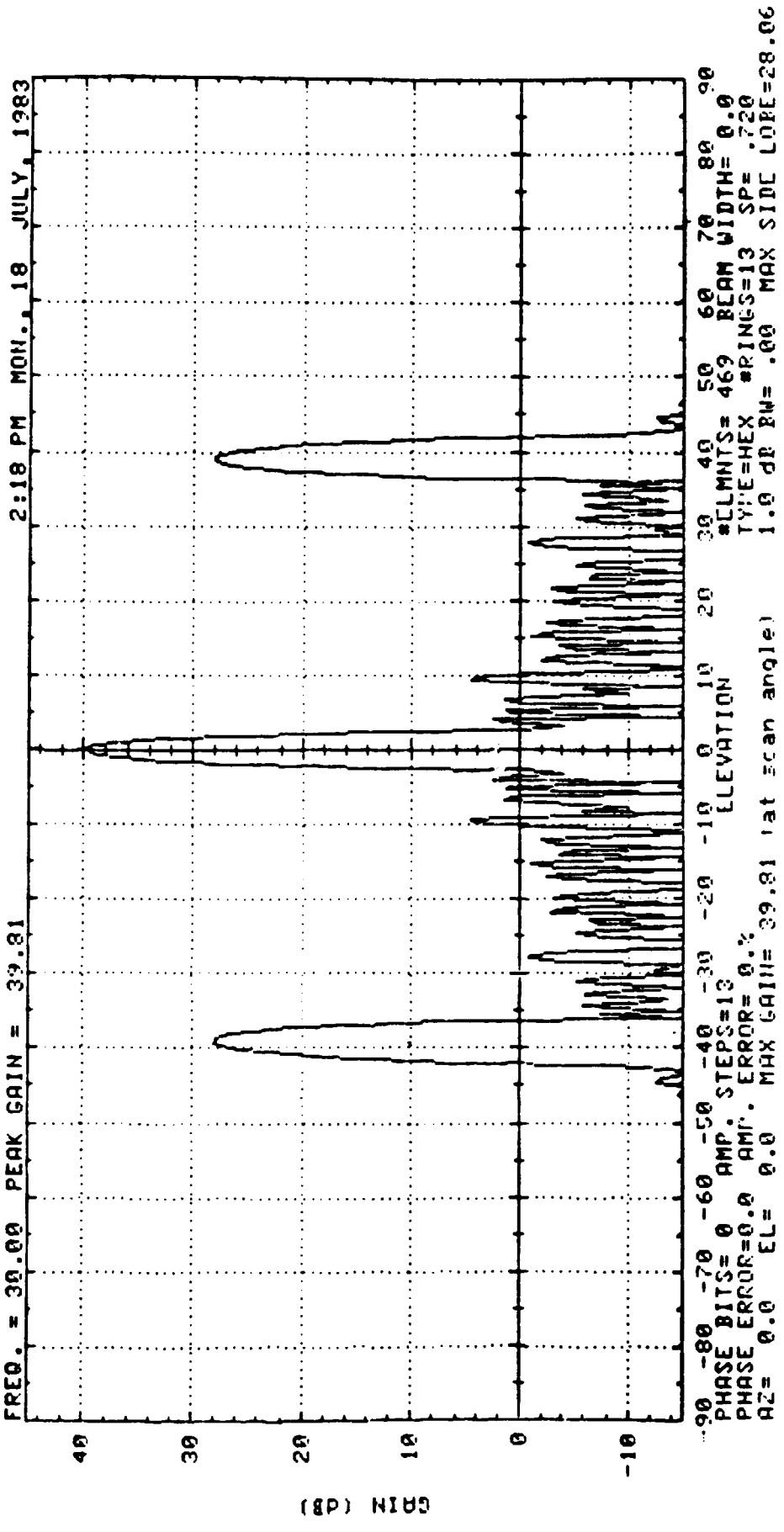
FREQ. = 30.00 PEAK GAIN = 39.81
2:18 PM MON., 18 JULY, 1983
GAIN (dB)
40
30
20
10
0
-10
-90 -80 -70 -60 -50 -40 -30 -20 -10 0 10 20 30 40 50 60 70 80 90
ELEVATION
PHASE BITS= 0 AMP. STEPS=13
PHASE ERROR=0.0 AMP. ERROR= 0.%
AZ= 0.0 EL= 0.0 MAX GAIN= 39.81 (at scan angle)
#ELMNTS= 469 BEAM WIDTH= 0.0
TYPE=HEX #RINGS=13 SP= .720
1.0 dB BW= .00 MAX SIDE LOBE=28.06

Fig 3.2-2

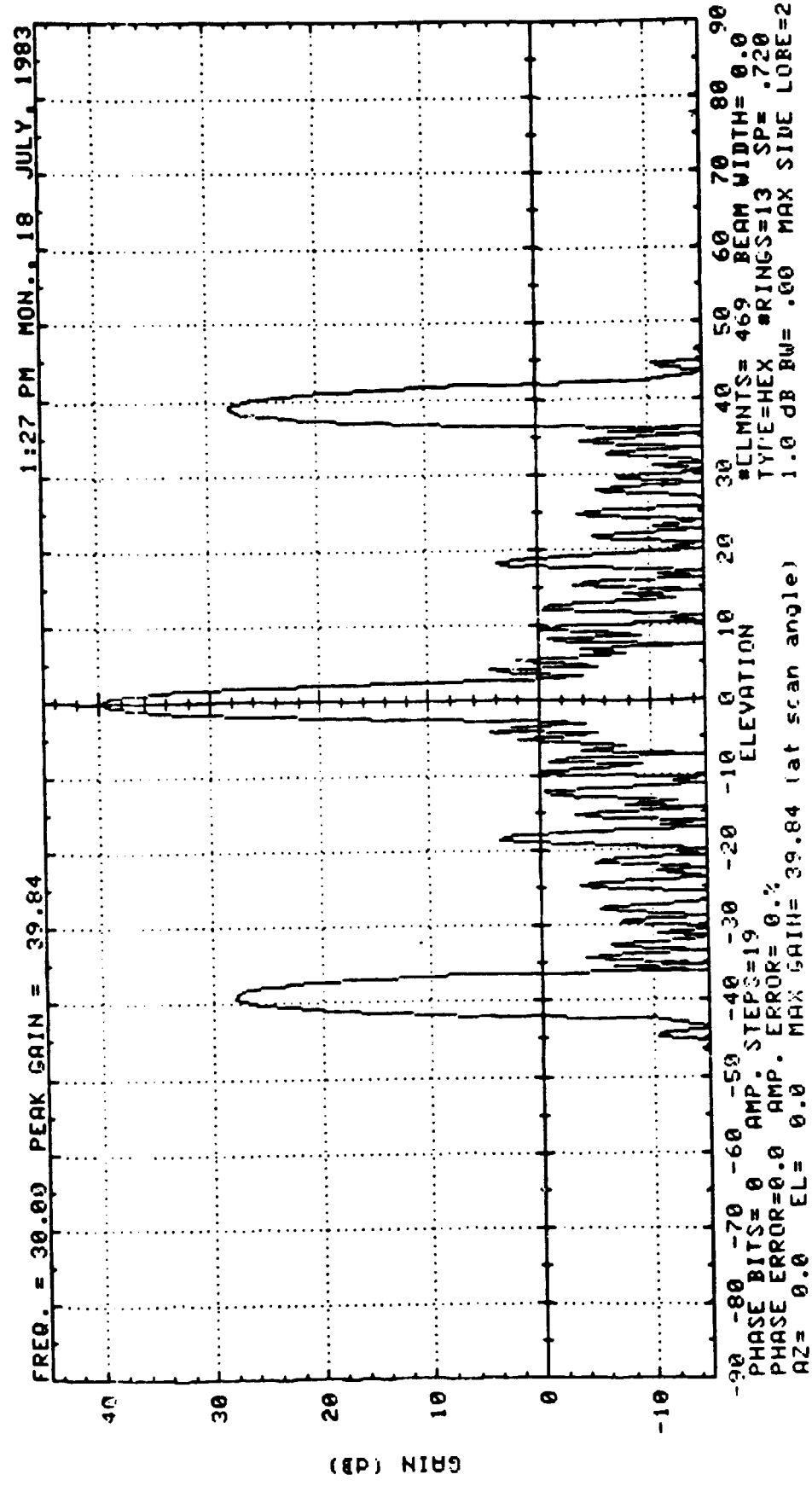
FREQ. = 30.00 PEAK GAIN = 39.84
1:27 PM MON., 18 JULY, 1983
GAIN (dB)
40
30
20
10
0
-10
-90 -80 -70 -60 -50 -40 -30 -20 -10 0 10 20 30 40 50 60 70 80 90
ELEVATION
PHASE BITS= 0 AMP. STEPS=19 #ELMNTS= 469 BEAM WIDTH= 0.0
PHASE ERROR=0.0 AMP. ERROR= 0.% TYPE=HEX #RINGS=13 SP= .720
AZ= 0.0 EL= 0.0 MAX GAIN= 39.84 (at scan angle) 1.0 dB BW= .00 MAX SIDE LOBE=28.09

FIG 3.2-3

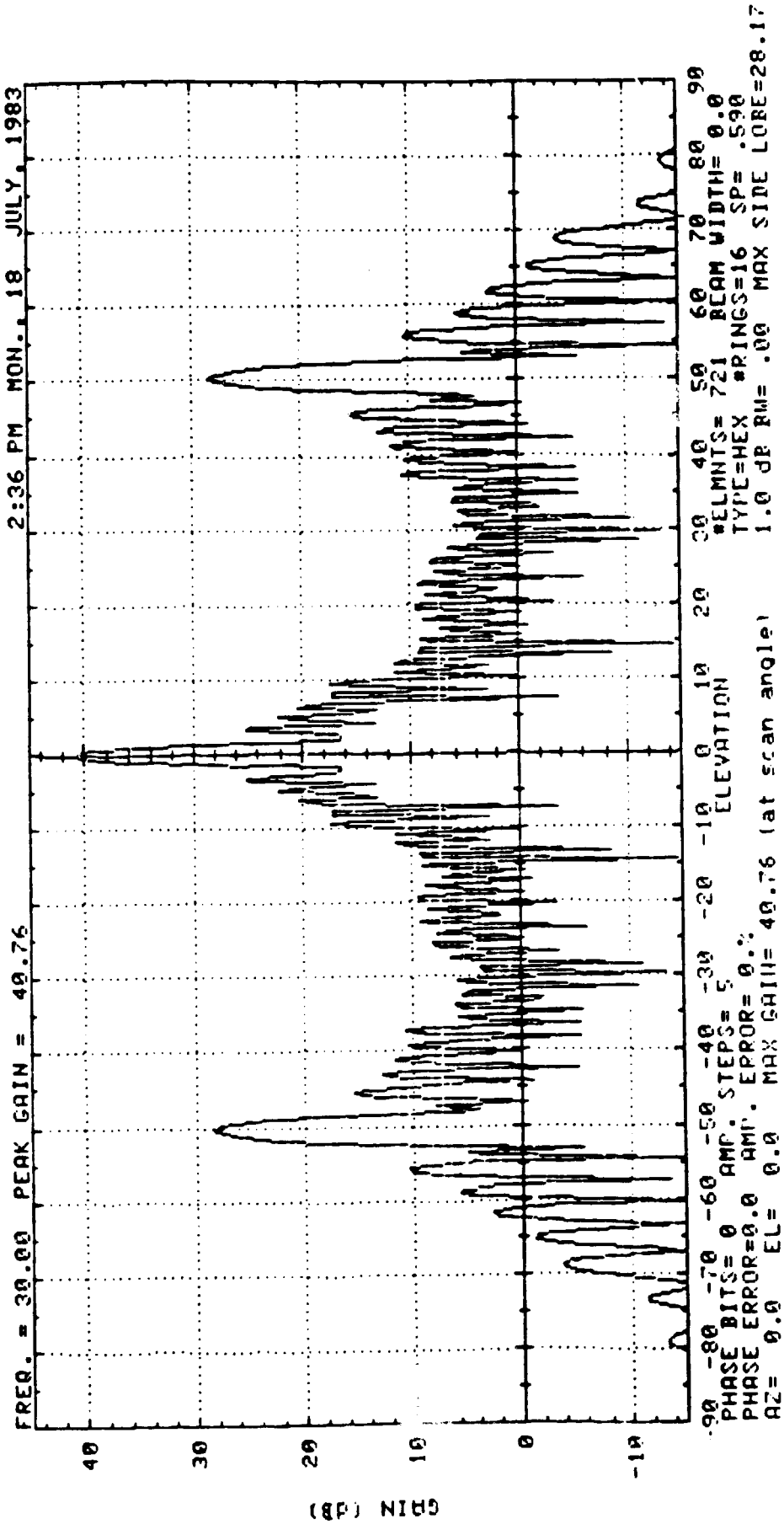
FREQ. = 30.00 PEAK GAIN = 40.76
2:36 PM MON., 18 JULY, 1983
GAIN (dB)
40
30
20
10
0
-10
-90 -80 -70 -60 -50 -40 -30 -20 -10 0 10 20 30 40 50 60 70 80 90
ELEVATION
PHASE BITS= 0 AMP. STEPS= 5
PHASE ERROR=0.0 AMP. ERROR= 0.%
AZ= 0.0 EL= 0.0 MAX GAIN= 40.76 (at scan angle)
#ELMNTS= 721 BEAM WIDTH= 0.0
TYPE=HEX #RINGS=16 SP= .590
1.0 dB RM= .00 MAX SIDE LOBE=28.17

FIG 3.2-4

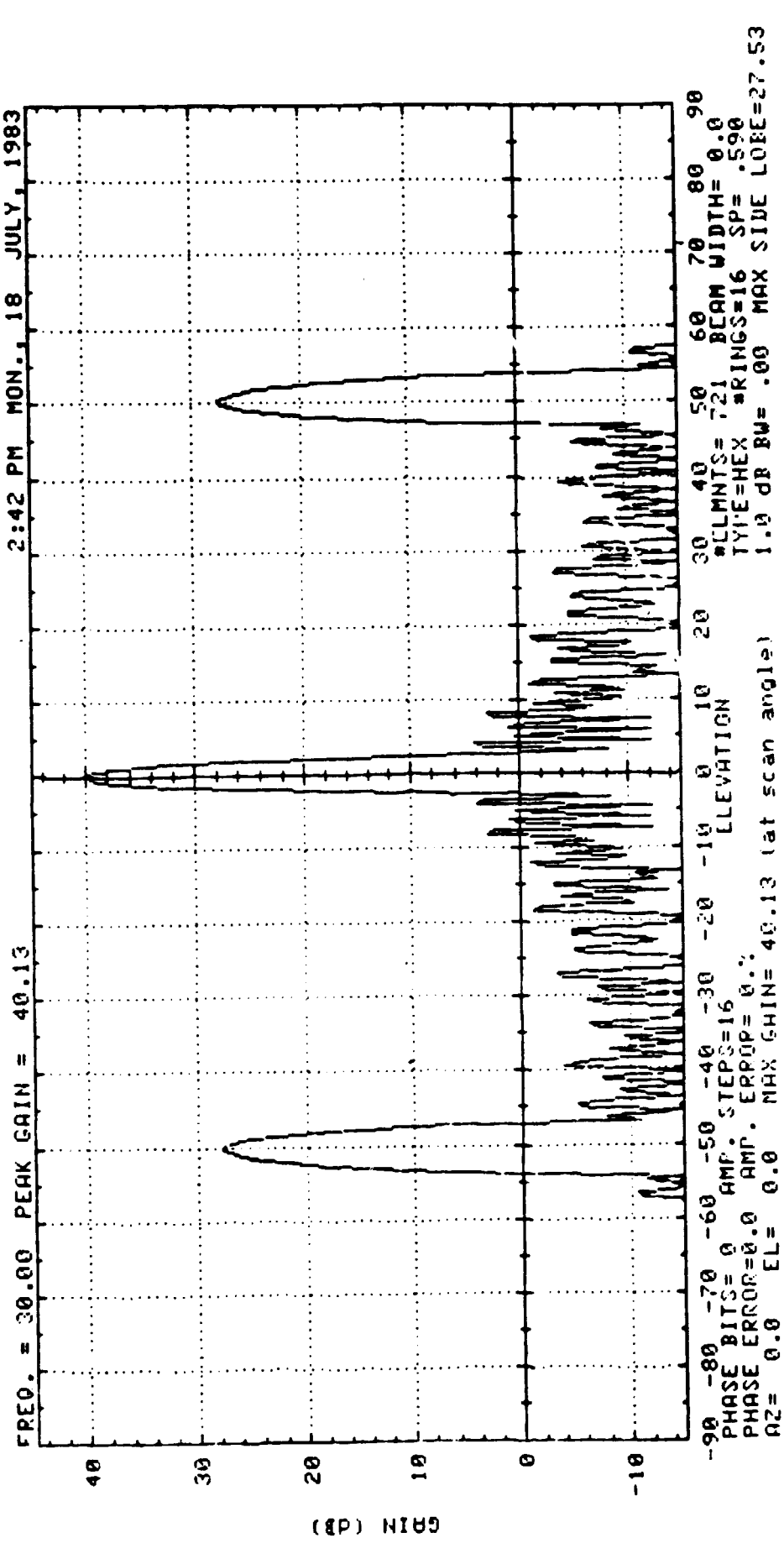
FREQ. = 30.00 PEAK GAIN = 40.13
2:42 PM MON., 18 JULY, 1983
GAIN (dB)
40
30
20
10
0
-10
-90 -80 -70 -60 -50 -40 -30 -20 -10 0 10 20 30 40 50 60 70 80 90
ELEVATION
PHASE BITS= 0 AMP. STEPS=16
PHASE ERROR=0.0 AMP. ERROR= 0.%
AZ= 0.0 EL= 0.0 MAX GAIN= 40.13 (at scan angle)
#ELMNTS= 721 BEAM WIDTH= 0.0
TYPE=HEX #RINGS=16 SP= .590
1.0 dB BW= .00 MAX SIDE LOBE=27.53

FIG. 3.2-5

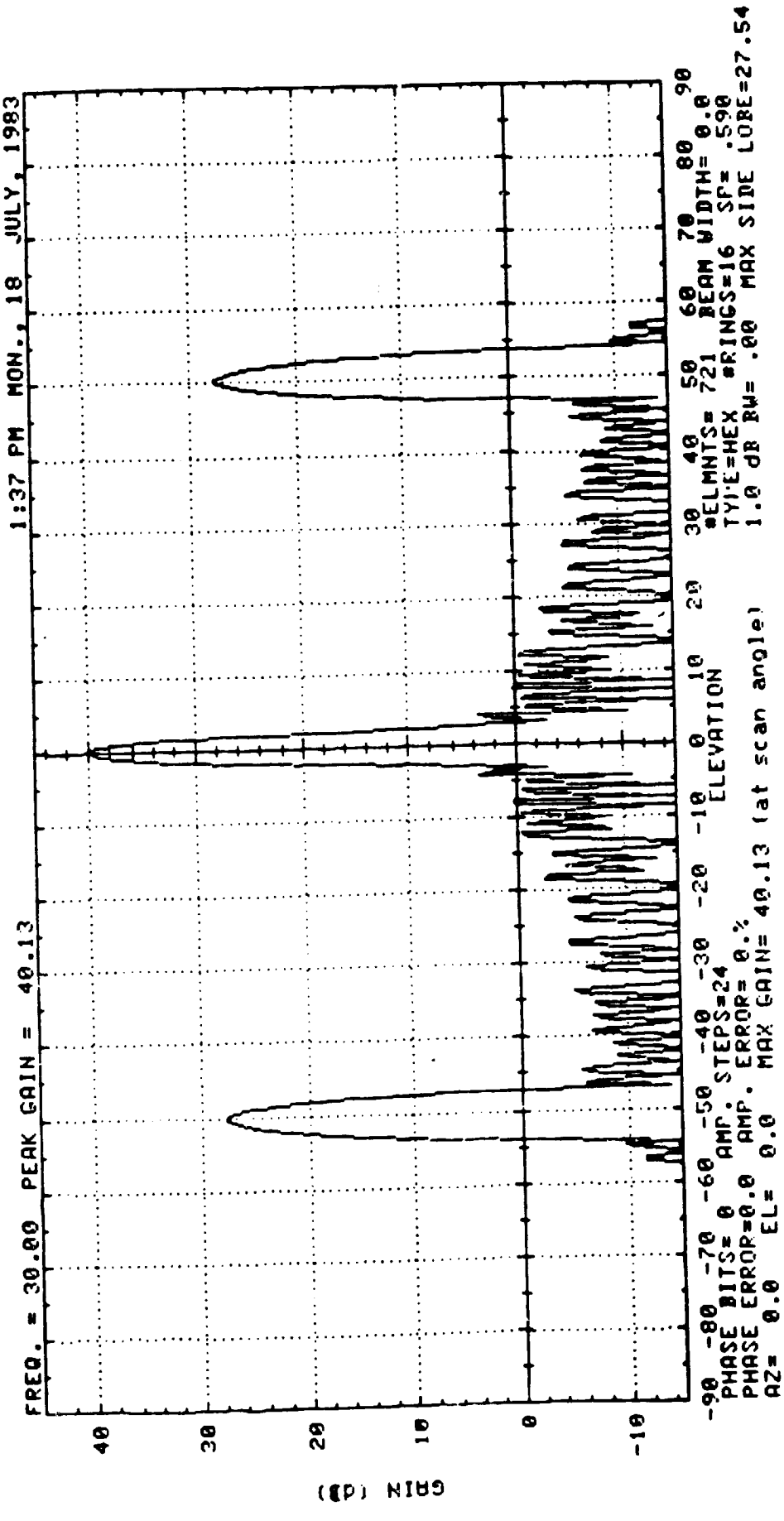
FREQ. = 30.00 PEAK GAIN = 40.13
1:37 PM MON., 18 JULY, 1983
GAIN (dB)
40
30
20
10
0
-10
-90 -80 -70 -60 -50 -40 -30 -20 -10 0 10 20 30 40 50 60 70 80 90
ELEVATION
PHASE BITS= 0 AMP. STEPS=24
PHASE ERROR=0.0 AMP. ERROR= 0.%
AZ= 0.0 EL= 0.0 MAX GAIN= 40.13 (at scan angle)
#ELMNTS= 721 BEAM WIDTH= 0.0
TYPE=HEX #RINGS=16 SP= .590
1.0 dB BW= .00 MAX SIDE LOBE=27.54

FIG. 3.2-6

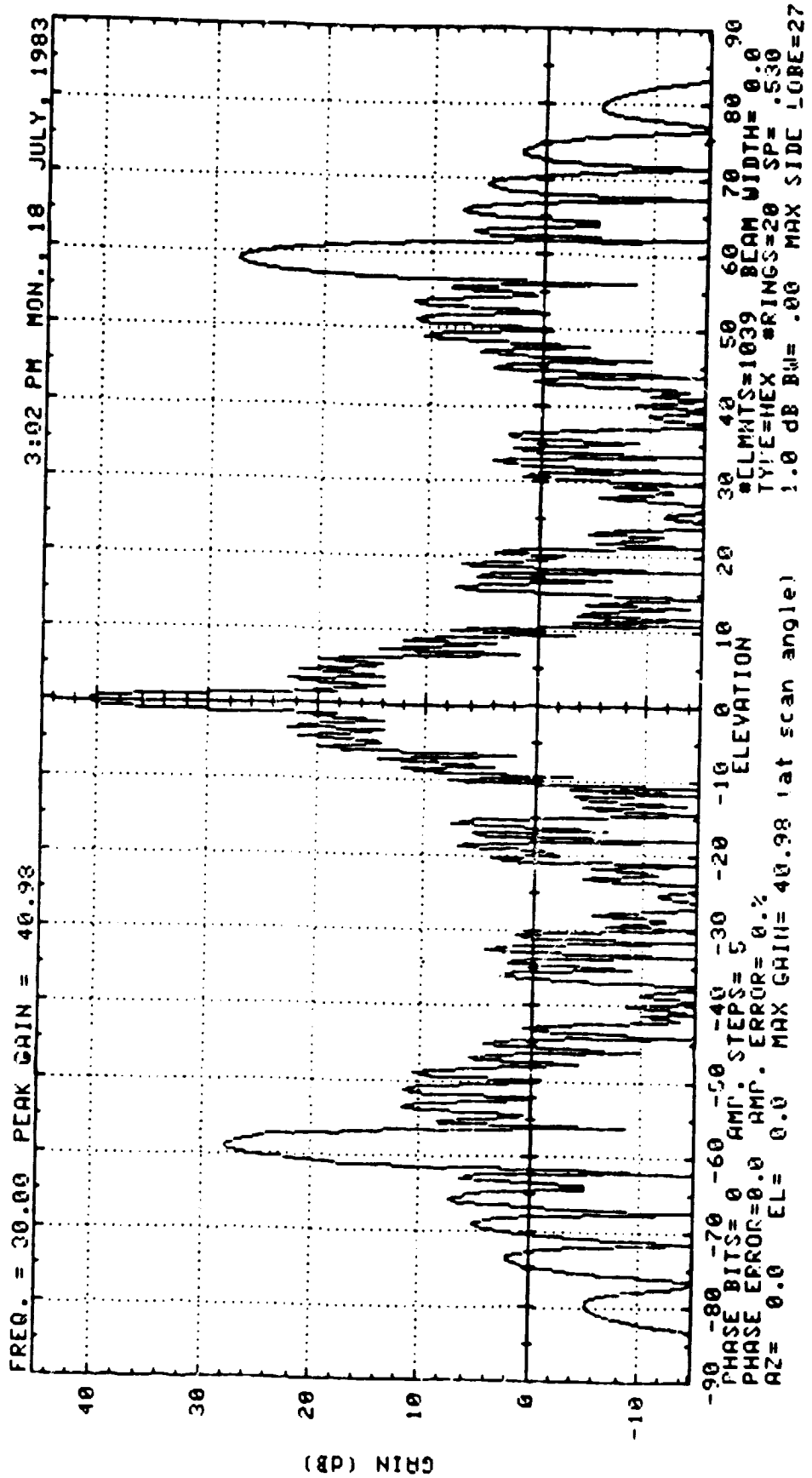
FREQ. = 30.00 PEAK GAIN = 40.98
3:02 PM MON., 18 JULY, 1983
GAIN (dB)
40
30
20
10
0
-10
-90 -80 -70 -60 -50 -40 -30 -20 -10 0 10 20 30 40 50 60 70 80 90
ELEVATION
PHASE BITS= 0 AMP. STEPS= 5
PHASE ERROR=0.0 AMP. ERROR= 0.%
AZ= 0.0 EL= 0.0 MAX GAIN= 40.98 (at scan angle)
#CLMNTS=1039 BEAM WIDTH= 0.0
TYPE=HEX #RINGS=20 SP= .530
1.0 dB BW= .00 MAX SIDE LOBE=27.89

Fig 3.2-7

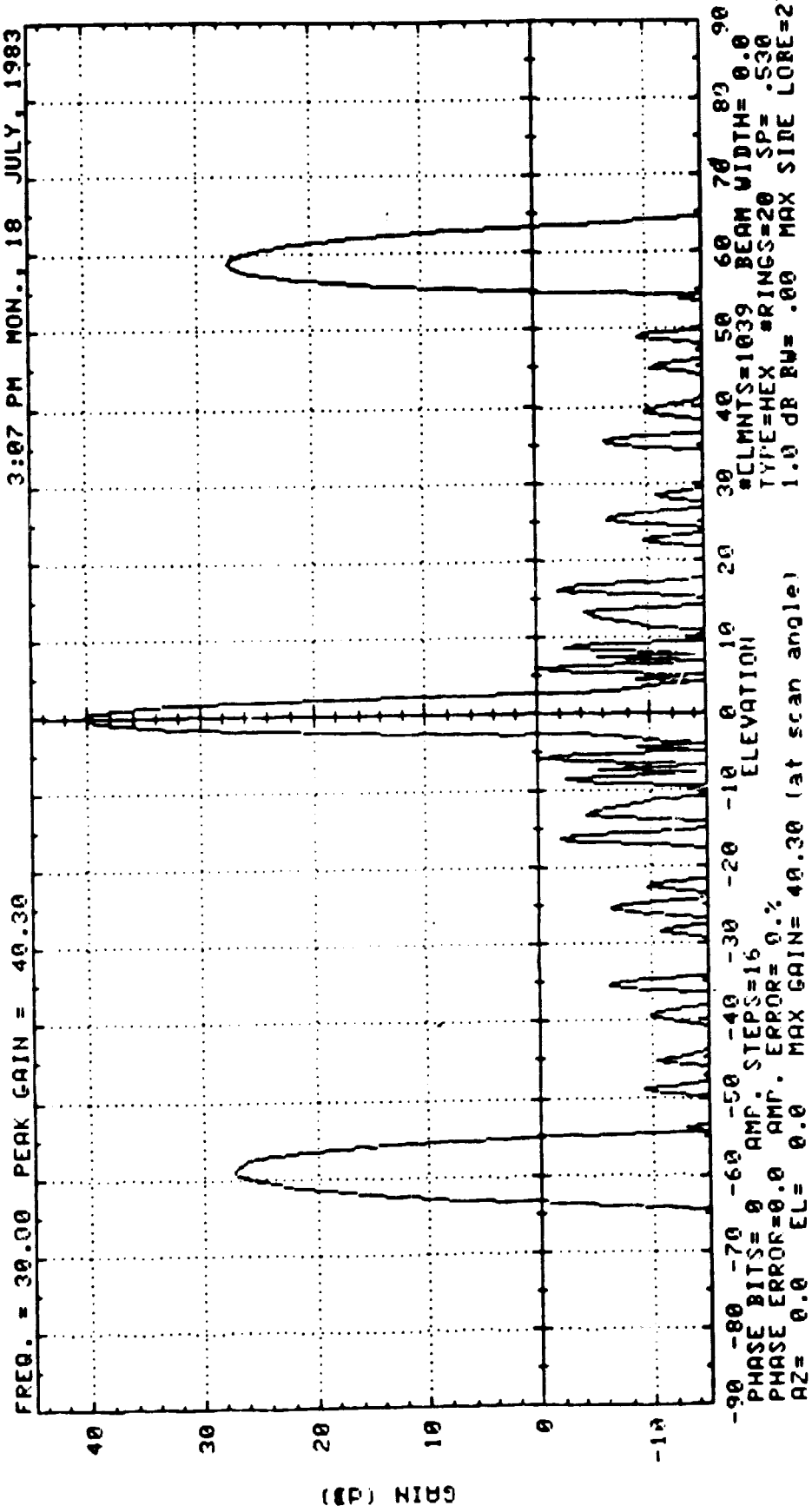
FREQ. = 39.00 PEAK GAIN = 40.30
3:07 PM MON., 18 JULY, 1983
PHASE BITS= 0 AMP. STEPS=16
PHASE ERROR=0.0 AMP. ERROR= 0.%
AZ= 0.0 EL= 0.0 MAX GAIN= 40.30 (at scan angle)
#CLMNTS=1039 BEAM WIDTH= 0.0
TYPE=HEX #RINGS=20 SP= .530
1.0 dB RW= .00 MAX SIDE LOBE=27.22
GAIN (dB)
ELEVATION
40
30
20
10
0
-10
-90 -80 -70 -60 -50 -40 -30 -20 -10 0 10 20 30 40 50 60 70 80 90

Fig. 3.2-8

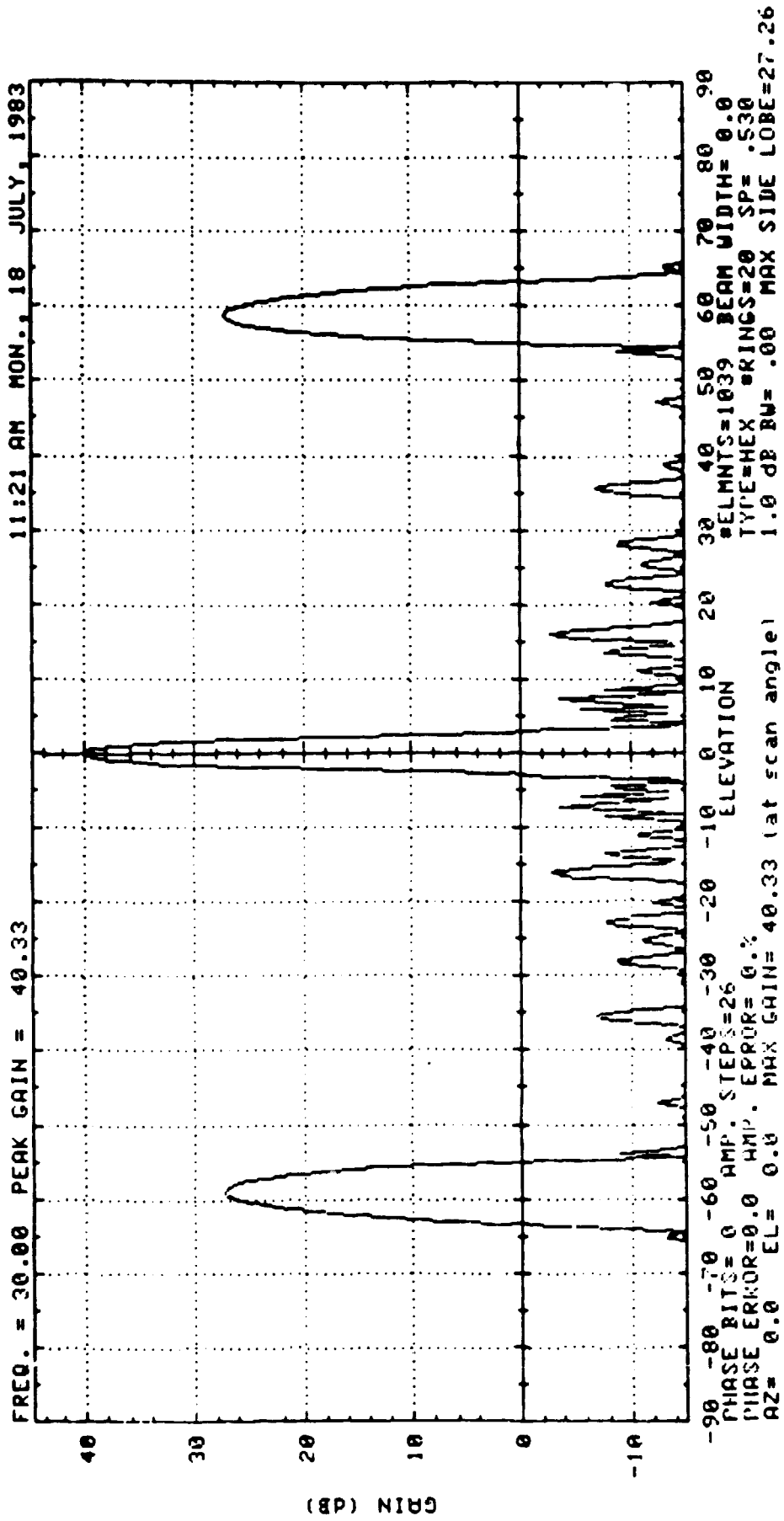
FREQ. = 30.00 PEAK GAIN = 40.33
11:21 AM MON., 18 JULY, 1983
GAIN (dB)
40
30
20
10
0
-10
-90 -80 -70 -60 -50 -40 -30 -20 -10 0 10 20 30 40 50 60 70 80 90
ELEVATION
#ELMNTS=1039 BEAM WIDTH= 0.0
TYPE=HEX #RINGS=20 SP= .530
1.0 dB BW= .00 MAX SIDE LOBE=27.26
PHASE BITS= 0 AMP. STEPS=26
PHASE ERROR=0.0 AMP. ERROR= 0.%
AZ= 0.0 EL= 0.0 MAX GAIN= 40.33 (at scan angle)

FIG. 3.2-9

PLOTS

FOR

SECTION 4

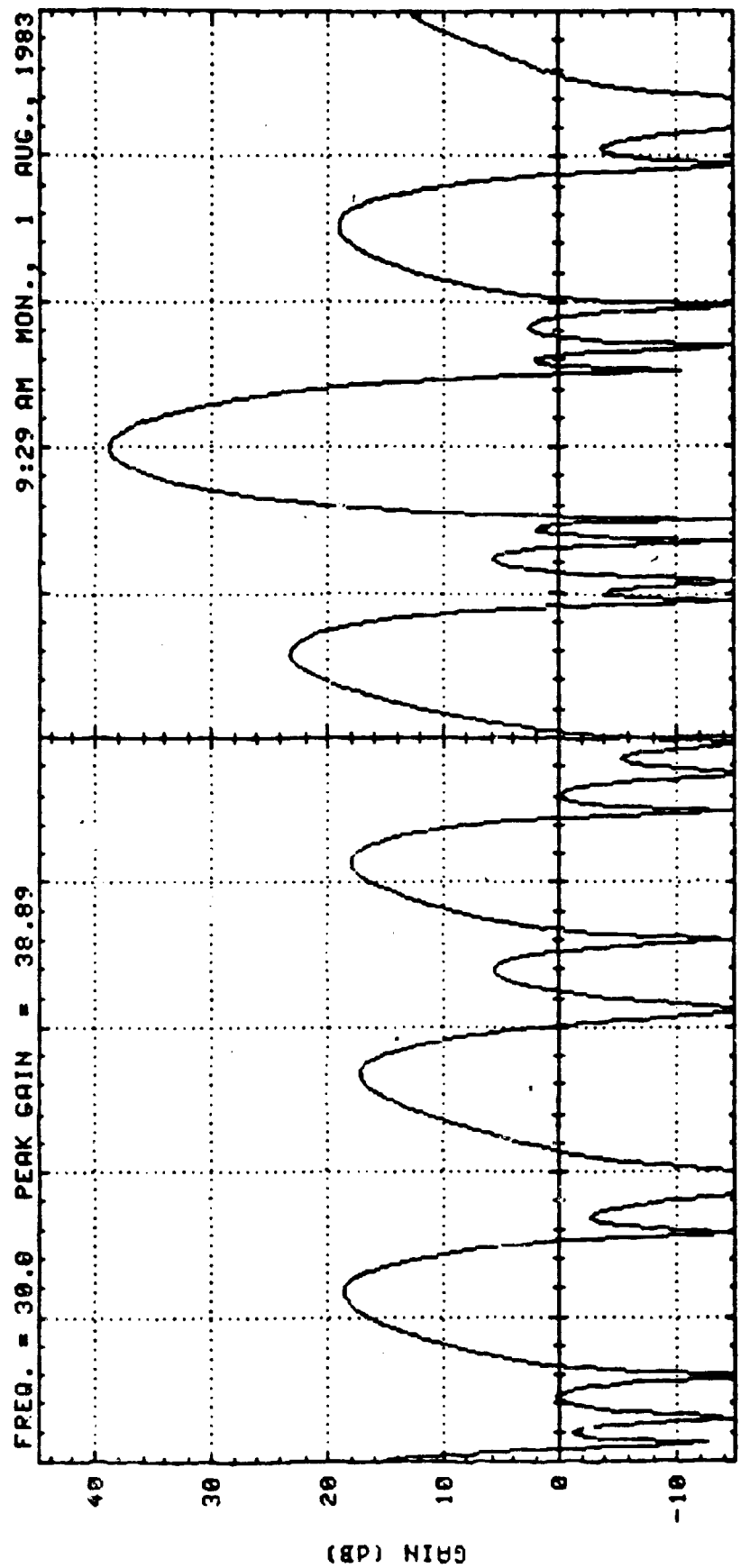
FREQ. = 30.0 PEAK GAIN = 38.89
9:29 AM MON., 1 AUG., 1983
GAIN (dB)
40
30
20
10
0
-10
-25 -20 -15 -10 -5 0 5 10 15 20 25
ELEVATION
PHASE BITS= 3 AMP. STEPS=19 #ELMNTS= 469 BEAM WIDTH= 0.0
PHASE ERROR=0.0 AMP. ERROR= 0.% TYPE=HEX #RINGS=13 SP= .720
AZ= 0.0 EL= 10.0 MAX GAIN= 38.89 (at scan angle) 3.0 dB BW= 1.50 MAX SIDE LOBE=-16.8

FIGURE 4.2-5

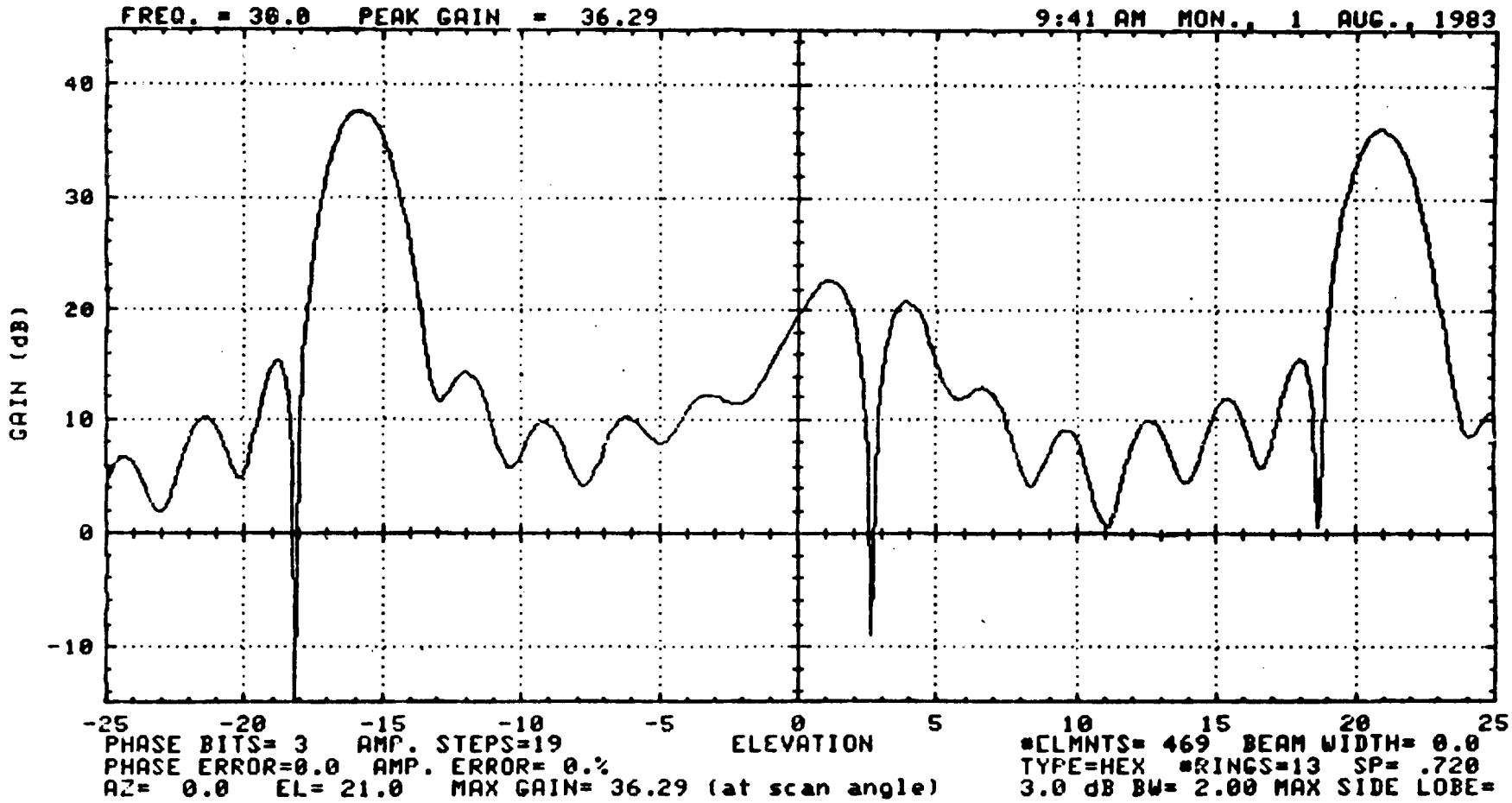
FREQ. = 30.0 PEAK GAIN = 36.29
9:41 AM MON., 1 AUG., 1983
GAIN (dB)
40
30
20
10
0
-10
-25 -20 -15 -10 -5 0 5 10 15 20 25
ELEVATION
PHASE BITS= 3 AMP. STEPS=19
PHASE ERROR=0.0 AMP. ERROR= 0.%
AZ= 0.0 EL= 21.0 MAX GAIN= 36.29 (at scan angle)
#ELMNTS= 469 BEAM WIDTH= 0.0
TYPE=HEX #RINGS=13 SP= .720
3.0 dB BW= 2.00 MAX SIDE LOBE= -2.3

FIGURE 4.2-6

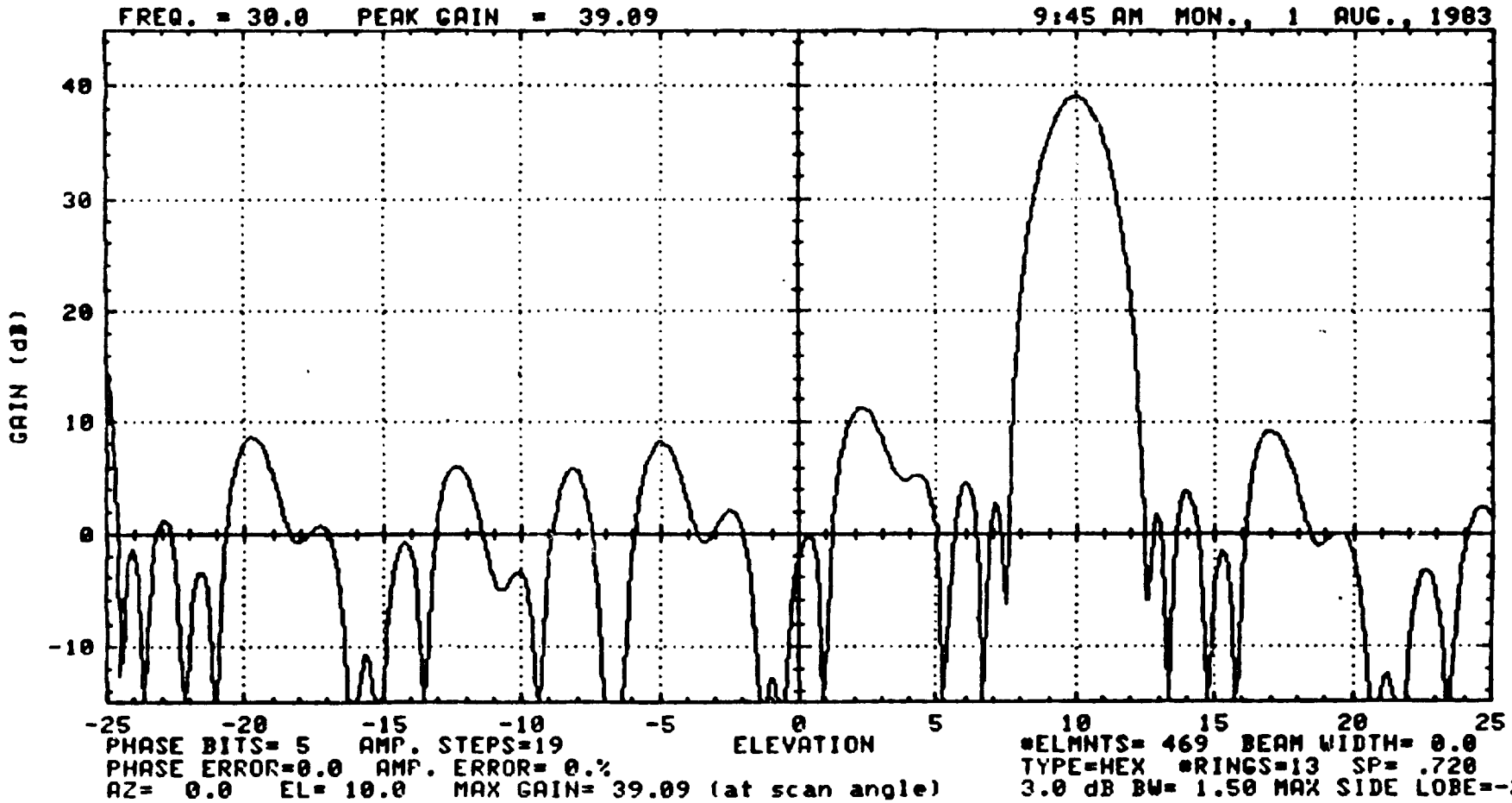
FREQ. = 30.0 PEAK GAIN = 39.09
9:45 AM MON., 1 AUG., 1983
GAIN (dB)
40
30
20
10
0
-10
-25 -20 -15 -10 -5 0 5 10 15 20 25
ELEVATION
PHASE BITS= 5 AMP. STEPS=19
PHASE ERROR=0.0 AMP. ERROR= 0.%
AZ= 0.0 EL= 10.0 MAX GAIN= 39.09 (at scan angle)
#ELMNTS= 469 BEAM WIDTH= 0.0
TYPE=HEX #RINGS=13 SP= .720
3.0 dB BW= 1.50 MAX SIDE LOBE=-24.6

FIGURE 4.2-7

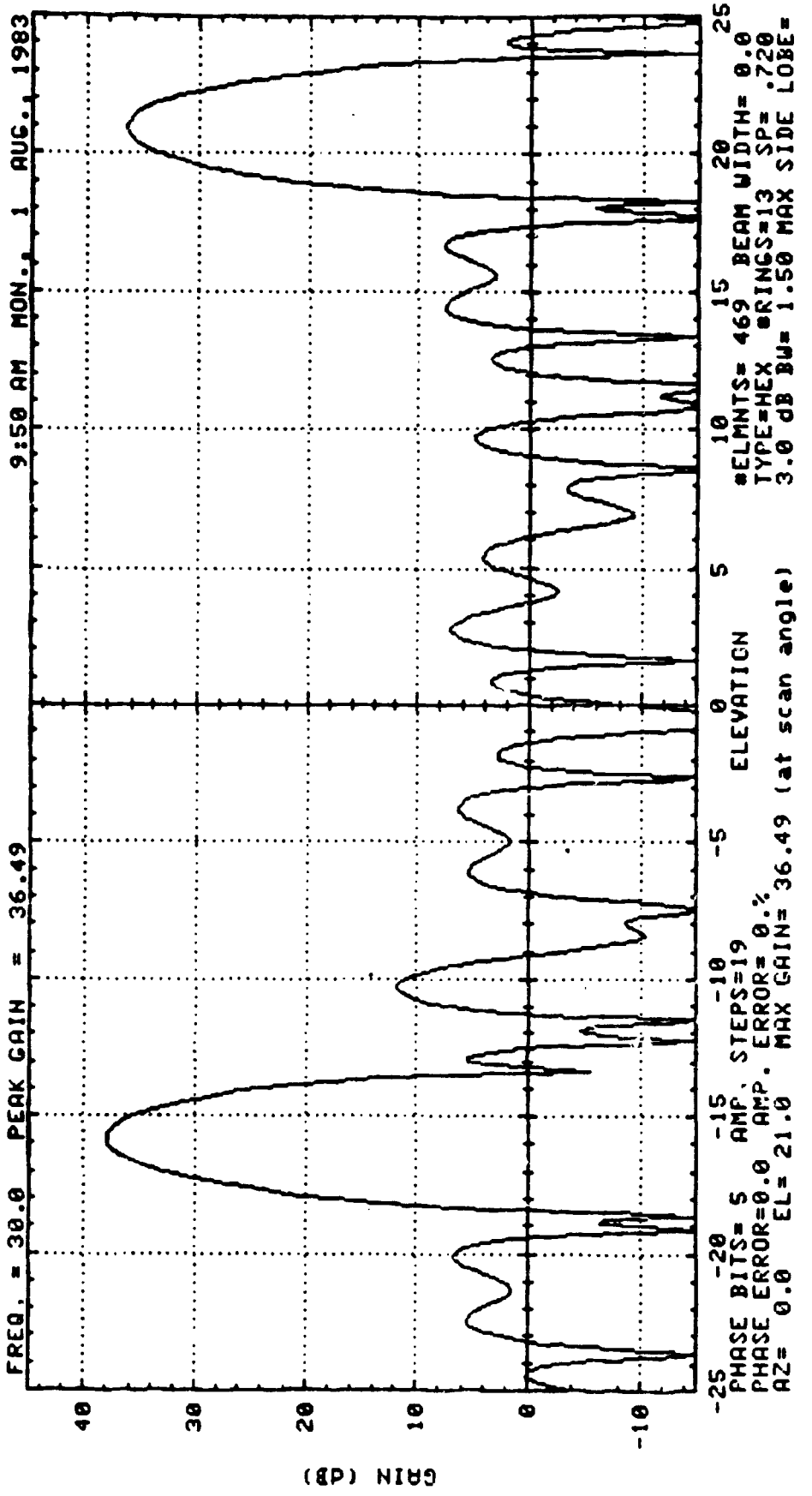
FREQ. = 30.0 PEAK GAIN = 36.49
9:50 AM MON., 1 AUG., 1983
GRIN (dB)
40
30
20
10
0
-10
-25 -20 -15 -10 -5 0 5 10 15 20 25
ELEVATION
PHASE BITS= 5 AMP. STEPS=19
PHASE ERROR=0.0 AMP. ERROR= 0.%
AZ= 0.0 EL= 21.0 MAX GAIN= 36.49 (at scan angle)
#ELMNTS= 469 BEAM WIDTH= 0.0
TYPE=HEX #RINGS=13 SP= .720
3.0 dB BW= 1.50 MAX SIDE LOBE= -2.1

FIGURE 4.2-8

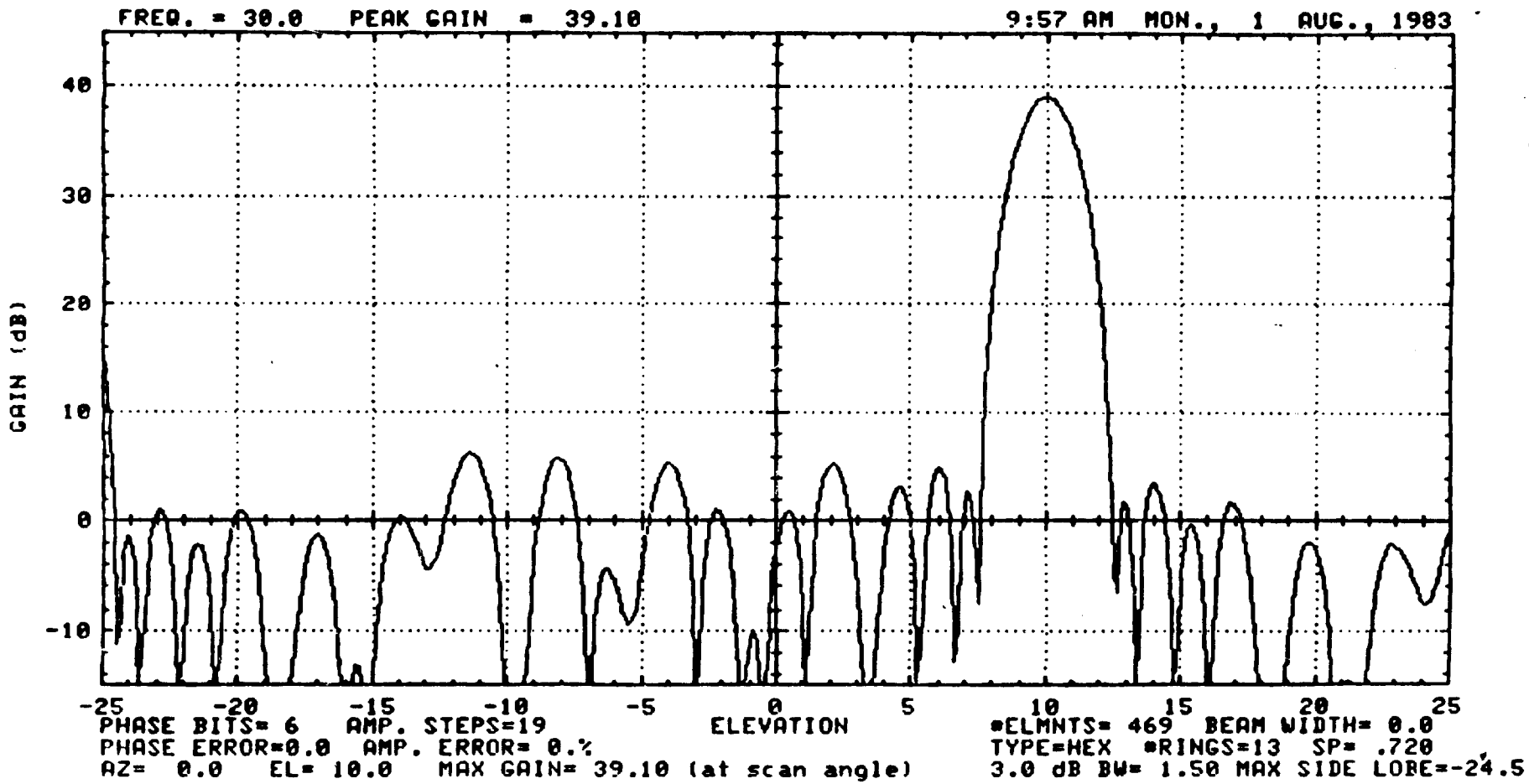
FREQ. = 30.0 PEAK GAIN = 39.10
9:57 AM MON., 1 AUG., 1983
GAIN (dB)
40
30
20
10
0
-10
-25 -20 -15 -10 -5 0 5 10 15 20 25
ELEVATION
PHASE BITS= 6 AMP. STEPS=19
PHASE ERROR=0.0 AMP. ERROR= 0.%
AZ= 0.0 EL= 10.0 MAX GAIN= 39.10 (at scan angle)
#ELMNTS= 469 BEAM WIDTH= 0.0
TYPE=HEX #RINGS=13 SP= .720
3.0 dB BW= 1.50 MAX SIDE LOBE=-24.5

FIGURE 4.2-9

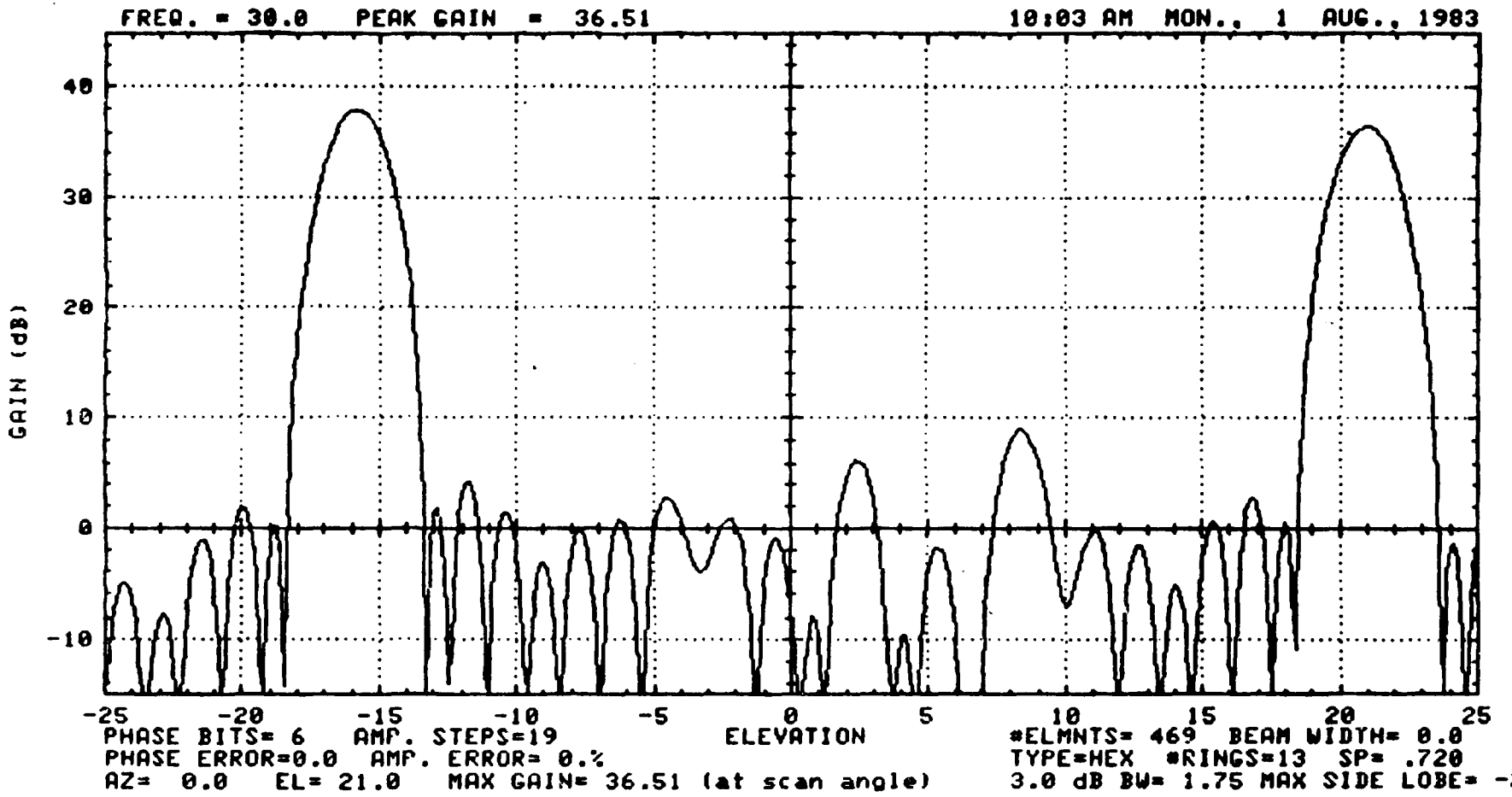
FREQ. = 30.0 PEAK GAIN = 36.51
10:03 AM MON., 1 AUG., 1983
GAIN (dB)
40
30
20
10
0
-10
-25 -20 -15 -10 -5 0 5 10 15 20 25
ELEVATION
PHASE BITS= 6 AMP. STEPS=19
PHASE ERROR=0.0 AMP. ERROR= 0.%
AZ= 0.0 EL= 21.0 MAX GAIN= 36.51 (at scan angle)
#ELMNTS= 469 BEAM WIDTH= 0.0
TYPE=HEX #RINGS=13 SP= .720
3.0 dB BW= 1.75 MAX SIDE LOBE= -2.1

FIGURE 4.2-10

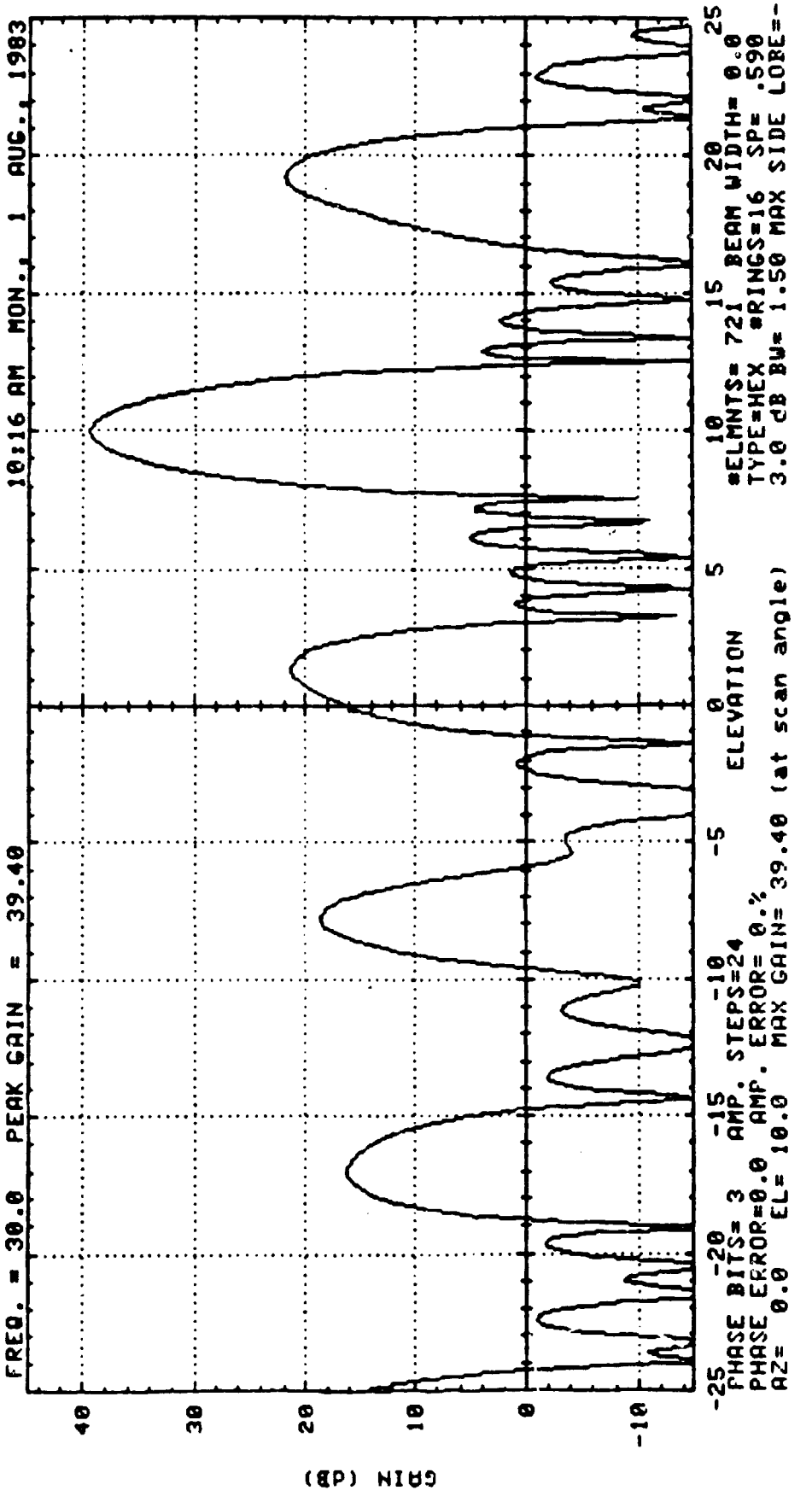
FREQ. = 30.0 PEAK GAIN = 39.40
10:16 AM MON., 1 AUG., 1983
GAIN (dB)
40
30
20
10
0
-10
-25 -20 -15 -10 -5 0 5 10 15 20 25
ELEVATION
PHASE BITS= 3 AMP. STEPS=24
PHASE ERROR=0.0 AMP. ERROR= 0.%
AZ= 0.0 EL= 10.0 MAX GAIN= 39.40 (at scan angle)
#ELMNTS= 721 BEAM WIDTH= 0.0
TYPE=HEX #RINGS=16 SP= .590
3.0 dB BW= 1.50 MAX SIDE LOBE=-18.2

FIGURE 4.2-1

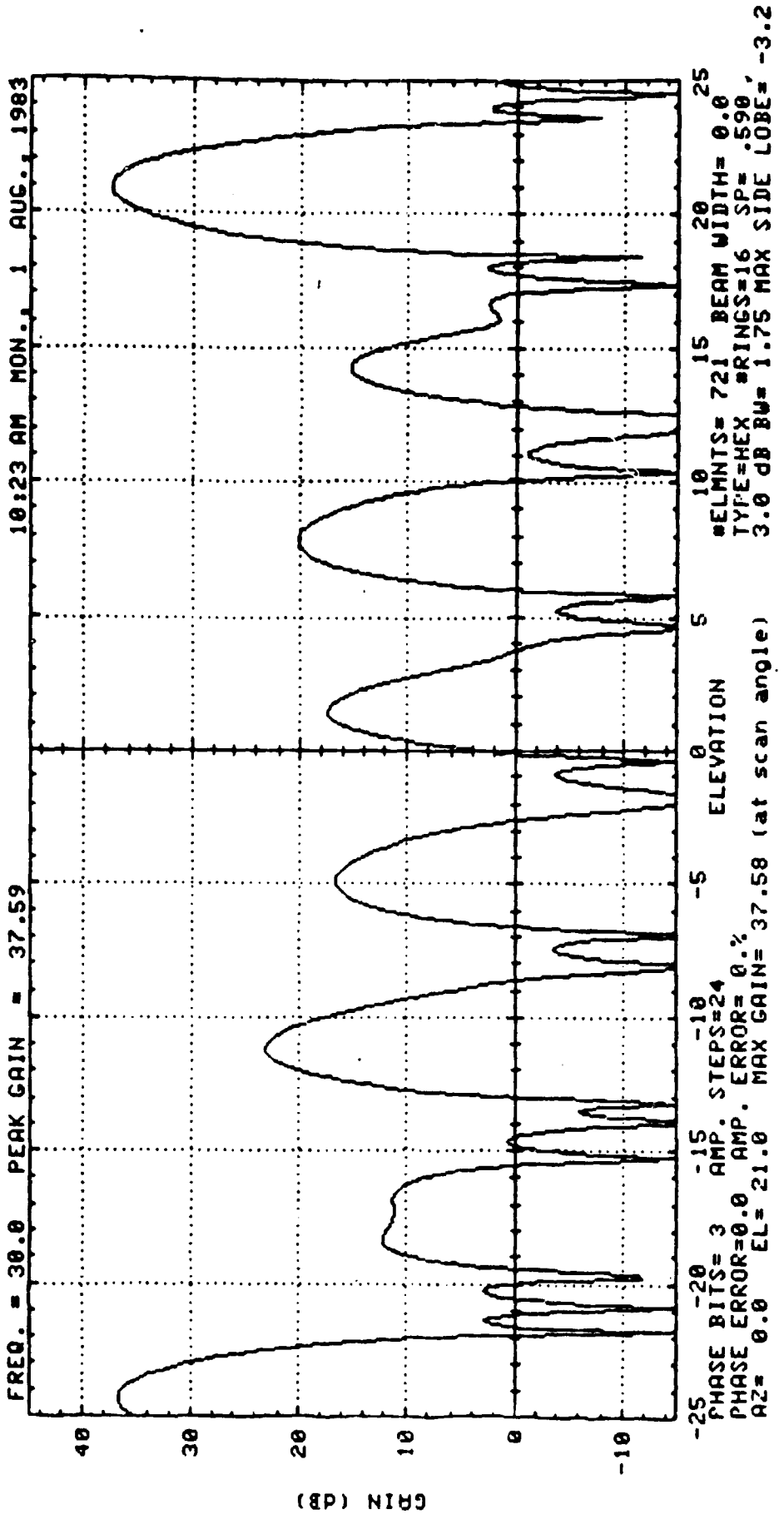
FREQ. = 30.0 PEAK GAIN = 37.59
10:23 AM MON., 1 AUG., 1983
GAIN (dB)
40
30
20
10
0
-10
-25 -20 -15 -10 -5 0 5 10 15 20 25
ELEVATION
PHASE BITS= 3 AMP. STEPS=24 #ELMNTS= 721 BEAM WIDTH= 0.0
PHASE ERROR=0.0 AMP. ERROR= 0.% TYPE=HEX #RINGS=16 SP= .590
AZ= 0.0 EL= 21.0 MAX GAIN= 37.58 (at scan angle) 3.0 dB BW= 1.75 MAX SIDE LOBE= -3.2

Figure 4.2-12

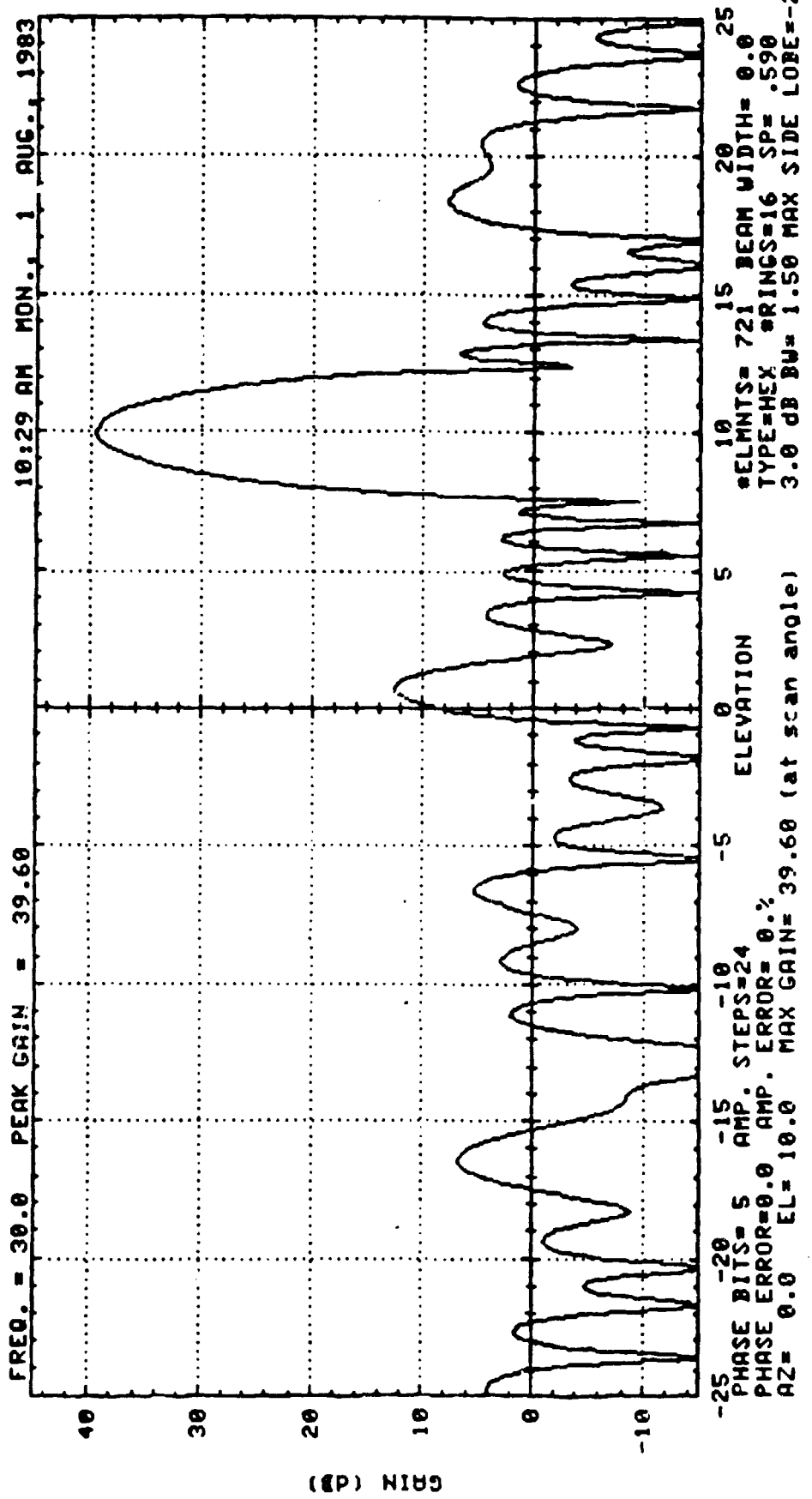
FREQ. = 30.0 PEAK GAIN = 39.60
10:29 AM MON., 1 AUG., 1983
GAIN (dB)
40
30
20
10
0
-10
-25 -20 -15 -10 -5 0 5 10 15 20 25
ELEVATION
PHASE BITS= 5 AMP. STEPS=24
PHASE ERROR=0.0 AMP. ERROR= 0.%
AZ= 0.0 EL= 10.0 MAX GAIN= 39.60 (at scan angle)
#ELMNTS= 721 BEAM WIDTH= 0.0
TYPE=HEX #RINGS=16 SP= .590
3.0 dB BW= 1.50 MAX SIDE LOBE=-27.3

FIGURE 4.2-13

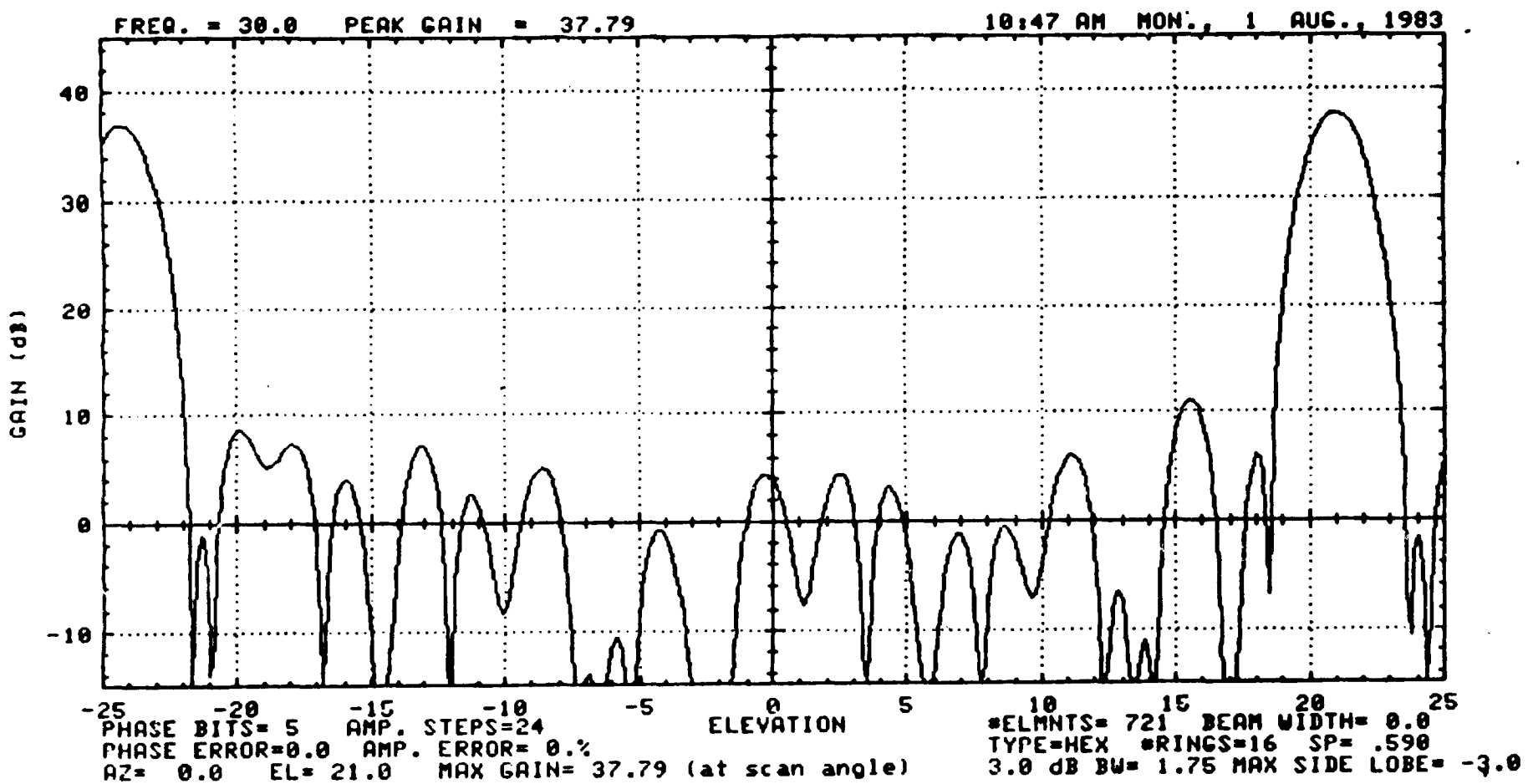
FREQ. = 30.0 PEAK GAIN = 37.79
10:47 AM MON., 1 AUG., 1983
GAIN (dB)
40
30
20
10
0
-10
-25 -20 -15 -10 -5 0 5 10 15 20 25
ELEVATION
PHASE BITS= 5 AMP. STEPS=24
PHASE ERROR=0.0 AMP. ERROR= 0.%
AZ= 0.0 EL= 21.0 MAX GAIN= 37.79 (at scan angle)
#ELMNTS= 721 BEAM WIDTH= 0.0
TYPE=HEX #RINGS=16 SP= .590
3.0 dB BW= 1.75 MAX SIDE LOBE= -3.0

FIGURE 4.2-14

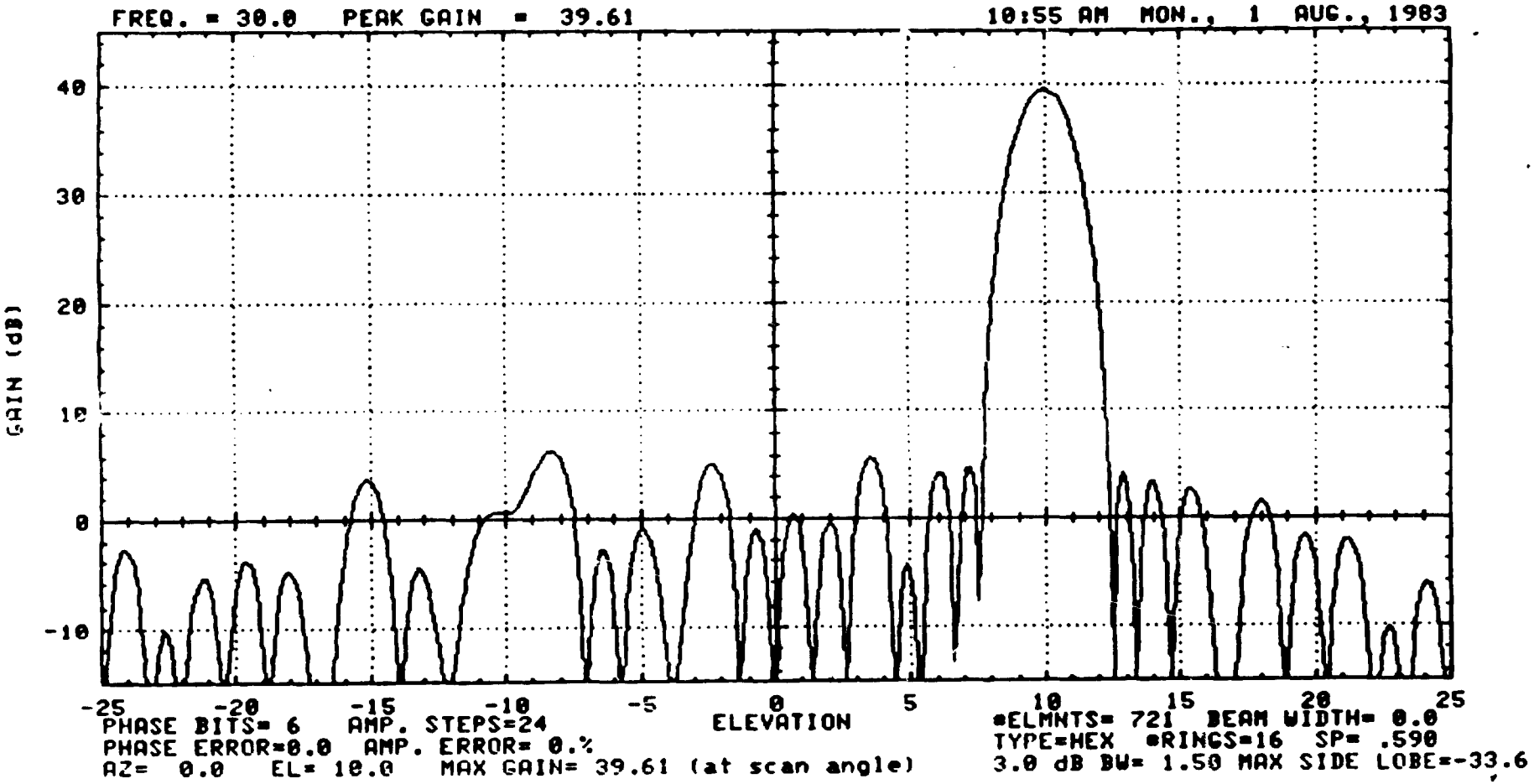
FREQ. = 30.0 PEAK GAIN = 39.61
10:55 AM MON., 1 AUG., 1983
GAIN (dB)
40
30
20
10
0
-10
-25 -20 -15 -10 -5 0 5 10 15 20 25
ELEVATION
PHASE BITS= 6 AMP. STEPS=24
PHASE ERROR=0.0 AMP. ERROR= 0.%
AZ= 0.0 EL= 10.0 MAX GAIN= 39.61 (at scan angle)
#ELMNTS= 721 BEAM WIDTH= 0.0
TYPE=HEX #RINGS=16 SP= .590
3.0 dB BW= 1.50 MAX SIDE LOBE=-33.6

FIGURE 4.2-15

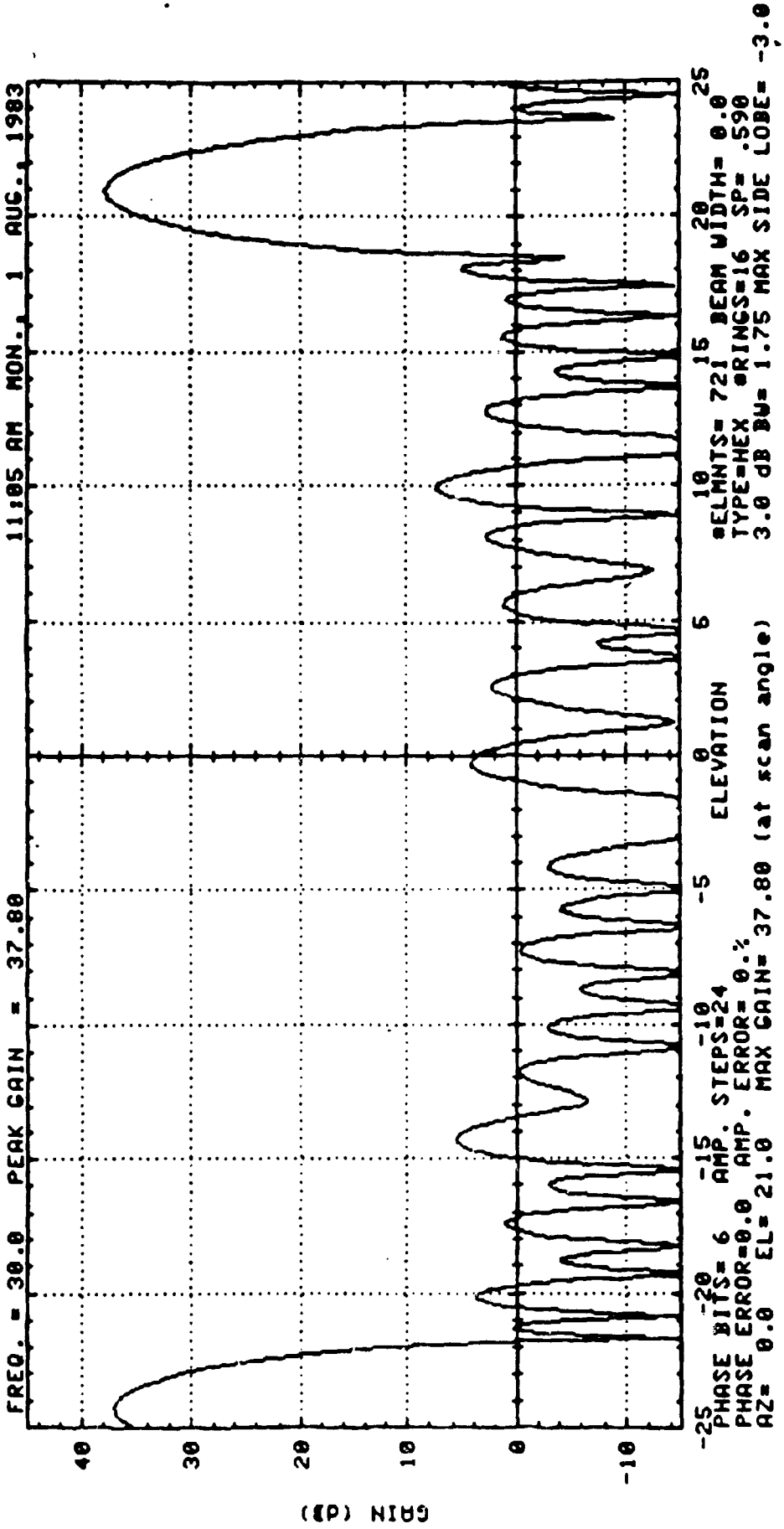
FREQ. = 30.0 PEAK GAIN = 37.80
11:05 AM MON., 1 AUG., 1983
GAIN (dB)
40
30
20
10
0
-10
-25 -20 -15 -10 -5 0 5 10 15 20 25
ELEVATION
PHASE BITS= 6 AMP. STEPS=24
PHASE ERROR=0.0 AMP. ERROR= 0.%
AZ= 0.0 EL= 21.0 MAX GAIN= 37.80 (at scan angle)
#ELMNTS= 721 BEAM WIDTH= 0.0
TYPE=HEX #RINGS=16 SP= .590
3.0 dB BW= 1.75 MAX SIDE LOBE= -3.0

FIGURE 4.2-16

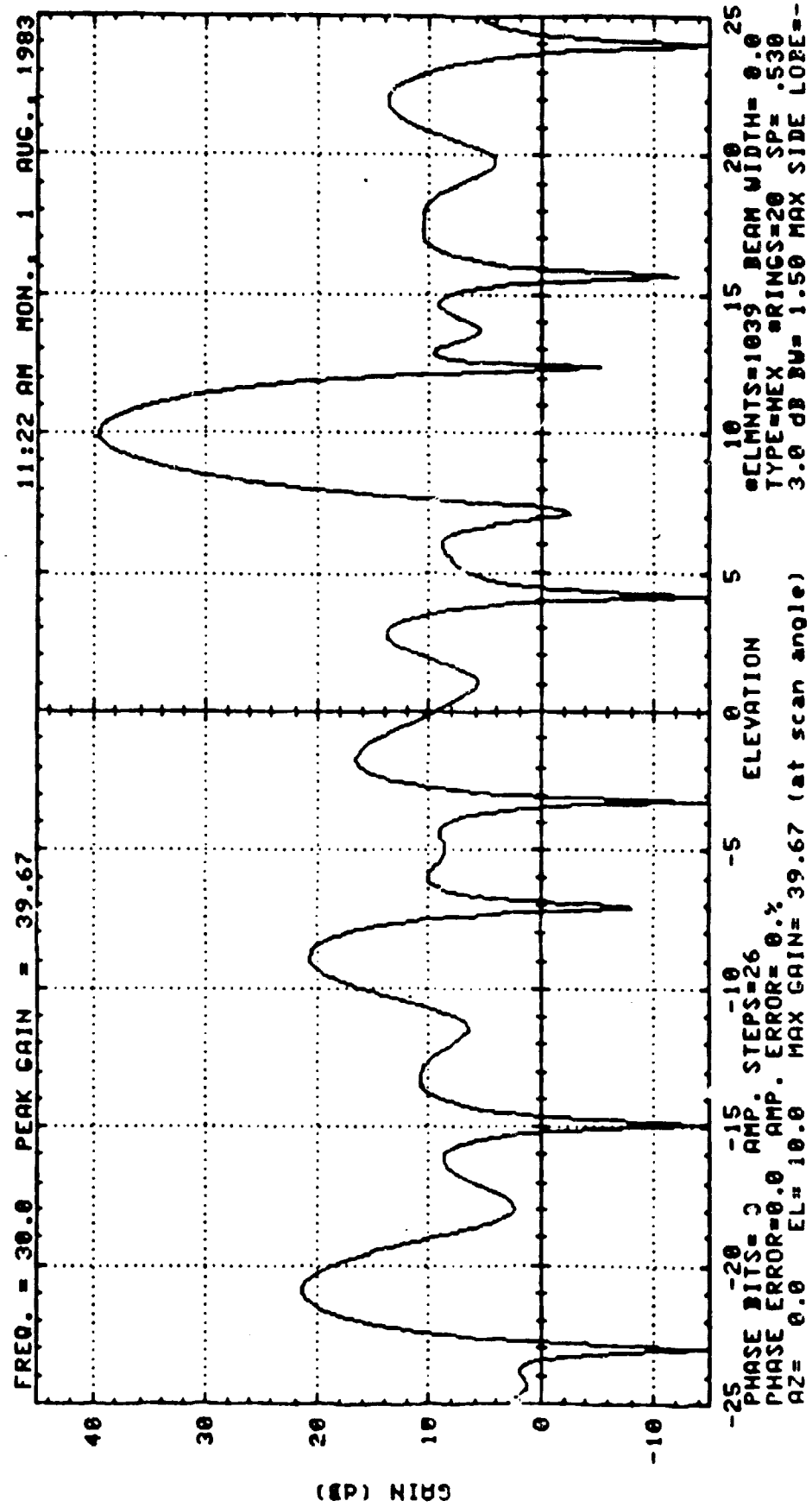
FREQ. = 30.0 PEAK GAIN = 39.67
11:22 AM MON., 1 AUG., 1983
GAIN (dB)
40
30
20
10
0
-10
-25 -20 -15 -10 -5 0 5 10 15 20 25
ELEVATION
PHASE BITS= 3 AMP. STEPS=26 #ELMNTS=1039 BEAM WIDTH= 0.0
PHASE ERROR=0.0 AMP. ERROR= 0.% TYPE=HEX #RINGS=20 SP= .530
AZ= 0.0 EL= 10.0 MAX GAIN= 39.67 (at scan angle) 3.0 dB BW= 1.50 MAX SIDE LOBE=-18.7

FIGURE 4.2-17

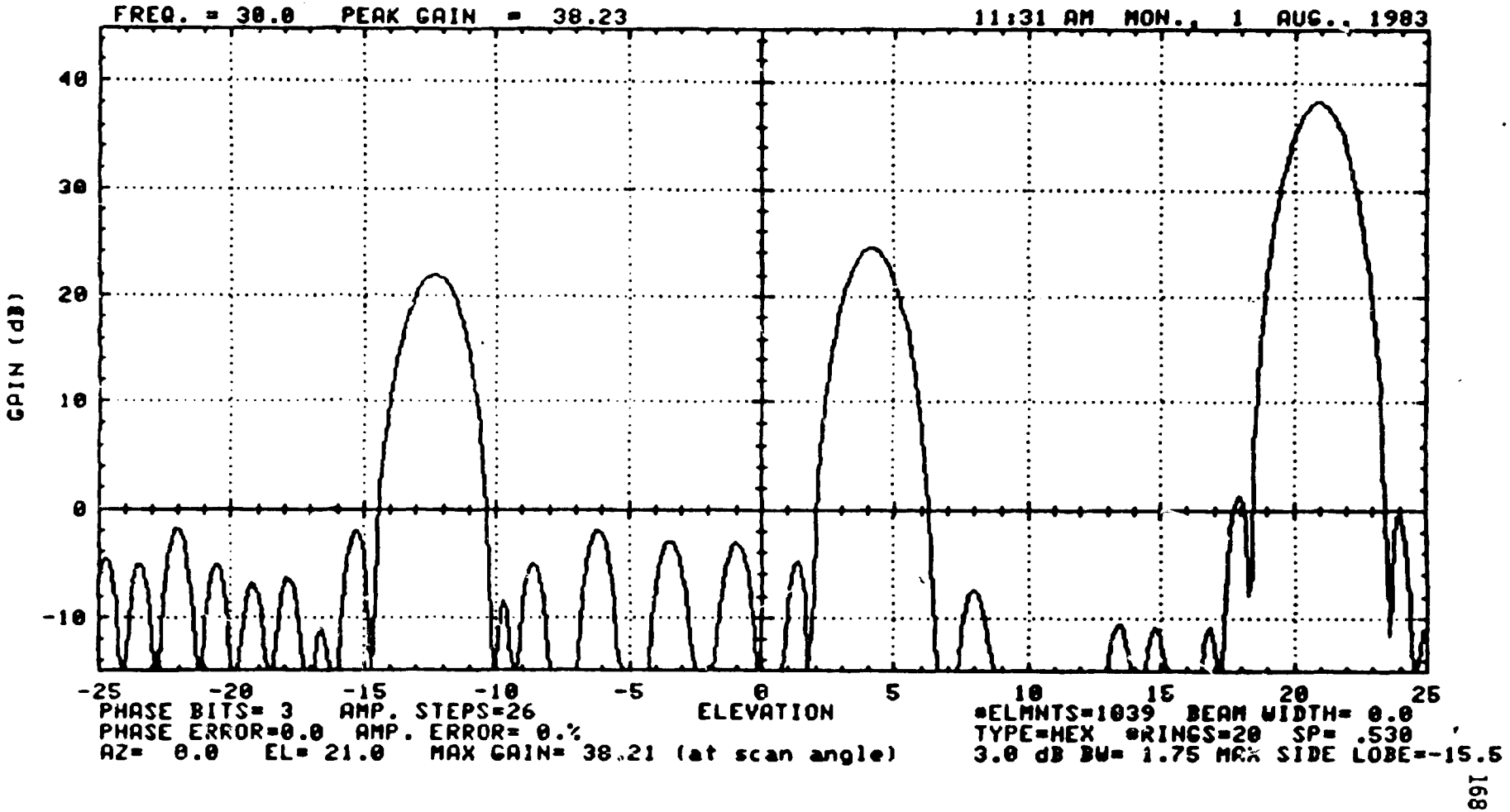

168

FIGURE 4.2-18

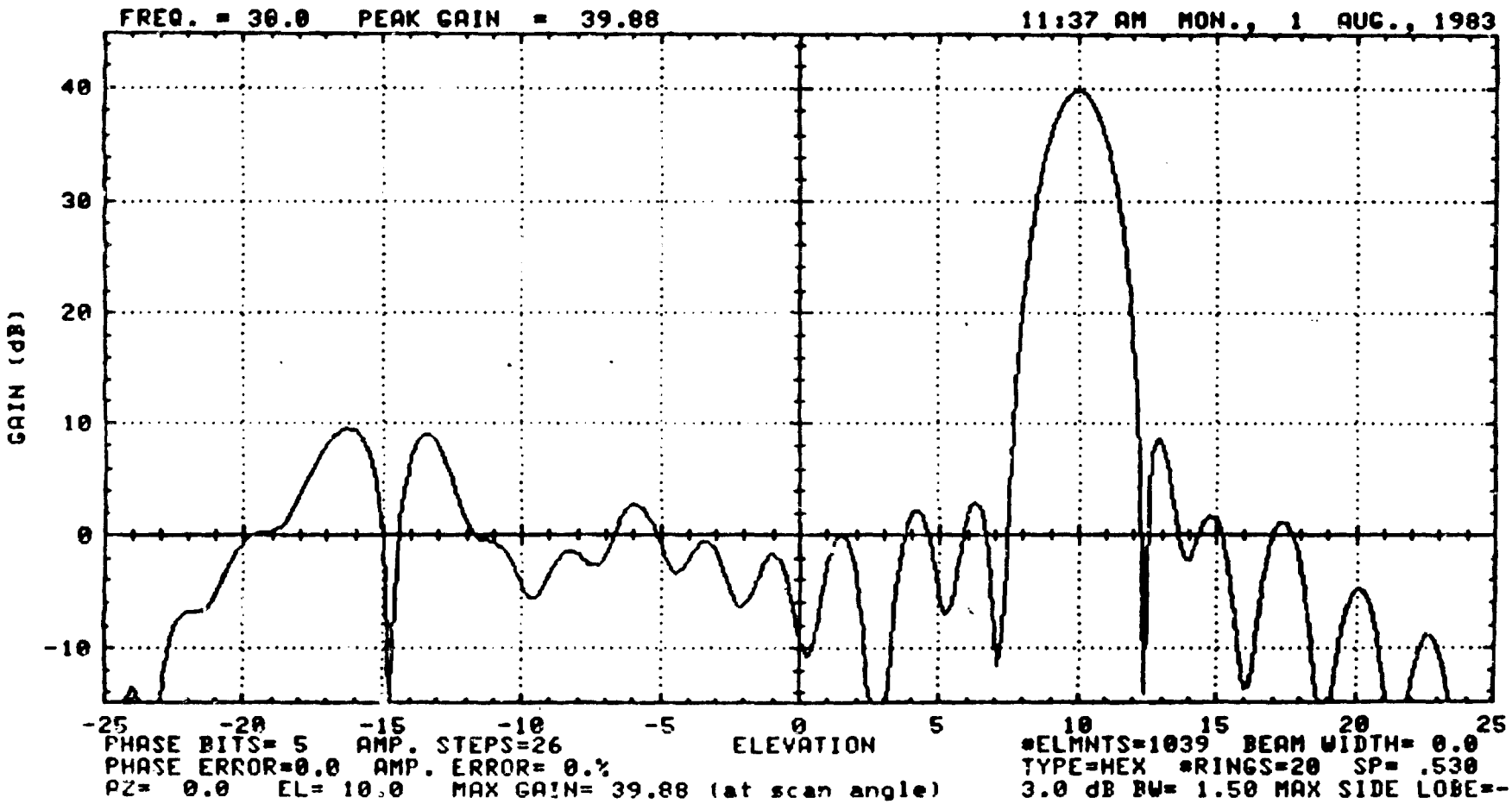
FREQ. = 30.0 PEAK GAIN = 39.88
11:37 AM MON., 1 AUG., 1983
GAIN (dB)
40
30
20
10
0
-10
-25 -20 -15 -10 -5 0 5 10 15 20 25
ELEVATION
PHASE BITS= 5 AMP. STEPS=26
PHASE ERROR=0.0 AMP. ERROR= 0.%
PZ= 0.0 EL= 10.0 MAX GAIN= 39.88 (at scan angle)
#ELMNTS=1039 BEAM WIDTH= 0.0
TYPE=HEX #RINGS=20 SP= .530
3.0 dB BW= 1.50 MAX SIDE LOBE=-30.4

FIGURE 4.2-19

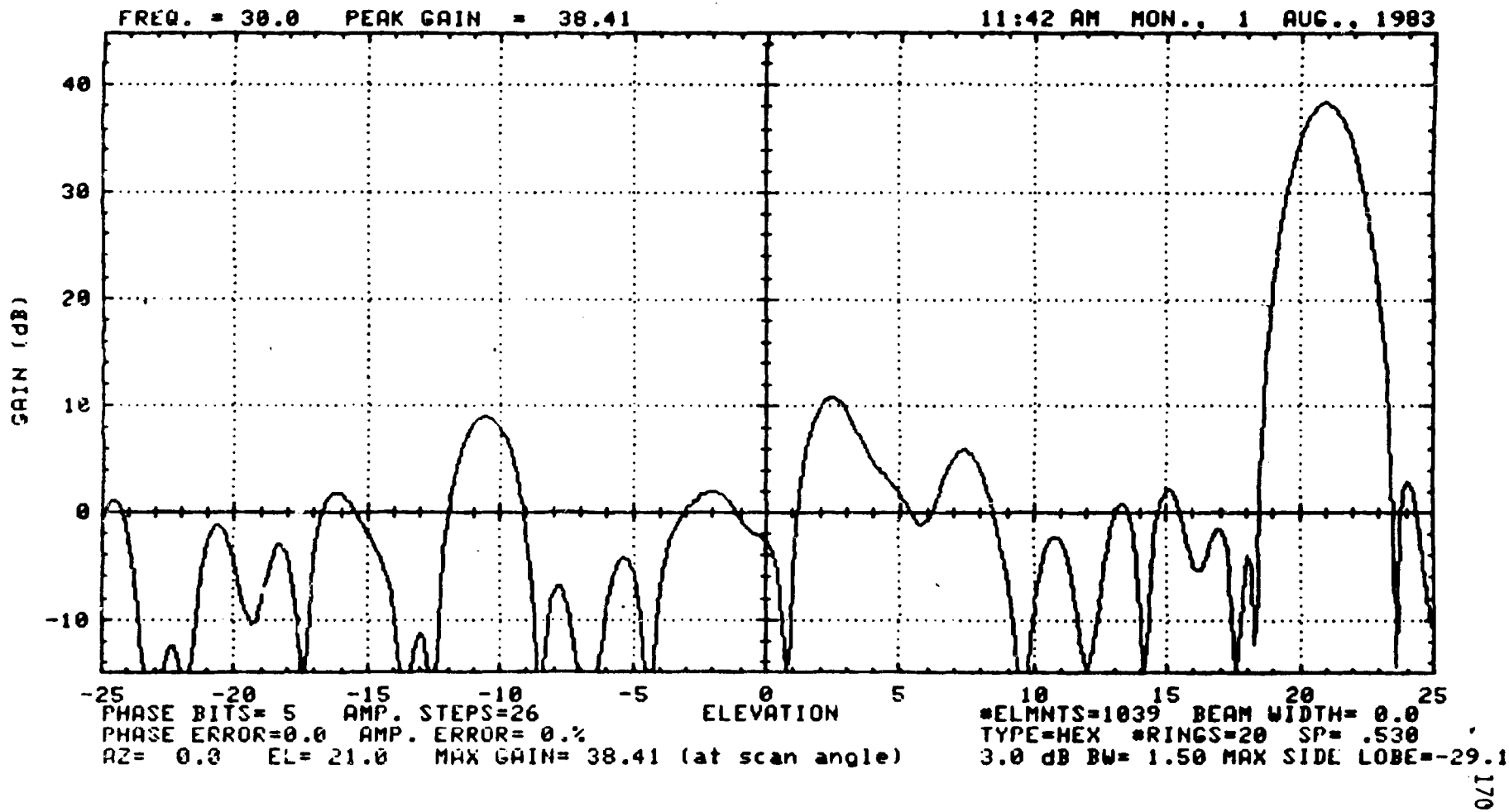

170

FIGURE 4.2-20

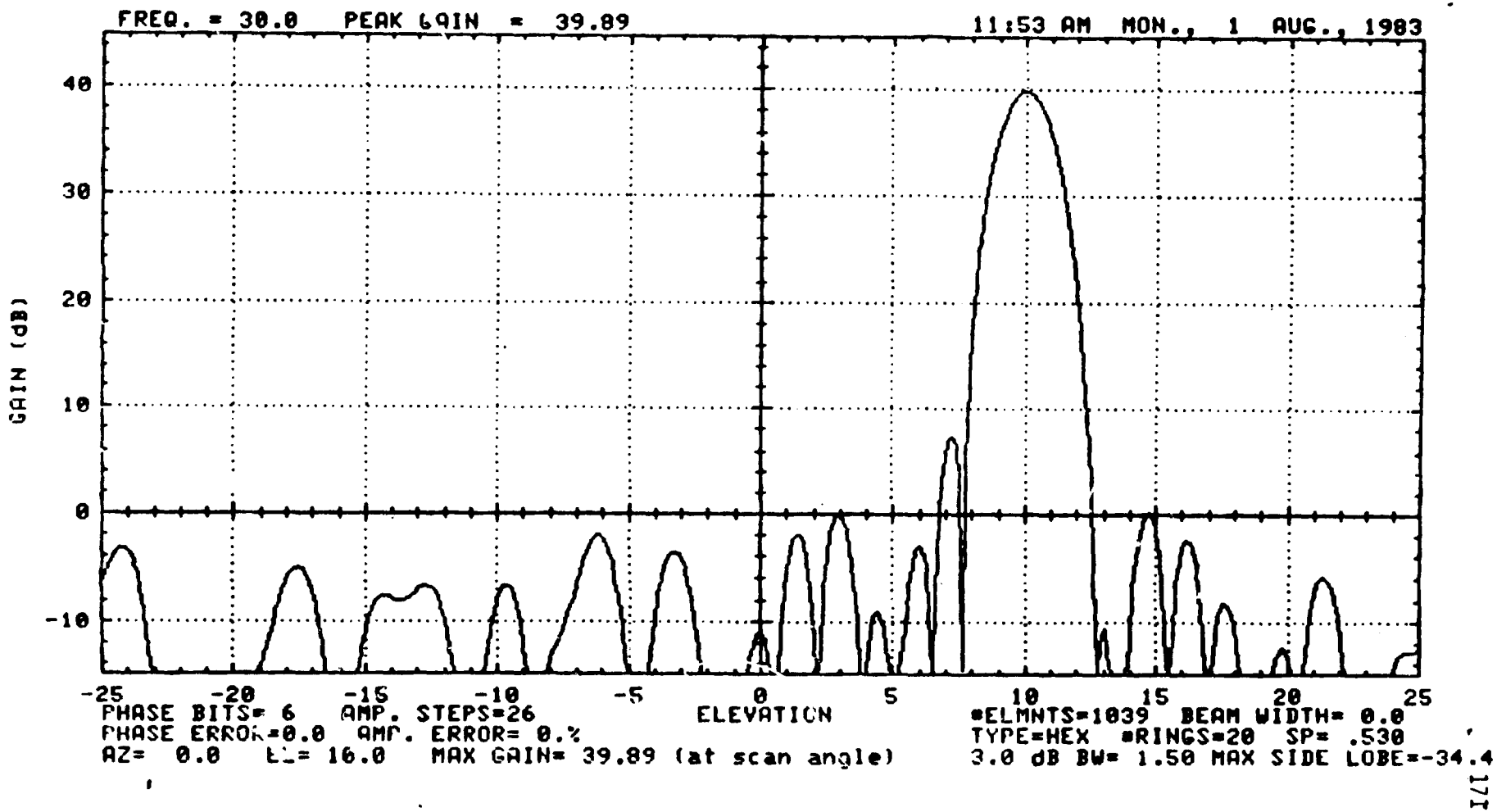
FREQ. = 30.0 PEAK GAIN = 39.89
11:53 AM MON., 1 AUG., 1983
GAIN (dB)
40
30
20
10
0
-10
-25 -20 -15 -10 -5 0 5 10 15 20 25
ELEVATION
PHASE BITS= 6 AMP. STEPS=26
PHASE ERROR=0.0 AMP. ERROR= 0.%
AZ= 0.0 EL= 16.0 MAX GAIN= 39.89 (at scan angle)
#ELMNTS=1039 BEAM WIDTH= 0.0
TYPE=HEX #RINGS=20 SP= .530
3.0 dB BW= 1.50 MAX SIDE LOBE=-34.4

FIGURE 4.2-21

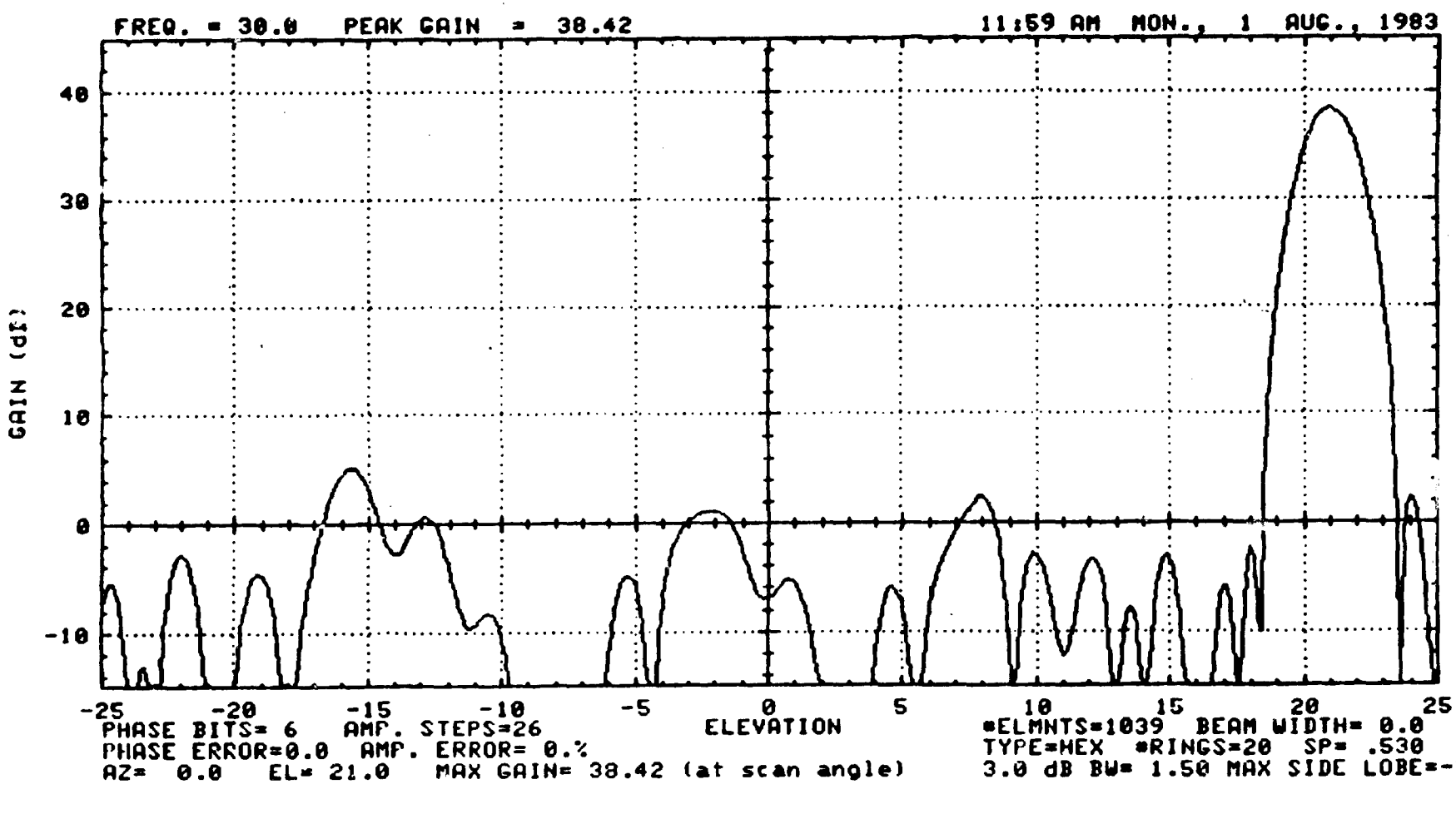
FREQ. = 30.0 PEAK GAIN = 38.42
11:59 AM MON., 1 AUG., 1983
GAIN (dB)
40
30
20
10
0
-10
-25 -20 -15 -10 -5 0 5 10 15 20 25
ELEVATION
PHASE BITS= 6 AMP. STEPS=26
PHASE ERROR=0.0 AMP. ERROR= 0.%
AZ= 0.0 EL= 21.0 MAX GAIN= 38.42 (at scan angle)
#ELMNTS=1039 BEAM WIDTH= 0.0
TYPE=HEX #RINGS=20 SP= .530
3.0 dB BW= 1.50 MAX SIDE LOBE=-34.9

FIGURE 4.2-22

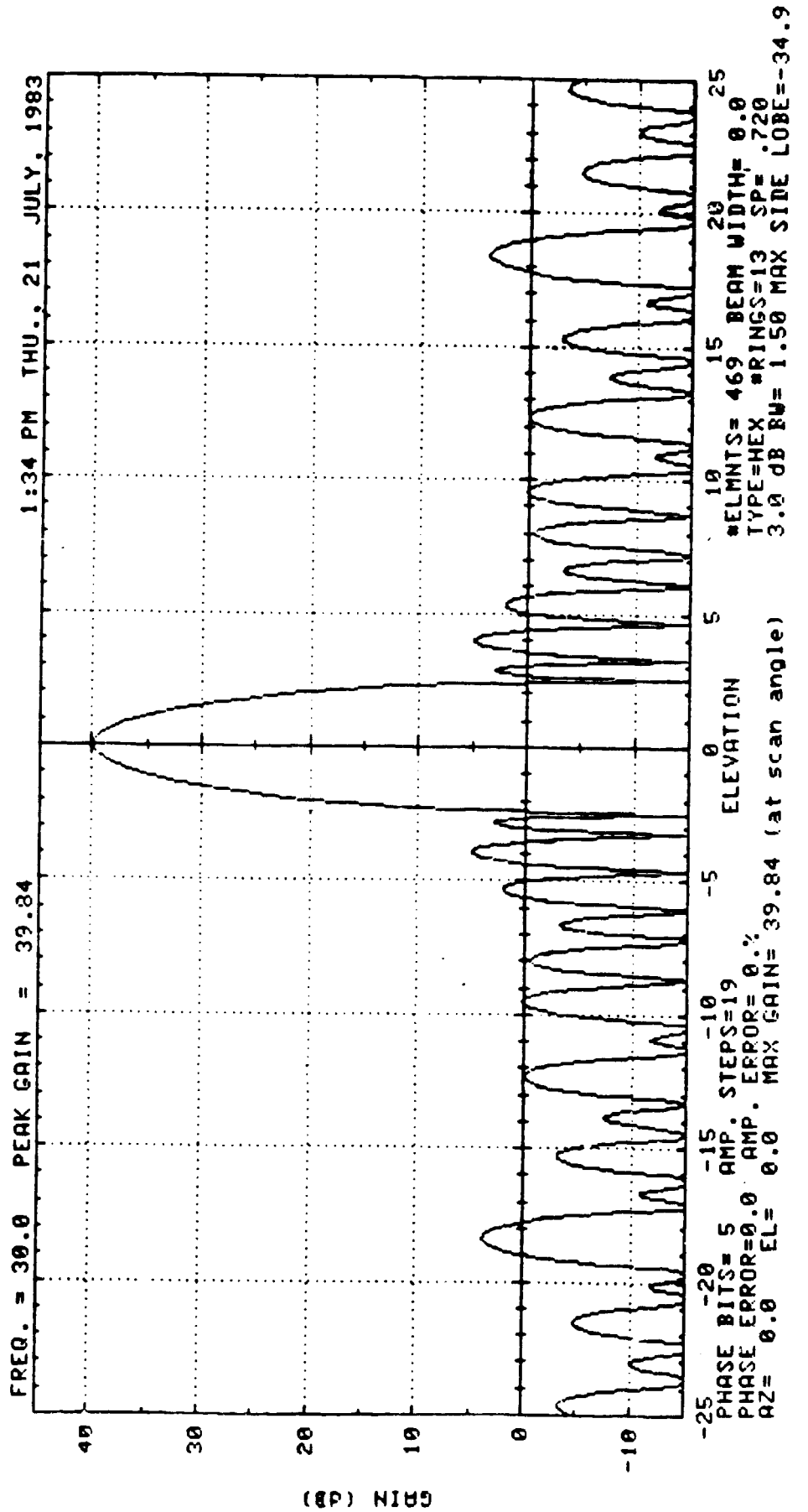
FREQ. = 30.0 PEAK GAIN = 39.84
1:34 PM THU., 21 JULY, 1983
GAIN (dB)
40
30
20
10
0
-10
-25 -20 -15 -10 -5 0 5 10 15 20 25
ELEVATION
PHASE BITS= 5 AMP. STEPS=19 *ELMNTS= 469 BEAM WIDTH= 0.0
PHASE ERROR=0.0 AMP. ERROR= 0.% TYPE=HEX *RINGS=13 SP= .720
AZ= 0.0 EL= 0.0 MAX GAIN= 39.84 (at scan angle) 3.0 dB BW= 1.50 MAX SIDE LOBE=-34.9

FIG. 4.2-25

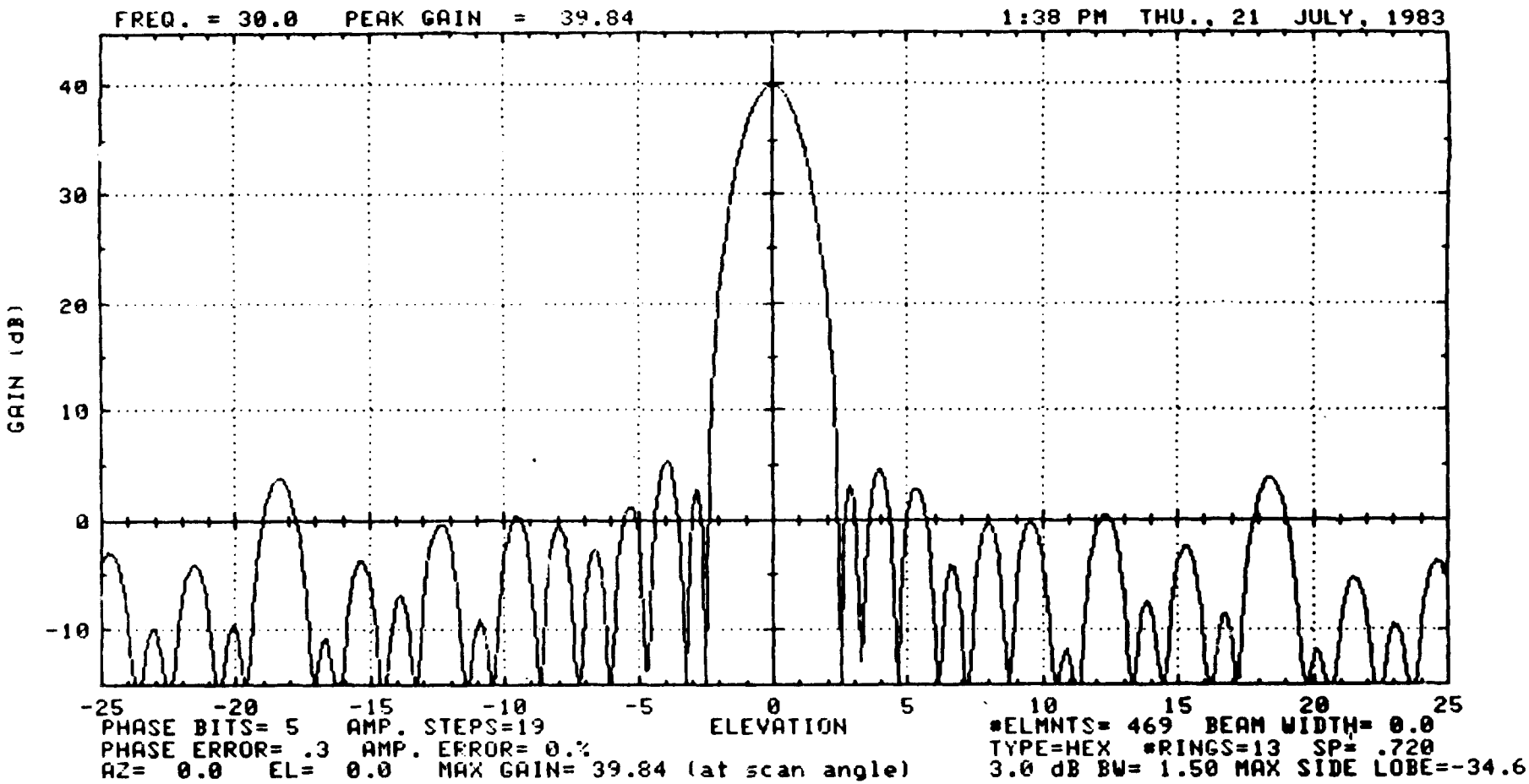
FREQ. = 30.0 PEAK GAIN = 39.84
1:38 PM THU., 21 JULY, 1983
GAIN (dB)
40
30
20
10
0
-10
-25 -20 -15 -10 -5 0 5 10 15 20 25
ELEVATION
PHASE BITS= 5 AMP. STEPS=19
PHASE ERROR= .3 AMP. ERROR= 0.%
AZ= 0.0 EL= 0.0 MAX GAIN= 39.84 (at scan angle)
#ELMNTS= 469 BEAM WIDTH= 0.0
TYPE=HEX #RINGS=13 SP= .720
3.0 dB BW= 1.50 MAX SIDE LOBE=-34.6

FIG 4.2-26

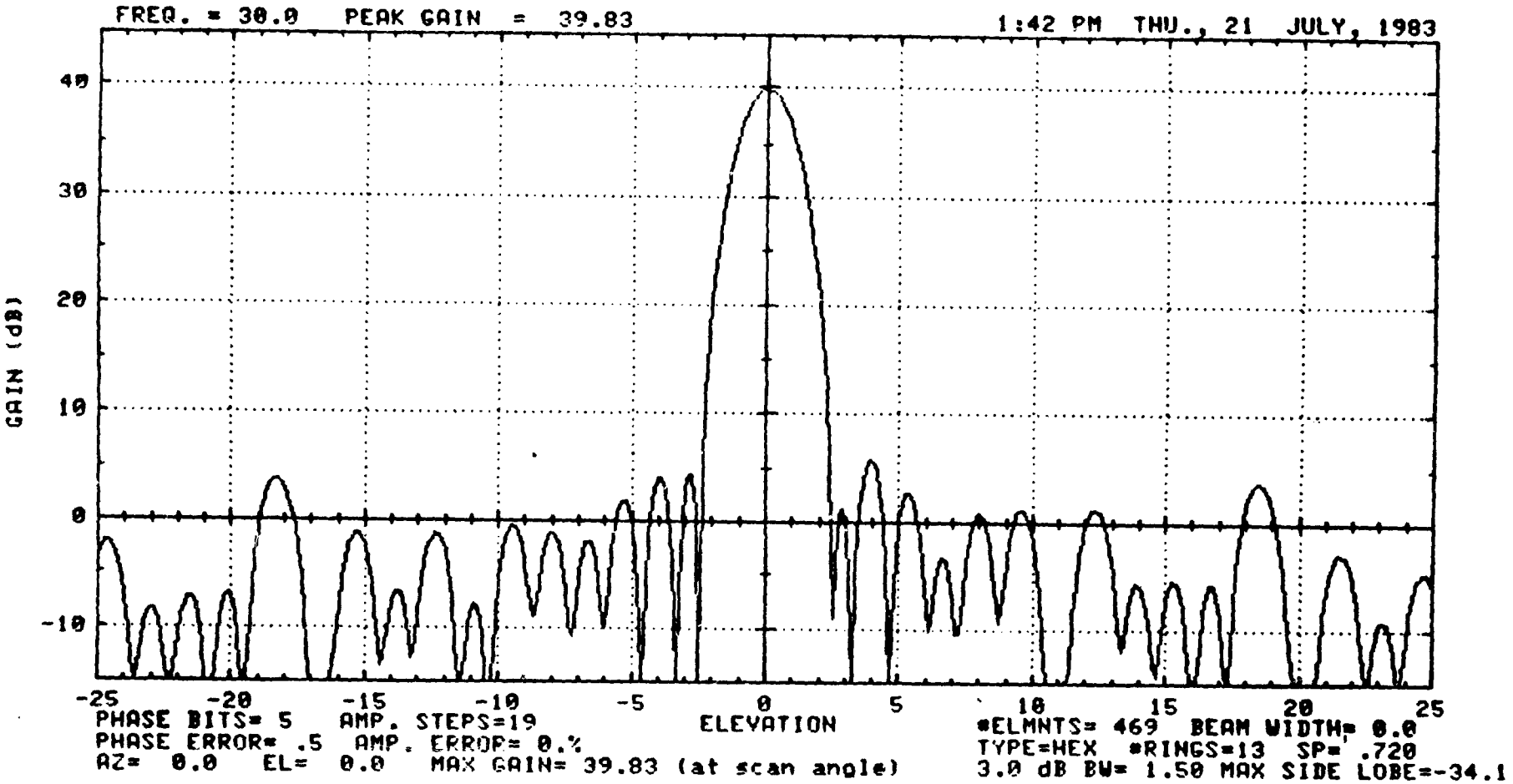
FREQ. = 30.0 PEAK GAIN = 39.83
1:42 PM THU., 21 JULY, 1983
GAIN (dB)
40
30
20
10
0
-10
-25 -20 -15 -10 -5 0 5 10 15 20 25
ELEVATION
PHASE BITS= 5 AMP. STEPS=19
PHASE ERROR= .5 AMP. ERROR= 0.%
AZ= 0.0 EL= 0.0 MAX GAIN= 39.83 (at scan angle)
#ELMNTS= 469 BEAM WIDTH= 0.0
TYPE=HEX #RINGS=13 SP= .720
3.0 dB BW= 1.50 MAX SIDE LOBE=-34.1

FIG 4.2-27

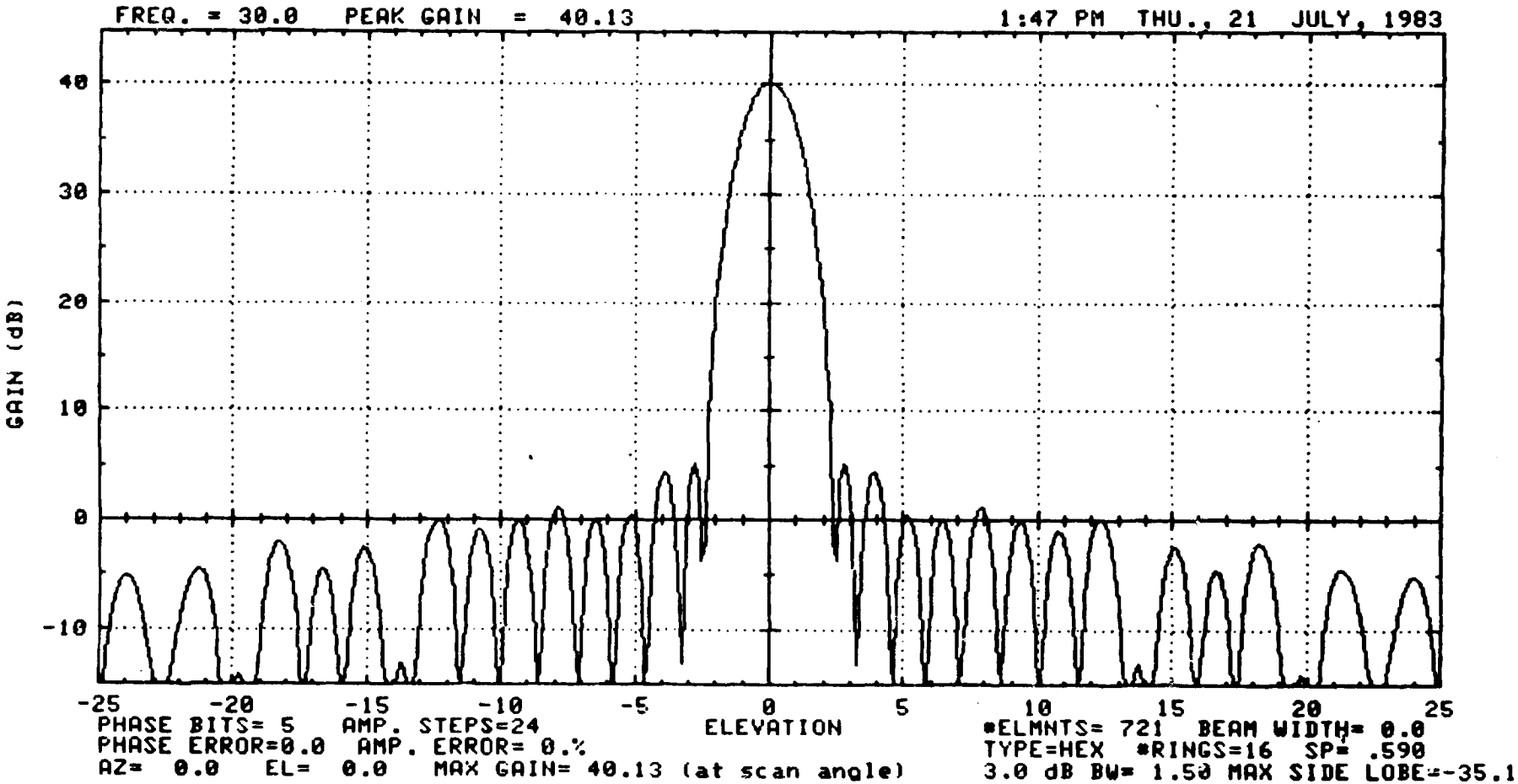
FREQ. = 30.0 PEAK GAIN = 40.13
1:47 PM THU., 21 JULY, 1983
GAIN (dB)
40
30
20
10
0
-10
-25 -20 -15 -10 -5 0 5 10 15 20 25
ELEVATION
PHASE BITS= 5 AMP. STEPS=24
PHASE ERROR=0.0 AMP. ERROR= 0.%
AZ= 0.0 EL= 0.0 MAX GAIN= 40.13 (at scan angle)
#ELMNTS= 721 BEAM WIDTH= 0.0
TYPE=HEX #RINGS=16 SP= .590
3.0 dB BW= 1.50 MAX SIDE LOBE=-35.1

FIG. 4.2-28

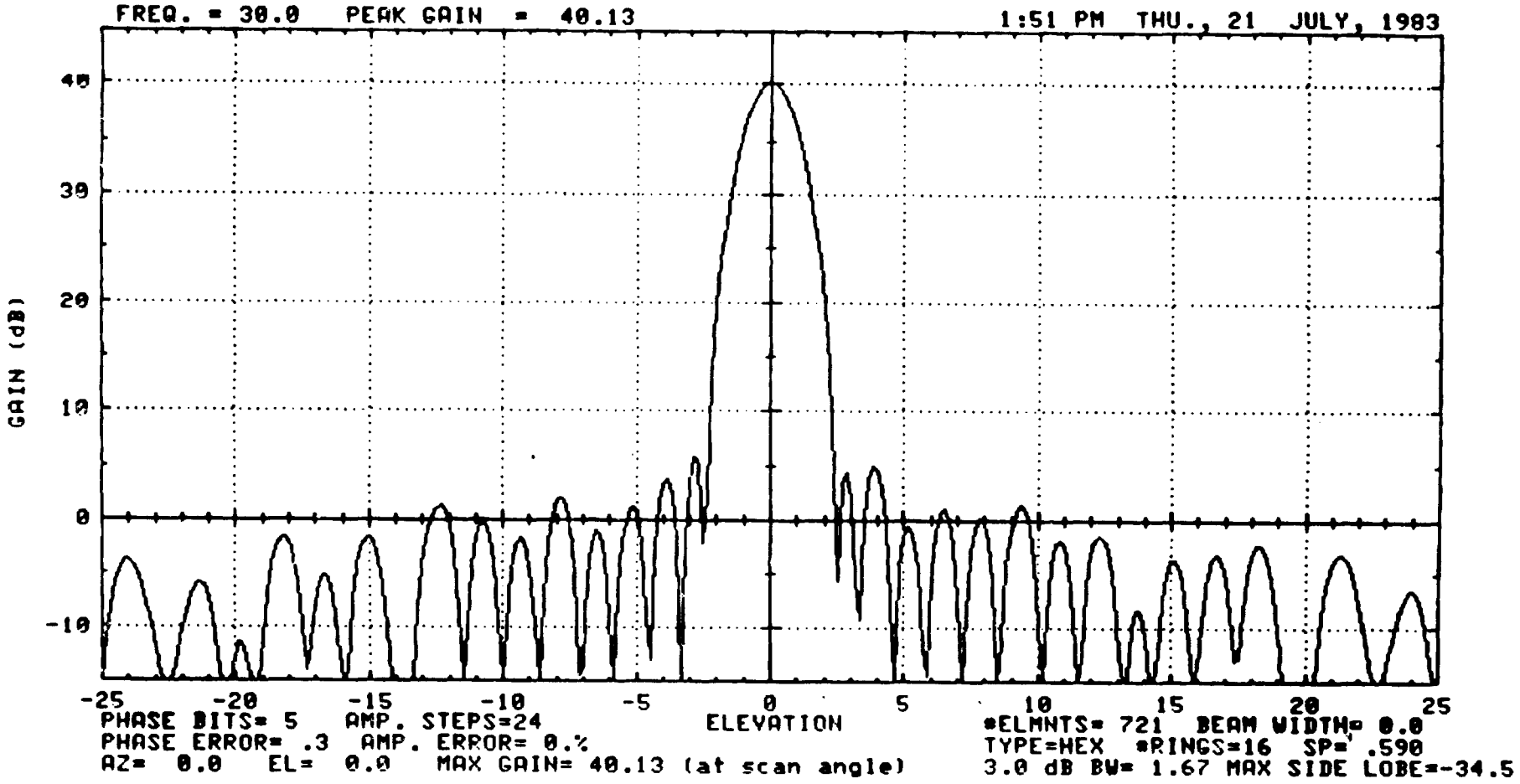
FREQ. = 30.0 PEAK GAIN = 40.13
1:51 PM THU., 21 JULY, 1983
GAIN (dB)
40
30
20
10
0
-10
-25 -20 -15 -10 -5 0 5 10 15 20 25
ELEVATION
PHASE BITS= 5 AMP. STEPS=24
PHASE ERROR= .3 AMP. ERROR= 0.%
AZ= 0.0 EL= 0.0 MAX GAIN= 40.13 (at scan angle)
#ELMNTS= 721 BEAM WIDTH= 0.0
TYPE=HEX #RINGS=16 SP= .590
3.0 dB BW= 1.67 MAX SIDE LOBE=-34.5

FIG. 4.2-29

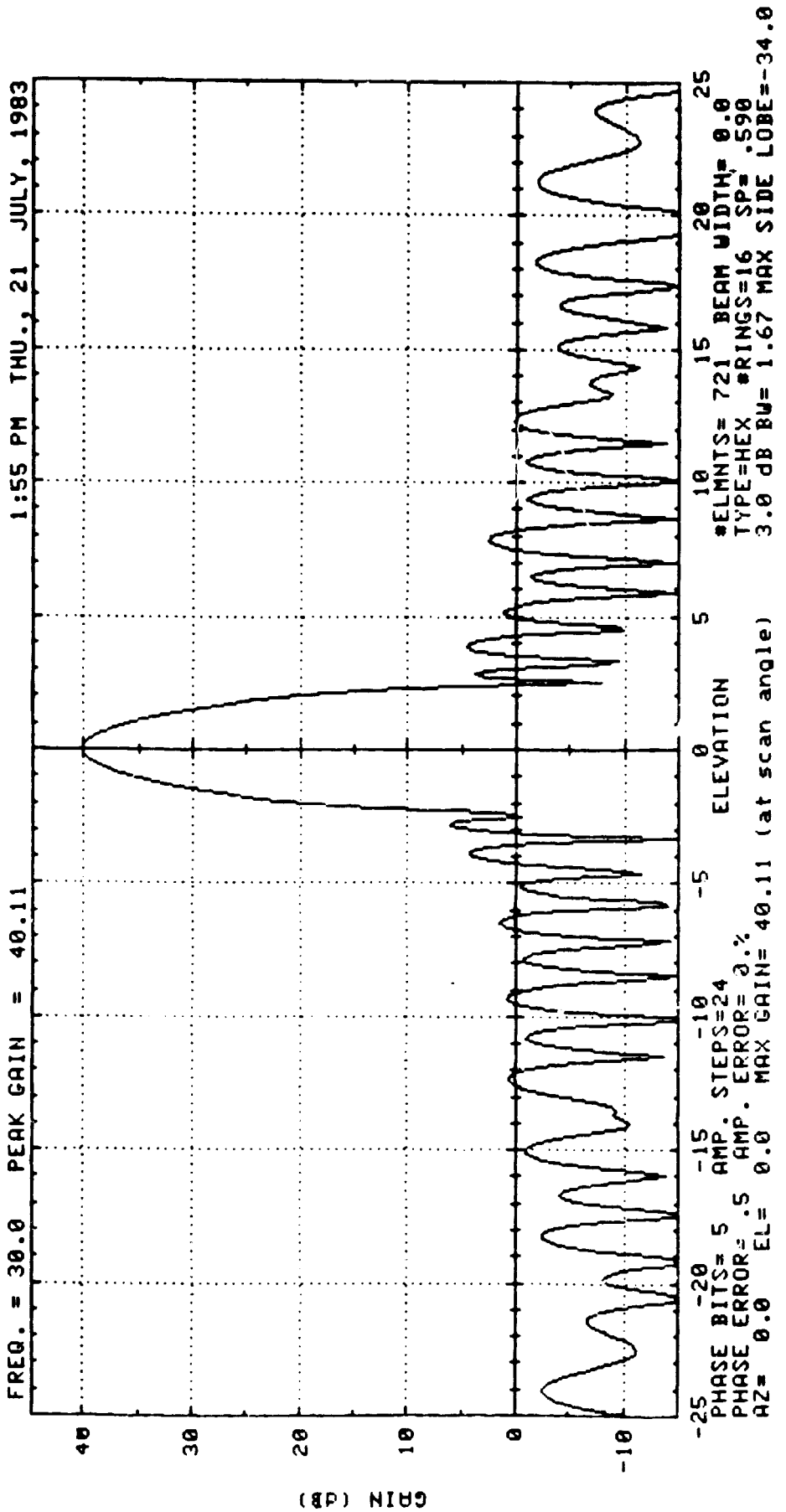
FREQ. = 30.0 PEAK GAIN = 40.11
1:55 PM THU., 21 JULY, 1983
GAIN (dB)
40
30
20
10
0
-10
-25 -20 -15 -10 -5 0 5 10 15 20 25
ELEVATION
PHASE BITS= 5 AMP. STEPS=24 *ELMNTS= 721 BEAM WIDTH= 0.0
PHASE ERROR= .5 AMP. ERROR= 0.% TYPE=HEX *RINGS=16 SP= .590
AZ= 0.0 EL= 0.0 MAX GAIN= 40.11 (at scan angle) 3.0 dB BW= 1.67 MAX SIDE LOBE=-34.0

FIG. 4.2-30

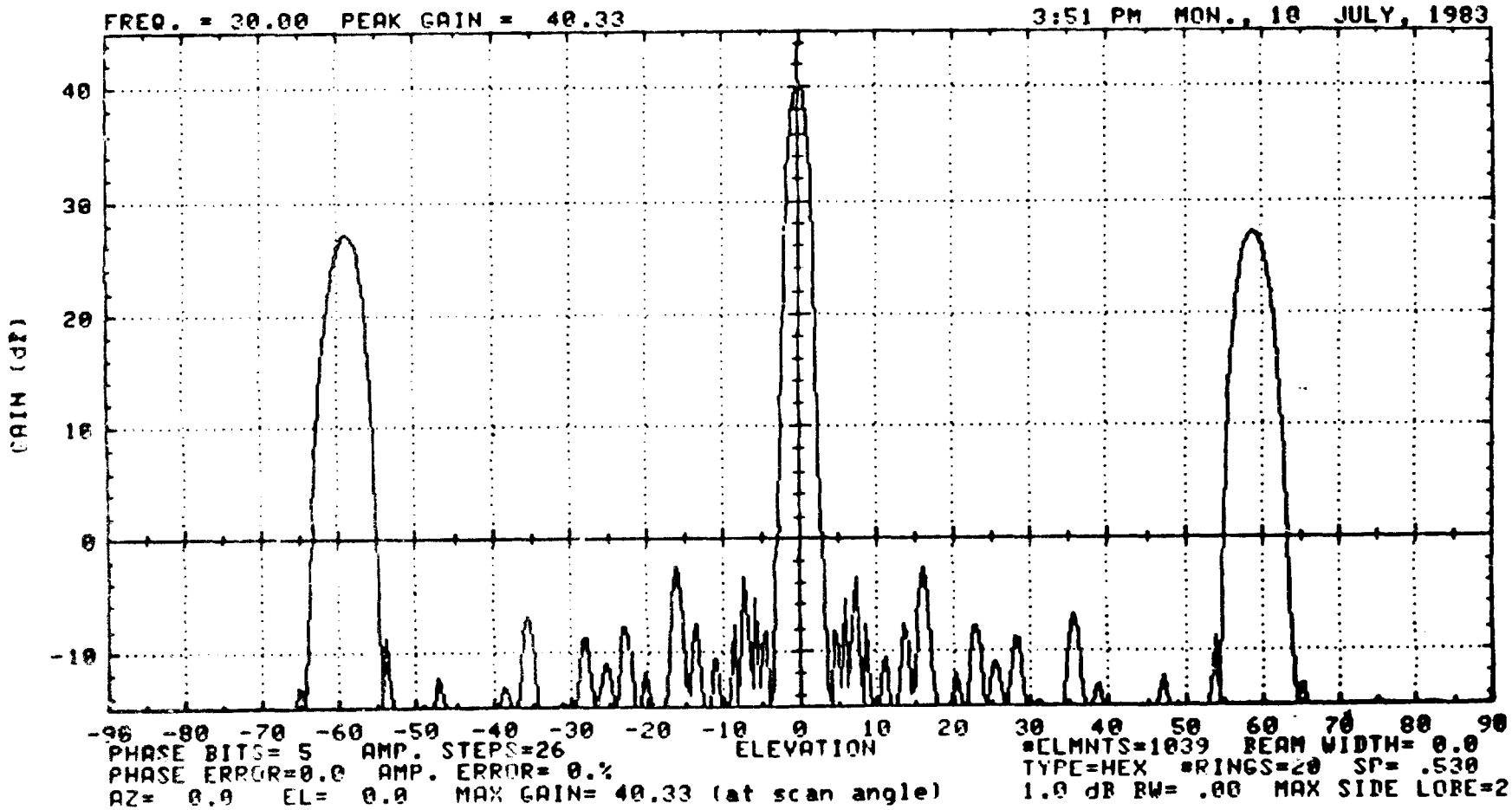
FREQ. = 30.00 PEAK GAIN = 40.33
3:51 PM MON., 10 JULY, 1983
GAIN (dB)
40
30
20
10
0
-10
-90 -80 -70 -60 -50 -40 -30 -20 -10 0 10 20 30 40 50 60 70 80 90
ELEVATION
PHASE BITS= 5 AMP. STEPS=26
PHASE ERROR=0.0 AMP. ERROR= 0.%
AZ= 0.0 EL= 0.0 MAX GAIN= 40.33 (at scan angle)
#ELMNTS=1039 BEAM WIDTH= 0.0
TYPE=HEX #RINGS=20 SP= .530
1.0 dB BW= .00 MAX SIDE LOBE=27.26

FIG 4.2-31

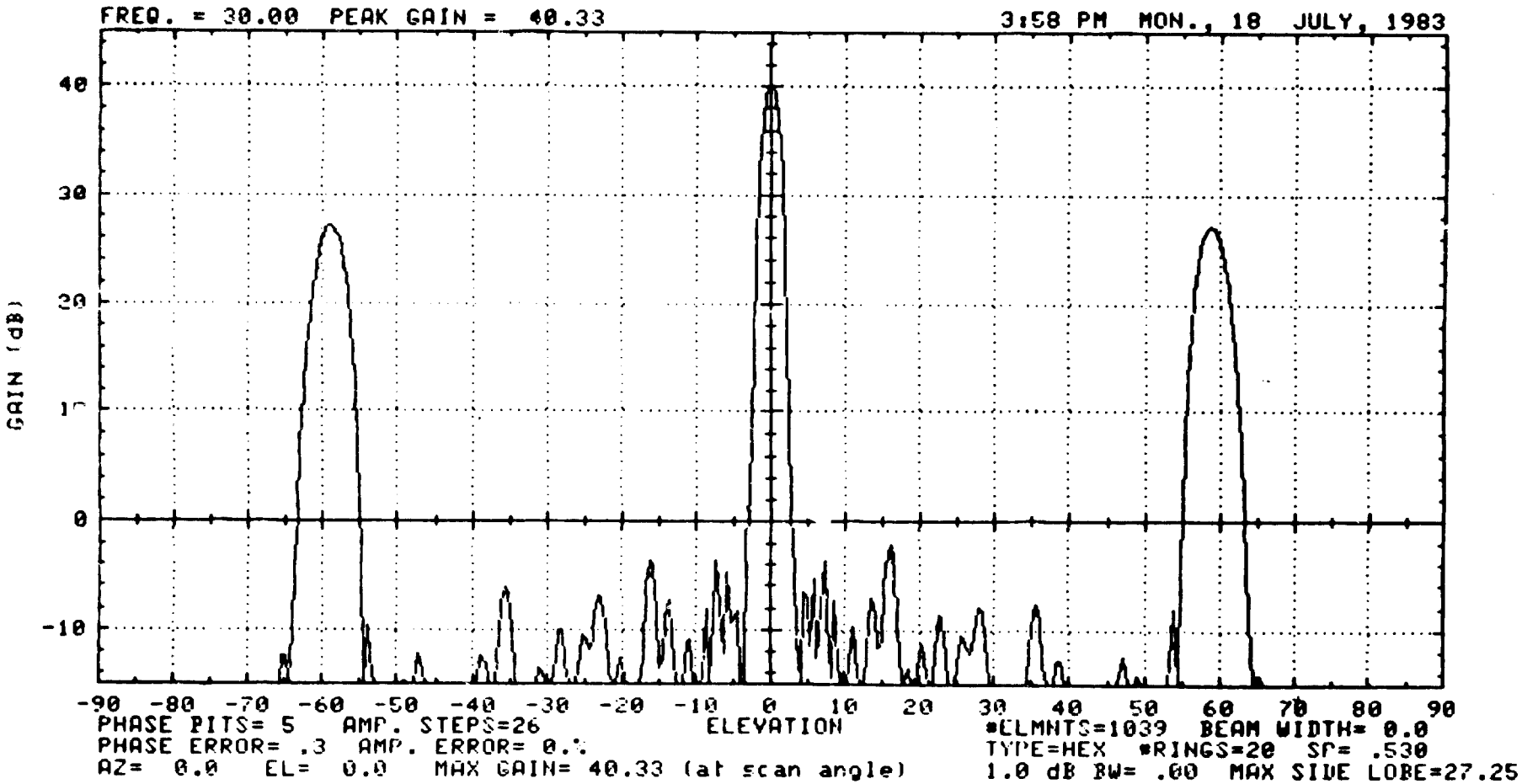
FREQ. = 30.00 PEAK GAIN = 40.33
3:58 PM MON., 18 JULY, 1983
GAIN (dB)
40
30
20
10
0
-10
-90 -80 -70 -60 -50 -40 -30 -20 -10 0 10 20 30 40 50 60 70 80 90
ELEVATION
PHASE BITS= 5 AMP. STEPS=26
PHASE ERROR= .3 AMP. ERROR= 0.%
AZ= 0.0 EL= 0.0 MAX GAIN= 40.33 (at scan angle)
#ELMNTS=1039 BEAM WIDTH= 0.0
TYPE=HEX #RINGS=20 SF= .530
1.0 dB BW= .00 MAX SIDE LOBE=27.25

FIG. 4.2-32

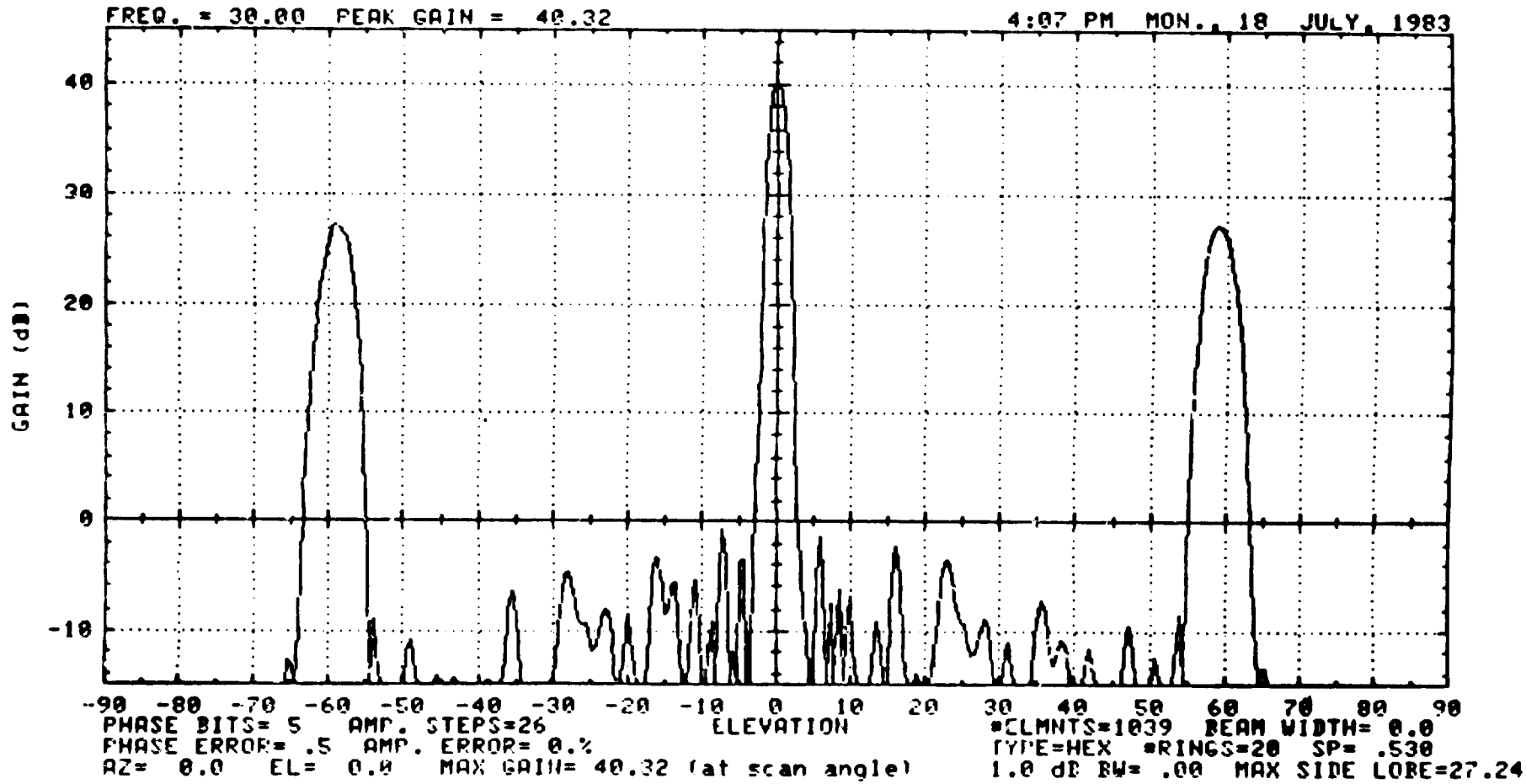
FREQ. = 30.00 PEAK GAIN = 40.32
4:07 PM MON., 18 JULY, 1983
GAIN (dB)
40
30
20
10
0
-10
-90 -80 -70 -60 -50 -40 -30 -20 -10 0 10 20 30 40 50 60 70 80 90
ELEVATION
PHASE BITS= 5 AMP. STEPS=26
PHASE ERROR= .5 AMP. ERROR= 0.%
AZ= 0.0 EL= 0.0 MAX GAIN= 40.32 (at scan angle)
#ELMNTS=1039 BEAM WIDTH= 0.0
TYPE=HEX #RINGS=20 SP= .530
1.0 dB BW= .00 MAX SIDE LOBE=27.24

FIG. 42-33

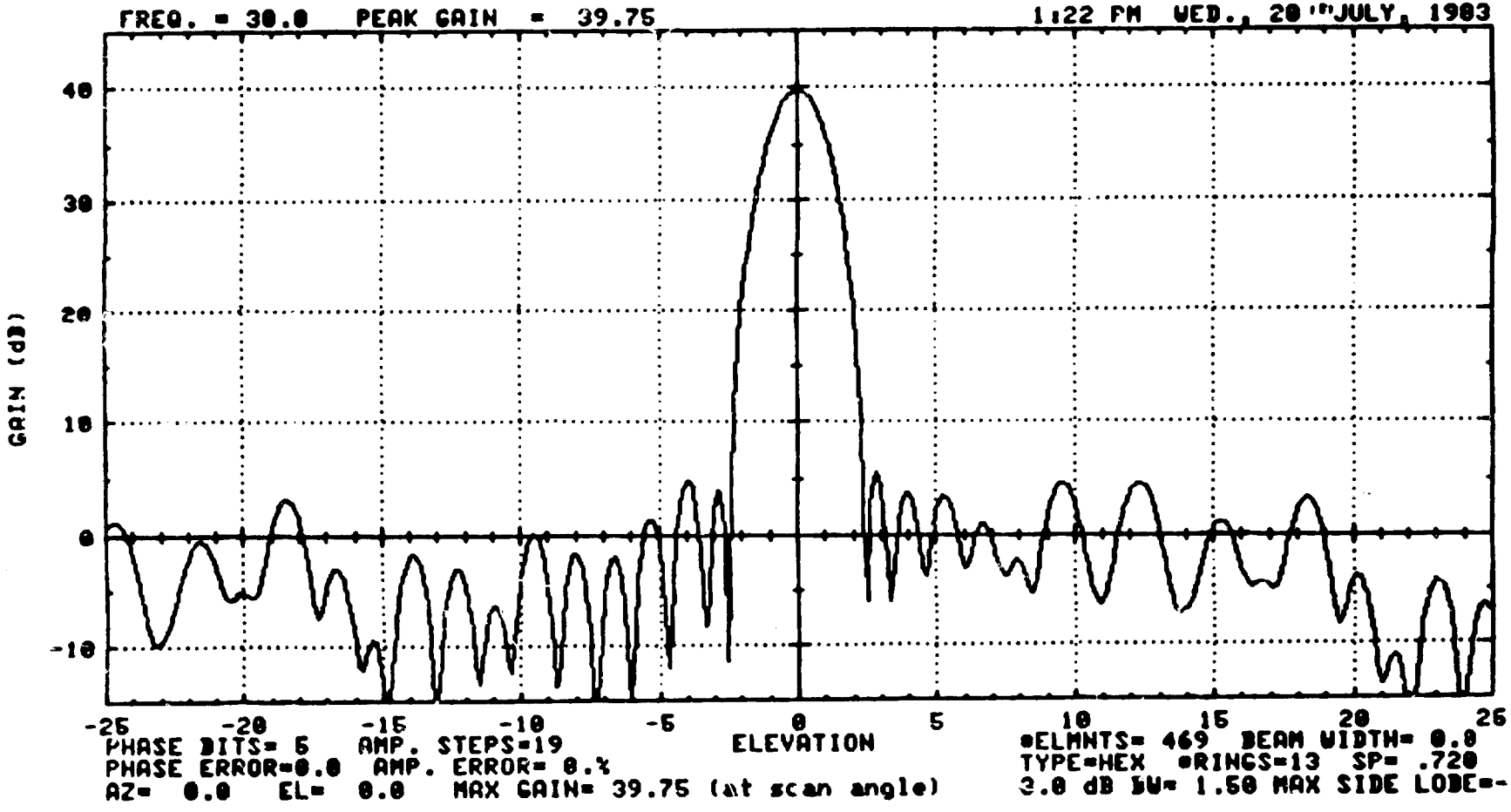

FIG. 4.2-40 3 FAILURES

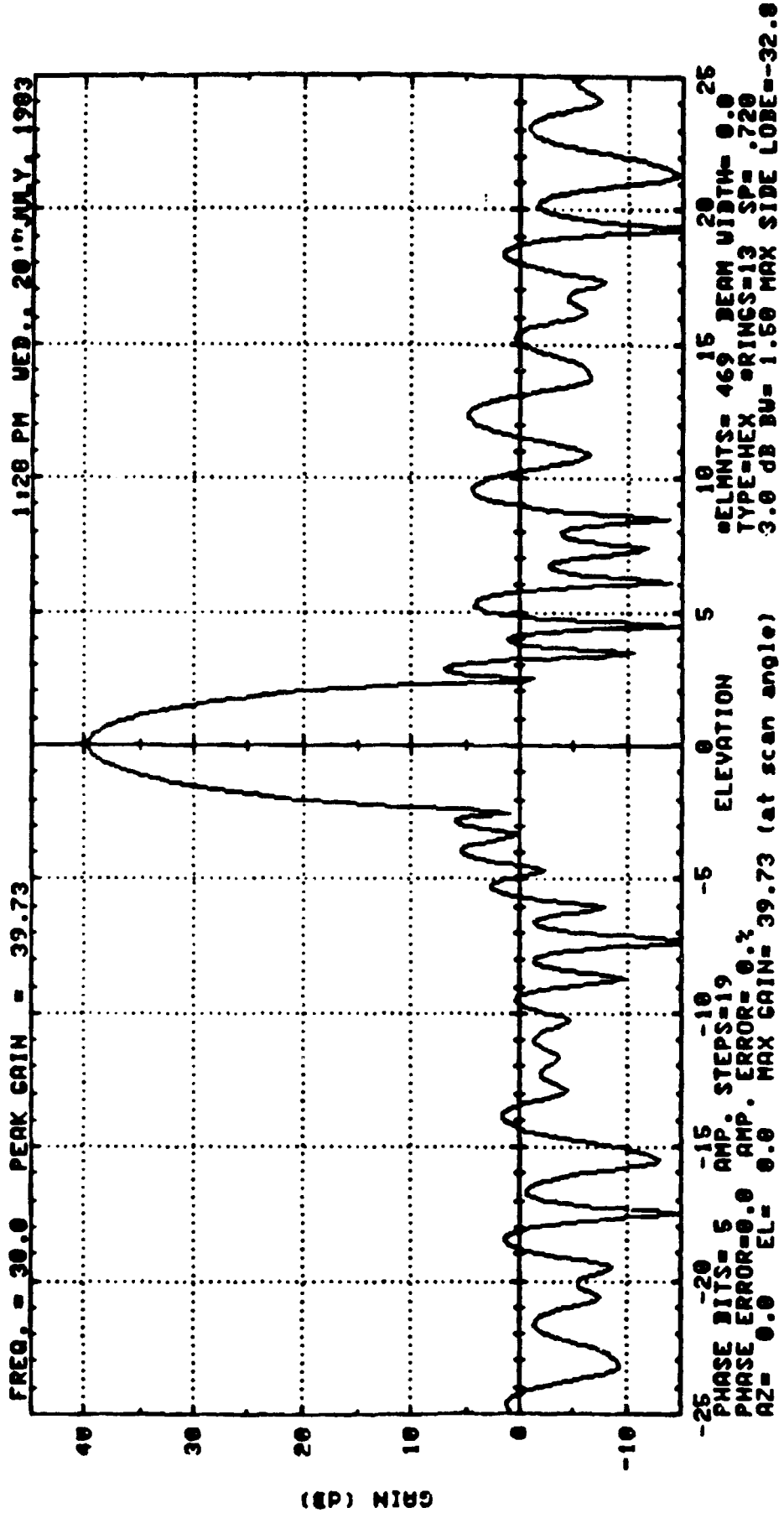

FIG. 4.2-44 5 FAILURES

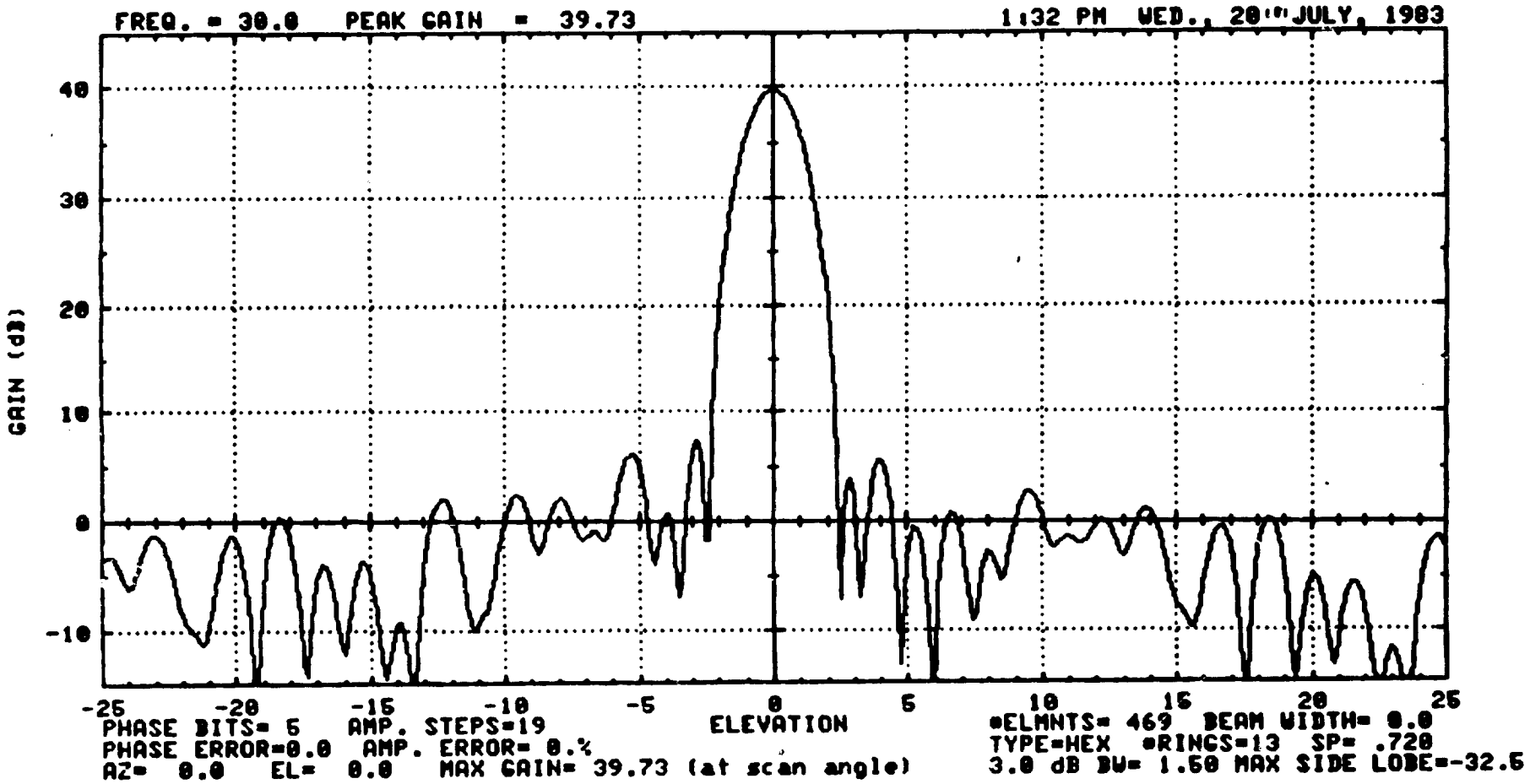

FIG. 4.2-42 8 FAILURES

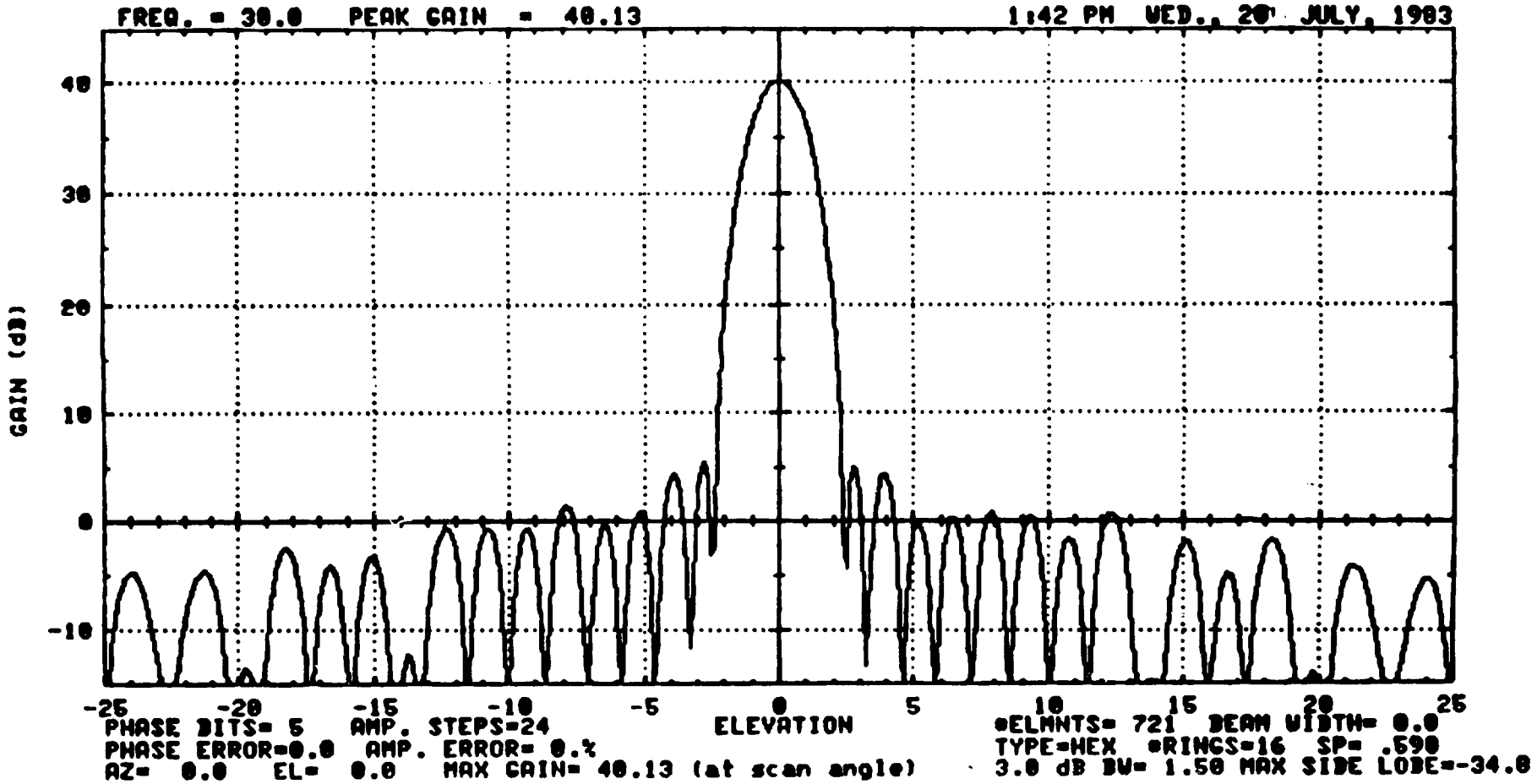

FIG. 4.2-43 3 FAILURES

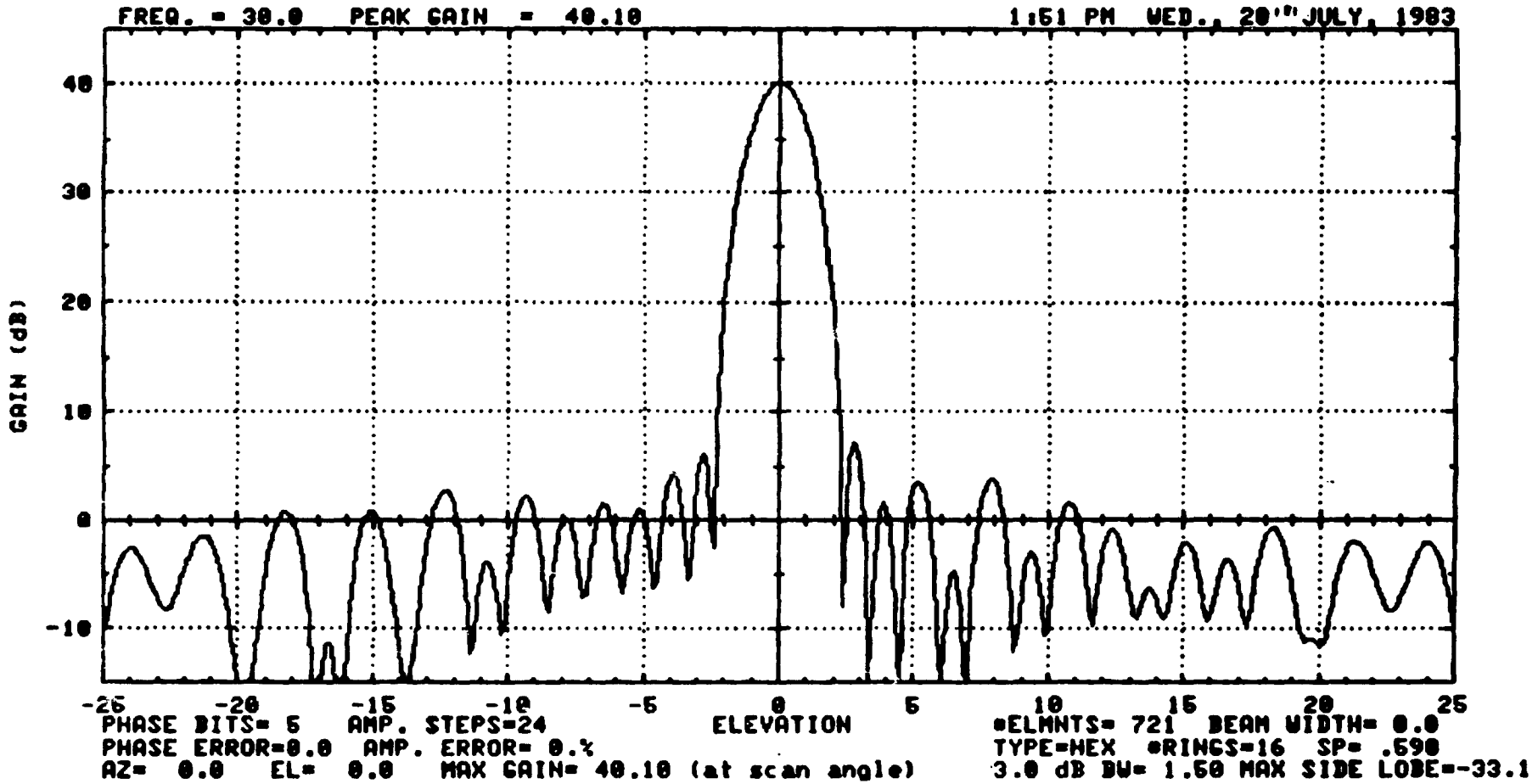

FIG. 4.2-44 , 5 FAILURES

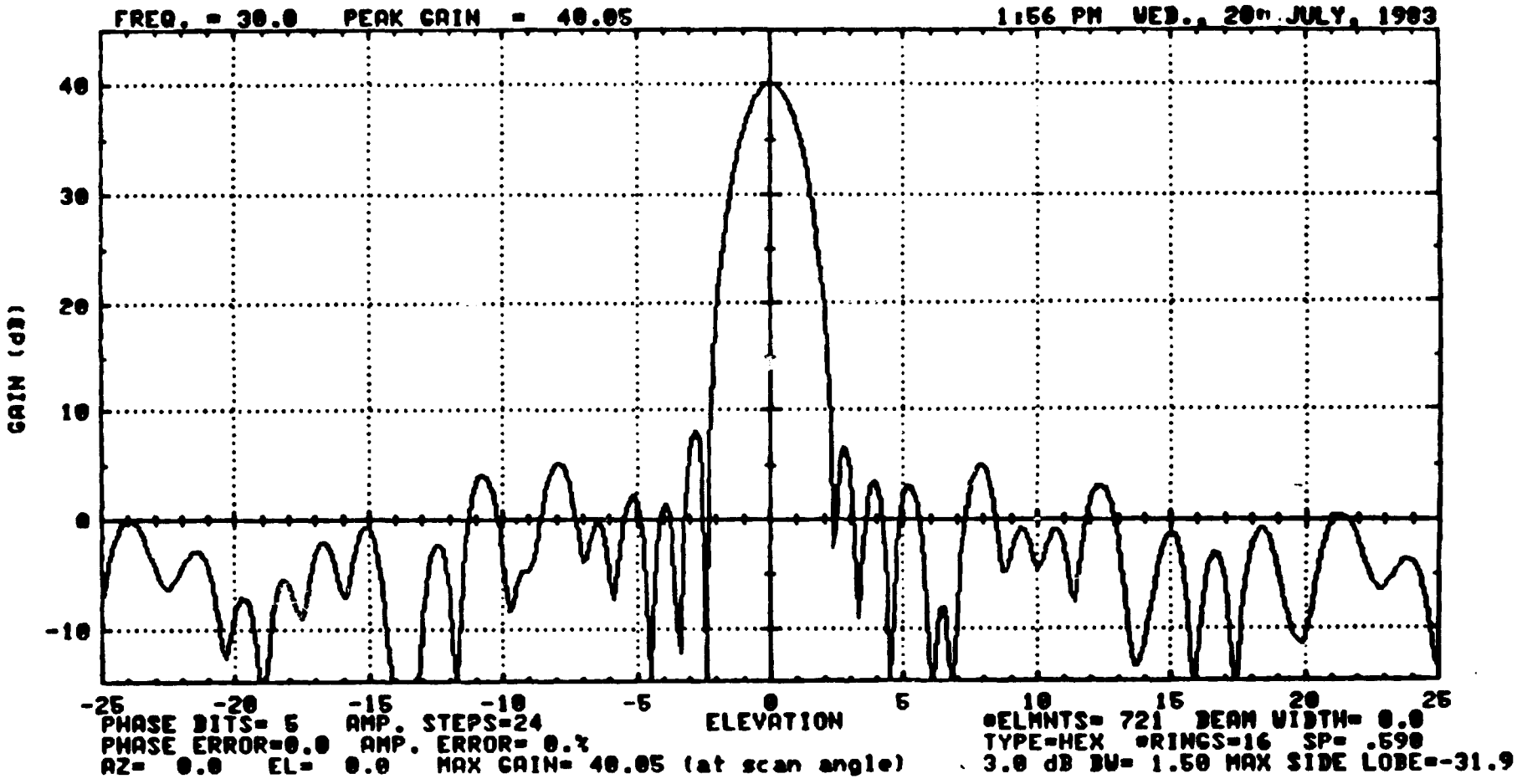

FIG. 4.2-45 8 FAILURES

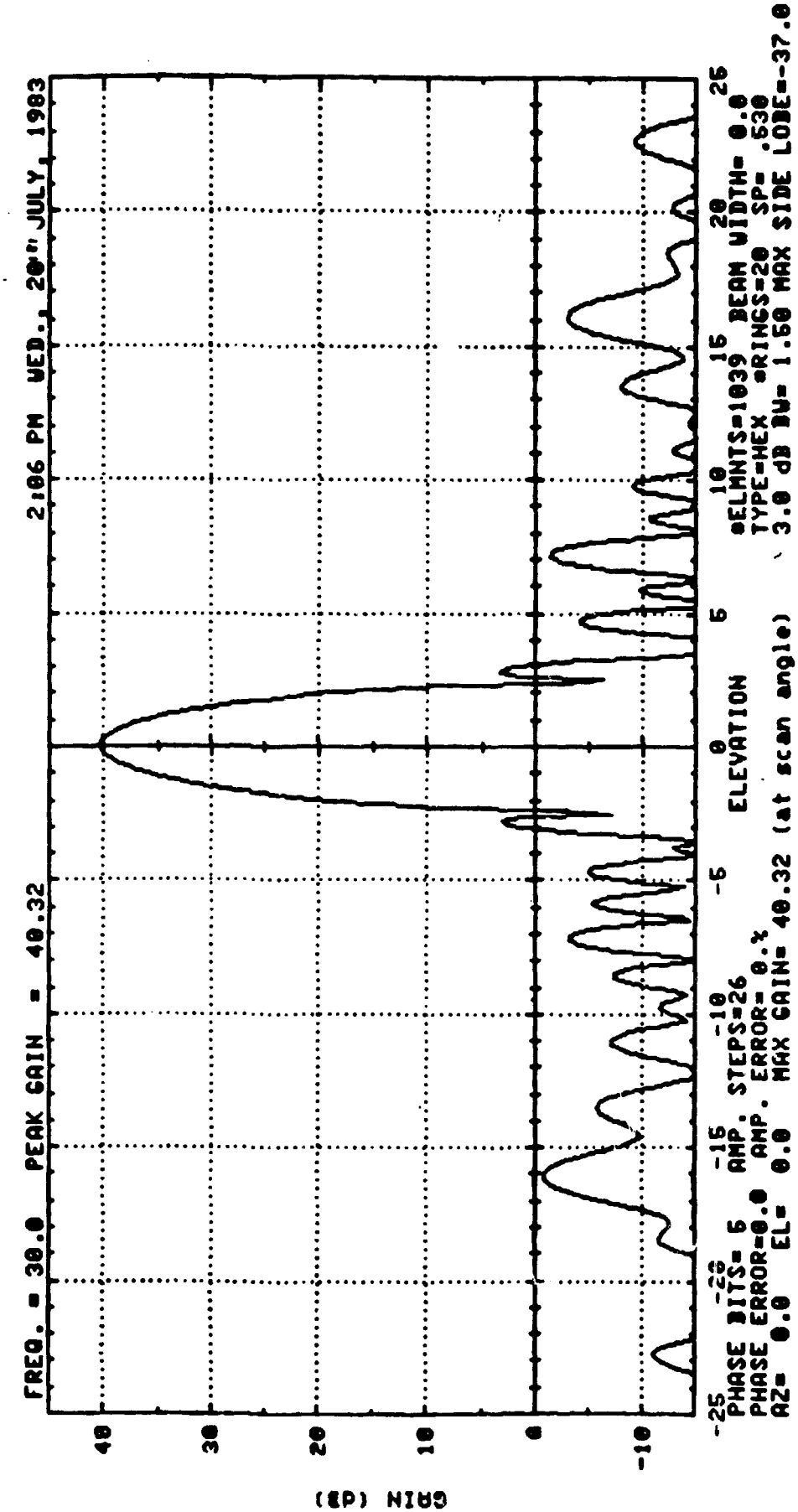

FIG. 4.2-46 3 FAILURES

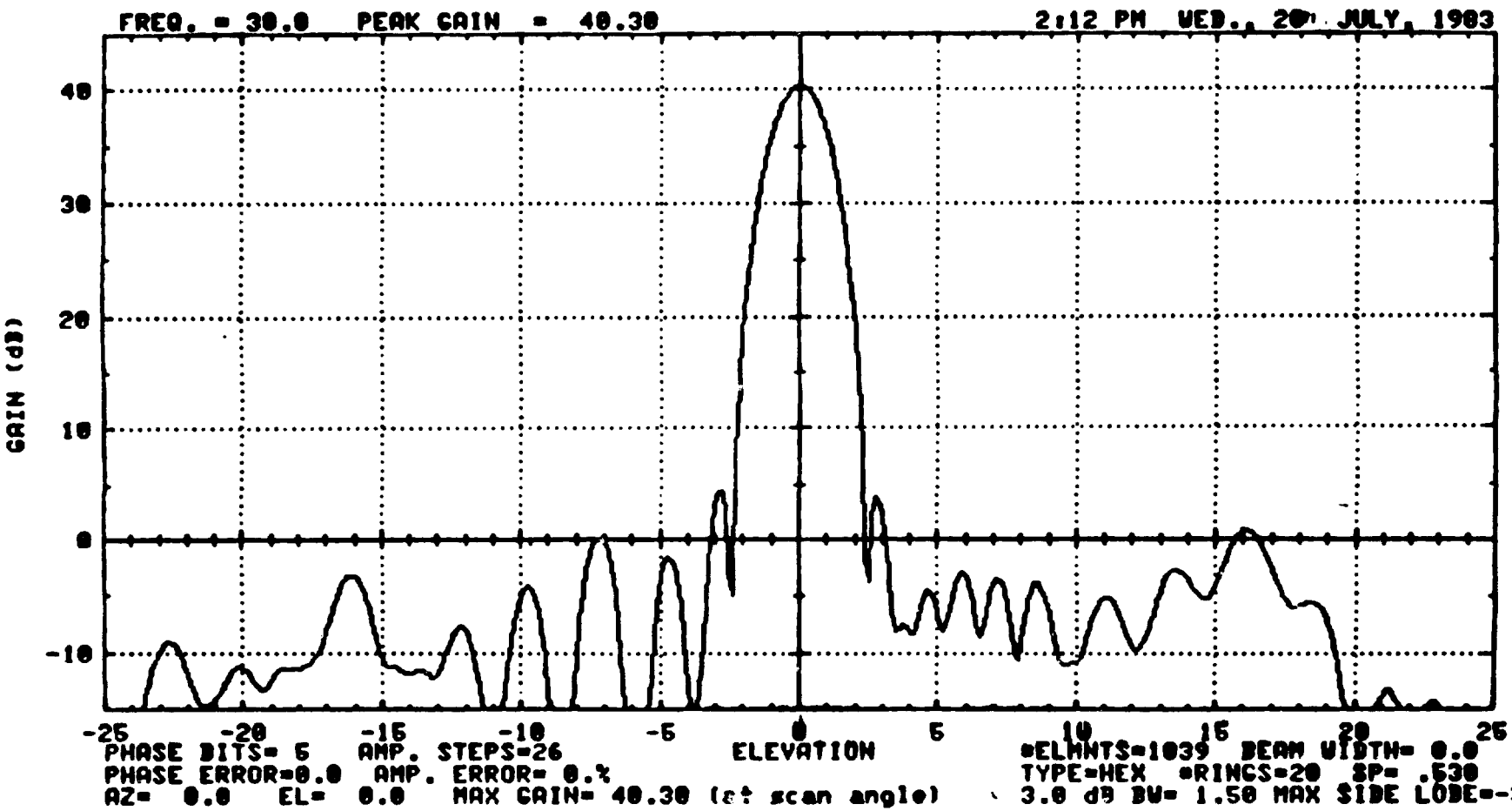

FIG. 4.2-47 5 FAILURES

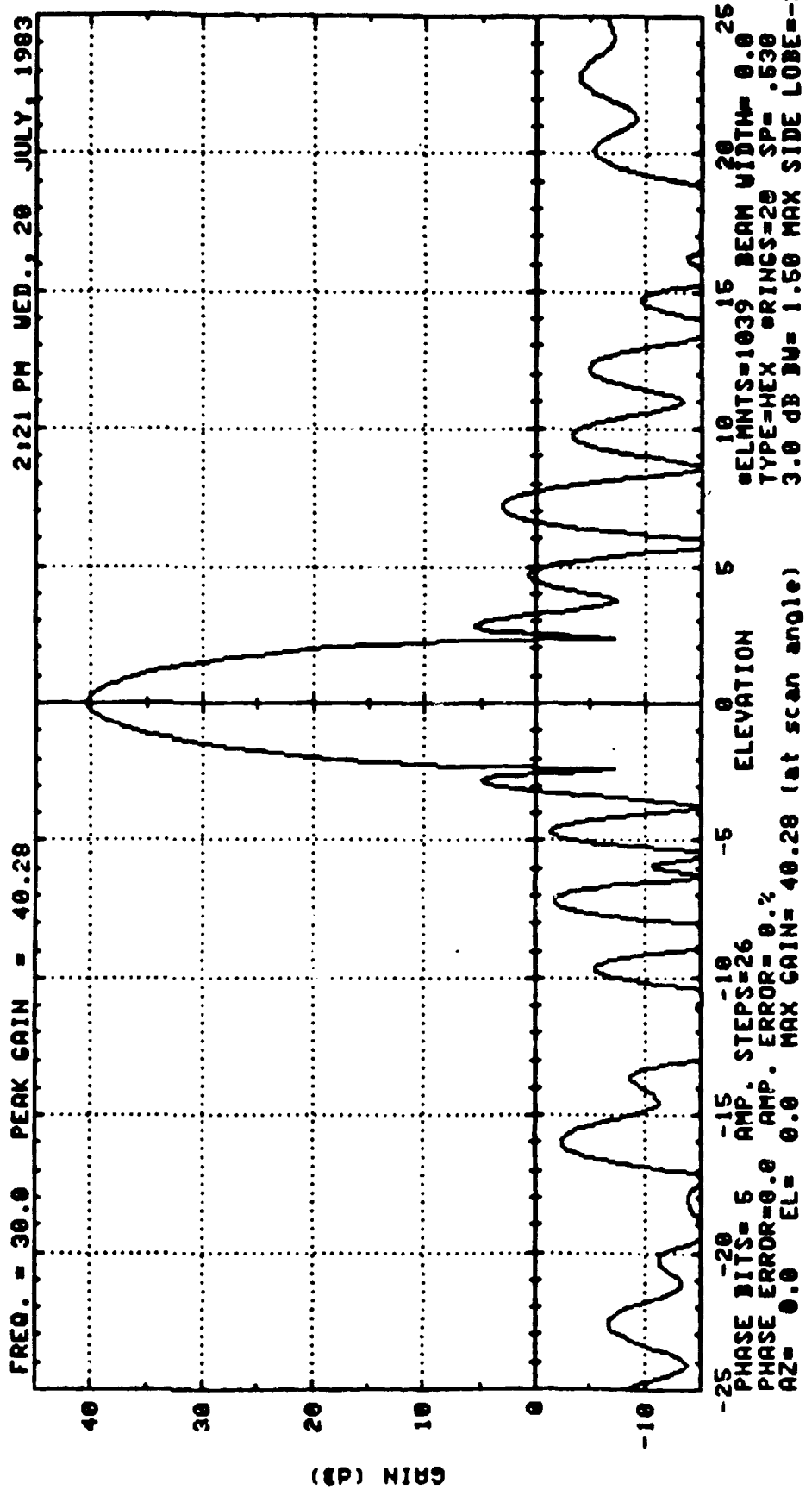

Fig. 4.2-48 8 FAILURES

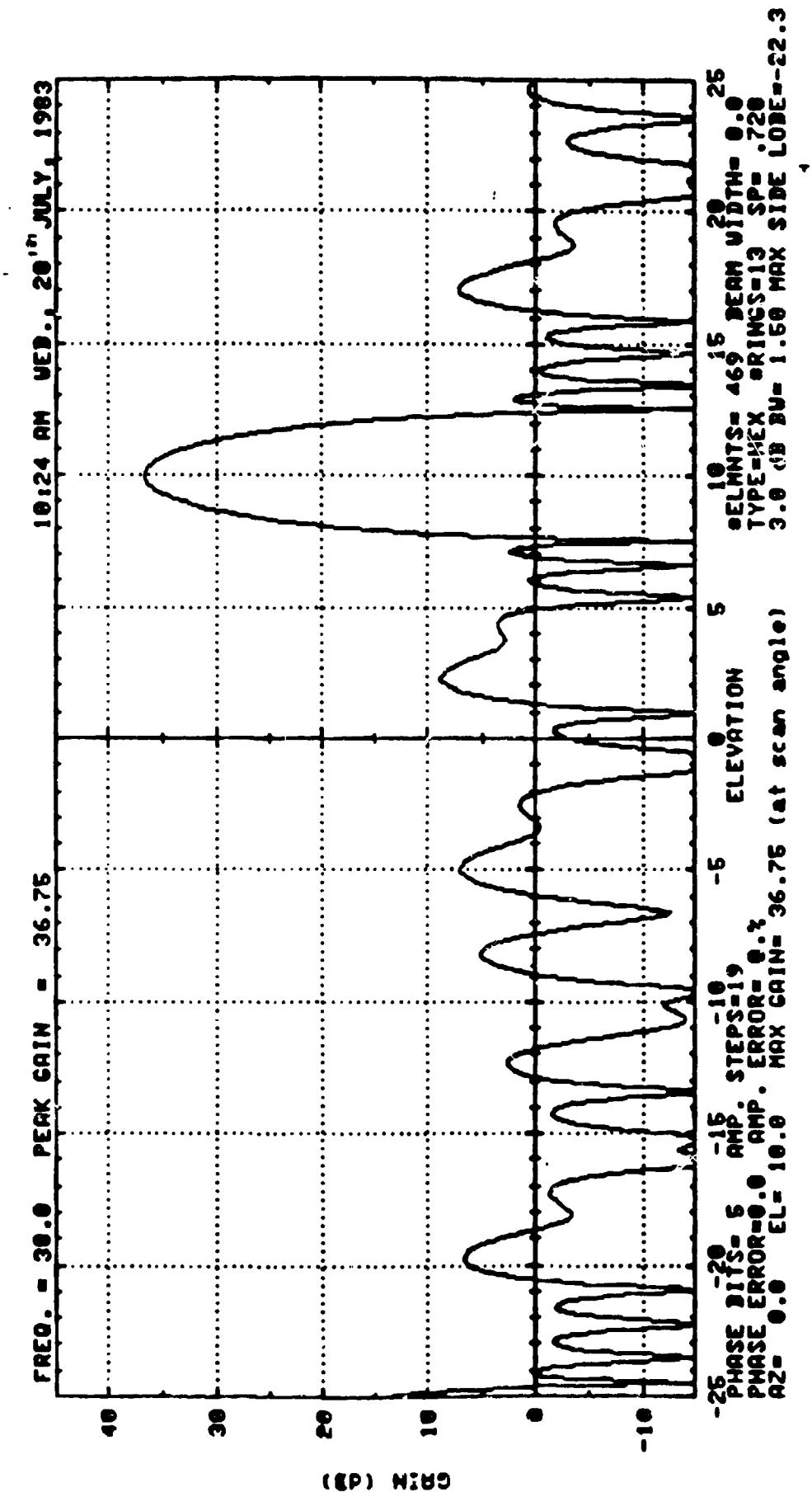

FIG. 4.2-49 3 FAILURES

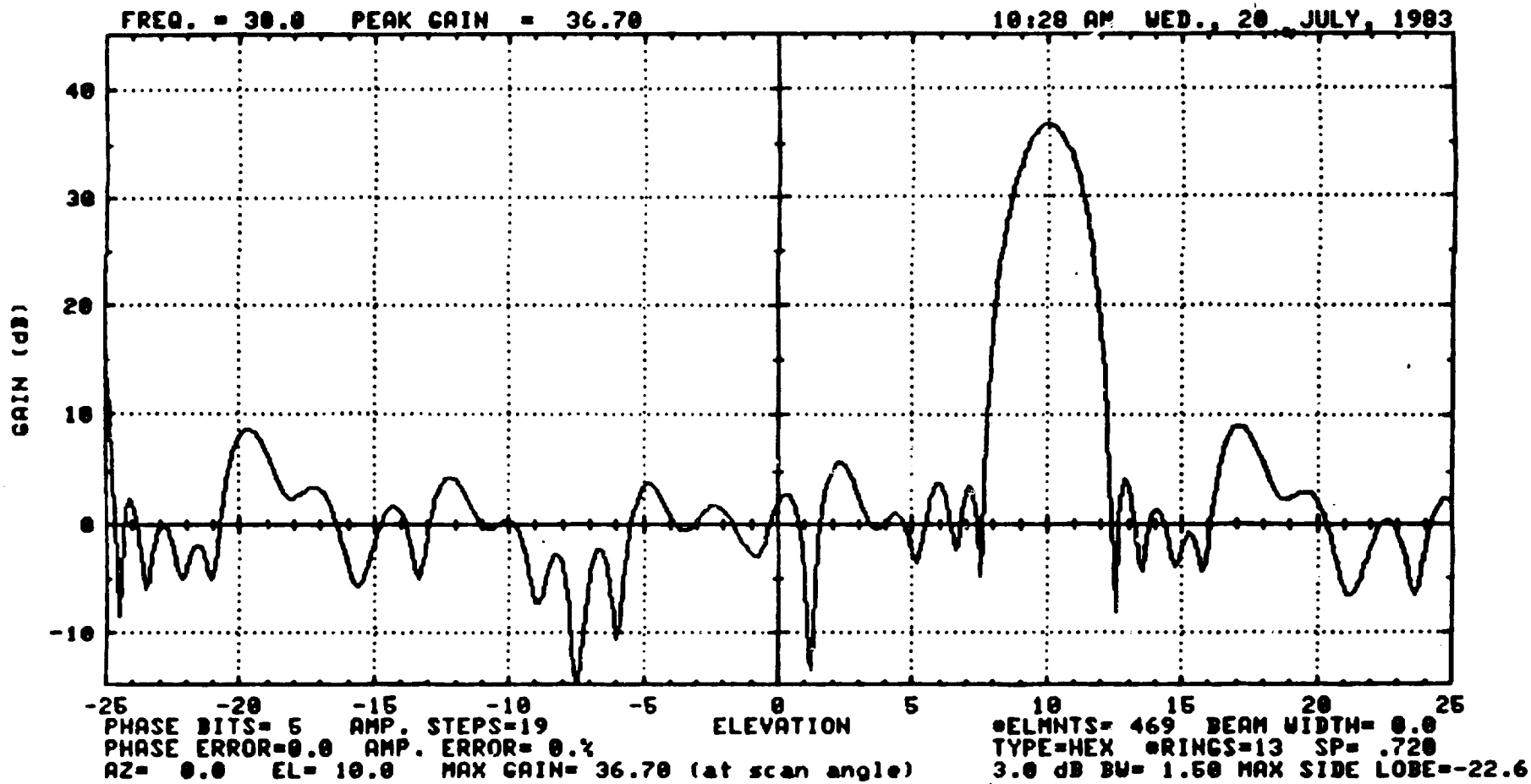

FIG. 4.2-50 5 FAILURES

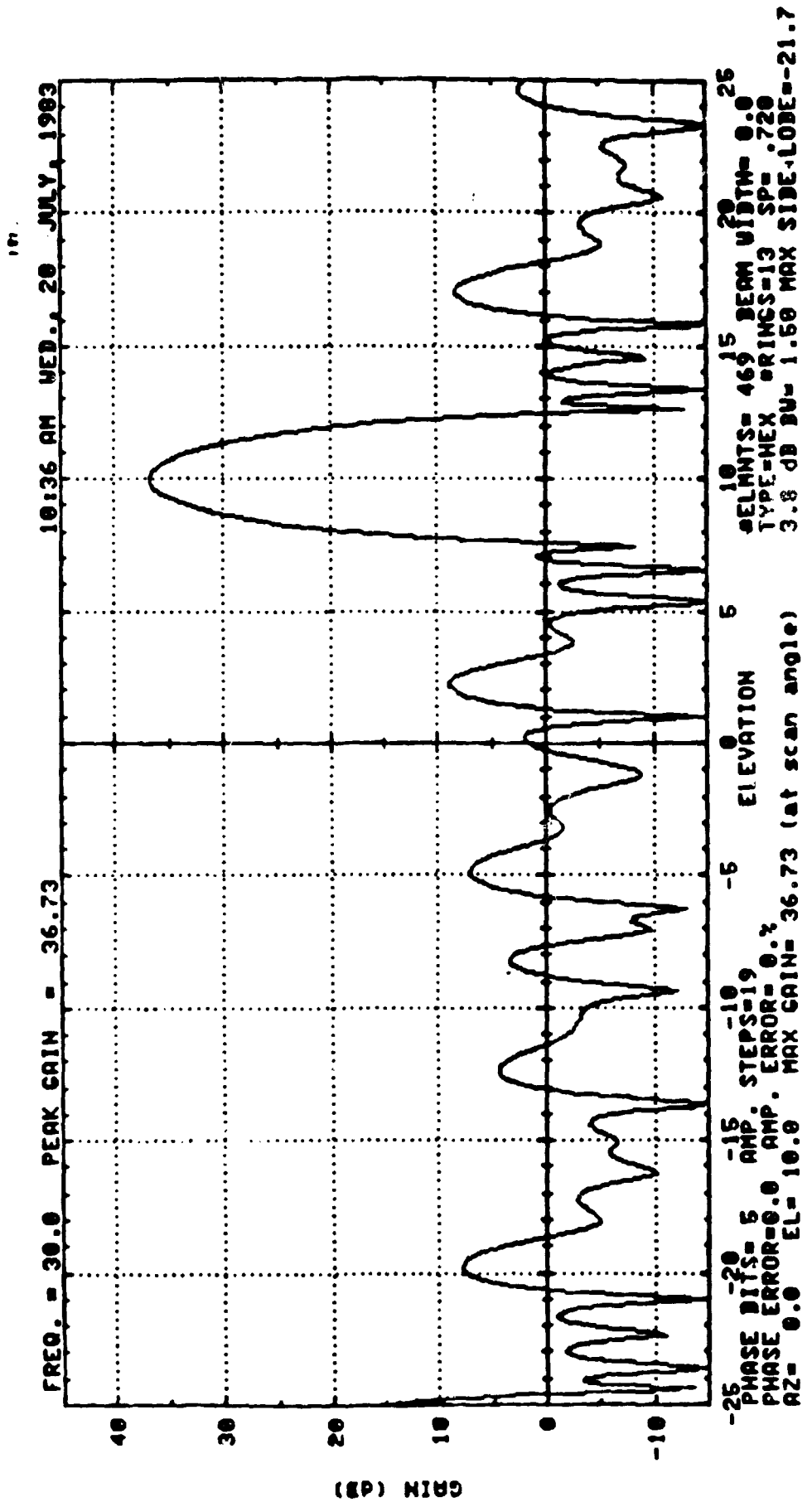

FIG. 4.2-51 8 FAILURES

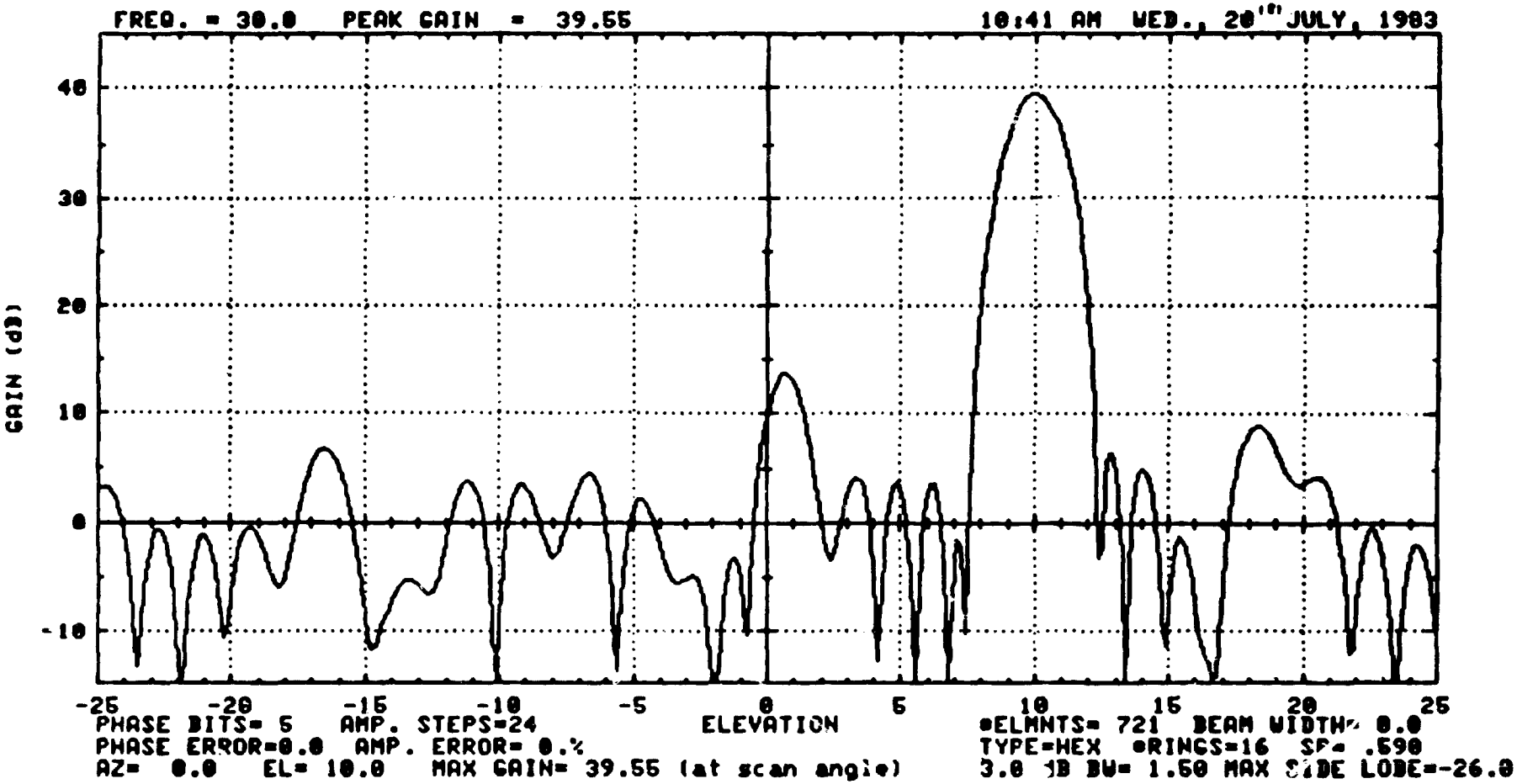

FIG. 4.2-52 3 FAILURES

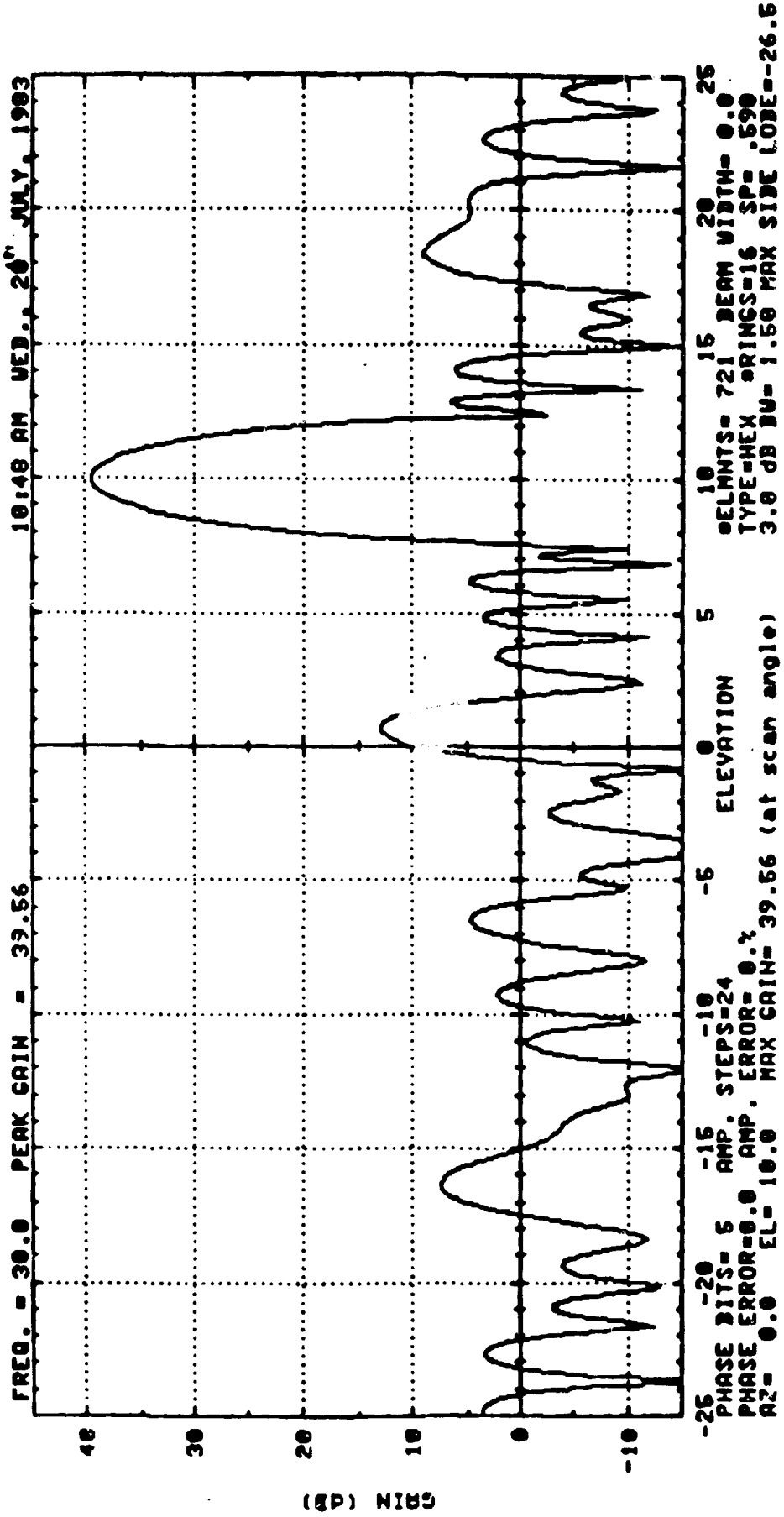

FIG 4.2-53 5 FAILURES

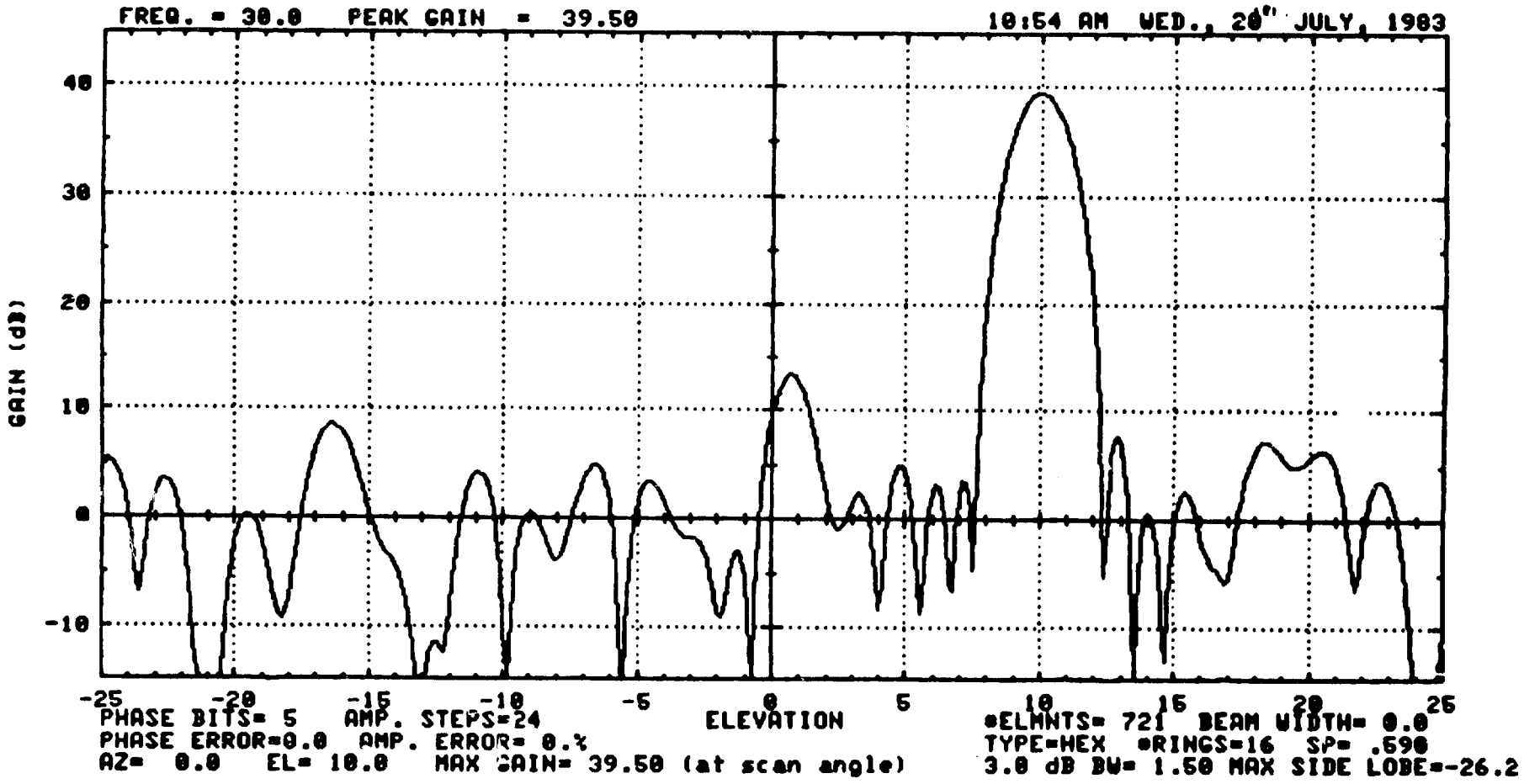

FIG. 4.2-54 8 FAILURES

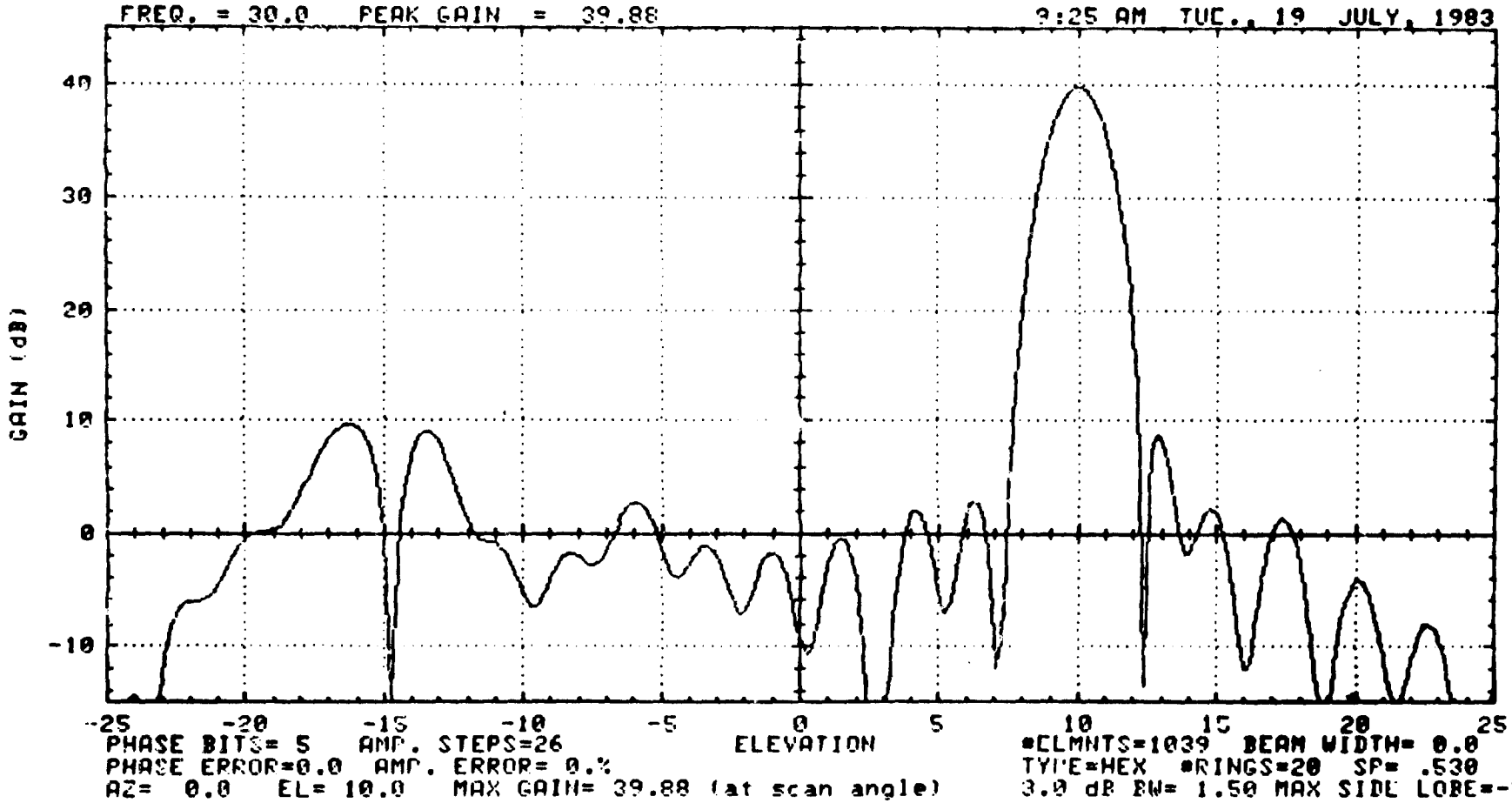

FIG. 4-2-55 3 FAILURES

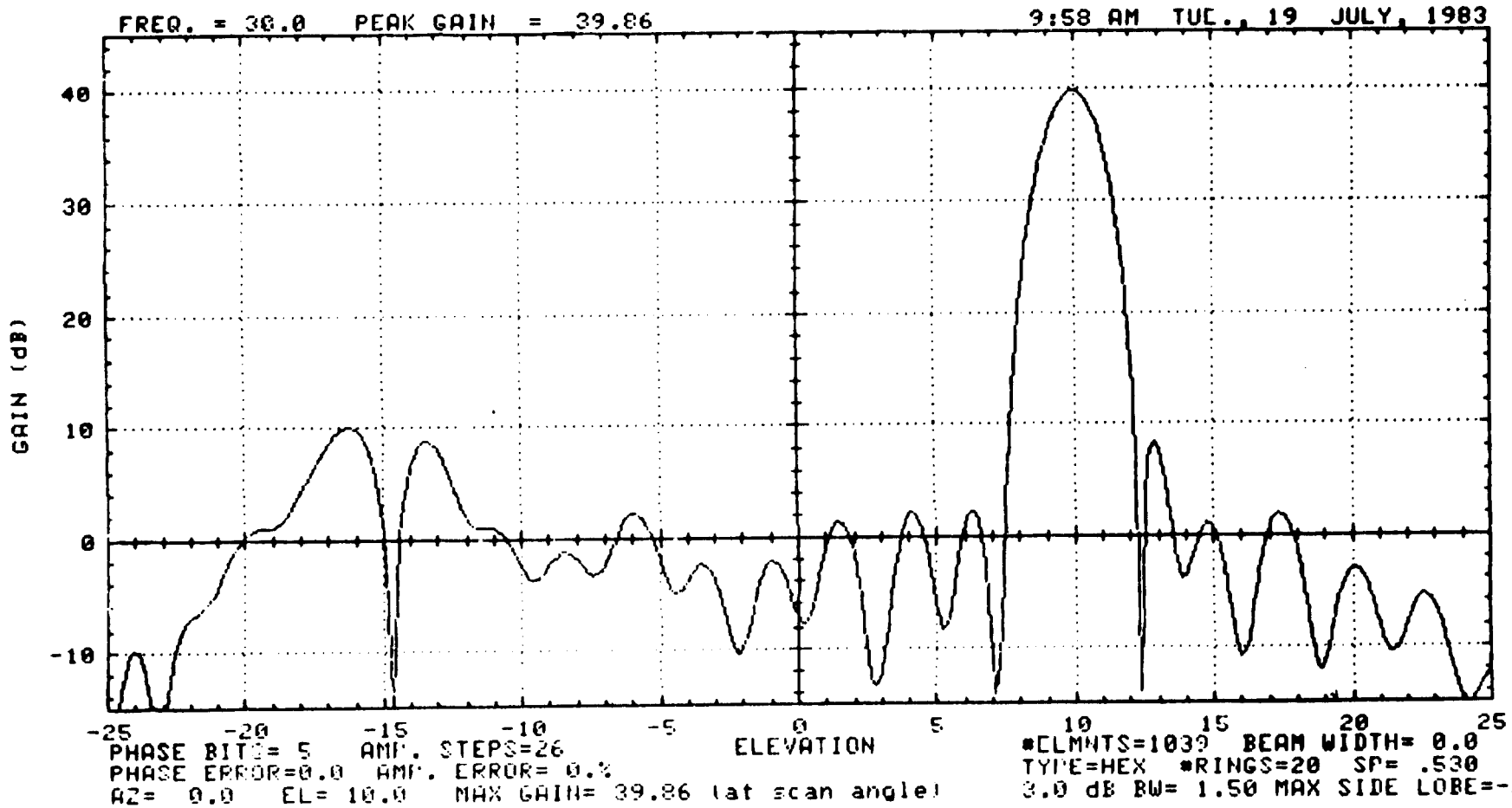

FIG 4.2-56 5 FAILURES

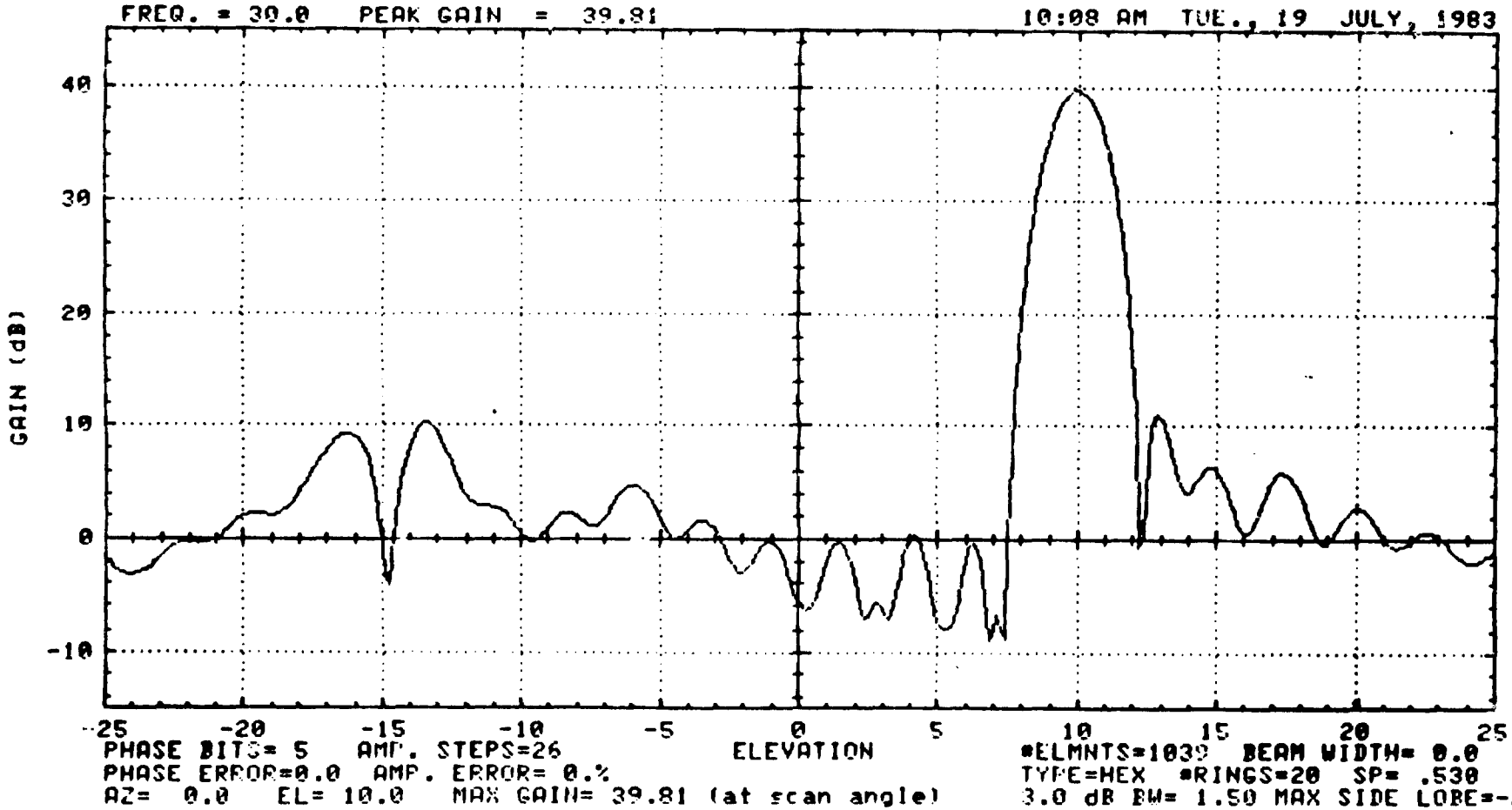

FIG. 4.2-57 8 FAILURES

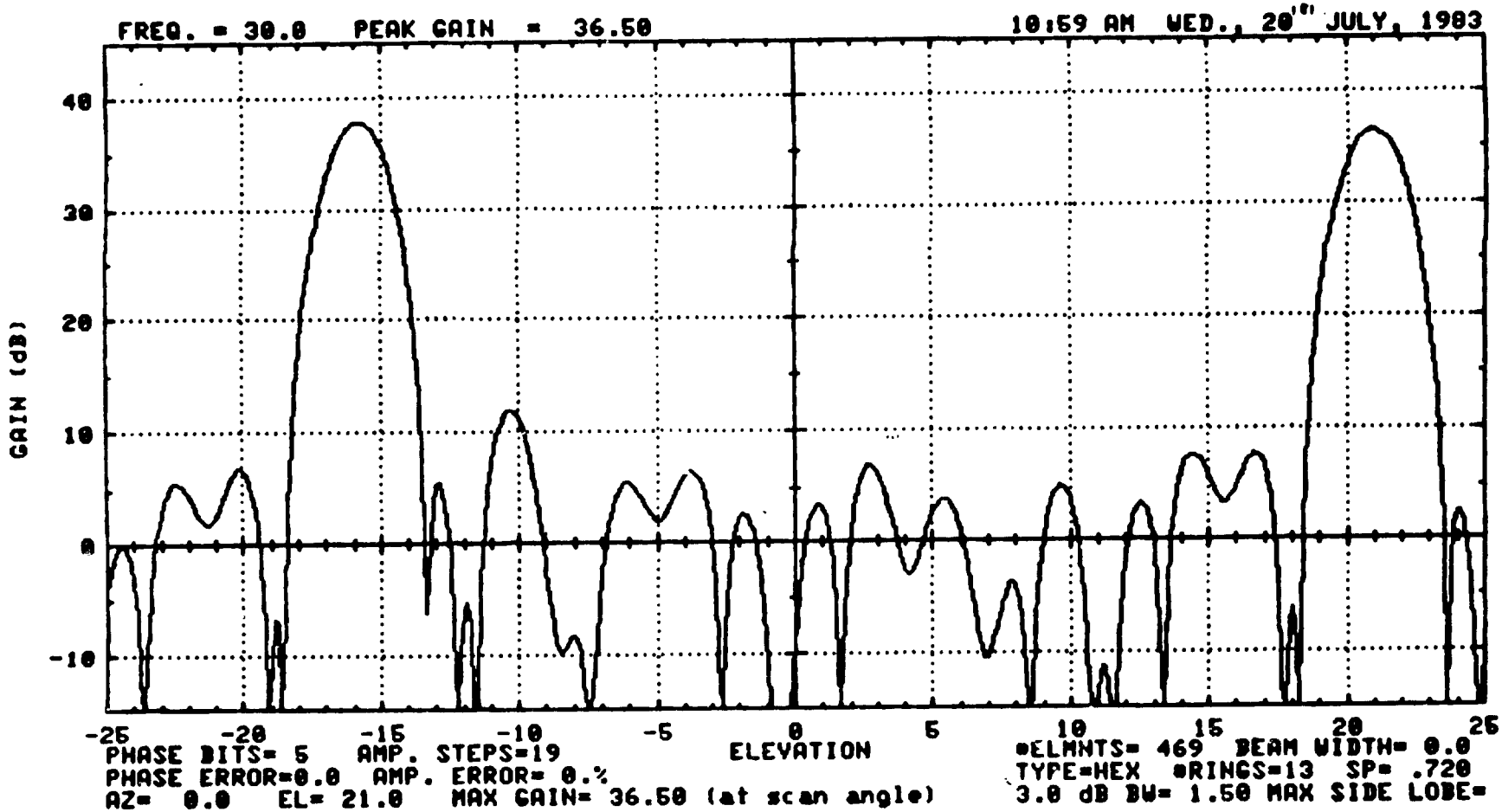

FIG. 42-58 3 FAILURES

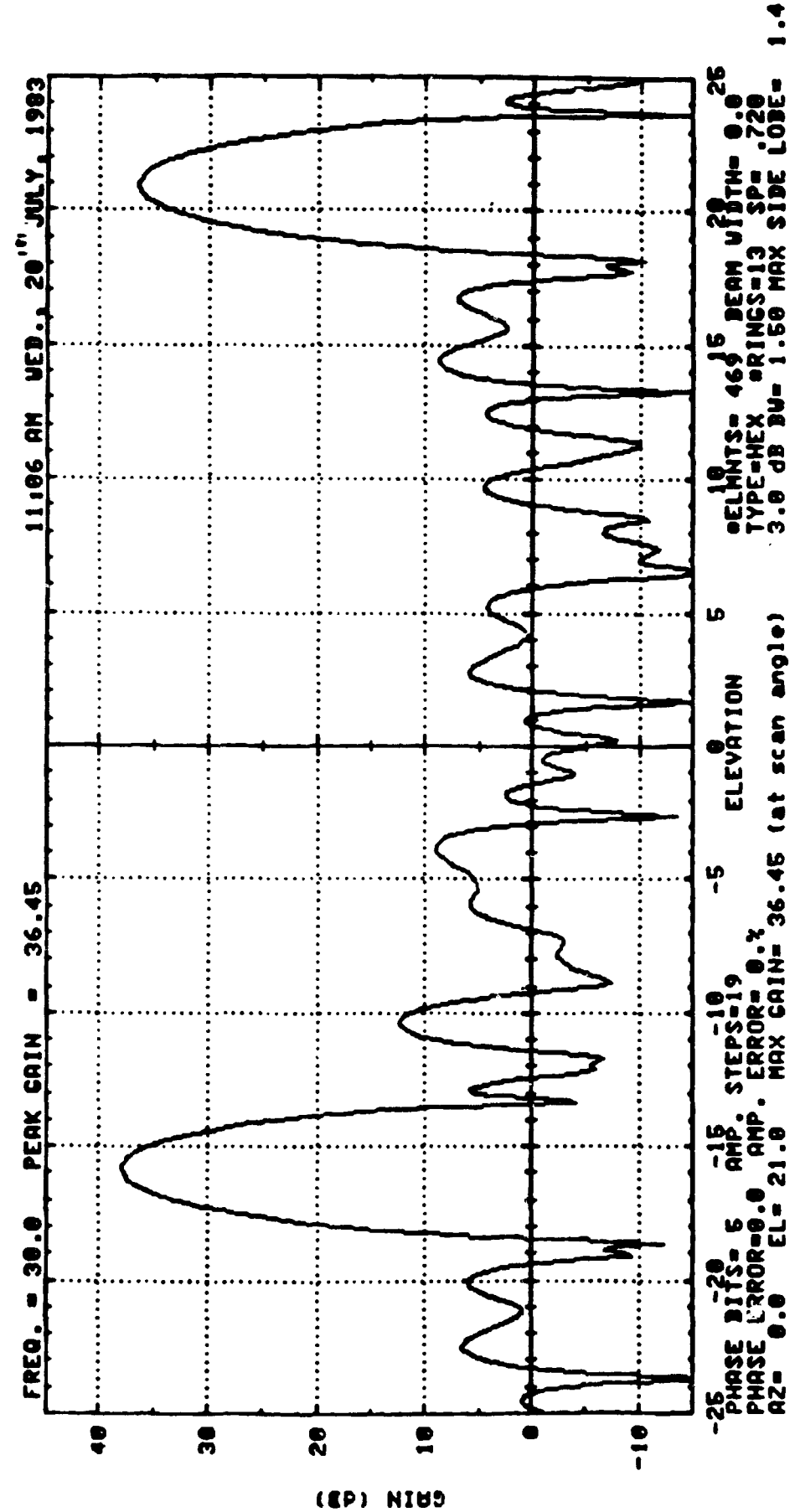

FIG. 4.2-59 5 FAILURES

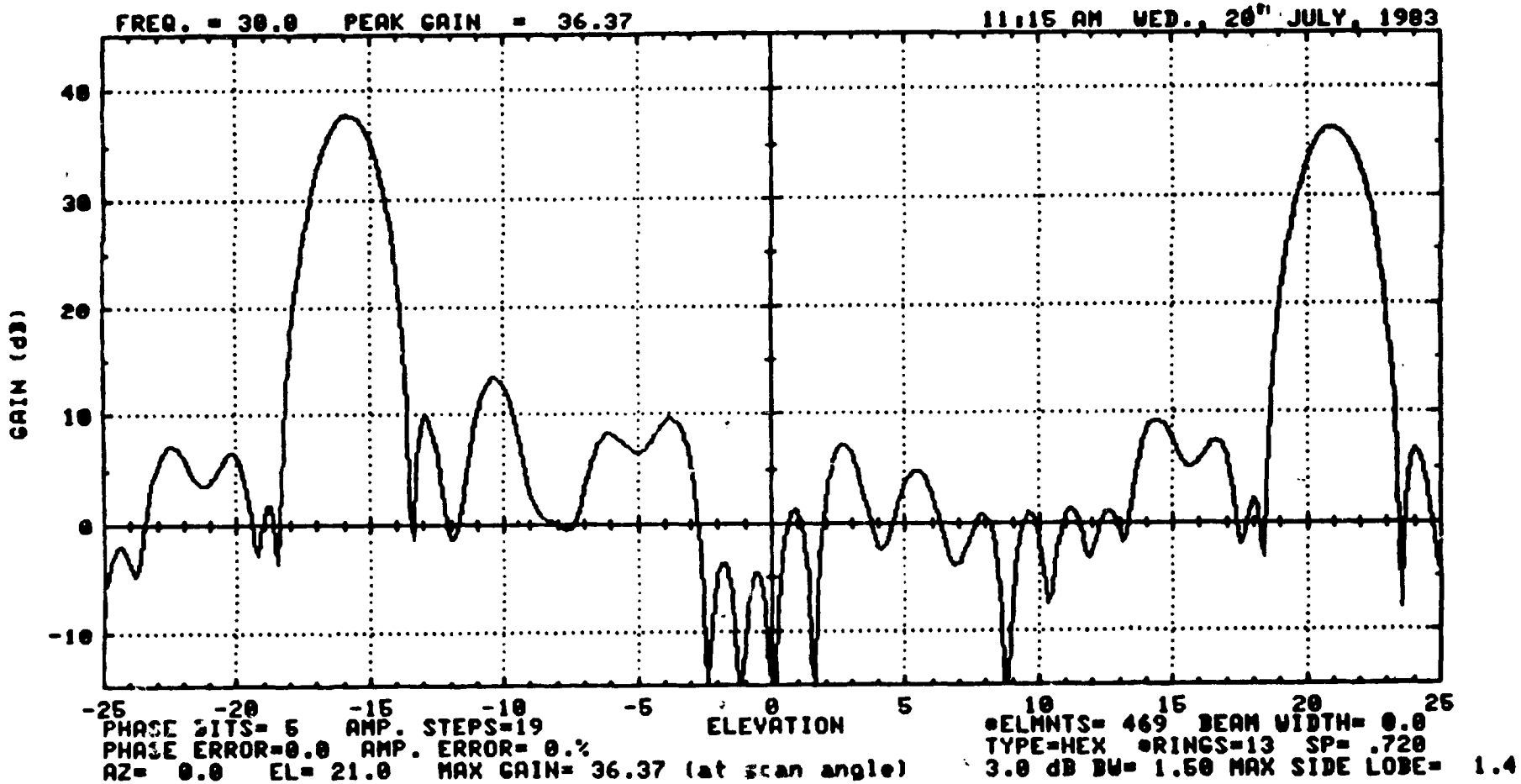

FIG. 4-2-61 8 FAILURES

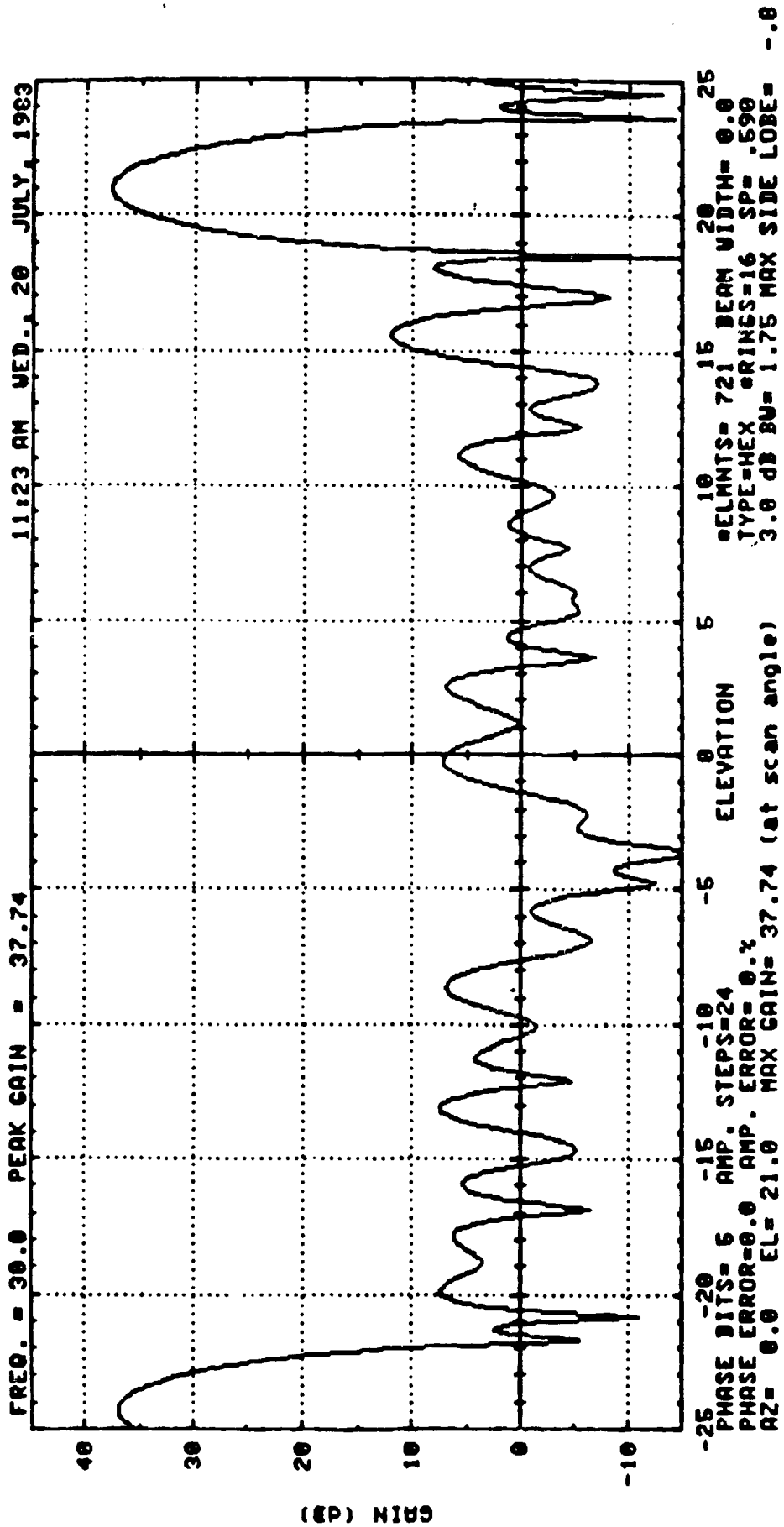

FIG 4.2-62 3 FAILURES

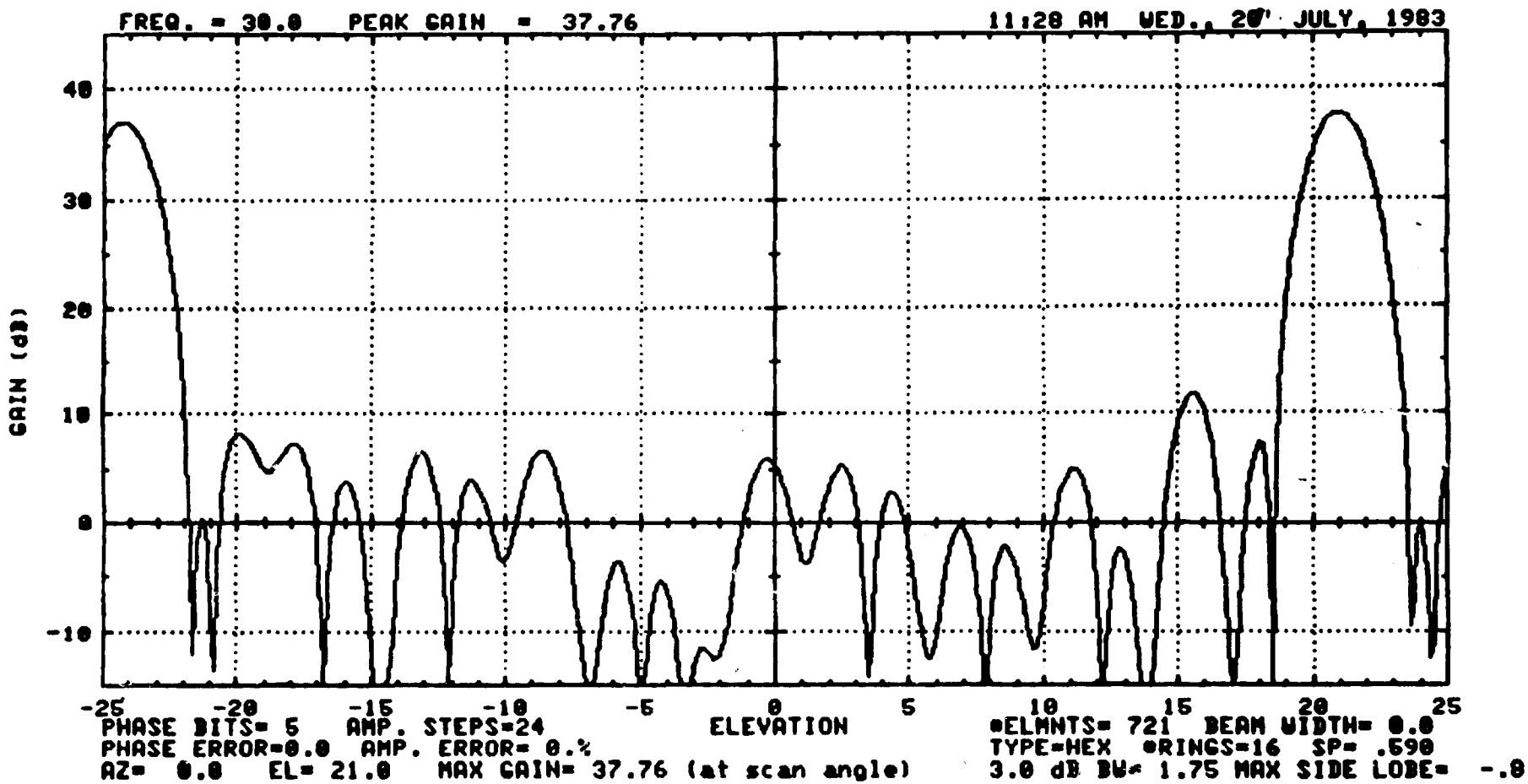

FIG. 4.2-63 5 FAILURES

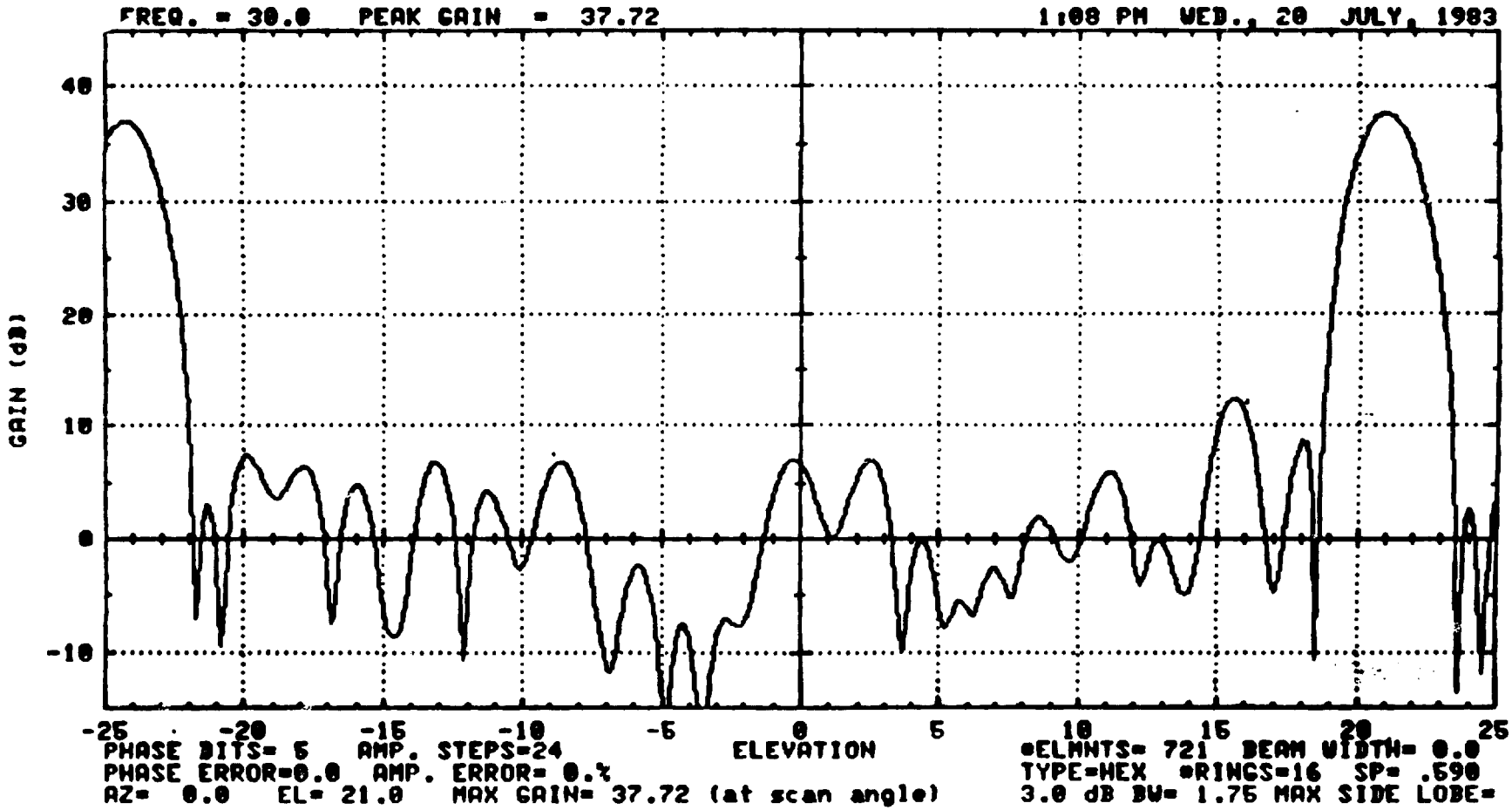

FIG. 4.2-64 8 FAILURES

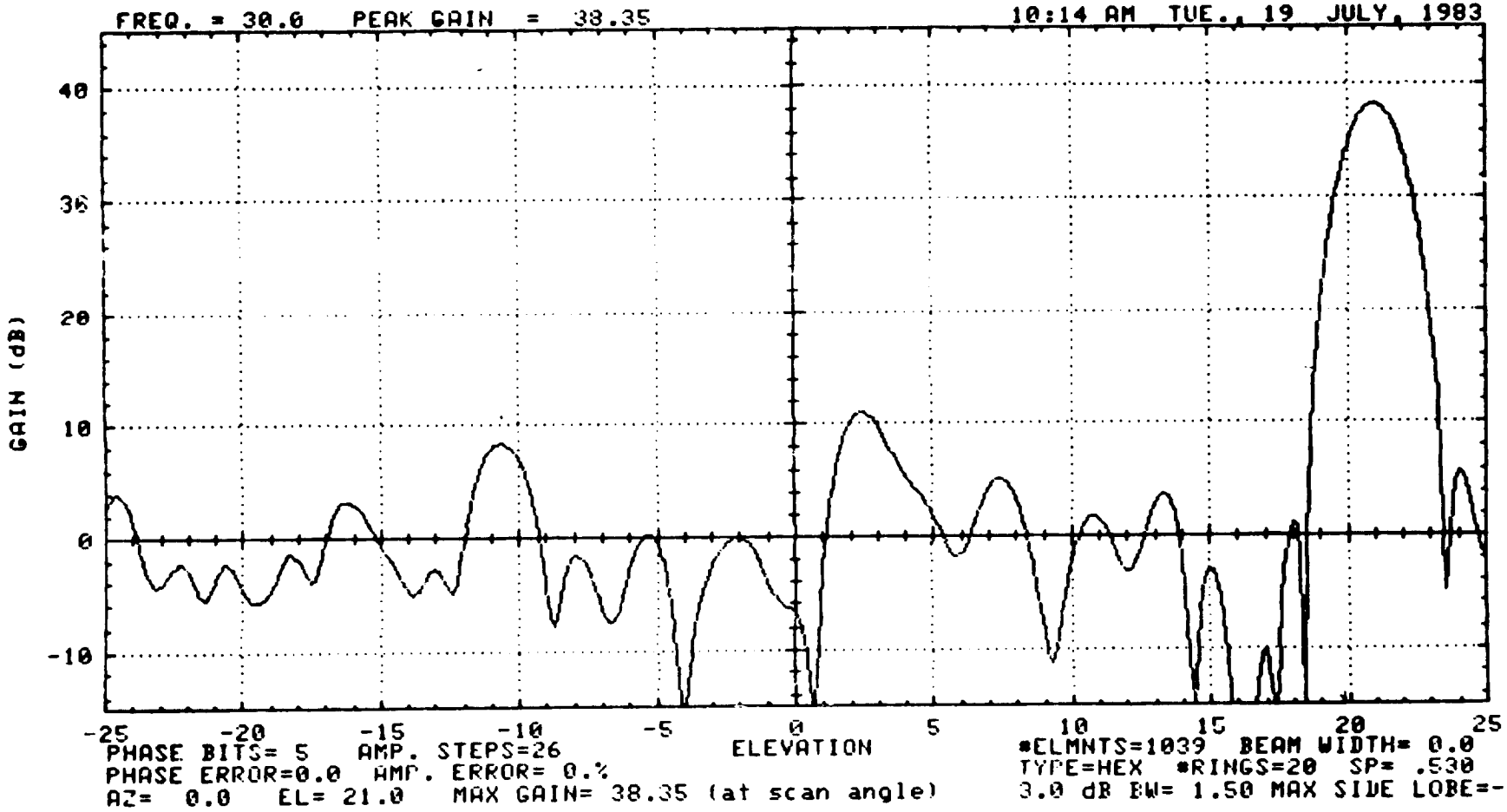

FIG. 4.2-65 3 FAILURES

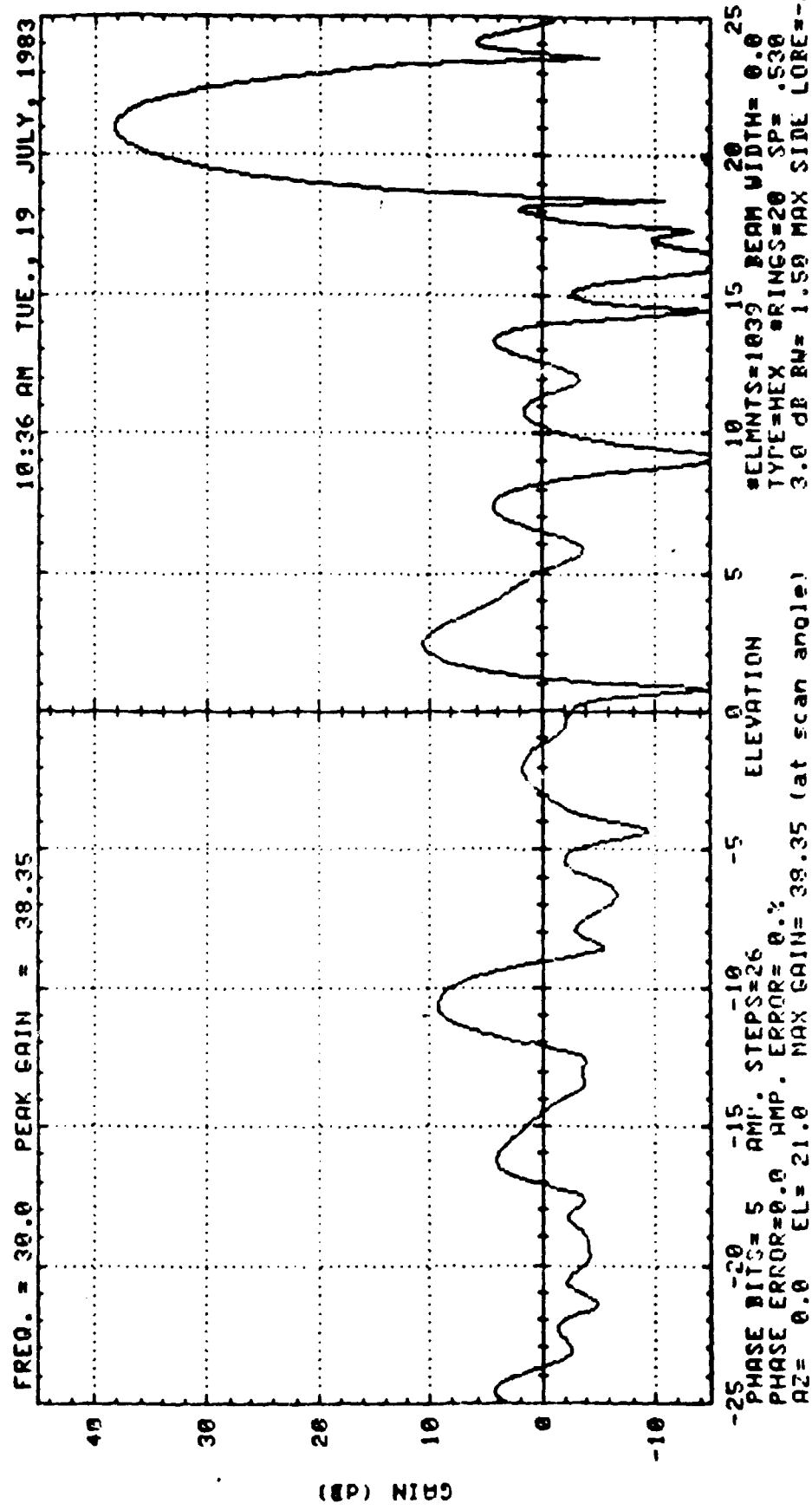

FIG 4.2-66 5 FAILURES

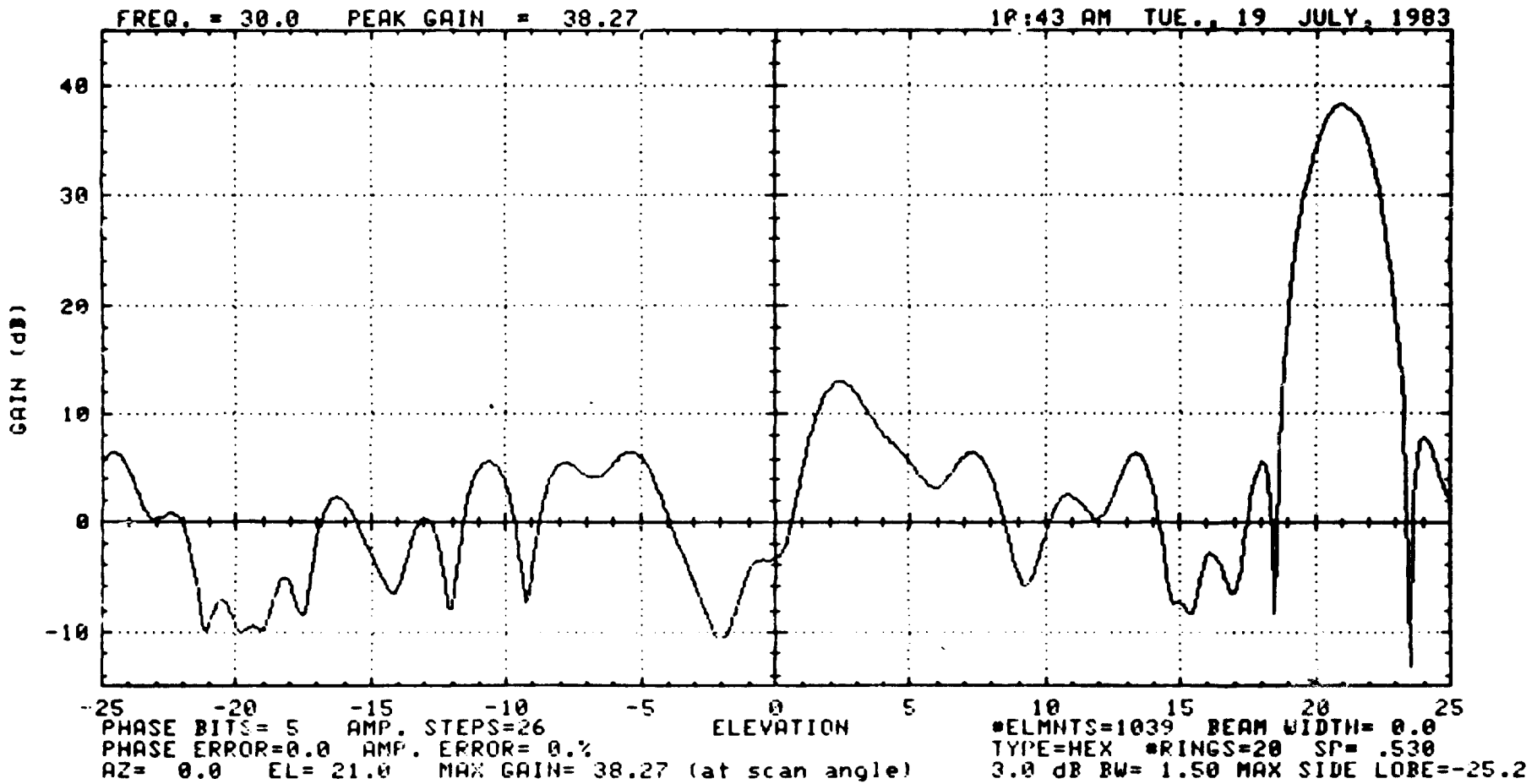

FIG. 4.2-67 8 FAILURES

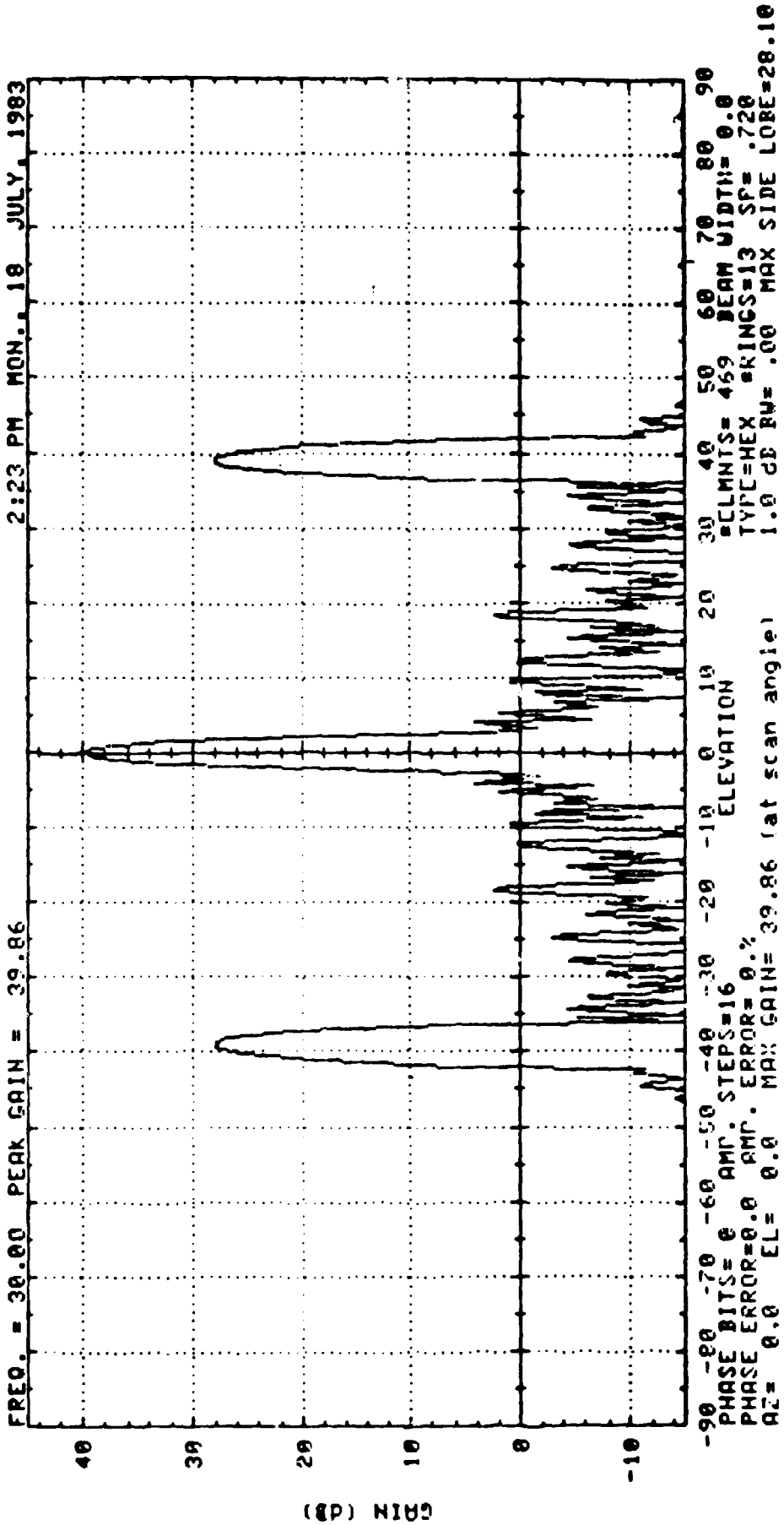
FREQ. = 30.00 PEAK GAIN = 39.86
2:23 PM MON., 18 JULY, 1983
GAIN (dB)
40
30
20
10
0
-10
-90 -80 -70 -60 -50 -40 -30 -20 -10 0 10 20 30 40 50 60 70 80 90
ELEVATION
PHASE BITS= 6 AMP. STEPS=16 #ELMNTS= 469 BEAM WIDTH= 0.0
PHASE ERROR=0.0 AMP. ERROR= 0.% TYPE=HEX #RINGS=13 SP= .720
AZ= 0.0 EL= 0.0 MAX GAIN= 39.86 (at scan angle) 1.0 dB BW= .00 MAX SIDE LOBE=28.10

FIG 4.2-70

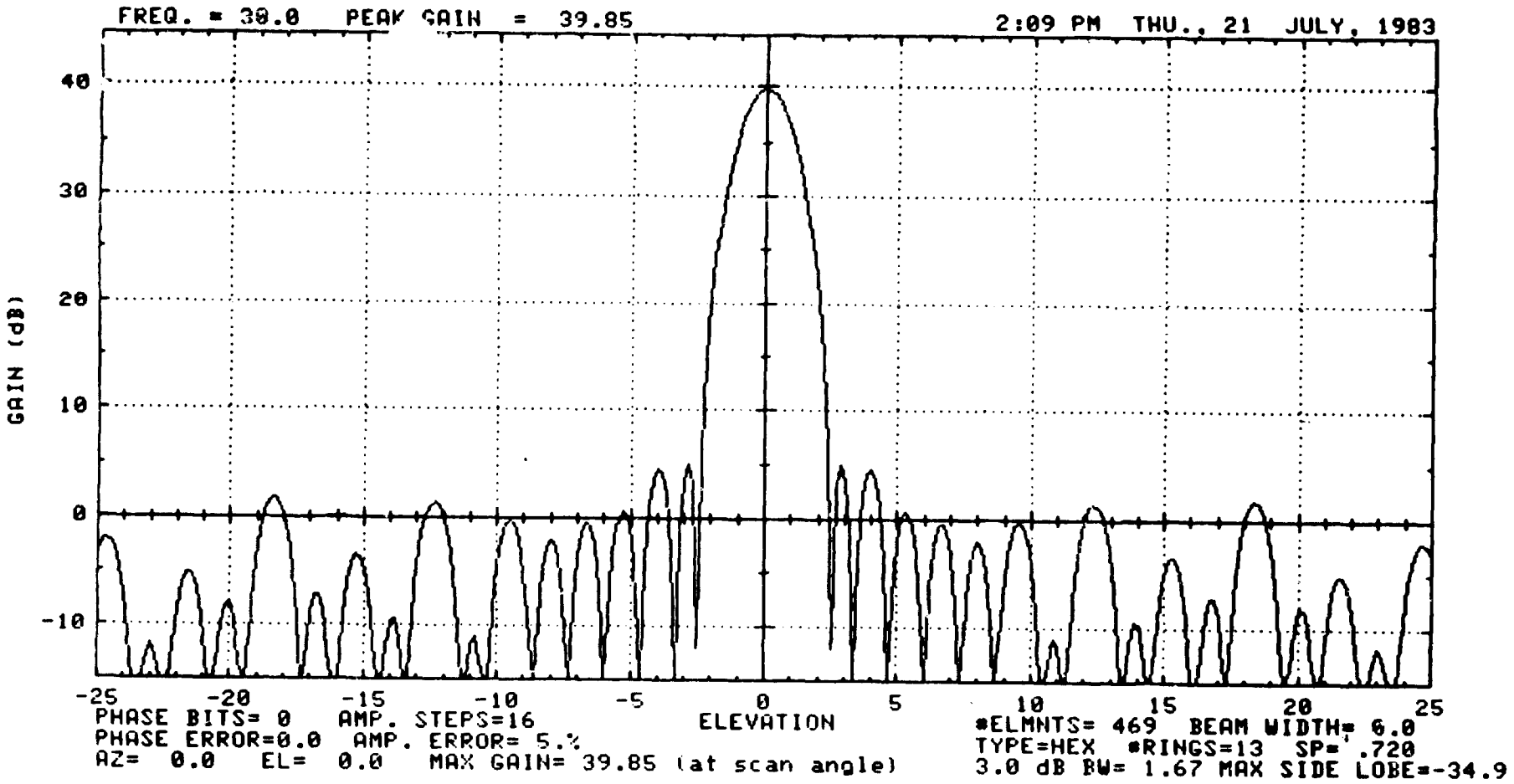
FREQ. = 30.0 PEAK GAIN = 39.85
2:09 PM THU., 21 JULY, 1983
GAIN (dB)
40
30
20
10
0
-10
-25 -20 -15 -10 -5 0 5 10 15 20 25
ELEVATION
PHASE BITS= 0 AMP. STEPS=16
PHASE ERROR=0.0 AMP. ERROR= 5.%
AZ= 0.0 EL= 0.0 MAX GAIN= 39.85 (at scan angle)
#ELMNTS= 469 BEAM WIDTH= 6.0
TYPE=HEX #RINGS=13 SP= .720
3.0 dB BW= 1.67 MAX SIDE LOBE=-34.9

FIG 4.2-71

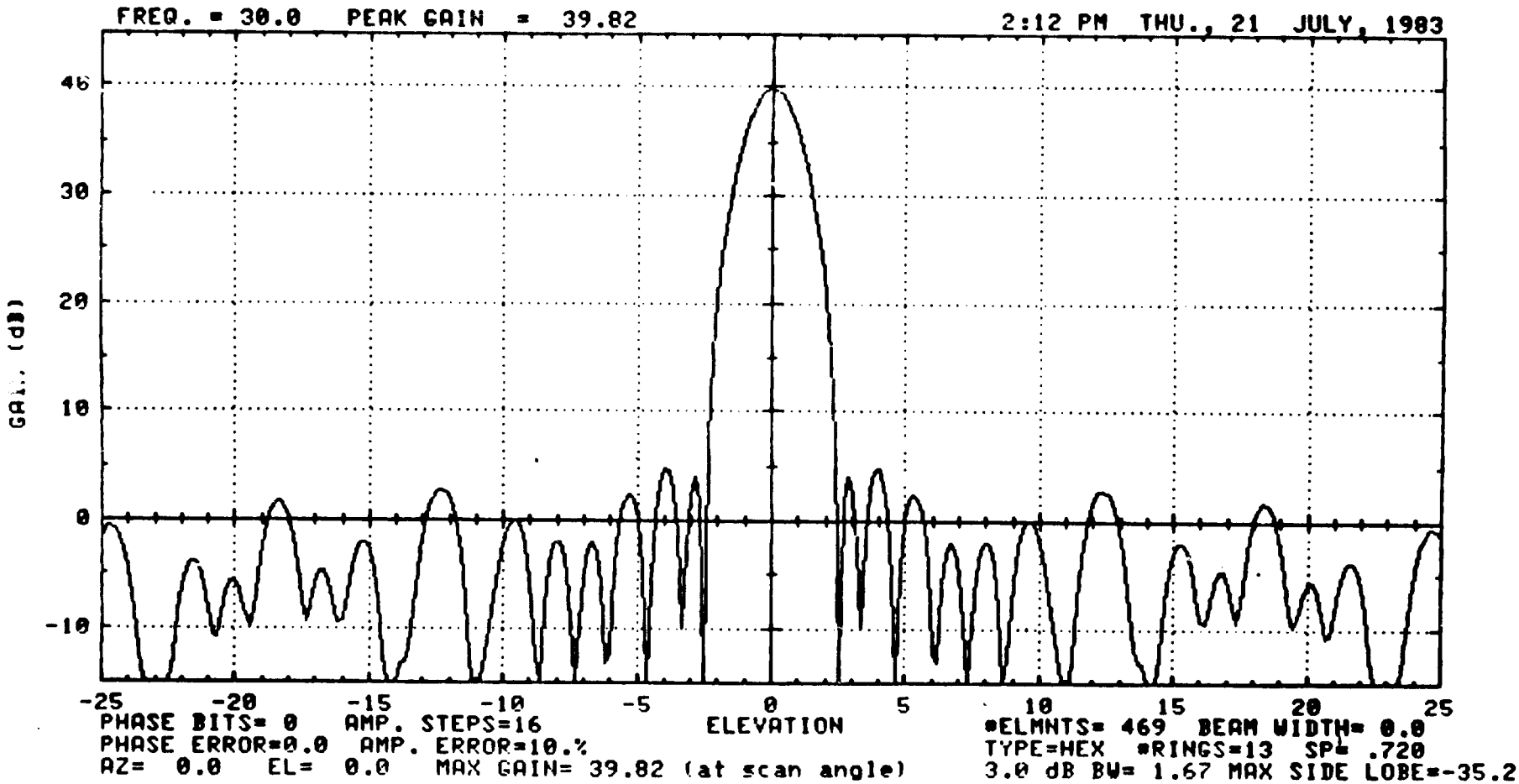
FREQ. = 30.0 PEAK GAIN = 39.82
2:12 PM THU., 21 JULY, 1983
GAIN (dB)
40
30
20
10
0
-10
-25 -20 -15 -10 -5 0 5 10 15 20 25
ELEVATION
PHASE BITS= 0 AMP. STEPS=16
PHASE ERROR=0.0 AMP. ERROR=10.%
AZ= 0.0 EL= 0.0 MAX GAIN= 39.82 (at scan angle)
#ELMNTS= 469 BEAM WIDTH= 0.0
TYPE=HEX #RINGS=13 SP= .720
3.0 dB BW= 1.67 MAX SIDE LOBE=-35.2

FIG 4 2-72

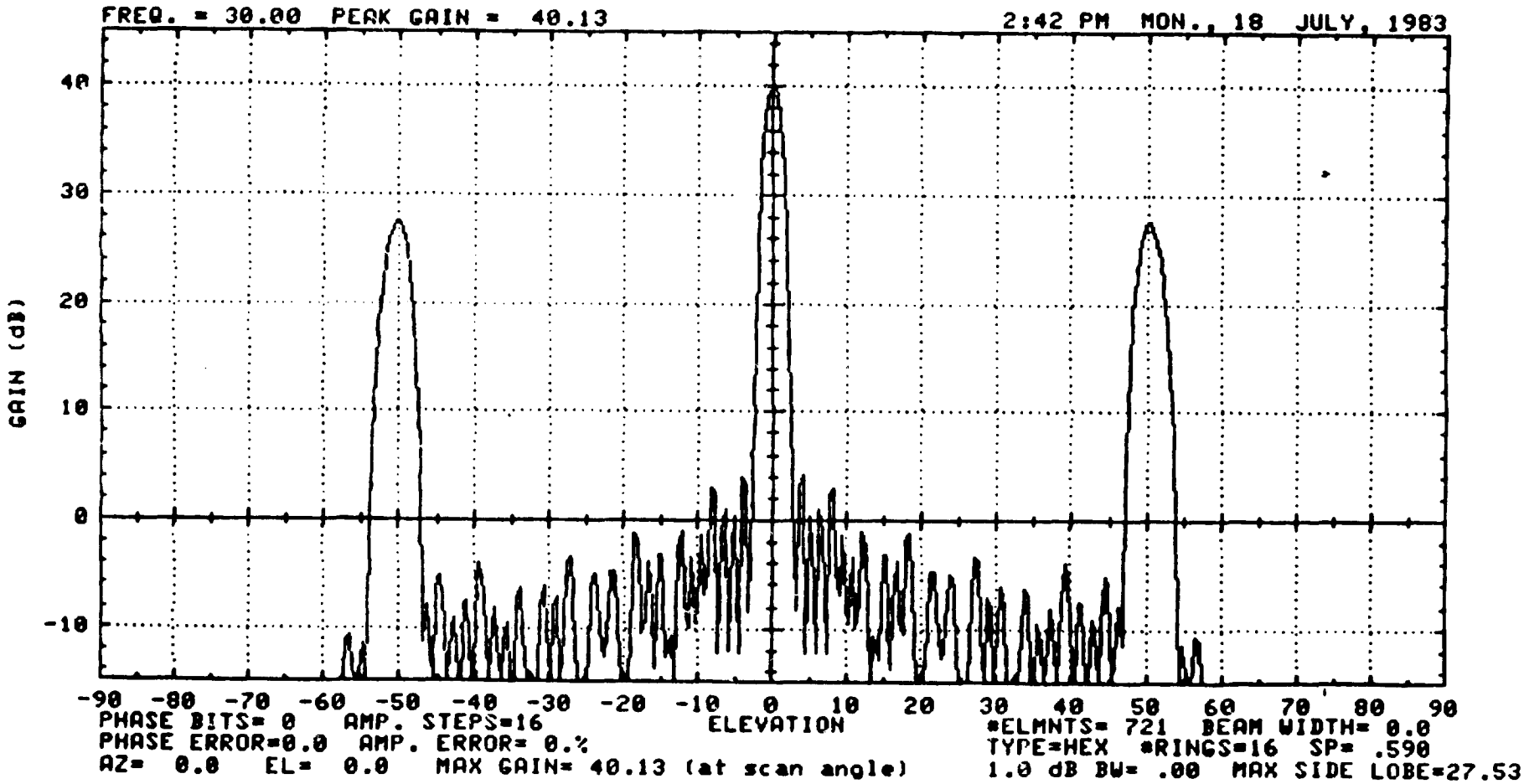
FREQ. = 30.00 PEAK GAIN = 40.13
2:42 PM MON., 18 JULY, 1983
GAIN (dB)
40
30
20
10
0
-10
-90 -80 -70 -60 -50 -40 -30 -20 -10 0 10 20 30 40 50 60 70 80 90
ELEVATION
PHASE BITS= 0 AMP. STEPS=16
PHASE ERROR=0.0 AMP. ERROR= 0.%
AZ= 0.0 EL= 0.0 MAX GAIN= 40.13 (at scan angle)
#ELMNTS= 721 BEAM WIDTH= 0.0
TYPE=HEX #RINGS=16 SP= .590
1.0 dB BW= .00 MAX SIDE LOBE=27.53

FIG. 4.2-73

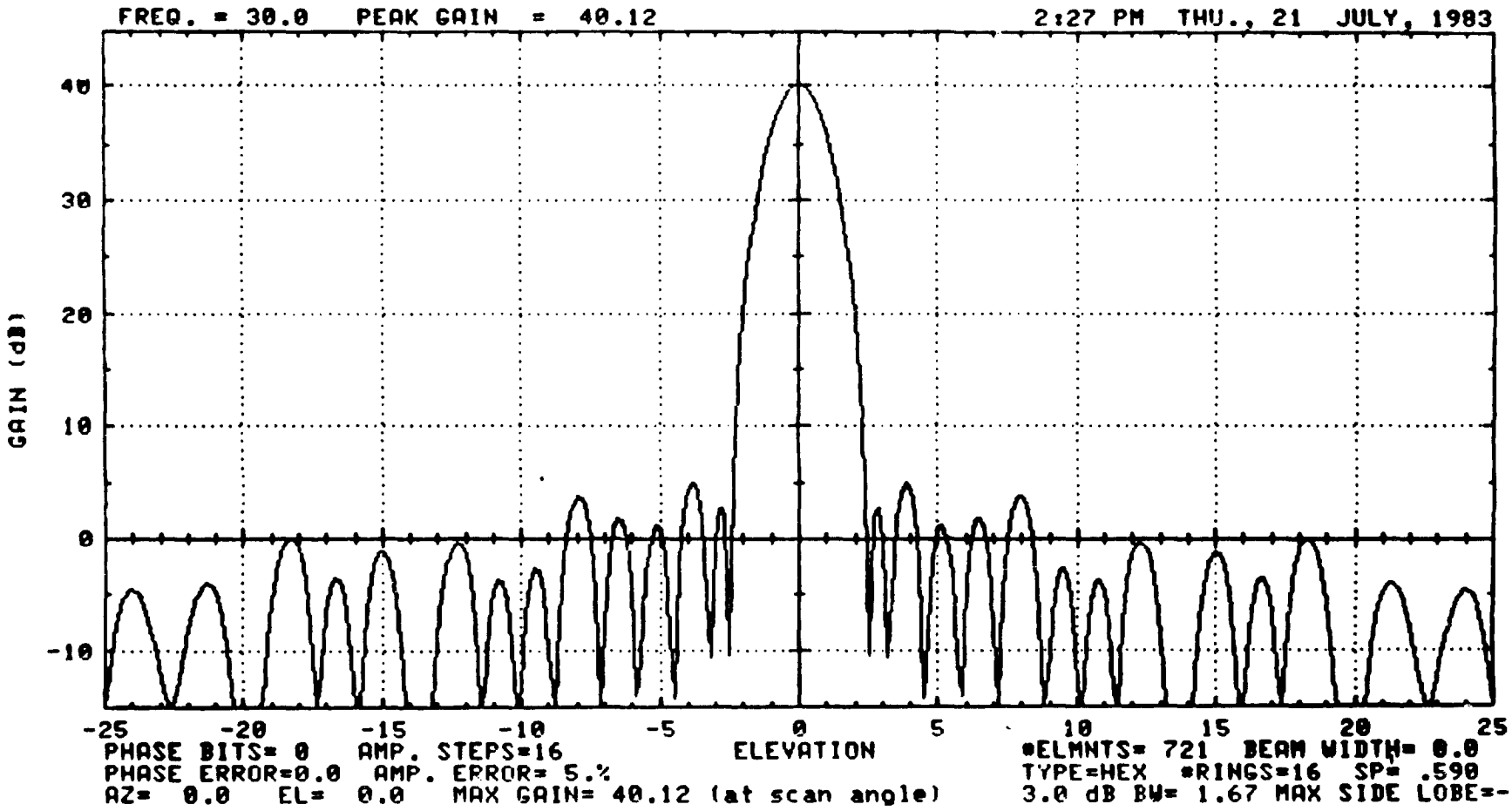
FREQ. = 30.0 PEAK GAIN = 40.12
2:27 PM THU., 21 JULY, 1983
GAIN (dB)
40
30
20
10
0
-10
-25 -20 -15 -10 -5 0 5 10 15 20 25
ELEVATION
PHASE BITS= 0 AMP. STEPS=16
PHASE ERROR=0.0 AMP. ERROR= 5.%
AZ= 0.0 EL= 0.0 MAX GAIN= 40.12 (at scan angle)
#ELMNTS= 721 BEAM WIDTH= 0.0
TYPE=HEX #RINGS=16 SP= .590
3.0 dB BW= 1.67 MAX SIDE LOBE=-35.1

FIG 42-74

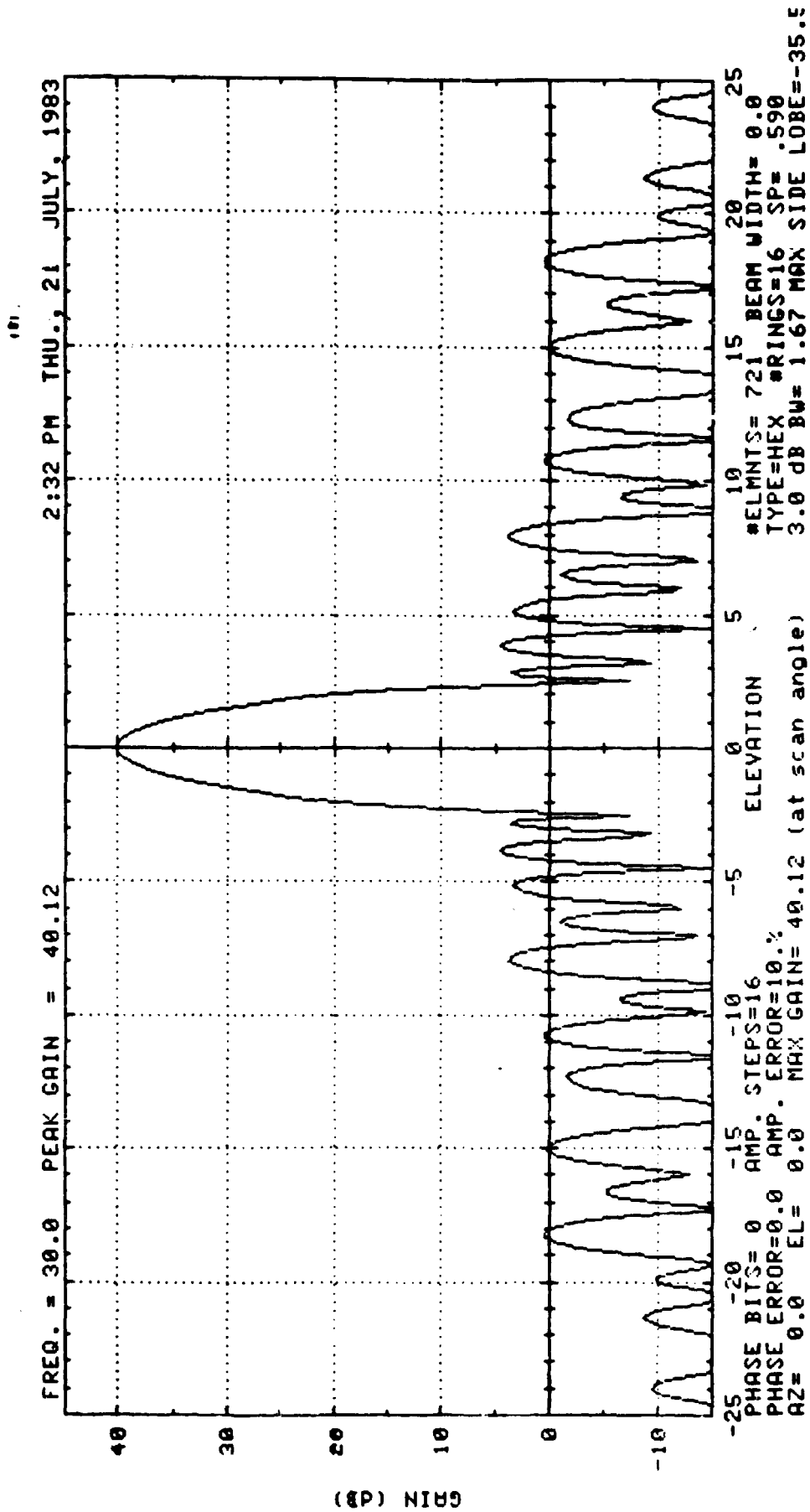
FREQ. = 30.0 PEAK GAIN = 40.12
2:32 PM THU., 21 JULY, 1983
GAIN (dB)
40
30
20
10
0
-10
-25 -20 -15 -10 -5 0 5 10 15 20 25
ELEVATION
PHASE BITS= 0 AMP. STEPS=16
PHASE ERROR=0.0 AMP. ERROR=10.%
AZ= 0.0 EL= 0.0 MAX GAIN= 40.12 (at scan angle)
#ELMNTS= 721 BEAM WIDTH= 0.0
TYPE=HEX #RINGS=16 SP= .590
3.0 dB BW= 1.67 MAX SIDE LOBE=-35.5

FIG. 4.2-75

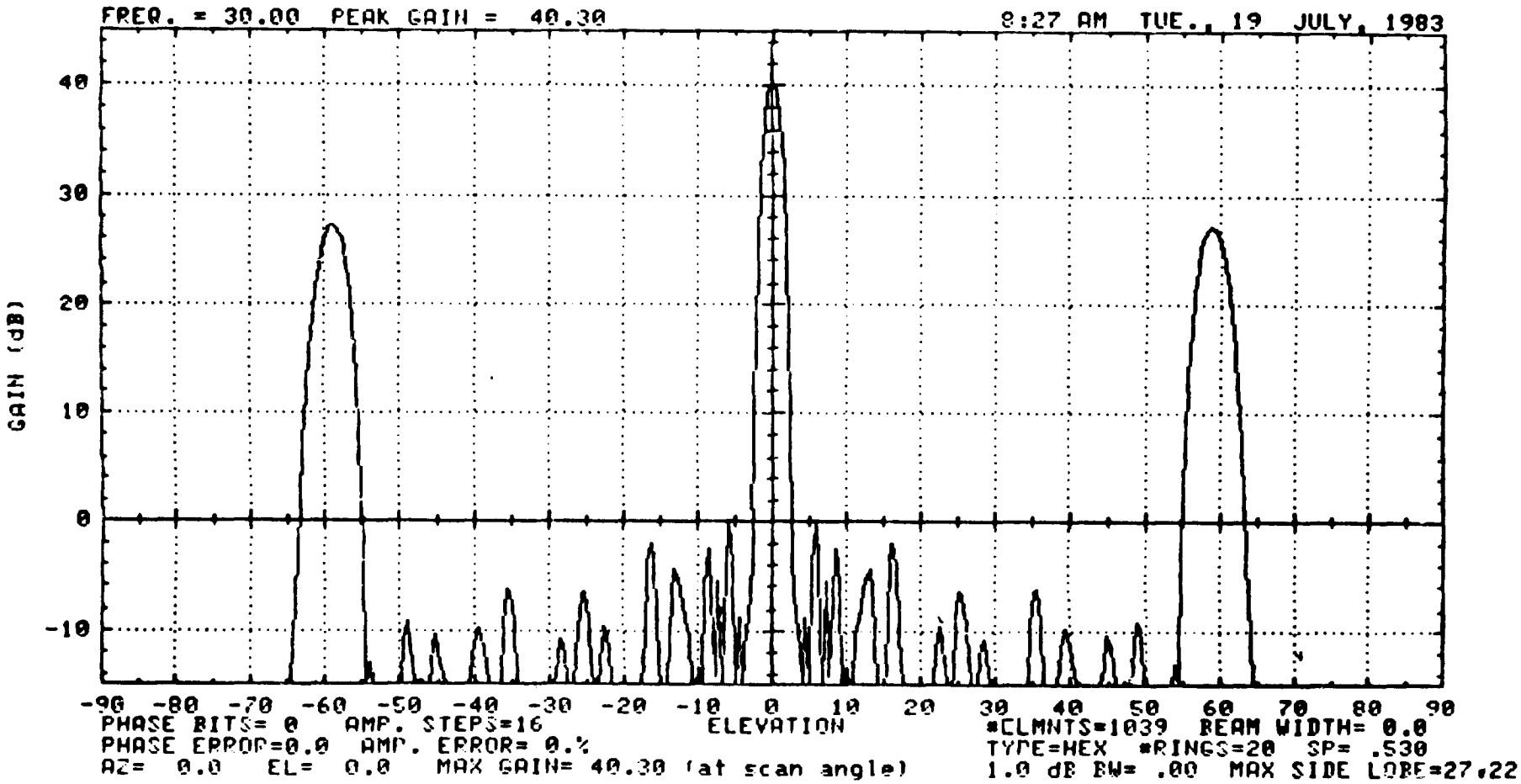
FREQ. = 30.00 PEAK GAIN = 40.30
8:27 AM TUE., 19 JULY, 1983
GAIN (dB)
40
30
20
10
0
-10
-90 -80 -70 -60 -50 -40 -30 -20 -10 0 10 20 30 40 50 60 70 80 90
ELEVATION
PHASE BITS= 0 AMP. STEPS=16
PHASE ERROR=0.0 AMP. ERROR= 0.%
AZ= 0.0 EL= 0.0 MAX GAIN= 40.30 (at scan angle)
#ELMNTS=1039 BEAM WIDTH= 0.0
TYPE=HEX #RINGS=20 SP= .530
1.0 dB BW= .00 MAX SIDE LOBE=27.22

FIG. 4.2-76

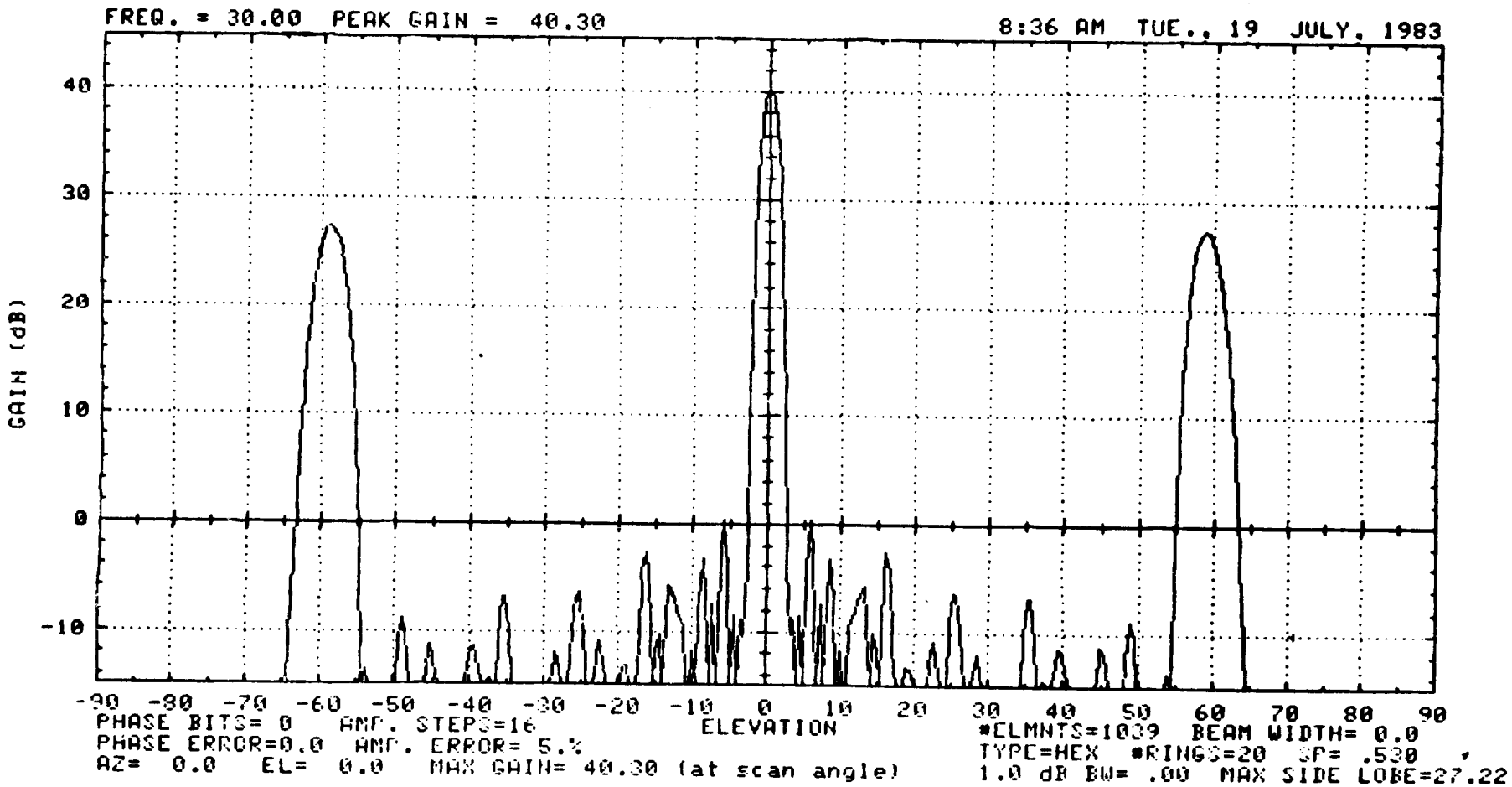
FREQ. = 30.00 PEAK GAIN = 40.30
8:36 AM TUE., 19 JULY, 1983
GAIN (dB)
40
30
20
10
0
-10
-90 -80 -70 -60 -50 -40 -30 -20 -10 0 10 20 30 40 50 60 70 80 90
ELEVATION
PHASE BITS= 0 AMP. STEPS=16
PHASE ERROR=0.0 AMP. ERROR= 5.%
AZ= 0.0 EL= 0.0 MAX GAIN= 40.30 (at scan angle)
#ELMNTS=1039 BEAM WIDTH= 0.0
TYPE=HEX #RINGS=20 SP= .530
1.0 dB BW= .00 MAX SIDE LOBE=27.22

FIG.4.2-77

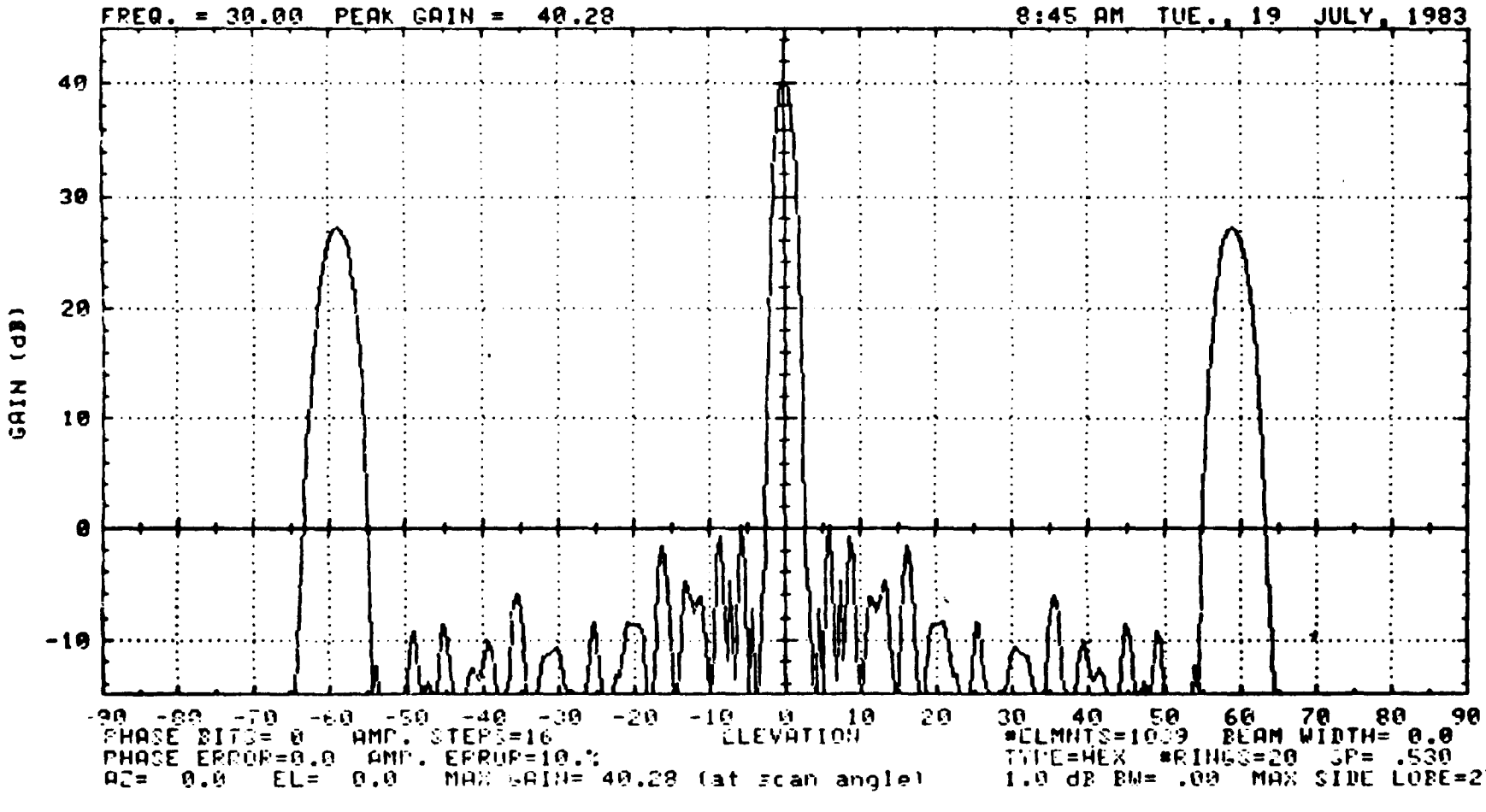
FREQ. = 30.00 PEAK GAIN = 40.28
8:45 AM TUE., 19 JULY, 1983
GAIN (dB)
40
30
20
10
0
-10
-90 -80 -70 -60 -50 -40 -30 -20 -10 0 10 20 30 40 50 60 70 80 90
ELEVATION
PHASE BITS= 0 AMP. STEPS=16
PHASE ERROR=0.0 AMP. ERROR=10.%
AZ= 0.0 EL= 0.0 MAX GAIN= 40.28 (at scan angle)
#ELMNTS=1009 BEAM WIDTH= 0.0
TYPE=HEX #RINGS=20 SP= .530
1.0 dB BW= .00 MAX SIDE LOBE=27.20

FIG 4.2-78

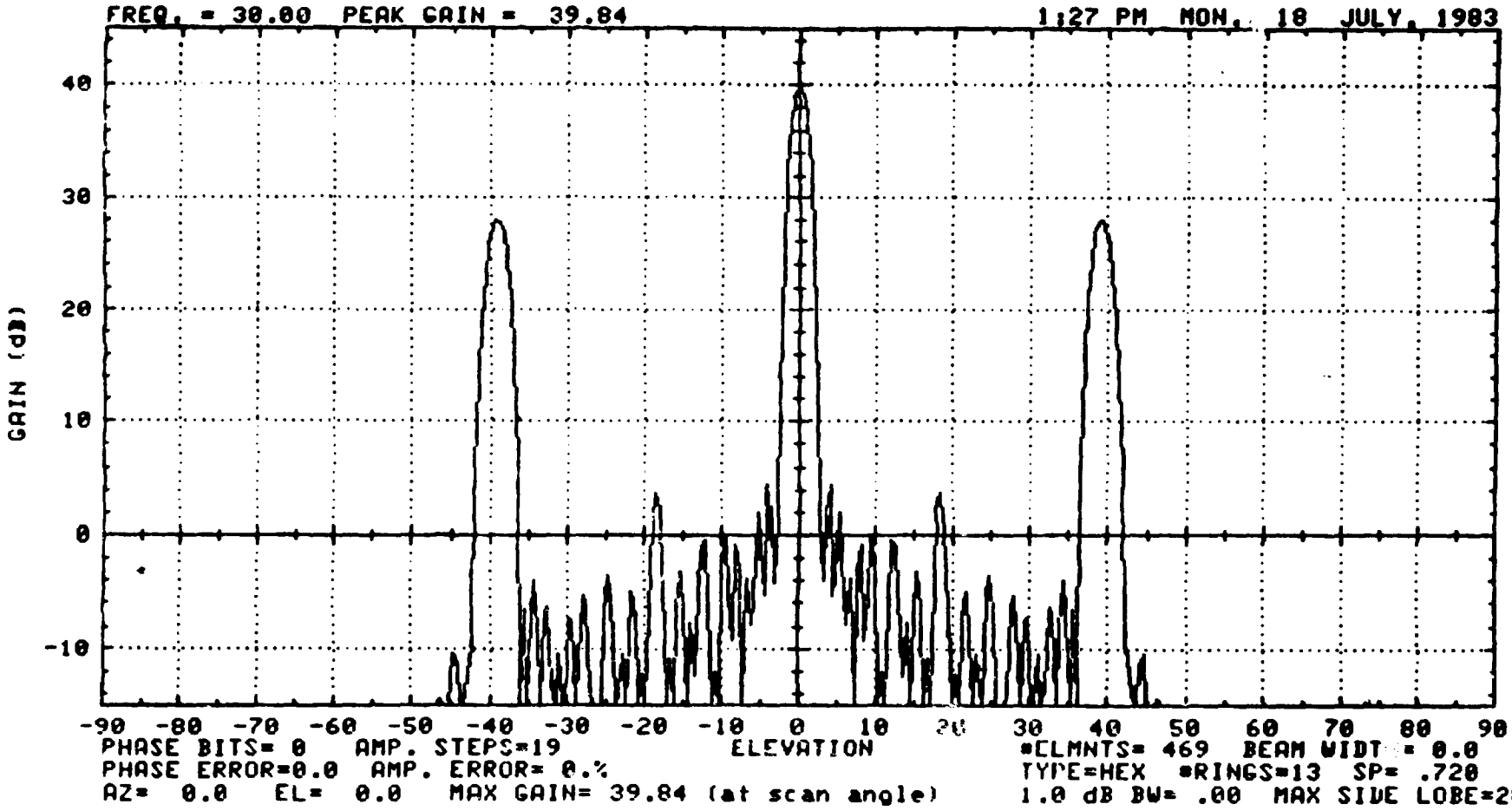
FREQ. = 30.00 PEAK GAIN = 39.84
1:27 PM MON. 18 JULY, 1983
GAIN (dB)
40
30
20
10
0
-10
-90 -80 -70 -60 -50 -40 -30 -20 -10 0 10 20 30 40 50 60 70 80 90
ELEVATION
PHASE BITS= 0 AMP. STEPS=19
PHASE ERROR=0.0 AMP. ERROR= 0.%
AZ= 0.0 EL= 0.0 MAX GAIN= 39.84 (at scan angle)
#ELMNTS= 469 BEAM WIDT = 0.0
TYPE=HEX #RINGS=13 SP= .720
1.0 dB BW= .00 MAX SIDE LOBE=28.09

Fig. 2-79

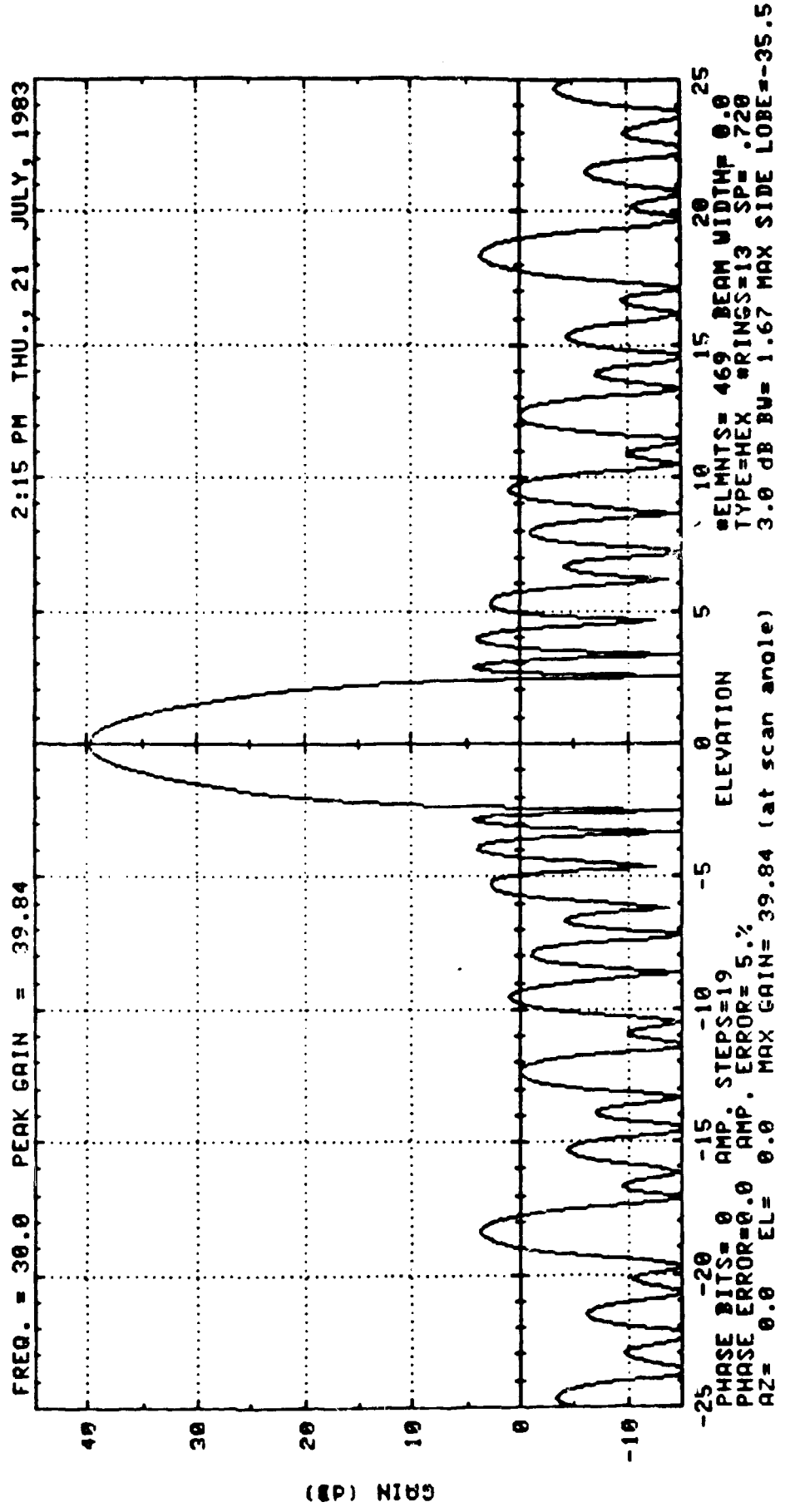
FREQ. = 30.0 PEAK GAIN = 39.84
2:15 PM THU., 21 JULY, 1983
GAIN (dB)
40
30
20
10
0
-10
-25 -20 -15 -10 -5 0 5 10 15 20 25
ELEVATION
PHASE BITS= 0 AMP. STEPS=19
PHASE ERROR=0.0 AMP. ERROR= 5.%
AZ= 0.0 EL= 0.0 MAX GAIN= 39.84 (at scan angle)
#ELMNTS= 469 BEAM WIDTH= 0.0
TYPE=HEX #RINGS=13 SP= .720
3.0 dB BW= 1.67 MAX SIDE LOBE=-35.5

Fig 4.2-80

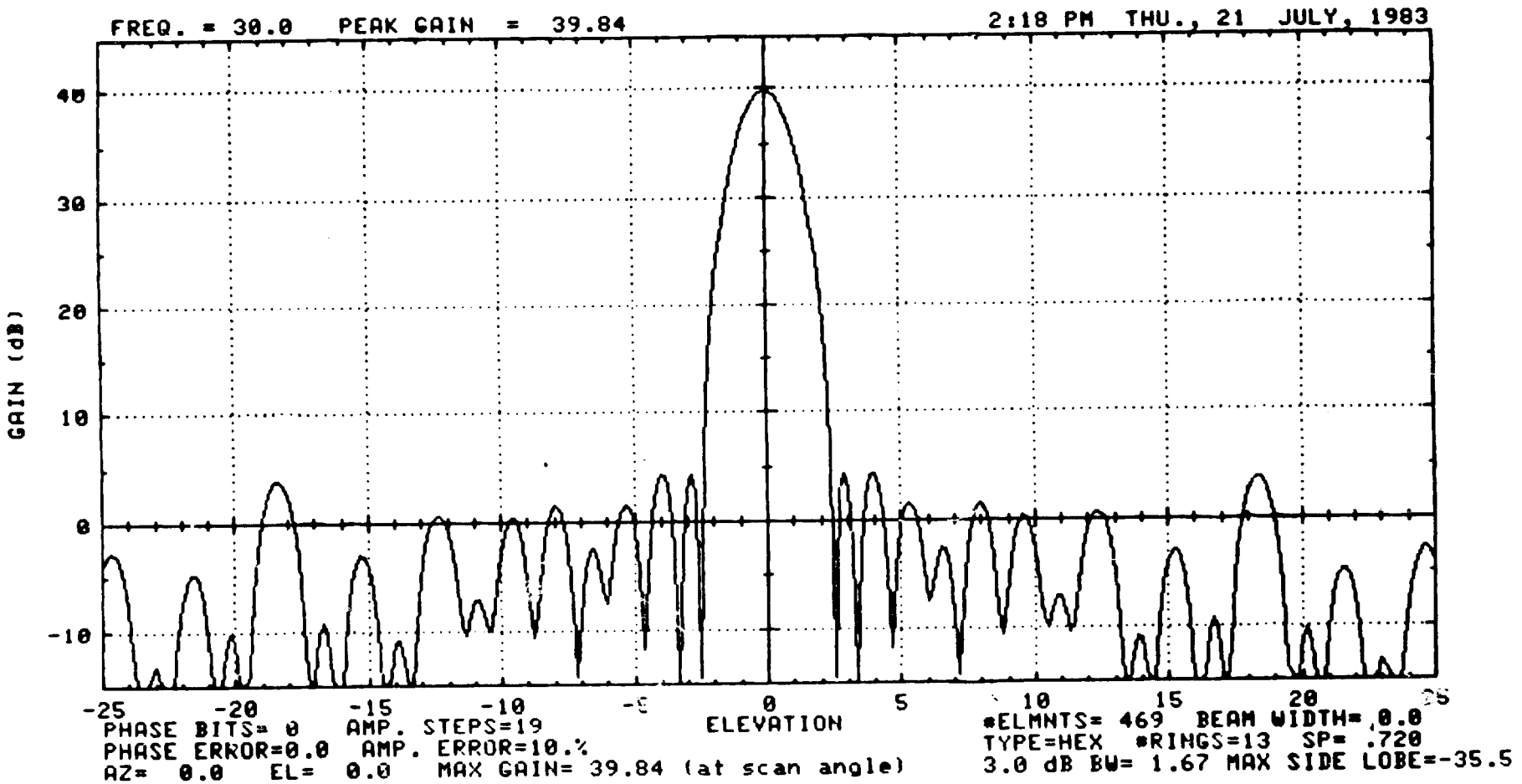
FREQ. = 30.0 PEAK GAIN = 39.84
2:18 PM THU., 21 JULY, 1983
GAIN (dB)
40
30
20
10
0
-10
-25 -20 -15 -10 -5 0 5 10 15 20 25
ELEVATION
PHASE BITS= 0 AMP. STEPS=19
PHASE ERROR=0.0 AMP. ERROR=10.%
AZ= 0.0 EL= 0.0 MAX GAIN= 39.84 (at scan angle)
#ELMNTS= 469 BEAM WIDTH= 0.0
TYPE=HEX #RINGS=13 SP= .720
3.0 dB BW= 1.67 MAX SIDE LOBE=-35.5

FIG. 4.2-81

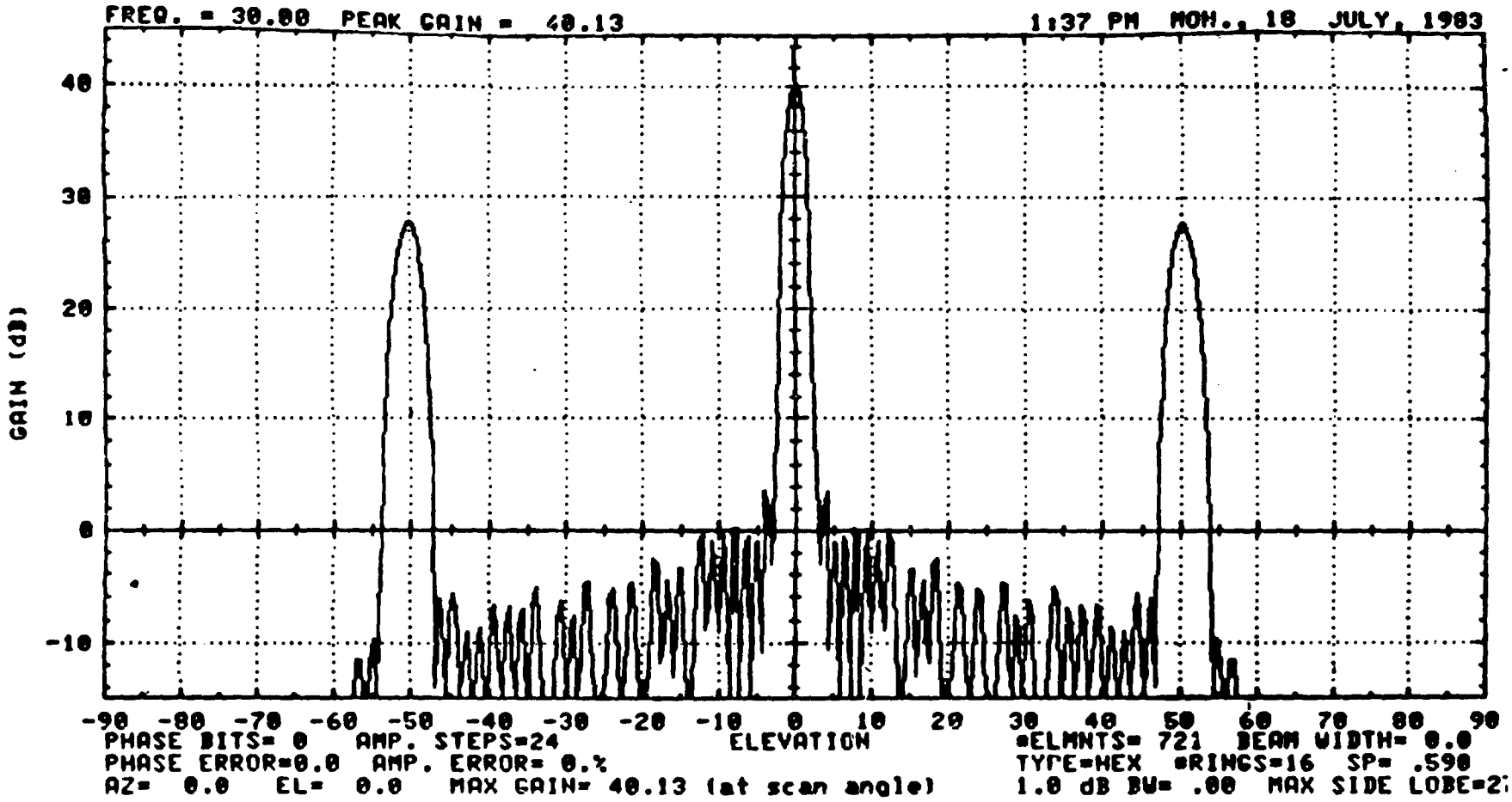
FREQ. = 30.00 PEAK GAIN = 40.13
1:37 PM MON., 18 JULY, 1983
GAIN (dB)
40
30
20
10
0
-10
-90 -80 -70 -60 -50 -40 -30 -20 -10 0 10 20 30 40 50 60 70 80 90
ELEVATION
PHASE BITS= 0 AMP. STEPS=24
PHASE ERROR=0.0 AMP. ERROR= 0.%
AZ= 0.0 EL= 0.0 MAX GAIN= 40.13 (at scan angle)
#ELMNTS= 721 BEAM WIDTH= 0.0
TYPE=HEX #RINGS=16 SP= .590
1.0 dB BW= .00 MAX SIDE LOBE=2

FIG. 4.2-82

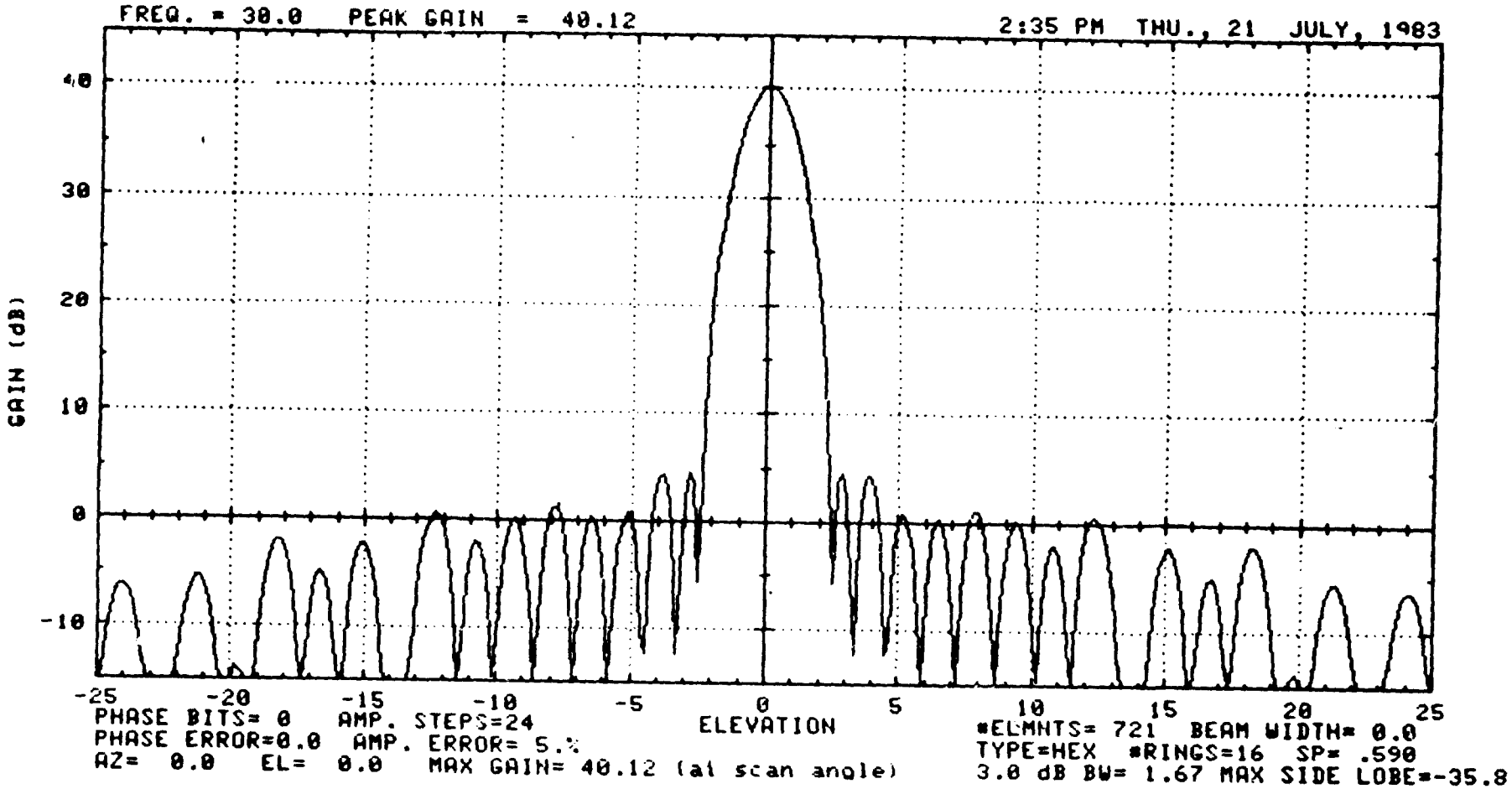
FREQ. = 30.0 PEAK GAIN = 40.12
2:35 PM THU., 21 JULY, 1983
GAIN (dB)
40
30
20
10
0
-10
-25 -20 -15 -10 -5 0 5 10 15 20 25
ELEVATION
PHASE BITS= 0 AMP. STEPS=24
PHASE ERROR=0.0 AMP. ERROR= 5.%
AZ= 0.0 EL= 0.0 MAX GAIN= 40.12 (at scan angle)
#ELMNTS= 721 BEAM WIDTH= 0.0
TYPE=HEX #RINGS=16 SP= .590
3.0 dB BW= 1.67 MAX SIDE LOBE=-35.8

FIG 4.2-83

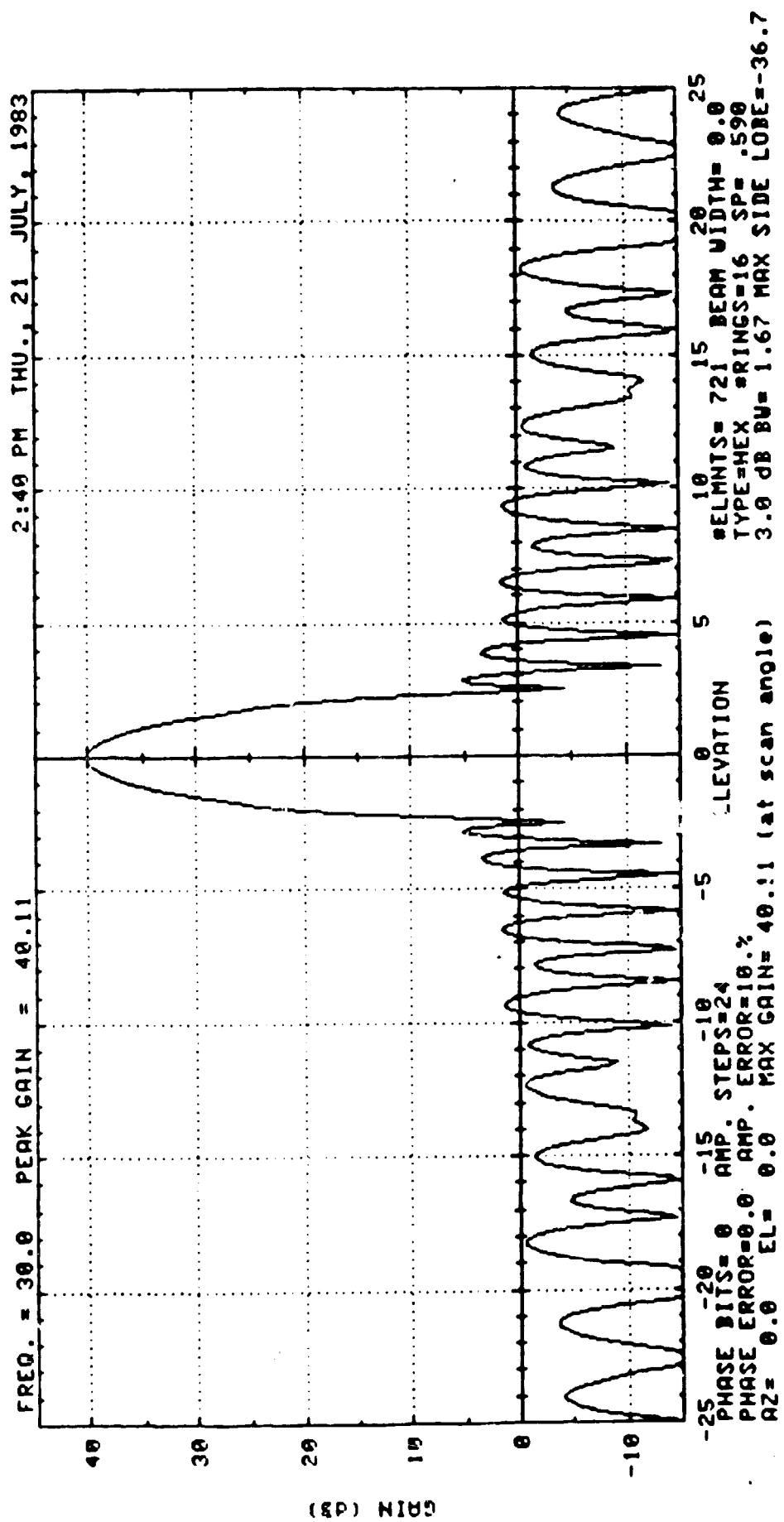
FREQ. = 30.0 PEAK GAIN = 40.11
2:40 PM THU., 21 JULY, 1983
GAIN (dB)
40
30
20
15
0
-10
-25 -20 -15 -10 -5 0 5 10 15 20 25
ELEVATION
PHASE BITS= 0 AMP. STEPS=24
PHASE ERROR=0.0 AMP. ERROR=10.%
AZ= 0.0 EL= 0.0 MAX GAIN= 40.11 (at scan angle)
#ELMNTS= 721 BEAM WIDTH= 0.0
TYPE=HEX #RINGS=16 SP= .590
3.0 dB BW= 1.67 MAX SIDE LOBE=-36.7

FIG. 4.2-84

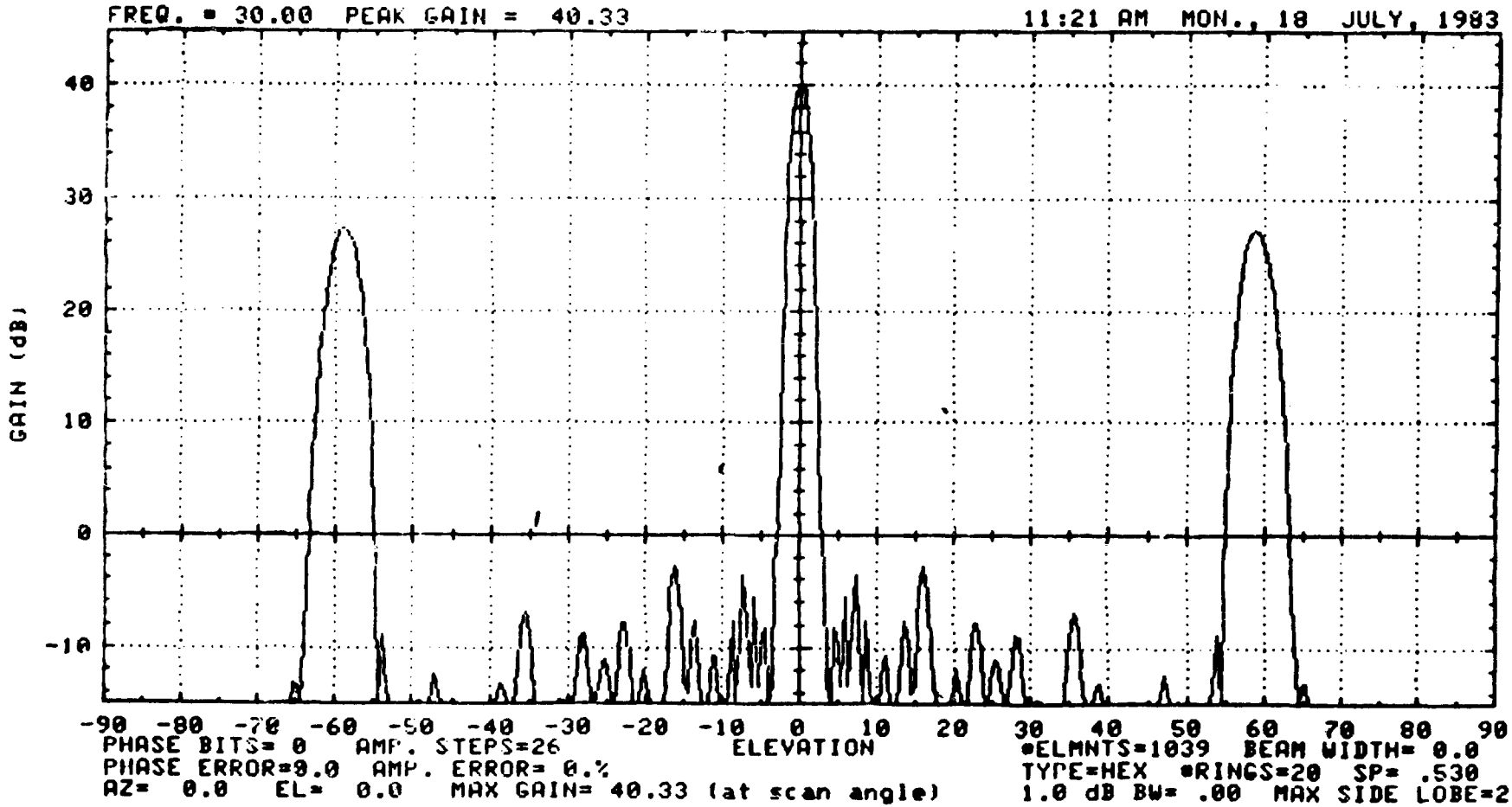
FREQ. = 30.00 PEAK GAIN = 40.33
11:21 AM MON., 18 JULY, 1983
GAIN (dB)
40
30
20
10
0
-10
-90 -80 -70 -60 -50 -40 -30 -20 -10 0 10 20 30 40 50 60 70 80 90
ELEVATION
PHASE BITS= 0 AMP. STEPS=26
PHASE ERROR=0.0 AMP. ERROR= 0.%
AZ= 0.0 EL= 0.0 MAX GAIN= 40.33 (at scan angle)
#ELMNTS=1039 BEAM WIDTH= 0.0
TYPE=HEX #RINGS=20 SP= .530
1.0 dB BW= .00 MAX SIDE LOBE=27.26

FIG. 42-85

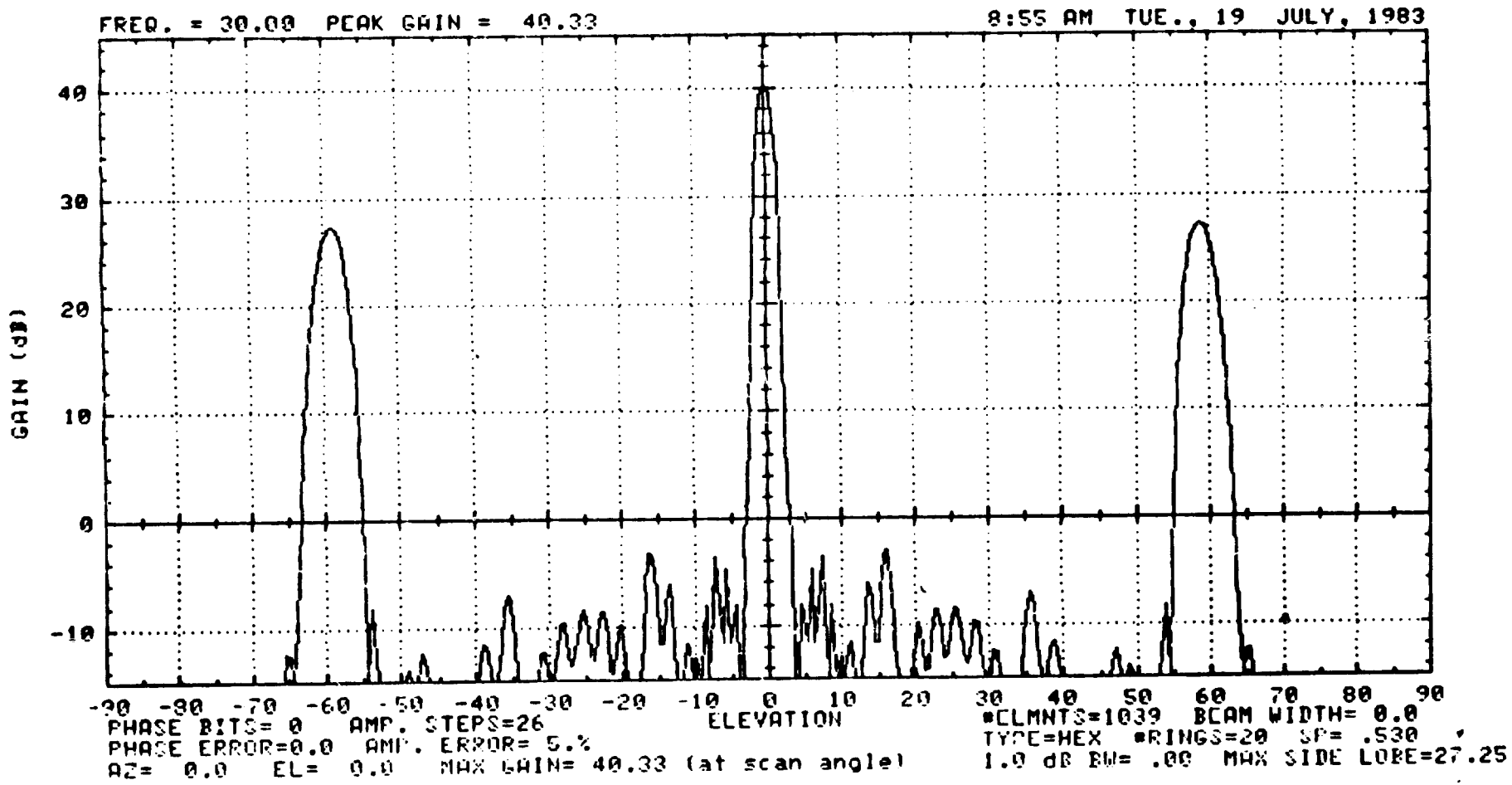
FREQ. = 30.00 PEAK GAIN = 40.33
8:55 AM TUE., 19 JULY, 1983
GAIN (dB)
40
30
20
10
0
-10
-90 -80 -70 -60 -50 -40 -30 -20 -10 0 10 20 30 40 50 60 70 80 90
ELEVATION
PHASE BITS= 0 AMP. STEPS=26
PHASE ERROR=0.0 AMP. ERROR= 5.%
AZ= 0.0 EL= 0.0 MAX GAIN= 40.33 (at scan angle)
#ELMNTS=1039 BEAM WIDTH= 0.0
TYPE=HEX #RINGS=20 SP= .530
1.0 dB BW= .00 MAX SIDE LOBE=27.25

FIG 4.2-86

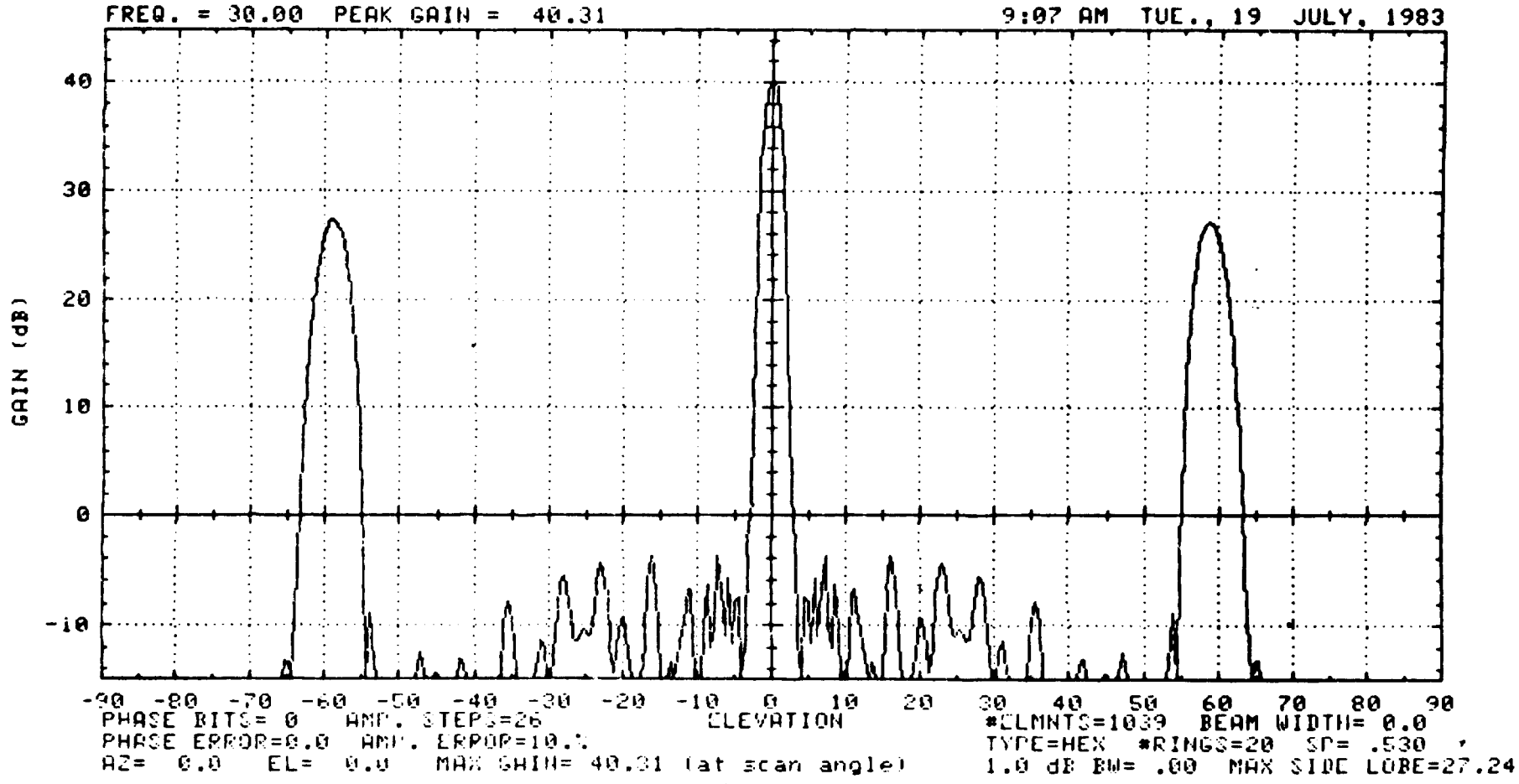
FREQ. = 30.00 PEAK GAIN = 40.31
9:07 AM TUE., 19 JULY, 1983
GAIN (dB)
40
30
20
10
0
-10
-90 -80 -70 -60 -50 -40 -30 -20 -10 0 10 20 30 40 50 60 70 80 90
ELEVATION
PHASE BITS= 0 AMP. STEPS=26
PHASE ERROR=0.0 AMP. ERROR=10.%
AZ= 0.0 EL= 0.0 MAX GAIN= 40.31 (at scan angle)
#ELMNTS=1039 BEAM WIDTH= 0.0
TYPE=HEX #RINGS=20 SP= .530
1.0 dB BW= .00 MAX SIDE LOBE=27.24

FIG. 4.2-87

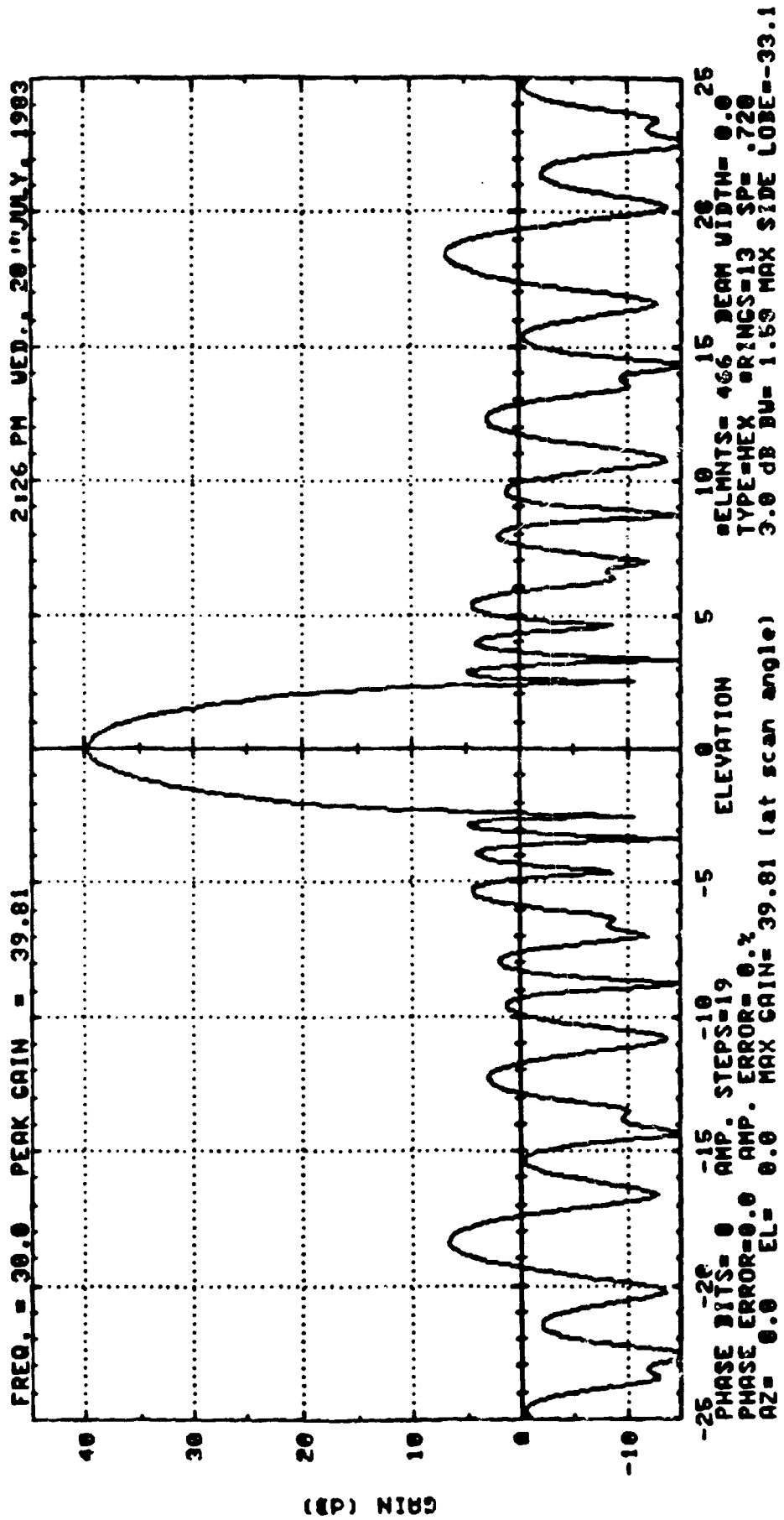

FIG. 4.2-94 3 FAILURES

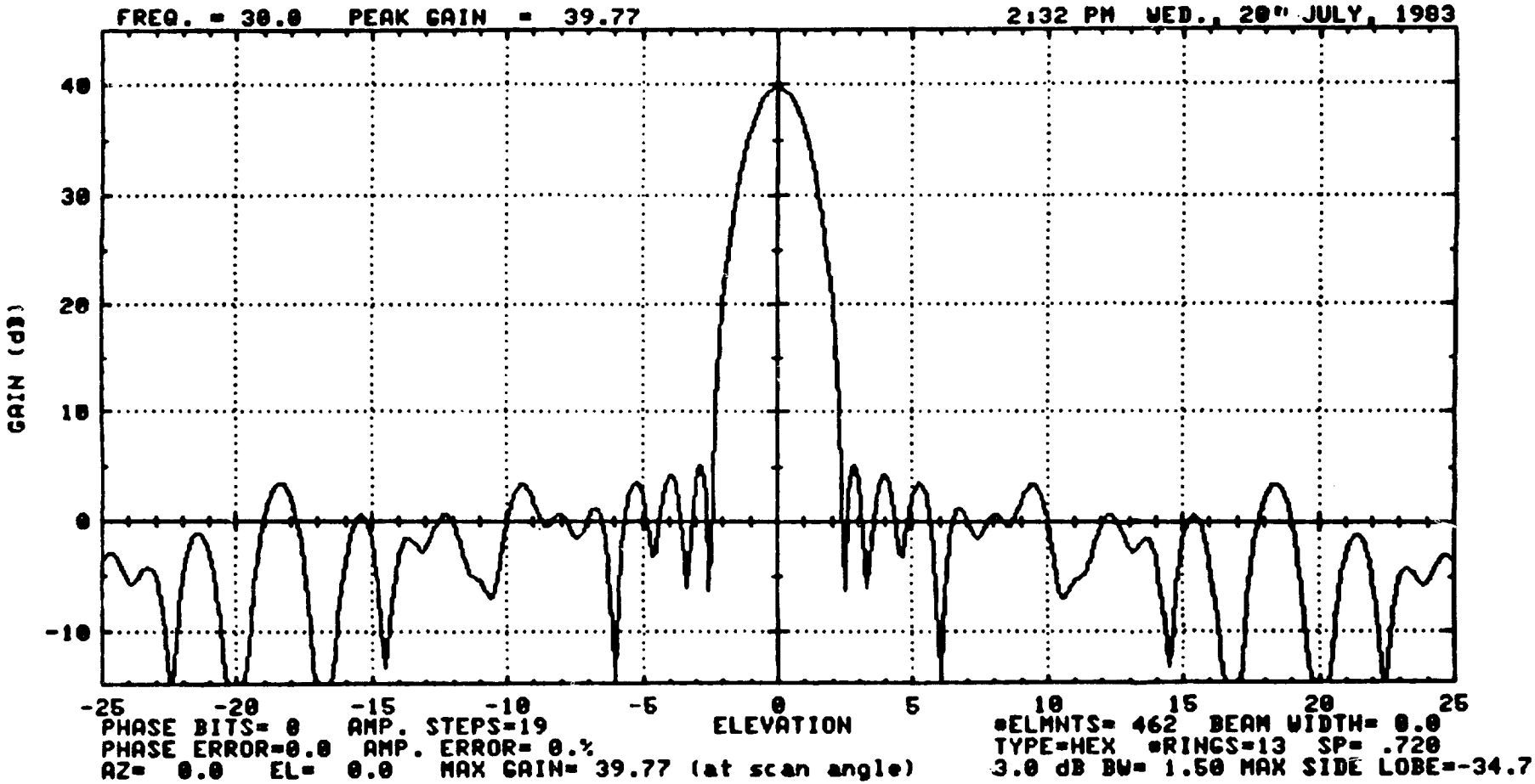

FIG. 4.2-95 7 FAILURES

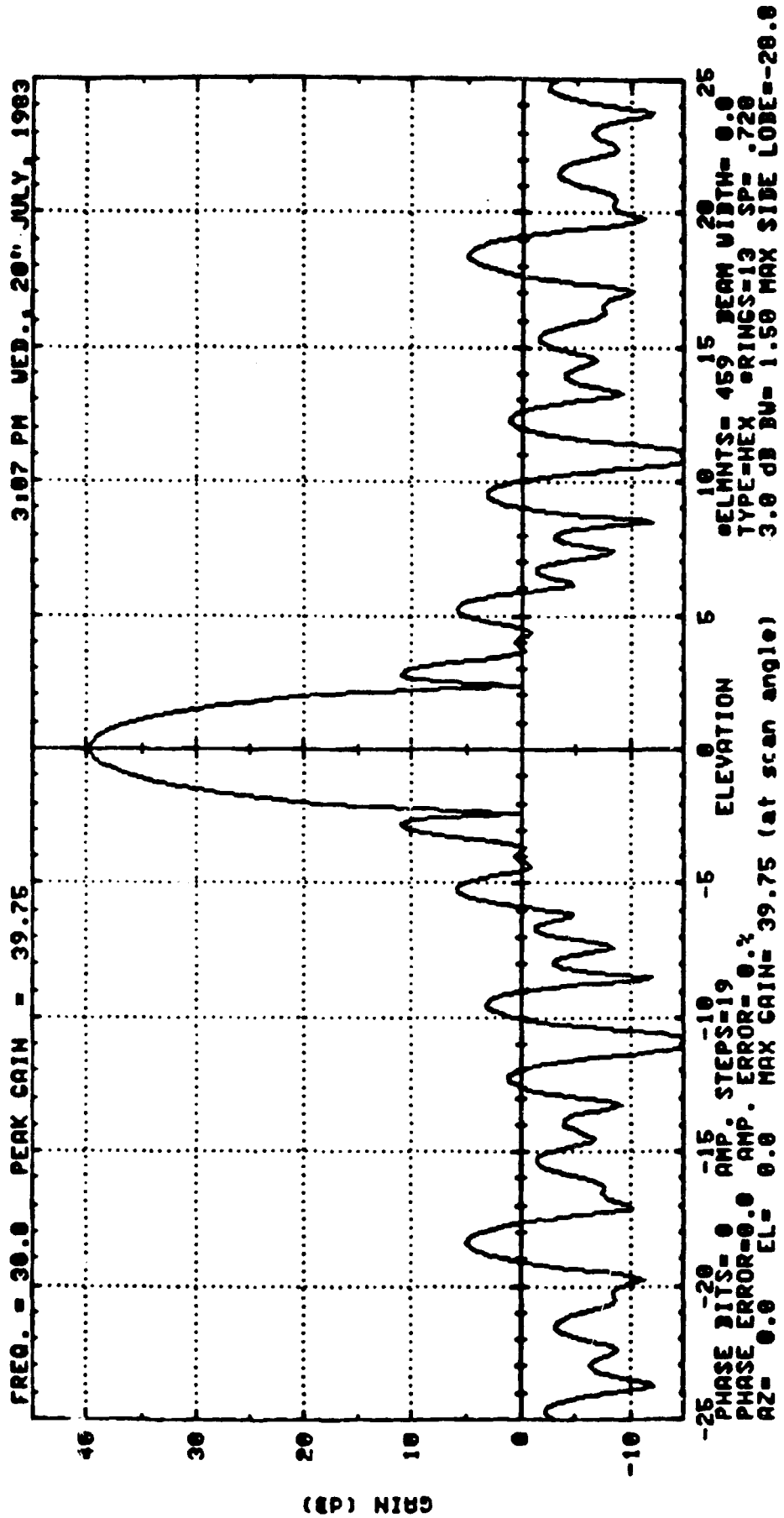

FIG. 4.2-96 10 FAILURES

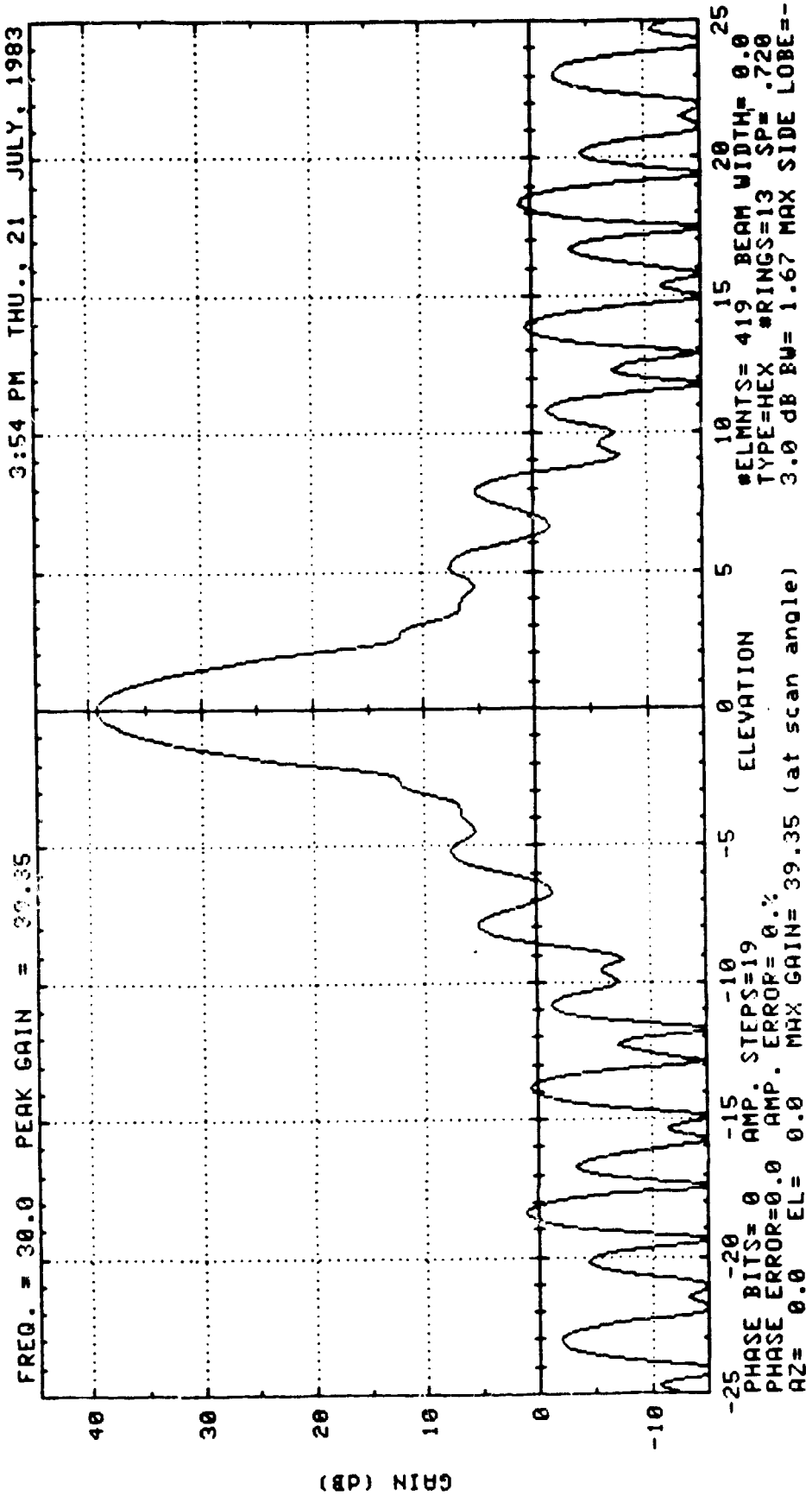

FIG.4.2-97 50 FAILURES

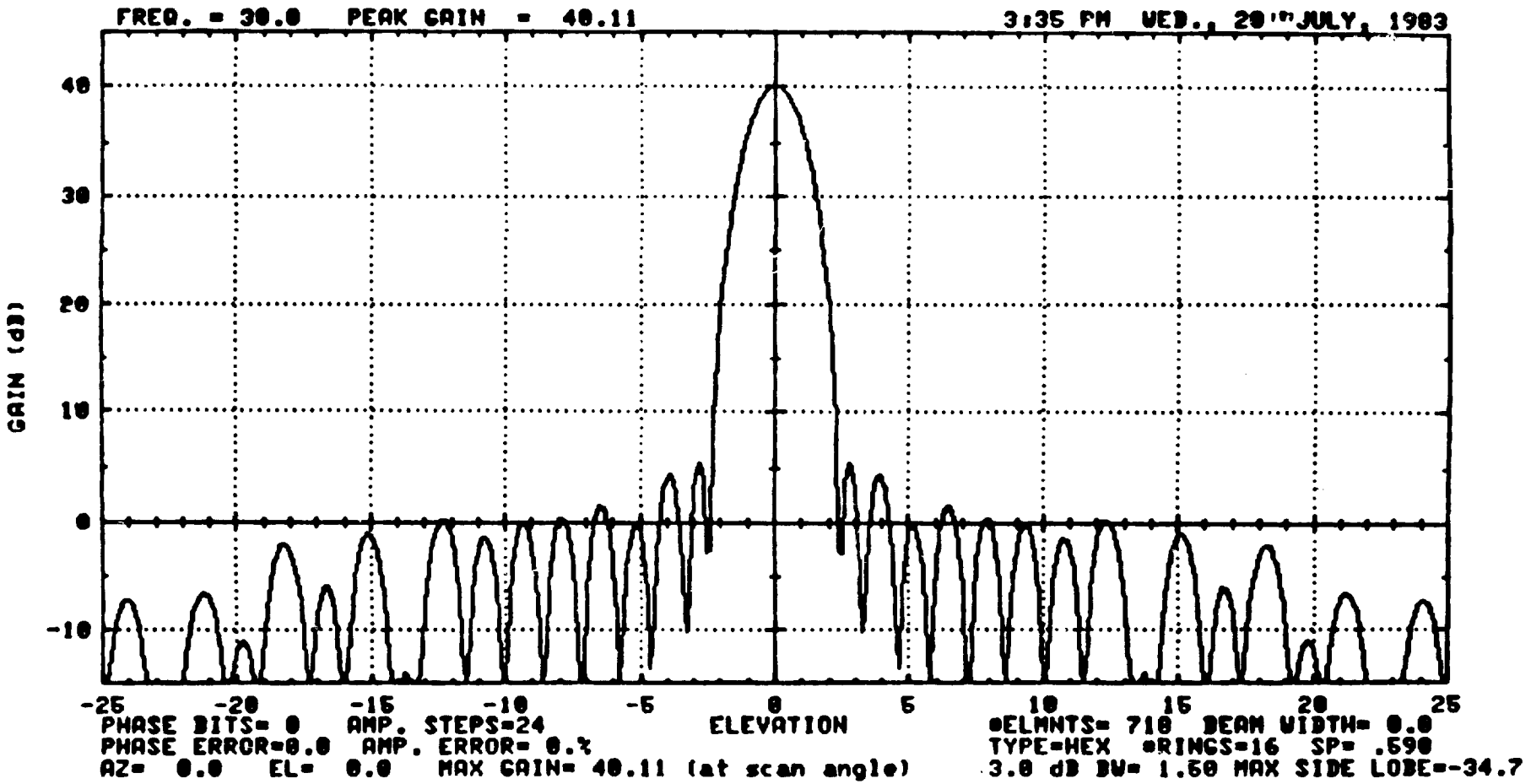

FIG. 4.2-98 3 FAILURES

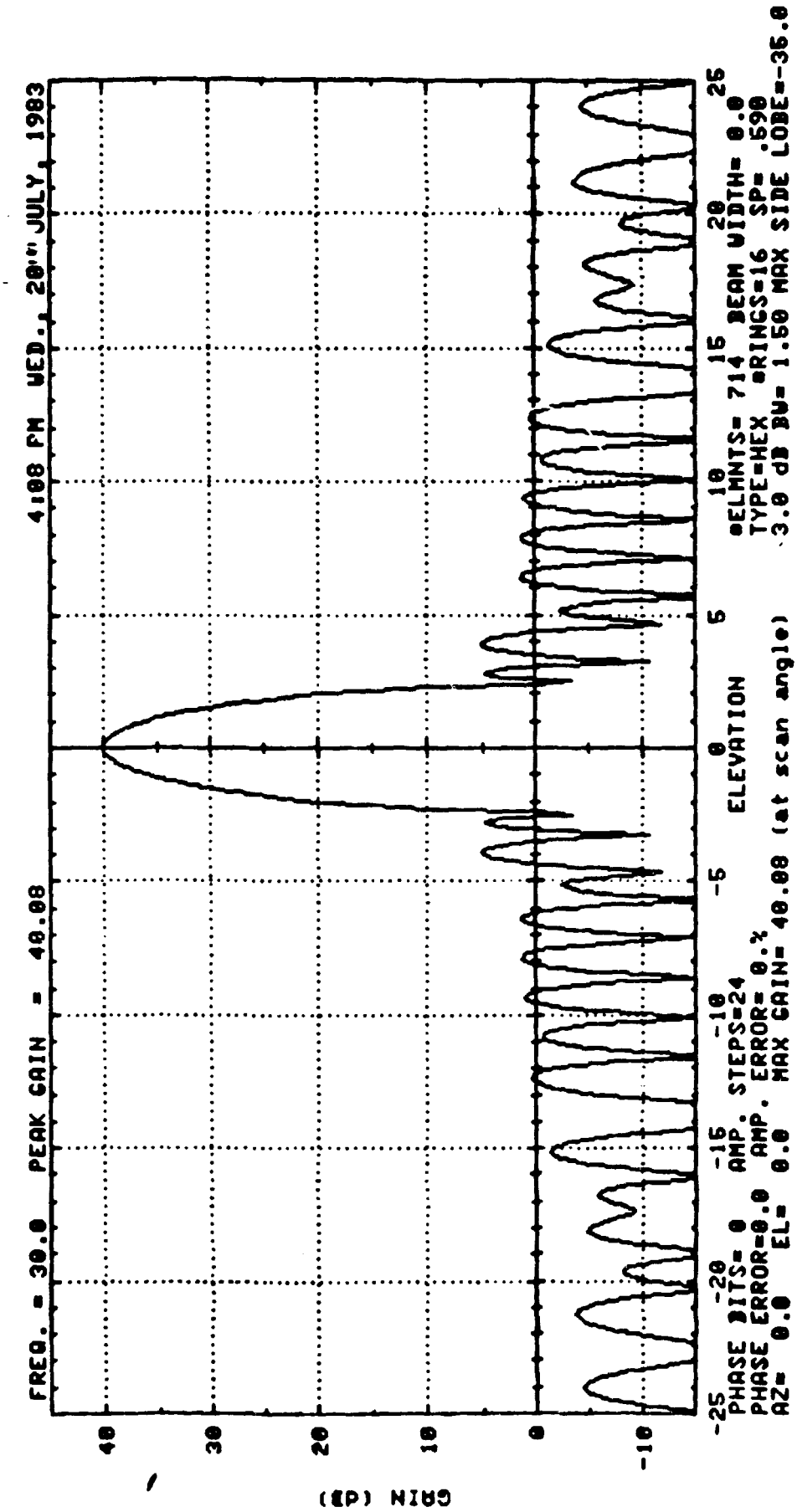

FIG 4.2-99 7 FAILURES

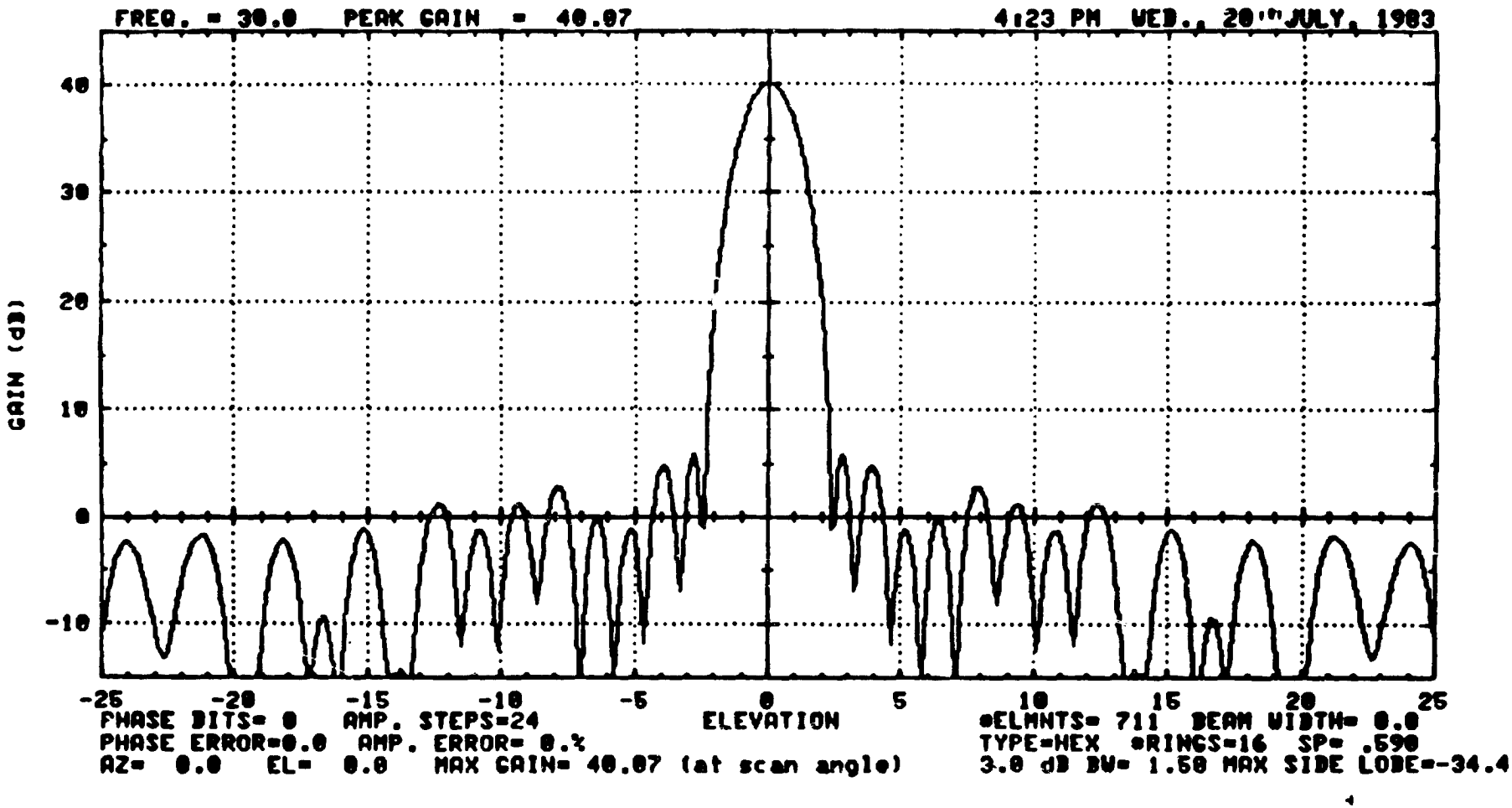

FIG 4.2-100 10 FAILURES

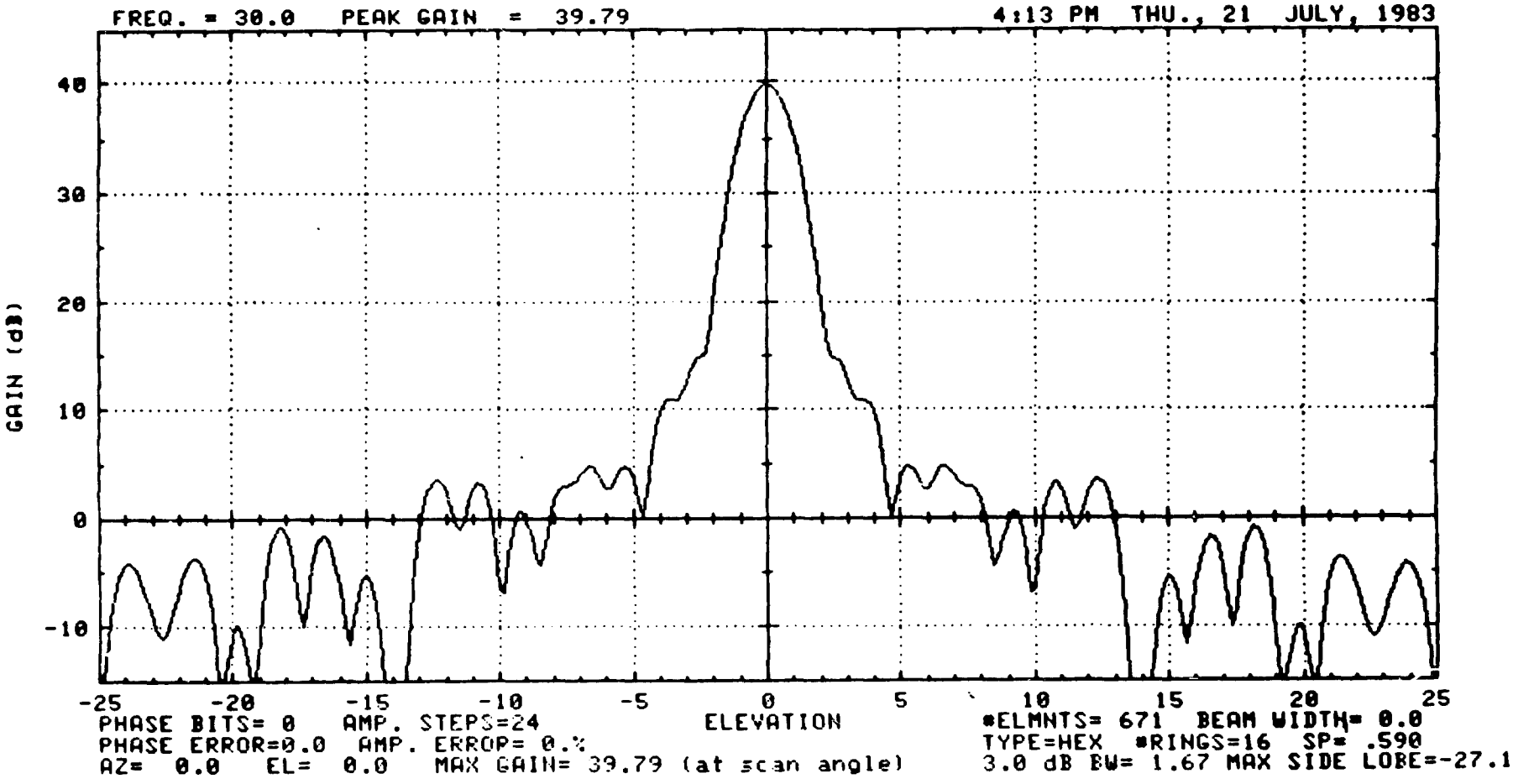

FIG. 4.2-101 50 FAILURES

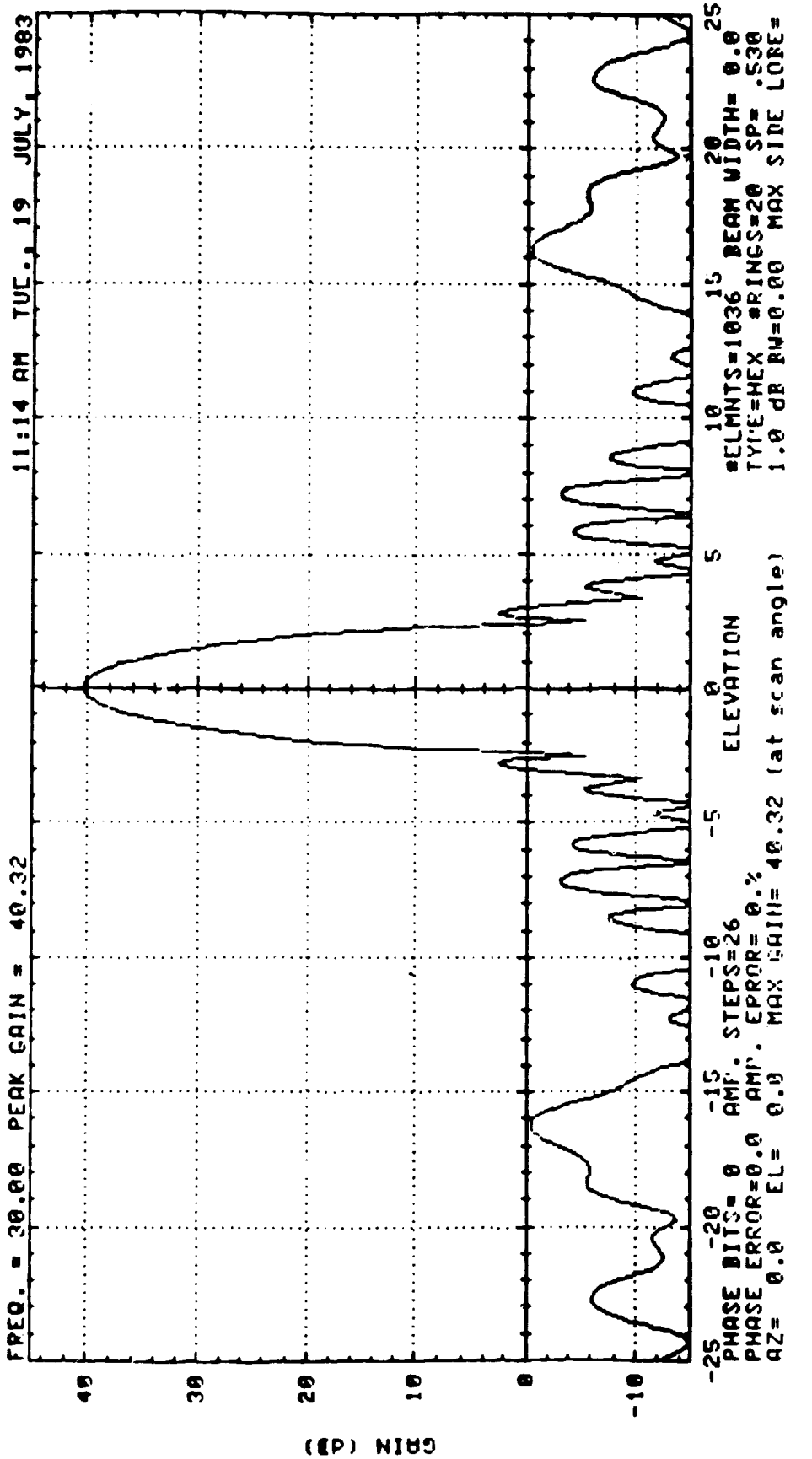

FIG 4.2-102 3 FAILURES

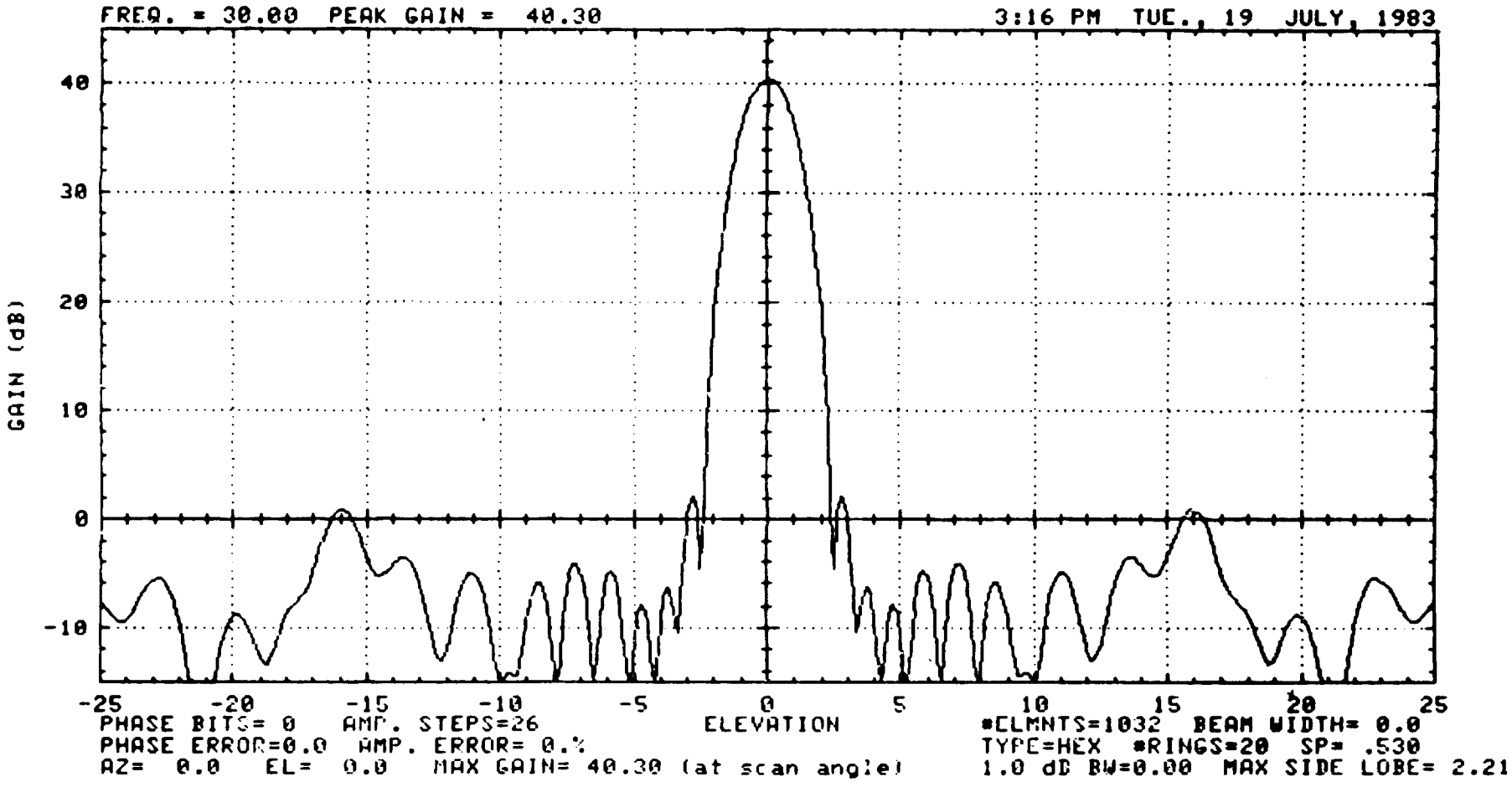

FIG. 4.2-103 7 FAILURES

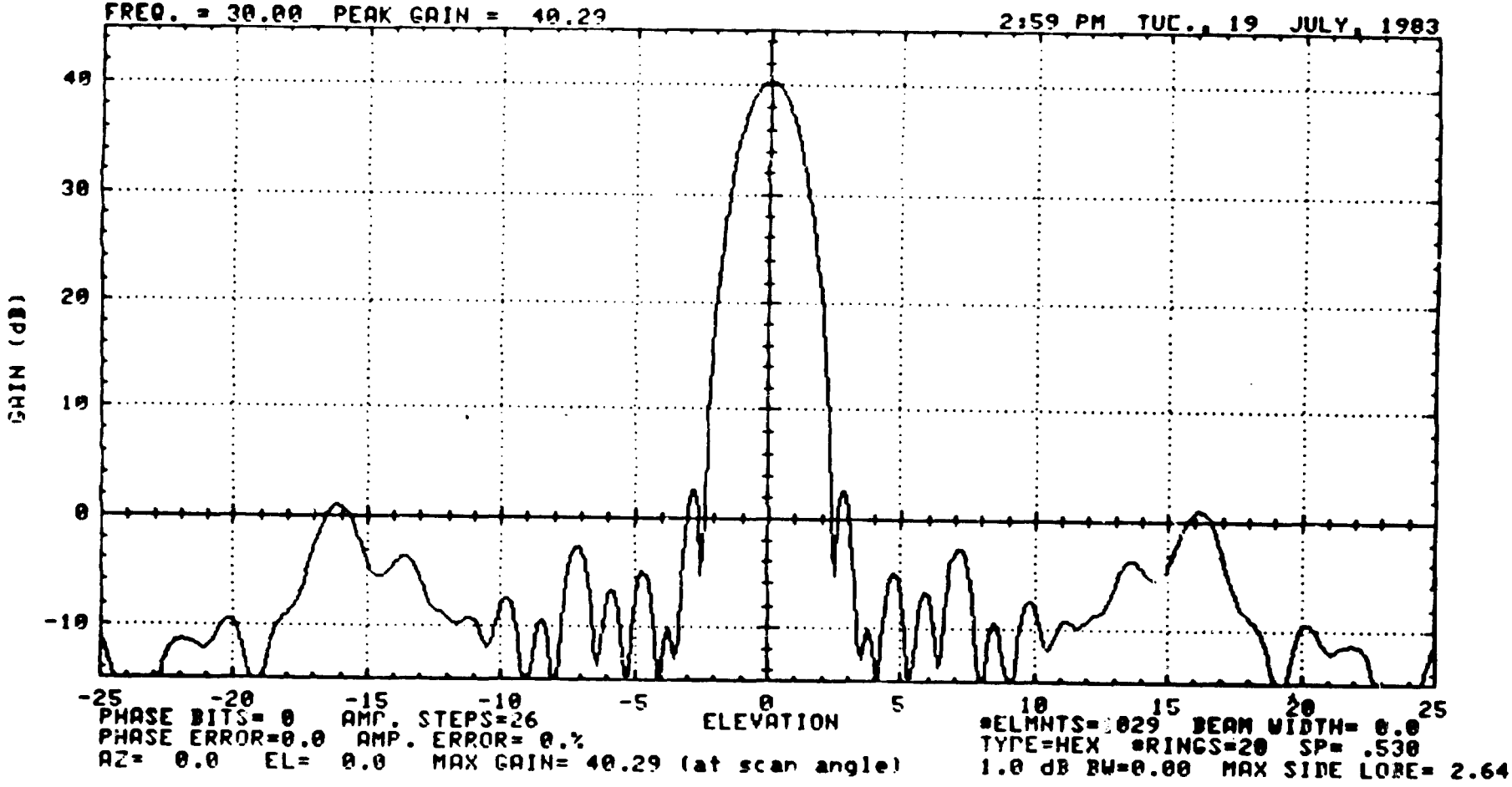

FIG 4.2-104 10 FAILURES

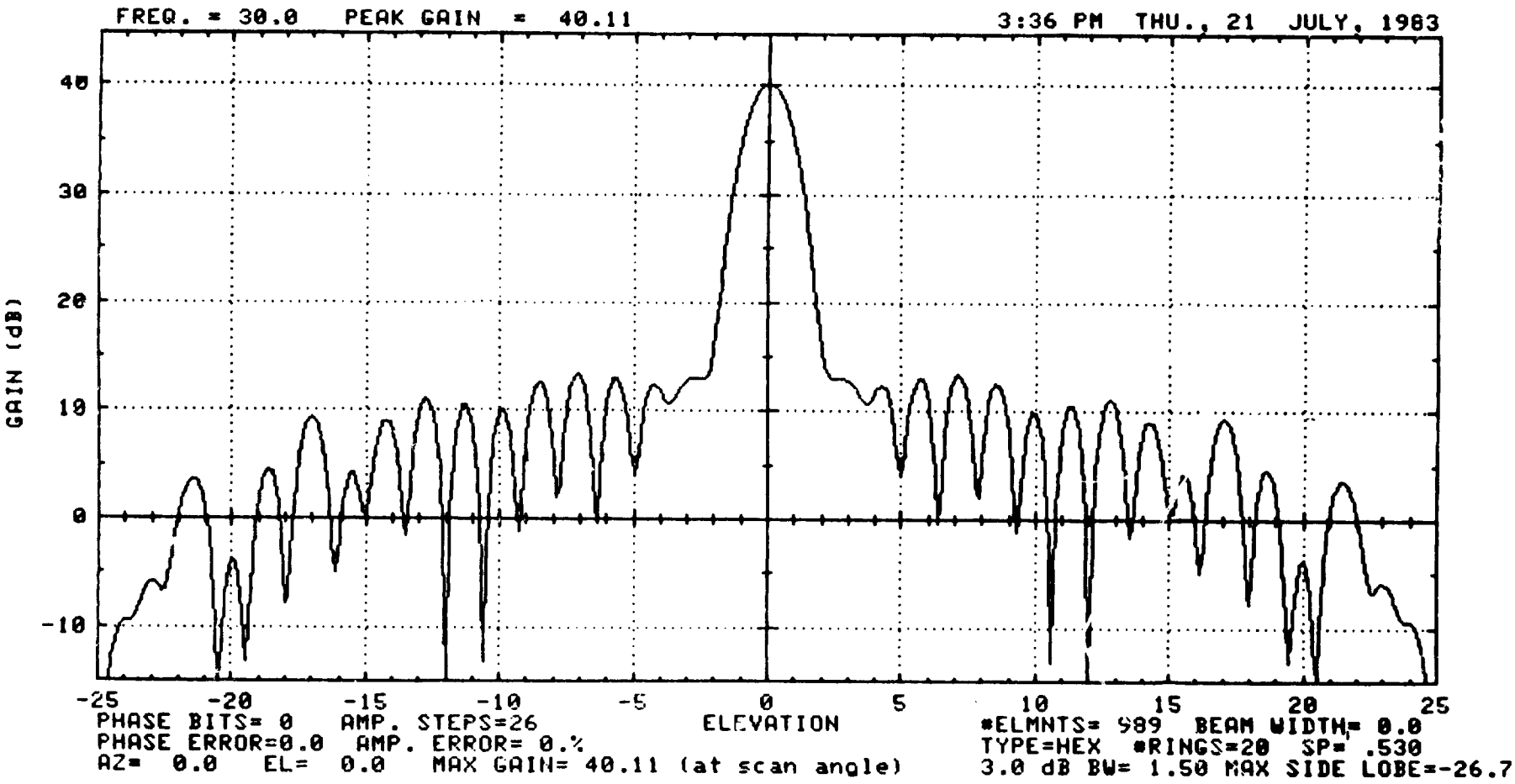

FIG. 4.2-105 50 FAILURES

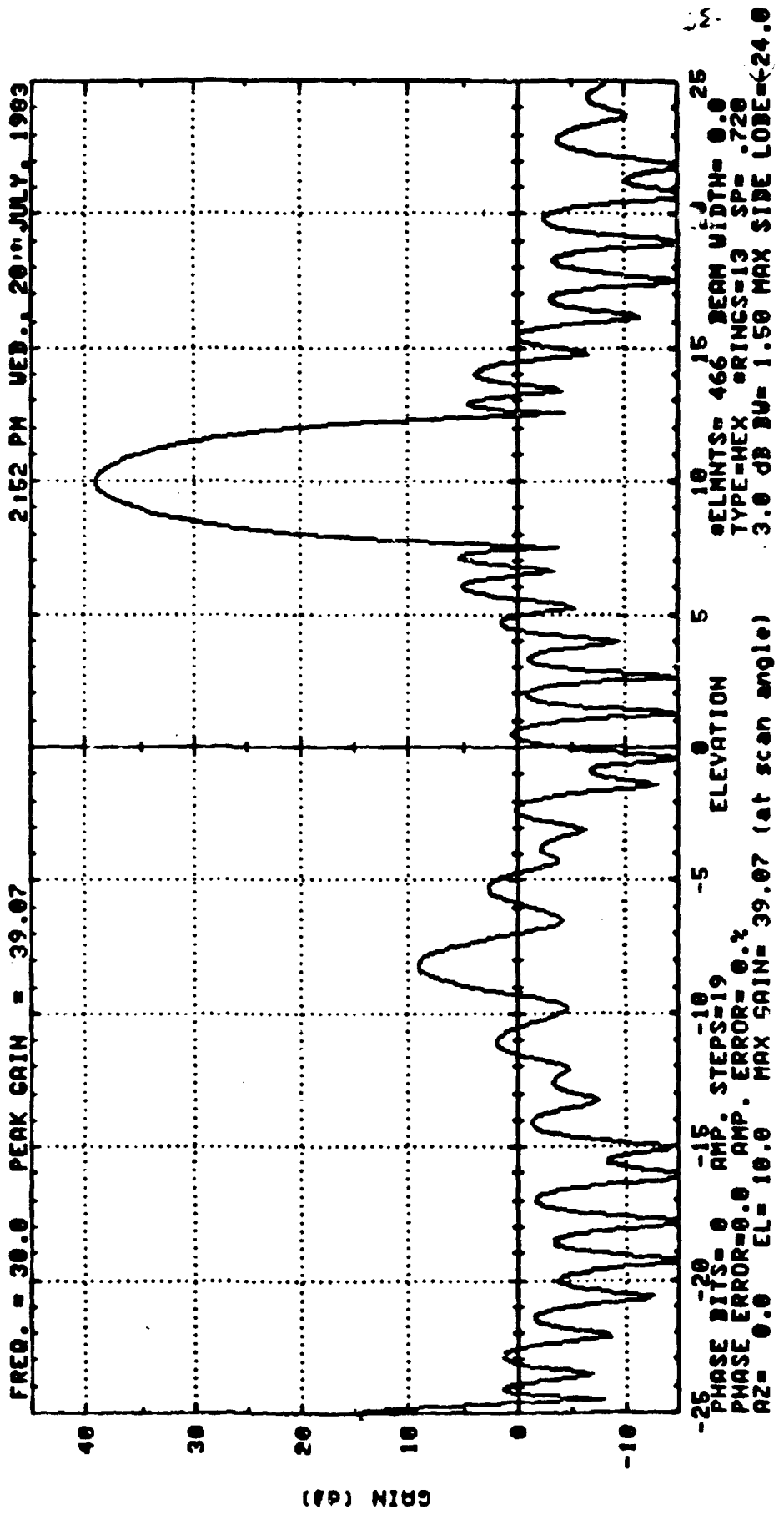

FIG. 4.2-106 3 FAILURES

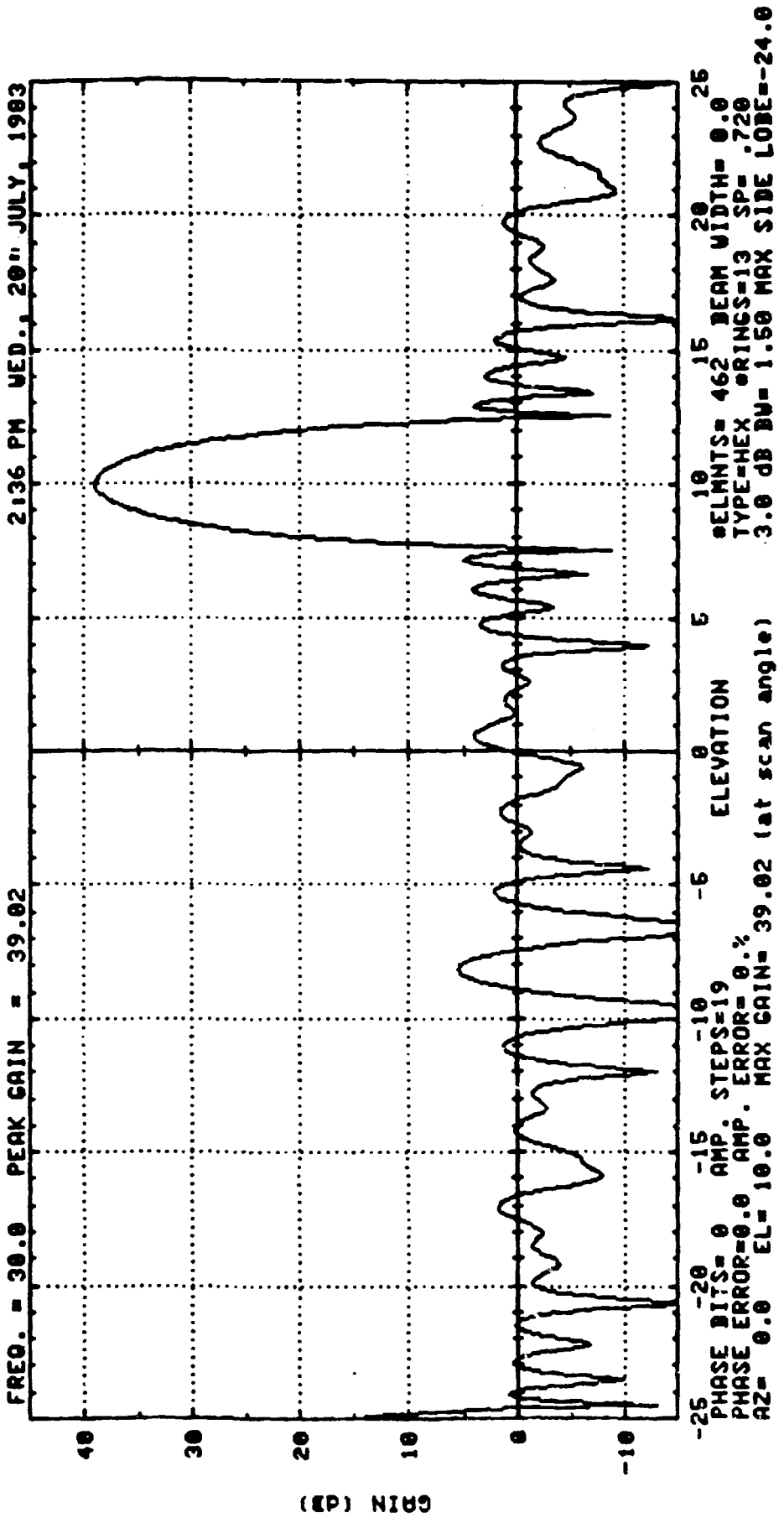

FIG. 4.2-107 7 FAILURES

5'87.

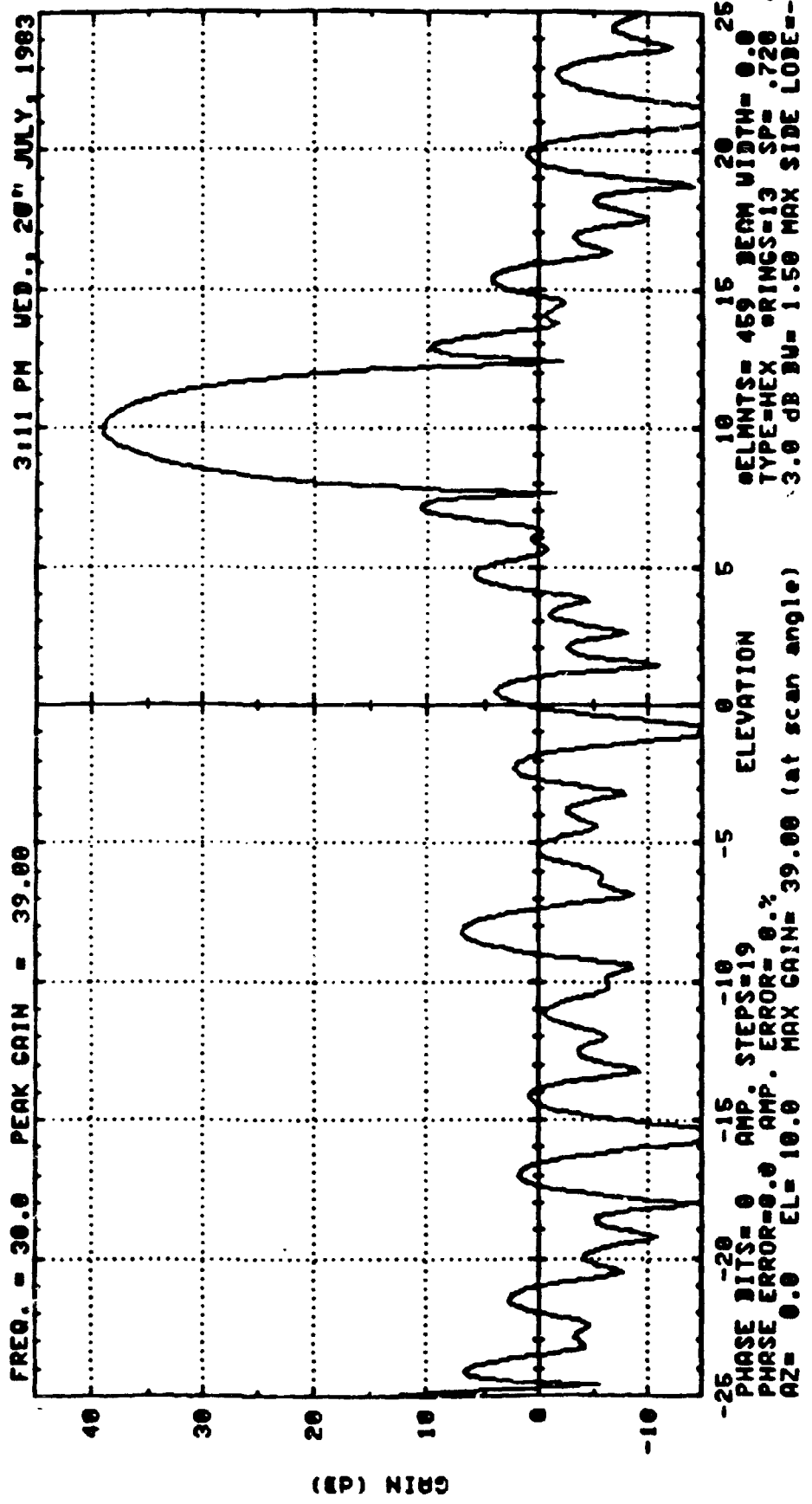

Fig 4.2-108 10 FAILURES

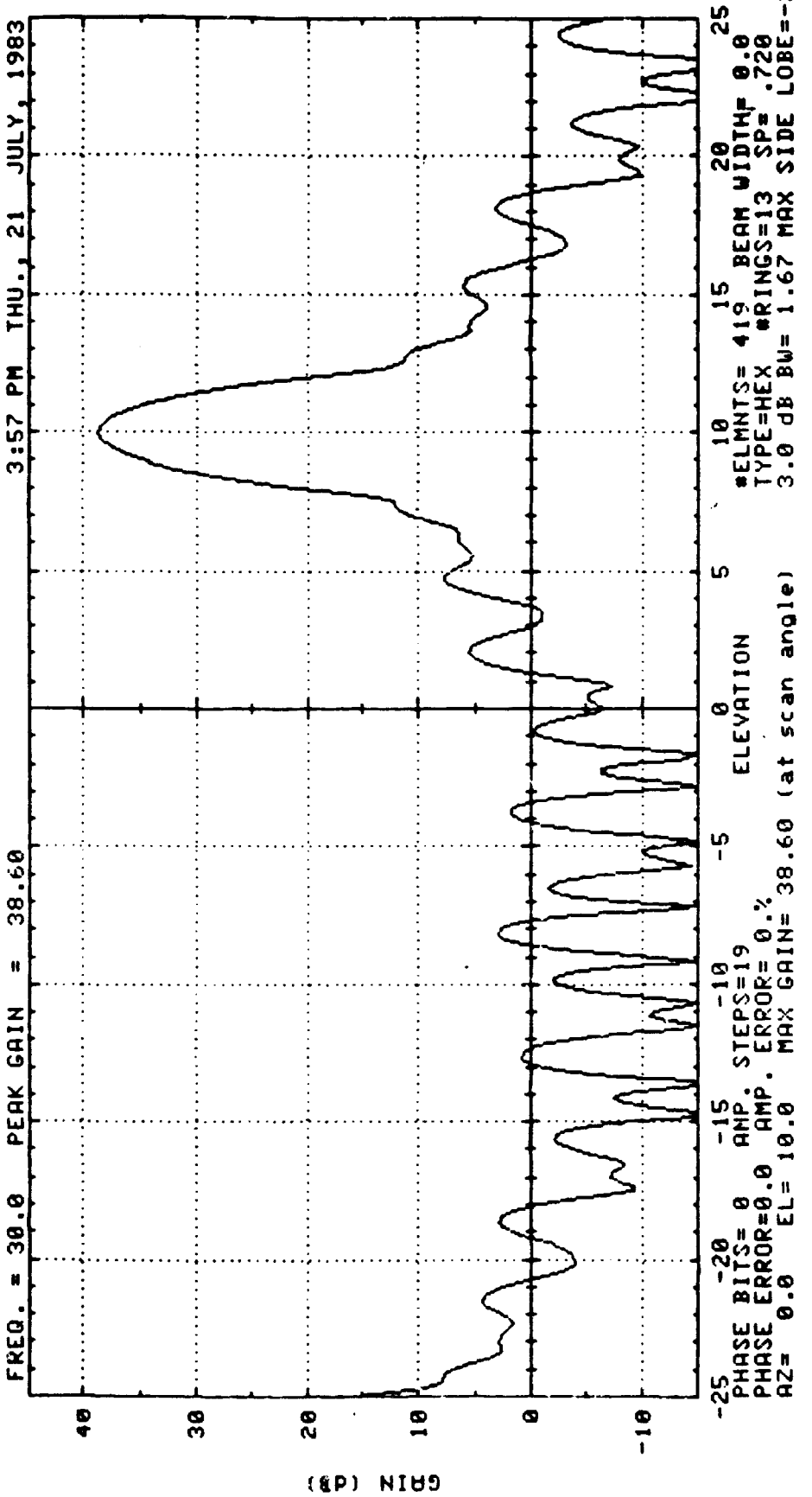

FIG. 4.2-109 50 FAILURES

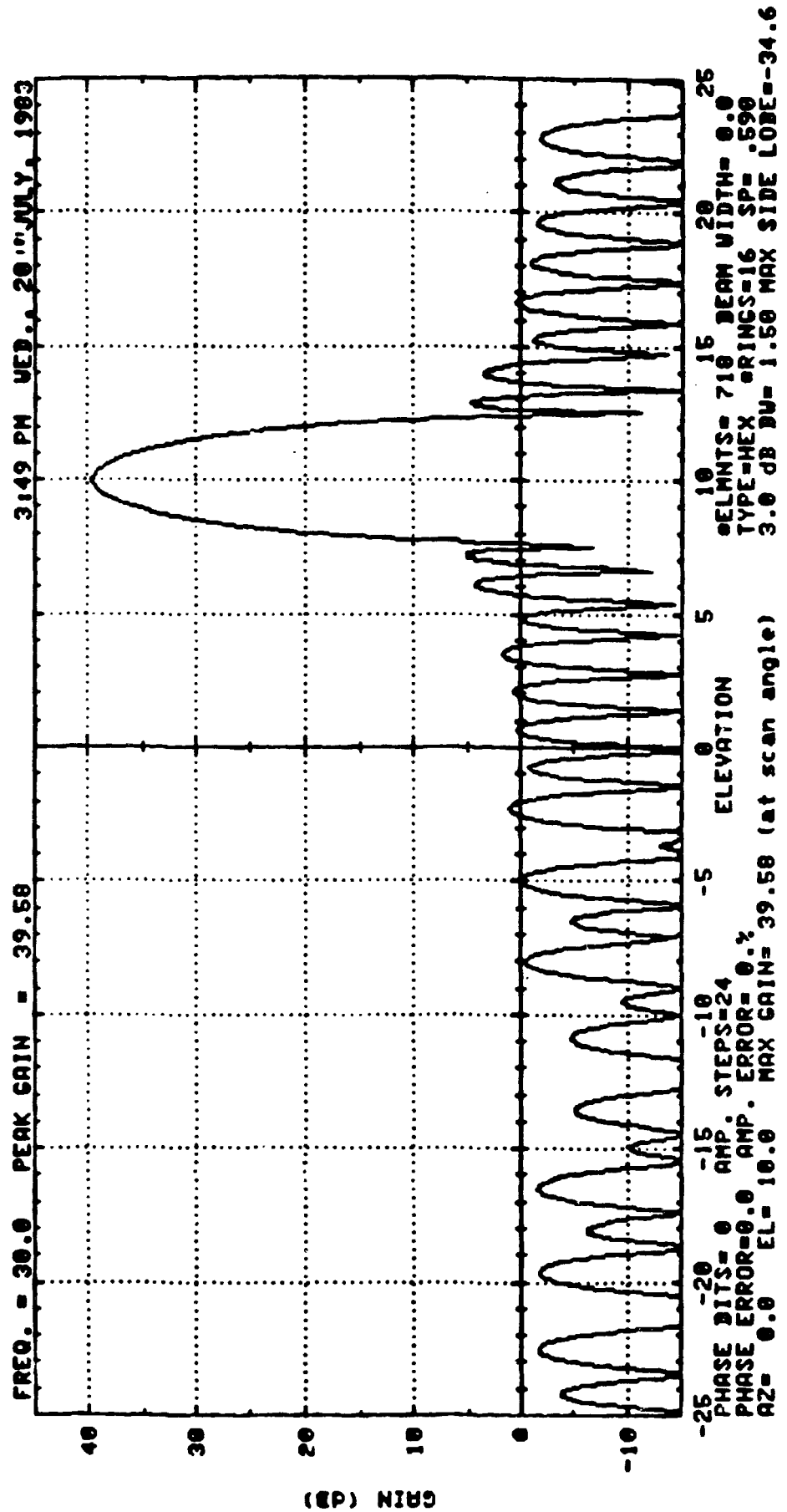

FIG. 4.2-110 3 FAILURES

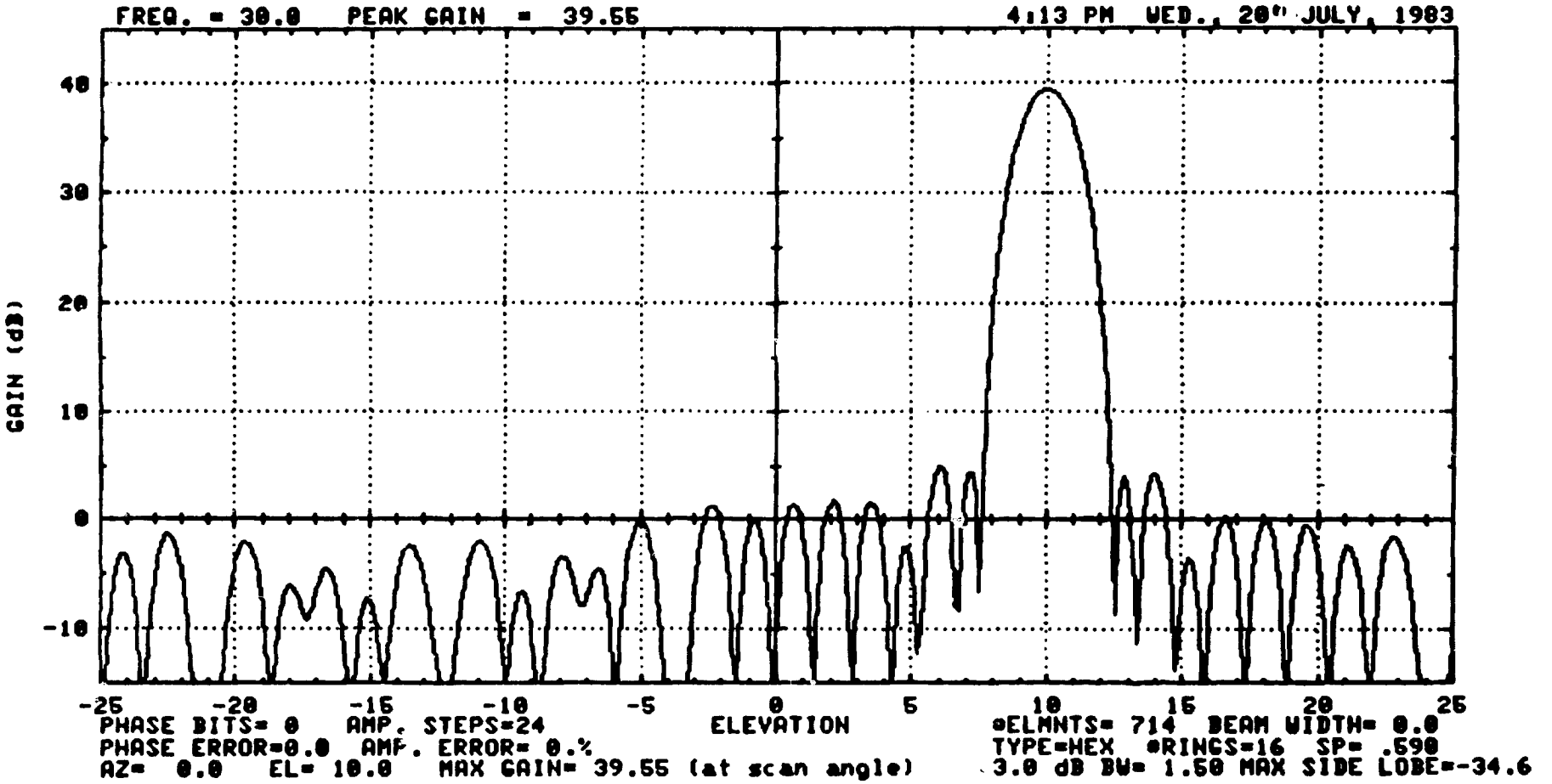

FIG. 4.2-111 7 FAILURES

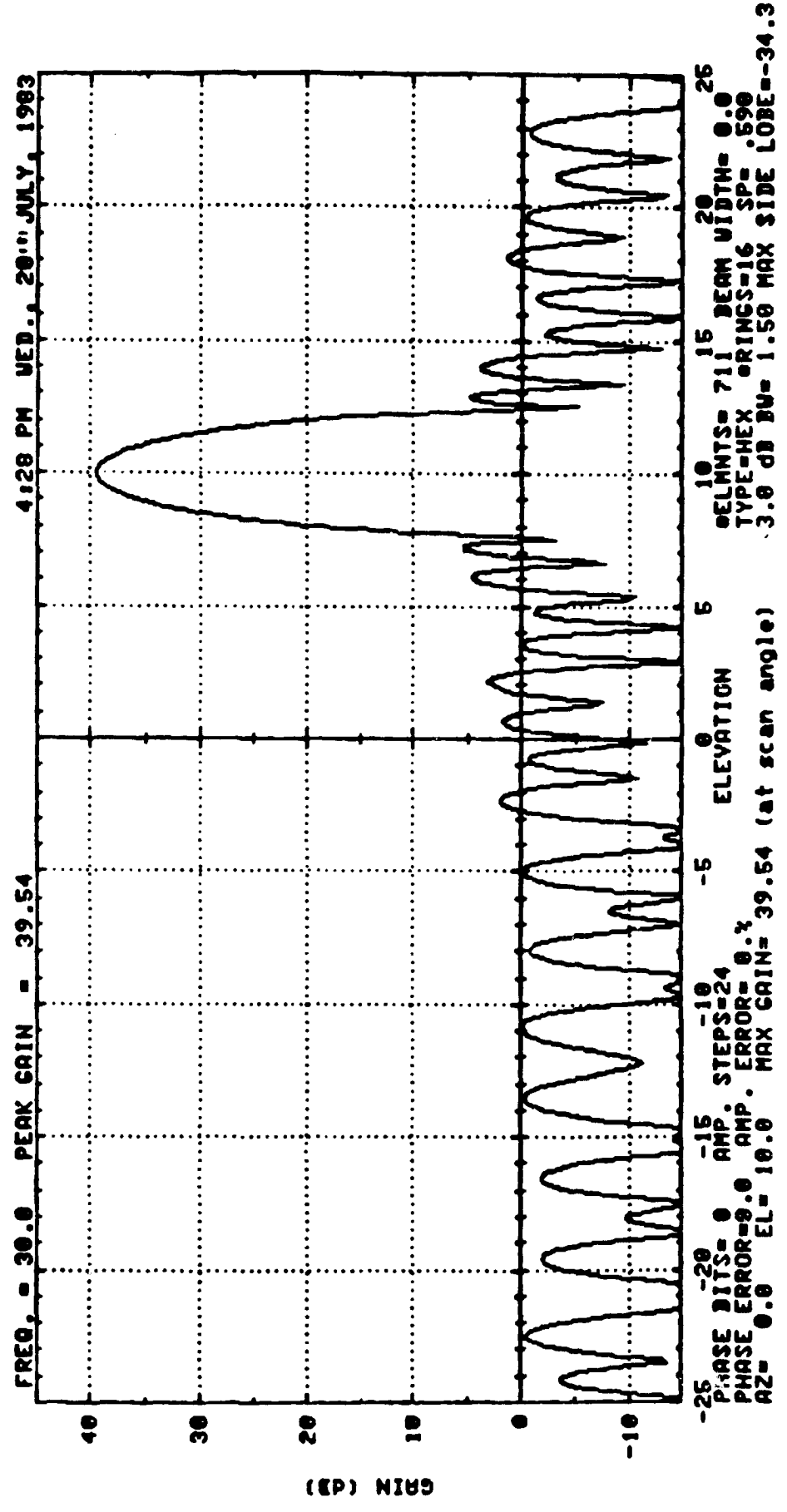

FIG 4.2-112 10 FAILURES

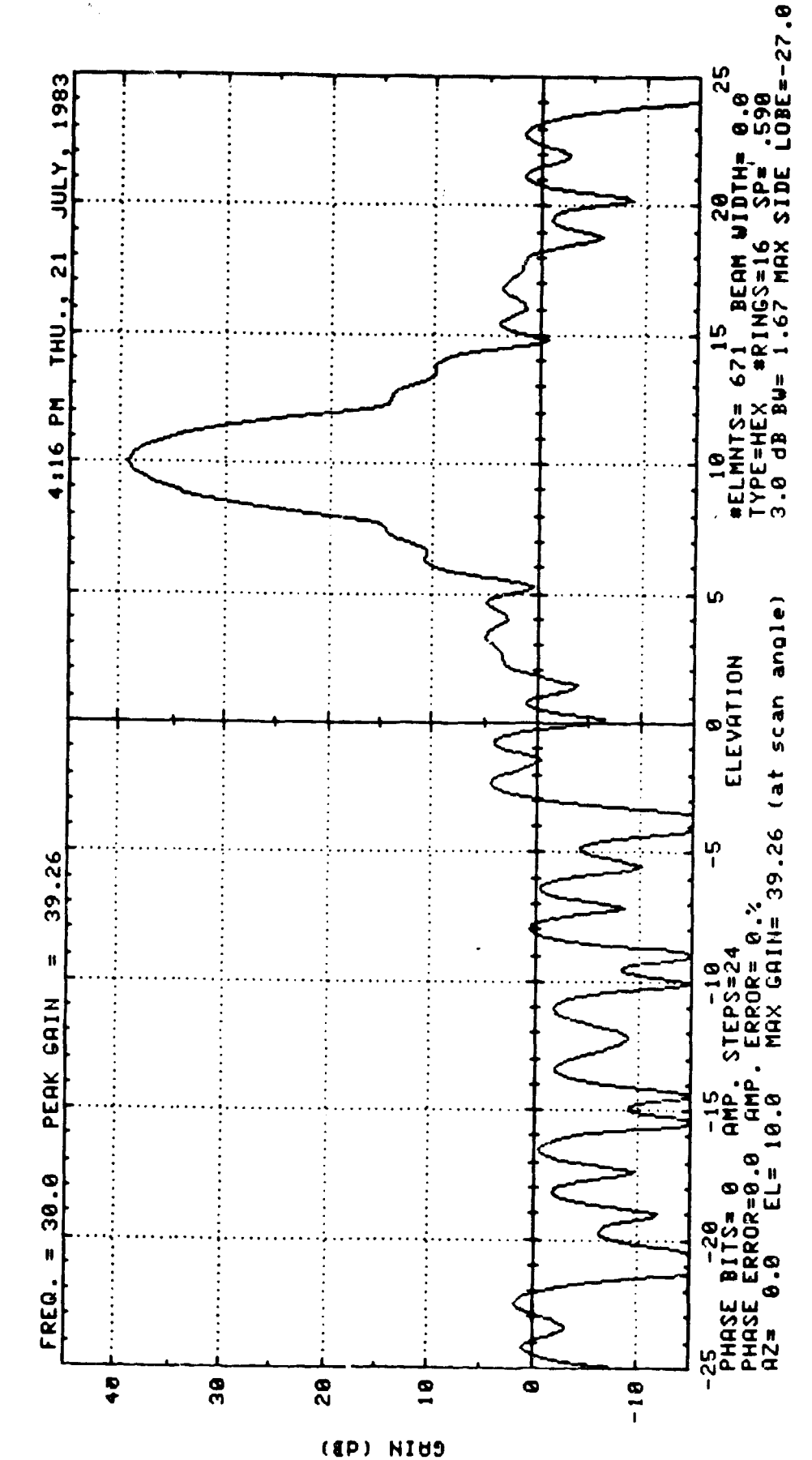

FIG 4.2-113 50 FAILURES

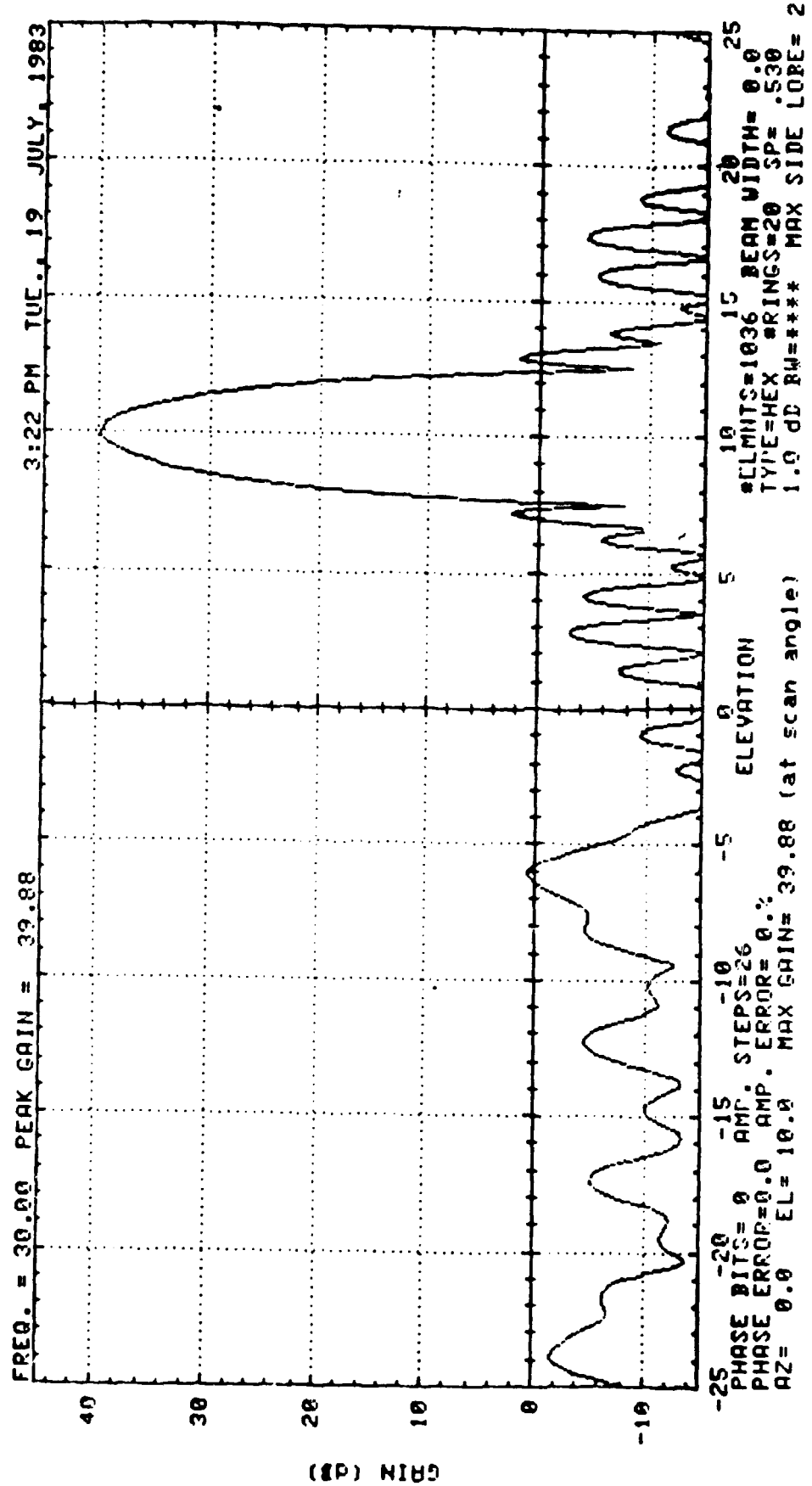

FIG. 4.2-114 3 FAILURES

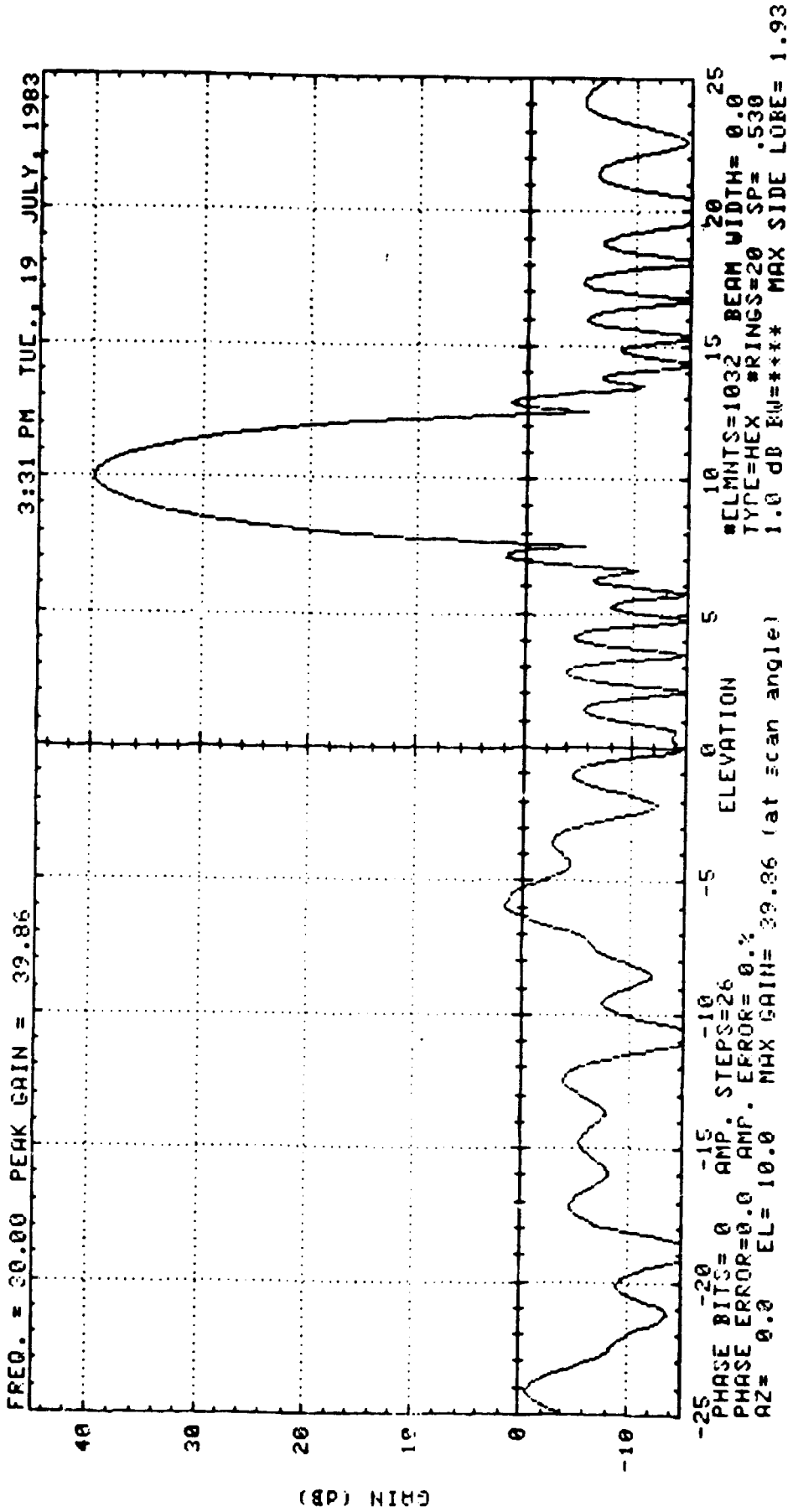

FIG. 4.2-115 7 FAILURES

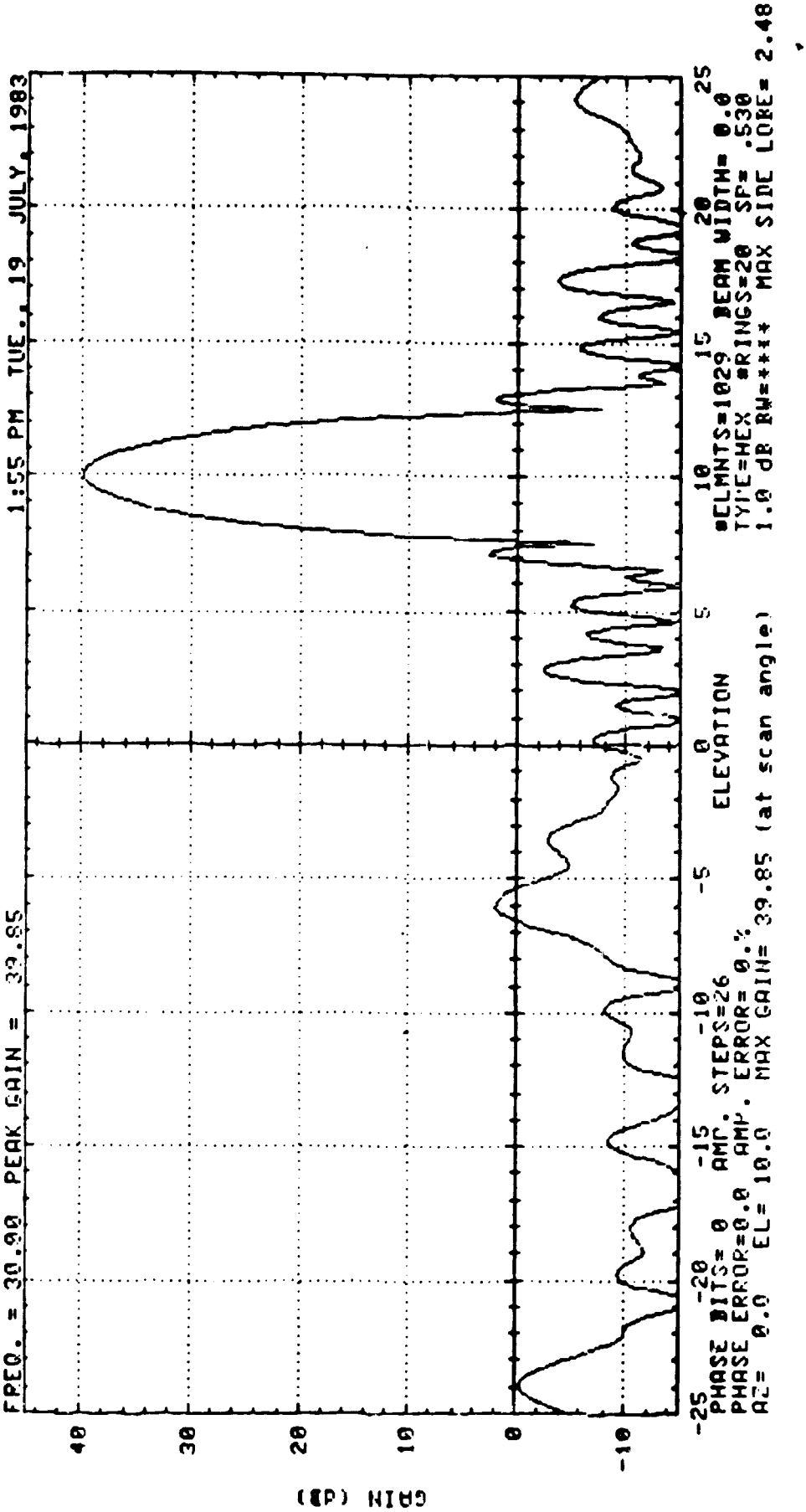

FIG. 4.2-116 10 FAILURES

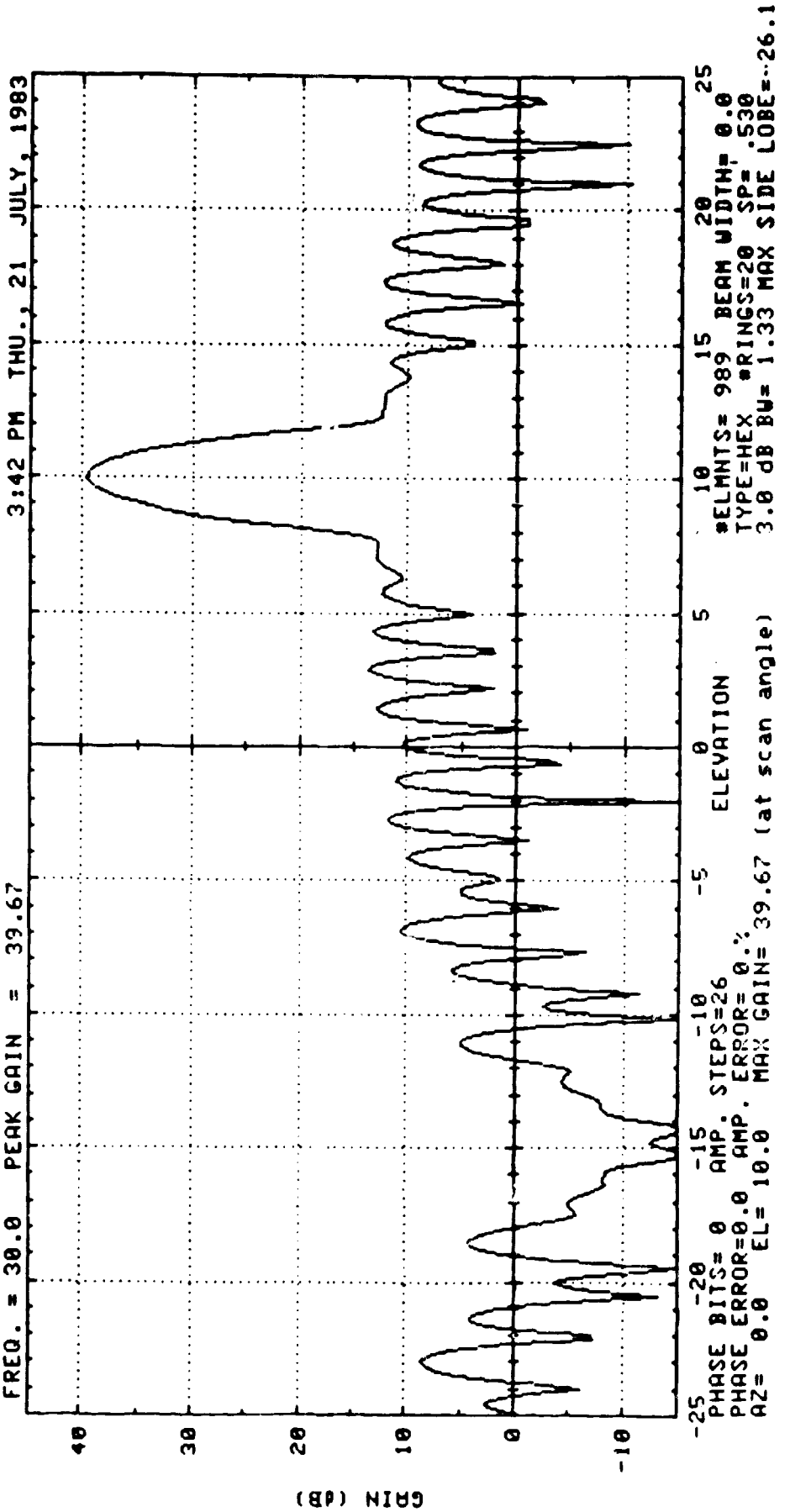

Fig 4.2-117 50 FAILURES

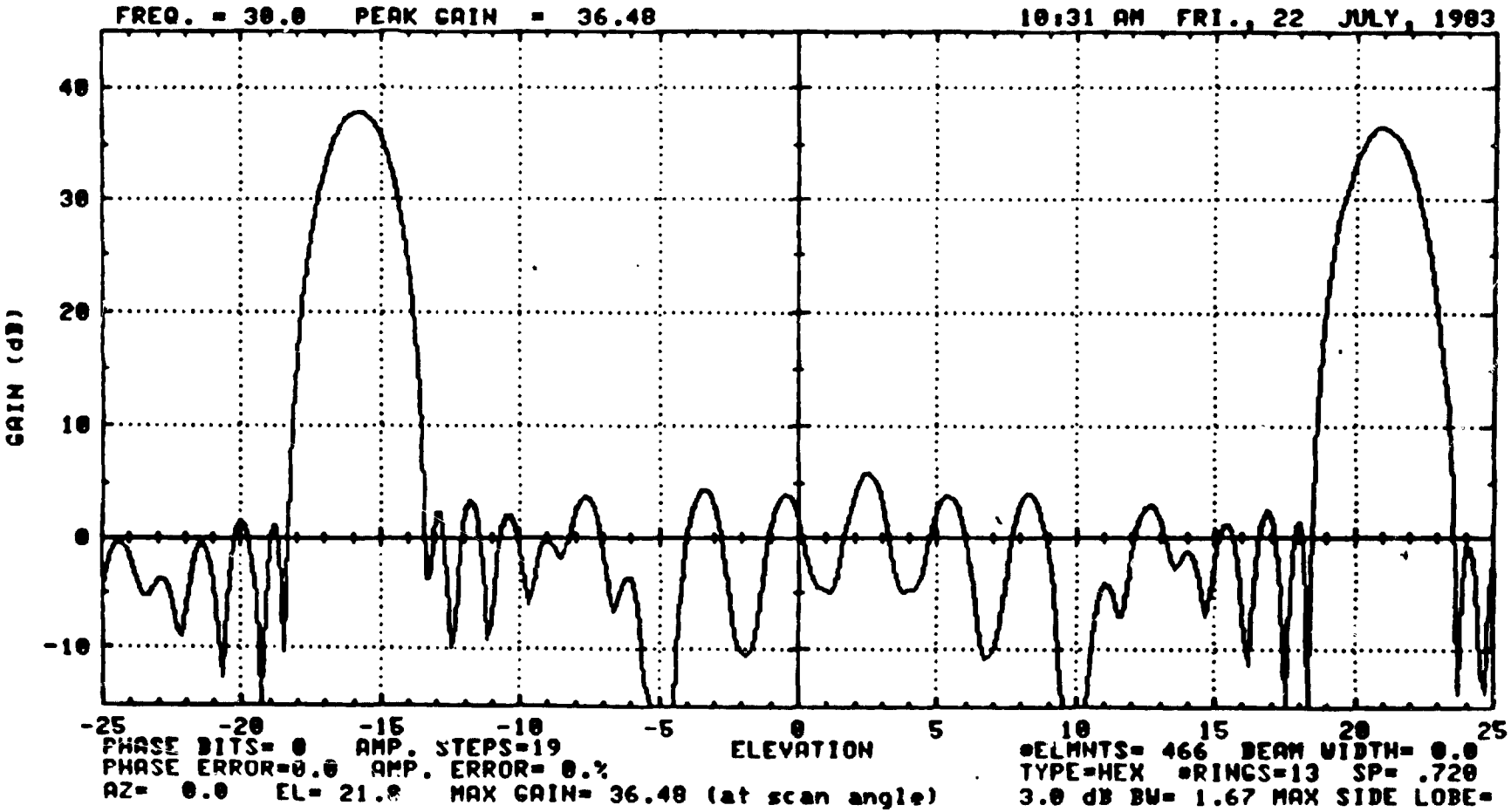

FIG. 4.2-118 3 FAILURES

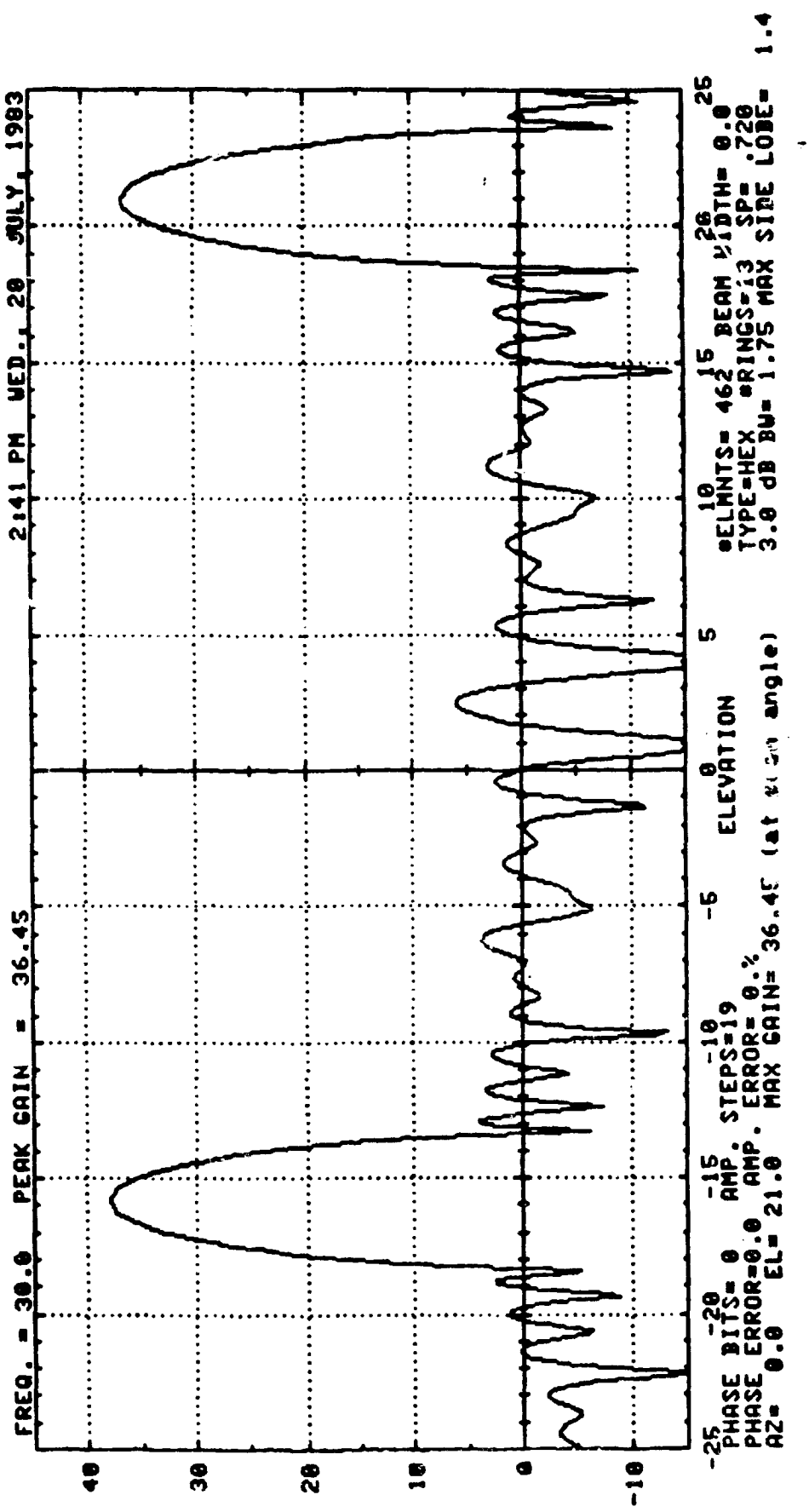

FIG 4.2-119 7 FAILURES

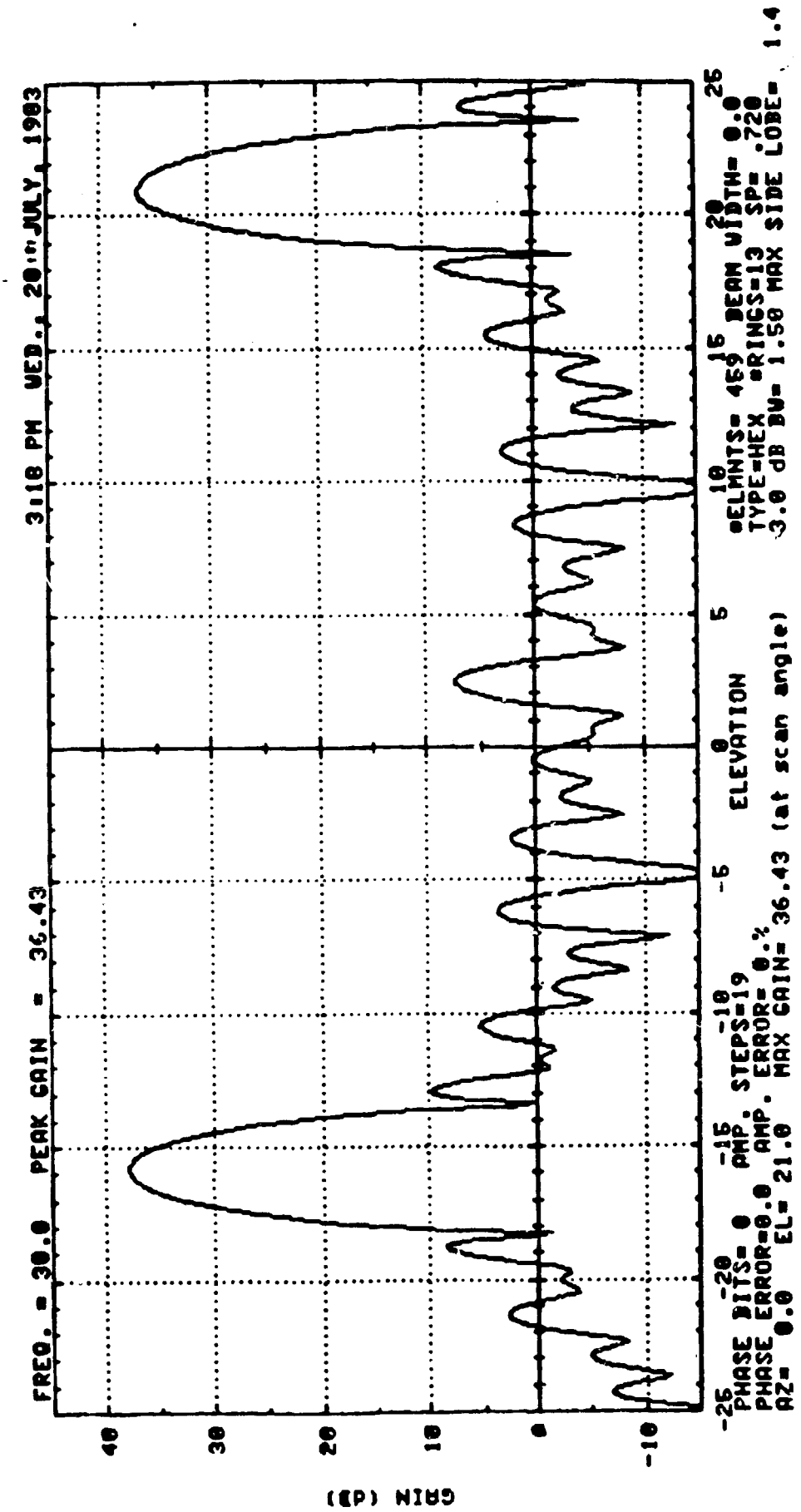

FIG. 42-120 10 FAILURES

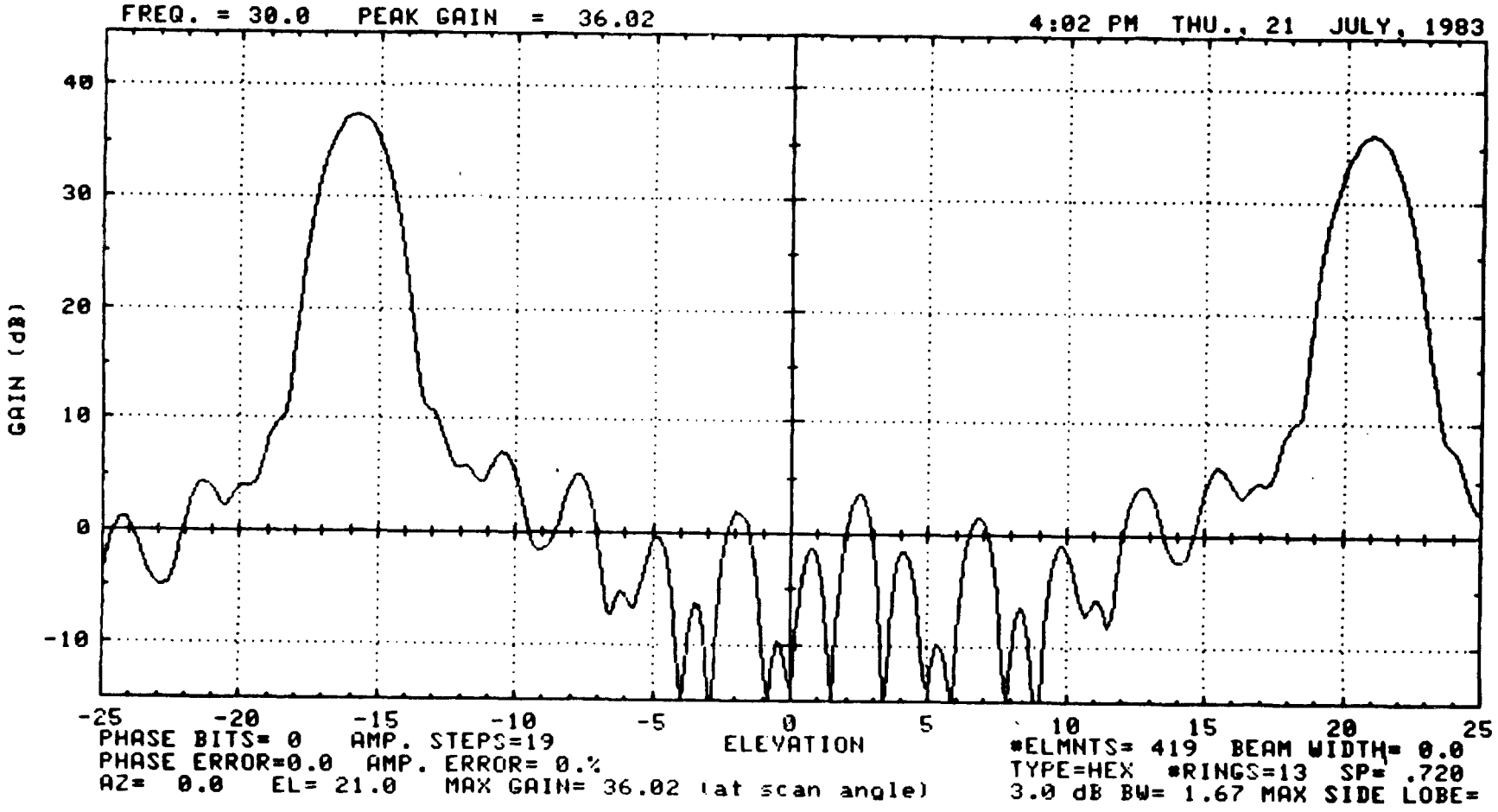

FIG 4.2-121 50 FAILURES

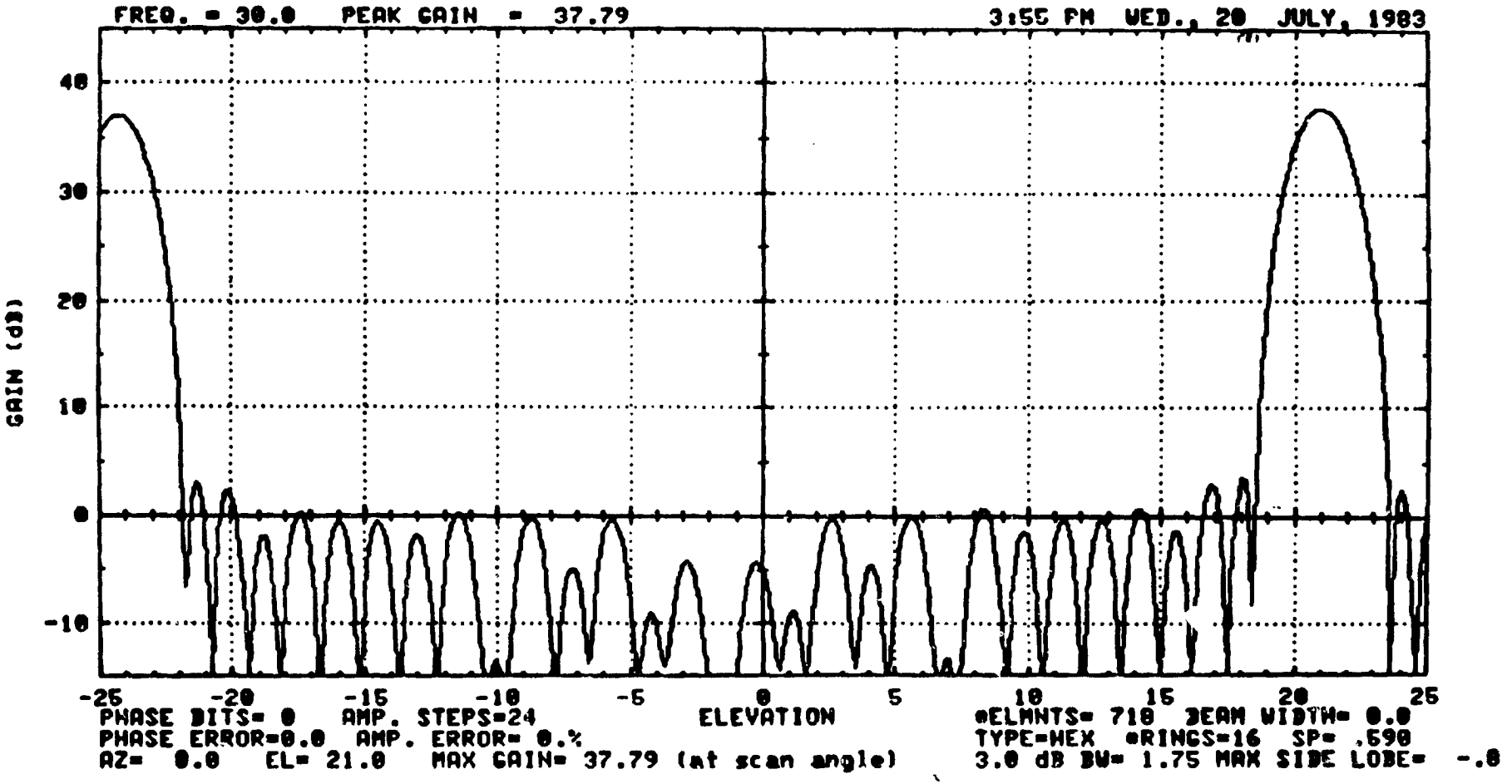

FIG 4.2-122 3 FAILURES

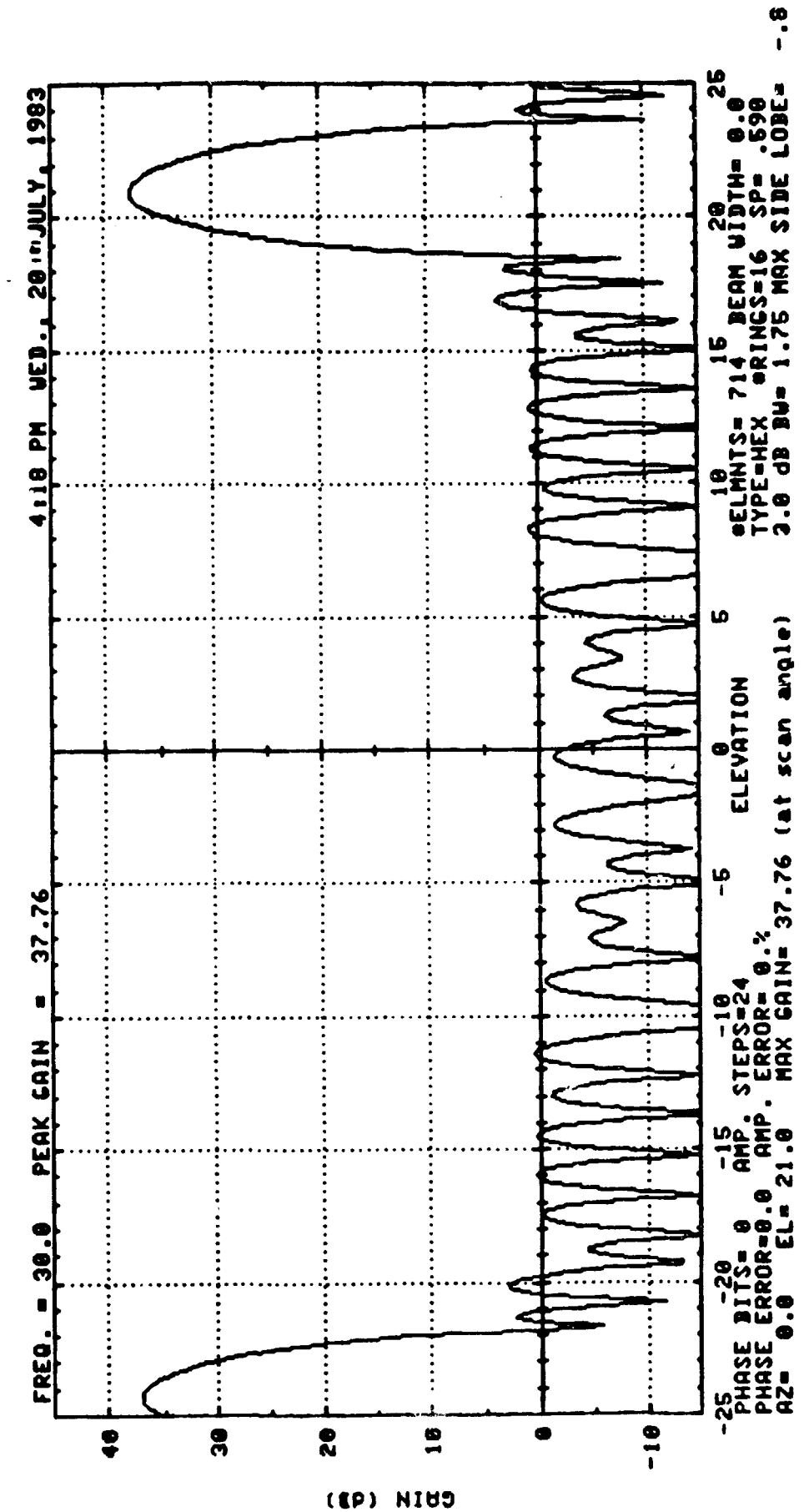

FIG 4.2-123 7 FAILURES

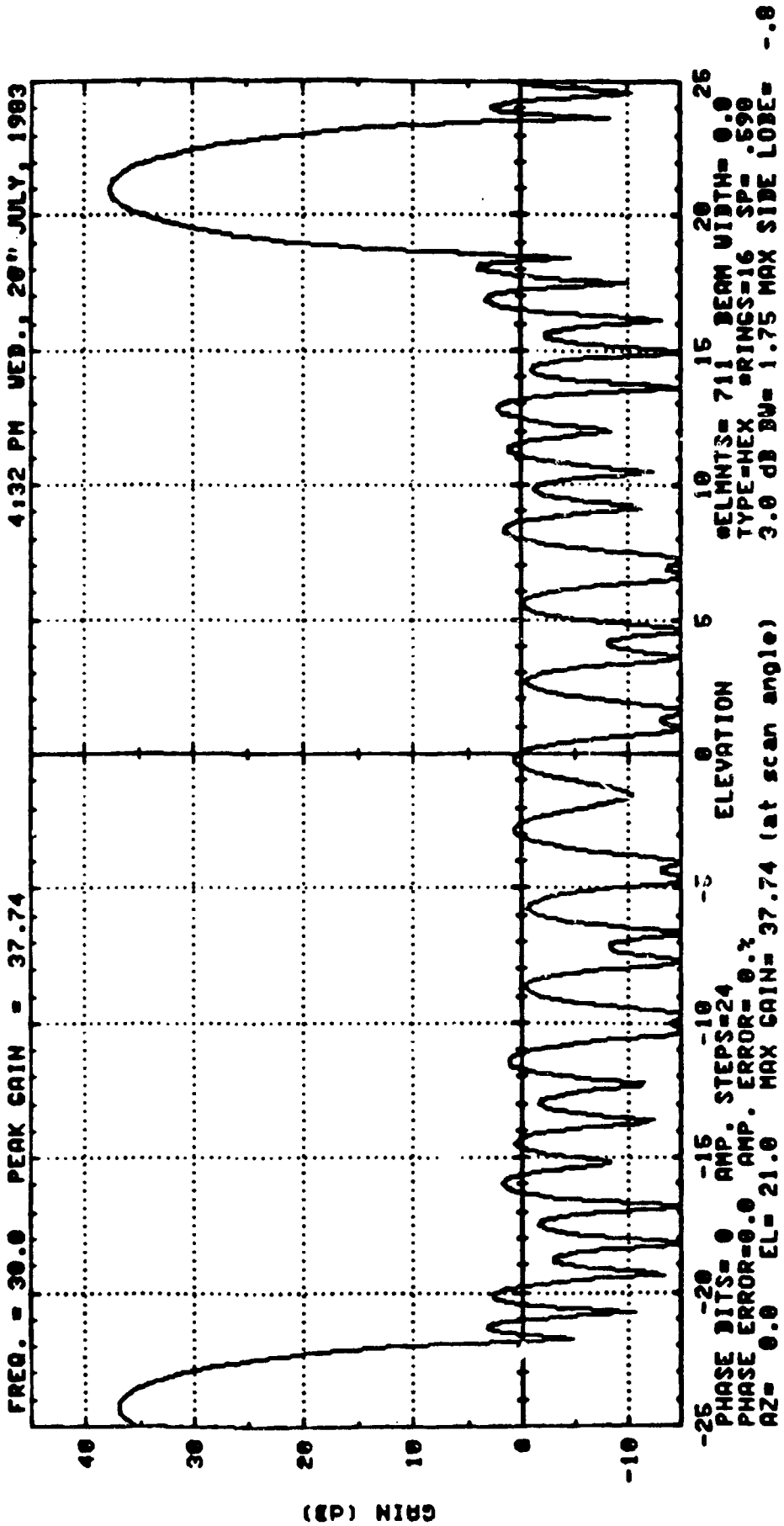

FIG. 4.2-124 10 FAILURES

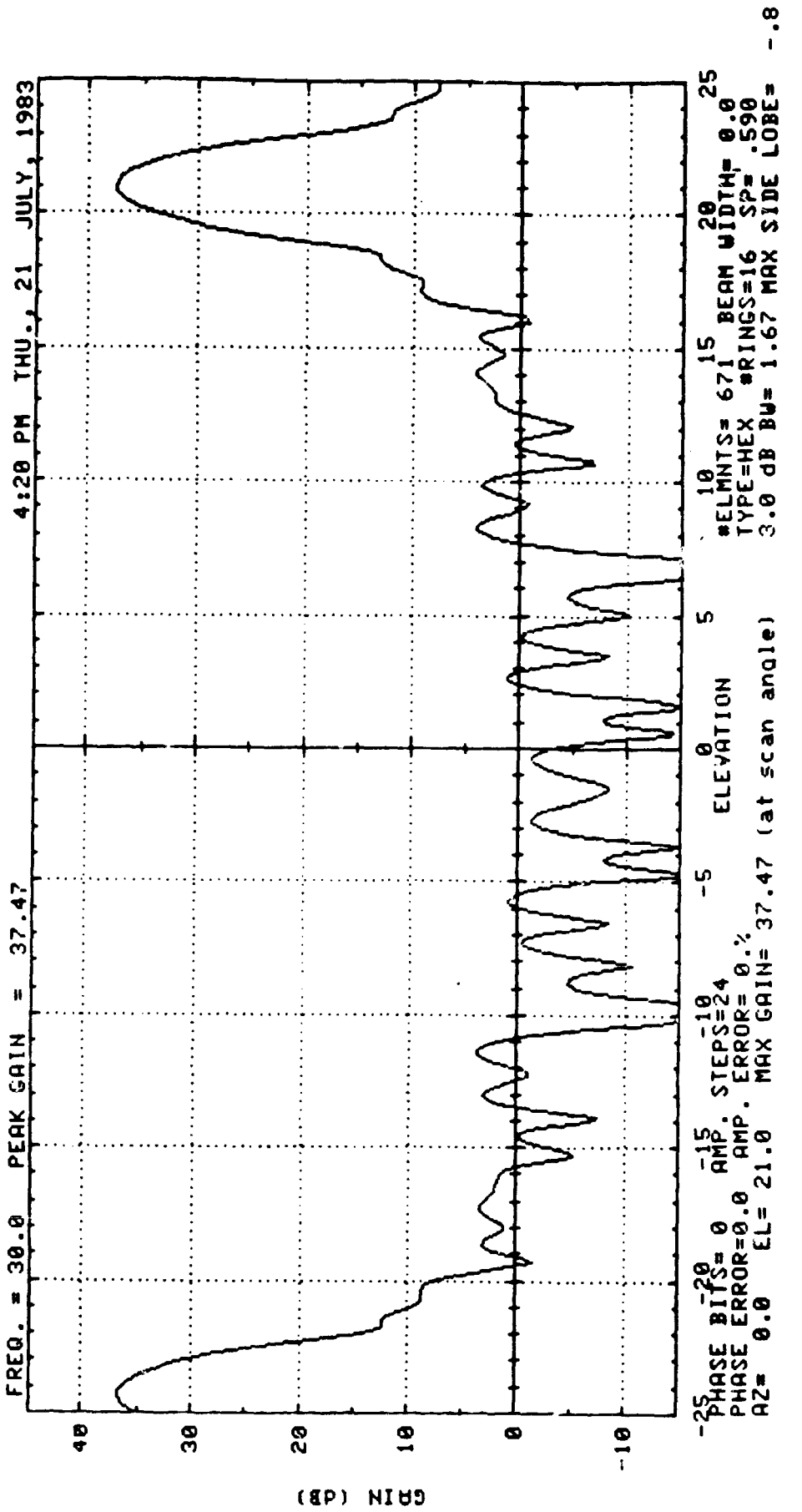

FIG. 4.2-125 50 FAILURES

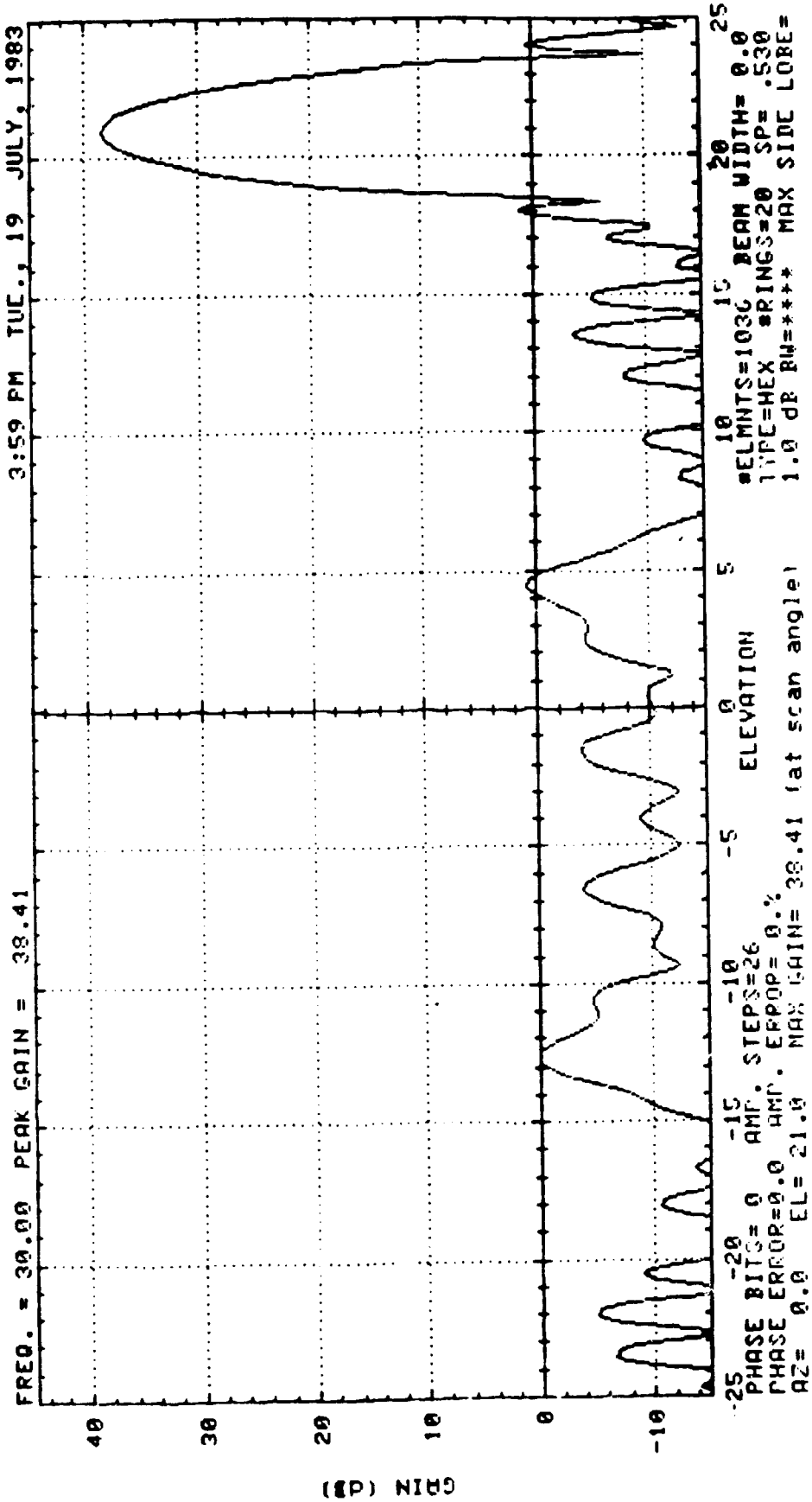

FIG. 4.2-126 3 FAILURES

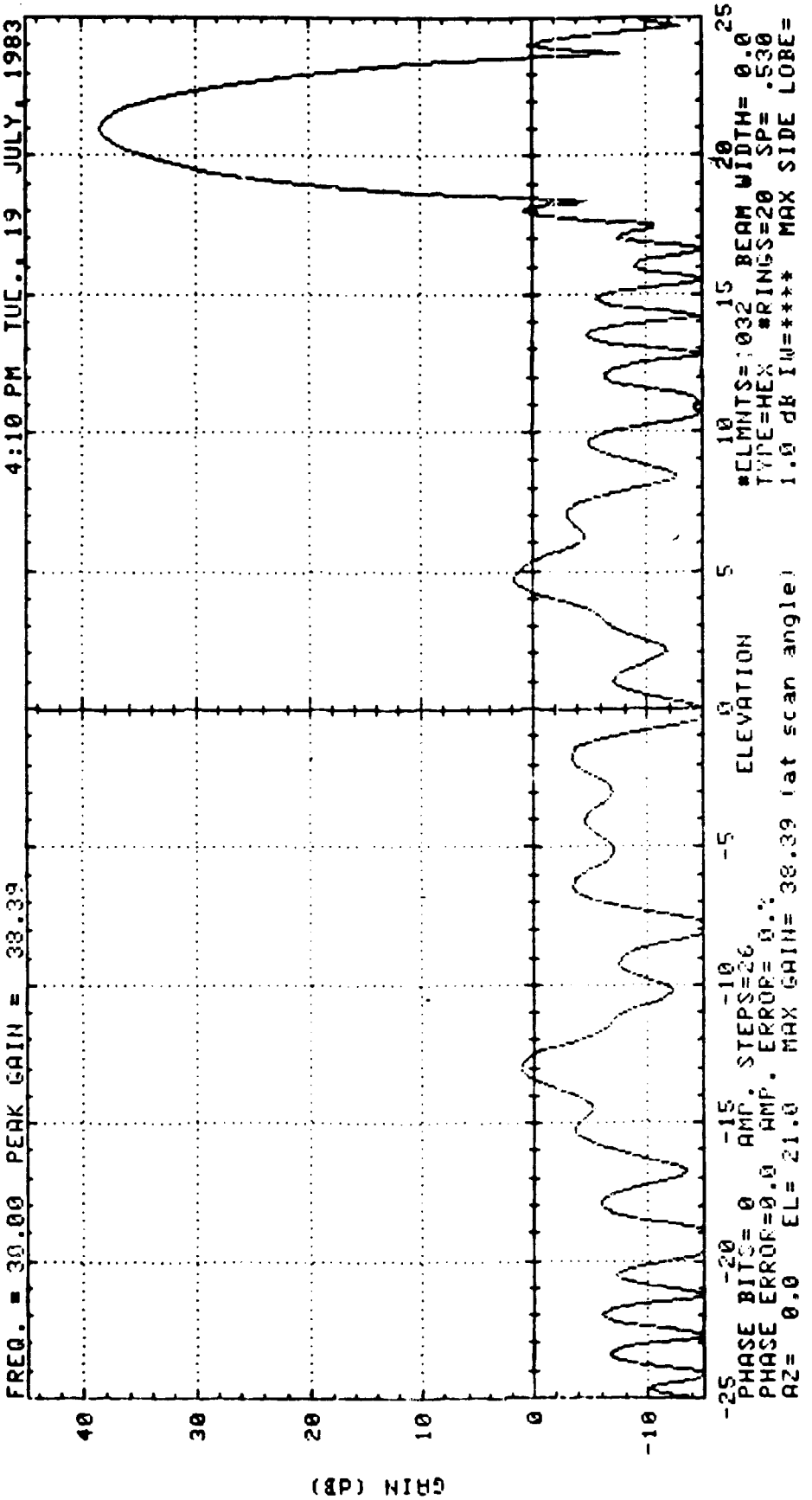

FIG 4.2-127 7 FAILURES

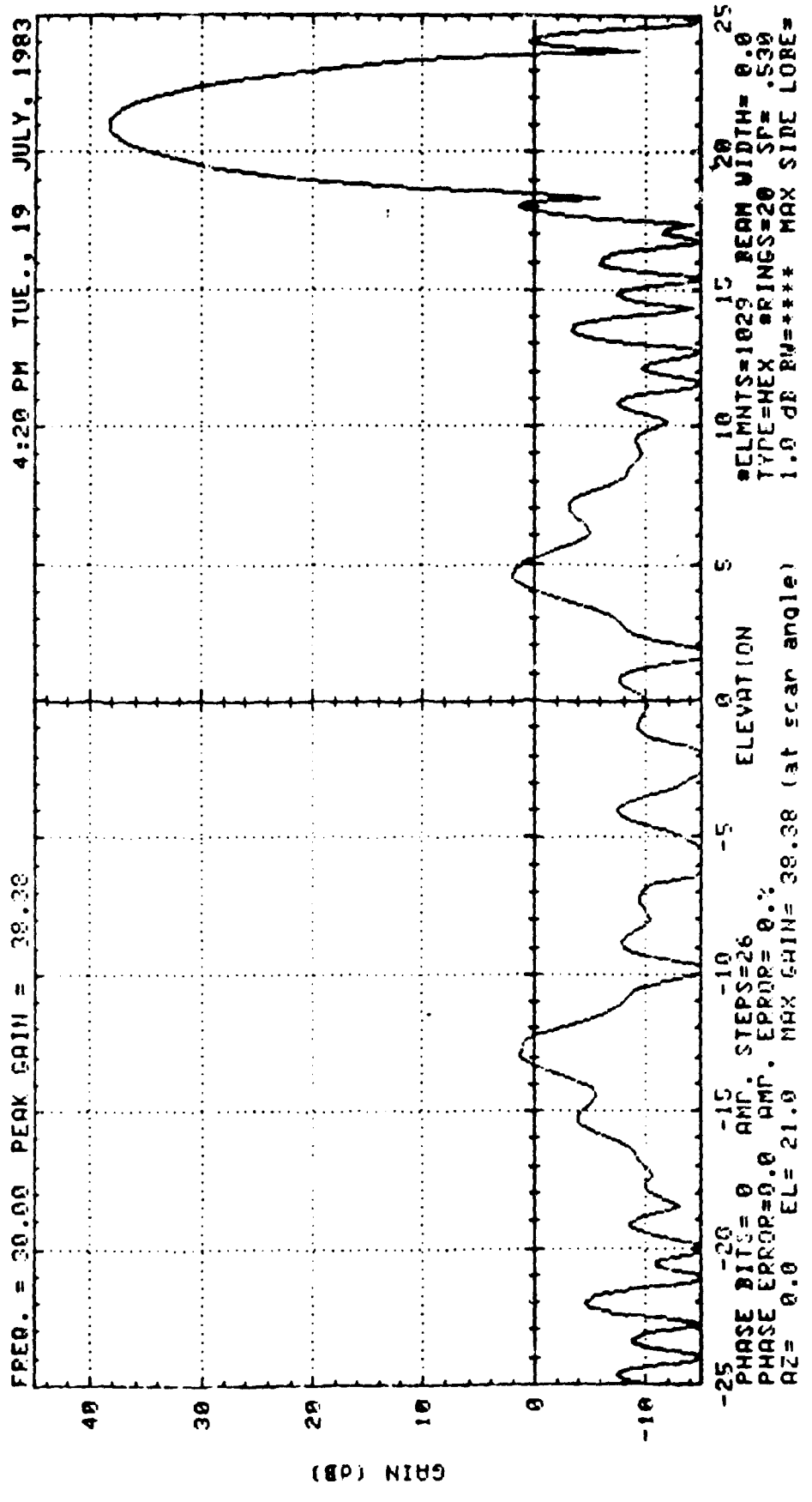

FIG 4.2-128 10 FAILURES

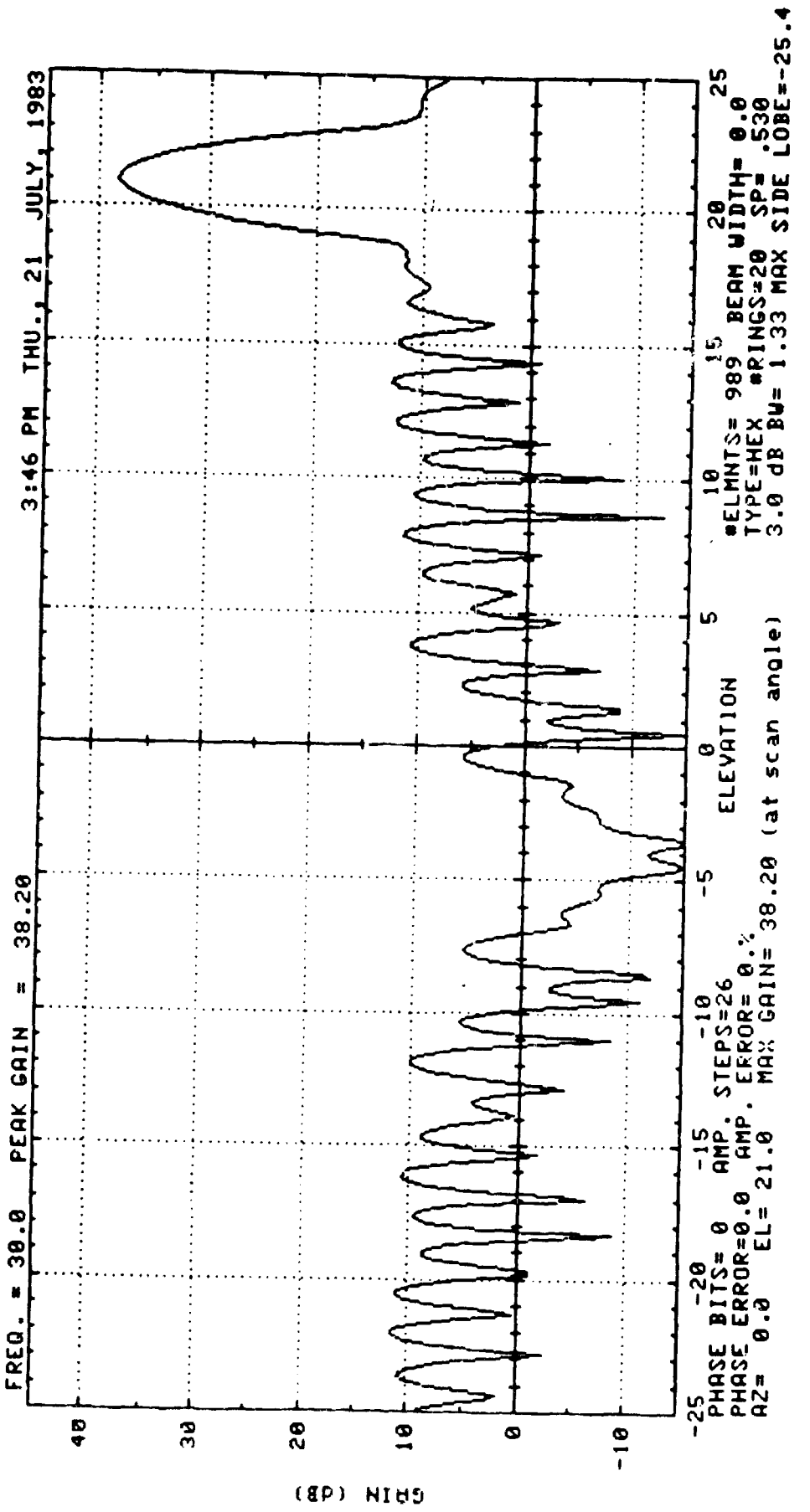

FIG 4.2-129 50 FAILURES

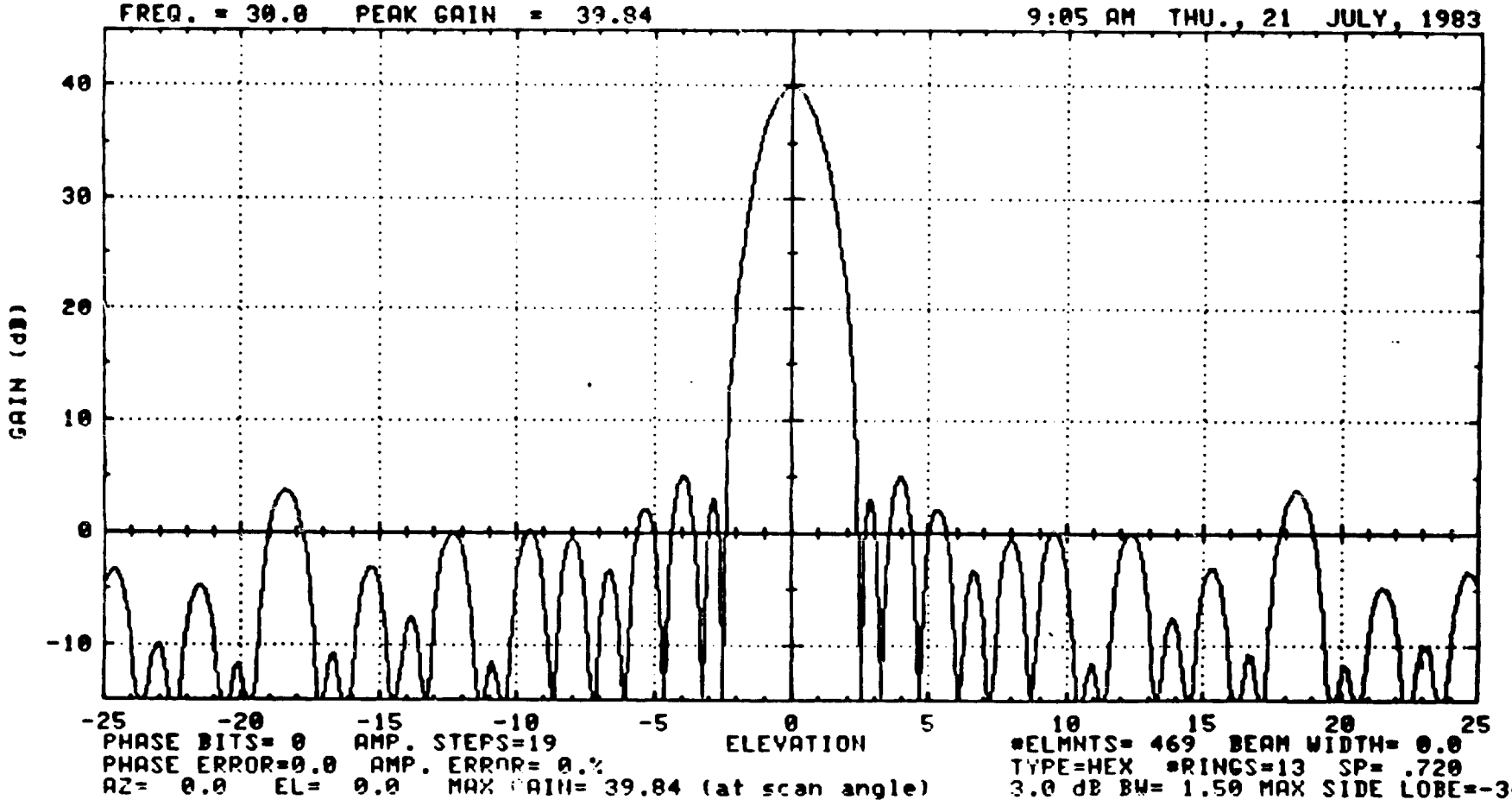
FREQ. = 30.0 PEAK GAIN = 39.84
9:05 AM THU., 21 JULY, 1983
GAIN (dB)
40
30
20
10
0
-10
-25 -20 -15 -10 -5 0 5 10 15 20 25
ELEVATION
PHASE BITS= 0 AMP. STEPS=19
PHASE ERROR=0.0 AMP. ERROR= 0.%
AZ= 0.0 EL= 0.0 MAX GAIN= 39.84 (at scan angle)
#ELMNTS= 469 BEAM WIDTH= 0.0
TYPE=HEX #RINGS=13 SP= .720
3.0 dB BW= 1.50 MAX SIDE LOBE=-34.9

FIG. 4.3-7

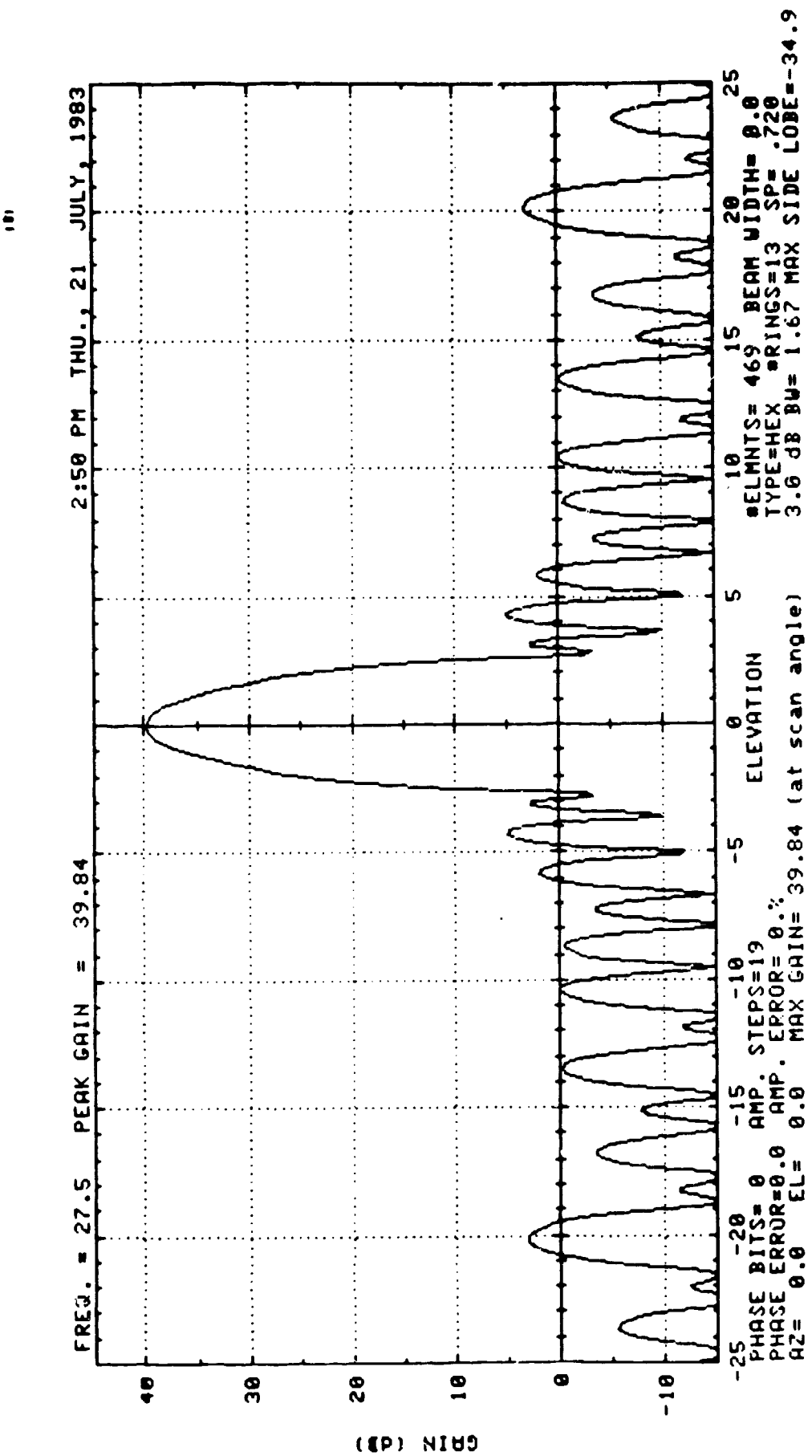
FREQ. = 27.5 PEAK GAIN = 39.84
2:50 PM THU., 21 JULY, 1983
GAIN (dB)
40
30
20
10
0
-10
-25 -20 -15 -10 -5 0 5 10 15 20 25
ELEVATION
PHASE BITS= 0 AMP. STEPS=19
PHASE ERROR=0.0 AMP. ERROR= 0.%
AZ= 0.0 EL= 0.0 MAX GAIN= 39.84 (at scan angle)
#ELMNTS= 469 BEAM WIDTH= 0.0
TYPE=HEX #RINGS=13 SP= .720
3.0 dB BW= 1.67 MAX SIDE LOBE=-34.9

FIG 43-8

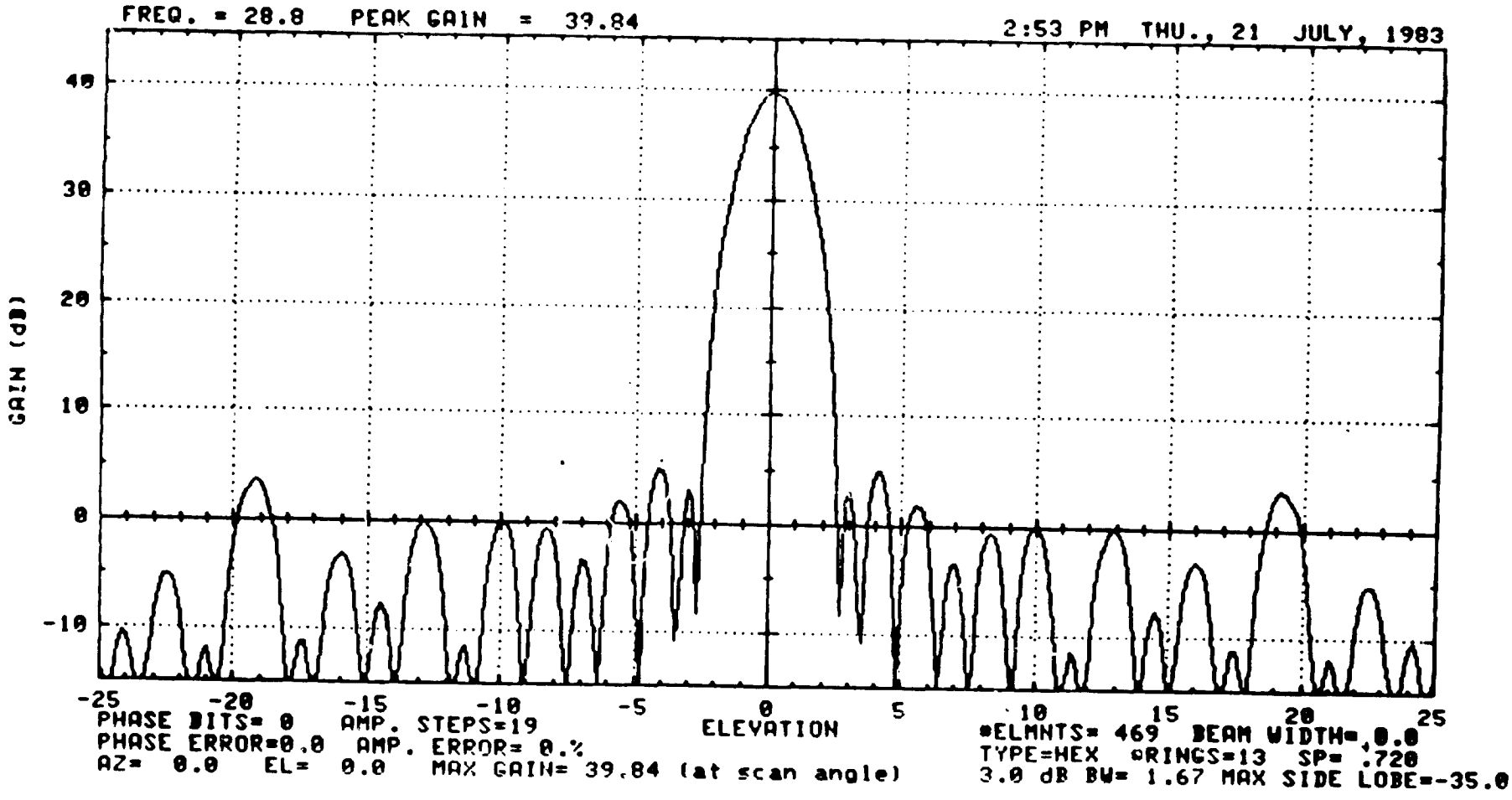
FREQ. = 28.8 PEAK GAIN = 39.84
2:53 PM THU., 21 JULY, 1983
GAIN (dB)
40
30
20
10
0
-10
-25 -20 -15 -10 -5 0 5 10 15 20 25
ELEVATION
PHASE BITS= 0 AMP. STEPS=19
PHASE ERROR=0.0 AMP. ERROR= 0.%
AZ= 0.0 EL= 0.0 MAX GAIN= 39.84 (at scan angle)
#ELMNTS= 469 BEAM WIDTH= 0.0
TYPE=HEX #RINGS=13 SP= .720
3.0 dB BW= 1.67 MAX SIDE LOBE=-35.0

FIG 4.3-9

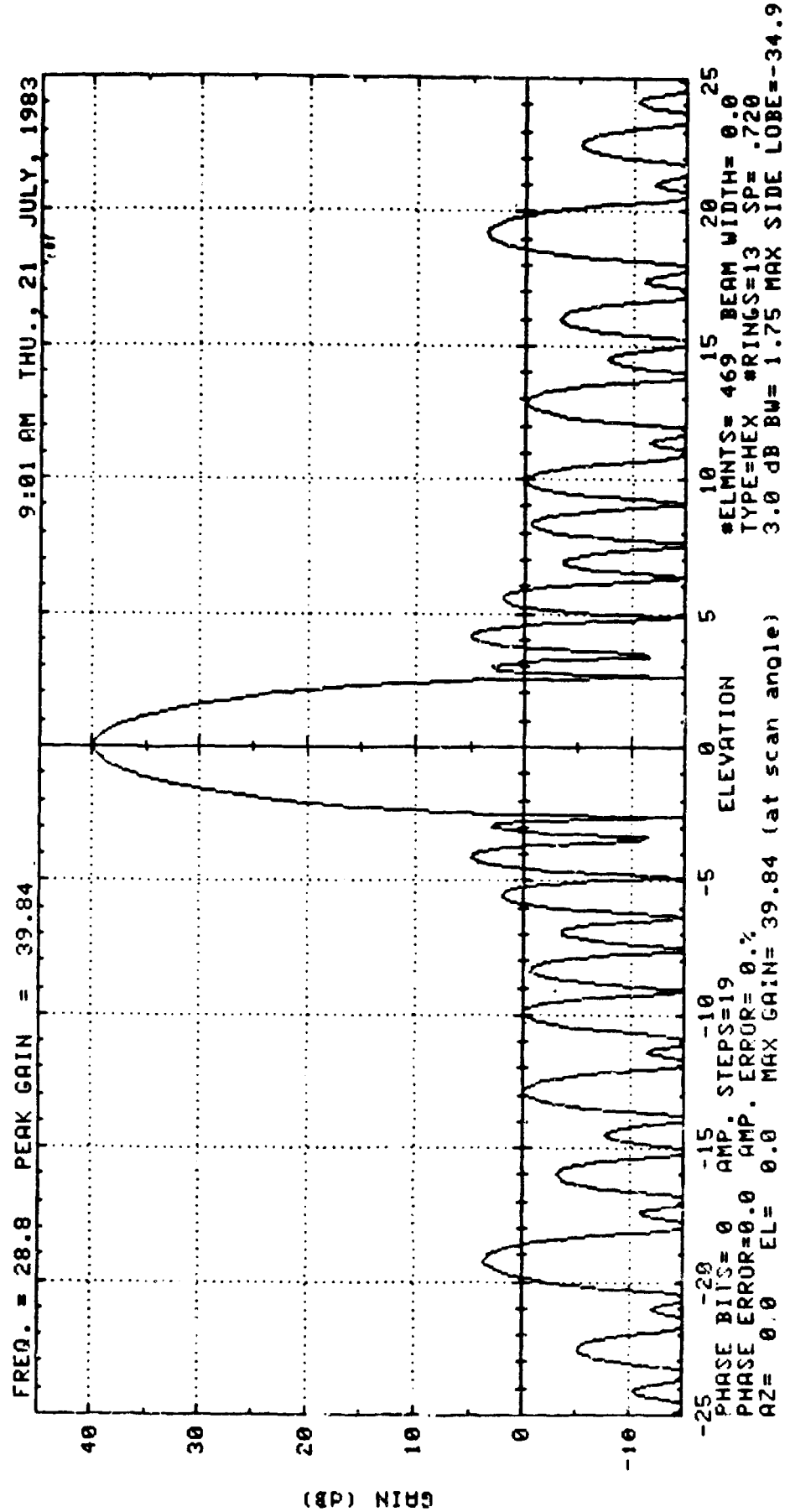
FREQ. = 28.8 PEAK GAIN = 39.84
9:01 AM THU., 21 JULY, 1983
GAIN (dB)
40
30
20
10
0
-10
-25 -20 -15 -10 -5 0 5 10 15 20 25
ELEVATION
PHASE BITS= 0 AMP. STEPS=19
PHASE ERROR=0.0 AMP. ERROR= 0.%
AZ= 0.0 EL= 0.0 MAX GAIN= 39.84 (at scan angle)
*ELMNTS= 469 BEAM WIDTH= 0.0
TYPE=HEX *RINGS=13 SP= .720
3.0 dB BW= 1.75 MAX SIDE LOBE=-34.9

Fig. 4.3-10

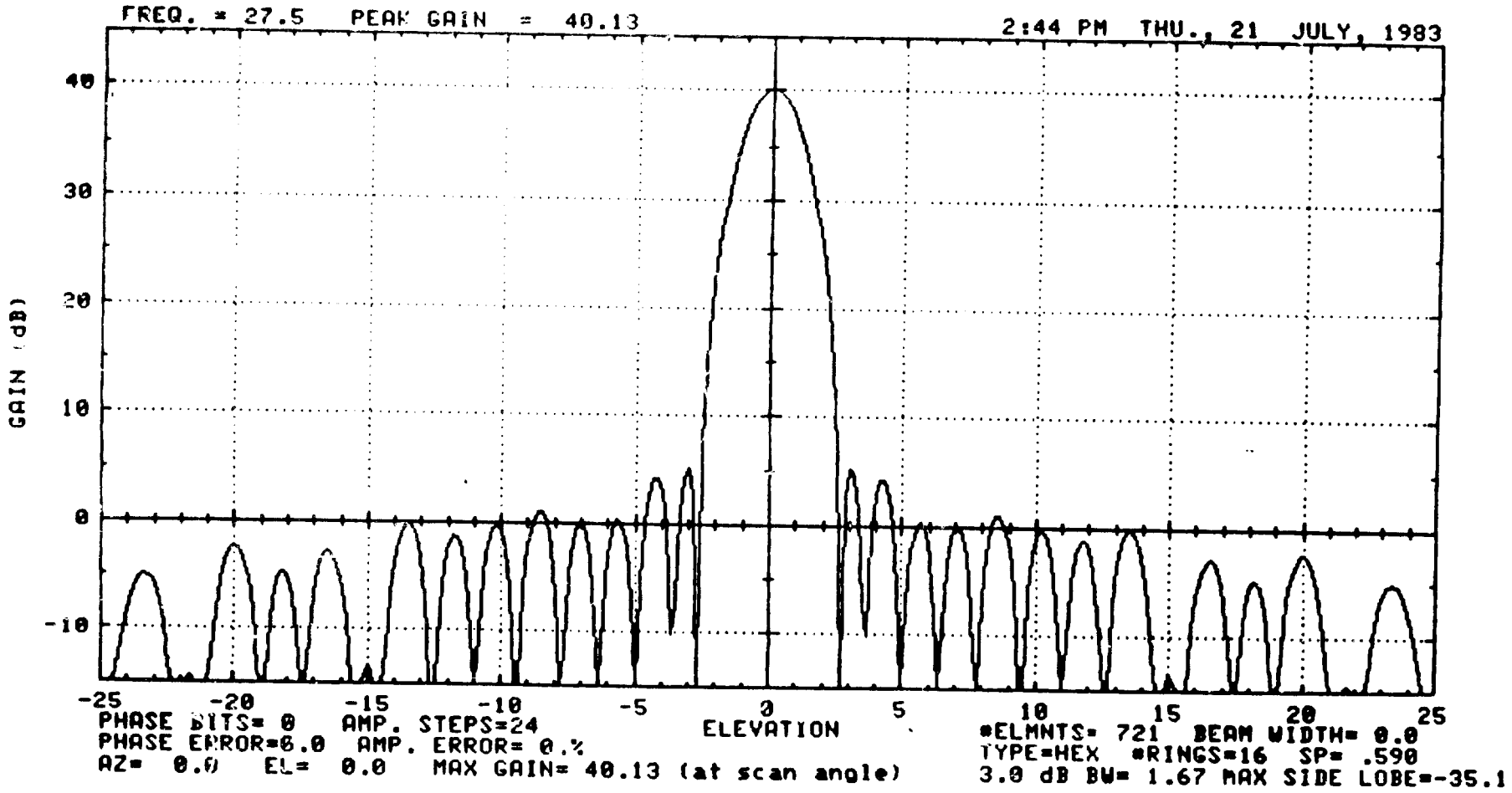
FREQ. = 27.5 PEAK GAIN = 40.13
2:44 PM THU., 21 JULY, 1983
GAIN (dB)
40
30
20
10
0
-10
-25 -20 -15 -10 -5 0 5 10 15 20 25
ELEVATION
PHASE BITS= 0 AMP. STEPS=24
PHASE ERROR=0.0 AMP. ERROR= 0.%
AZ= 0.0 EL= 0.0 MAX GAIN= 40.13 (at scan angle)
#ELMNTS= 721 BEAM WIDTH= 0.0
TYPE=HEX #RINGS=16 SP= .590
3.0 dB BW= 1.67 MAX SIDE LOBE=-35.1

FIG. 4.3-11

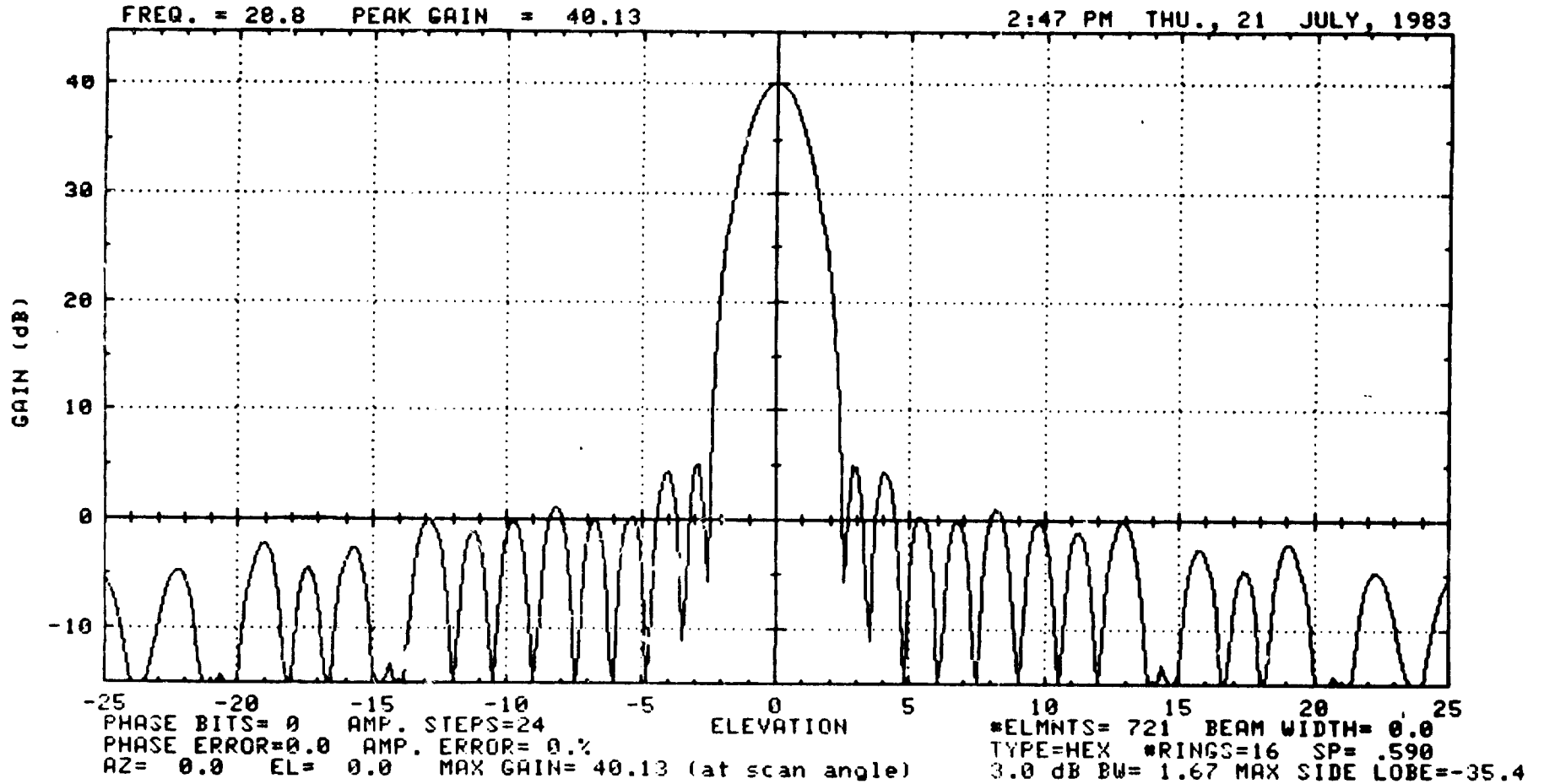
FREQ. = 28.8 PEAK GAIN = 40.13
2:47 PM THU., 21 JULY, 1983
GAIN (dB)
40
30
20
10
0
-10
-25 -20 -15 -10 -5 0 5 10 15 20 25
ELEVATION
PHASE BITS= 0 AMP. STEPS=24
PHASE ERROR=0.0 AMP. ERROR= 0.%
AZ= 0.0 EL= 0.0 MAX GAIN= 40.13 (at scan angle)
#ELMNTS= 721 BEAM WIDTH= 0.0
TYPE=HEX #RINGS=16 SP= .590
3.0 dB BW= 1.67 MAX SIDE LOBE=-35.4

FIG. 4.3-12

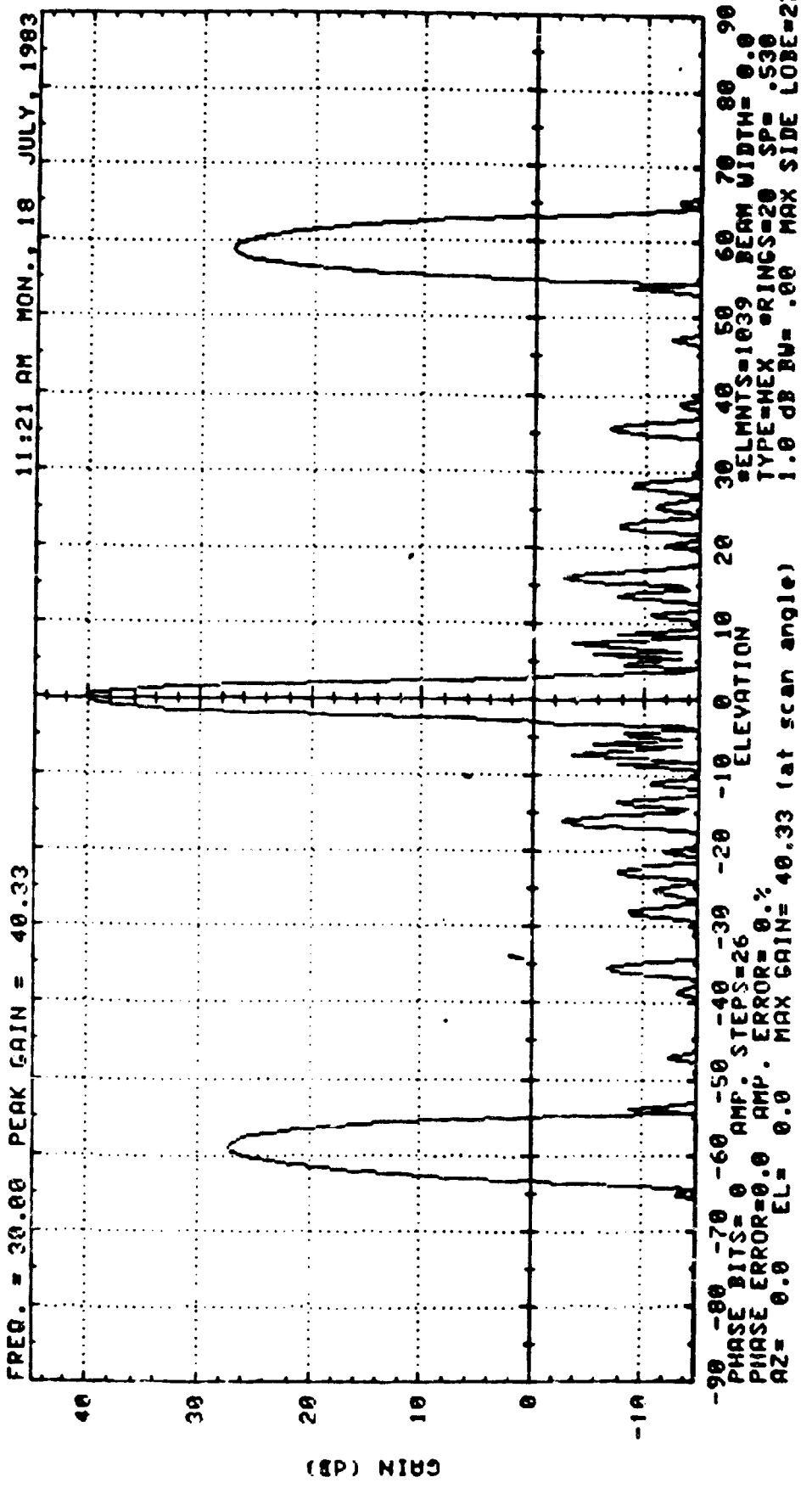
FREQ. = 30.00 PEAK GAIN = 40.33
11:21 AM MON., 18 JULY, 1983
GAIN (dB)
40
30
20
10
0
-10
-90 -80 -70 -60 -50 -40 -30 -20 -10 0 10 20 30 40 50 60 70 80 90
ELEVATION
PHASE BITS= 0 AMP. STEPS=26 *ELMNTS=1039 BEAM WIDTH= 0.0
PHASE ERROR=0.0 AMP. ERROR= 0.% TYPE=HEX *RINGS=20 SP= .530
AZ= 0.0 EL= 0.0 MAX GAIN= 40.33 (at scan angle) 1.0 dB BW= .00 MAX SIDE LOBE=27.26

FIG 4.3-13

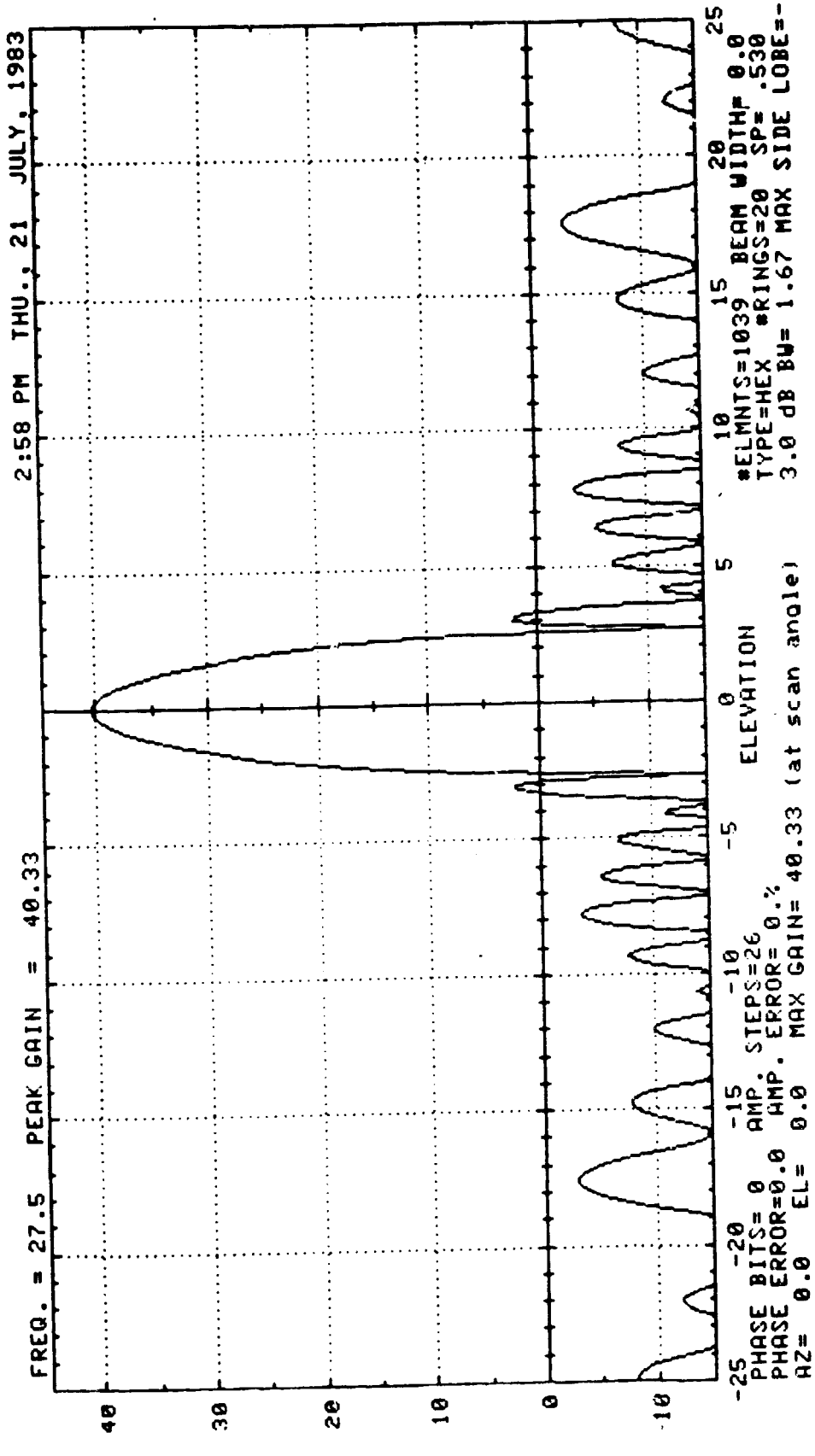
FREQ. = 27.5 PEAK GAIN = 40.33
2:58 PM THU., 21 JULY, 1983
GAIN (dB)
40
30
20
10
0
-10
-25 -20 -15 -10 -5 0 5 10 15 20 25
ELEVATION
PHASE BITS= 0 AMP. STEPS=26
PHASE ERROR=0.0 AMP. ERROR= 0.%
AZ= 0.0 EL= 0.0 MAX GAIN= 40.33 (at scan angle)
#ELMNTS=1039 BEAM WIDTH= 0.0
TYPE=HEX #RINGS=20 SP= .530
3.0 dB BW= 1.67 MAX SIDE LOBE=-38.1

FIG. 4.3-14

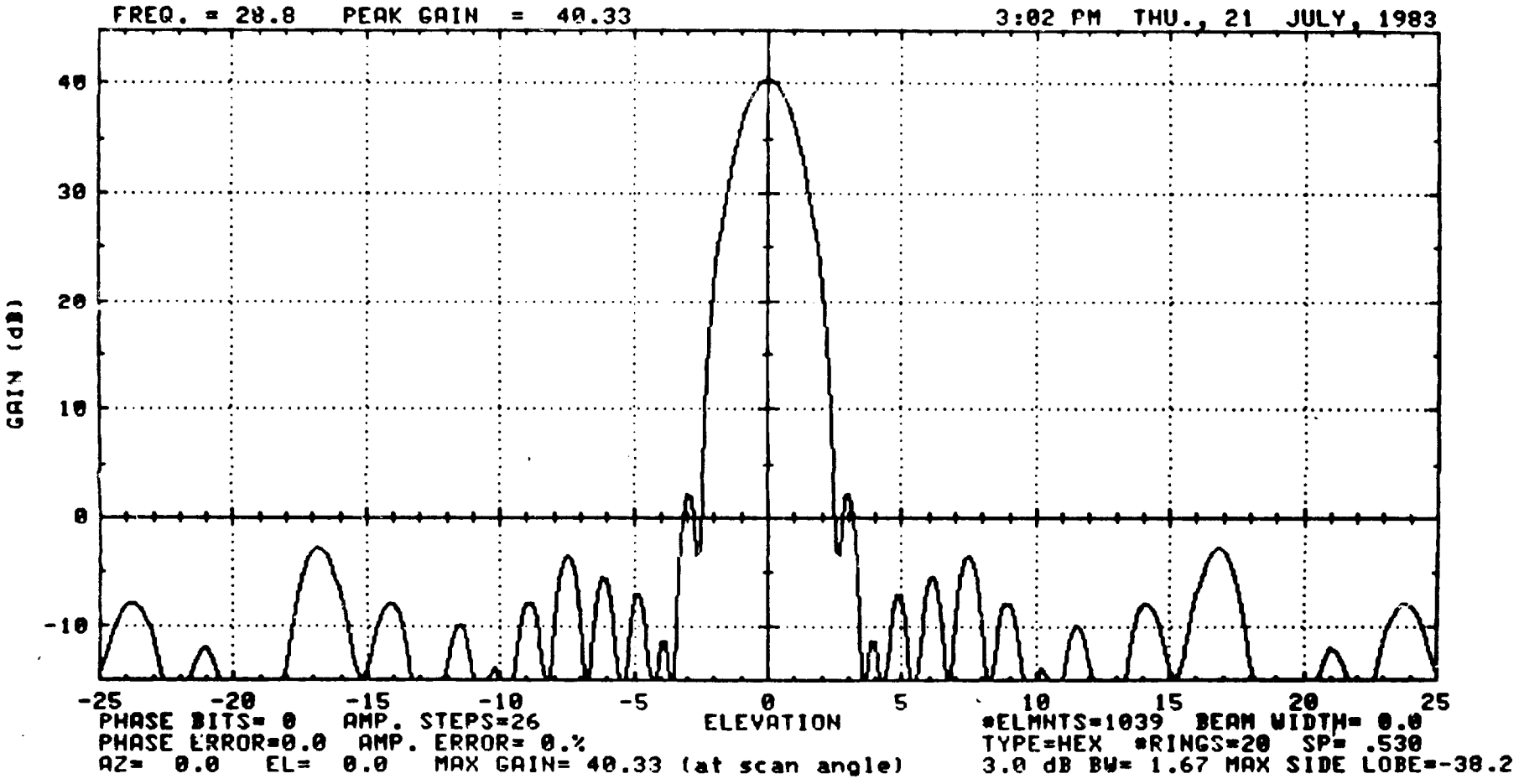
FREQ. = 28.8 PEAK GAIN = 40.33
3:02 PM THU., 21 JULY, 1983
GAIN (dB)
40
30
20
10
0
-10
-25 -20 -15 -10 -5 0 5 10 15 20 25
ELEVATION
PHASE BITS= 0 AMP. STEPS=26
PHASE ERROR=0.0 AMP. ERROR= 0.%
AZ= 0.0 EL= 0.0 MAX GAIN= 40.33 (at scan angle)
#ELMNTS=1039 BEAM WIDTH= 0.0
TYPE=HEX #RINGS=20 SP= .530
3.0 dB BW= 1.67 MAX SIDE LOBE=-38.2

FIG. 4.3-15

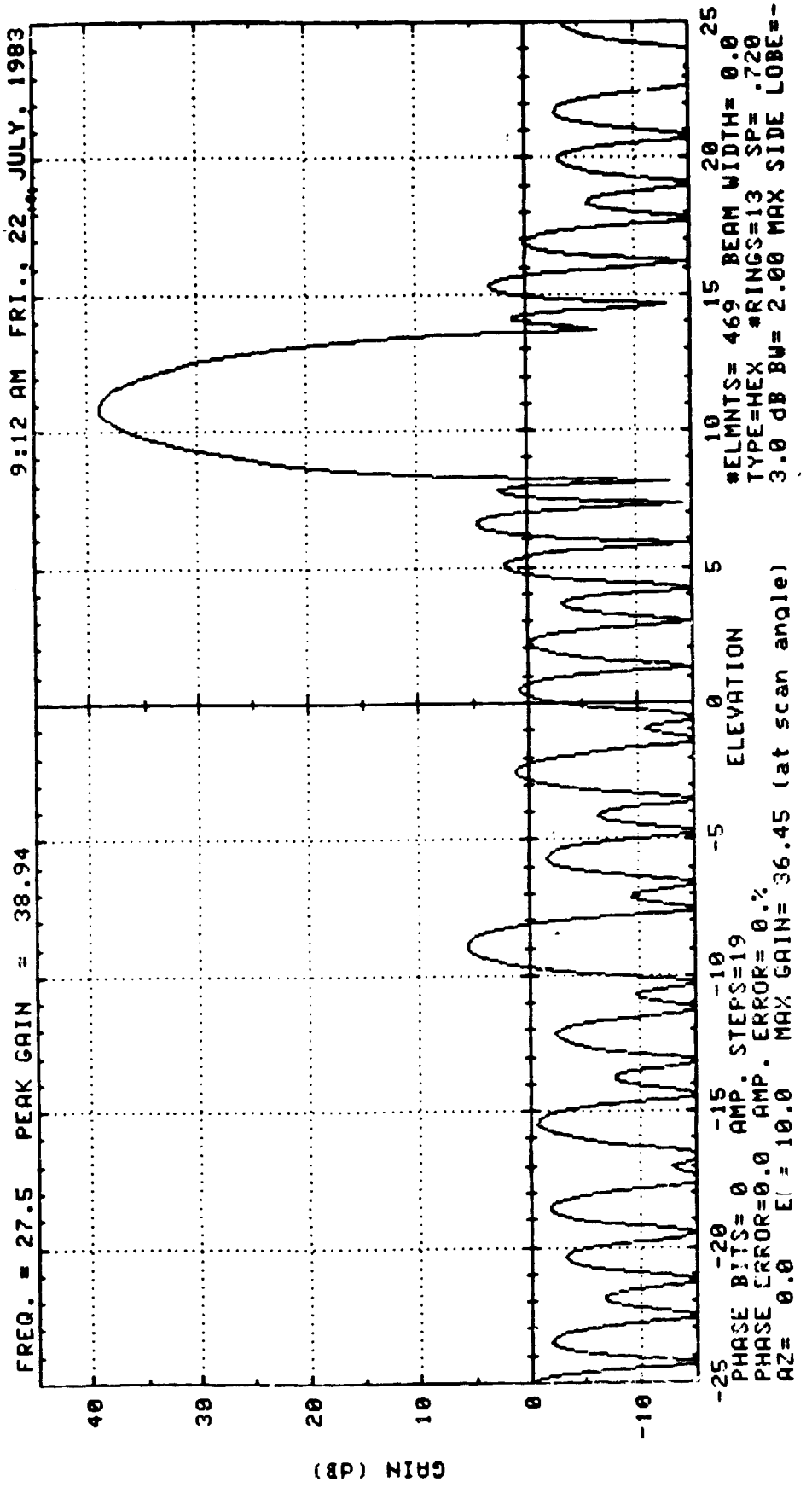
FREQ. = 27.5 PEAK GAIN = 38.94
9:12 AM FRI., 22 JULY, 1983
GAIN (dB)
40
30
20
10
0
-10
-25 -20 -15 -10 -5 0 5 10 15 20 25
ELEVATION
PHASE BITS= 0 AMP. STEPS=19
PHASE ERROR=0.0 AMP. ERROR= 0.%
AZ= 0.0 EL= 10.0 MAX GAIN= 36.45 (at scan angle)
*ELMNTS= 469 BEAM WIDTH= 0.0
TYPE=HEX *RINGS=13 SP= .720
3.0 dB BW= 2.00 MAX SIDE LOBE=-16.3

FIG. 4.3-16

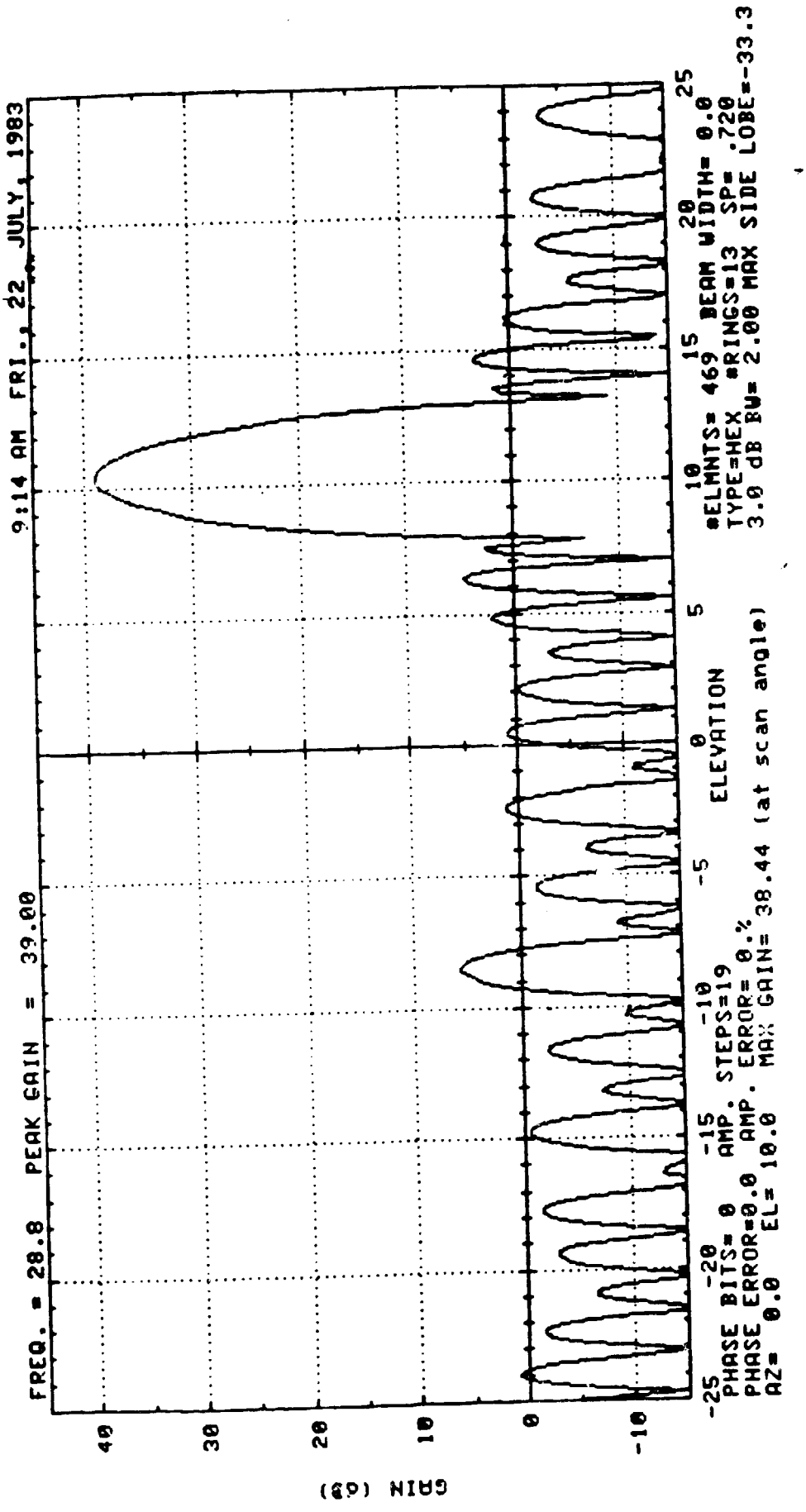
FREQ. = 28.8 PEAK GAIN = 39.00
9:14 AM FRI., 22 JULY, 1983
GAIN (dB)
40
30
20
10
0
-10
-25 -20 -15 -10 -5 0 5 10 15 20 25
ELEVATION
PHASE BITS= 0 AMP. STEPS=19
PHASE ERROR=0.0 AMP. ERROR= 0.%
AZ= 0.0 EL= 10.0 MAX GAIN= 38.44 (at scan angle)
#ELMNTS= 469 BEAM WIDTH= 0.0
TYPE=HEX #RINGS=13 SP= .720
3.0 dB BW= 2.00 MAX SIDE LOBE=-33.3

FIG. 4.3-17

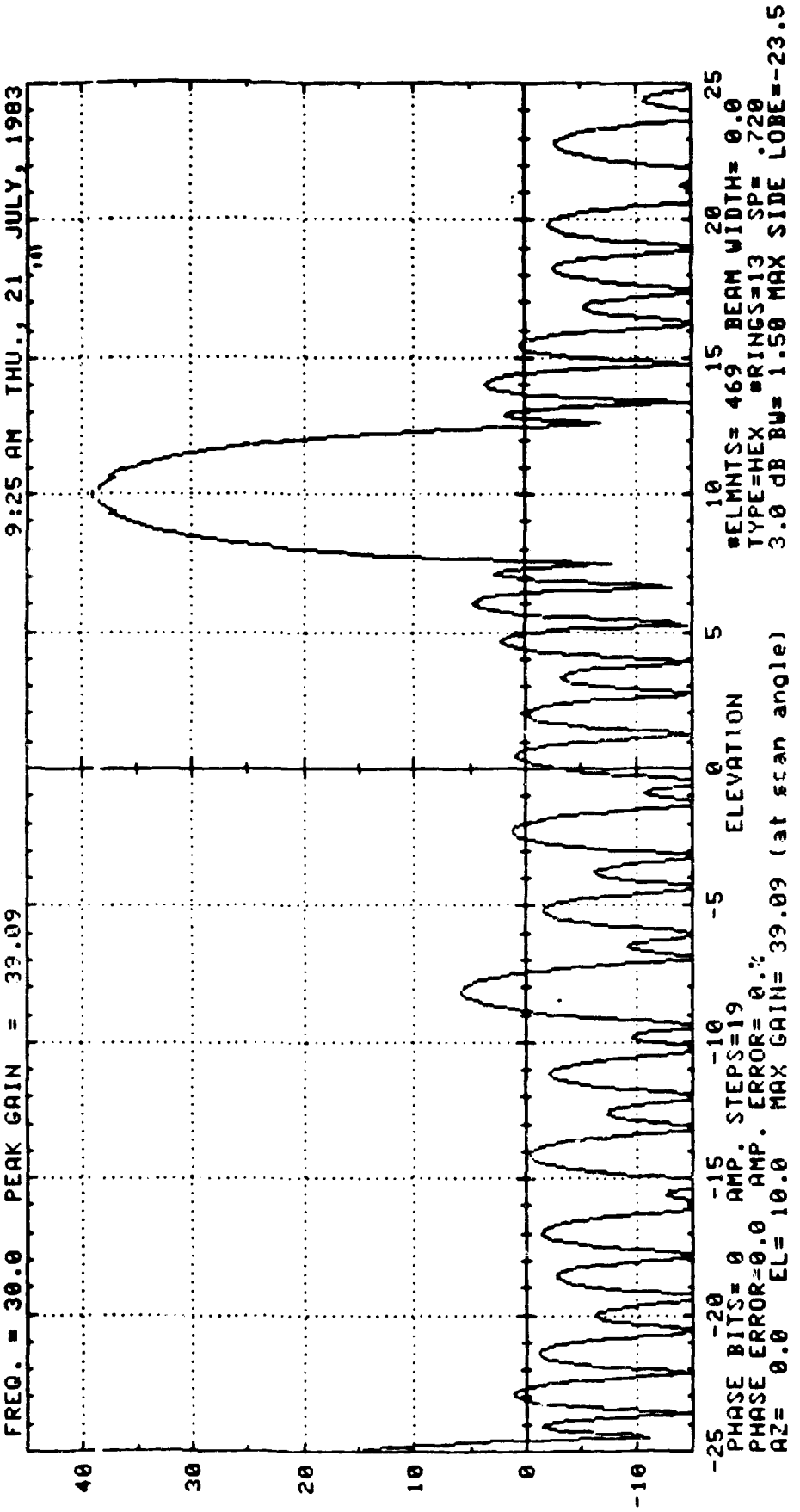
FREQ. = 30.0 PEAK GAIN = 39.09
9:25 AM THU., 21 JULY, 1983
GAIN (dB)
40
30
20
10
0
-10
-25 -20 -15 -10 -5 0 5 10 15 20 25
ELEVATION
PHASE BITS= 0 AMP. STEPS=19
PHASE ERROR=0.0 AMP. ERROR= 0.%
AZ= 0.0 EL= 10.0 MAX GAIN= 39.09 (at scan angle)
#ELMNTS= 469 BEAM WIDTH= 0.0
TYPE=HEX #RINGS=13 SP= .720
3.0 dB BW= 1.50 MAX SIDE LOBE=-23.5

Fig. 4.3-18

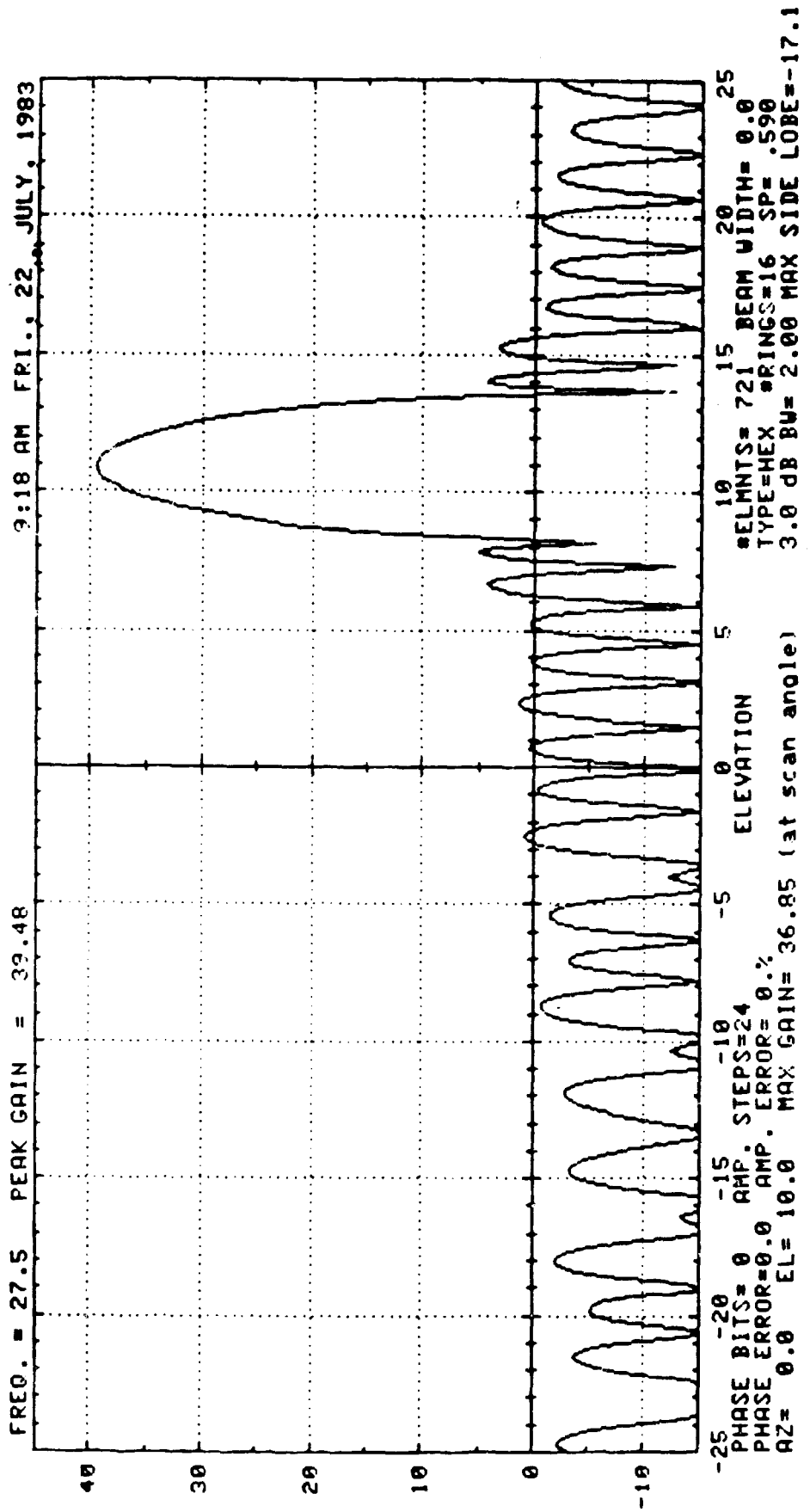
FREQ. = 27.5 PEAK GAIN = 39.48
9:18 AM FRI., 22 JULY, 1983
GAIN (dB)
40
30
20
10
0
-10
-25 -20 -15 -10 -5 0 5 10 15 20 25
ELEVATION
PHASE BITS= 0 AMP. STEPS=24
PHASE ERROR=0.0 AMP. ERROR= 0.%
AZ= 0.0 EL= 10.0 MAX GAIN= 36.85 (at scan angle)
#ELMNTS= 721 BEAM WIDTH= 0.0
TYPE=HEX #RINGS=16 SP= .590
3.0 dB BW= 2.00 MAX SIDE LOBE=-17.1

Fig 4.3-19

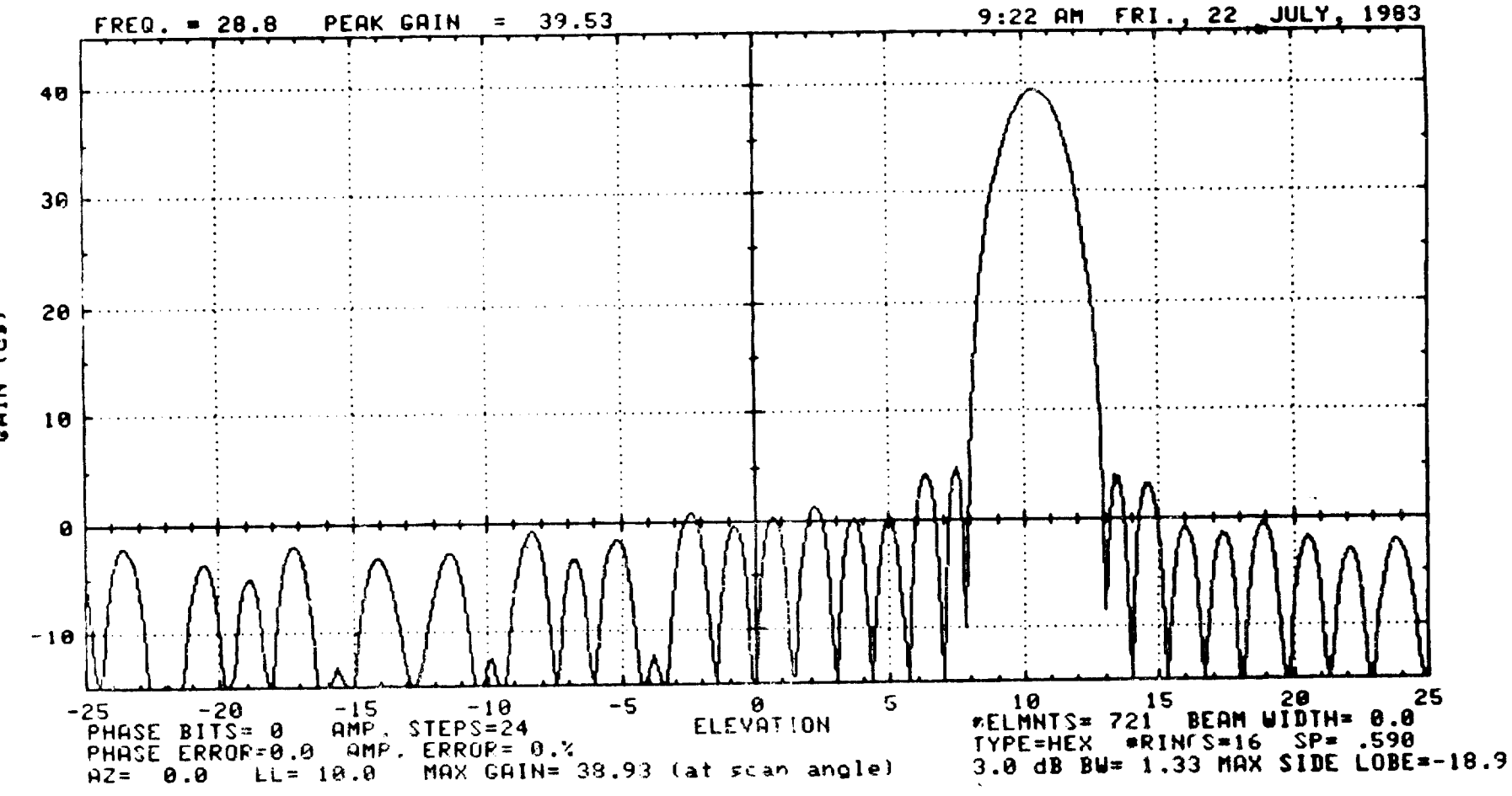
FREQ. = 28.8 PEAK GAIN = 39.53
9:22 AM FRI., 22 JULY, 1983
40
30
20
10
0
-10
-25 -20 -15 -10 -5 0 5 10 15 20 25
ELEVATION
PHASE BITS= 0 AMP. STEPS=24
PHASE ERROR=0.0 AMP. ERROR= 0.%
AZ= 0.0 EL= 10.0 MAX GAIN= 38.93 (at scan angle)
#ELMNTS= 721 BEAM WIDTH= 0.0
TYPE=HEX #RINGS=16 SP= .590
3.0 dB BW= 1.33 MAX SIDE LOBE=-18.9

FIG. 43-20

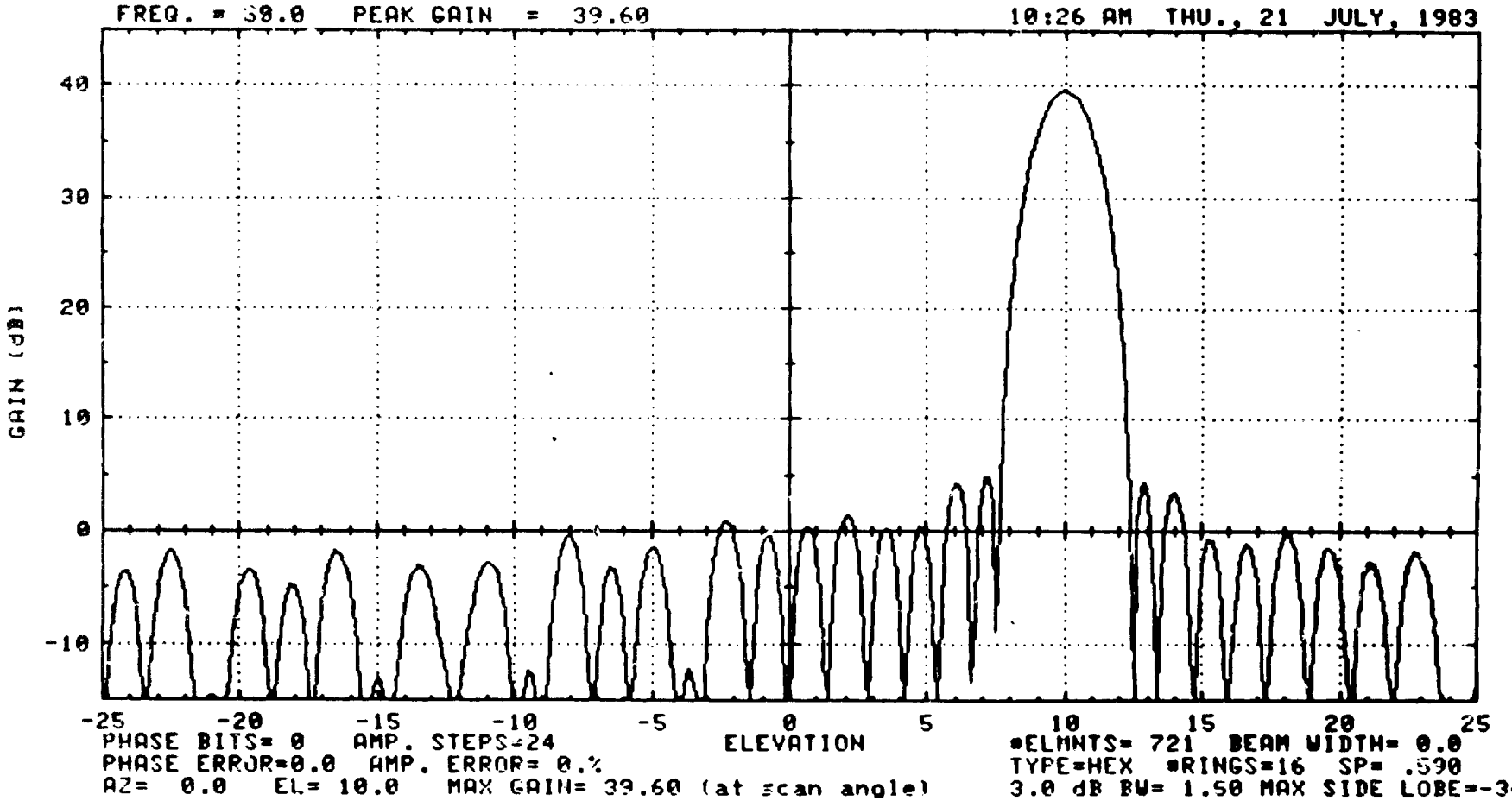
FREQ. = 30.0 PEAK GAIN = 39.60
10:26 AM THU., 21 JULY, 1983
GAIN (dB)
40
30
20
10
0
-10
-25 -20 -15 -10 -5 0 5 10 15 20 25
ELEVATION
PHASE BITS= 0 AMP. STEPS=24
PHASE ERROR=0.0 AMP. ERROR= 0.%
AZ= 0.0 EL= 10.0 MAX GAIN= 39.60 (at scan angle)
#ELMNTS= 721 BEAM WIDTH= 0.0
TYPE=HEX #RINGS=16 SP= .590
3.0 dB BW= 1.50 MAX SIDE LOBE=-34.9

FIG 43-21

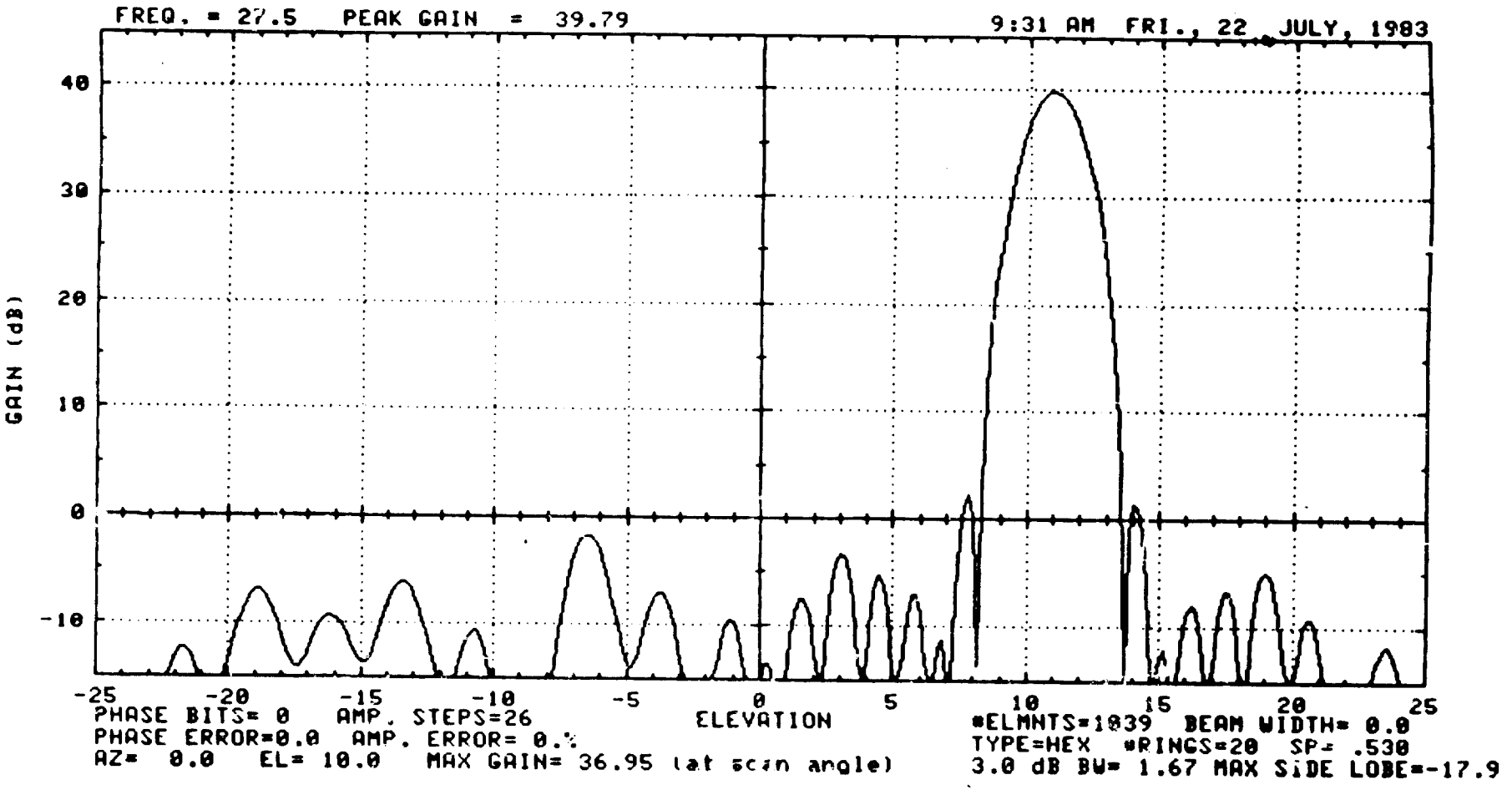
FREQ. = 27.5 PEAK GAIN = 39.79
9:31 AM FRI., 22 JULY, 1983
GAIN (dB)
40
30
20
10
0
-10
-25 -20 -15 -10 -5 0 5 10 15 20 25
ELEVATION
PHASE BITS= 0 AMP. STEPS=26
PHASE ERROR=0.0 AMP. ERROR= 0.%
AZ= 0.0 EL= 10.0 MAX GAIN= 36.95 (at scan angle)
#ELMNTS=1039 BEAM WIDTH= 0.0
TYPE=HEX #RINGS=20 SP= .530
3.0 dB BW= 1.67 MAX SIDE LOBE=-17.9

FIG. 4-3-22

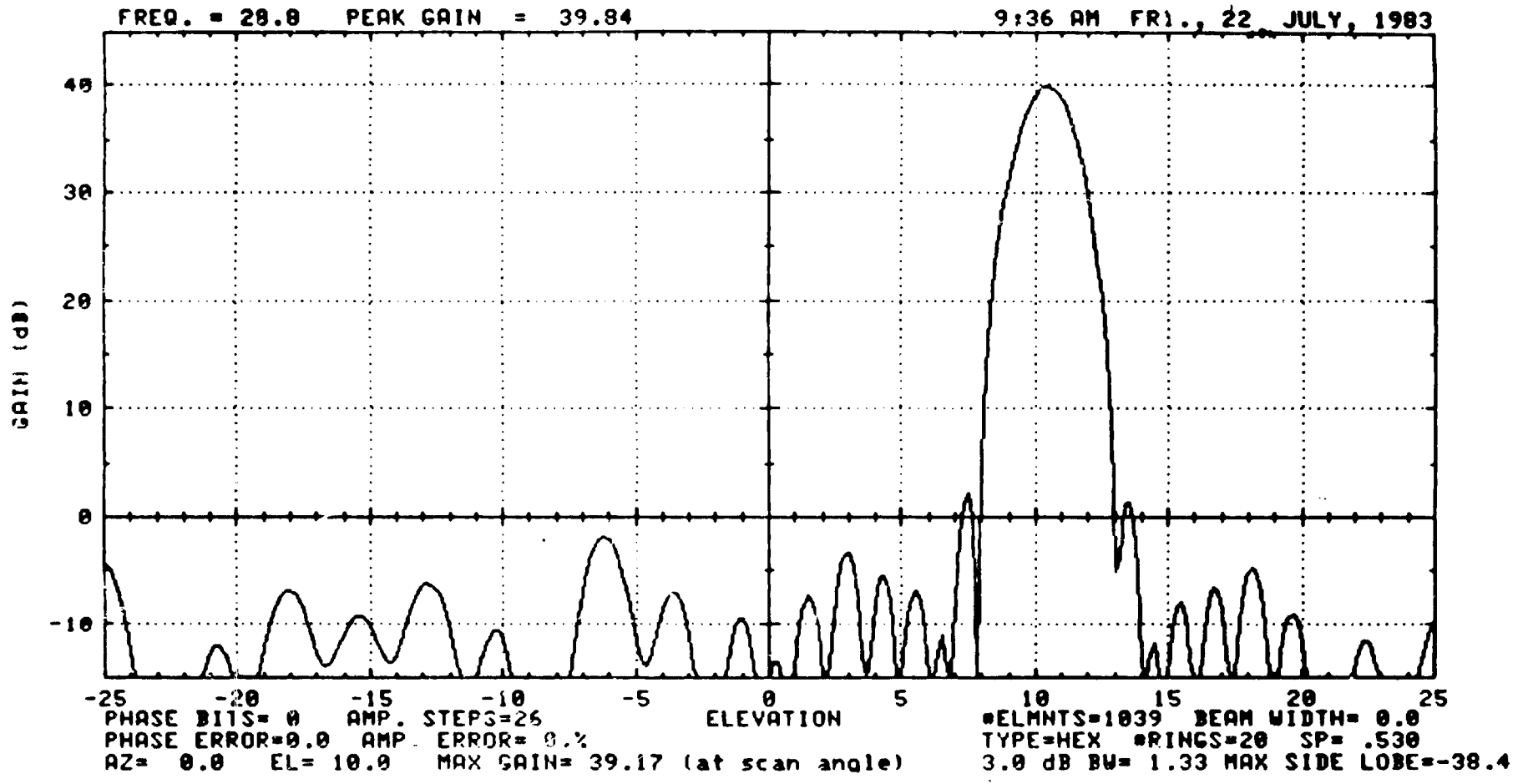
FREQ. = 28.0 PEAK GAIN = 39.84
9:36 AM FRI., 22 JULY, 1983
GAIN (dB)
40
30
20
10
0
-10
-25 -20 -15 -10 -5 0 5 10 15 20 25
ELEVATION
PHASE BITS= 0 AMP. STEPS=26
PHASE ERROR=0.0 AMP. ERROR= 0.%
AZ= 0.0 EL= 10.0 MAX GAIN= 39.17 (at scan angle)
#ELMNTS=1039 BEAM WIDTH= 0.0
TYPE=HEX #RINGS=20 SP= .530
3.0 dB BW= 1.33 MAX SIDE LOBE=-38.4

FIG. 4.3-23

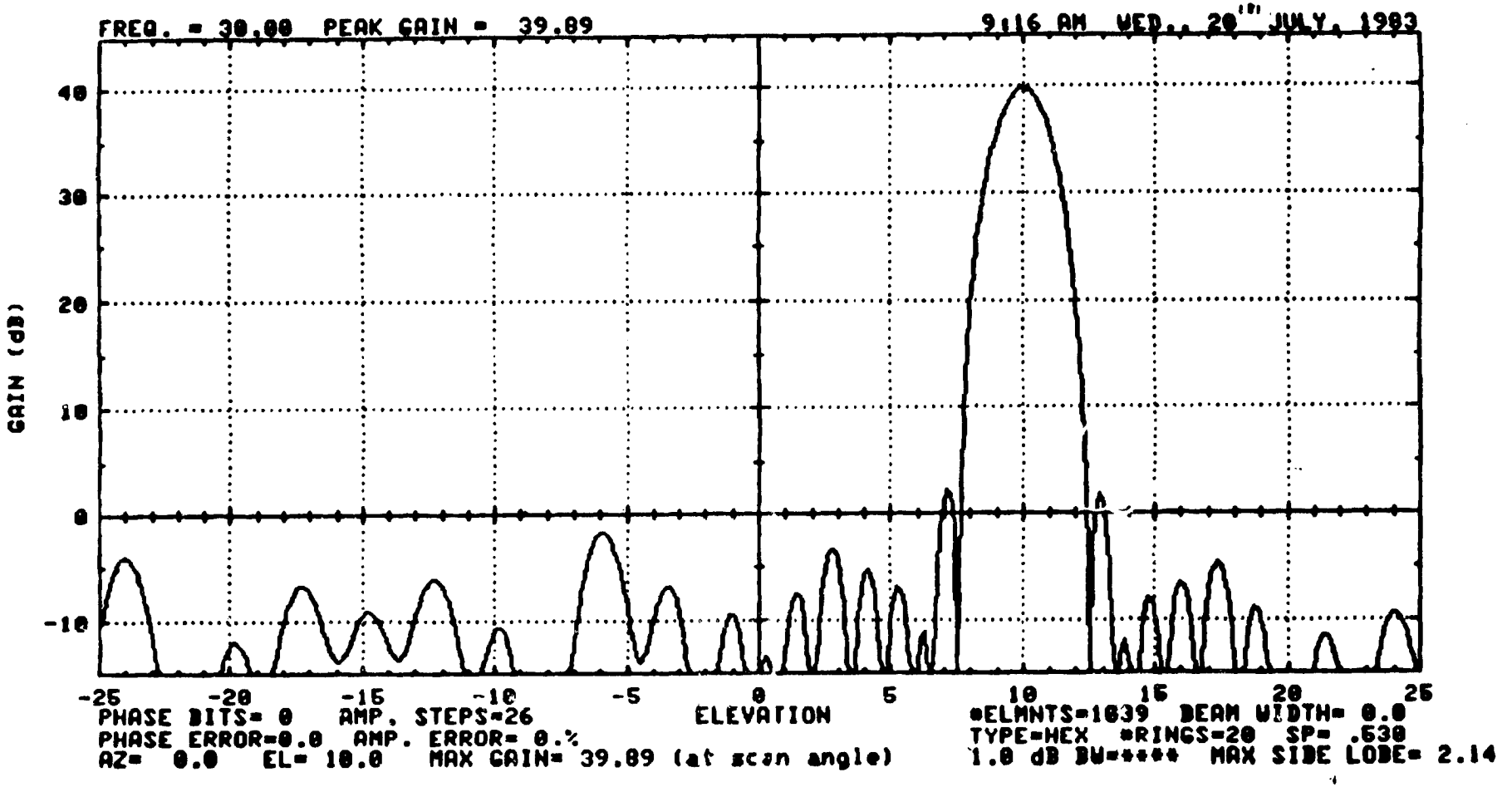
FREQ. = 30.00 PEAK GAIN = 39.89
9:16 AM WED., 20TH JULY, 1983
GAIN (dB)
40
30
20
10
0
-10
-25 -20 -15 -10 -5 0 5 10 15 20 25
ELEVATION
PHASE BITS= 0 AMP. STEPS=26
PHASE ERROR=0.0 AMP. ERROR= 0.%
AZ= 0.0 EL= 10.0 MAX GAIN= 39.89 (at scan angle)
#ELMNTS=1039 BEAM WIDTH= 0.0
TYPE=HEX #RINGS=20 SP= .530
1.0 dB BW=**** MAX SIDE LOBE= 2.14

FIG. 4.3-24

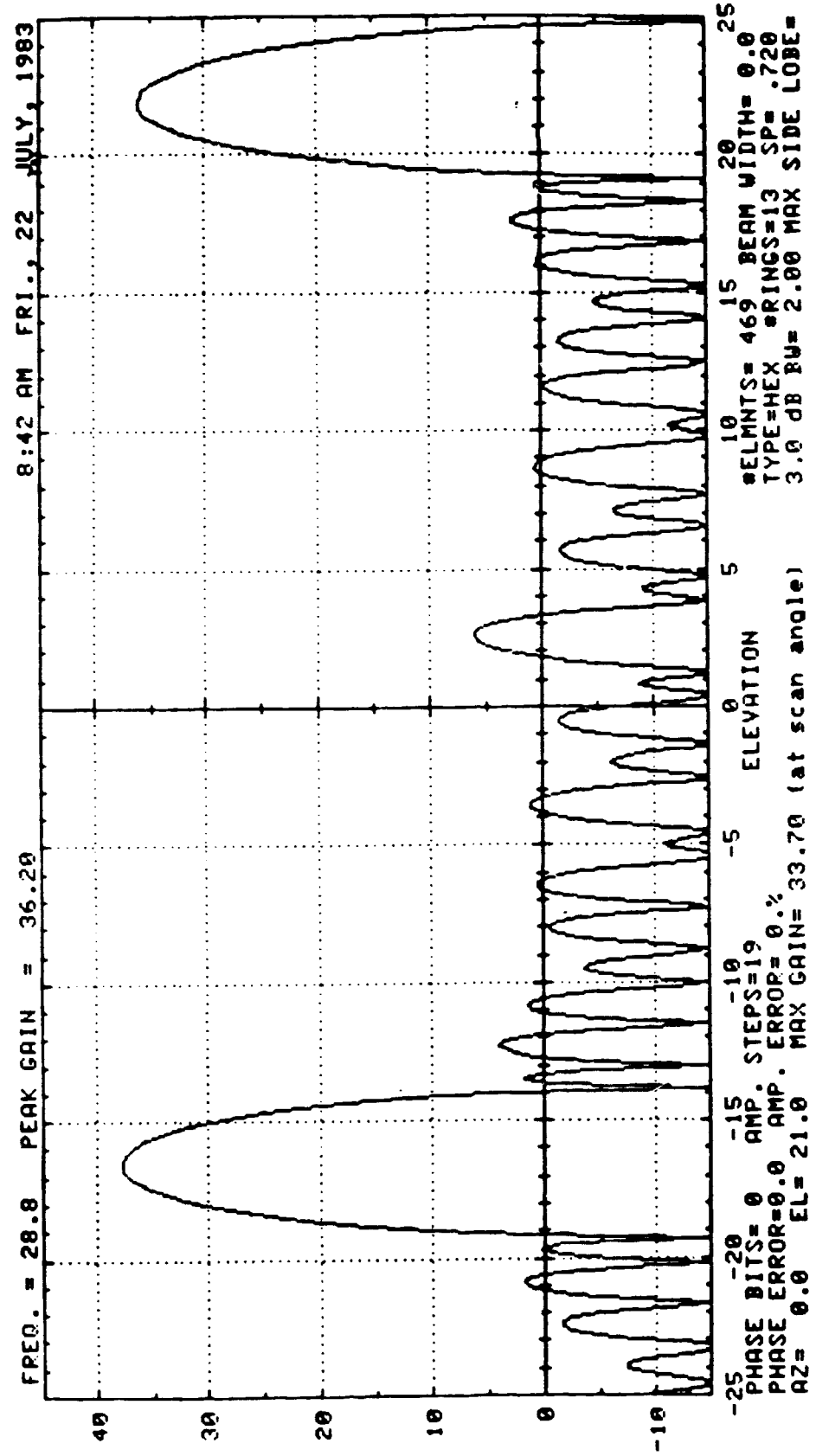
8:42 AM FRI., 22 JULY, 1983
FREQ. = 28.8 PEAK GAIN = 36.20
PHASE BITS= 0 AMP. STEPS=19
PHASE ERROR=0.0 AMP. ERROR= 0.%
AZ= 0.0 EL= 21.0 MAX GAIN= 33.70 (at scan angle)
#ELMNTS= 469 BEAM WIDTH= 0.0
TYPE=HEX #RINGS=13 SP= .720
3.0 dB BW= 2.00 MAX SIDE LOBE= 1.6
GAIN (dB)
ELEVATION
40
30
20
10
0
-10
-25
-20
-15
-10
-5
0
5
10
15
20
25

FIG. 4.3-25

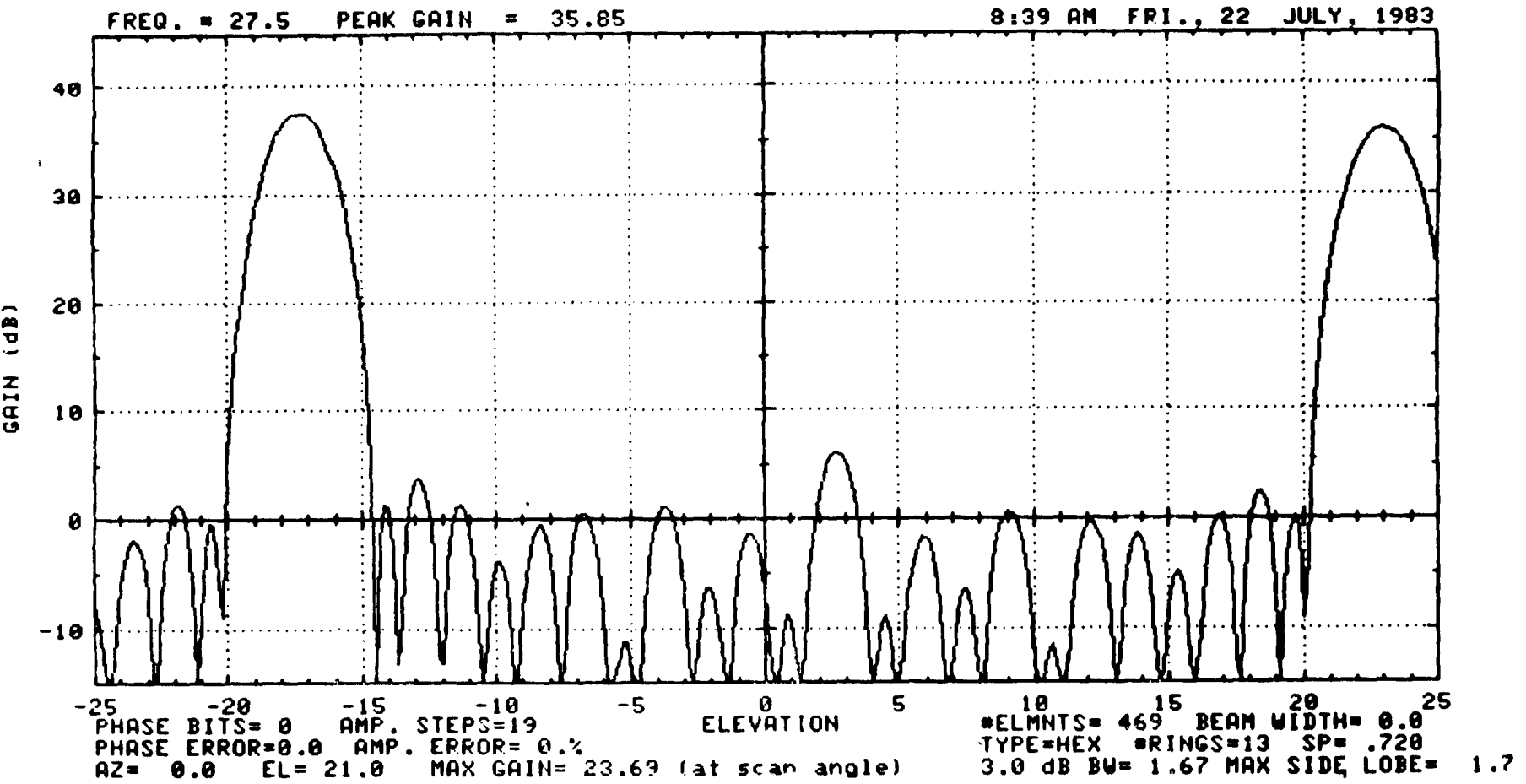
FREQ. = 27.5 PEAK GAIN = 35.85
8:39 AM FRI., 22 JULY, 1983
GAIN (dB)
40
30
20
10
0
-10
-25 -20 -15 -10 -5 0 5 10 15 20 25
ELEVATION
PHASE BITS= 0 AMP. STEPS=19
PHASE ERROR=0.0 AMP. ERROR= 0.%
AZ= 0.0 EL= 21.0 MAX GAIN= 23.69 (at scan angle)
#ELMNTS= 469 BEAM WIDTH= 0.0
TYPE=HEX #RINGS=13 SP= .720
3.0 dB BW= 1.67 MAX SIDE LOBE= 1.7

Fig 4.3-26

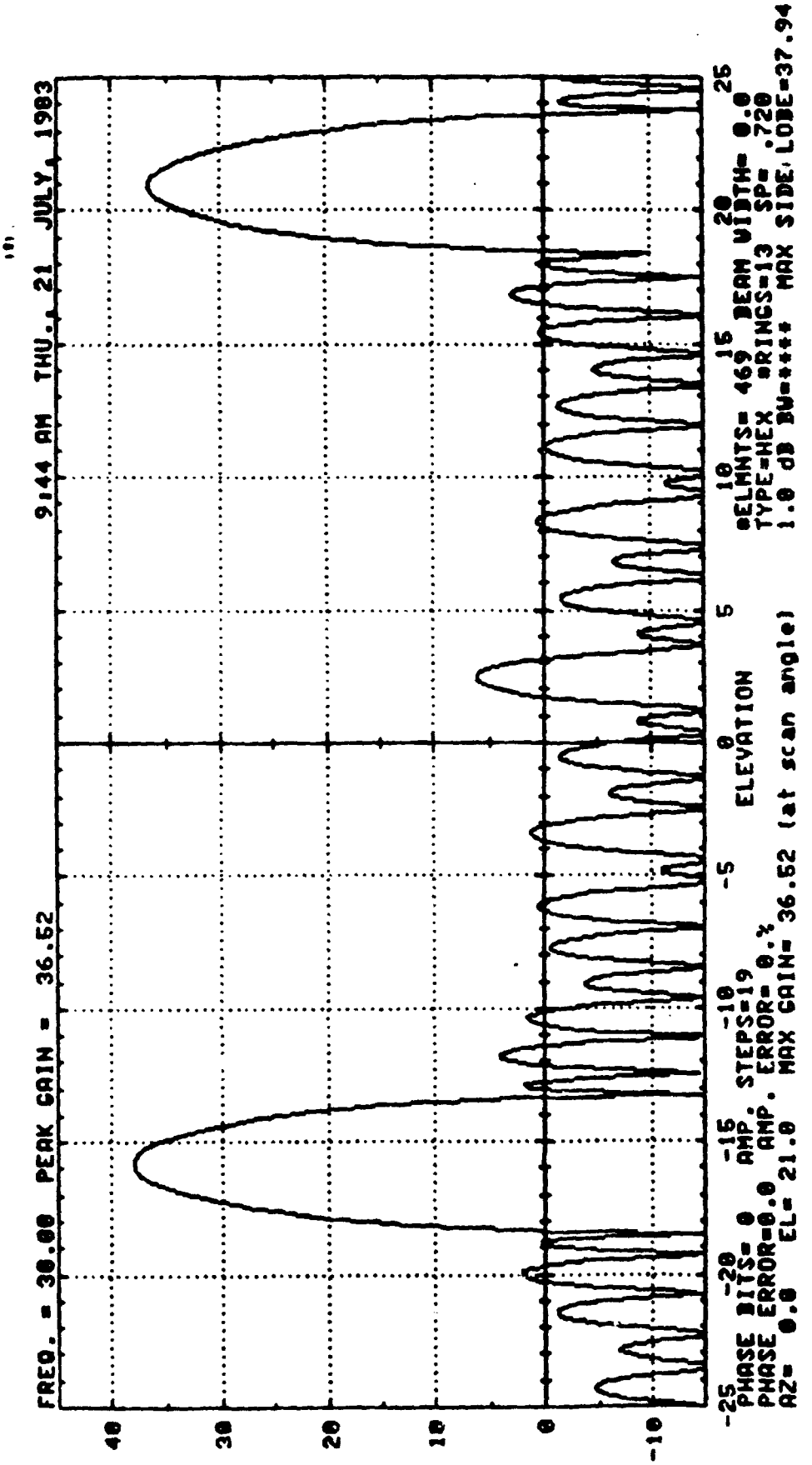
FREQ. = 30.00 PEAK GAIN = 36.52
9:44 AM THU., 21 JULY, 1983
GAIN (dB)
40
30
20
10
0
-10
-25 -20 -15 -10 -5 0 5 10 15 20 25
ELEVATION
PHASE BITS= 0 AMP. STEPS=19
PHASE ERROR=0.0 AMP. ERROR= 0.%
AZ= 0.0 EL= 21.0 MAX GAIN= 36.52 (at scan angle)
#ELMNTS= 469 BEAM WIDTH= 0.0
TYPE=HEX #RINGS=13 SP= .720
1.0 dB BW=**** MAX SIDE LOBE=37.94

Fig. 4.3-27

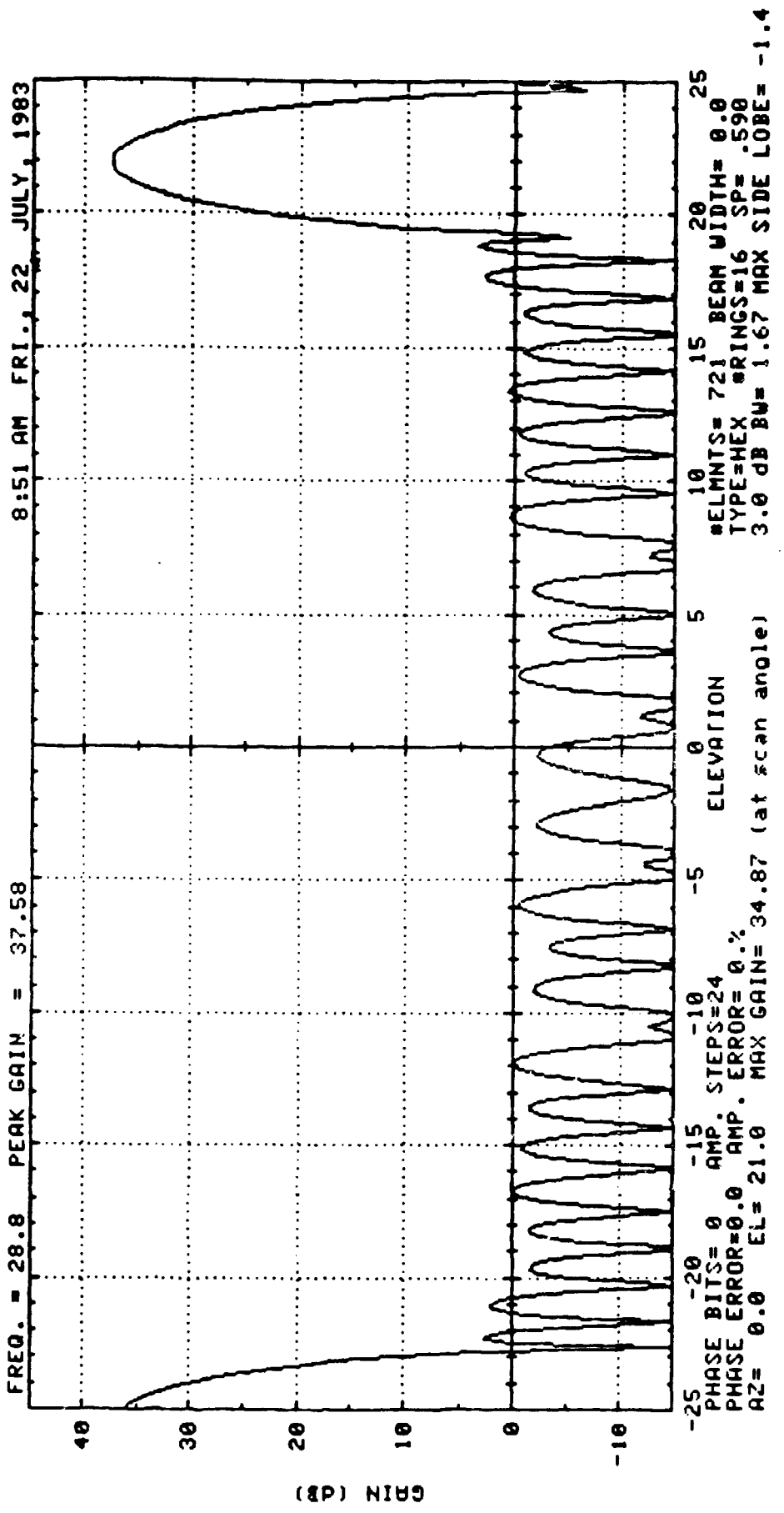
FREQ. = 28.8 PEAK GAIN = 37.58
8:51 AM FRI., 22 JULY, 1983
GAIN (dB)
40
30
20
10
0
-10
-25 -20 -15 -10 -5 0 5 10 15 20 25
ELEVATION
PHASE BITS= 0 AMP. STEPS=24
PHASE ERROR=0.0 AMP. ERROR= 0.%
AZ= 0.0 EL= 21.0 MAX GAIN= 34.87 (at scan angle)
#ELMNTS= 721 BEAM WIDTH= 0.0
TYPE=HEX #RINGS=16 SP= .590
3.0 dB BW= 1.67 MAX SIDE LOBE= -1.4

FIG. 43-28

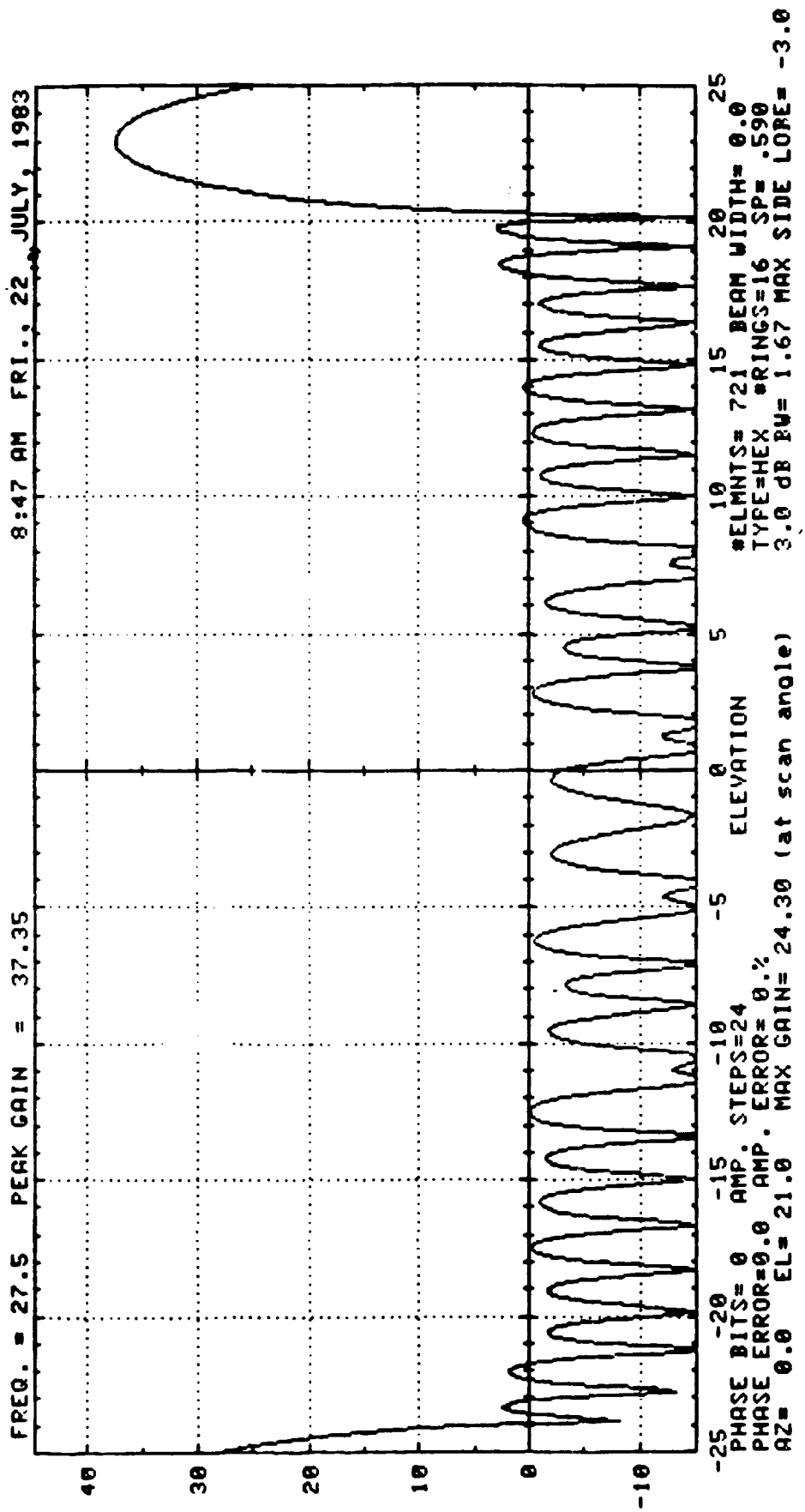
FREQ. = 27.5 PEAK GAIN = 37.35
8:47 AM FRI., 22 JULY, 1983
GAIN (dB)
40
30
20
10
0
-10
-25 -20 -15 -10 -5 0 5 10 15 20 25
ELEVATION
PHASE BITS= 0 AMP. STEPS=24
PHASE ERROR=0.0 AMP. ERROR= 0.%
AZ= 0.0 EL= 21.0 MAX GAIN= 24.30 (at scan angle)
*ELMNTS= 721 BEAM WIDTH= 0.0
TYPE=HEX *RINGS=16 SP= .590
3.0 dB BW= 1.67 MAX SIDE LORE= -3.0

Fig. 4.3-29

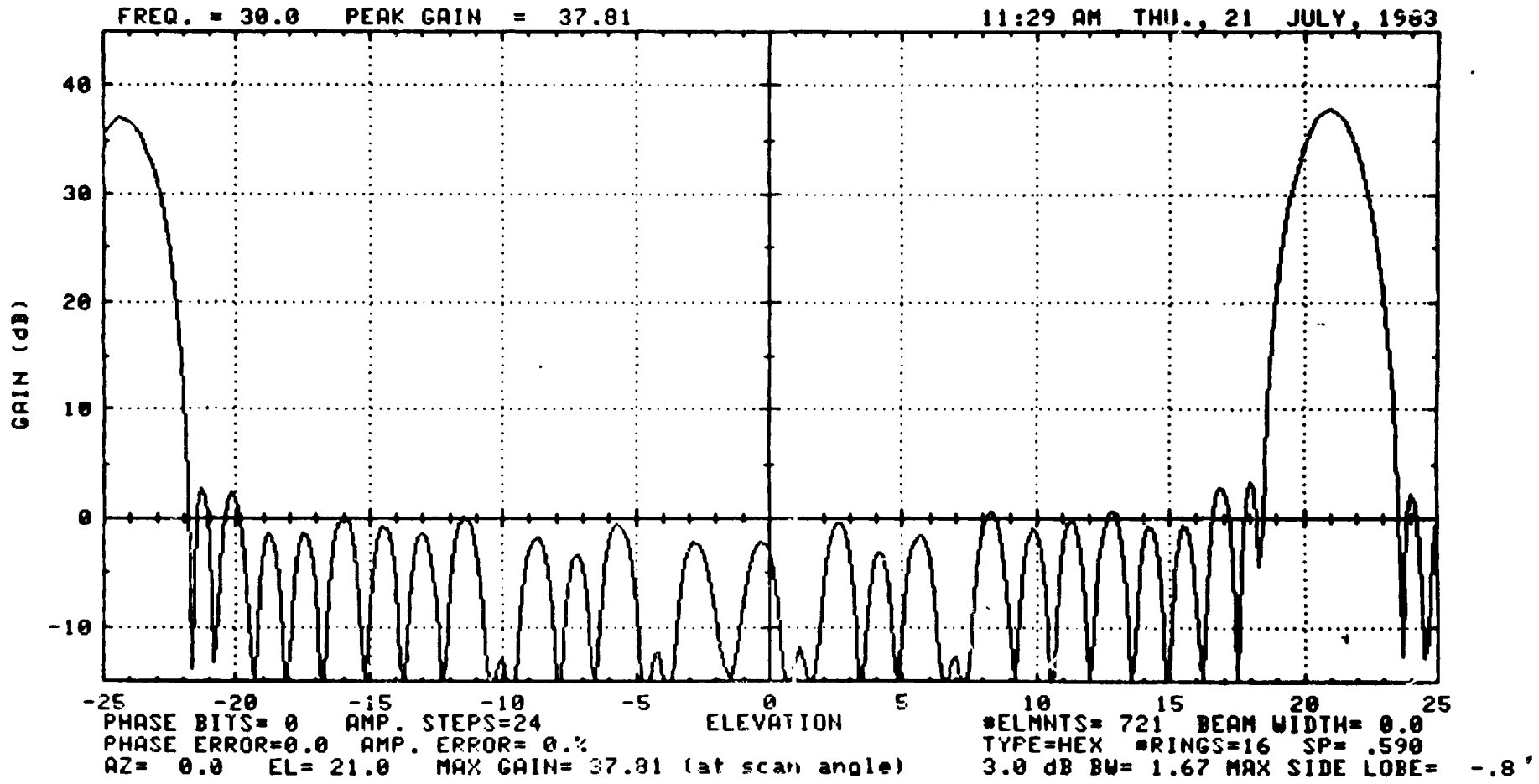
FREQ. = 30.0 PEAK GAIN = 37.81
11:29 AM THU., 21 JULY, 1983
GAIN (dB)
40
30
20
10
0
-10
-25 -20 -15 -10 -5 0 5 10 15 20 25
ELEVATION
PHASE BITS= 0 AMP. STEPS=24
PHASE ERROR=0.0 AMP. ERROR= 0.%
AZ= 0.0 EL= 21.0 MAX GAIN= 37.81 (at scan angle)
#ELMNTS= 721 BEAM WIDTH= 0.0
TYPE=HEX #RINGS=16 SP= .590
3.0 dB BW= 1.67 MAX SIDE LOBE= -.8

FIG. 43-30

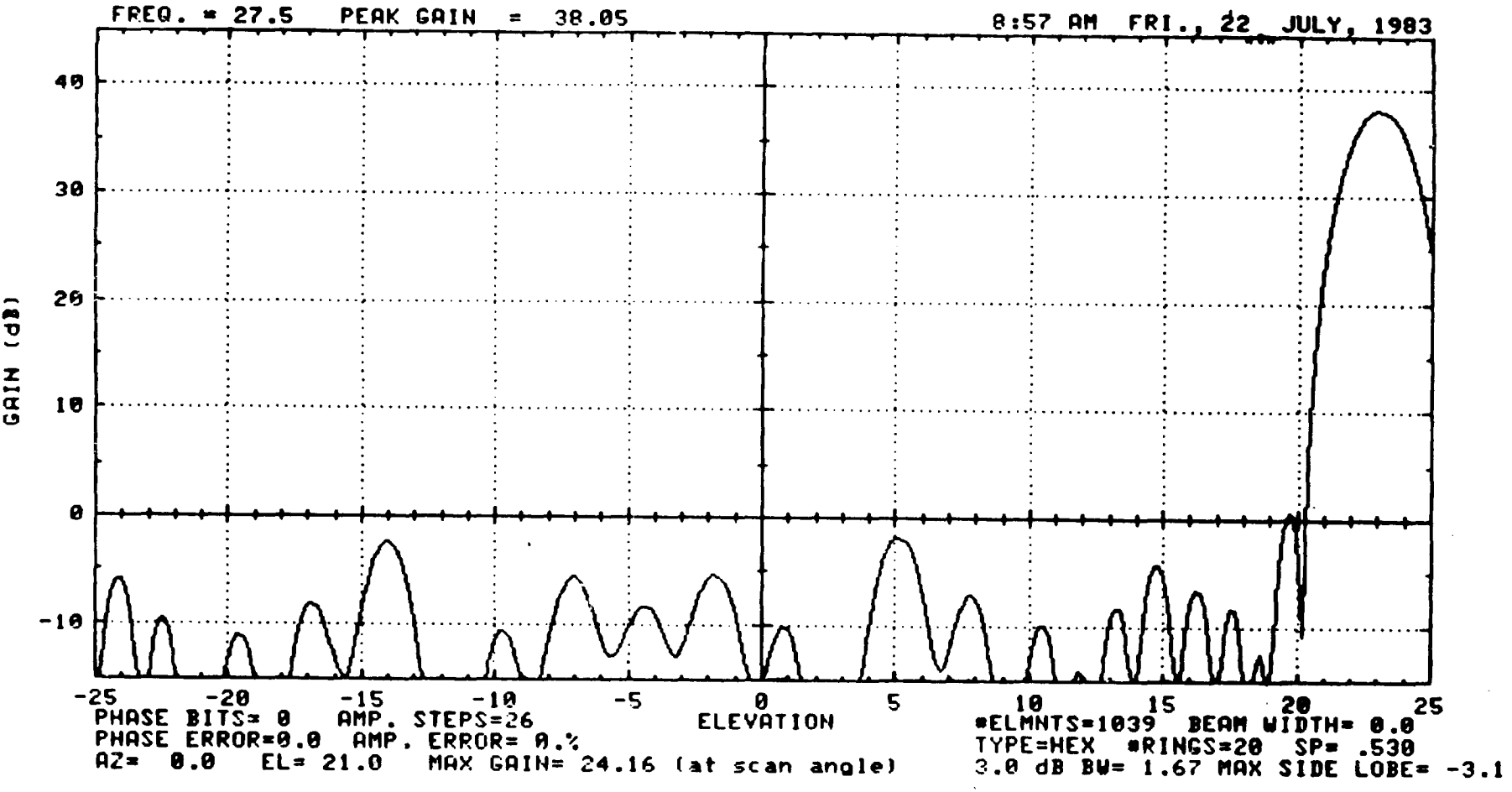
FREQ. = 27.5 PEAK GAIN = 38.05
8:57 AM FRI., 22 JULY, 1983
GAIN (dB)
40
30
20
10
0
-10
-25 -20 -15 -10 -5 0 5 10 15 20 25
ELEVATION
PHASE BITS= 0 AMP. STEPS=26
PHASE ERROR=0.0 AMP. ERROR= 0.%
AZ= 0.0 EL= 21.0 MAX GAIN= 24.16 (at scan angle)
#ELMNTS=1039 BEAM WIDTH= 0.0
TYPE=HEX #RINGS=20 SP= .530
3.0 dB BW= 1.67 MAX SIDE LOBE= -3.1

FIG 4.3-31

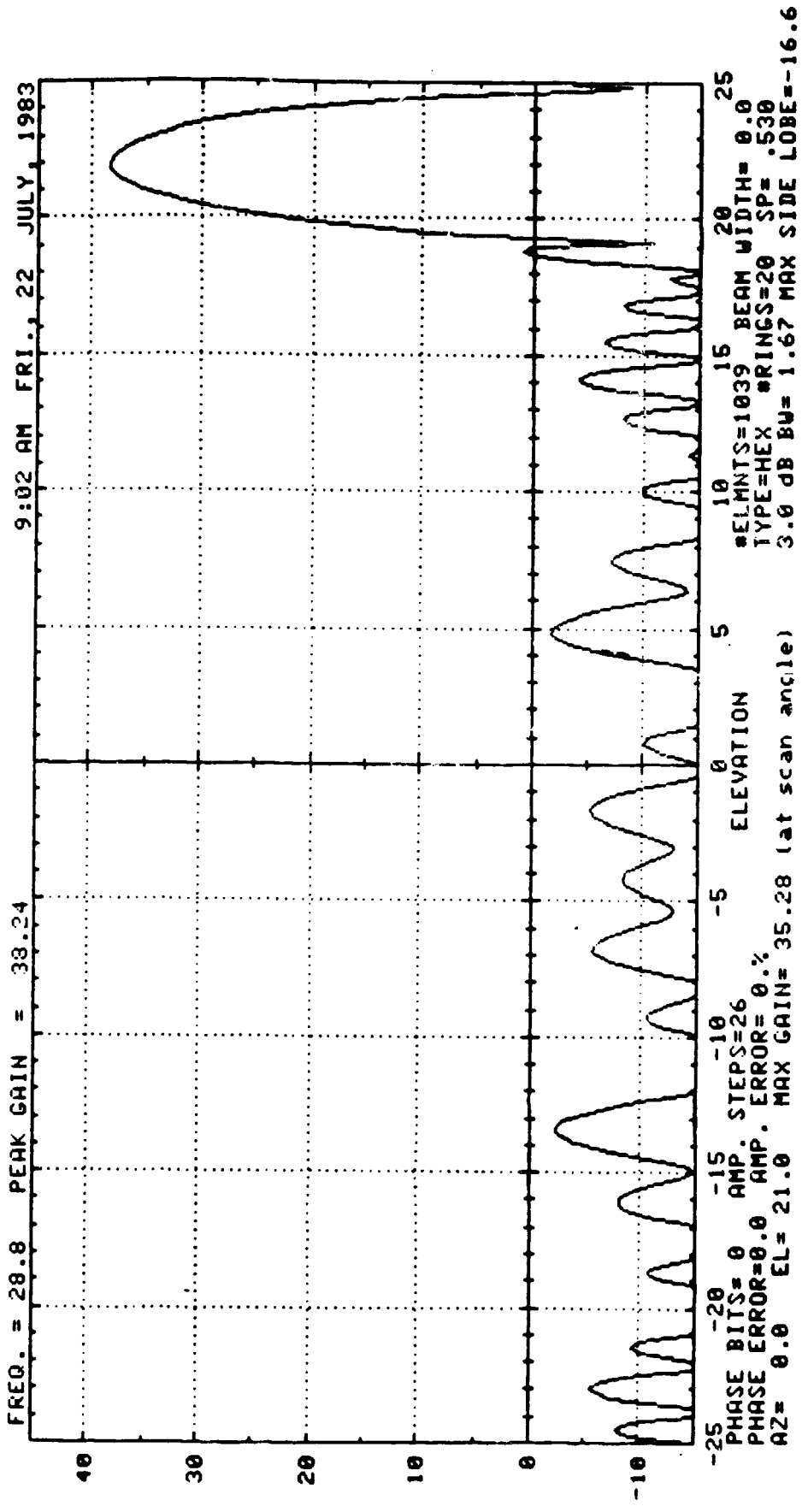
FREQ. = 28.8 PEAK GAIN = 38.24
9:02 AM FRI., 22 JULY, 1983
GAIN (dB)
40
30
20
10
0
-10
-25 -20 -15 -10 -5 0 5 10 15 20 25
ELEVATION
PHASE BITS= 0 AMP. STEPS=26
PHASE ERROR=0.0 AMP. ERROR= 0.%
AZ= 0.0 EL= 21.0 MAX GAIN= 35.28 (at scan angle)
#ELMNTS=1039 BEAM WIDTH= 0.0
TYPE=HEX #RINGS=20 SP= .530
3.0 dB BW= 1.67 MAX SIDE LOBE=-16.6

FIG. 4.3-32

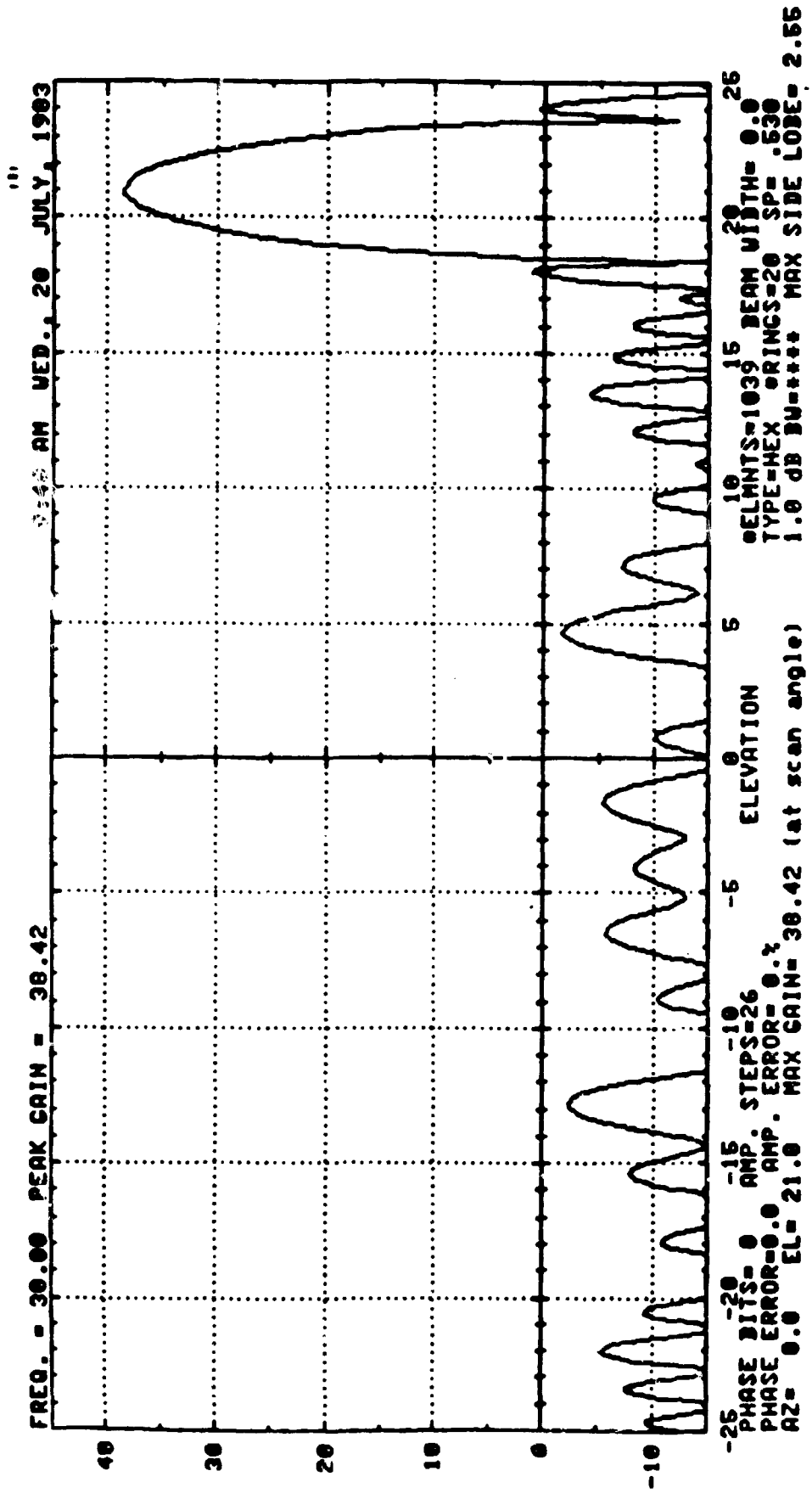
FREQ. = 30.00 PEAK GAIN = 38.42
AM WED., 20 JULY, 1983
GAIN (dB)
40
30
20
10
0
-10
-25 -20 -15 -10 -5 0 5 10 15 20 25
ELEVATION
PHASE BITS= 0 AMP. STEPS=26
PHASE ERROR=0.0 AMP. ERROR= 0.%
AZ= 0.0 EL= 21.0 MAX GAIN= 38.42 (at scan angle)
•ELMNTS=1039 BEAM WIDTH= 0.0
TYPE=HEX •RINGS=20 SP= .530
1.0 dB BW=**** MAX SIDE LOBE= 2.55

FIG. 4.3-33

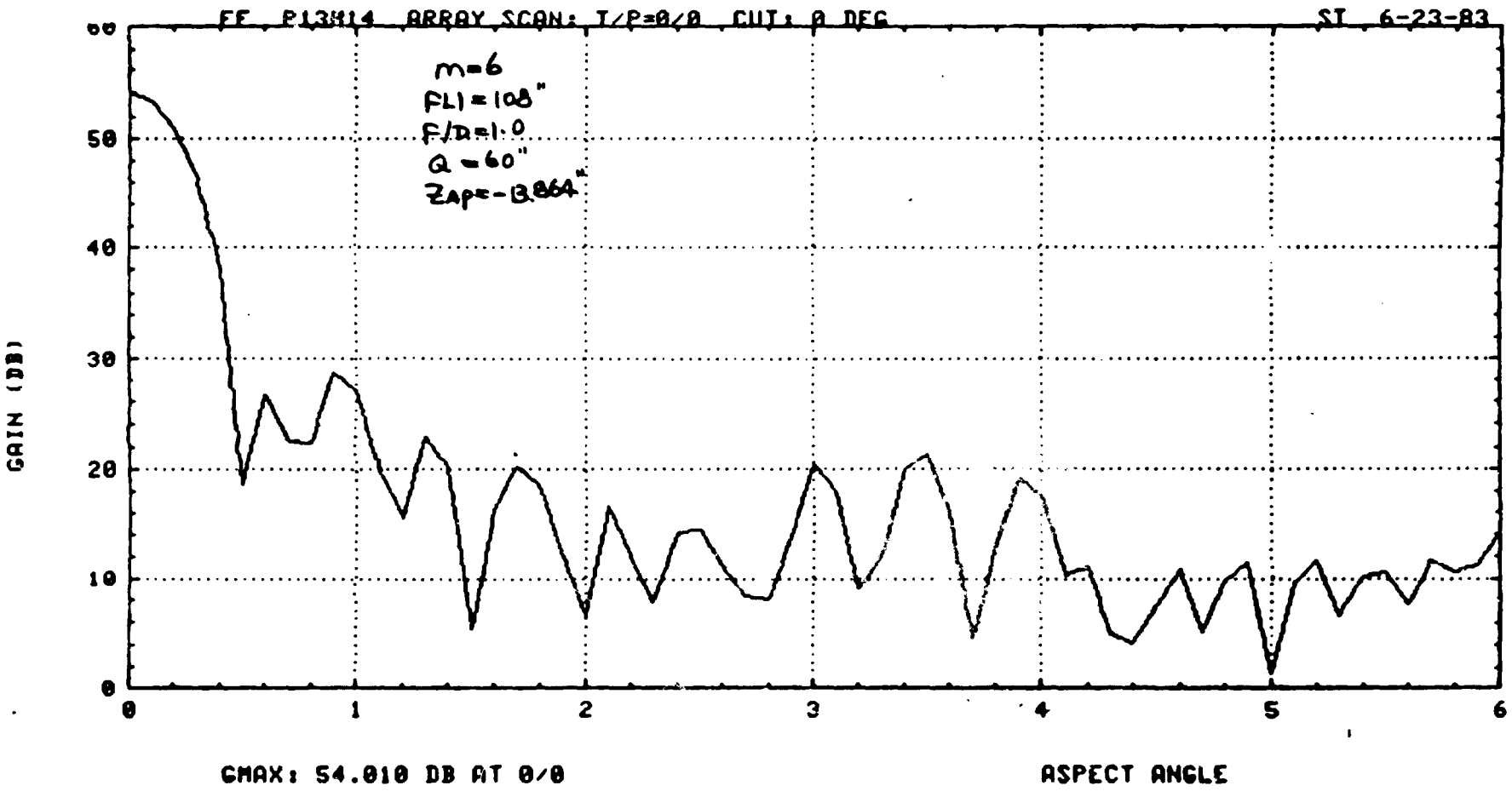
FF P13H14 ARRAY SCAN: T/P=0/0 CUT: 0 DEG
ST 6-23-83
m=6
FL1=108"
F/D=1.0
Q=60"
Zap=-13.864"
GAIN (DB)
60
50
40
30
20
10
0
0
1
2
3
4
5
6
GMAX: 54.010 DB AT 0/0
ASPECT ANGLE

Fig 5.31

PLOTS

FOR

SECTION 5

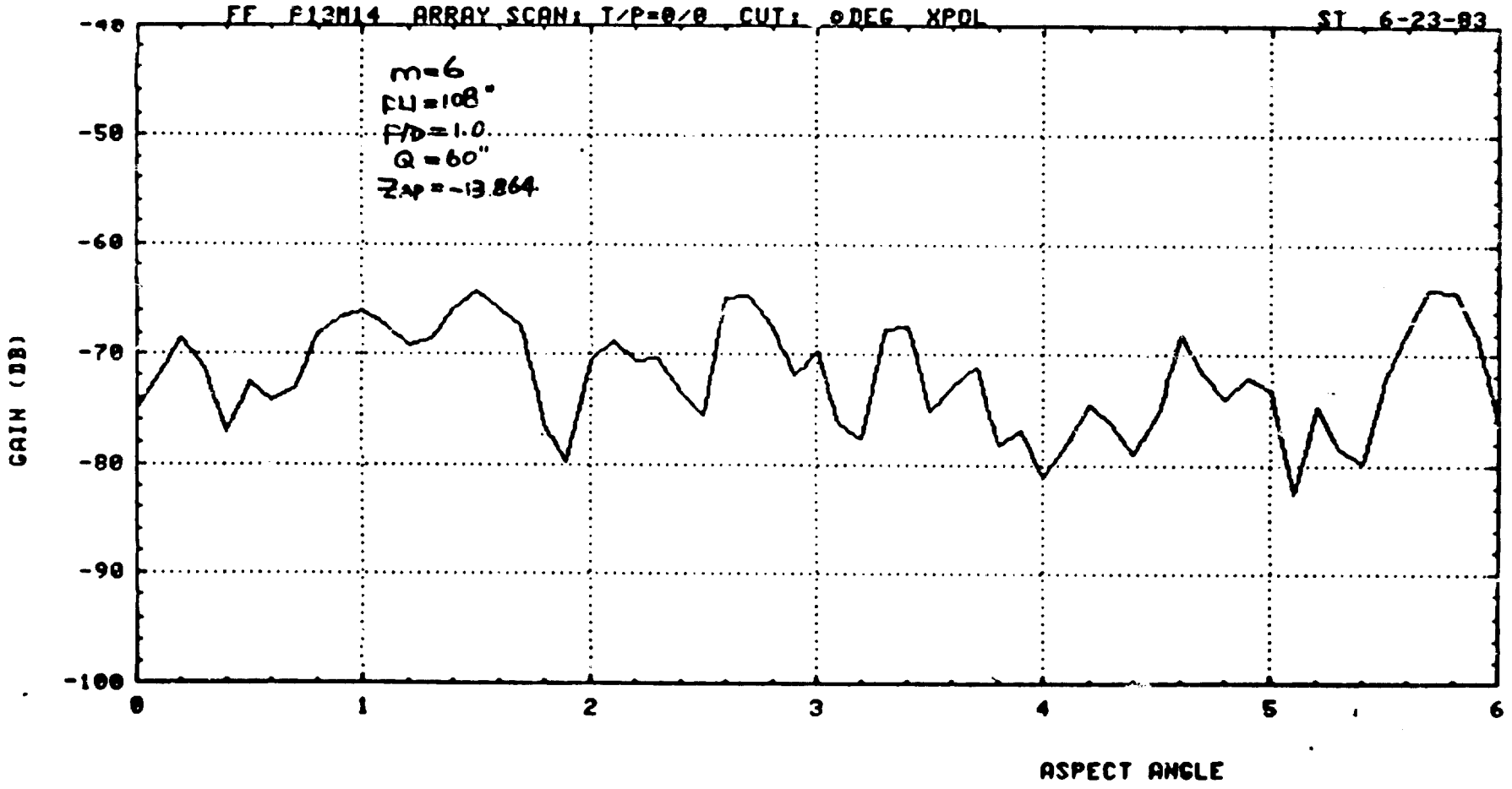
FF F13M14 ARRAY SCAN: T/P=0/0 CUT: 0 DEG XPOL
ST 6-23-83
m=6
PW=108°
F/D=1.0
Q=60"
ZAP=-13.864
GAIN (DB)
-40
-50
-60
-70
-80
-90
-100
0
1
2
3
4
5
6
ASPECT ANGLE

FIG 5.3

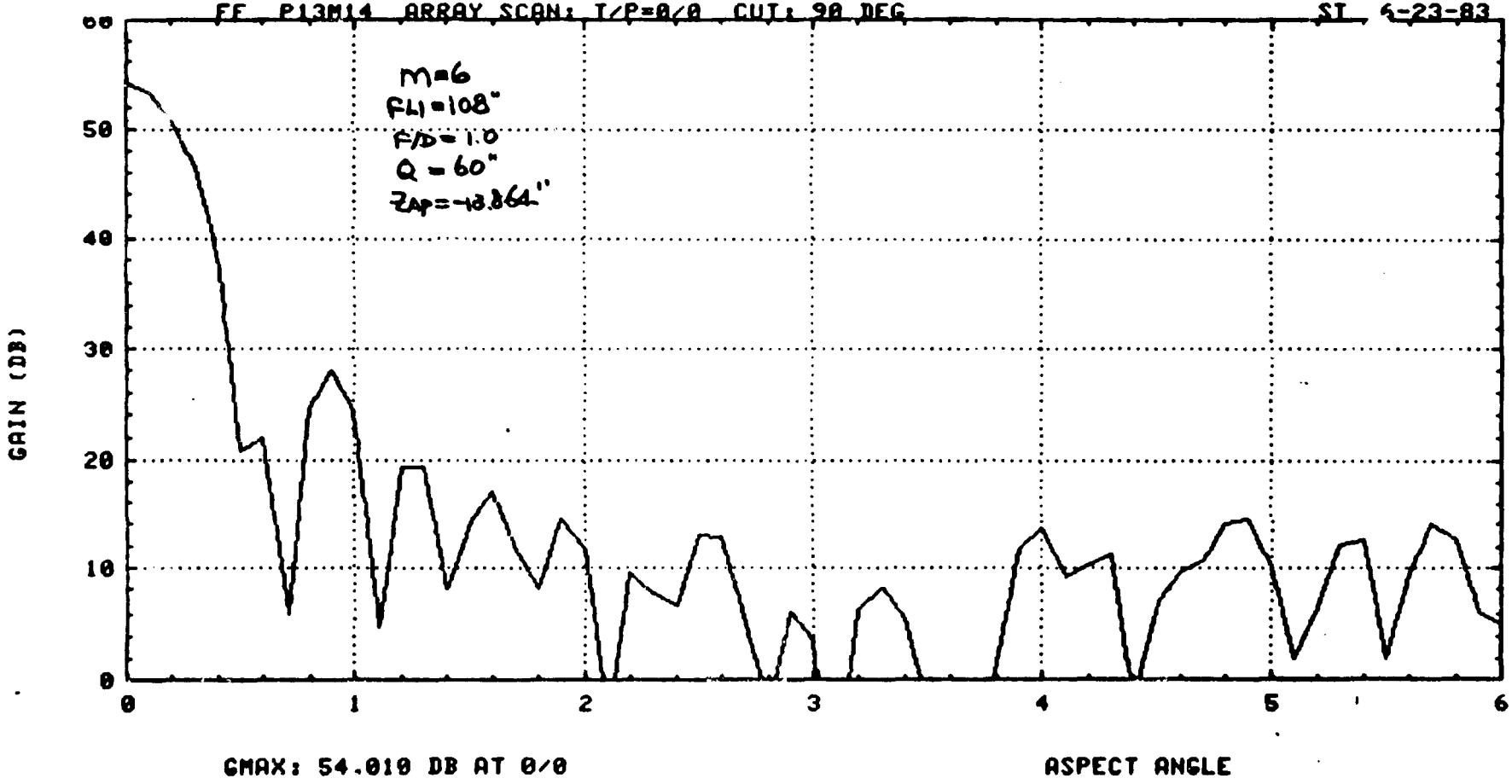
FF P13M14 ARRAY SCAN: I/P=0/0 CUT: 90 DEG
SI 4-23-83
M=6
FLI=108"
F/D=1.0
Q=60"
ZAP=-13.864"
GAIN (DB)
60
50
40
30
20
10
0
0
1
2
3
4
5
6
GMAX: 54.010 DB AT 0/0
ASPECT ANGLE

FIG 5.3-3

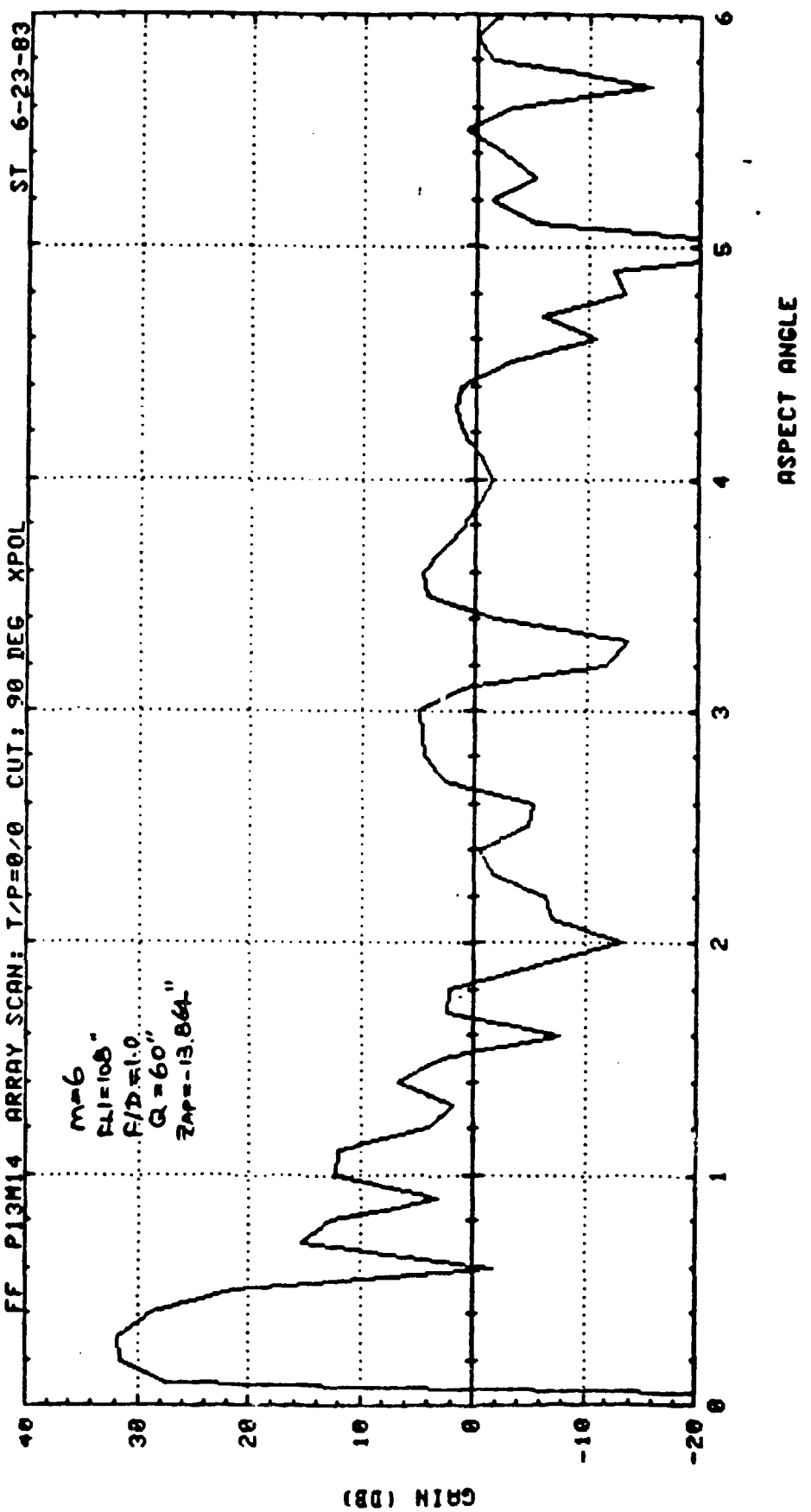
FF P13M14 ARRAY SCAN: T/P=0/0 CUT: 90 DEG XPOL
ST 6-23-83
m=6
n=108
F/D=1.0
Q=60"
Zap=-13.864"
GAIN (DB)
ASPECT ANGLE
40
30
20
10
0
-10
-20
0
1
2
3
4
5
6

FIG 5.3-4.

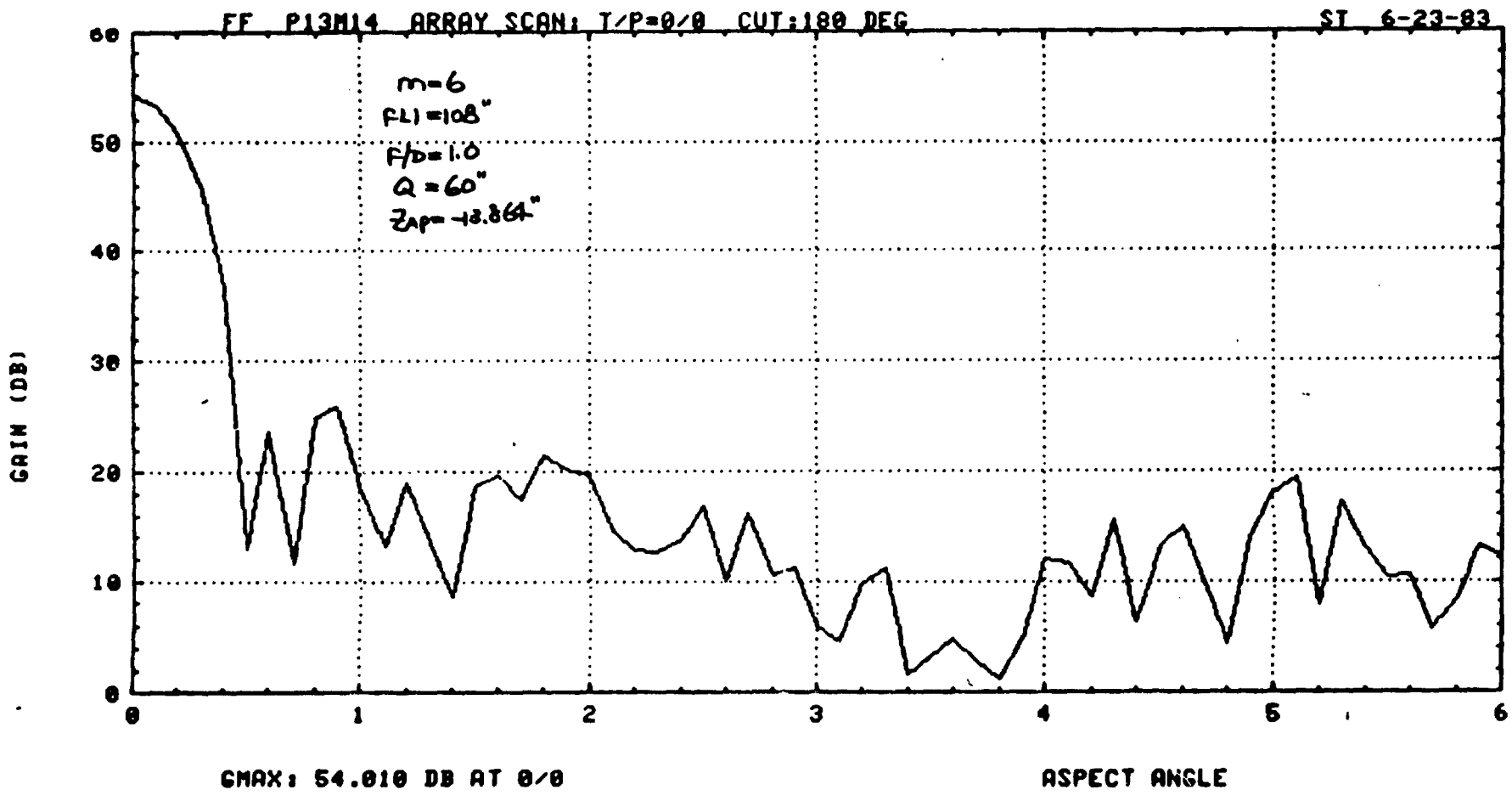
FF P13M14 ARRAY SCAN: T/P=0/0 CUT:180 DEG
ST 6-23-83
m=6
FLI=108"
F/D=1.0
Q=60"
Zap=-13.864"
GAIN (DB)
60
50
40
30
20
10
0
0
1
2
3
4
5
6
GMAX: 54.010 DB AT 0/0
ASPECT ANGLE

FIG 5.3-5

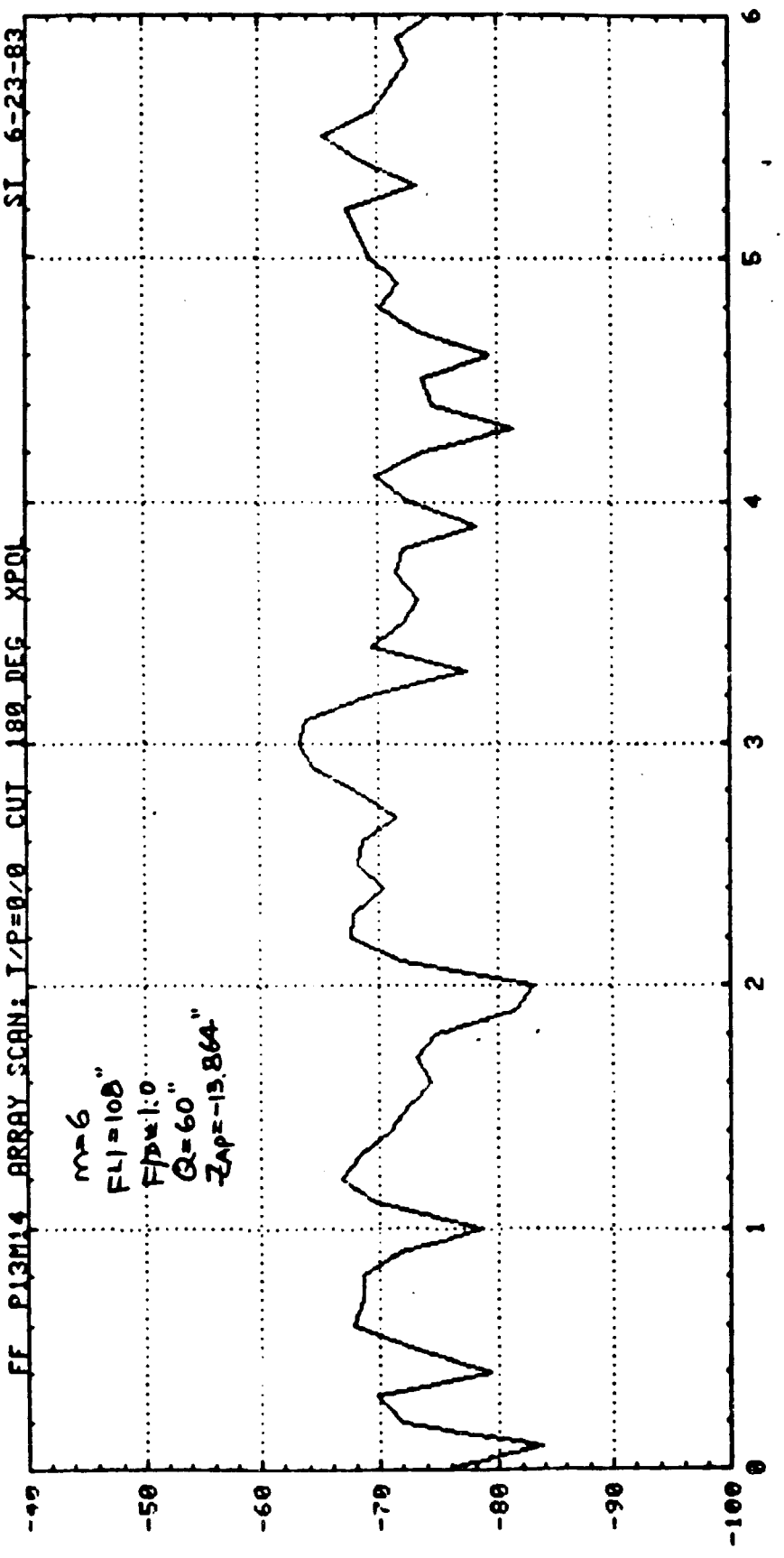
FF P13M14 ARRAY SCAN: I/P=0/0 CUT 180 DEG XPOL
SI 6-23-83
M=6
FL1=108"
F/D=1.0
Q=60"
ZAP=-13.864"
GAIN (DB)
ASPECT ANGLE
-40
-50
-60
-70
-80
-90
-100
0
1
2
3
4
5
6

FIG 5.3-6

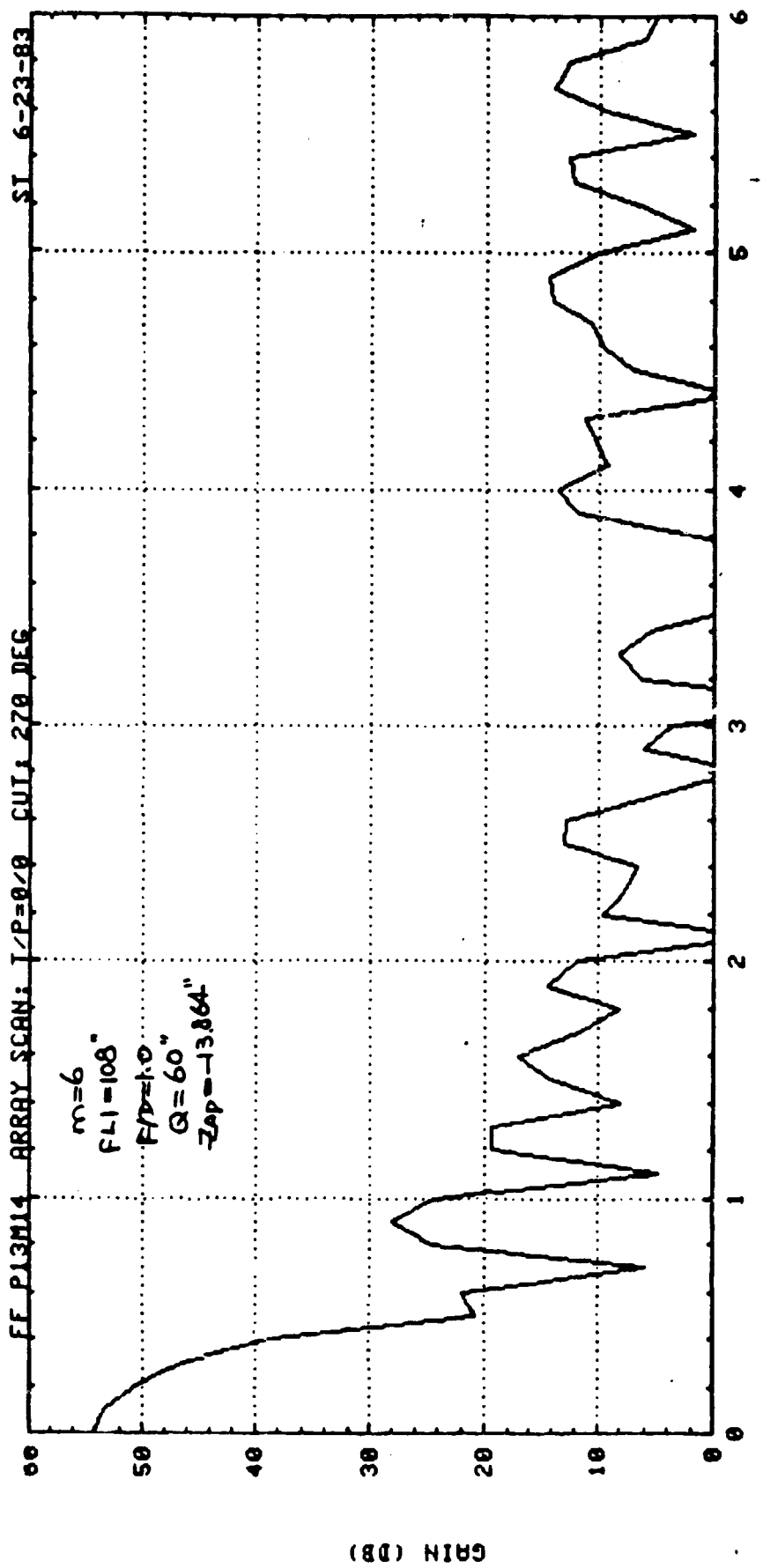
FF P13M14 ARRAY SCAN: I/P=0/0 CUT: 270 DEG
ST 6-23-83
m=6
FL1=108"
F/D=1.0
Q=60"
Zap=-13.864"
GRAIN (DB)
ASPECT ANGLE
GMAX: 54.010 AT 0/0
60
50
40
30
20
10
0
0
1
2
3
4
5
6

FIG. 5.3-7

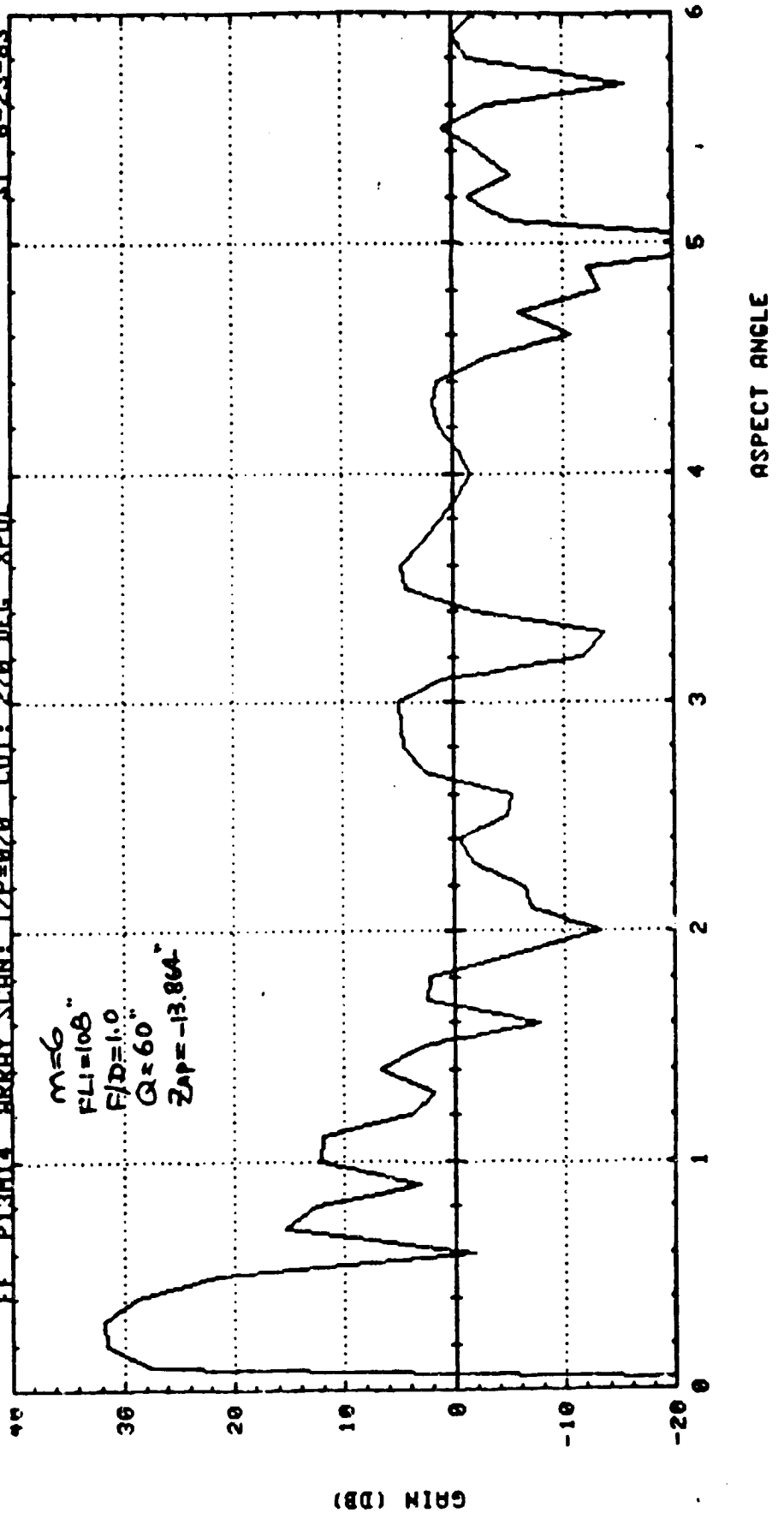
FF P13N14 ARRAY SCAN: I/P=0/0 CUT: 270 DEG XPOL
ST 6-23-83
M=6
FL=108"
F/D=1.0
Q=60"
Zp=-13.864"
GAIN (DB)
ASPECT ANGLE
40
30
20
10
0
-10
-20
0
1
2
3
4
5
6

FIG 5.3-8

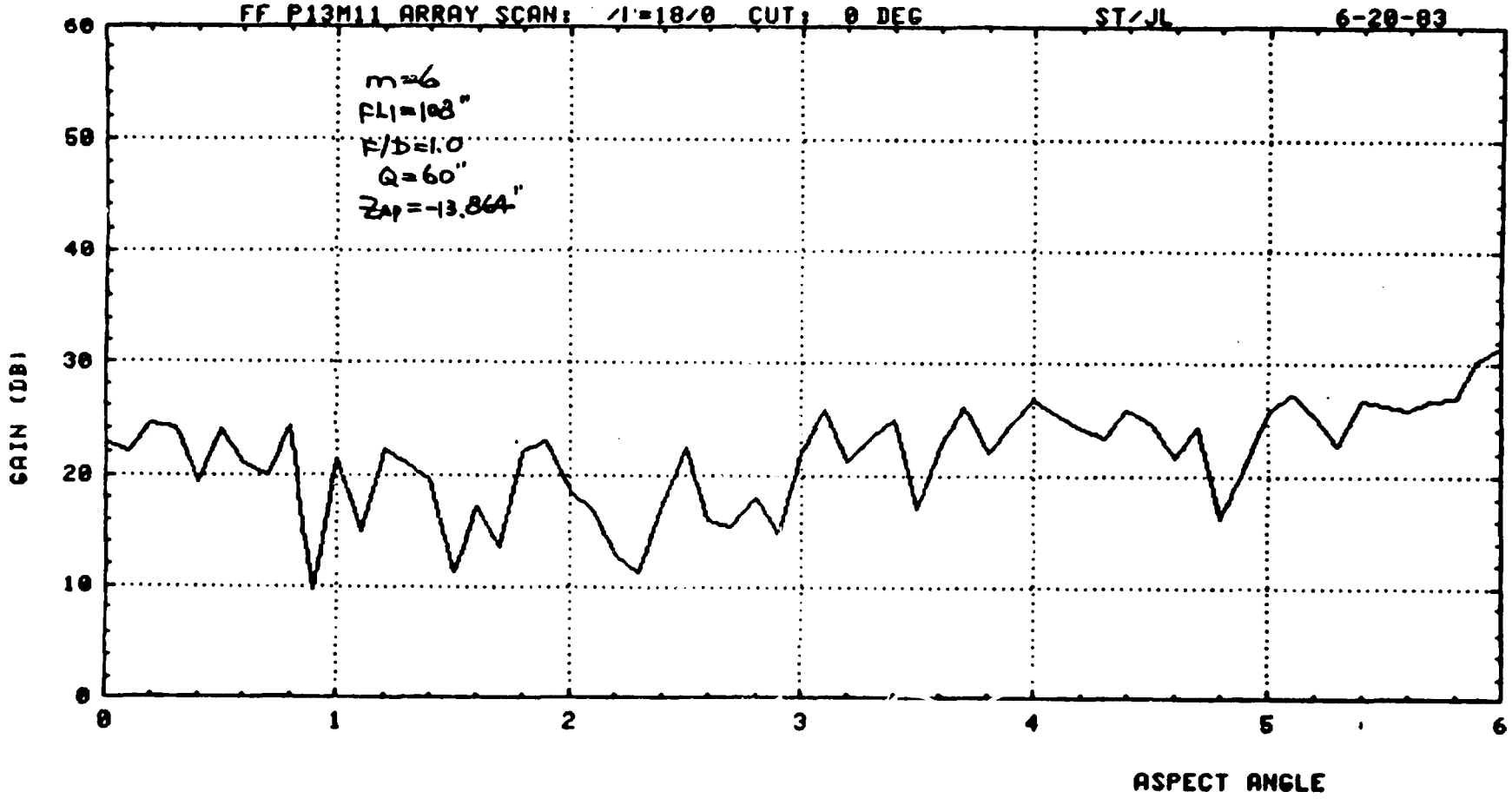
FF P13M11 ARRAY SCAN: λ=18/0 CUT: 0 DEG ST/JL 6-20-83
m=6
FL1=108"
F/D=1.0
Q=60"
Zap=-13.864"
GAIN (DBI)
60
50
40
30
20
10
0
0
1
2
3
4
5
6
ASPECT ANGLE

FIG 3-9

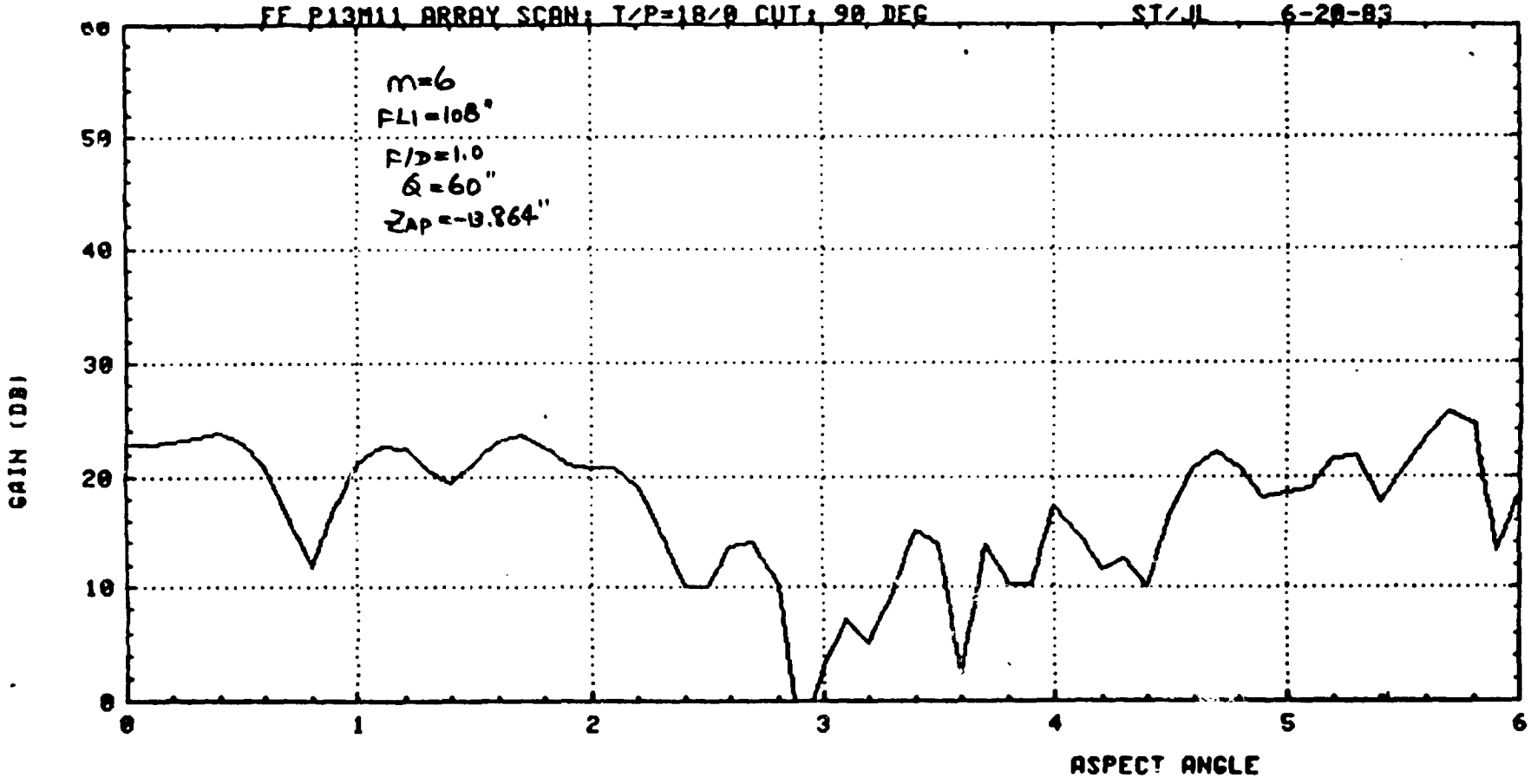
FF P13M11 ARRAY SCAN; T/P=18/0 CUT; 90 DEG
ST/JL 6-28-83
m=6
FLI=108"
F/D=1.0
Q=60"
ZAP=-13.864"
GAIN (DB)
60
50
40
30
20
10
0
0
1
2
3
4
5
6
ASPECT ANGLE

FIG 5.3-10

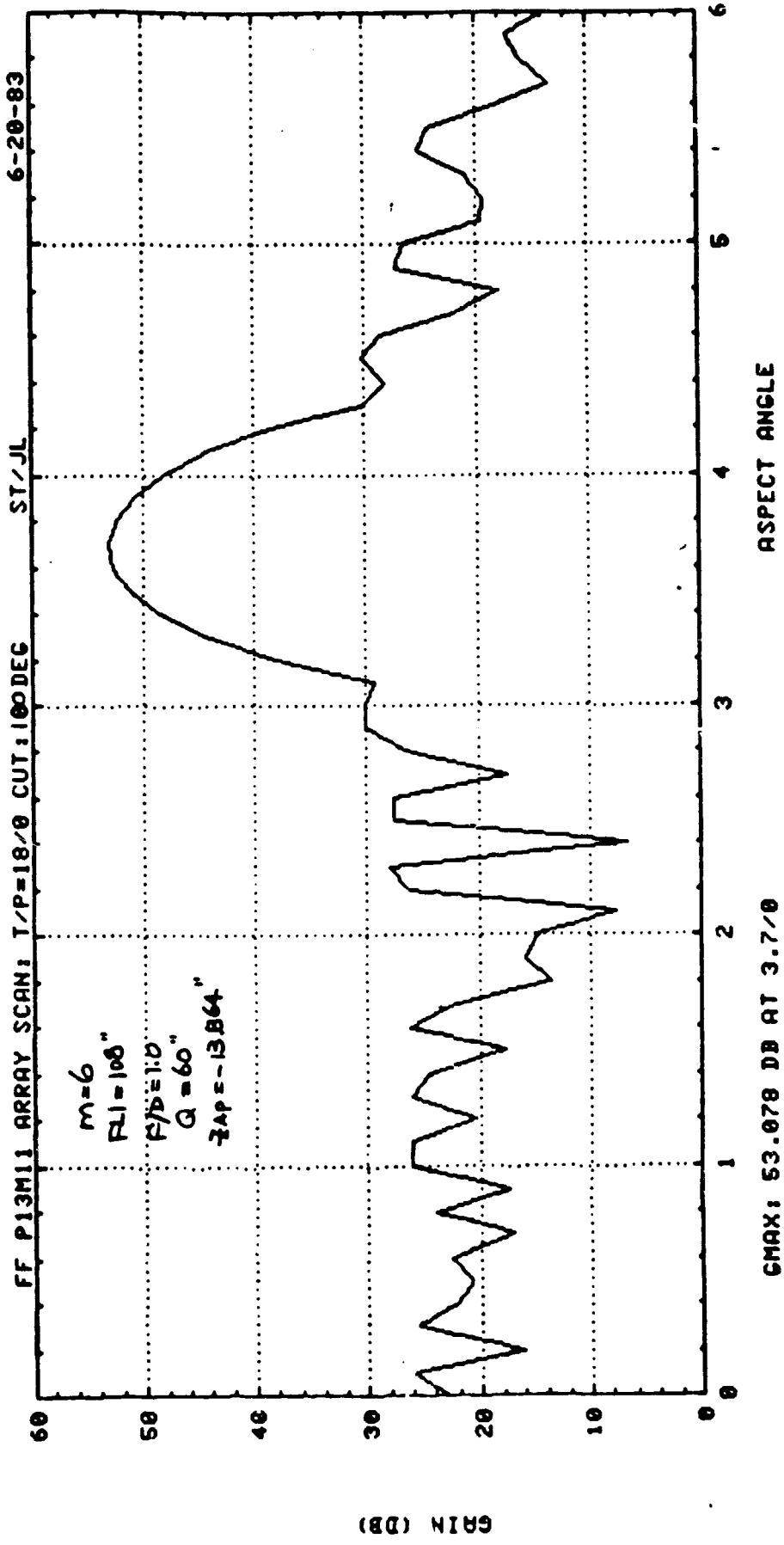
FF P13M11 ARRAY SCAN: T/P=18/0 CUT:180DEG
6-20-83
ST/JL
m=6
RL=108"
F/D=1.0
Q=60"
ZAP=-13.864"
GMAX: 53.078 DB AT 3.7/0
GAIN (DB)
ASPECT ANGLE
60
50
40
30
20
10
0
0
1
2
3
4
5
6

FIG 5.3.11

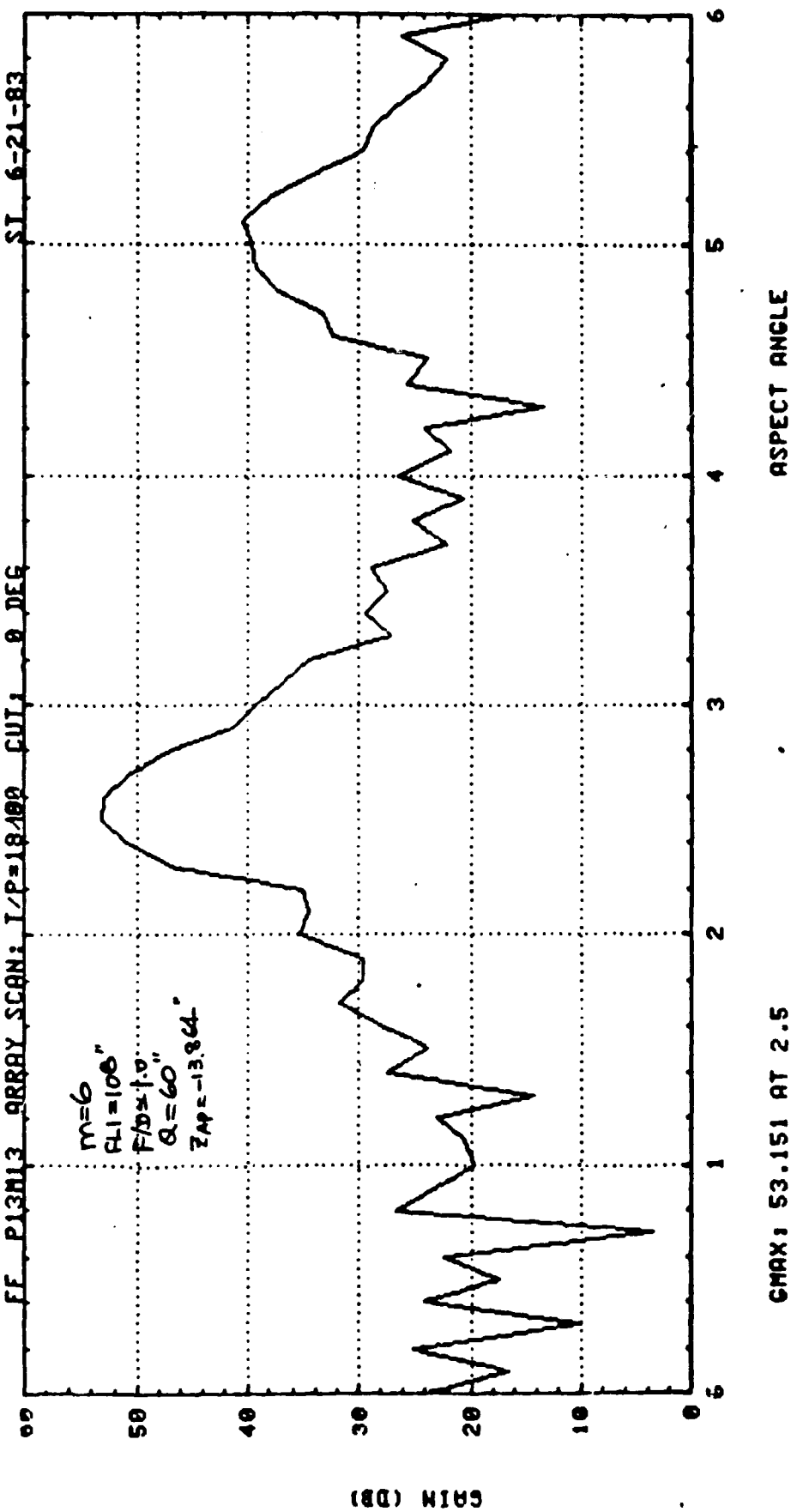
FF P13M13 ARRAY SCAN: I/P=18.00 CUT: 0 DEG SI 6-21-83
m=6
FLI=108"
F/D=1.0
Q=60"
ZAP=-13.84"
GMAX: 53.151 AT 2.5
ASPECT ANGLE
GAIN (DB)
0
10
20
30
40
50
60
1
2
3
4
5
6

FIG 5.3-12

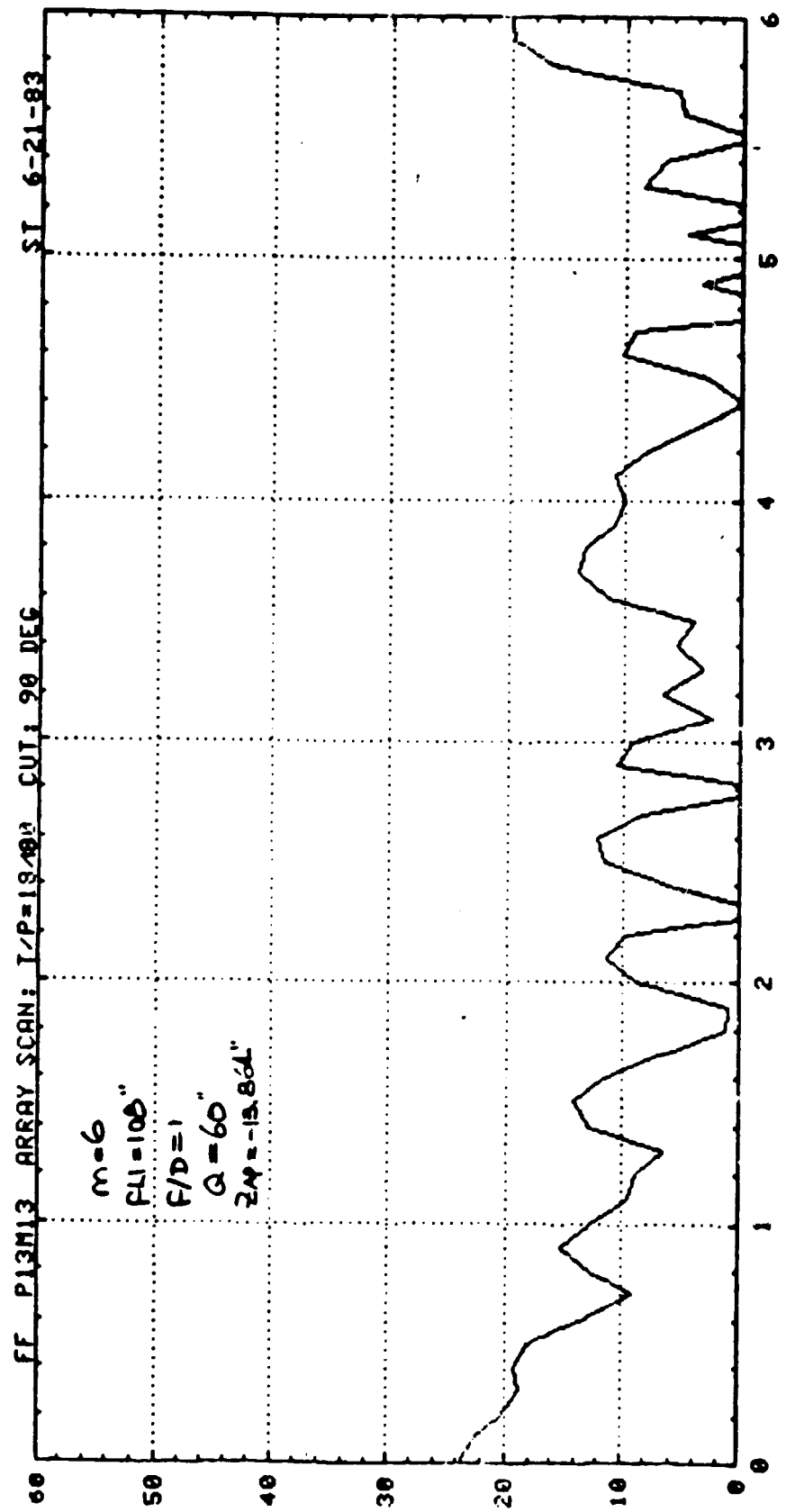
FF P13M13 ARRAY SCAN: I/P=1.48@ CUT 90 DEG
ST 6-21-83
m=6
FLI=10B"
F/D=1
Q=60"
2M=-13.86L"
GAIN (DB)
ASPECT ANGLE
0
10
20
30
40
50
60
1
2
3
4
5
6

FIG 5.3-13

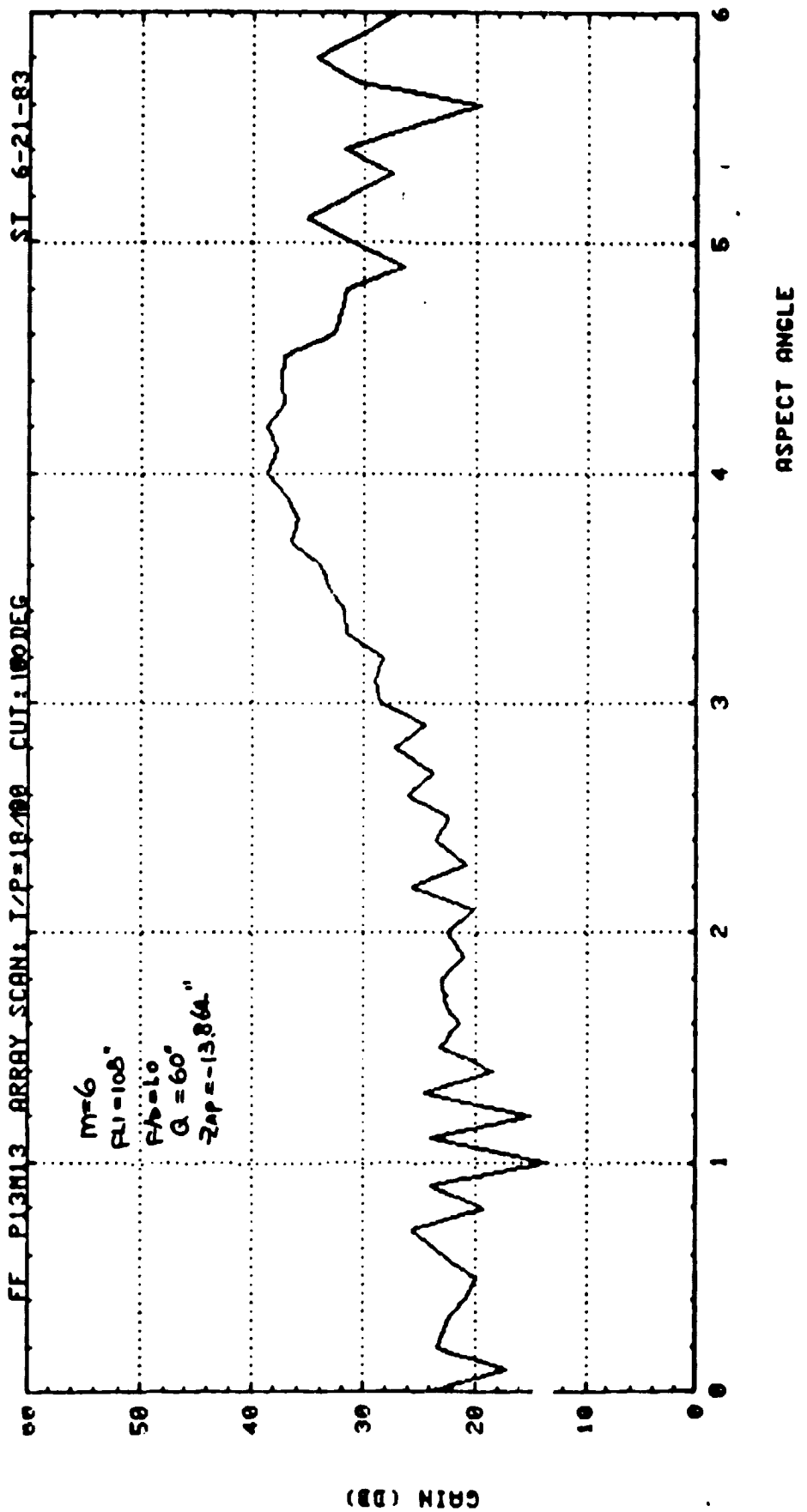
FF P13M13 ARRAY SCAN: I/P=18.00 CUT: 180 DEG ST 6-21-83
m=6
AU=108°
Fb=1.0
Q = 60°
Zap=-13.864"
GAIN (DB)
ASPECT ANGLE
60
50
40
30
20
10
0
0
1
2
3
4
5
6

FIG 5.3-14

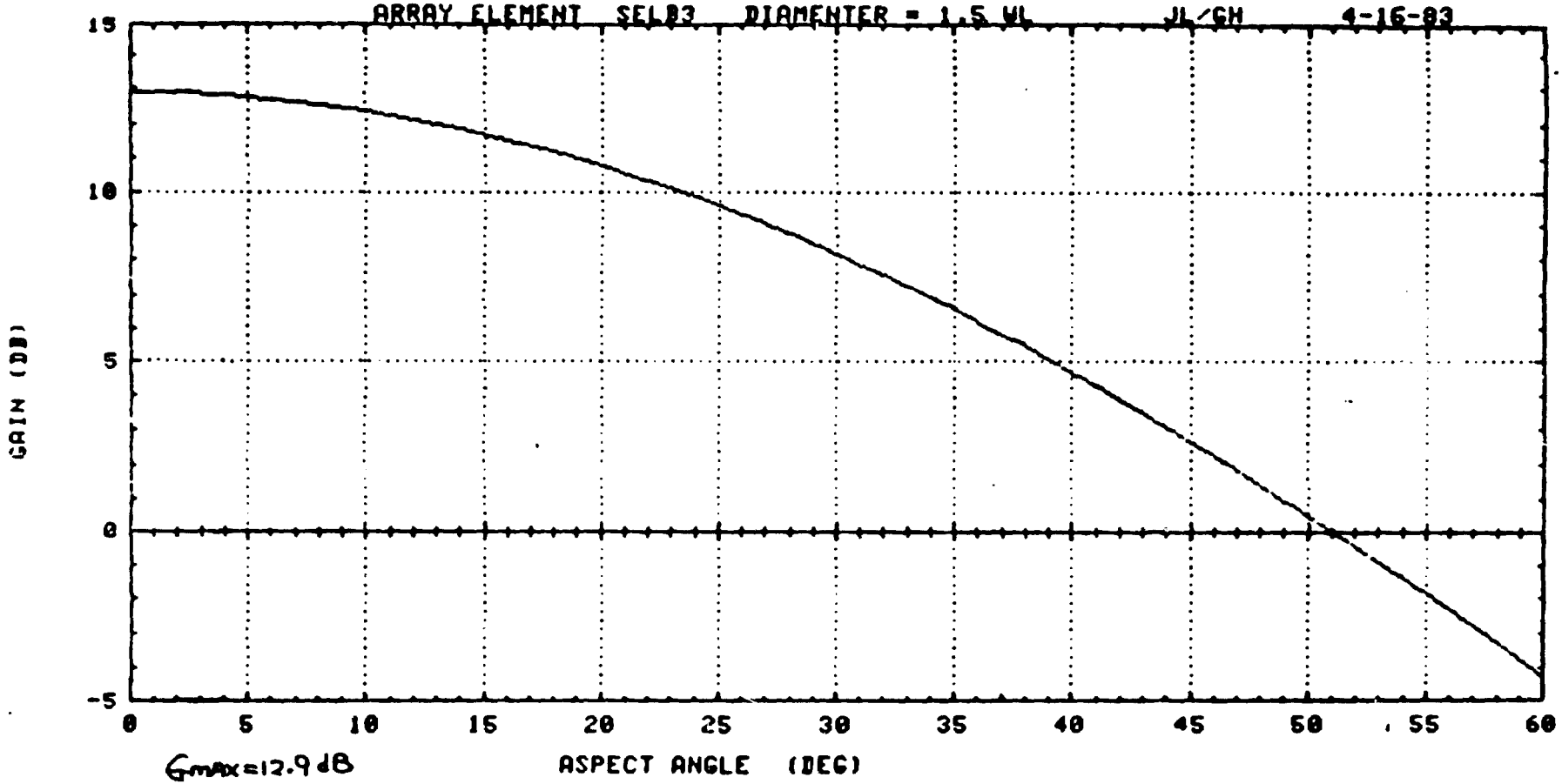

ELEMENT (0.59° DIA.) FOR 16 RING HEX

FIG 5.3-15

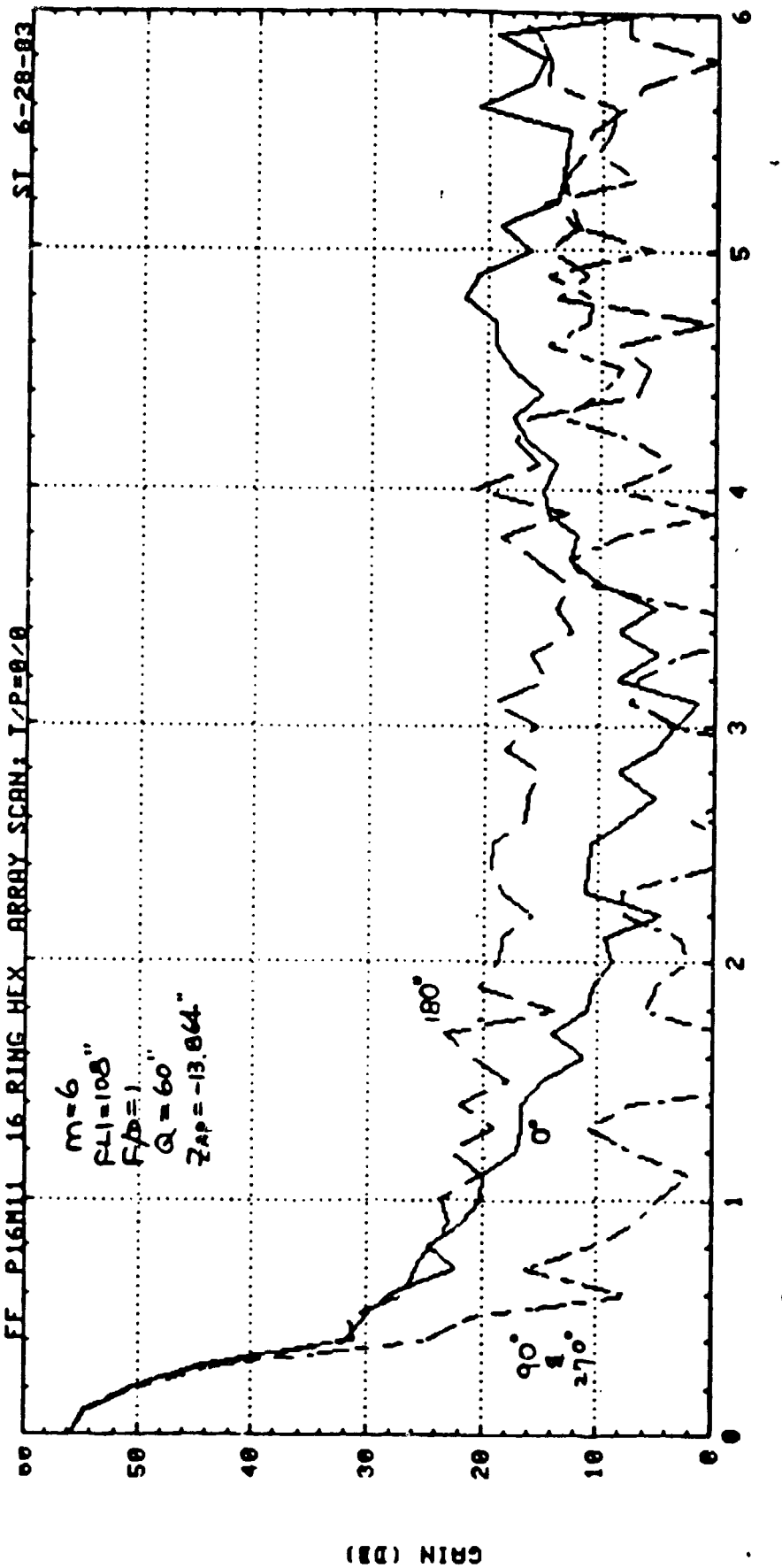
FF PIGMIJ 16 RING HEX ARRAY SCAN: I/P=0/0
SI 6-28-83
m=6
PLI=108"
F/D=1
Q=60"
Zap=-13.864"
180°
0°
90°
270°
GMAX = 55.7 dB
GAIN (DB)
ASPECT ANGLE
60
50
40
30
20
10
0
0
1
2
3
4
5
6

FIG 3.6

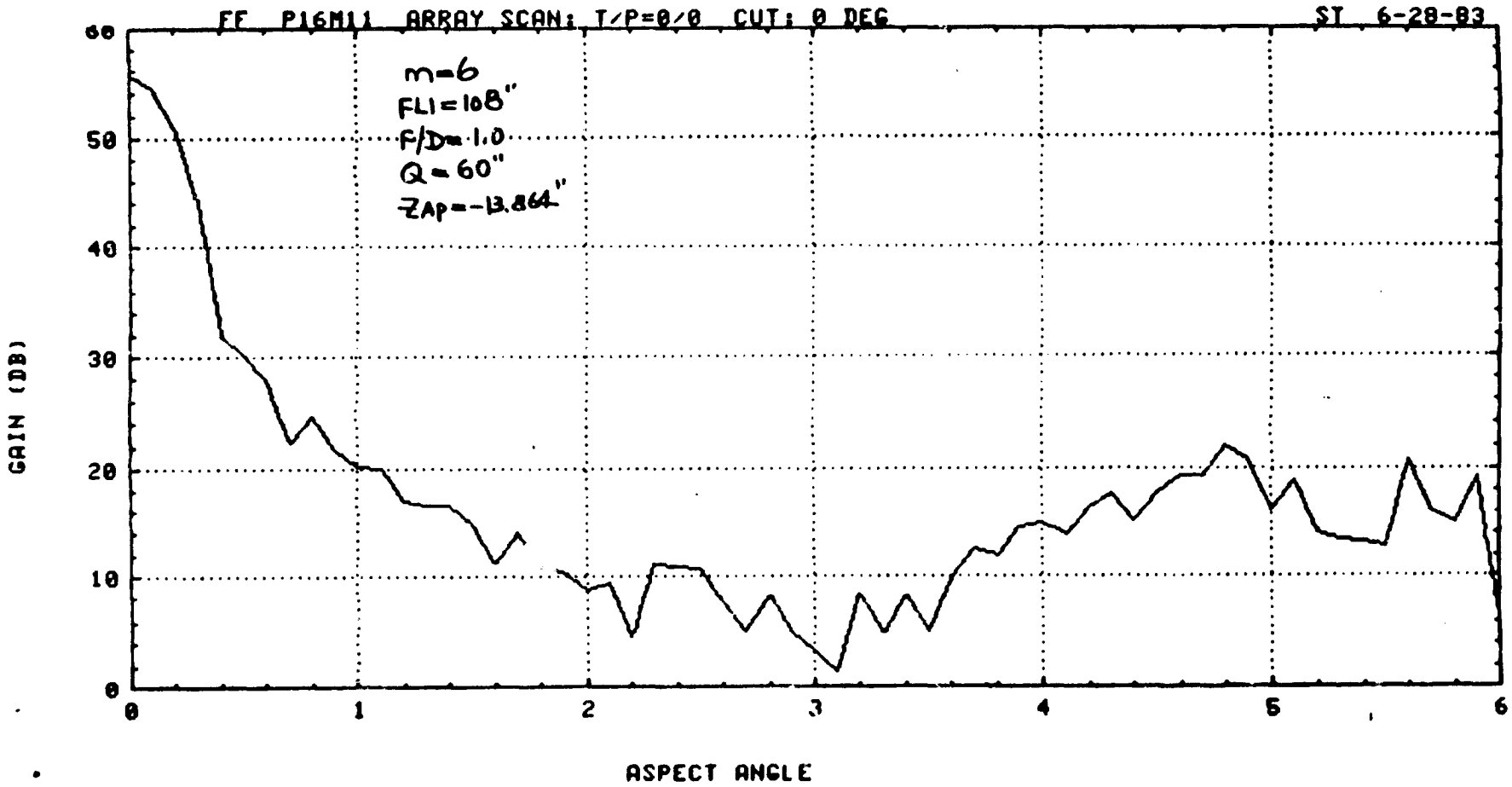
FF P16M11 ARRAY SCAN: T/P=0/0 CUT: 0 DEG
ST 6-28-83
m=6
FLI=108"
F/D=1.0
Q=60"
ZAp=-13.864"
GAIN (DB)
60
50
40
30
20
10
0
0
1
2
3
4
5
6
ASPECT ANGLE

FIG 4.3-17

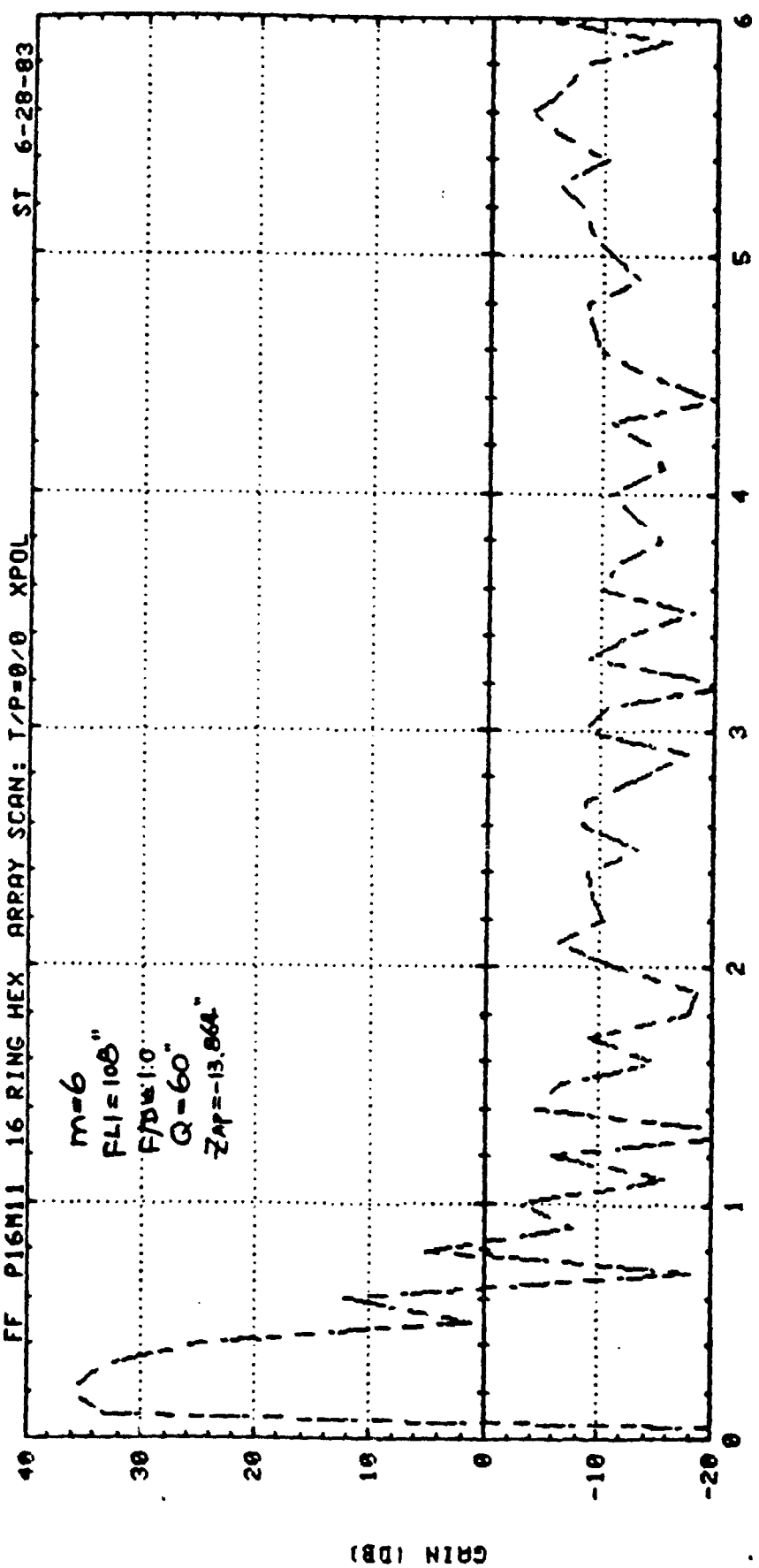
FF P16N11 16 RING HEX ARRAY SCAN: T/P=0/0 XPOL
ST 6-28-83
m=6
FL1=108"
F/D=1.0
Q=60"
ZAP=-13.864"
GAIN (DB)
ASPECT ANGLE
40
30
20
10
0
-10
-20
0
1
2
3
4
5
6

FIG 5.3-18

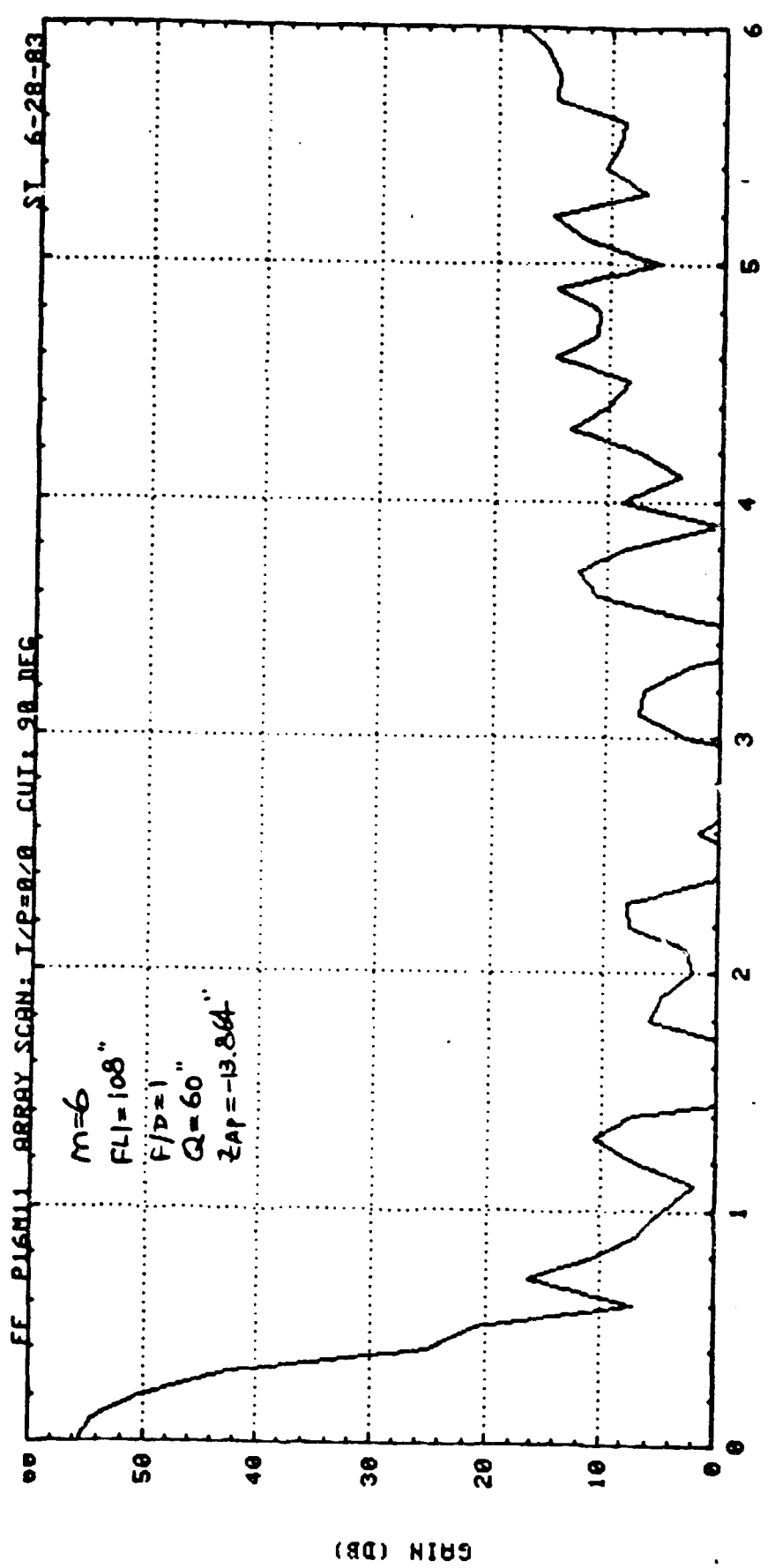
FF PLANAR ARRAY SCAN: I/P=0/0 CUT: 90 DEG
SI 6-28-83
m=6
FLI=108"
F/D=1
Q=60"
ZAP=-13.864"
GAIN (DB)
ASPECT ANGLE
60
50
40
30
20
10
0
0
1
2
3
4
5
6

FIG 3-19

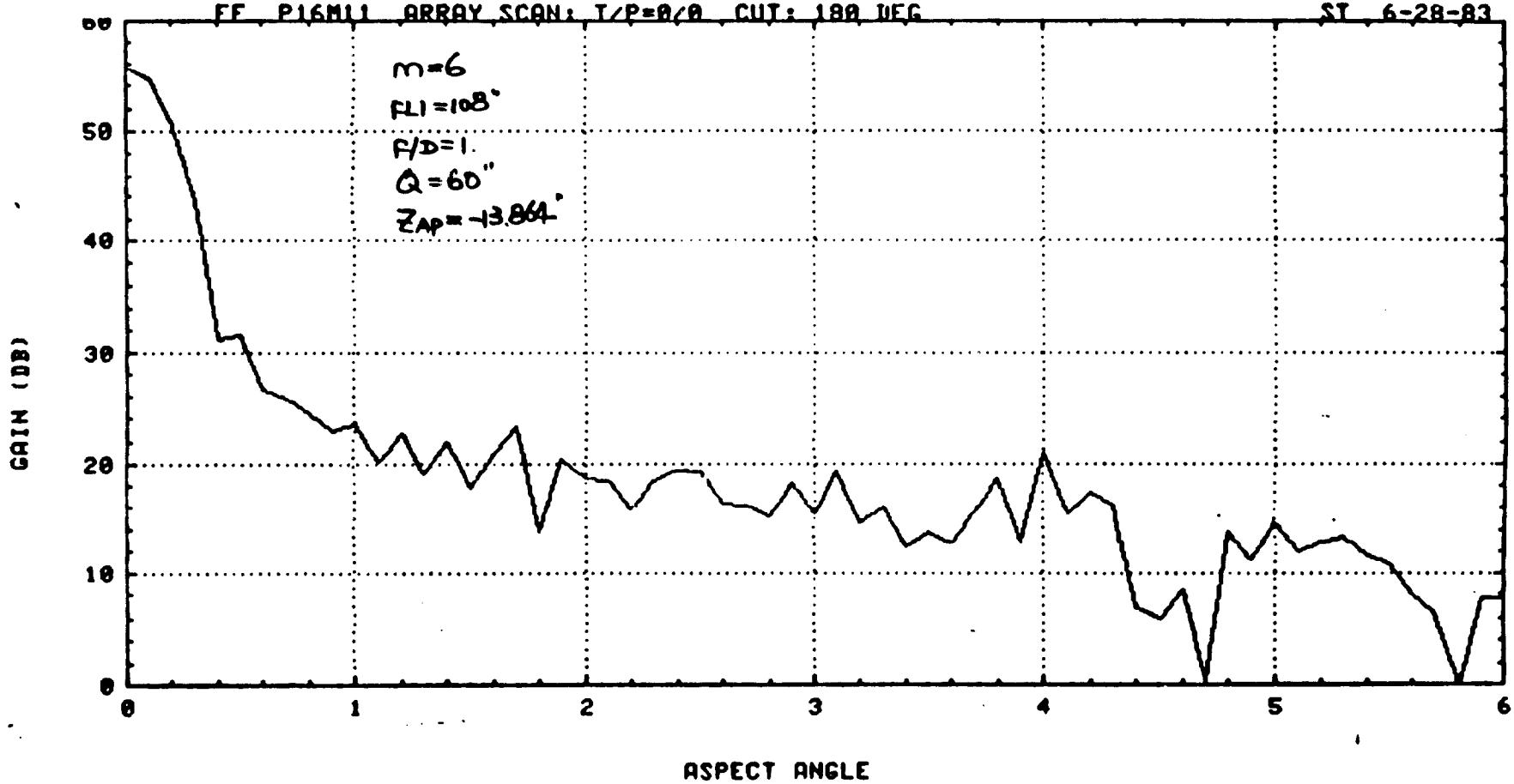
FF P16M11 ARRAY SCAN: T/P=0/0 CUT: 180 DEG
ST 6-28-83
m=6
FLI=108"
F/D=1.
Q=60"
ZAP=-13.864"
GAIN (DB)
60
50
40
30
20
10
0
0
1
2
3
4
5
6
ASPECT ANGLE

FIG 53-20

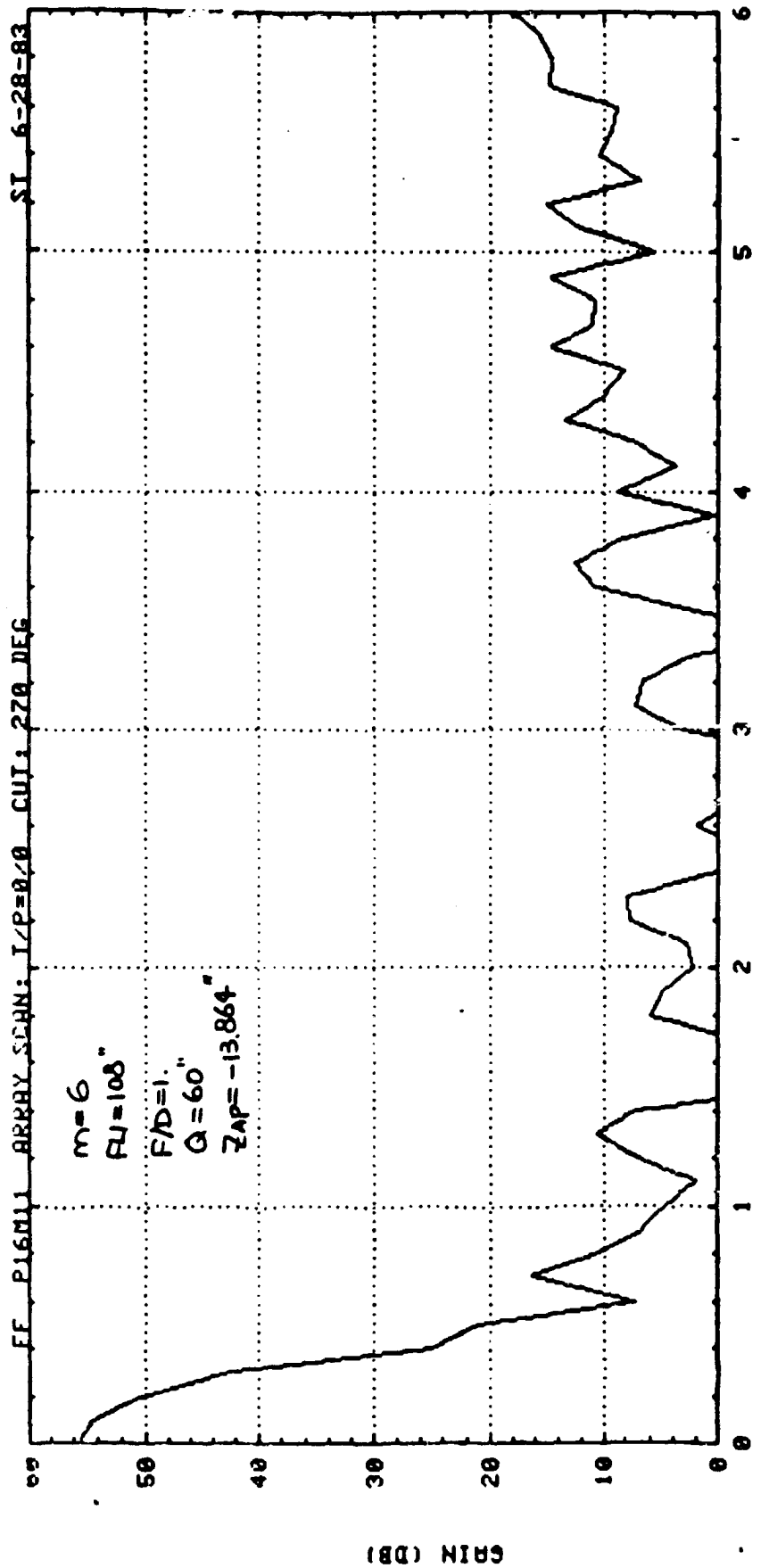
EE PIGMI ARRAY SCAN: I/P=0/0 CUT: 270 DEG
ST 6-28-83
m=6
AU=108"
F/D=1.
Q=60"
Zap=-13.864"
GAIN (DB)
ASPECT ANGLE
60
50
40
30
20
10
0
0
1
2
3
4
5
6

FIG 5.3-21

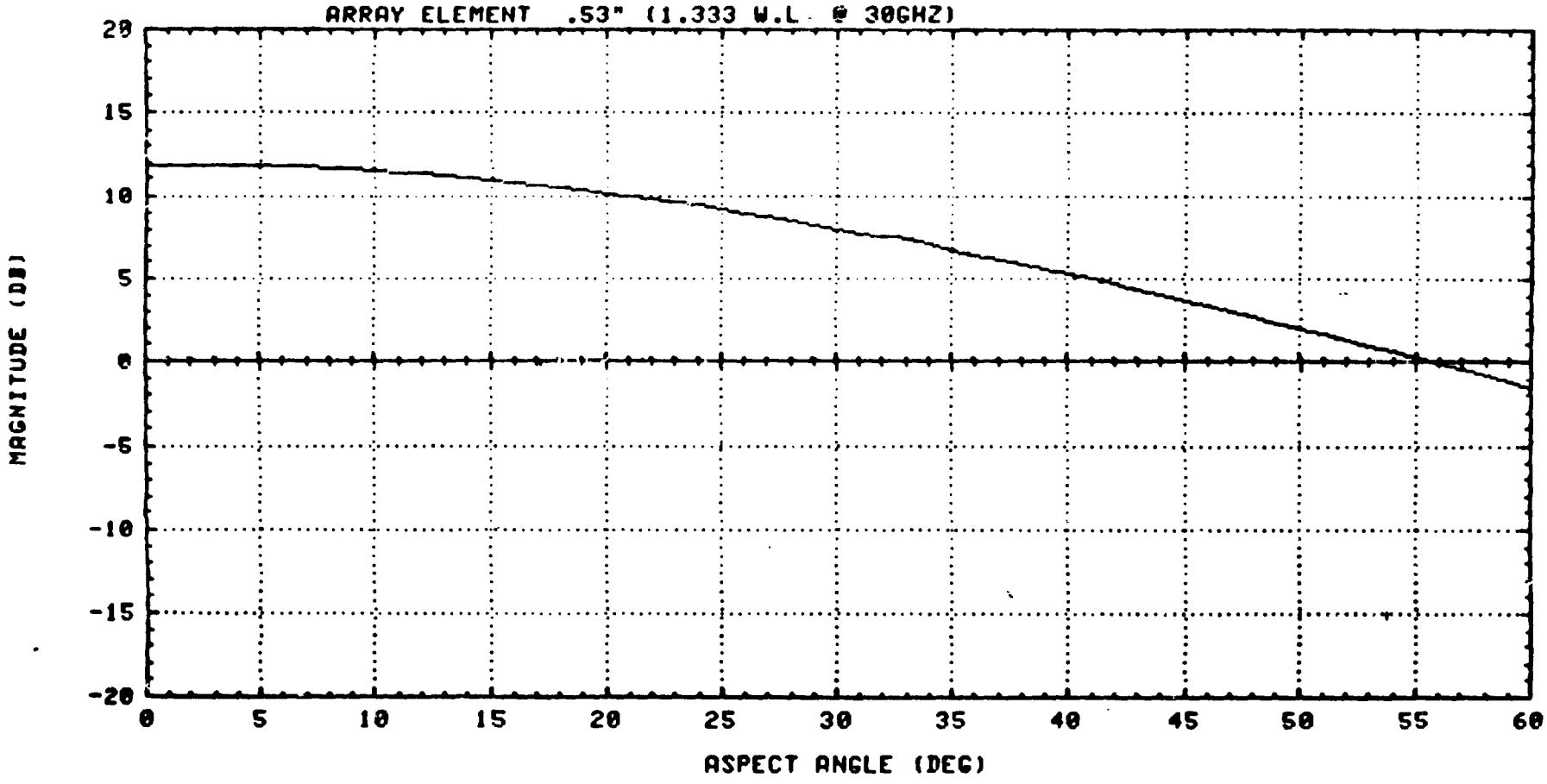

ELEMENT FOR 20 RING HEX ARRAY

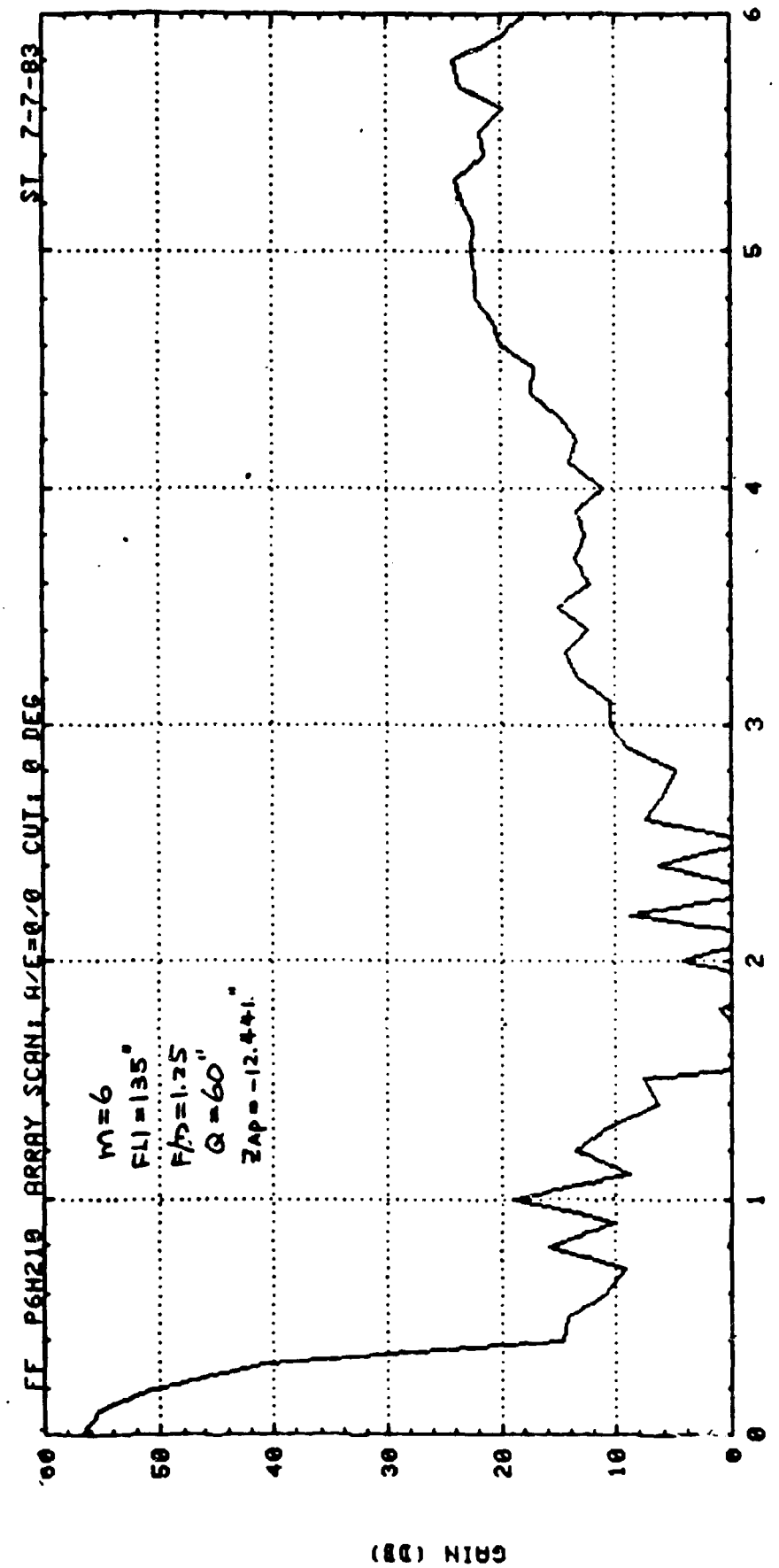
FF P6H210 ARRAY SCAN: H/E=0/0 CUT: 0 DEG
ST 7-7-83
M=6
FLI=135"
F/D=1.25
Q=60"
ZAp=-12.441"
CMAX: 56.749 DB
GAIN (DB)
ASPECT ANGLE
0
10
20
30
40
50
60
1
2
3
4
5
6

FIG 5.3-23

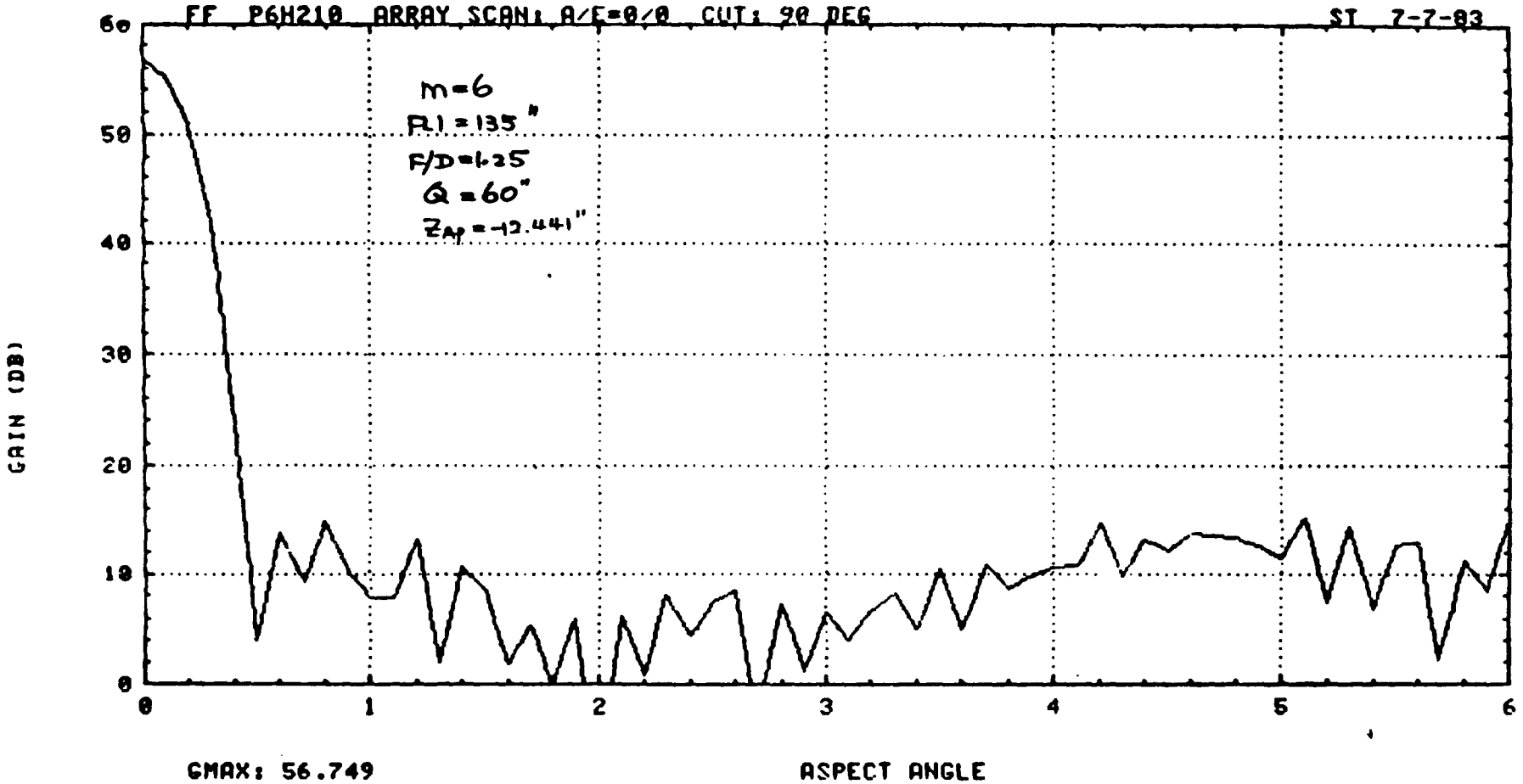
FF P6H210 ARRAY SCAN: A/E=0/0 CUT: 90 DEG
ST 7-7-83
m=6
R1=135"
F/D=1.25
Q=60"
ZAP=-12.441"
GAIN (DB)
60
50
40
30
20
10
0
0
1
2
3
4
5
6
GMAX: 56.749
ASPECT ANGLE

FIG 7.3-24

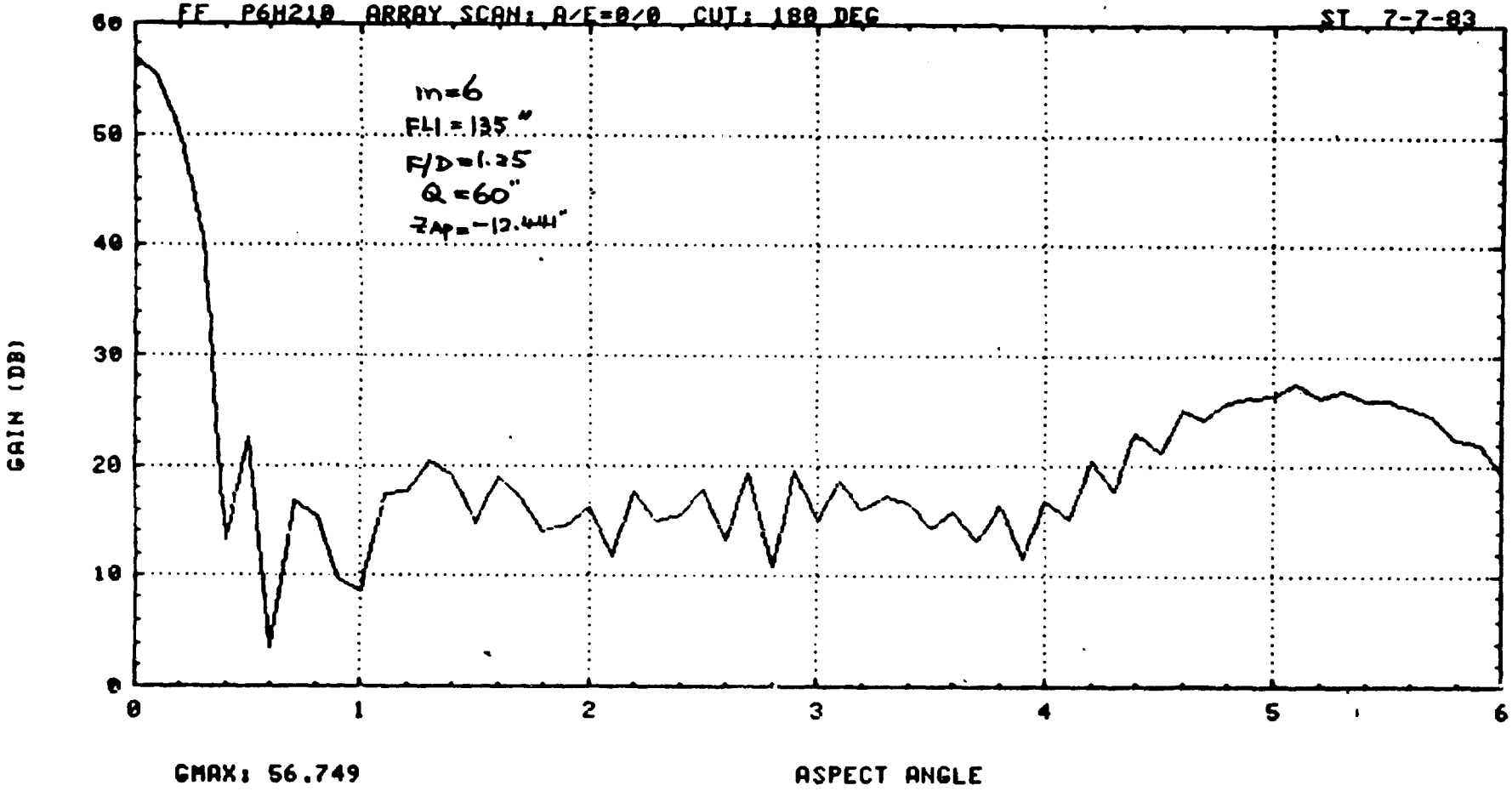
FF P6H210 ARRAY SCAN: A/E=0/0 CUT: 180 DEG
ST 7-7-83
m=6
FLI=135"
F/D=1.25
Q=60"
ZAp=-12.441"
GAIN (DB)
60
50
40
30
20
10
0
0
1
2
3
4
5
6
GMAX: 56.749
ASPECT ANGLE

FIG 5.3-25

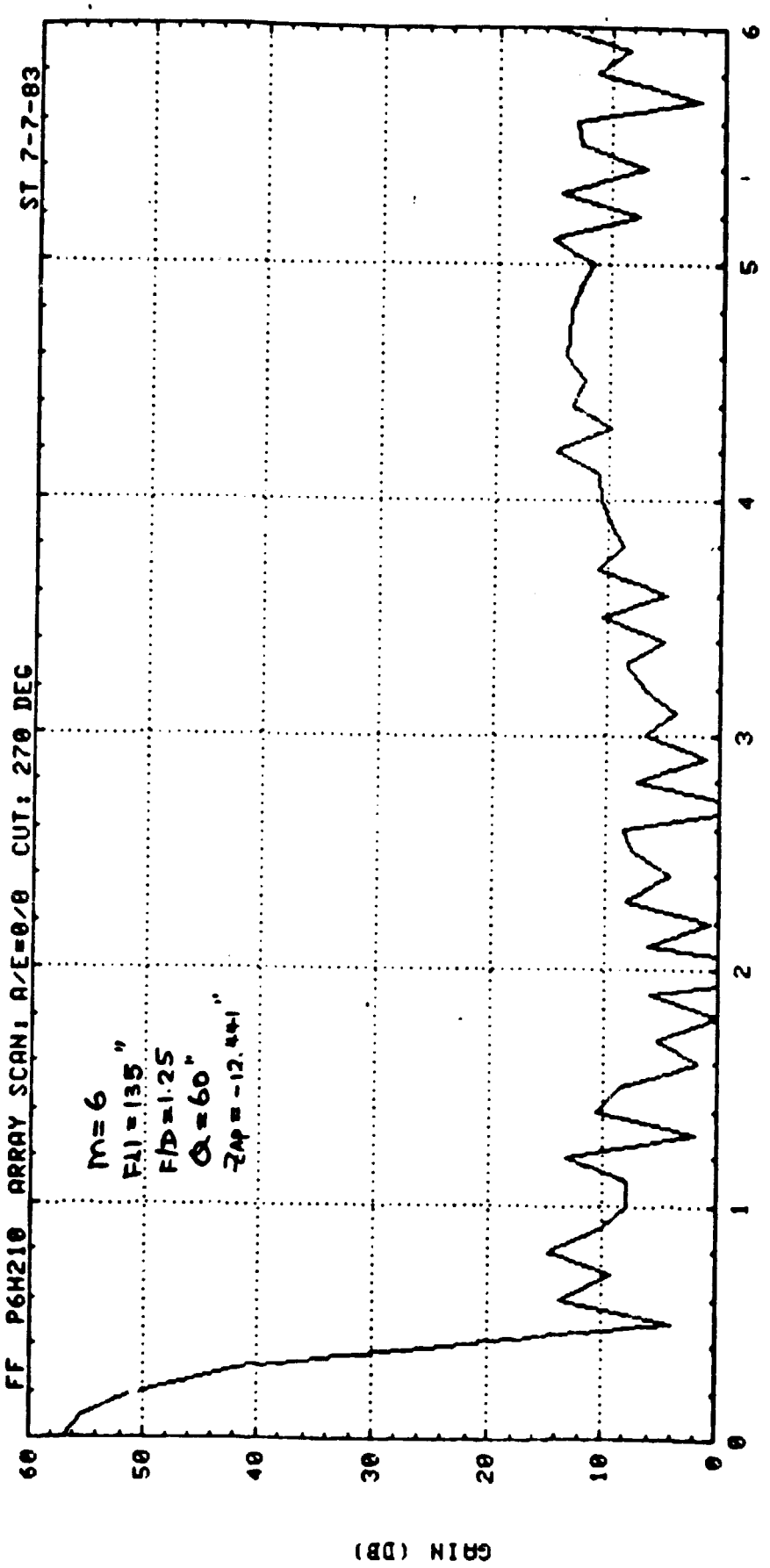
FF P6H210 ARRAY SCAN: A/E=0/0 CUT: 270 DEC
ST 7-7-83
m=6
Fu=135"
Fb=1.25
Q=60"
Zp=-12.441"
GAIN (DB)
ASPECT ANGLE
GMAX: 56.749 DB
0
10
20
30
40
50
60
1
2
3
4
5
6

FIG 5.3-26

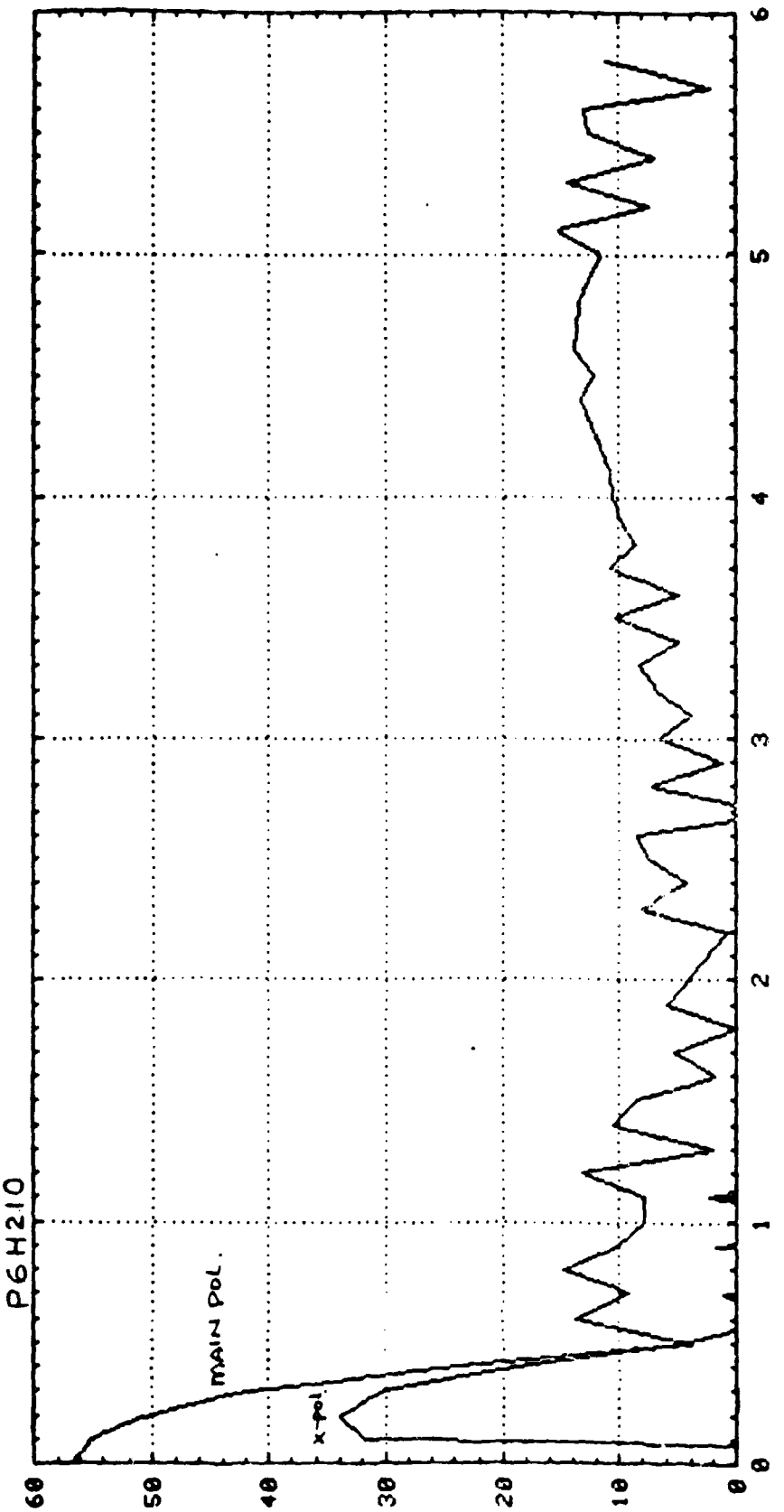

FIG 5.3-27

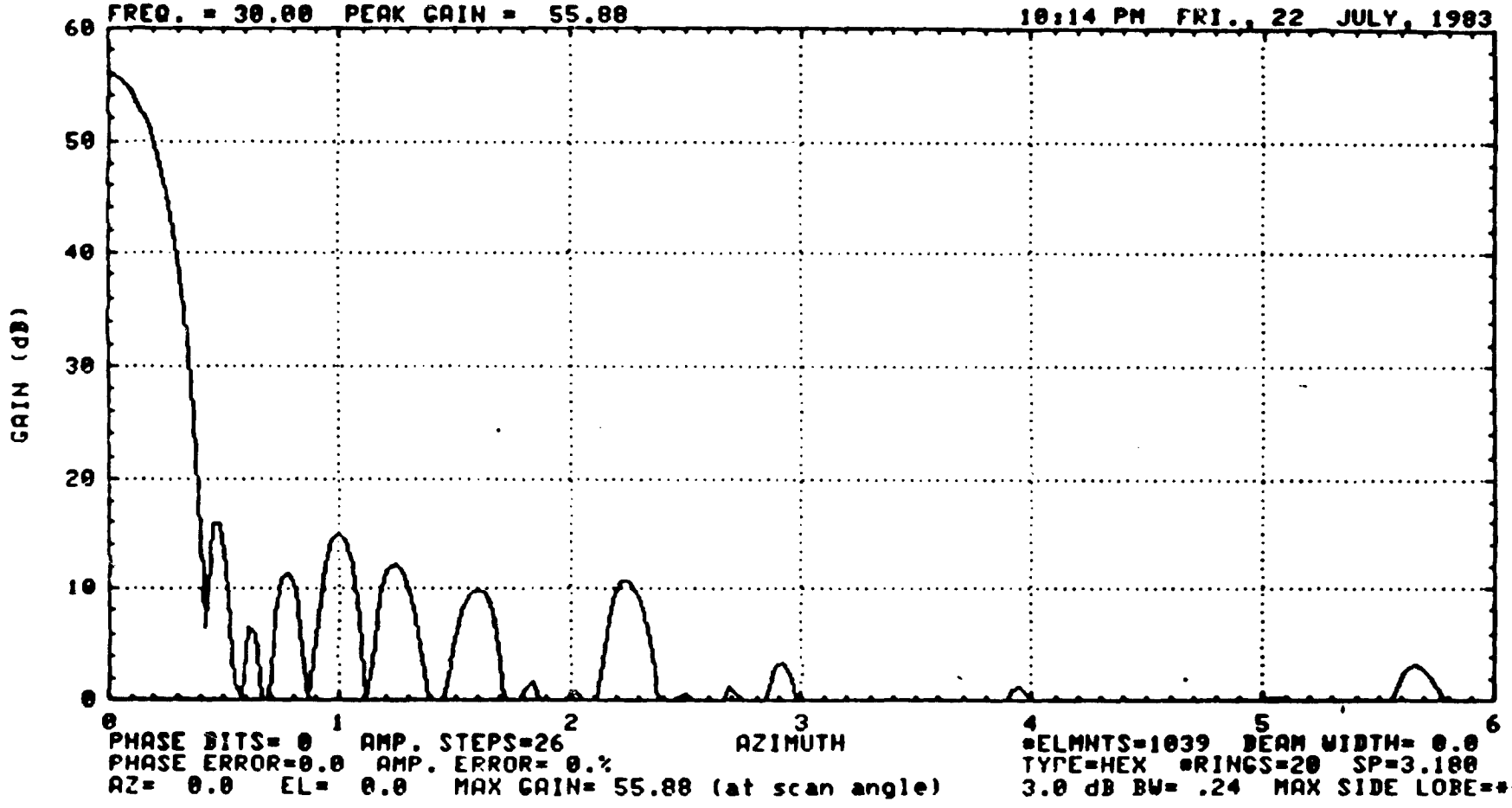

ELEMENT HORN ENLARGED 6 TIMES, FOR IMAGING CONCEPT VERIFICATION
AZ-CUT, ARRAY PATTERN

FIG 5.3-28

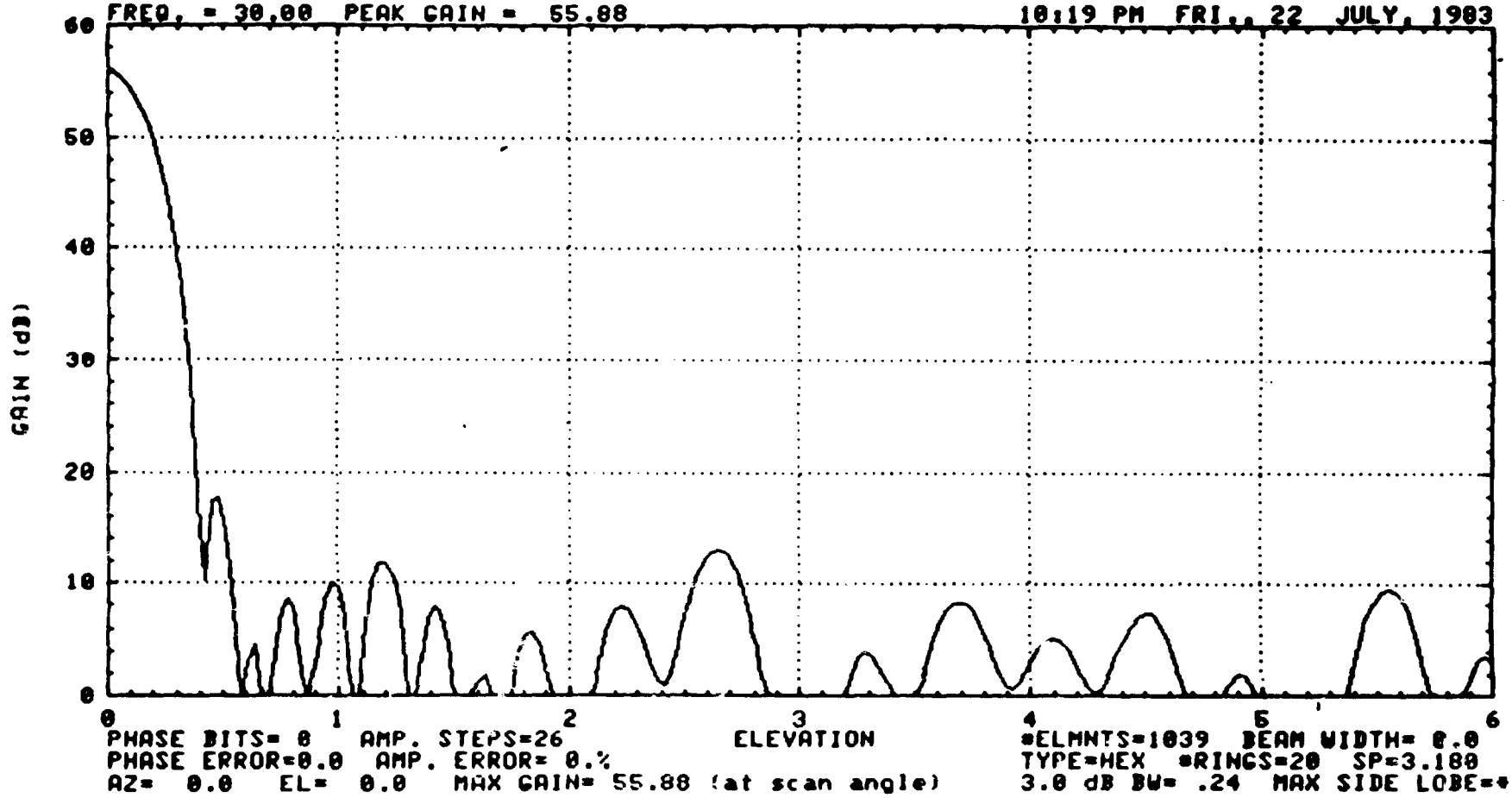

ELEMENT HORN ENLARGED 6 TIMES, FOR IMAGING CONCEPT VERIFICATION

EL-CUT, ARRAY PATTERN

FIG 5.3-29

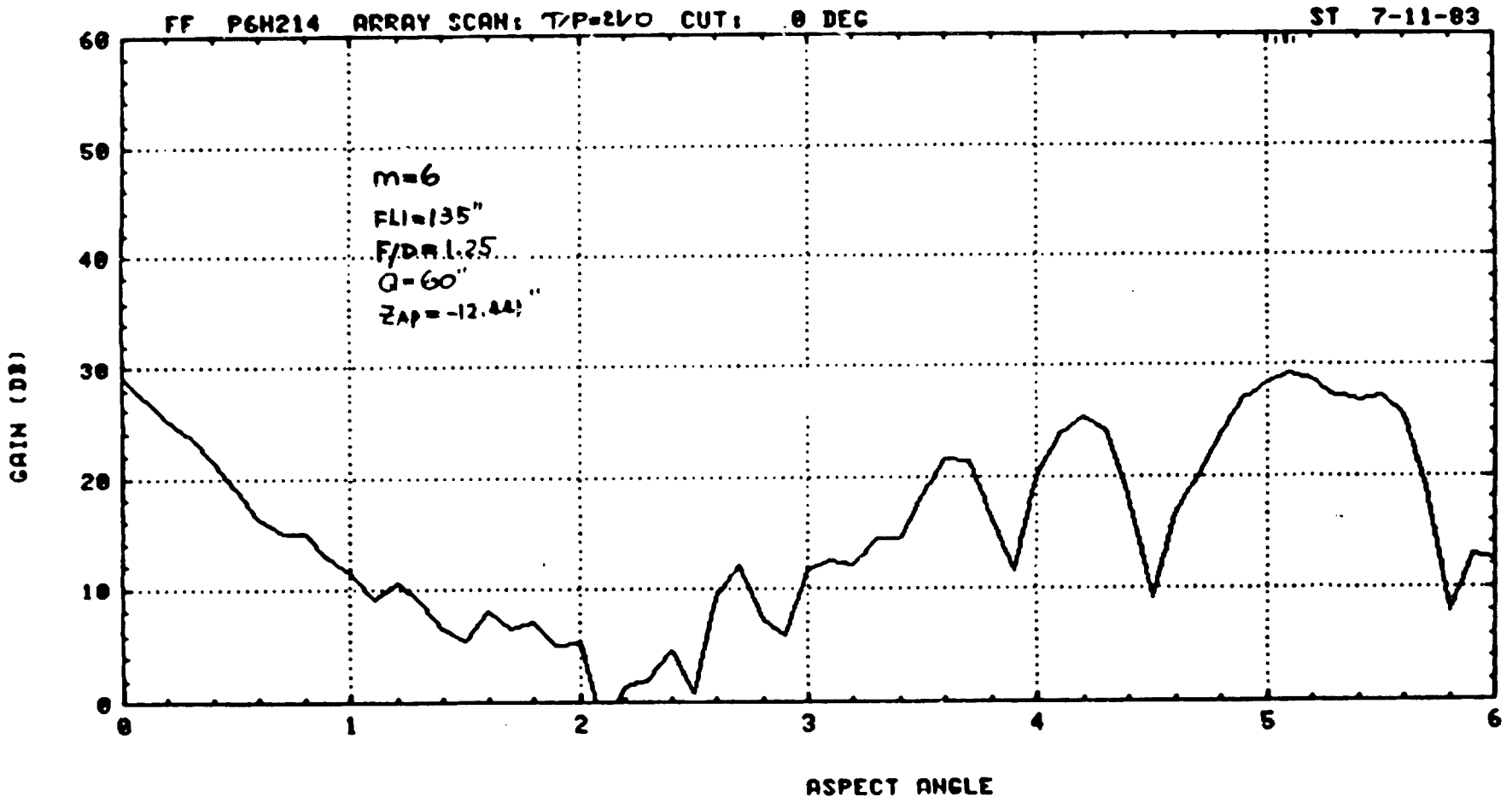
FF P6H214 ARRAY SCAN: T/P=2V0 CUT: 0 DEG
ST 7-11-83
m=6
FLI=135"
F/D=1.25
Q=60"
ZAP=-12.441"
GAIN (DB)
60
50
40
30
20
10
0
0
1
2
3
4
5
6
ASPECT ANGLE

Fig 5.3-30

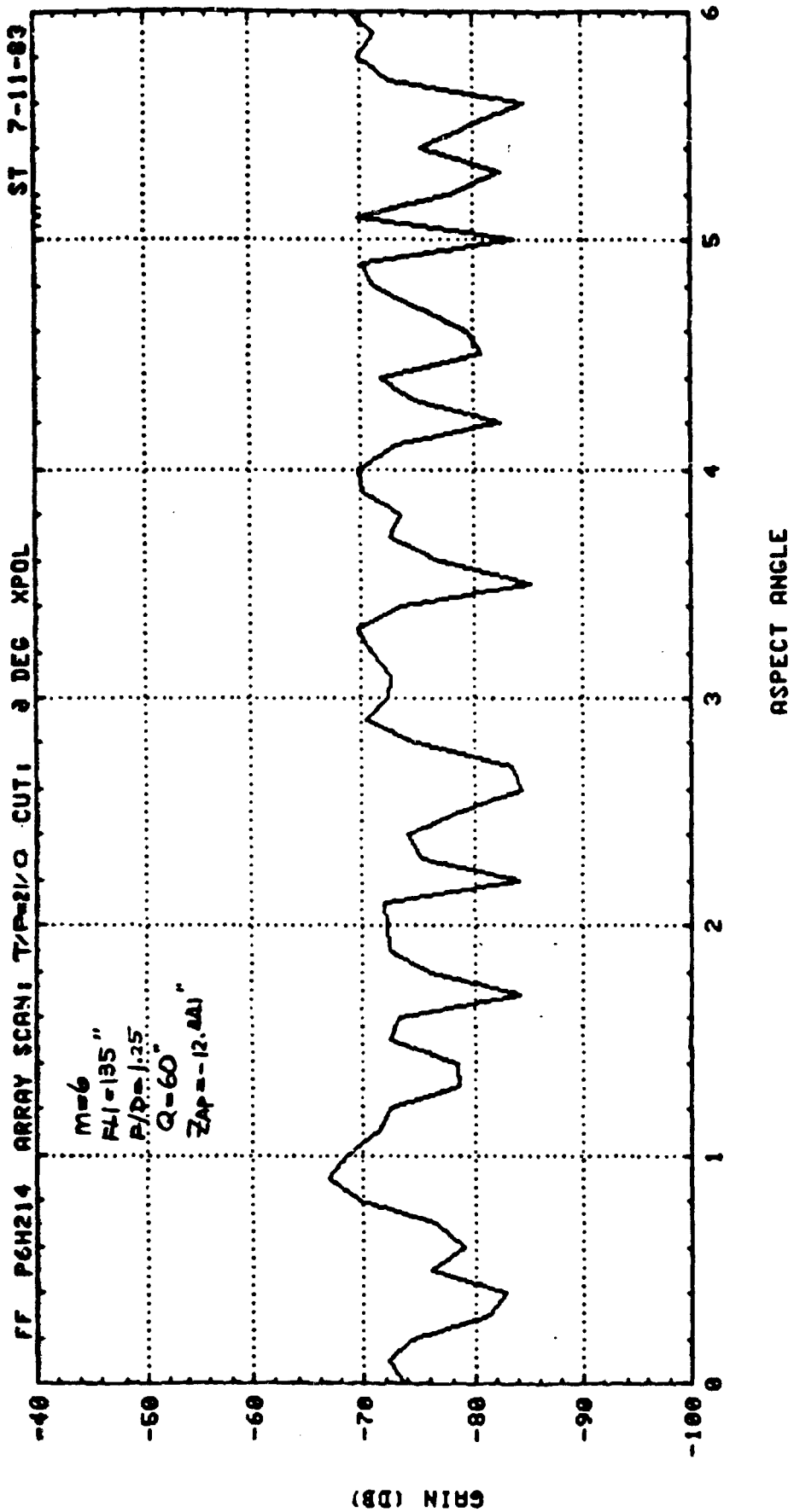
FF P6H214 ARRAY SCAN: T/P=21/0 CUT: 0 DEG XPOL
ST 7-11-83
m=6
AI=135"
P/P=1.25
Q=60"
Zap=-12.81"
GAIN (DB)
-40
-50
-60
-70
-80
-90
-100
0
1
2
3
4
5
6
ASPECT ANGLE

FIG 5.3-31

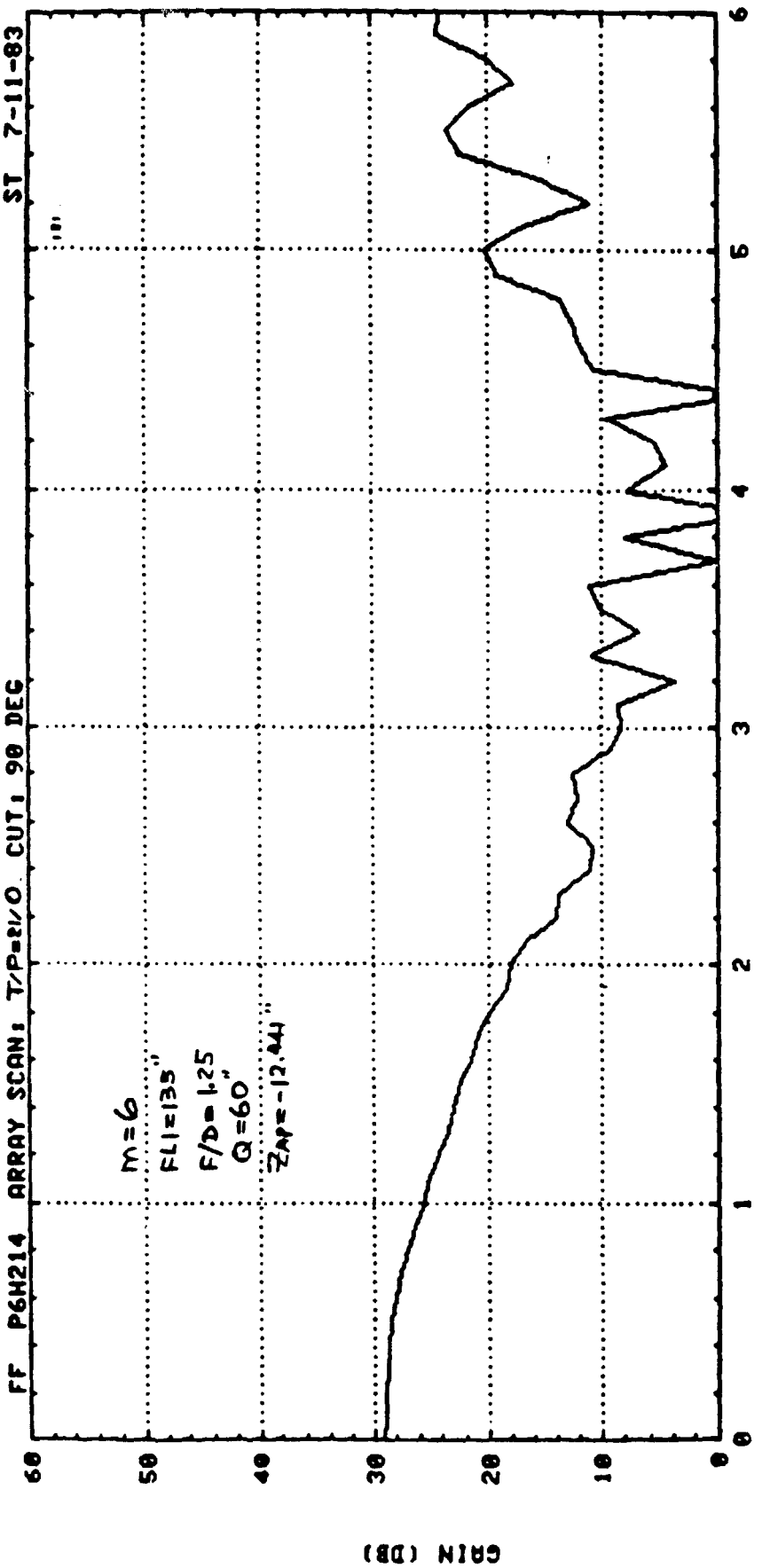
FF P6H214 ARRAY SCAN: T/P=21/0 CUT: 90 DEG
ST 7-11-83
M=6
FL1=135"
F/D=1.25
Q=60"
ZAP=-12.44"
GAIN (DB)
ASPECT ANGLE
60
50
40
30
20
10
0
0
1
2
3
4
5
6

FIG 5.3-32

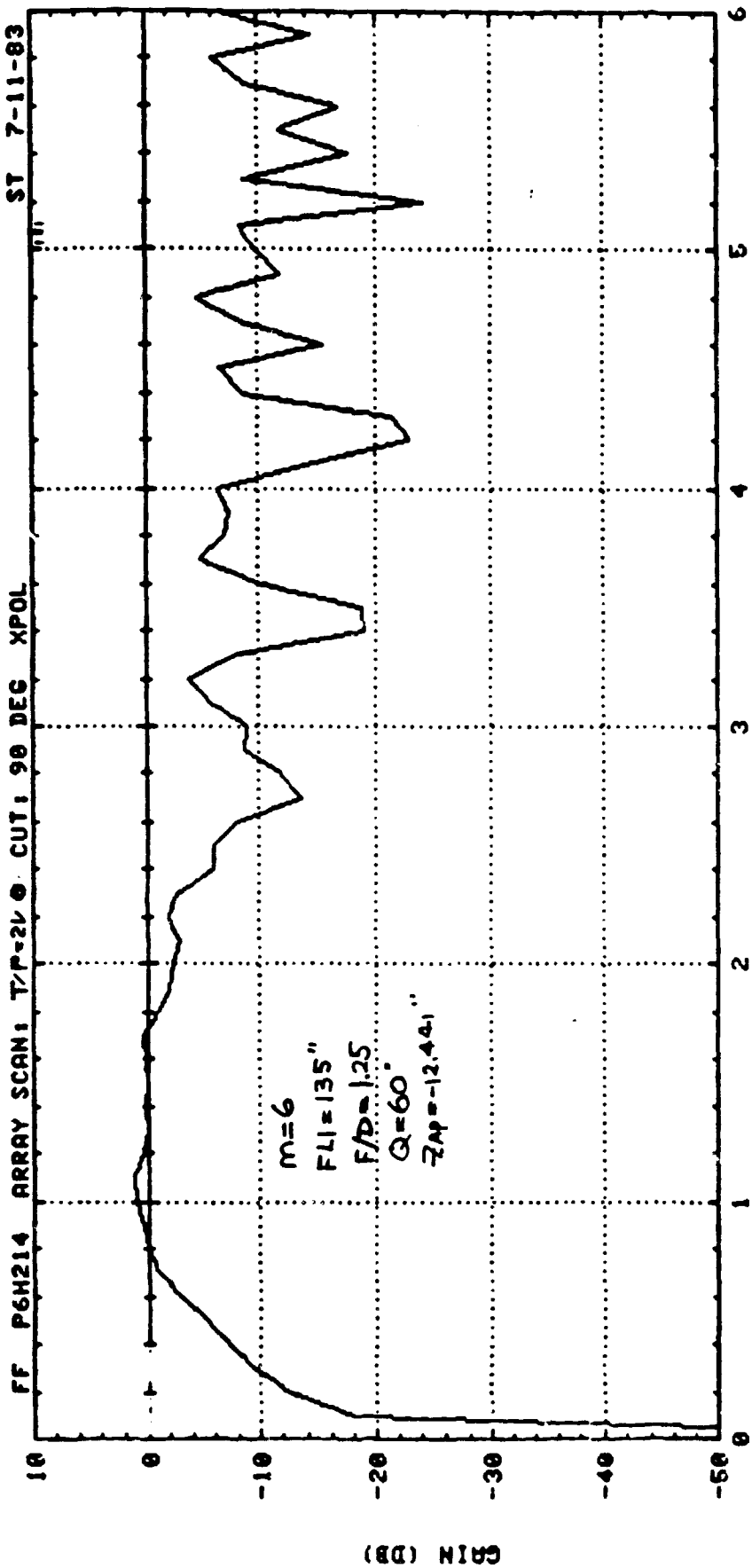
FF P6H214 ARRAY SCAN: T/P-2V @ CUT: 90 DEG XPOL
ST 7-11-83
m=6
FLI=135"
F/D=1.25
Q=60°
ZM=-12.441"
GAIN (DB)
ASPECT ANGLE
10
0
-10
-20
-30
-40
-50
0
1
2
3
4
5
6

FIG 5.3-33

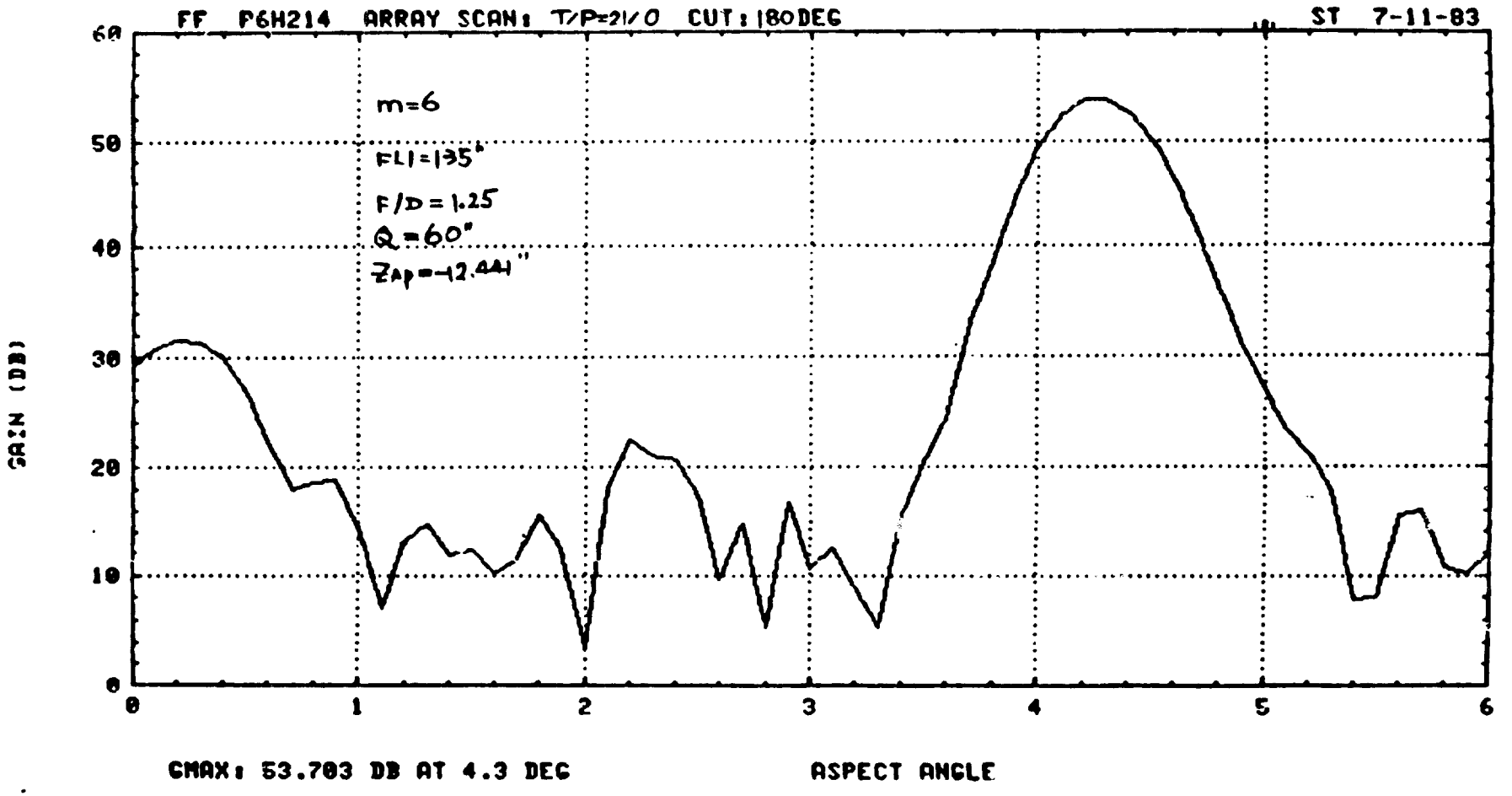
FF P6H214 ARRAY SCAN: T/P=21/0 CUT: 180DEG
ST 7-11-83
m=6
FLI=135"
F/D=1.25
Q=60"
ZAP=-12.441"
GAIN (DB)
60
50
40
30
20
10
0
0
1
2
3
4
5
6
GMAX: 53.703 DB AT 4.3 DEG
ASPECT ANGLE

FIG 5.3-34

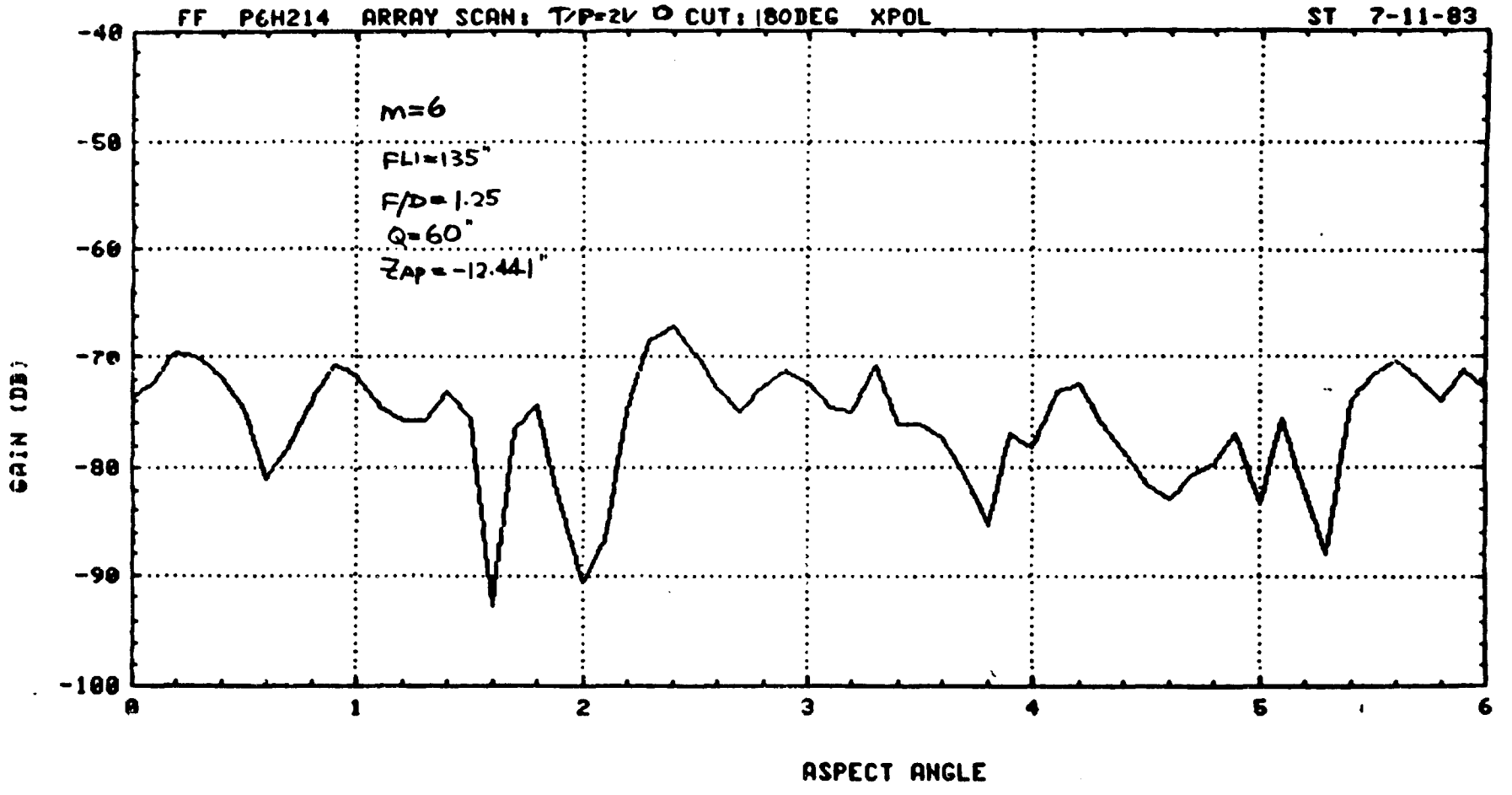
FF P6H214 ARRAY SCAN: T/P=2V Φ CUT: 180DEG XPOL
ST 7-11-83
m=6
FL1=135"
F/D=1.25
Q=60"
ZAP=-12.441"
GAIN (DB)
-40
-50
-60
-70
-80
-90
-100
0
1
2
3
4
5
6
ASPECT ANGLE

FIG 5.3-35

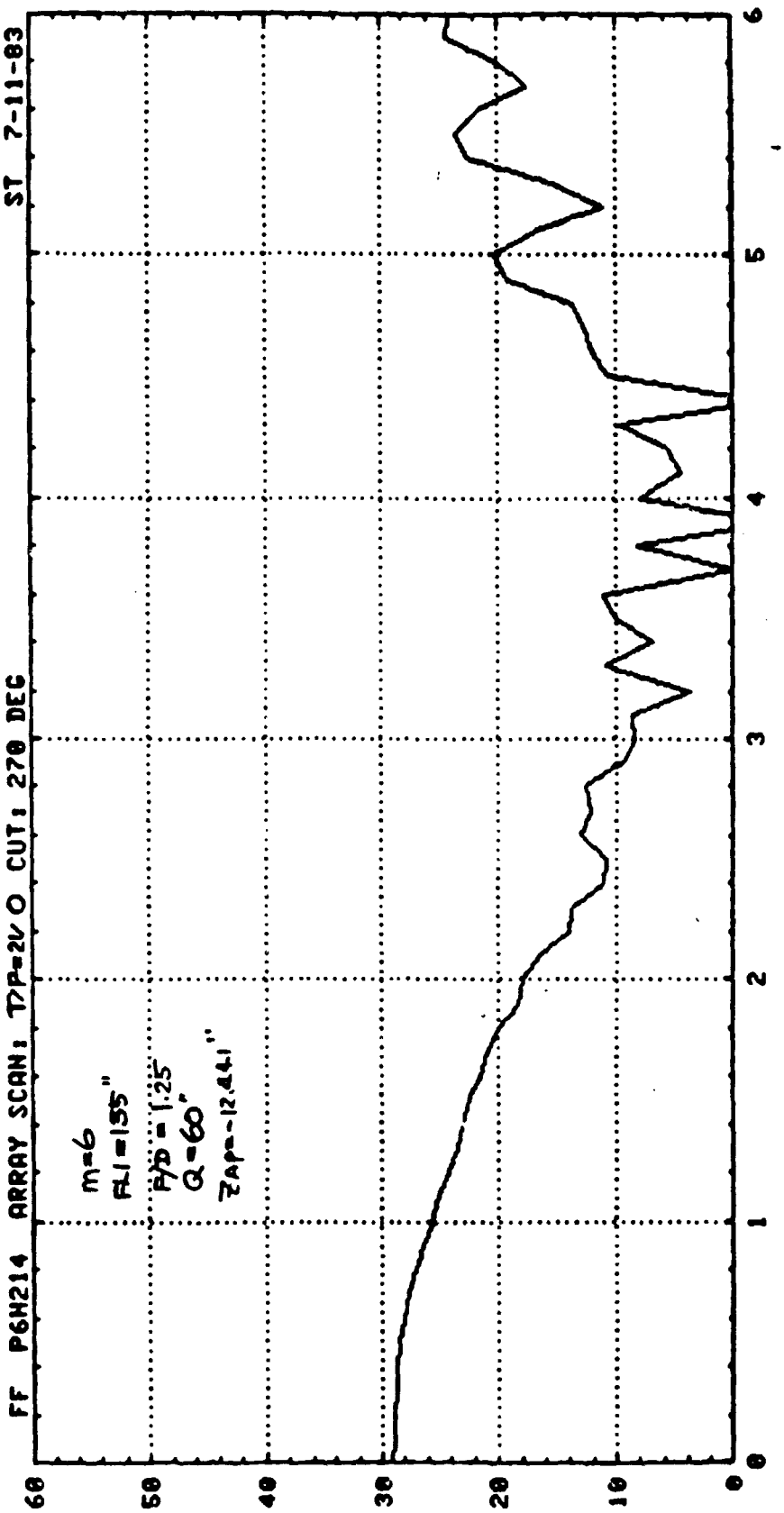
FF P6H214 ARRAY SCAN: TP=270 CUT: 270 DEG
ST 7-11-83
m=6
AL=135"
B/b=1.25
Q=60°
Zap=-12.441"
GAIN (DB)
ASPECT ANGLE
60
50
40
30
20
10
0
0
1
2
3
4
5
6

FIG 5.3-36

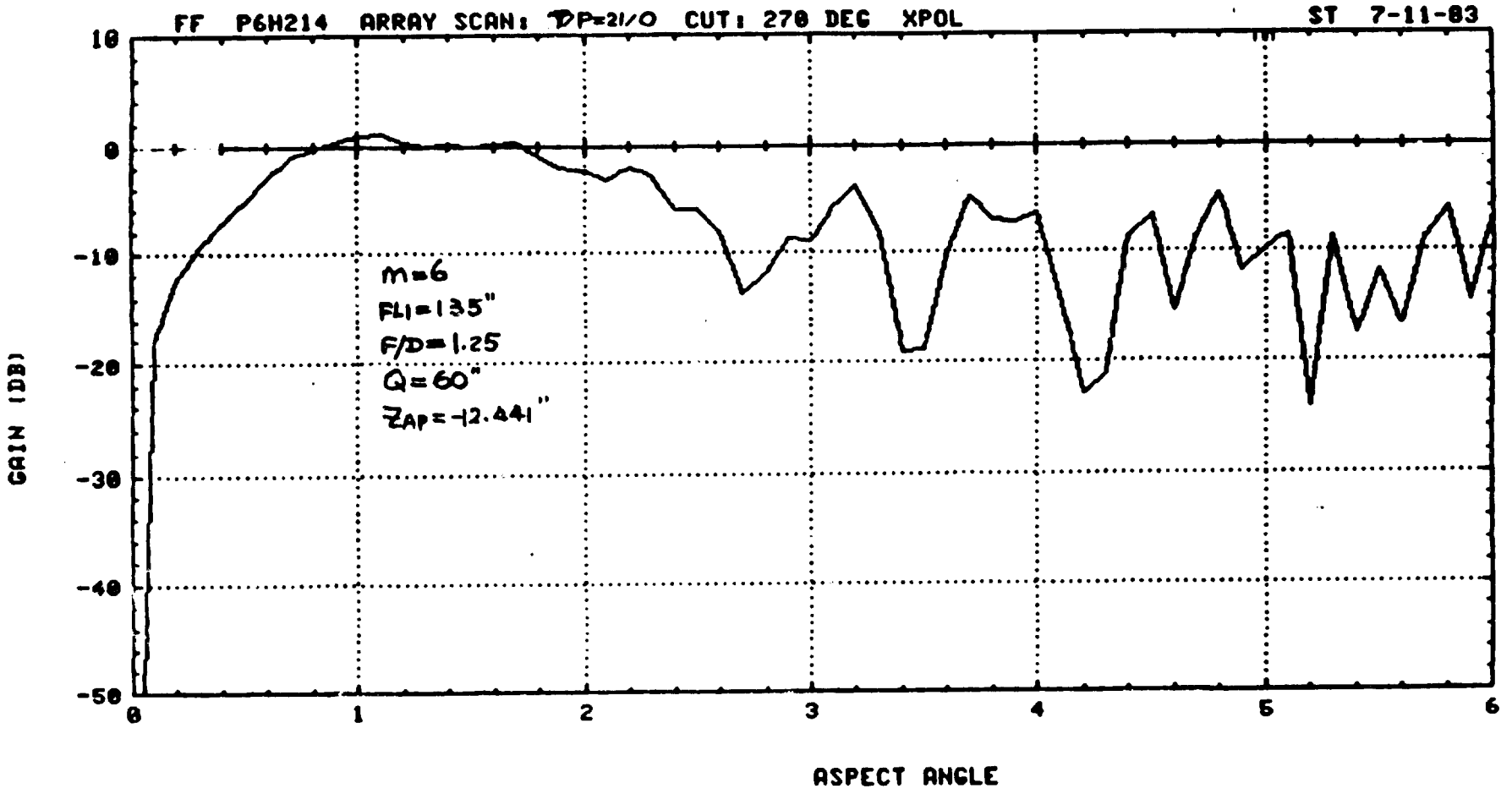
FF P6H214 ARRAY SCAN: ΦP=210 CUT: 270 DEG XPOL
ST 7-11-83
m=6
FLI=135"
F/D=1.25
Q=60"
ZAP=-12.441"
GAIN (DB)
ASPECT ANGLE
10
0
-10
-20
-30
-40
-50
0
1
2
3
4
5
6

FIG 5.3-37

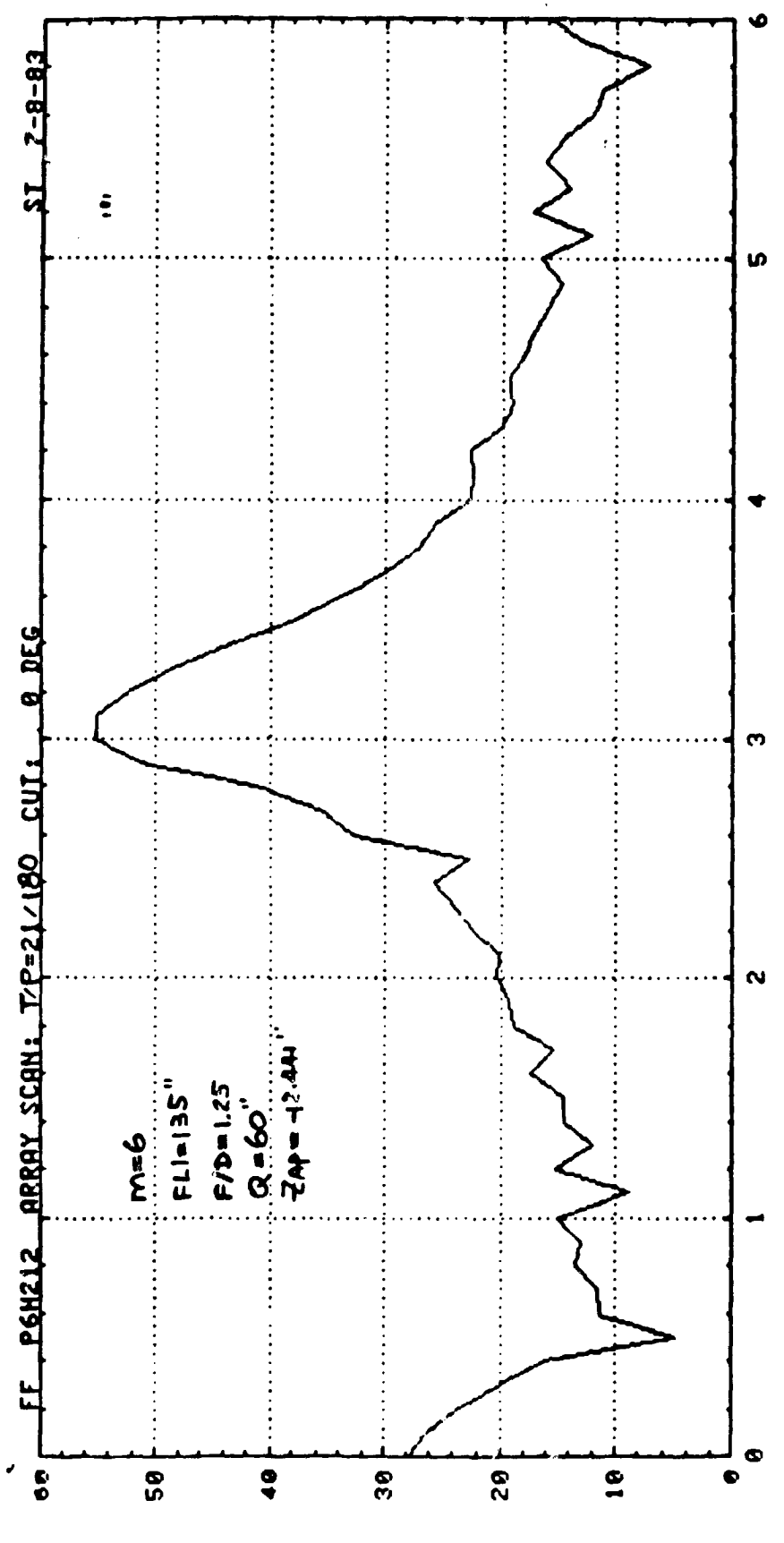
FF P6H212 ARRAY SCAN: T/P=21/180 CUT: 0 DEG SI 2-8-83
m=6
FLI=135"
F/D=1.25
Q=60"
ZAP=-12.4W'
GMAX: 55.045 DB AT 3.00 DEG
GAIN (DB)
ASPECT ANGLE
60
50
40
30
20
10
0
0
1
2
3
4
5
6

Fig 53-38

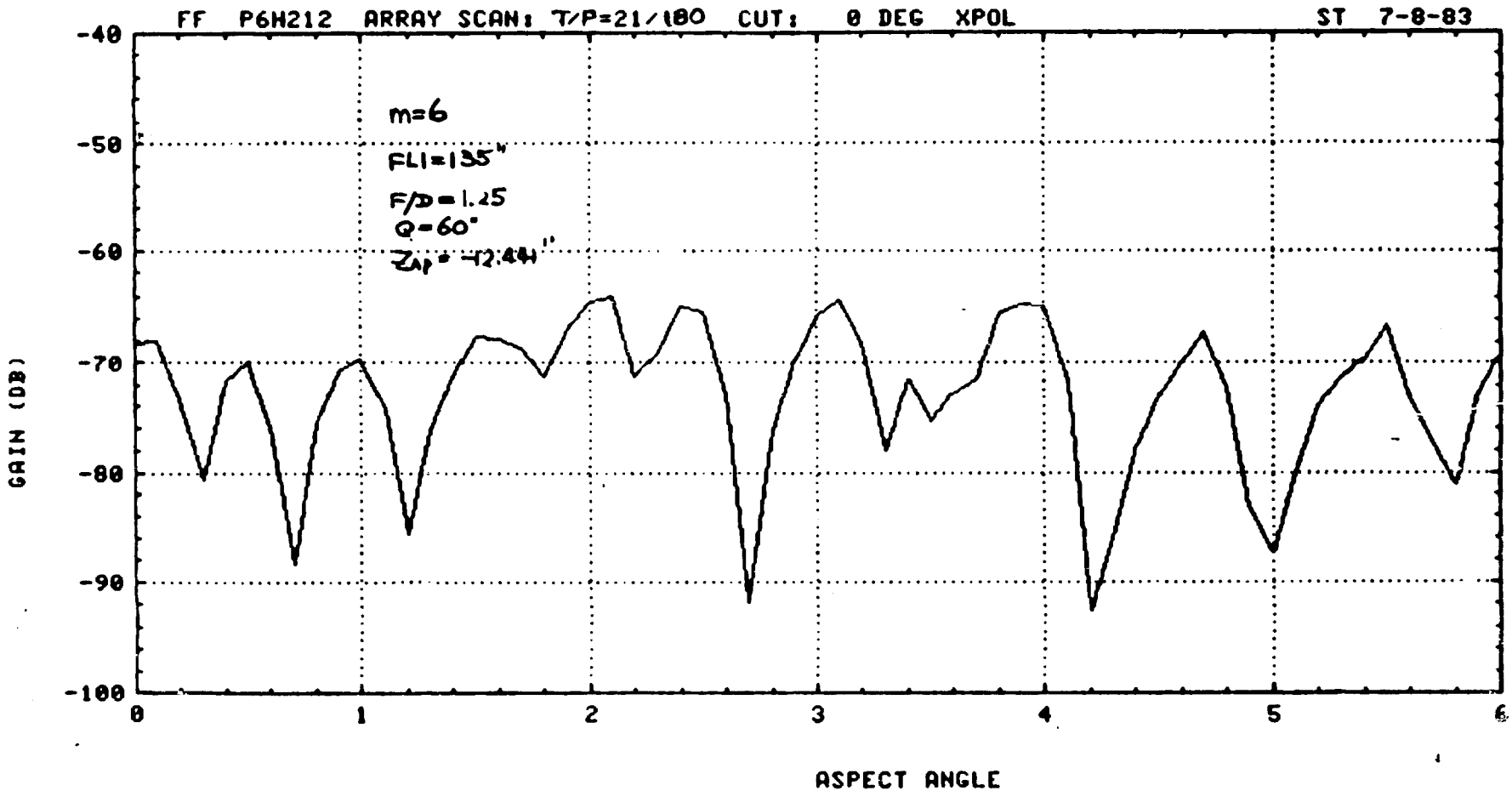
FF P6H212 ARRAY SCAN: T/P=21/180 CUT: 0 DEG XPOL ST 7-8-83
m=6
FLI=135"
F/D=1.25
Q=60°
ZAP=-12.44"
-40
-50
-60
-70
-80
-90
-100
GAIN (DB)
0
1
2
3
4
5
6
ASPECT ANGLE

FIG 5.3-39

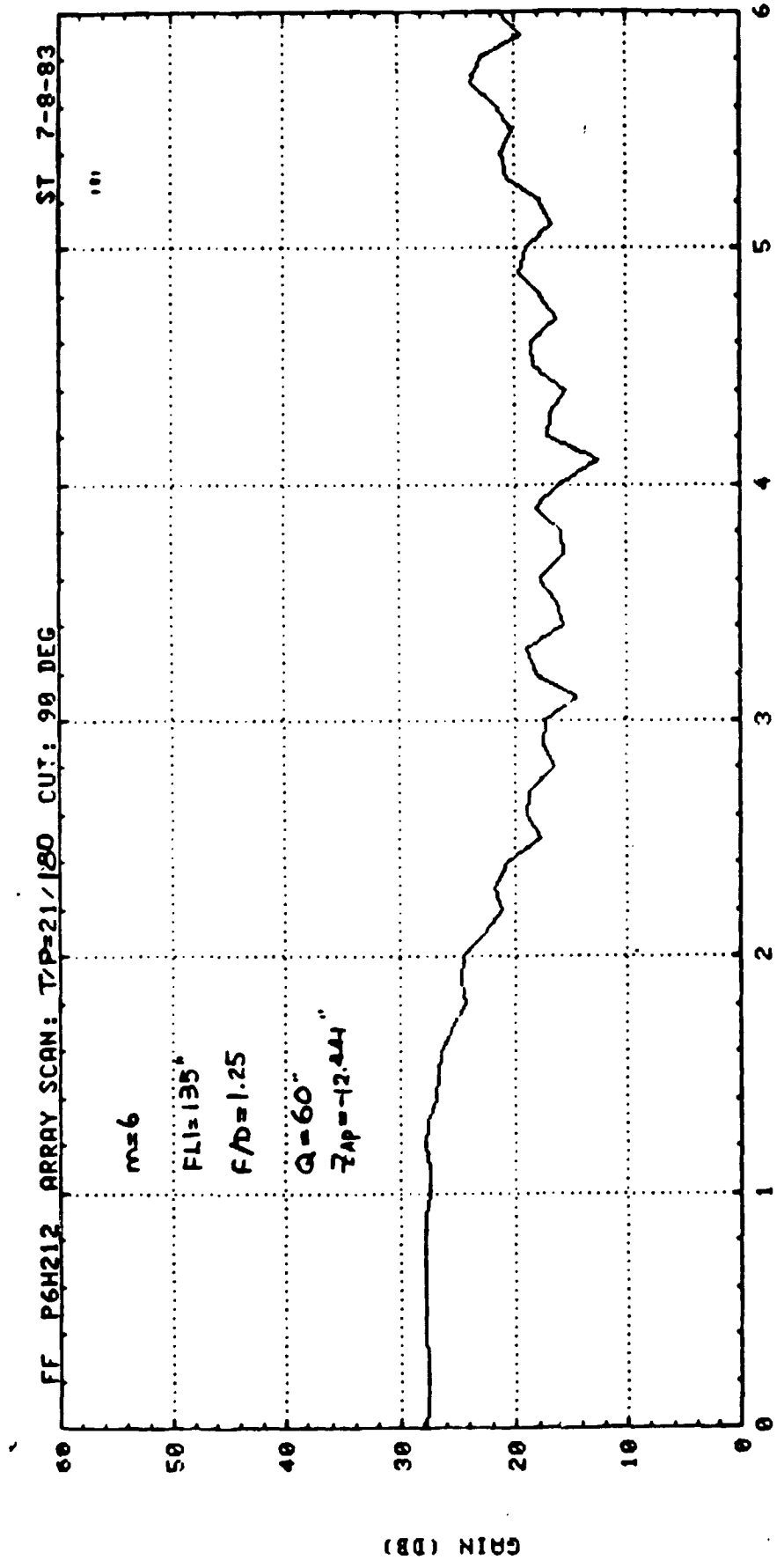
FF P6H212 ARRAY SCAN: T/P=21/180 CUT: 90 DEG
ST 7-8-83
m=6
FL1=135"
F/D=1.25
Q=60"
ZAP=-12.444"
GMAX: 27.908 DB AT .50 DEG
GAIN (DB)
ASPECT ANGLE
0
10
20
30
40
50
60
1
2
3
4
5
6

FIG 5.3-40

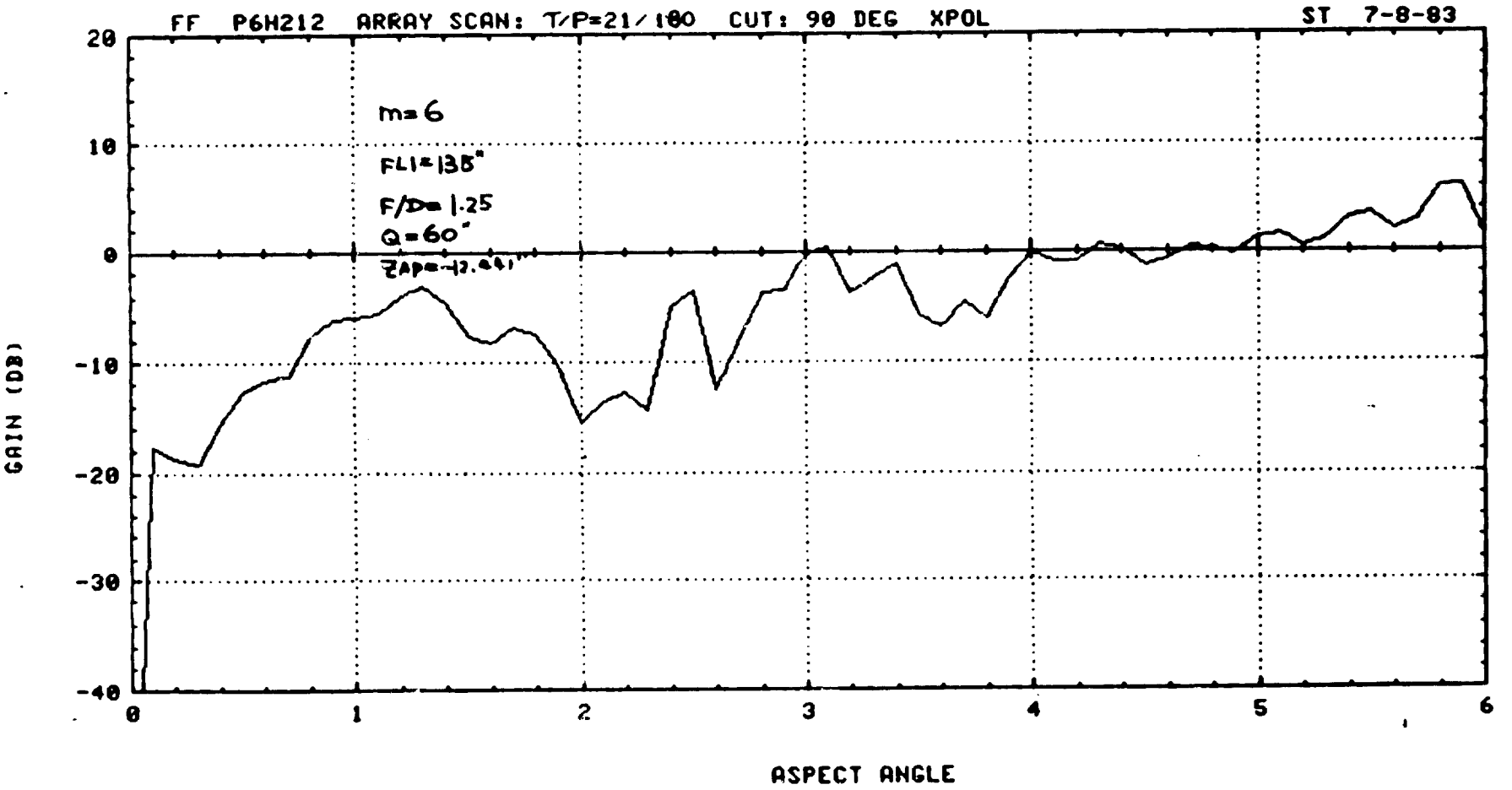
FF P6H212 ARRAY SCAN: T/P=21/180 CUT: 90 DEG XPOL
ST 7-8-83
m=6
FL1=135"
F/D=1.25
Q=60°
ZAP=-12.641"
GAIN (DB)
20
10
0
-10
-20
-30
-40
0
1
2
3
4
5
6
ASPECT ANGLE

FIG 5.3-41

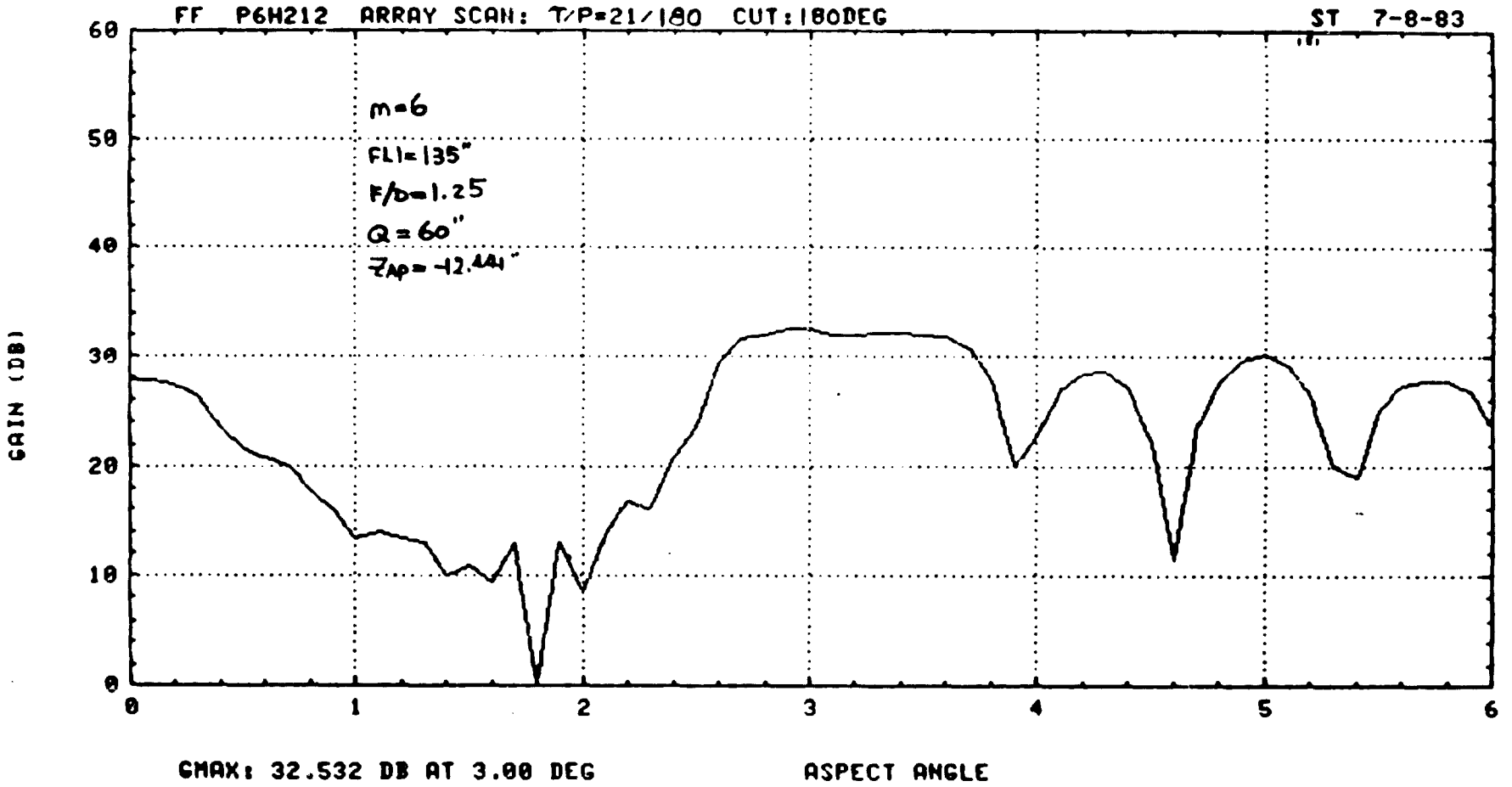
FF P6H212 ARRAY SCAN: T/P=21/180 CUT:180DEG
ST 7-8-83
m=6
FL1=135"
F/D=1.25
Q=60"
ZAP=-12.441"
GAIN (DB)
60
50
40
30
20
10
0
0
1
2
3
4
5
6
GMAX: 32.532 DB AT 3.00 DEG
ASPECT ANGLE

FIG 5.3-42

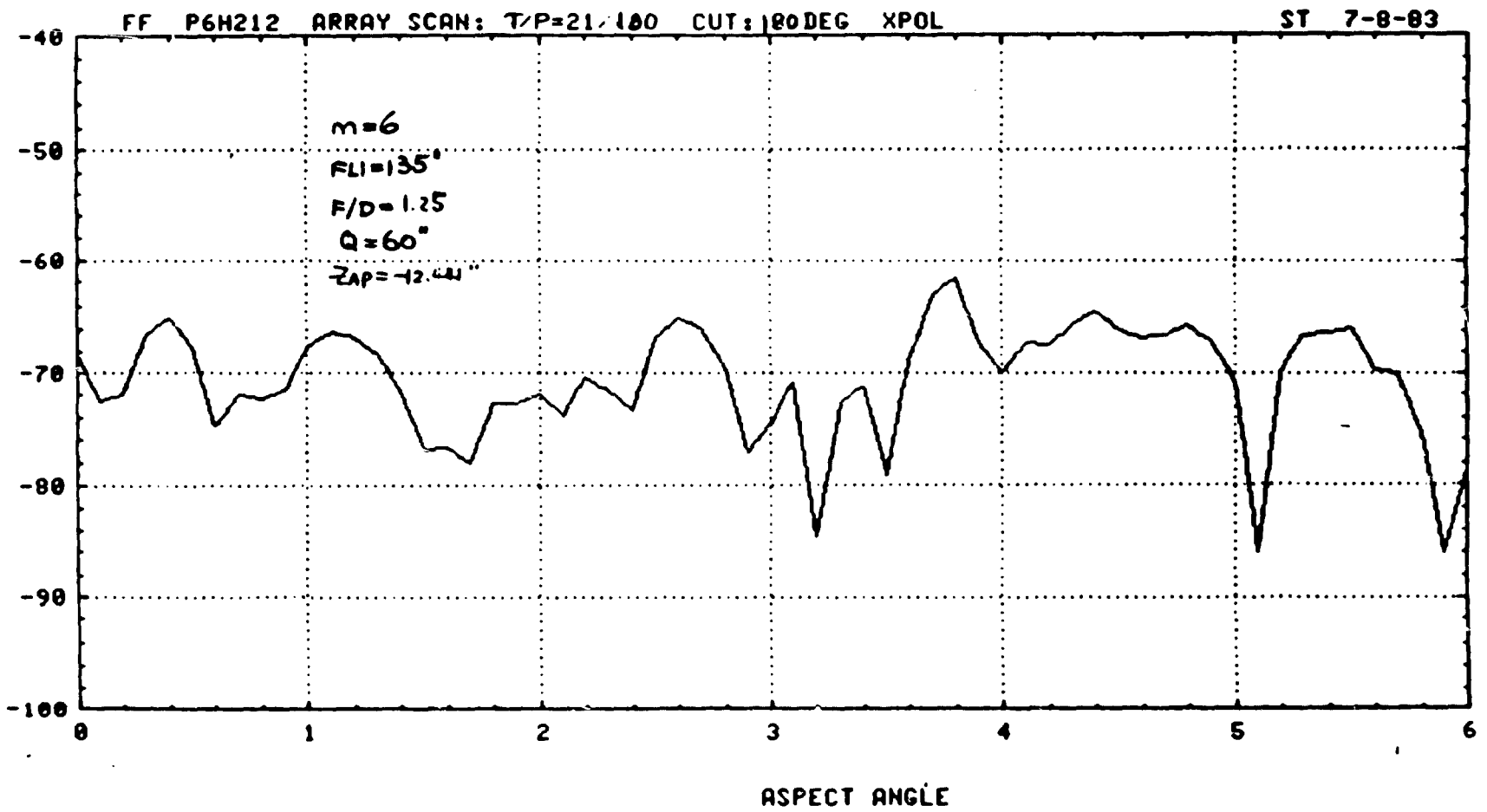
FF P6H212 ARRAY SCAN: T/P=21/180 CUT: 180 DEG XPOL
ST 7-8-83
m=6
FLI=135°
F/D=1.25
Θ=60°
ZAP=-12.441"
-40
-50
-60
-70
-80
-90
-100
GAIN (DB)
0
1
2
3
4
5
6
ASPECT ANGLE

FIG 5.3-43

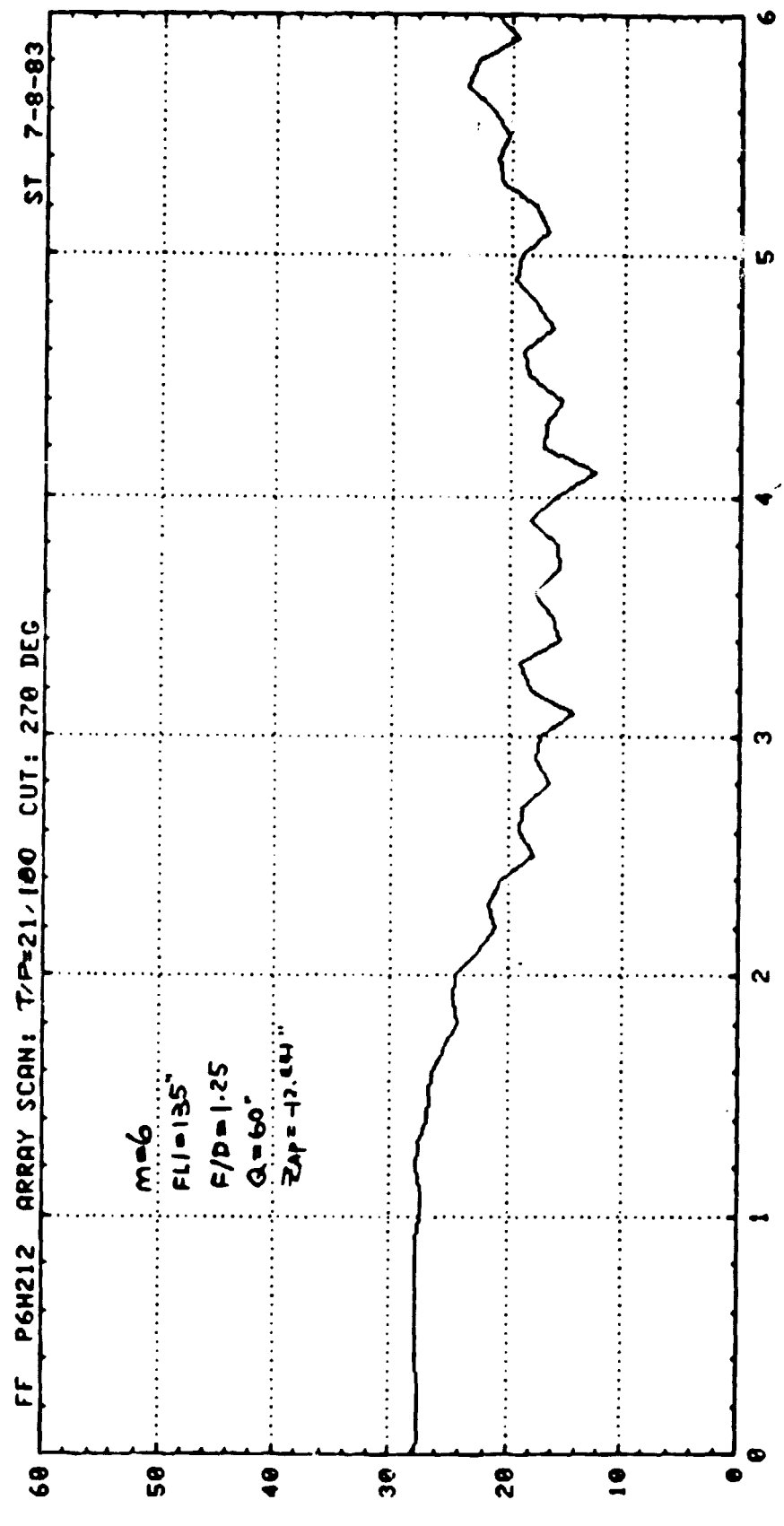
FF P6H212 ARRAY SCAN: T/R=21/100 CUT: 270 DEG ST 7-8-83
m=6
FL1=135"
F/D=1.25
Q=60°
ZAP=-13.64"
GAIN (DB)
60
50
40
30
20
10
0
0
1
2
3
4
5
6
ASPECT ANGLE
GMAX: 27.908 DB AT .50 DEG

FIG 53-44

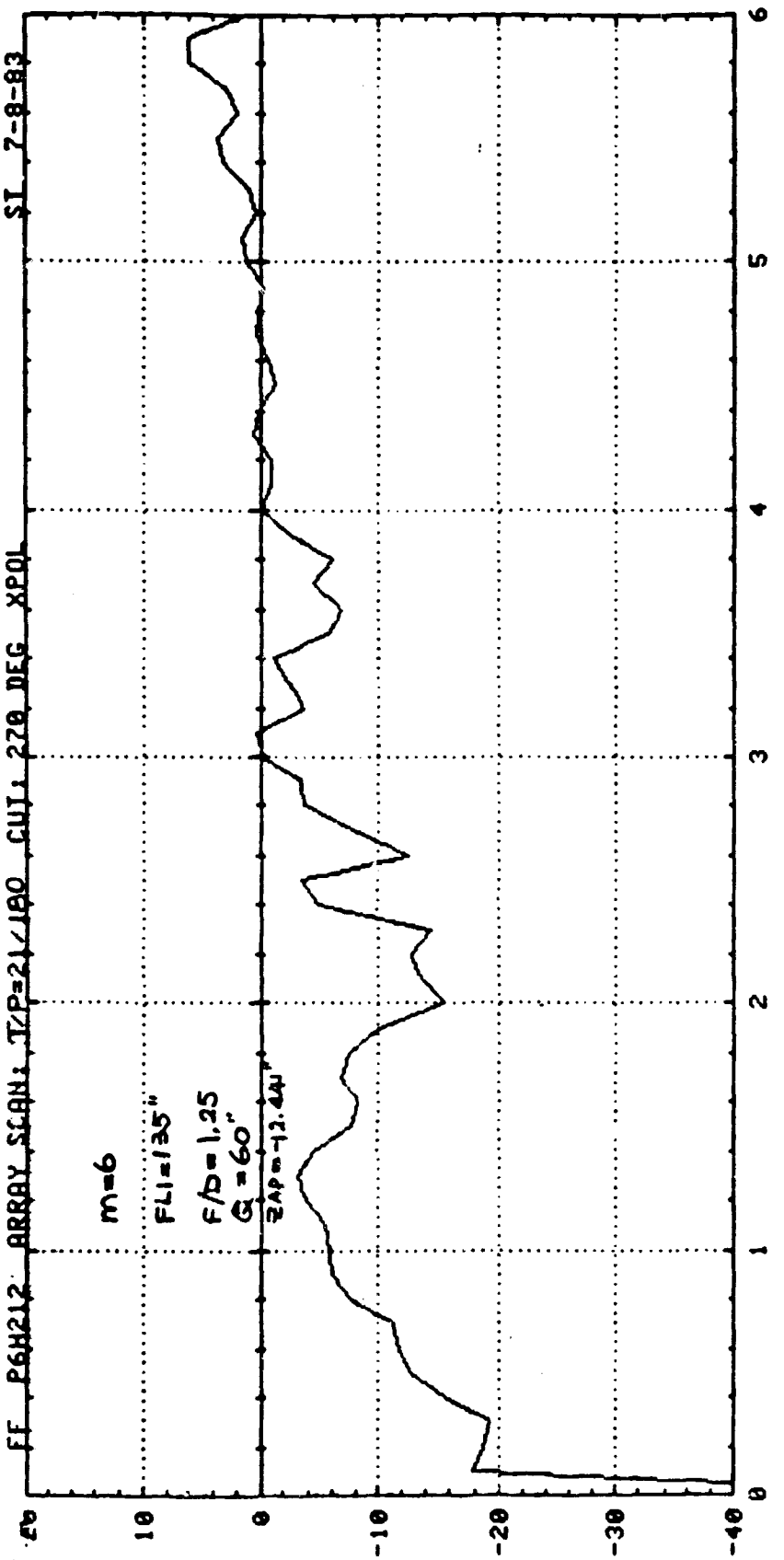
FF P6H212 ARRAY SCAN: T/P=21/180 CUT: 270 DEG XPOL SI 7-8-83
m=6
FL1=135"
F/D=1.25
Q=60"
ZAP=12.44"
GAIN (DB)
ASPECT ANGLE
10
0
-10
-20
-30
-40
0
1
2
3
4
5
6

FIG 5.3-45

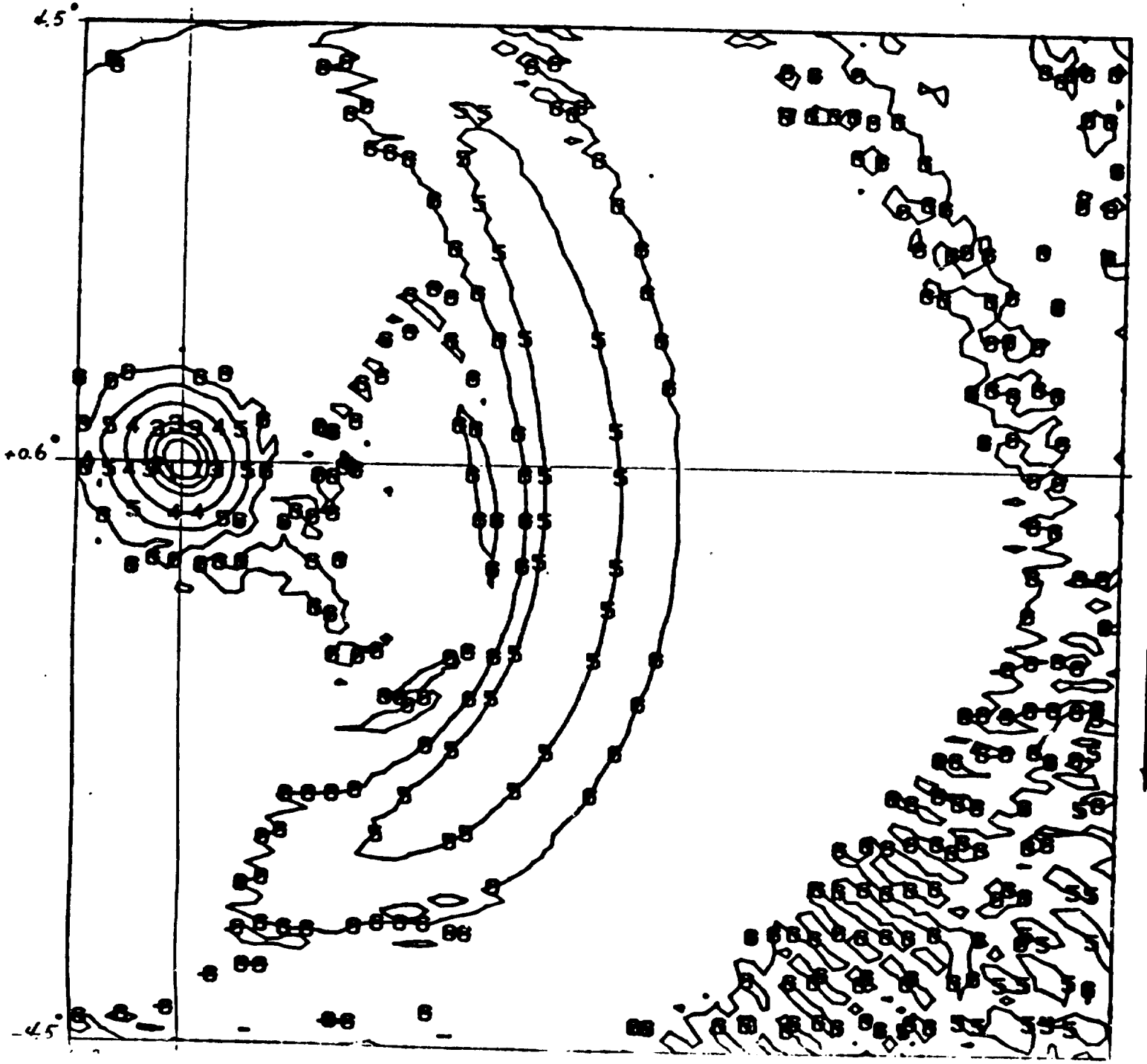

"

MAIN POL. = YP

ARRAY SCAN:

(21°, 0°)
A E

SYSTEM FF:

MAIN POL. (YP)

G_{MAX} = 54.43 dB

@ (-3.6°, +0.6°)

MAIN DISH
OFFSET
DIRECTION

m=6
FLI=135"
F/D=1.25
Q=60"
ZAP=-12.441"

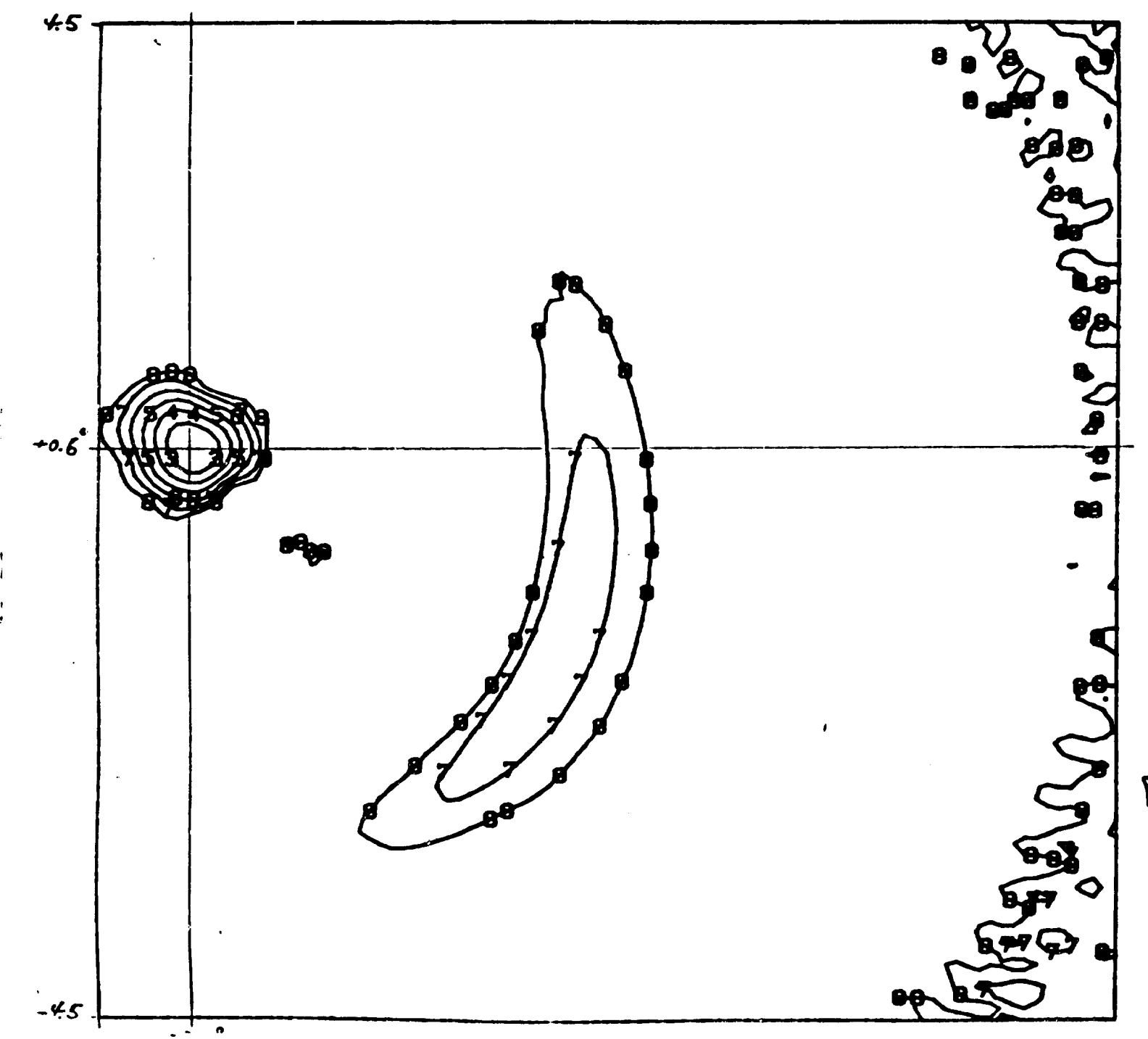

10 15 20 25 3[illegible]

"MAIN POL. = YP

A E

ARRAY SCAN: (21°, 0°)

SYSTEM FF:

* CROSS POL:

G_{MAX} = 39.43 dB

@ (-3.6°, +0.6°)

MAIN DISH OFFSET DIRECTION

m=6
FLI=135"
F/D=1.25
Q=60"
Zap=-12.441

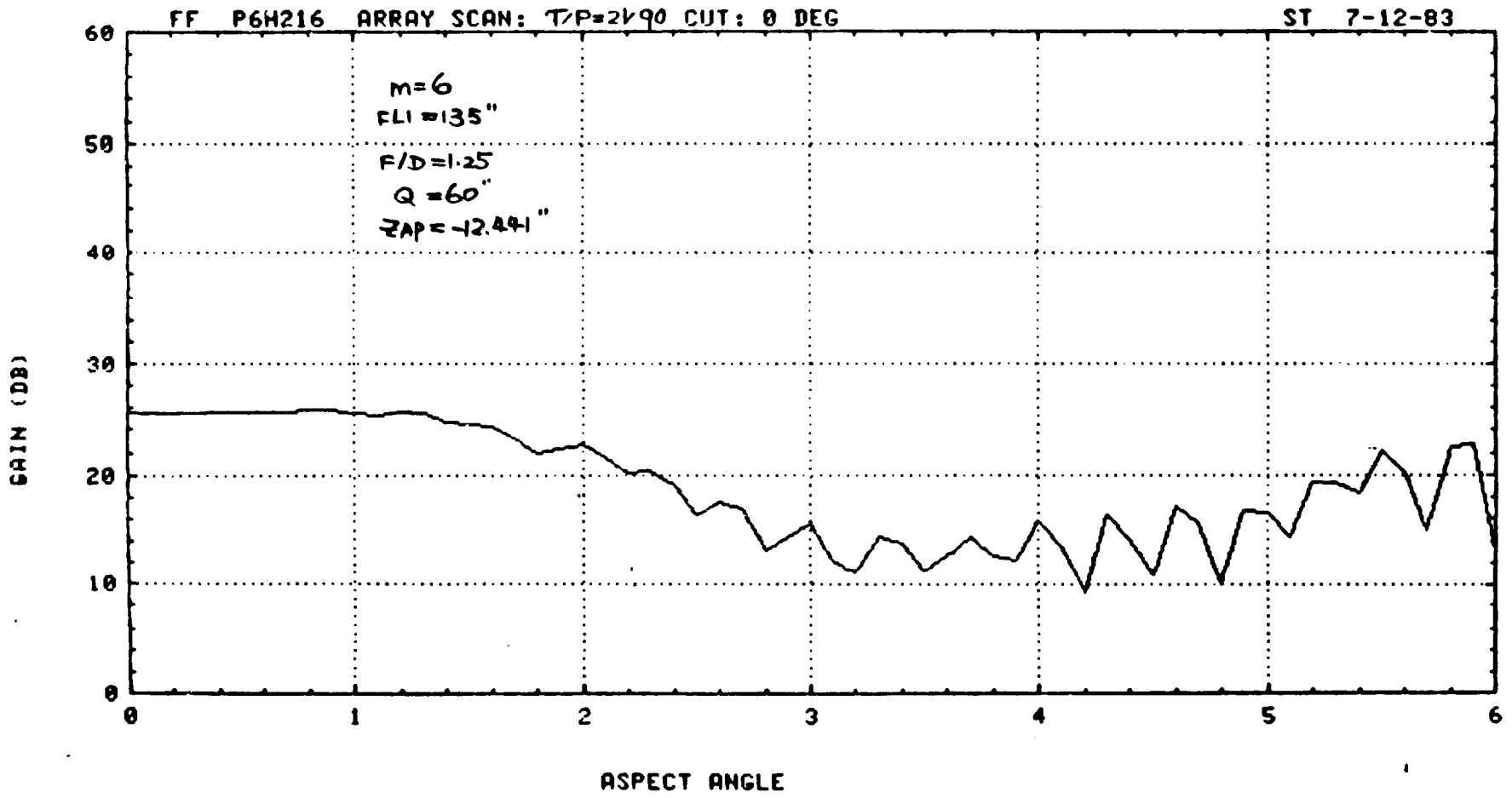
FF P6H216 ARRAY SCAN: T/P=2V90 CUT: 0 DEG
ST 7-12-83
m=6
FLI =135"
F/D=1.25
Q =60"
ZAP=-12.441"
GAIN (DB)
60
50
40
30
20
10
0
0
1
2
3
4
5
6
ASPECT ANGLE

FIG 5.3-48

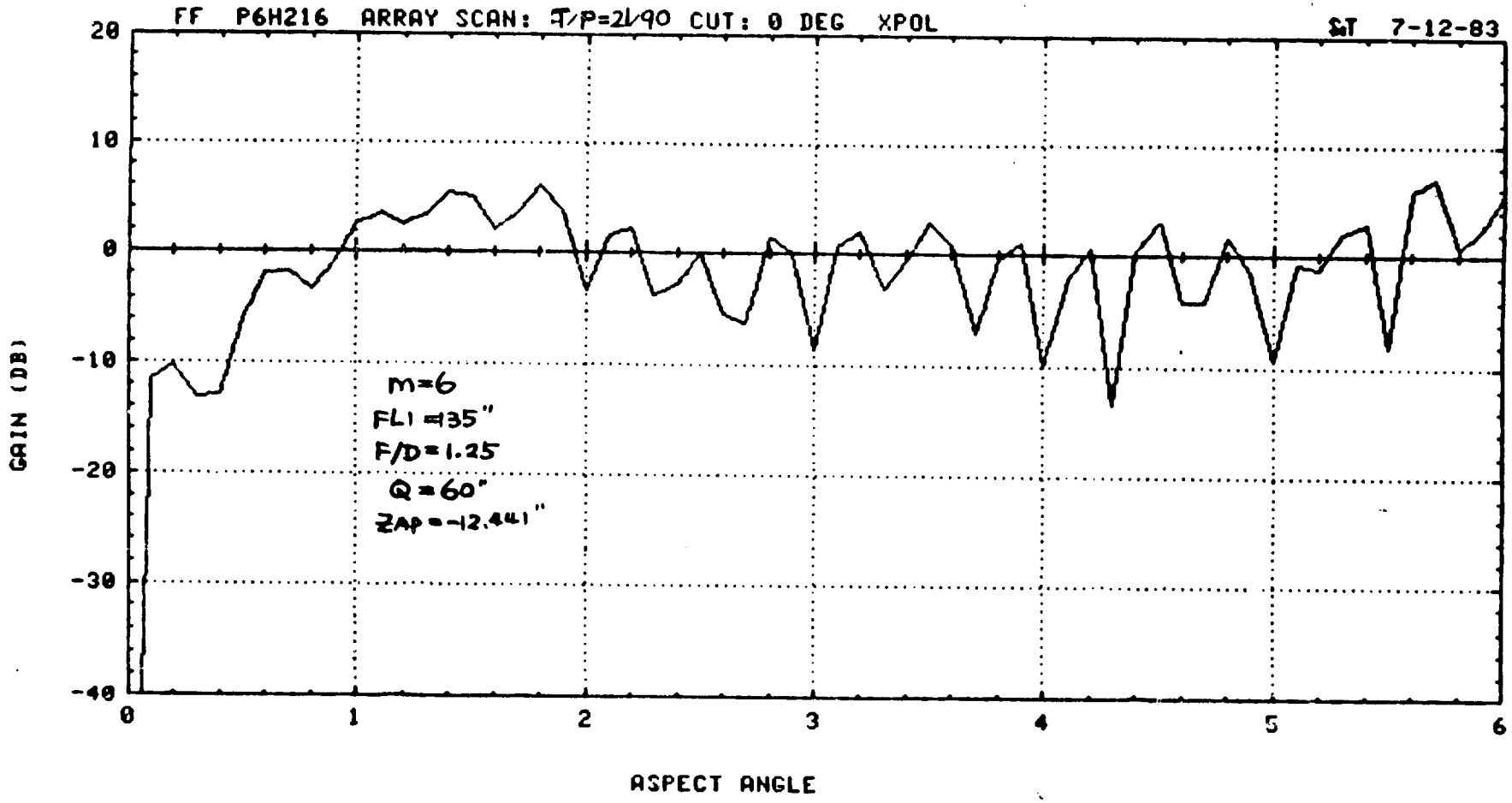
FF P6H216 ARRAY SCAN: T/P=2/90 CUT: 0 DEG XPOL
S&T 7-12-83
20
10
0
-10
-20
-30
-40
GAIN (DB)
0
1
2
3
4
5
6
ASPECT ANGLE
m=6
FL1 =135"
F/D=1.25
Q=60"
ZAP=-12.441"

FIG 5.3-49

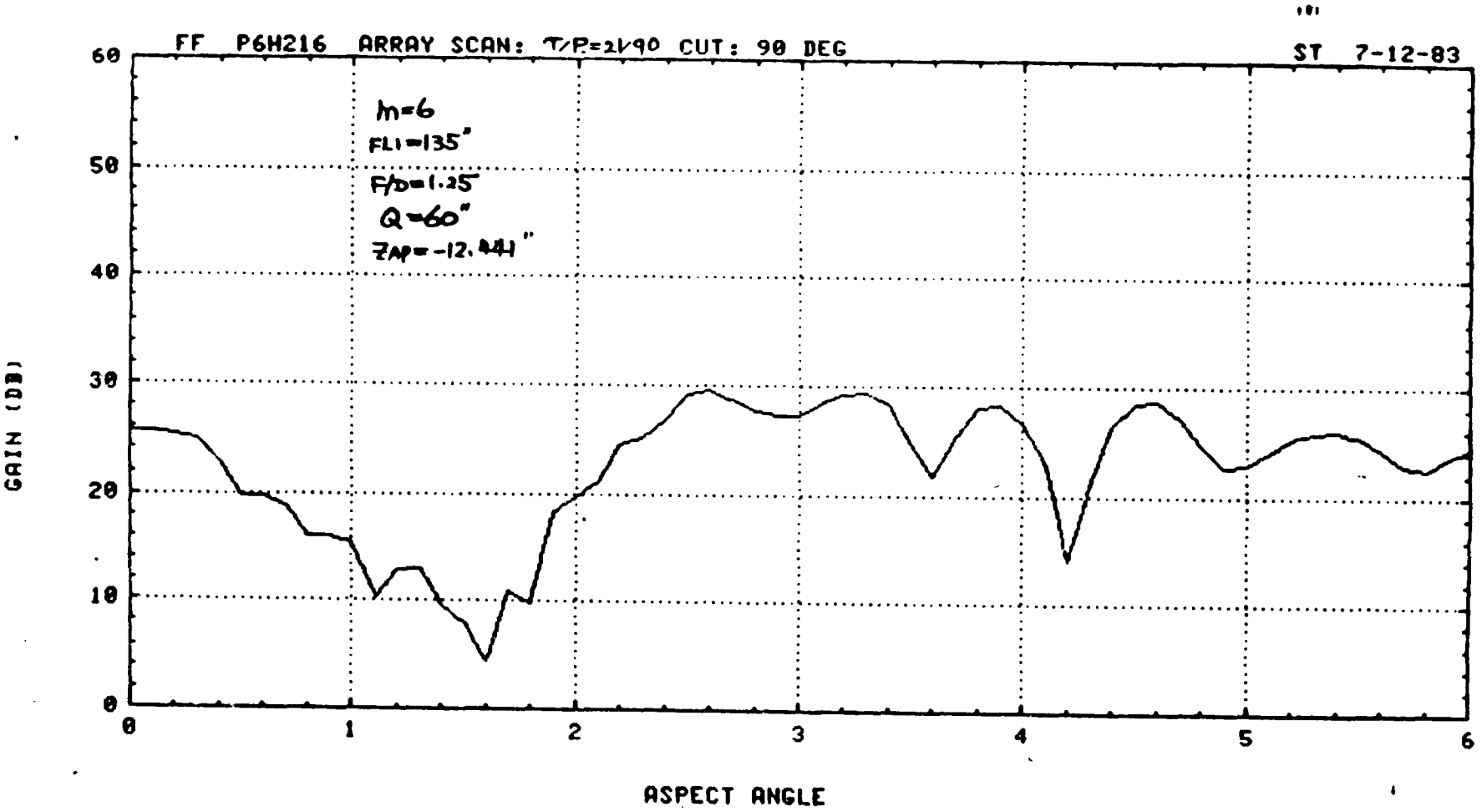
FF P6H216 ARRAY SCAN: T/P=2/90 CUT: 90 DEG
ST 7-12-83
n=6
FL1=135"
F/D=1.25
Q=60"
ZAP=-12.441"
GAIN (DB)
ASPECT ANGLE
60
50
40
30
20
10
0
0
1
2
3
4
5
6

FIG 5.3-50

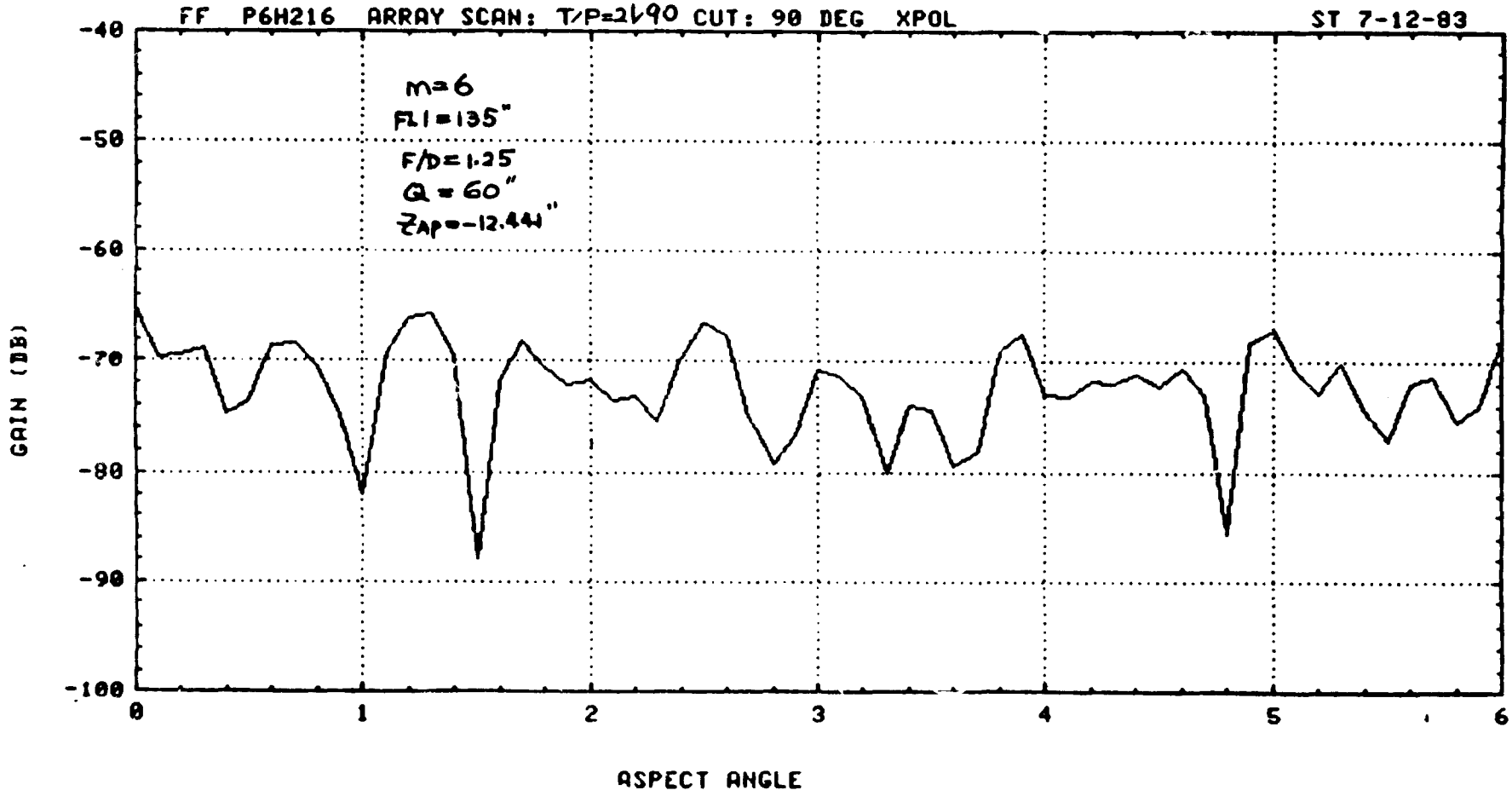
FF P6H216 ARRAY SCAN: T/P=2190 CUT: 90 DEG XPOL
ST 7-12-83
m=6
FL1=135"
F/D=1.25
Q=60"
ZAP=-12.441"
GAIN (DB)
-40
-50
-60
-70
-80
-90
-100
0
1
2
3
4
5
6
ASPECT ANGLE

FIG 5.3-51

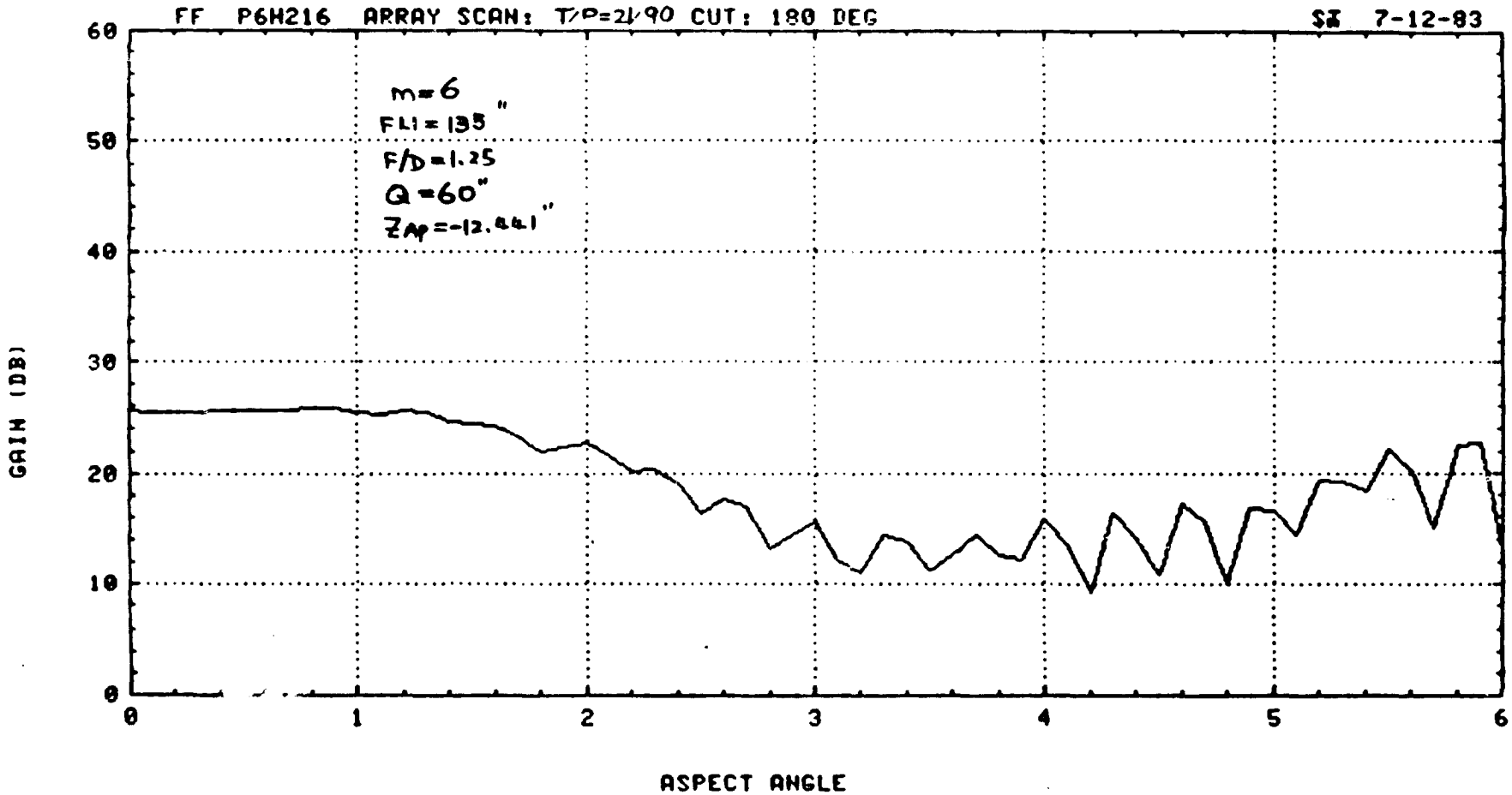
FF P6H216 ARRAY SCAN: T/P=21/90 CUT: 180 DEG
SI 7-12-83
m=6
FLI=135"
F/D=1.25
Q=60"
ZAP=-12.441"
GAIN (DB)
60
50
40
30
20
10
0
0
1
2
3
4
5
6
ASPECT ANGLE

Fig 3.3-52

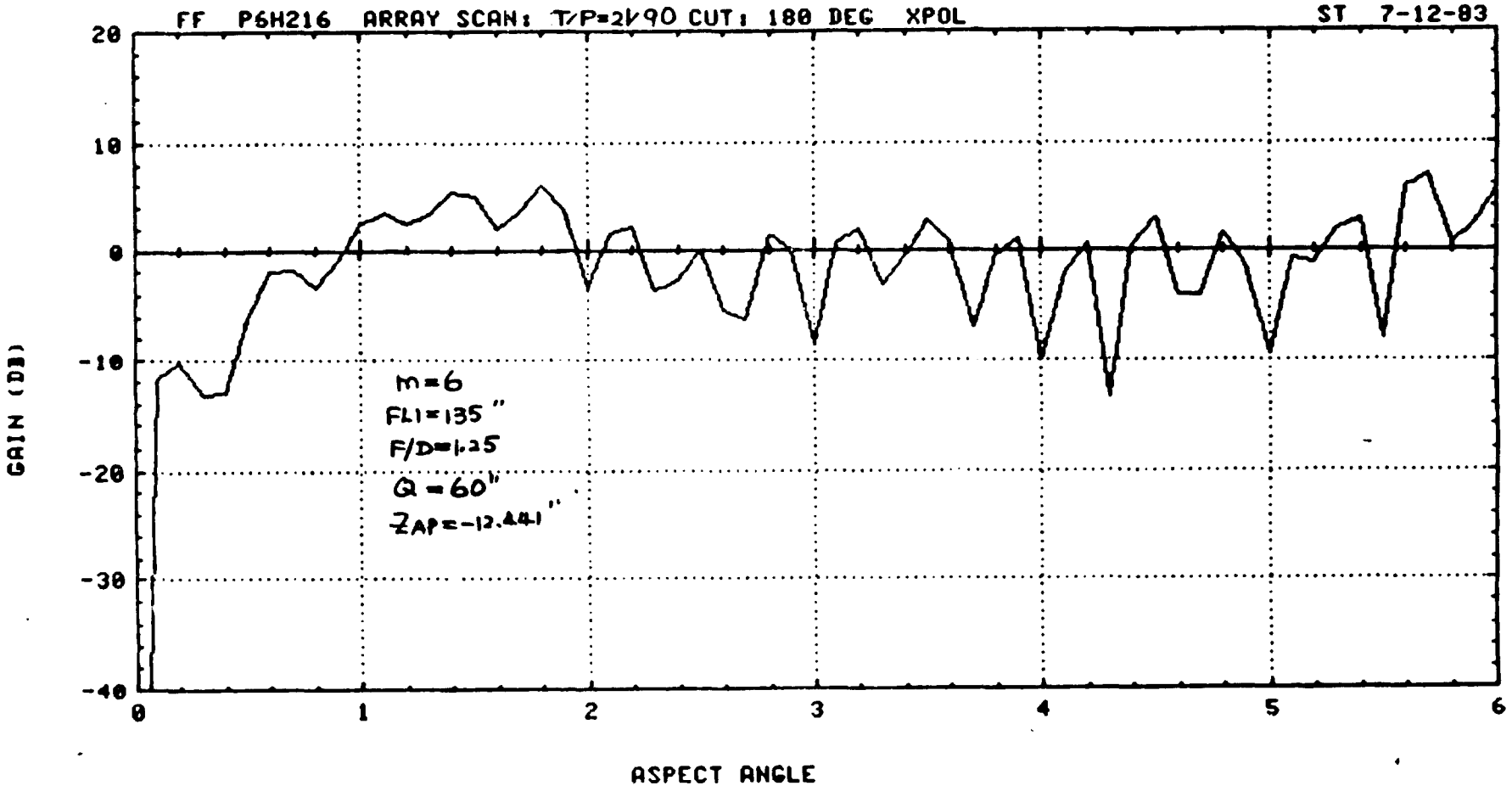
FF P6H216 ARRAY SCAN: T/P=2/90 CUT: 180 DEG XPOL
ST 7-12-83
20
10
0
-10
-20
-30
-40
0
1
2
3
4
5
6
GAIN (DB)
ASPECT ANGLE
m=6
FL1=135"
F/D=1.25
Q=60"
ZAP=-12.441"

FIG 5.3-53

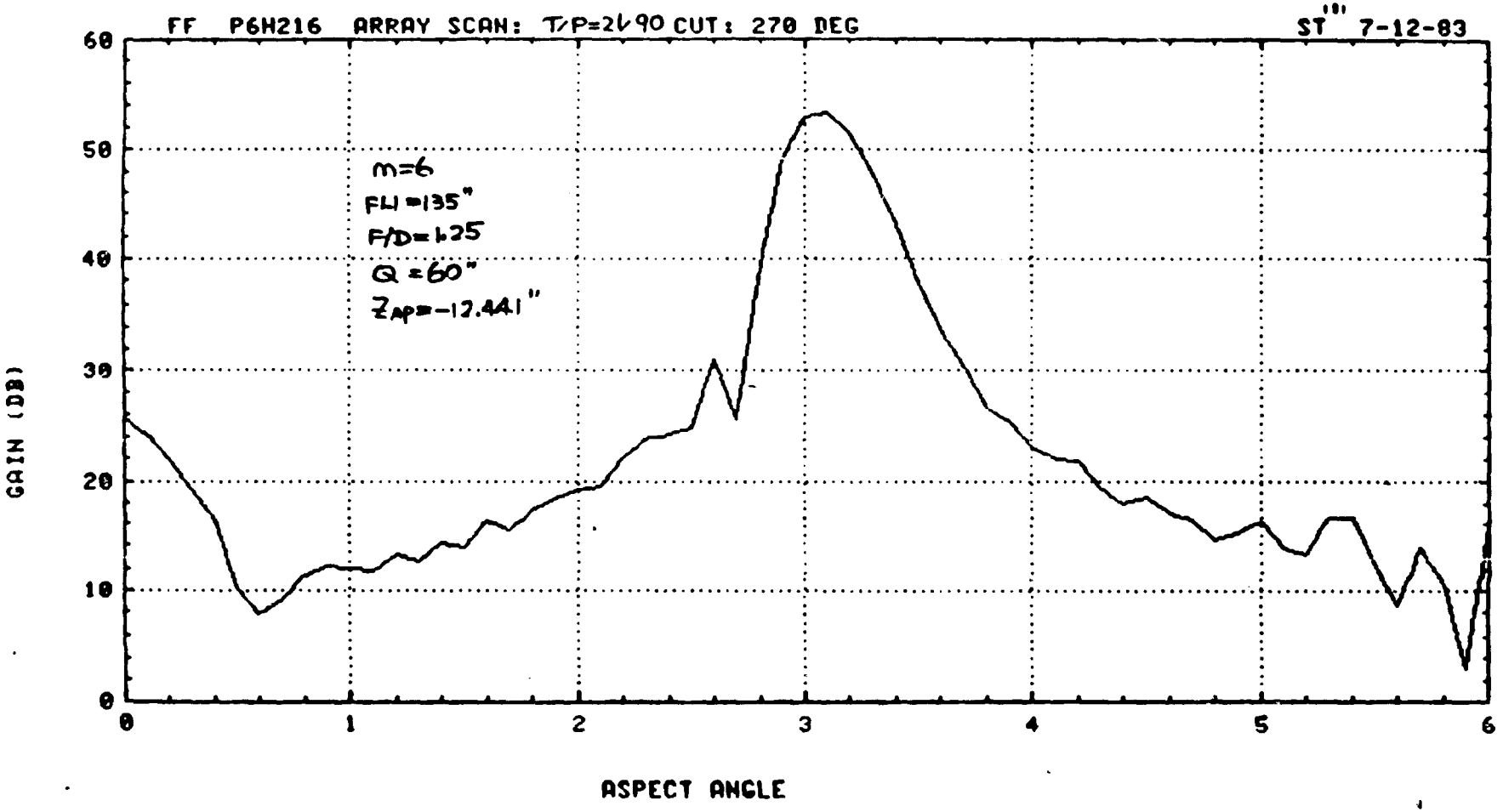
FF P6H216 ARRAY SCAN: T/P=2690 CUT: 270 DEG
ST 7-12-83
m=6
FLI=135"
F/D=1.25
Q=60"
ZAP=-12.441"
GAIN (DB)
ASPECT ANGLE
0
10
20
30
40
50
60
0
1
2
3
4
5
6

FIG 5.3-54

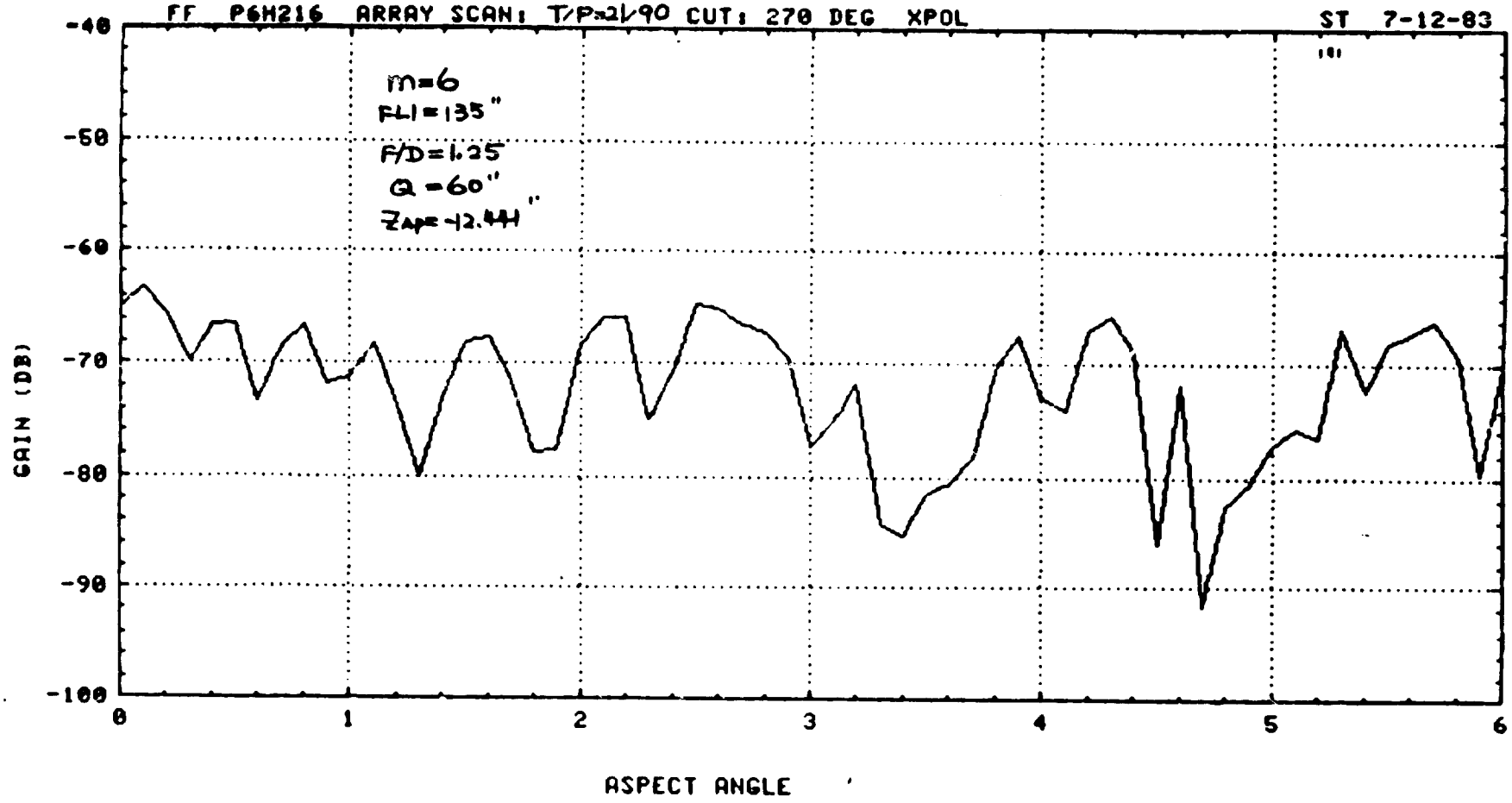
FF P6M216 ARRAY SCAN: T/P=21/90 CUT: 270 DEG XPOL
ST 7-12-83
m=6
FLI=135"
F/D=1.25
Q=60"
ZAp=-12.441"
GAIN (DB)
-40
-50
-60
-70
-80
-90
-100
0
1
2
3
4
5
6
ASPECT ANGLE

FIG 3-55

BLAZ15
Y POL 27 42 46.51
6 LEVELS 3 6 10 20 30 40
IBXD = 3 IBYD = 5

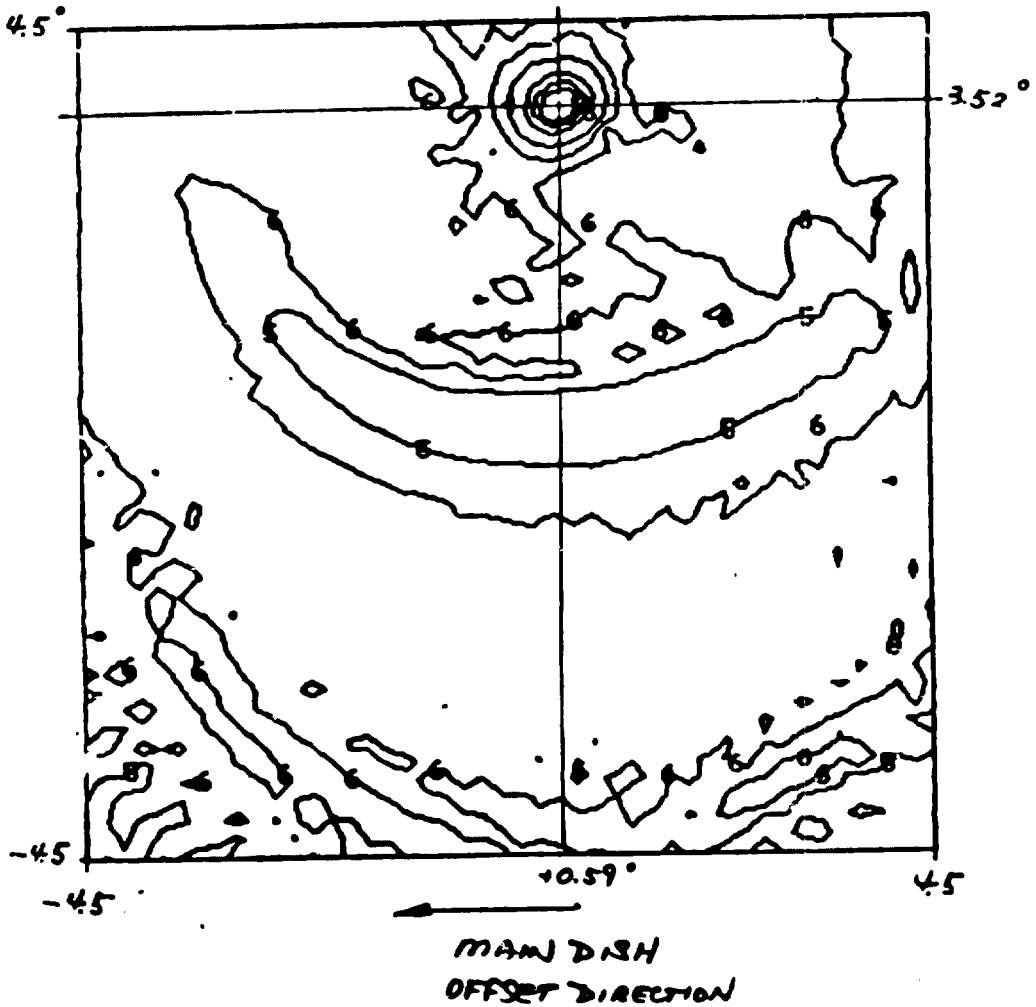

MAIN POL. = XP

ARRAY SCAN: 21° IN ASYMMETRY PLANE
(21°, 0°)
A E

G_{MAX} = 46.51 @ (-3.52, .59)
A E

M=6
FLI = 135"
F/D = 1.25
Q = 60"
ZAP = -12.44"

FIG 5.3-56

BLAZIS
X POL 27 41 36.30
6 LEVELS 3 6 10 20 30 40
IBXO=3 IBYO=5

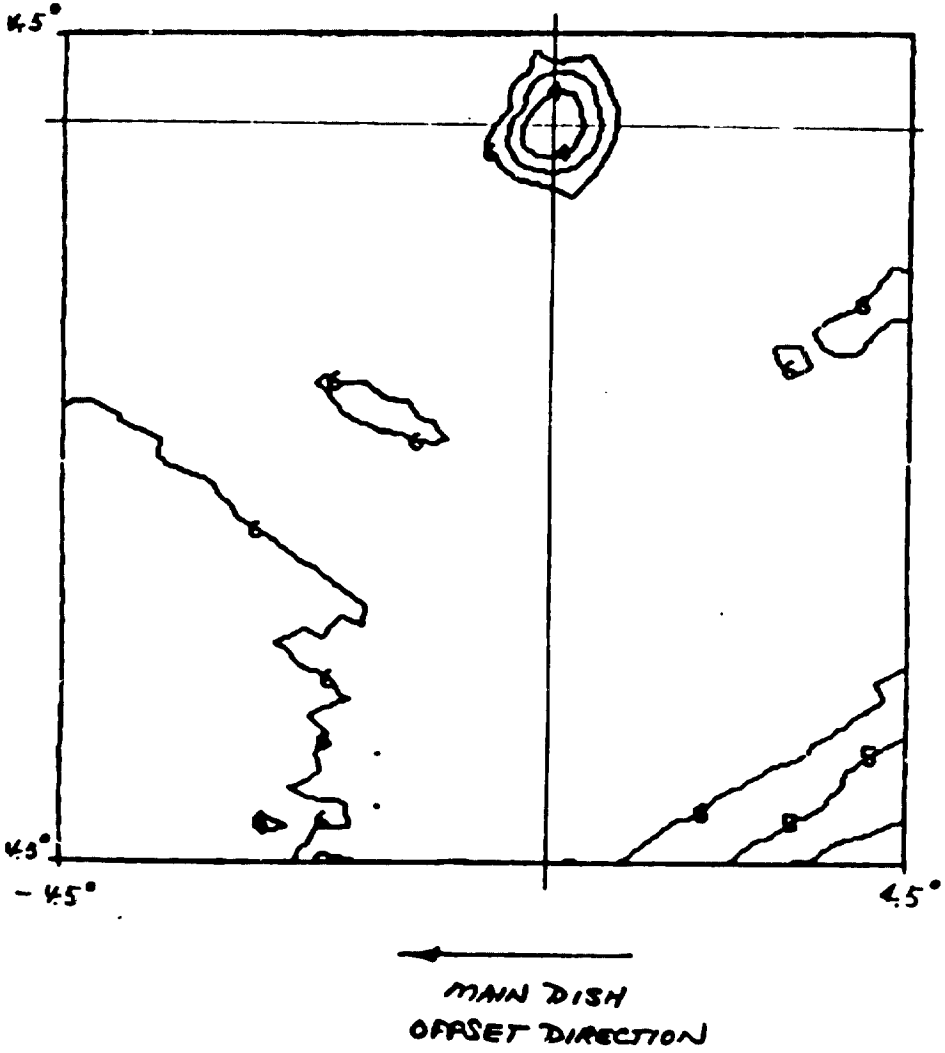

MAIN POL. = XP

ARRAY SCAN: (21, 0)
A E

FF (CROSS POL):

G_{MAX} = 36.3 dB @ (-3.52, 0.59)

- m=6
FL1 = 135"
F/D = 1.25
Q = 60"
ZAP = -12.441"

FIG 5.3-57

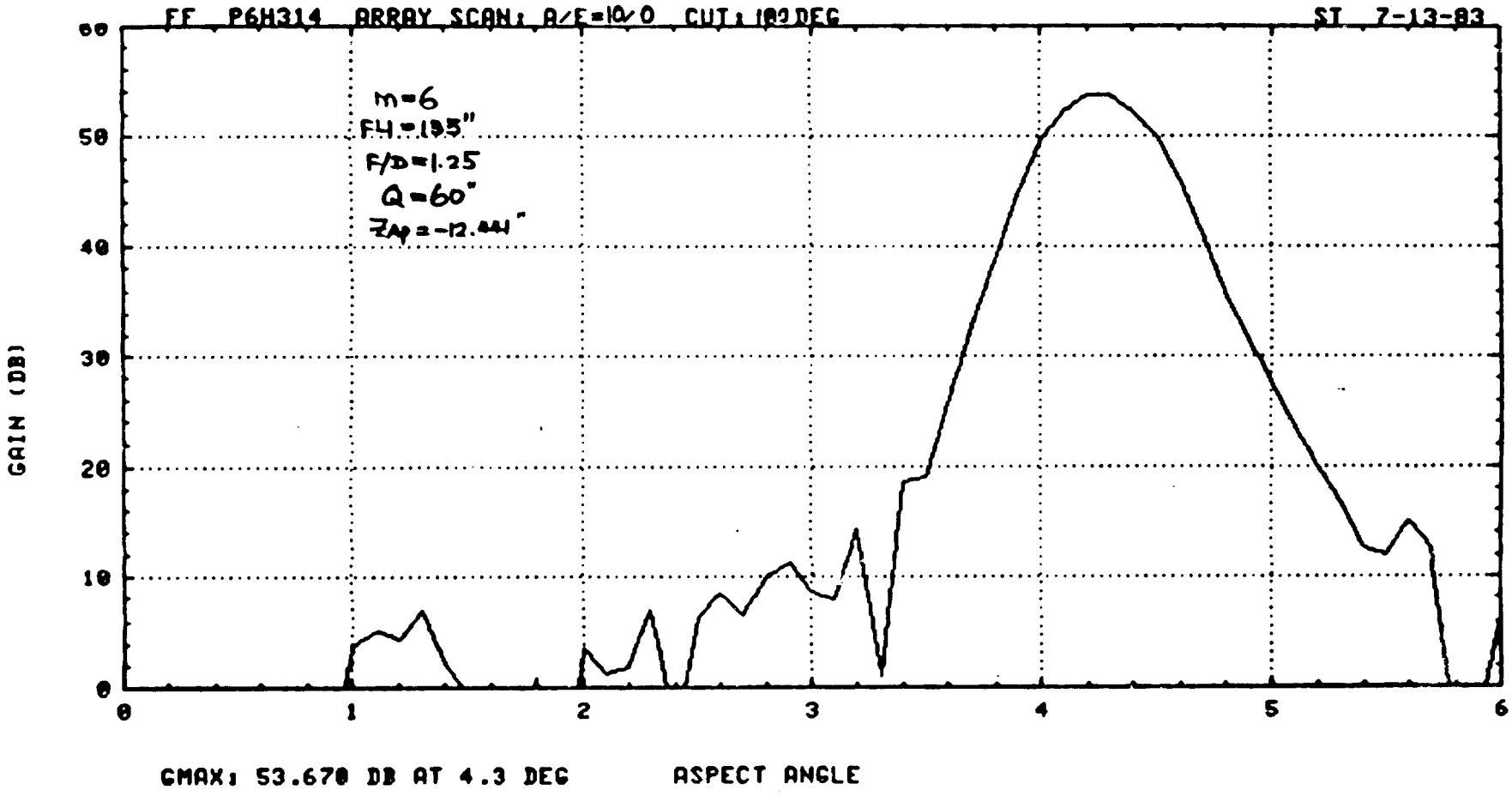
FF P6H314 ARRAY SCAN: A/E=10/0 CUT: 180 DEG
SI 7-13-83
m=6
F4=195"
F/D=1.25
Q=60°
ZAp=-12.441"
GAIN (DB)
60
50
40
30
20
10
0
0
1
2
3
4
5
6
GMAX: 53.670 DB AT 4.3 DEG
ASPECT ANGLE

FIG. 53-58

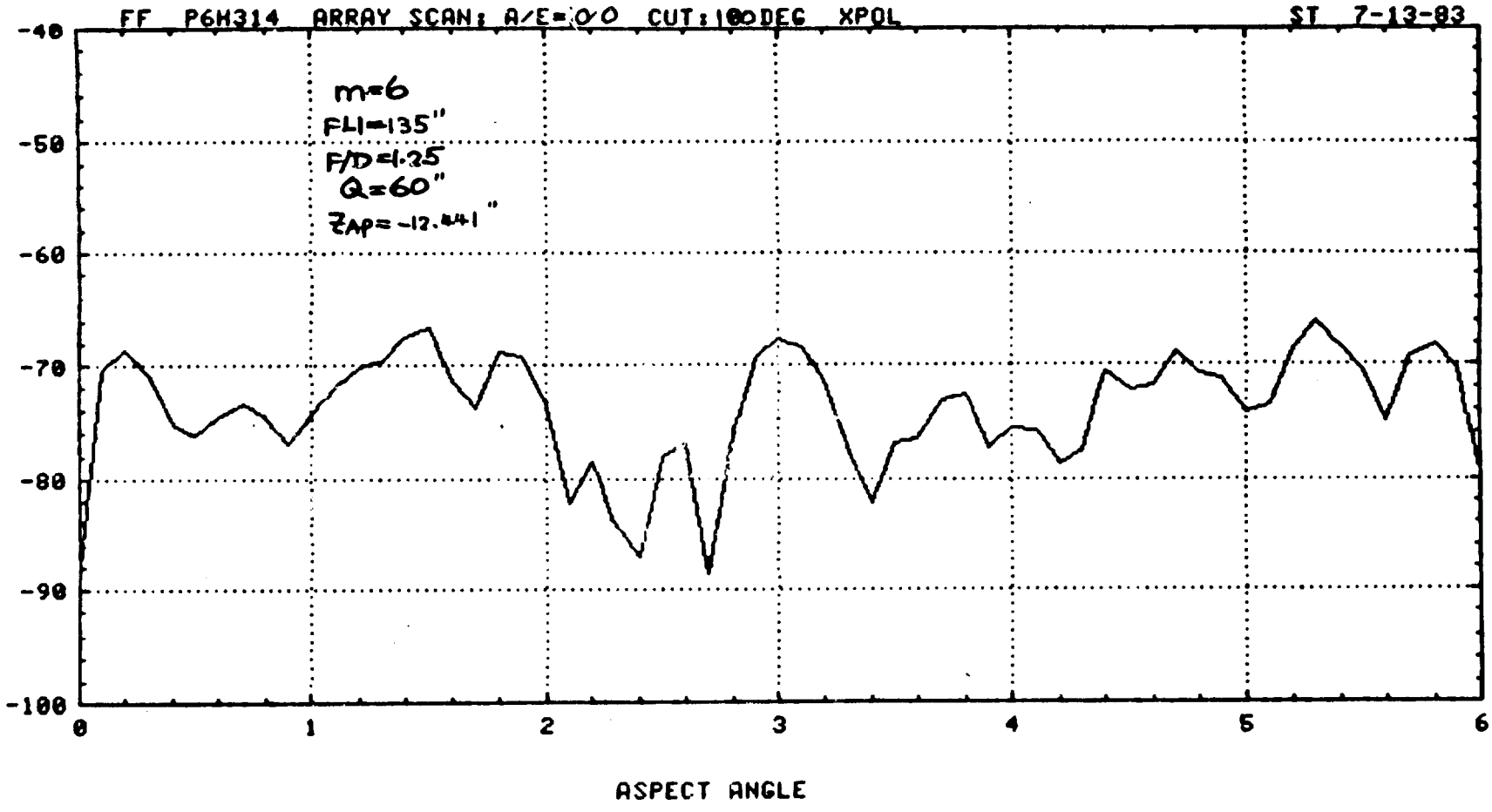
FF P6M314 ARRAY SCAN: A/E=0.0 CUT:180DEG XPOL
ST 7-13-83
m=6
FLI=135"
F/D=1.25
Q=60"
ZAP=-12.441"
-40
-50
-60
-70
-80
-90
-100
0
1
2
3
4
5
6
ASPECT ANGLE

FIG. 5.3-59

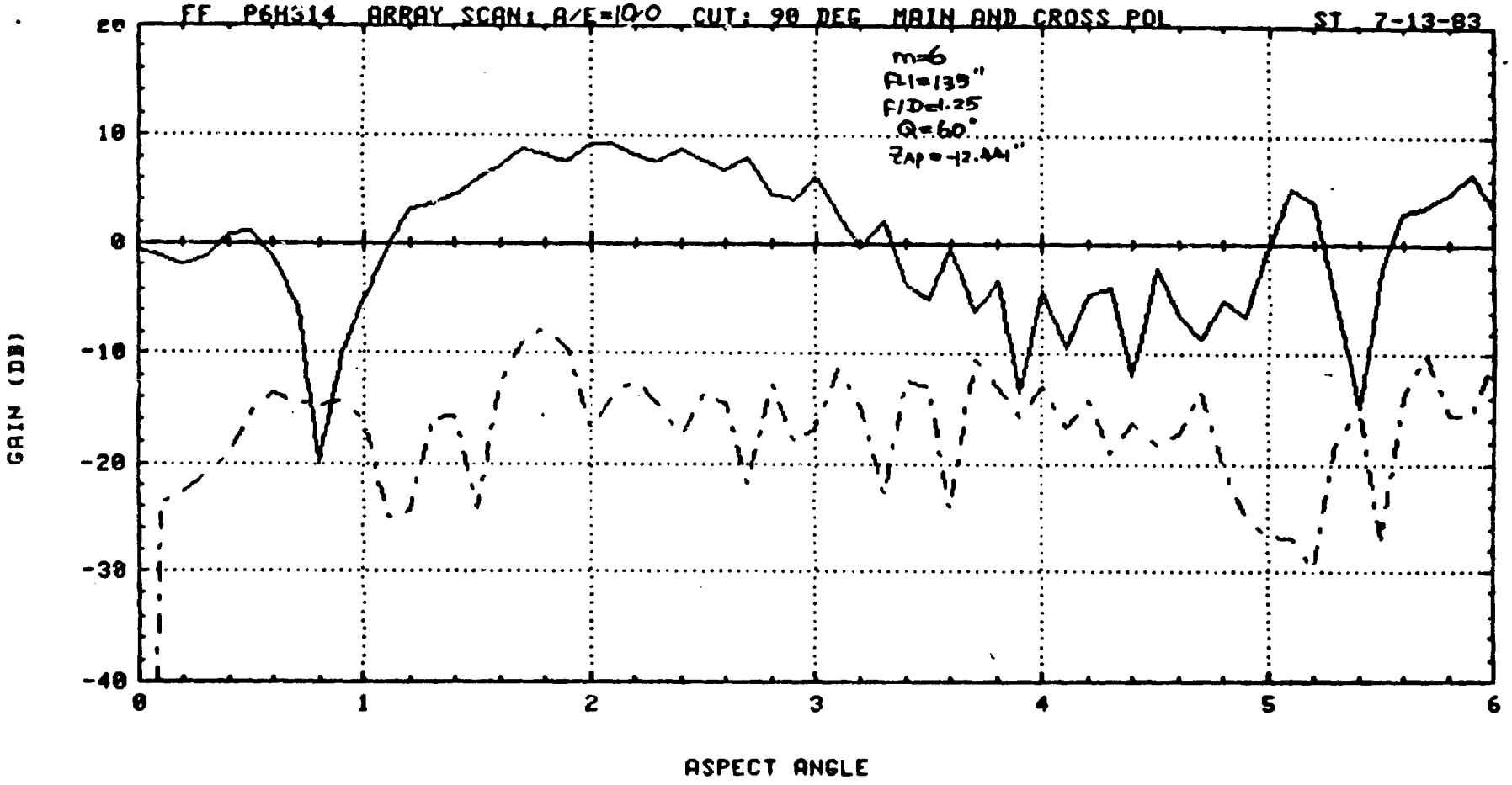
FF P6H314 ARRAY SCAN; A/E=1.0 CUT: 90 DEG MAIN AND CROSS POL ST 7-13-83
m=6
R1=139"
F/D=1.25
Q=60°
ZAp=-12.441"
20
10
0
-10
-20
-30
-40
GAIN (DB)
0
1
2
3
4
5
6
ASPECT ANGLE

FIG. 5.3-60

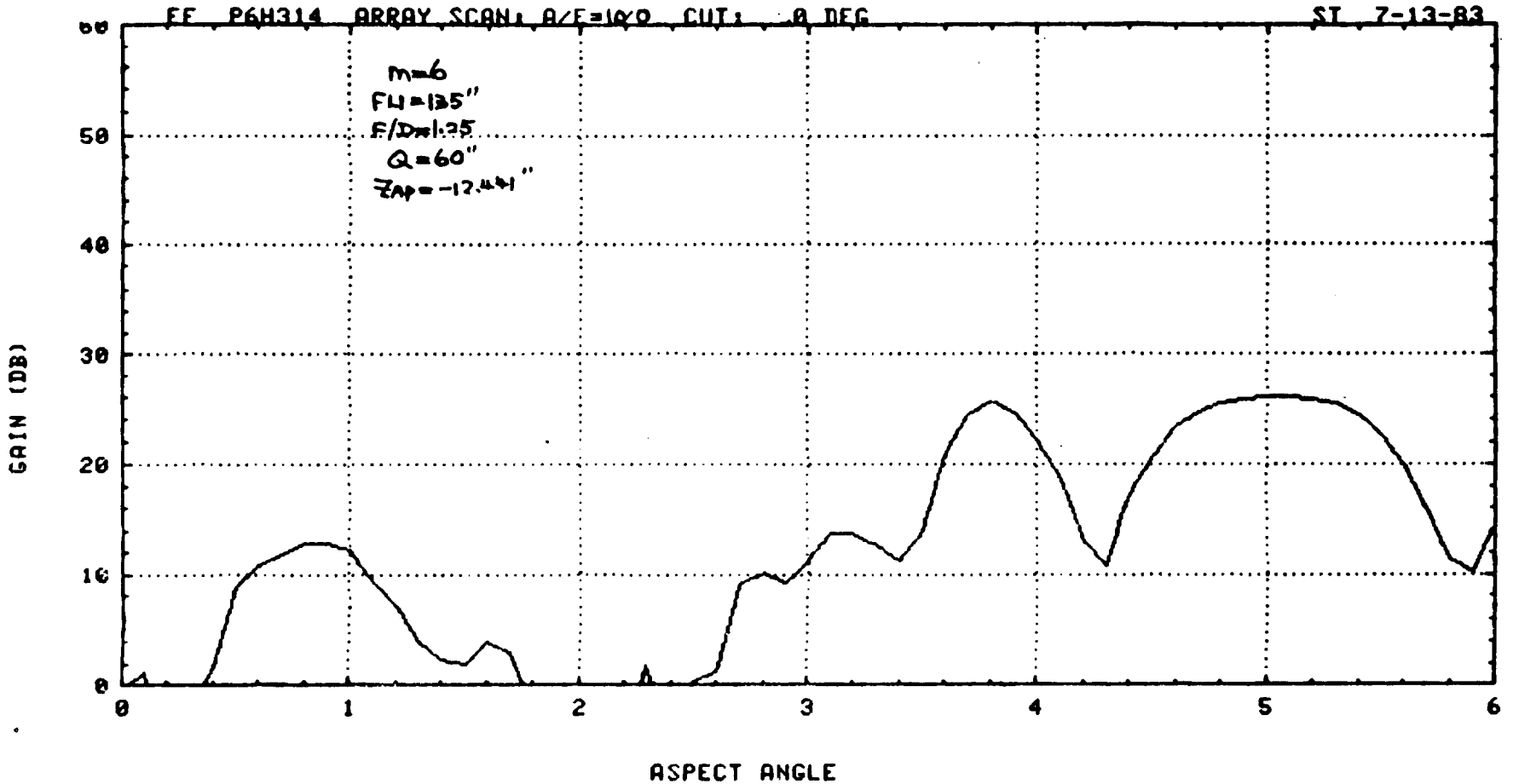
FF P6H314 ARRAY SCAN: A/E=10/0 CUT: 0 DEG ST 7-13-83
m=6
FH=135"
F/D=1.25
Q=60"
ZAP=-12.441"
60
50
40
30
20
10
0
GAIN (DB)
0
1
2
3
4
5
6
ASPECT ANGLE

FIG. 5.3-61

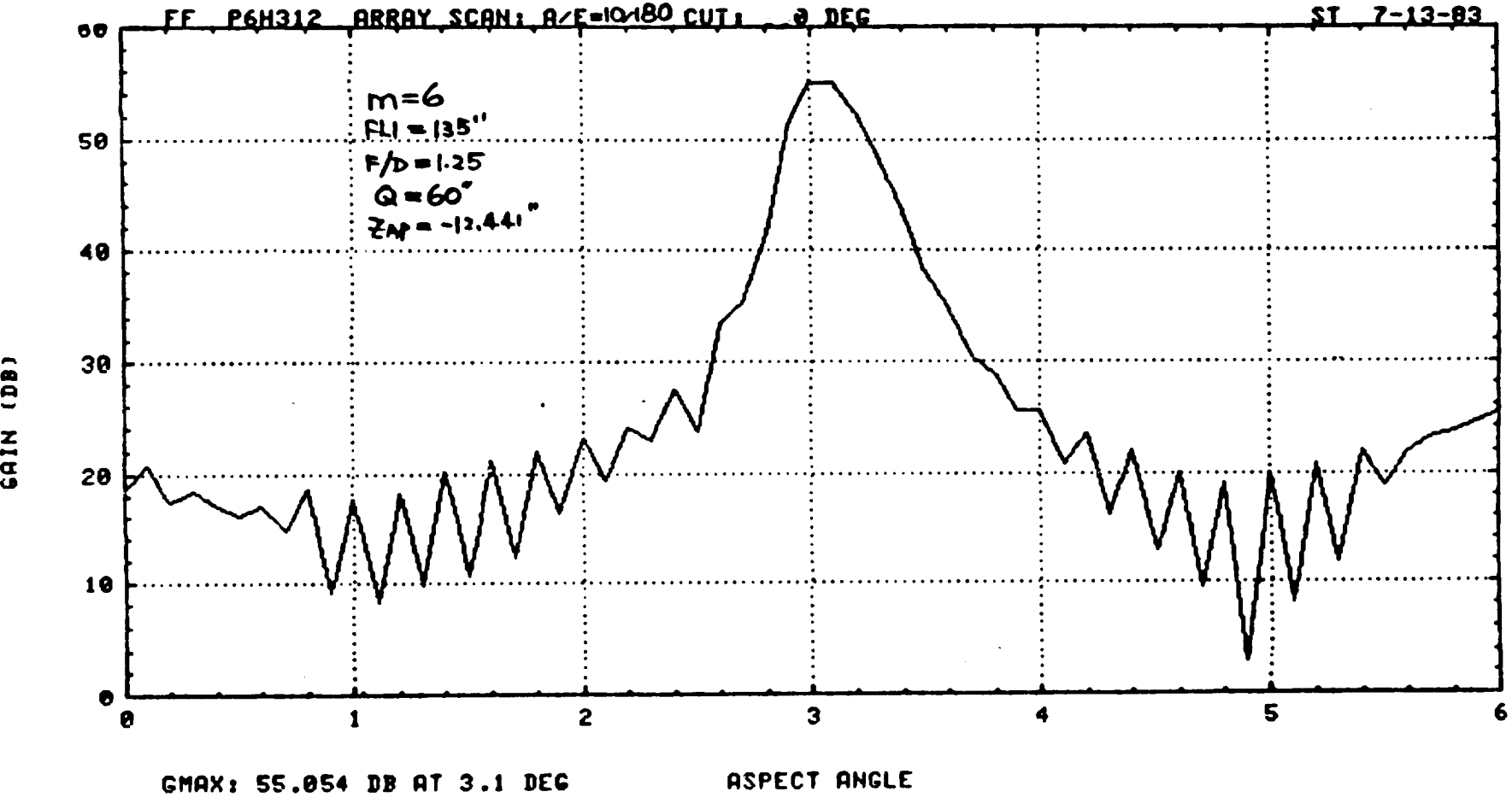
FF P6H312 ARRAY SCAN: A/E=10/180 CUT: 0 DEG
ST 7-13-83
m=6
FLI=135"
F/D=1.25
Q=60°
ZM=-12.441"
GAIN (DB)
60
50
40
30
20
10
0
0
1
2
3
4
5
6
GMAX: 55.054 DB AT 3.1 DEG
ASPECT ANGLE

FIG. 5.3-62

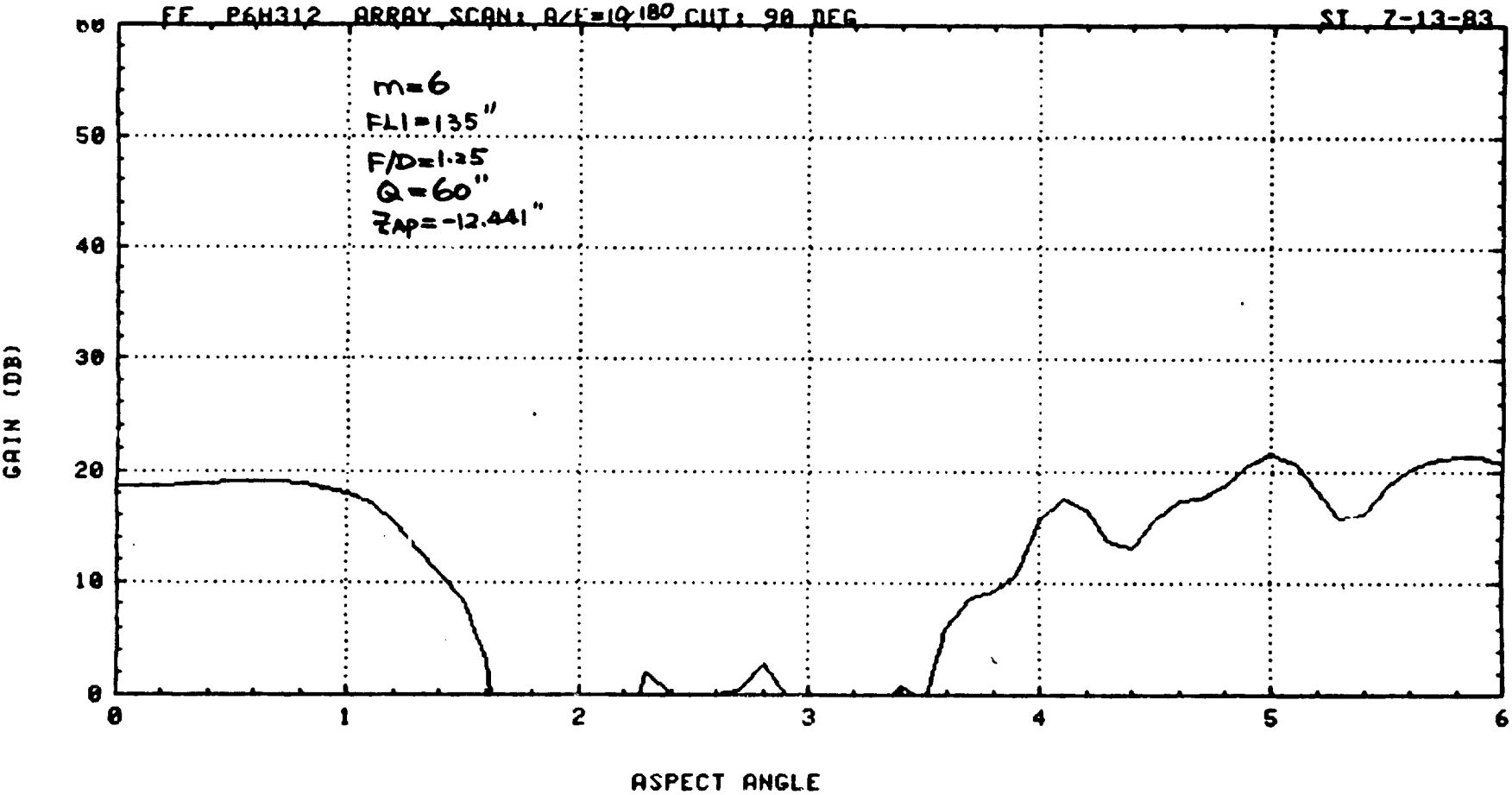
FF P6H312 ARRAY SCAN: A/E=10/180 CUT: 90 DEG
SI 7-13-83
m=6
FLI=135"
F/D=1.25
Q=60"
ZAp=-12.441"
60
50
40
30
20
10
0
GAIN (DB)
0
1
2
3
4
5
6
ASPECT ANGLE

FIG. 5.3-63

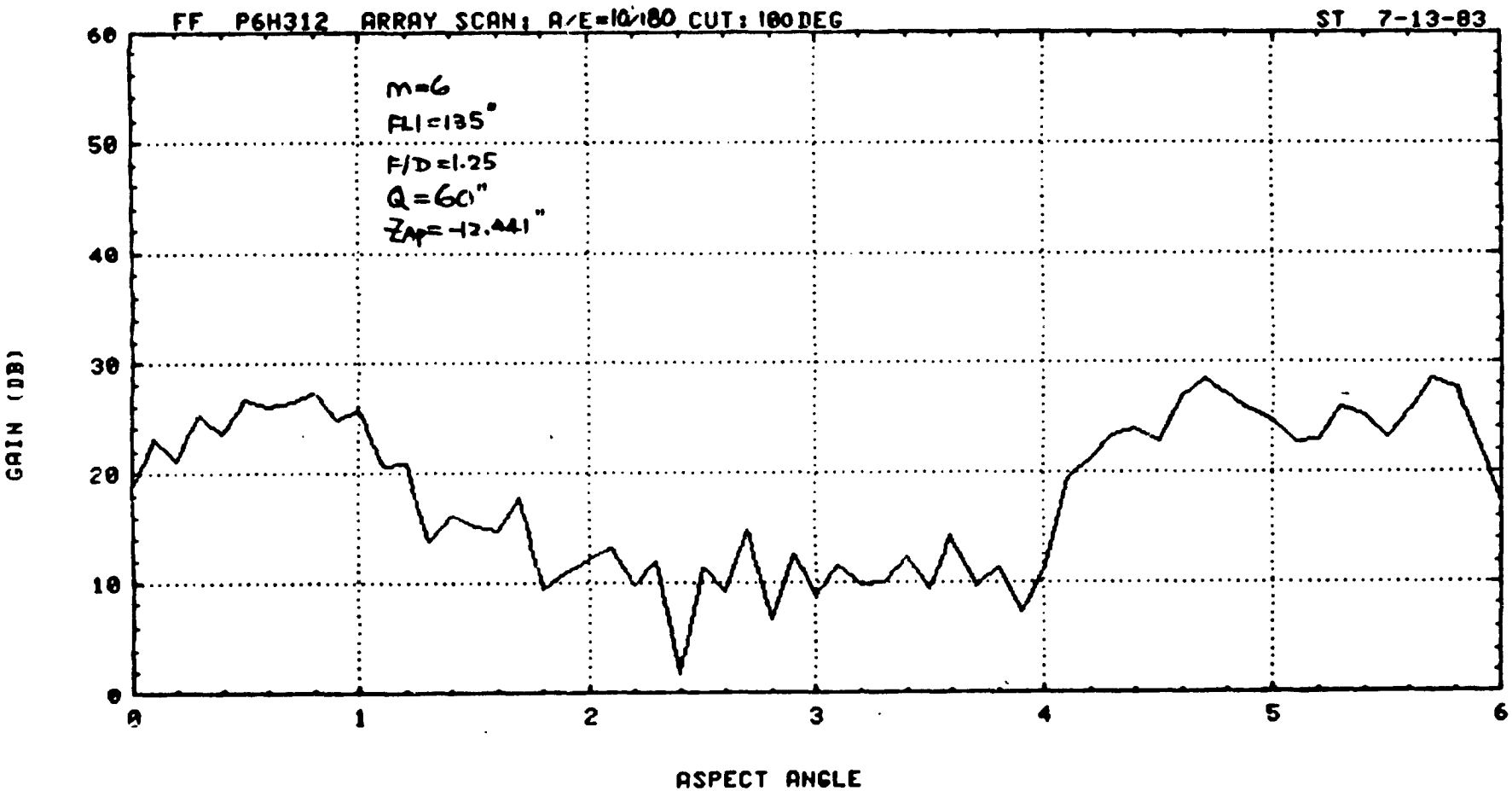
FF P6H312 ARRAY SCAN; A/E=10/180 CUT: 180 DEG
ST 7-13-83
m=6
FLI=135"
F/D=1.25
Q=60"
ZAp=-12.441"
GAIN (DB)
60
50
40
30
20
10
0
0
1
2
3
4
5
6
ASPECT ANGLE

FIG. 5.3 -64

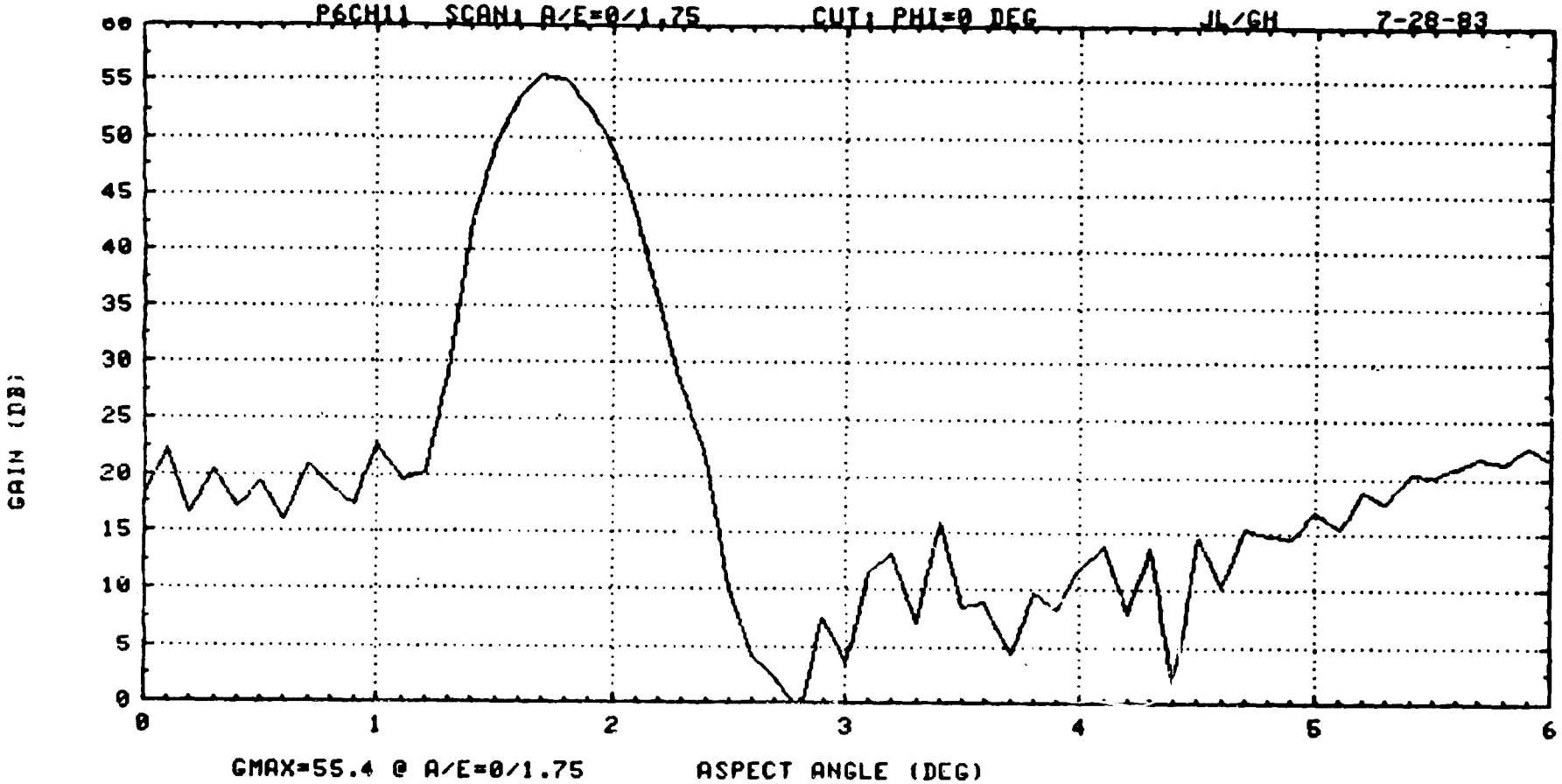
P6CH11 SCAN: A/E=0/1.75
CUT: PHI=0 DEG
JL/GH
7-28-83
GAIN (DB)
60
55
50
45
40
35
30
25
20
15
10
5
0
0
1
2
3
4
5
6
GMAX=55.4 @ A/E=0/1.75
ASPECT ANGLE (DEG)

FIG. 5.3-65

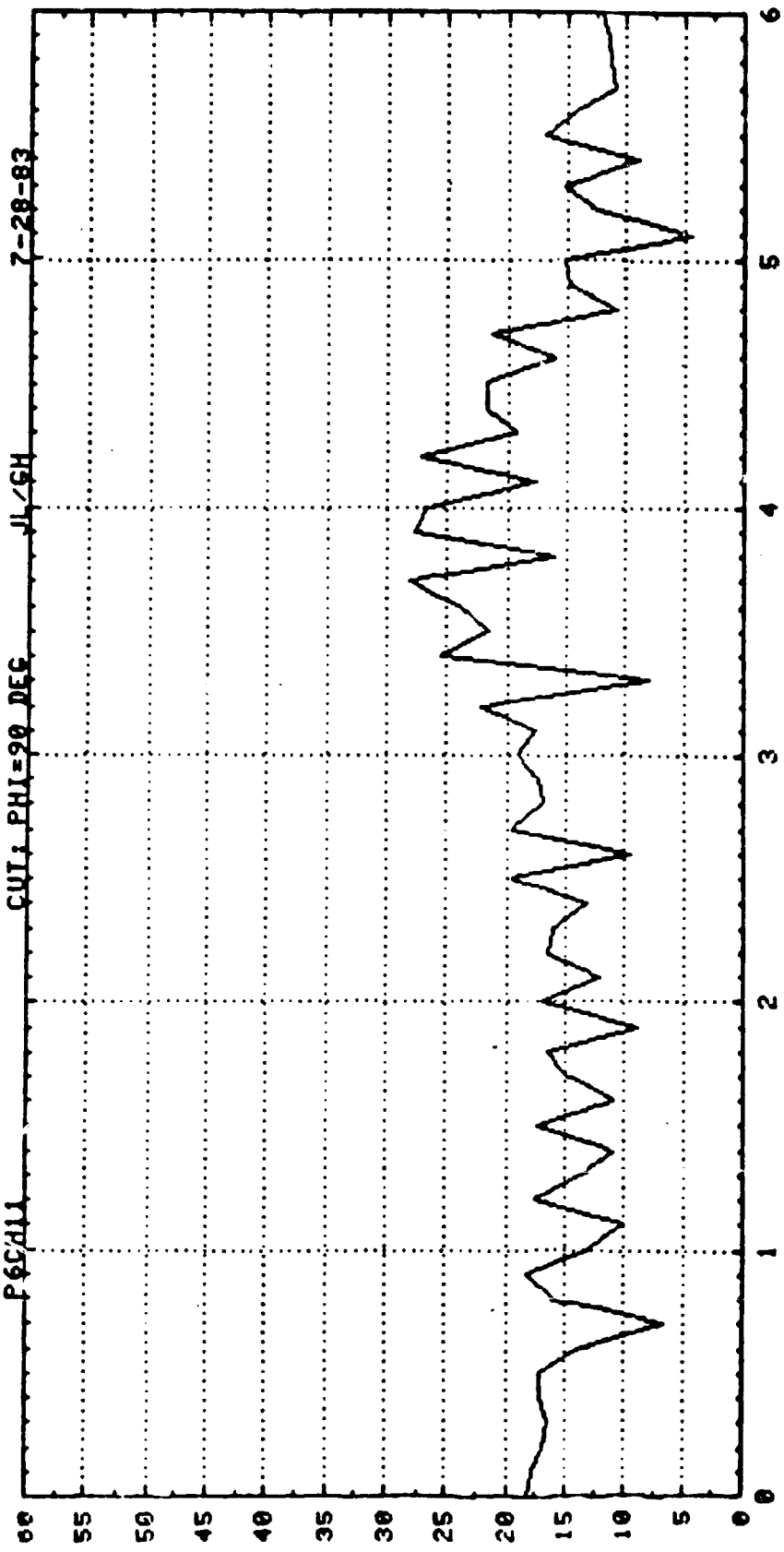
P6CUT
CUT: PHI=90 DEG
11/6H
7-28-83
GRIN (DB)
60
55
50
45
40
35
30
25
20
15
10
5
0
0
1
2
3
4
5
6
ASPECT (DEG)
GMAX=55.4 DB

FIG. 5.3-66

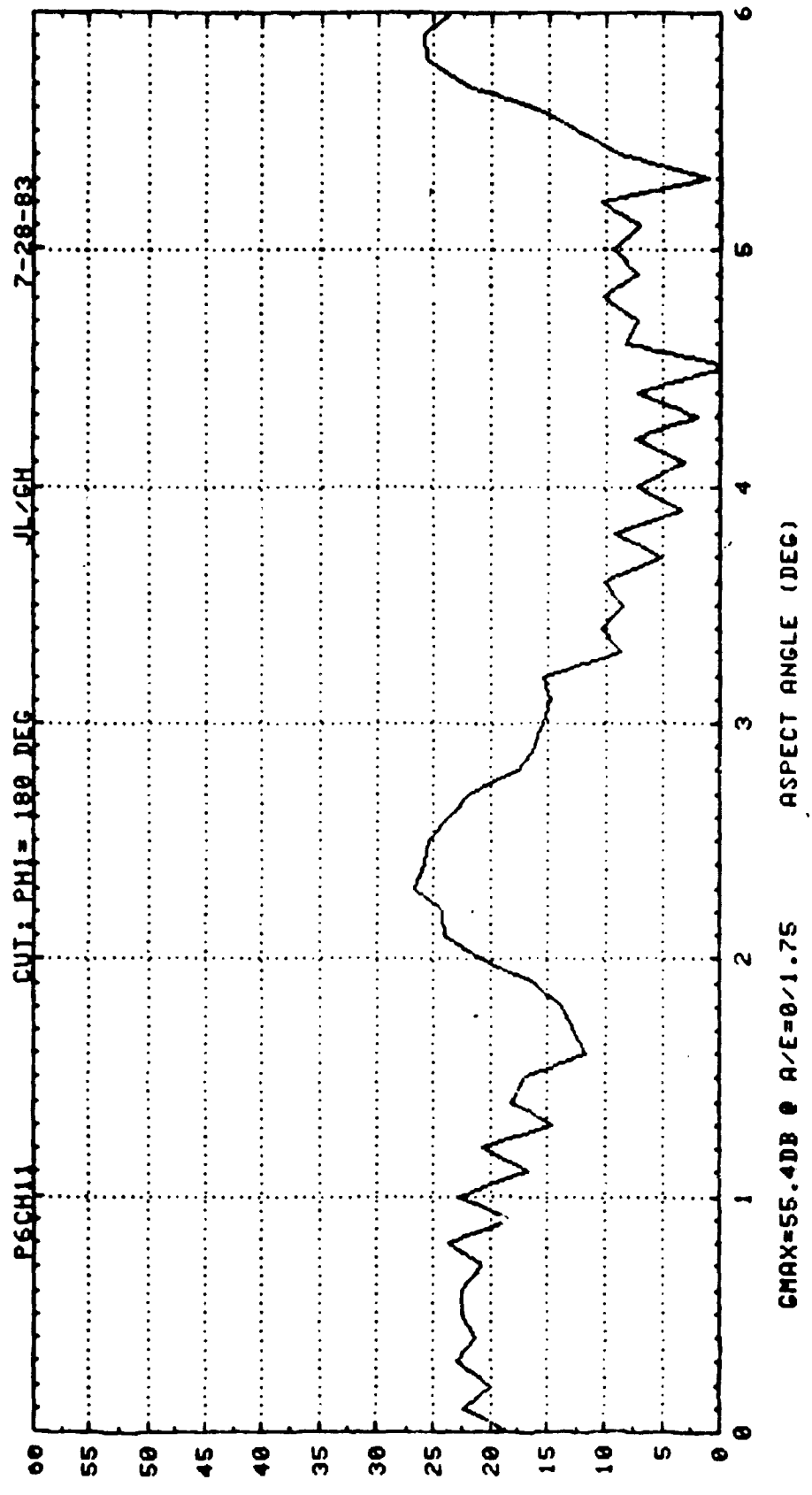
P6CH11
CUT: PHI= 180 DEG
JL/GH
7-28-83
GRIN (DB)
00
55
50
45
40
35
30
25
20
15
10
5
0
0
1
2
3
4
5
6
GMAX=55.4DB @ A/E=0/1.75
ASPECT ANGLE (DEG)

FIG. 5.3-67

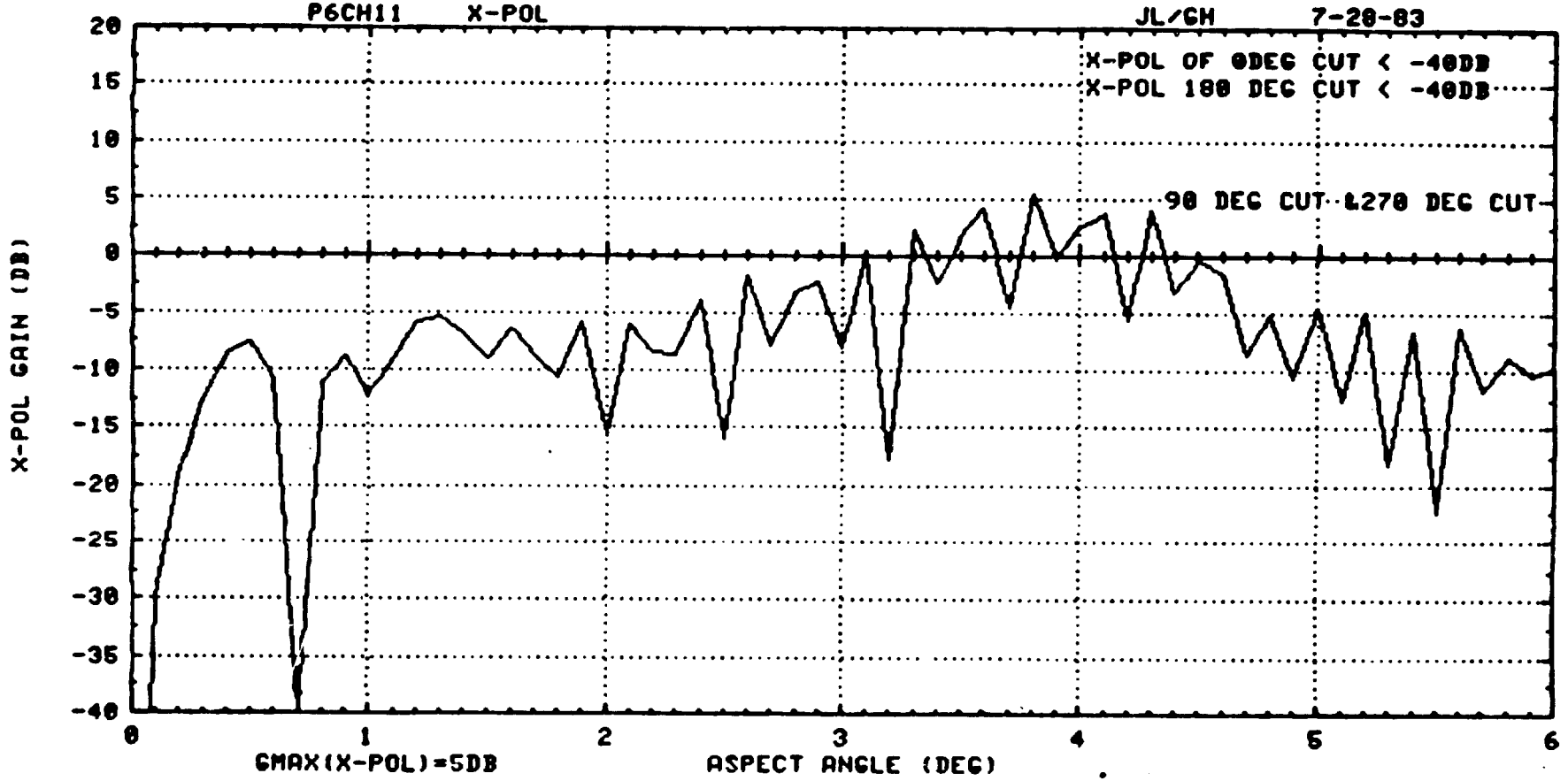
P6CH11 X-POL
JL/GH 7-28-83
X-POL OF 0DEG CUT < -40DB
X-POL 180 DEG CUT < -40DB
90 DEG CUT &270 DEG CUT
X-POL GAIN (DB)
20
15
10
5
0
-5
-10
-15
-20
-25
-30
-35
-40
0
1
2
3
4
5
6
GMAX(X-POL)=5DB
ASPECT ANGLE (DEG)

FIG. 5.3-68

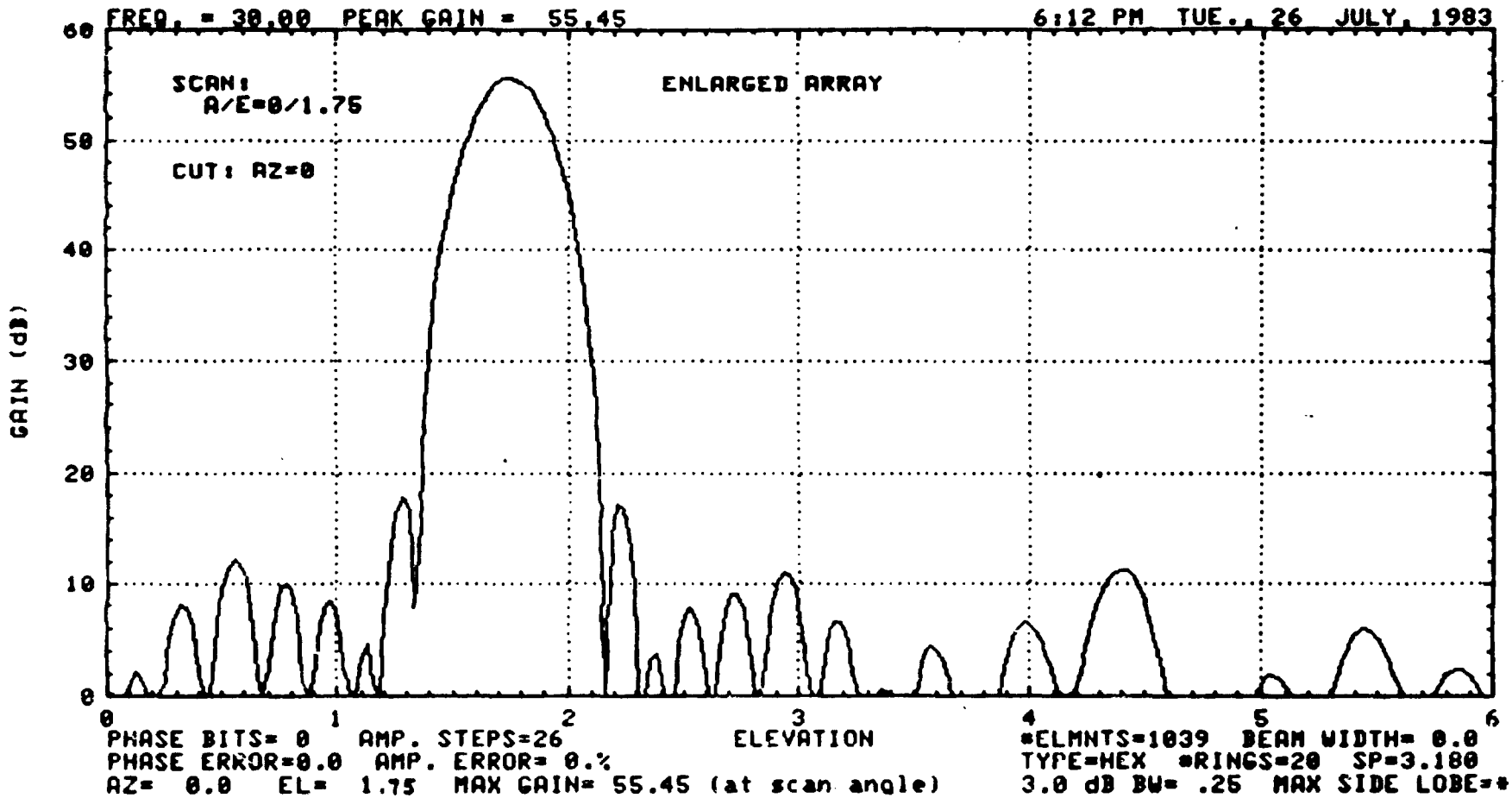
FREQ. = 30.00 PEAK GAIN = 55.45
6:12 PM TUE., 26 JULY, 1983
SCAN:
A/E=0/1.75
ENLARGED ARRAY
CUT: AZ=0
GAIN (dB)
60
50
40
30
20
10
0
0
1
2
3
4
5
6
ELEVATION
PHASE BITS= 0 AMP. STEPS=26
PHASE ERROR=0.0 AMP. ERROR= 0.%
AZ= 0.0 EL= 1.75 MAX GAIN= 55.45 (at scan angle)
#ELMNTS=1039 BEAM WIDTH= 0.0
TYPE=HEX #RINGS=20 SP=3.180
3.0 dB BW= .25 MAX SIDE LOBE=*****

FIG. 5.3-69

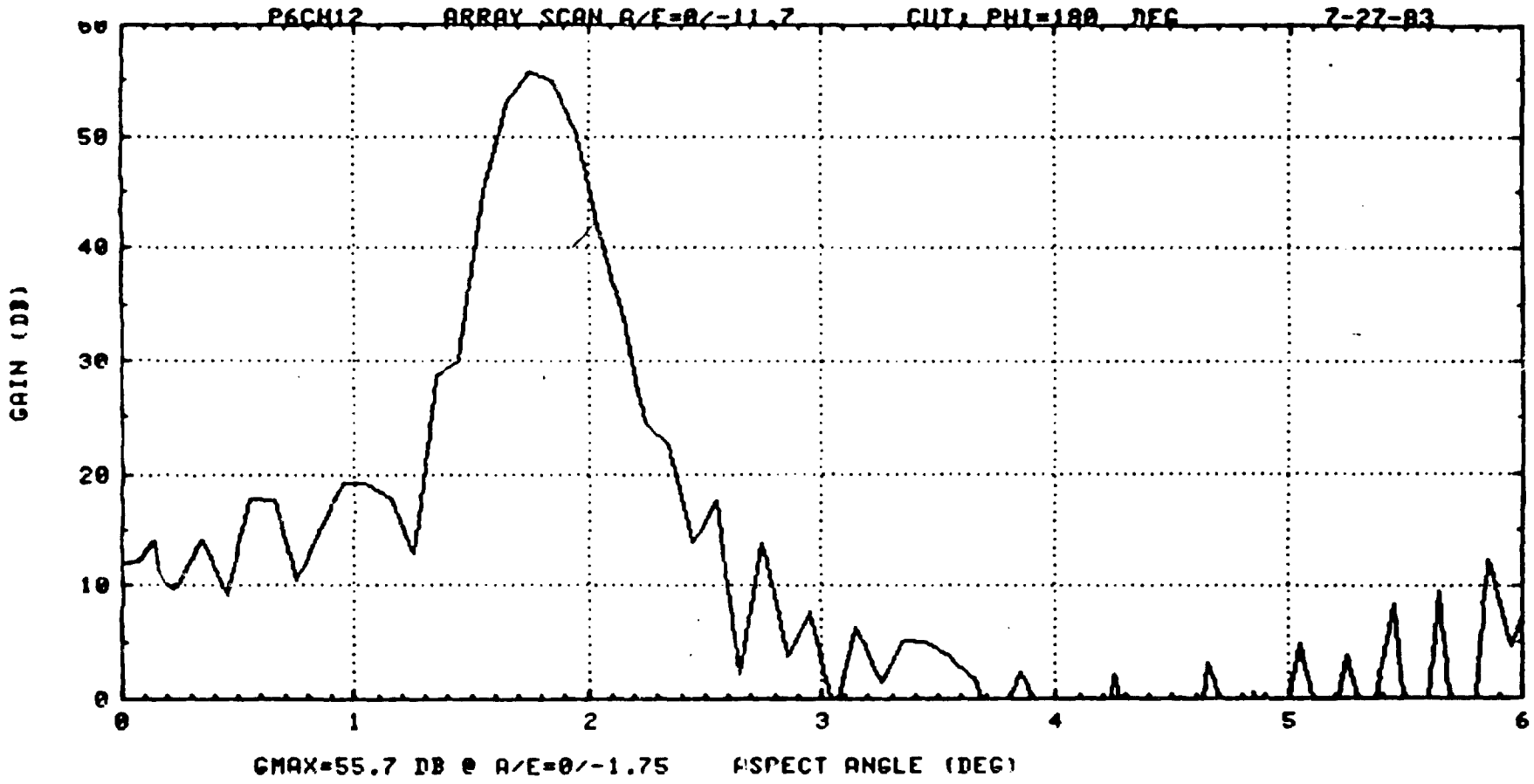
P6CH12 ARRAY SCAN A/E=0/-11.7 CUT: PHI=180 DEG 7-27-83
60
50
40
30
20
10
0
GAIN (DB)
0
1
2
3
4
5
6
GMAX=55.7 DB @ A/E=0/-1.75 ASPECT ANGLE (DEG)

FIG. 5.3-70

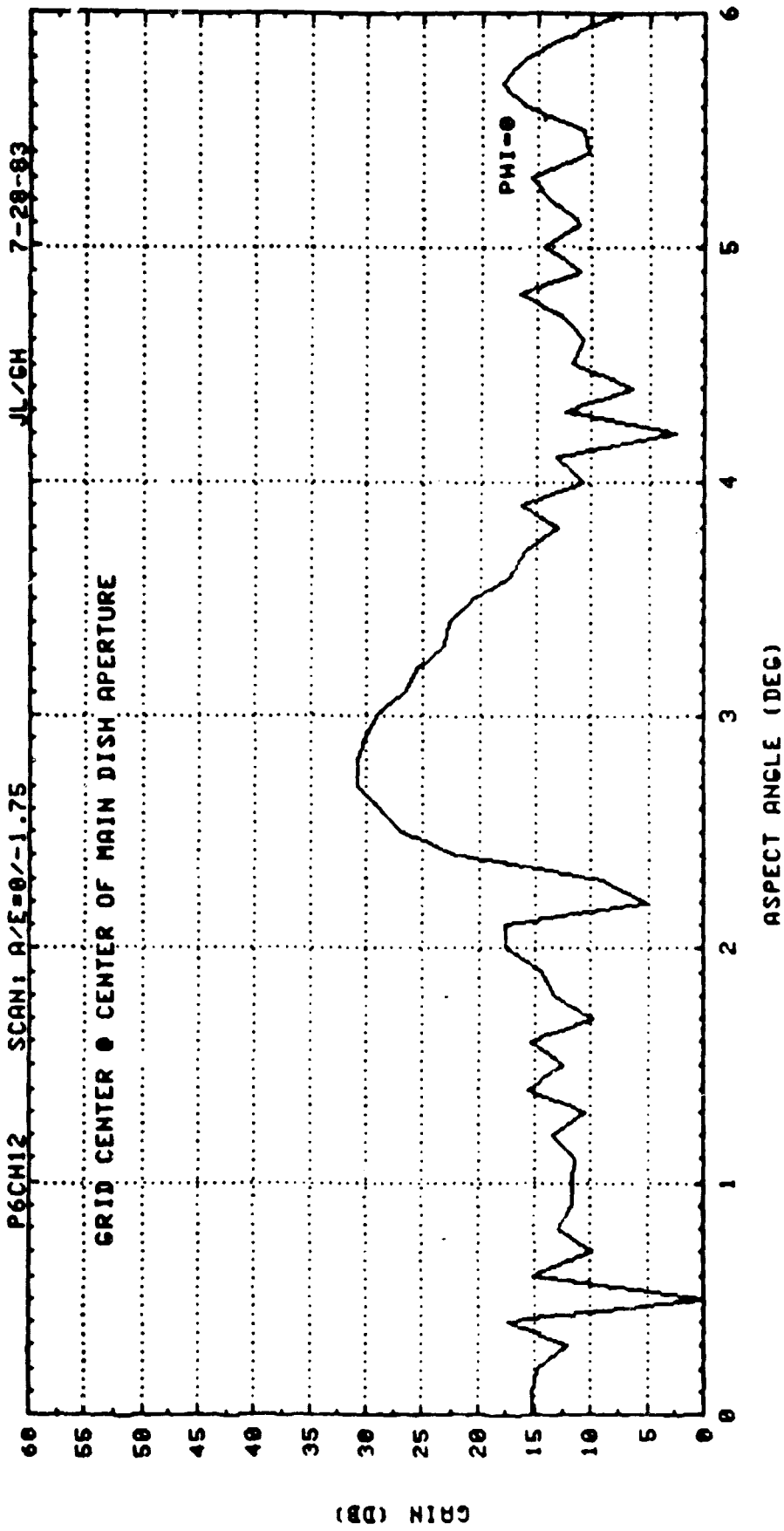
P6CH12 SCAN: A/E=0/-1.75 JL/GH 7-28-83
GRID CENTER ● CENTER OF MAIN DISH APERTURE
PHI=0
GAIN (DB)
ASPECT ANGLE (DEG)
60
55
50
45
40
35
30
25
20
15
10
5
0
0
1
2
3
4
5
6

F.G. 5.3-71

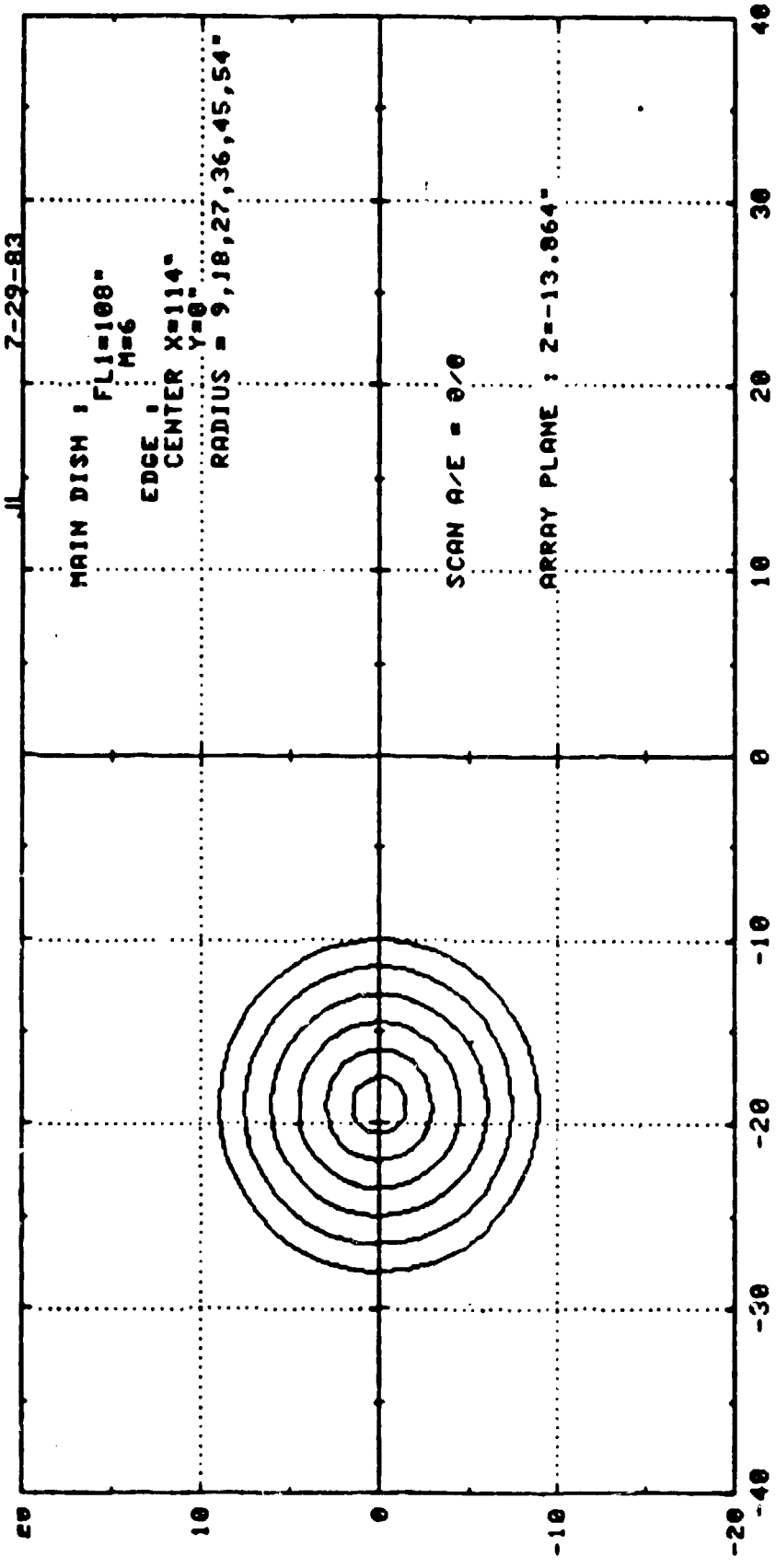

MAIN DISH IMAGES IN THE ARRAY PLANE--UNSCANNED CASE

FIG. 5.3-72